University of Alberta

Conformational analysis of galactofuranosides using NMR spectroscopy and computational chemistry

by

Michele R. Richards

A thesis submitted to the Faculty of Graduate Studies and Research
in partial fulfillment of the requirements for the degree of

Doctor of Philosophy

Chemistry

Fall 2012
Edmonton, Alberta

Dedicated to Jesse R. Davis, who did not attend college but made certain all his grandchildren were able to.

Abstract

The five-membered ring, or furanose, form of galactose is not found in mammalian systems. However, it is commonly found in pathogenic organisms, including *Aspergillus fumigatus*, *Campylobacter jejuni*, and *Mycobacterium tuberculosis*. In many of these organisms, galactofuranose (Gal*f*) is essential for virulence or viability. For example, a major component of the mycobacterial cell wall is the mycolyl-arabinogalactan (mAG) complex, which contains 30–35 alternating β-(1→5)- and β-(1→6)-linked Gal*f* moieties. The enzyme that synthesizes most of the galactan portion of mAG, GlfT2, is bifunctional, forming both β-(1→5)- and β-(1→6)-bonds in a single active site. The exact mechanism of the regiochemistry of bond formation catalyzed by GlfT2 has not been established, but accurate predictions of the conformation of short galactan oligomers would allow us to determine key carbohydrate-protein interactions with these furanose sugars.

The inherent flexibility of the furanose ring makes it difficult to model with current methods. This thesis presents improved tools for determining the conformation of the monosaccharides, methyl α- and β-D-Gal*f*, as well as Gal*f*-containing trisaccharides, which are model systems for the mycobacterial mAG complex. Specifically, we have evaluated the gas-phase the potential energy surfaces (PES) for both monosaccharides. We then compared the low energy conformations from the PES to the solution-state conformation determined from nuclear magnetic resonance (NMR) spectra and the program PSEUROT. For the

α-anomer, there was good agreement between the gas-phase conformation and the PSEUROT results; however, the PSEUROT approach failed for the β-anomer.

To overcome the limitations in PSEUROT, we turned to molecular dynamics (MD) simulations of the monosaccharides. Average vicinal proton–proton coupling constants were determined from the MD simulations, via newly developed Gal*f*-specific Karplus relationships. Most of the calculated vicinal coupling constants agreed well with the corresponding experimental values, except those of the C4–C5 bond. Therefore, we adjusted the force field terms associated with this bond, and the new parameters improved the agreement between experiment and simulation for C4–C5 bond in the monosaccharides. However, the new terms did not affect the C4–C5 bond for β-(1→5)-linked residues in the Gal*f*-containing trisaccharides.

Acknowledgements

First, I would like to thank my advisor, Prof. Todd Lowary, for his support over past several years. I am fortunate to have a mentor who helped me to develop the skills needed for this project and still gave me enough freedom to explore my own ideas.

I sincerely thank Profs. Alex Brown, Gabriel Hanna, and Mariusz Klobukowski for their advice when I ran into the inevitable road blocks. I am grateful to the NMR facility – in particular Dr. Albin Otter and Mr. Mark Miskolzie – for setting up the new experiments needed for my research. I also thank Prof. Christine Syzmanski for her patience in these last few months.

I am privileged to have worked with a great group of people in the Lowary lab. I would particularly like to thank Dr. Hashem Taha for getting me started and commiserating through the "notebook of fail". Without my talented synthetic colleagues – Mr. Yu Bai, Mr. Simon Byrns, Dr. Maju Joe, and Dr. Chunjuan Liu – I would not have had any molecules to study. I am also grateful to Mr. Myles Poulin for helpful discussions and proofreading.

My time at the UofA would not have been nearly as enjoyable without my classmates, especially Ms. Sara Bonderoff, Dr. Jessie Key, Ms. Stéphanie Lessard, Dr. Tiffany MacDougall, Dr. Avena Ross, and Dr. Erin Sullivan.

Finally, I would like to thank my family for their constant love and support. I would not have made it this far without the encouragement from my husband, Christopher Cairo.

Table of Contents

List of Tables

List of Figures

List of Abbreviations

$^{3}J_{C,H}$	Three-bond carbon-proton coupling constant
$^{3}J_{H,H}$	Three-bond proton-proton coupling constant
All*f*	Allofuranose
AMBER	Assisted Model Building with Energy Refinement
Ara*f*	Arabinofuranose
Ara*p*	Arabinopyranose
B3LYP	Becke 3-parameter Lee-Yang-Parr
DFT	Density Functional Theory
E	Envelope
eq.	Equation
EXSIDE	Excitation-Sculptured Indirect-Detection Experiment
FAD	Flavin Adenine Dinucleotide
Gal*f*	Galactofuranose
Gal*f*NAc	2-Acetamido-2-deoxy-D-galactofuranose
Gal*p*	Galactopyranose
Gal*p*NAc	2-Acetamido-2-deoxy-D-galactopyranose
GalPUT	Galactose-1-phosphate Uridinyltransferase
ge-CSSF	Gradient-enhanced Chemical Shift Selective Filtering
Glc*f*	Glucofurnaose
Glc*p*	Glucopyranose
GlfT1	Galactosyltransferase 1
GlfT2	Galactosyltransferase 2

Gul*f*	Gulofuranose
HPLC	High Pressure Liquid Chromatography
IC_{50}	Half-maximal Inhibitory Concentration
J	Coupling Constant
K_d	Dissociation Constant
mAG	Mycolyl Arabinogalactan
Man*p*	Mannopyranose
MD	Molecular Dynamics
MIC	Minimum Inhibitory Concentration
MM	Molecular Mechanics
MMCSA	Metropolis Monte Carlo Simulated Annealing
MP2	Second-order Møller–Plesset perturbation theory
NMR	Nuclear Magnetic Resonance
NOE	Nuclear Overhauser Effect
P	Pseudorotational phase angle
PES	Potential Energy Surface
PIX	Positional Isotope Exchange
PMF	Potential of Mean Force
RESP	Restrained Electrostatic Potential
QM	Quantum Mechanics
RMS	Root Mean Square
RMSD	Root Mean Square Deviation
RMSE	Root Mean Squared Error
S_N2	Bimolecular Nucleophilic Substitution
STD	Saturation Transfer Difference

TOCSY	Total Correlation Spectroscopy
UDP	Uridine Diphosphate
UGM	UDP-Galactopyranose Mutase
UMP	Uridine Monophosphate
WHAM	Weighted Histogram Analysis Method
α-Gal*f*	Alpha Galactofuranose
β-Gal*f*	Beta Galactofuranose
$\Delta\nu$	Chemical shift difference in Hz
ϕ_m	Psuedorotational ring puckering

Chapter 1:

Biosynthesis of galactofuranose-containing polysaccharides

A portion of this chapter was published as a review article in a peer-reviewed journal:

Richards, M. R.; Lowary, T. L. *ChemBioChem* **2009**, *10*, 1920–1938.[1]

1.1. Introduction

Galactose is an important component in many mammalian glycoconjugates, including the ABO blood group antigens, the glycosaminoglycan keratan sulfate, and glycolipids such as GM1 and GM3.[2] In mammals, galactose is found solely in the six-membered ring form as galactopyranose (Gal*p*); in contrast, galactose is found both as Gal*p* and as galactofuranose (Gal*f*), the five-membered ring form, in bacteria, protozoa, and fungi. Examples of a few glycoconjugates from pathogenic organisms are illustrated in Figure 1.1. Many of these organisms that produce Gal*f* are pathogenic; thus, targeting Gal*f* biosynthesis might lead to novel, specific therapies, and we propose that a detailed understanding of their conformational properties is essential to successfully exploiting them as drug targets. The design of inhibitors for many enzyme systems has benefited from a detailed understanding of the substrate's conformational preferences.[3,4] The furanose ring is much more flexible than the pyranose ring,[5-7] but conformational models of the former are not well refined. Our objective has been to elucidate the conformational preferences of Gal*f* through NMR spectroscopy and computational chemistry.

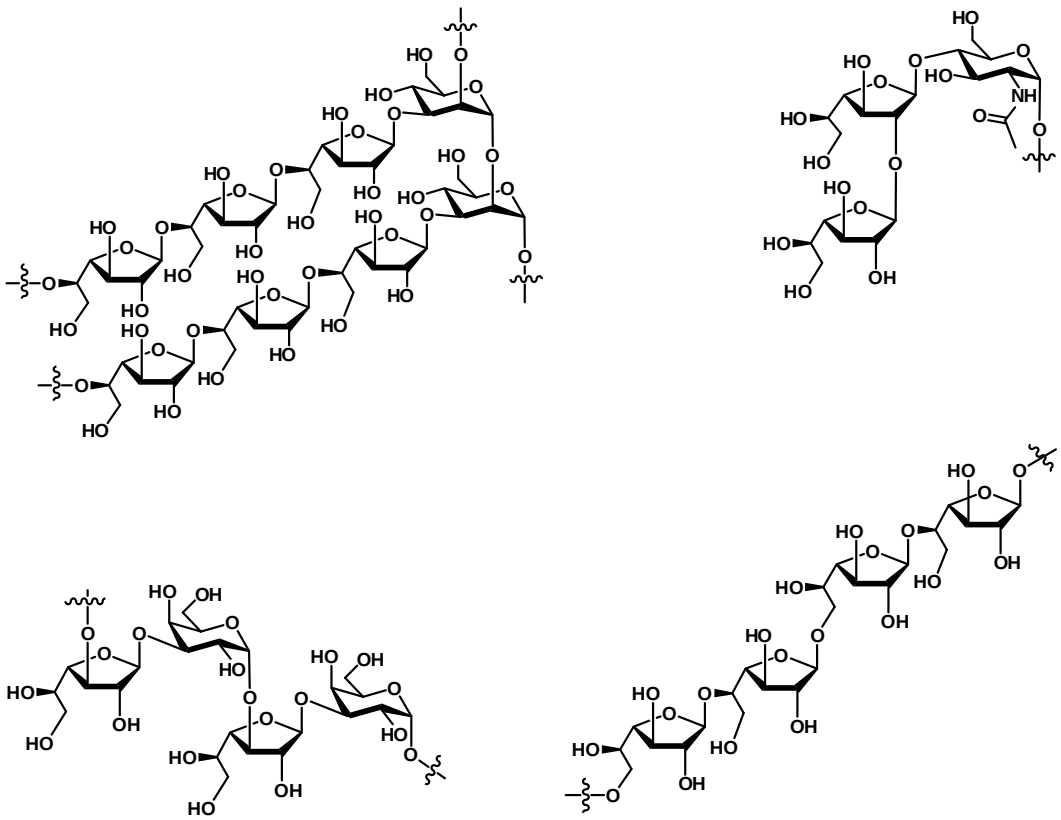

Figure 1.1. Portions of glycoconjugates containing galactofuranose from pathogenic organisms (clockwise, from top right): galactomanan from *Aspergillus fumigatus*, mucin-like proteins from *Trypanosoma cruzi*, arabinogalactan from *Mycobacterium tuberculosis*, and galactan I from *Klebsiella pneumoniae.*

This chapter focuses on the enzymes responsible for Gal*f* biosynthesis, particularly the one that create the furanose ring (UDP-galactopyranose mutase, UGM).[8] UGM is central to galactofuranose metabolism; most organisms cannot use exogenous Gal*f,* and UDP-Gal*f* appears to be the biological source of Gal*f* residues in polysaccharides.[9] Readers are also alerted to other reviews by Houseknecht and Lowary,[10] Pedersen and Turco,[11] Peltier et al.,[12] von Itzstein,[13] and Tefsen et al.[14] that also discuss the chemistry and biology of Gal*f.*

The earlier review by Peltier et al.[12] includes an extensive list of Gal*f*-containing polysaccharides and the organisms that produce them. These are,

therefore, not catalogued here. To highlight just a few examples: the major structural component of the *Mycobacterium tuberculosis* cell wall contains a galactan chain of 30–35 Gal*f* units,[15] and the biosynthesis of the galactan is essential for viability.[16] The O-antigens of both *Escherichia coli* and *Klebsiella pneumoniae* contain β-D-Gal*f* as part of lipopolysaccharides.[9,17] Several Gal*f*-containing glycoconjugates have been found in *Trypanosoma cruzi*, the causative agent of Chagas disease, including glycoinositolphopholipids,[18,19] lipopeptido-phosphoglycans,[20] and mucin-like proteins.[21] The galactomannan of *Aspergillus fumigatus* also contains Gal*f*,[22] and this polysaccharide is used for clinical detection of fungal infections.[23,24] Finally, halting Gal*f* biosynthesis in *Leishmania major* attenuates its virulence.[25]

Since the earlier review's publication, several other oligosaccharides with Gal*f* have been identified in algae, bacteria, fungi, lichen, marine sponges, and nematodes. Analysis of cell-wall glycoproteins from the green alga *Chlamydomonas reinhardtii* revealed polysaccharides similar to those found in plants: α-D-Gal*f*-(1→2)-β-L-Ara*f*-(1→2)-β-L-Ara*f*-(1→4)-hydroxyproline and 3-*O*-methyl-β-L-Ara*f*-(1→5)-α-D-Gal*f*-(1→2)-β-L-Ara*f*-(1→2)-β-L-Ara*f*-(1→4)-hydroxyproline.[26] The core arabinose disaccharide seems to be conserved between plants and algae, and glycosylation of hydroxyproline in proteins of plants has been shown to stabilize polyproline type II helices.[27] The lipopolysaccharide from *Citrobacter freundii*, a bacterium that causes enteritis, contains the same repeating unit as galactan I from *K. pneumoniae*: [→3)-β-D-Gal*f*-(1→3)-α-D-Gal*p*(1→].[28] Cell-wall polysaccharides from the

cyanobacterium *Nostoc commune* contain linear chains of three to nine β-(1→6)-linked Gal*f* residues.[29] A complex polysaccharide containing Gal*f* at branch points (Figure 1.2) was identified from the fungus *Neotestudina rosati*, an organism that causes severe subcutaneous infections that often lead to deformity.[30] A similar, less branched polysaccharide was found in the water-soluble extract from the lichen species *Lichina pygmaea* and *L. confinis*; it too is composed of a main chain of α-(1→6)-linked mannose, with substitution at O2 or at both O2 and O4 positions with the less common α-Gal*f* residues.[31] A glycosphingolipid vesparioside B from the marine sponge *Spheciospongia vesparia* was identified containing both α- and β-Gal*f* components: α-D-Gal*f*-(1→3)-[α-D-Gal*f*-(1→2)]-β-D-Gal*f*-(1→3)-α-D-Gal*p*-(1→2)-α-D-Ara*p*-(1→6)-β-D-Glc*p*.[32] Interestingly, in this last example, the authors assigned the anomeric configurations for the furanosides through three-bond proton-proton coupling constants by comparing the values from the ^{1}H NMR spectrum to values determined via quantum mechanical calculations. A terminal α-D-Gal*f* residue was found in the exopolysaccharide produced by *Bifidobacteriaum animalis* subsp. *lactis*, a probiotic often present in dairy products.[33] Recently, galactomannans were isolated from a group fungi that infect insects – *Lecanicillium muscarium*, *Beauveria bassiana*, *Beauveria brogniartii*, and *Cordyceps sphingum* – that all contain Gal*f* in β-(1→2)-linkages to the mannan.[34]

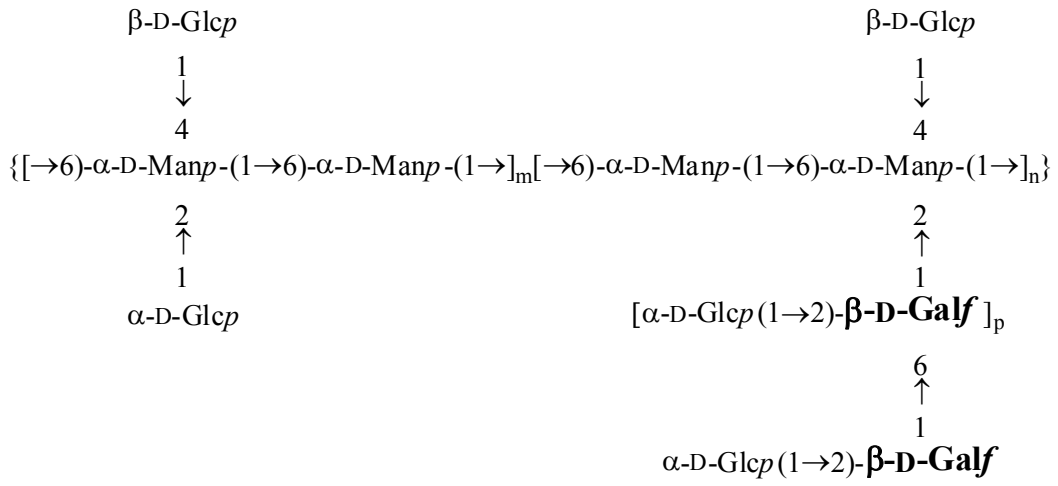

Figure 1.2. Complex Gal*f*-containing polysaccharide isolation from *Neotestudina rosati.*

1.2. Biosynthesis of galactofuranose residues

Several enzymes involved in Gal*f* polysaccharide synthesis have been identified and characterized in detail – a mutase that provides the starting material (UDP-Gal*f*) for elongating galactan chains, two galactosyltransferase enzymes from *Mycobacterium tuberculosis*, and *exo*-galactofuranosidases.

1.2.1. UDP-galactopyranose mutates (UGM)

Because Gal*f* is not present in glycoconjugates in mammals, Gal*f* metabolism is an attractive therapeutic target for the treatment of diseases caused by *Mycobacteria* spp., *Leishmania* spp., *Trypanosoma cruzi*, *E. coli*, and *Klebsiella* spp., among others.[11,13] These pathogenic organisms all use the same building block for synthesizing Gal*f*-containing polysaccharides: uridine diphosphogalactofuranose (UDP-Gal*f*, **1.2**, Figure 1.3). This sugar nucleotide is produced from UDP-Glc*p* by the enzymes UDP-glucose 4-epimerase (generating

UDP-Gal*p*, **1.1**) and UDP-galactopyranose mutase (UGM), which catalyzes the transformation of UDP-Gal*p* to UDP-Gal*f*.[35] The gene encoding UGM was first identified in *E. coli* 1996,[9] followed shortly by its identification in *K. pneumoniae*[17] and *M. tuberculosis*.[36] More recently, UGM was identified in the eukaryotes *Aspergillus fumigatus*,[37] *Cryptococcus neoformans*, *Leishmania major*,[38] *Trypanosoma cruzi*,[36,39] and *Caenorhabditis elegans*.[40] There is only about 20% homology between the eukaryotic and prokaryotic proteins, though the sequence identity is similar for the active site amino acids.[39] A homologue of UGM from *Campylobacter jejuni* has also been characterized, and this enzyme can catalyze the reaction from UDP-2-acetamido-2-deoxy-D-galactopyranose (UDP-Gal*p*NAc) to UDP-2-acetamido-2-deoxy-D-galactofuranose (UDP-Gal*f*NAc), in addition to the reaction from UDP-Gal*p* to UDP-Gal*f*.[41]

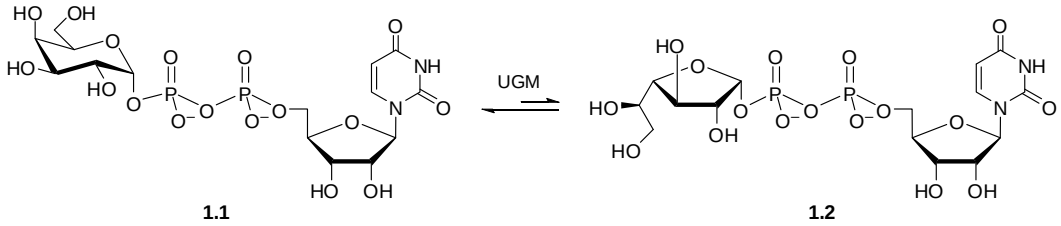

Figure 1.3. The reaction catalyzed by UDP-galactopyranose mutase (UGM).

Besides not being present in mammals, UGM is also crucial for the survival of these organisms. For example, when UGM is not expressed in *L. major*, its virulence is attenuated[25] and no lipophosphoglycan is produced.[42] In fact, when mice were infected with *L. major* clones lacking UGM, they showed a dramatic reduction in onset of symptoms (nine weeks versus three weeks for wild-type).[42] When UGM is deleted from *A. niger*, colony growth is altered.[25] In *A.*

fumigatus, UGM deletion leads to thinner cell walls, increased susceptibility to antifungals, attenuated virulence, and reduced growth.[43] Deletion of UGM in *C. elegans* results in larval lethality.[40] This evidence suggests that UGM is an attractive therapeutic target. Also, if UGM is overexpressed in *M. bovis*, the organism displays increased resistance to isoniazid, one of the front-line drugs used to treat tuberculosis.[44]

1.2.2. UGM structure and mechanism

There has been significant effort toward understanding the mechanism of UGM. Naismith and coworkers reported the first crystal structure of UGM from *E. coli* in 2001.[45,46] Site-directed mutagenesis and comparison with other flavin and nucleotide binding domains identified key amino acid contacts: W156 stacks against uridine; R247 and R278 form ionic interactions with the diphosphate; and Y181, Y311, and Y346 are important for substrate binding, potentially forming hydrogen bonds with the carbohydrate ring. In 2005, Naismith and coworkers solved additional crystal structures of UGM with FAD bound – from *M. tuberculosis* in the oxidized (inactive) state, as well as from *K. pneumoniae* in both the oxidized (inactive) and reduced (active) states.[8] These structures are quite similar to the *E. coli* enzyme, with < 1.2 Å root mean square deviation (RMSD) for the 330 α-carbons in the proteins. The major differences seen in the structures are in the flexible loop. This loop is in the "closed" form in the *E. coli* structure, lying in the cleft occupied by the FAD cofactor; whereas, the loop is in the solvent-exposed, "open" form in the *M. tuberculosis* and *K. pneumoniae* structures. Further site-directed mutagenesis studies identified a key arginine

residue on the mobile loop necessary for catalysis – R170 in *E. coli*.[47] When this residue is mutated to alanine, UGM no longer catalyzes the reaction. Docking studies and molecular dynamics simulations indicate that R170 forms an electrostatic interaction with the β-phosphoryl group of UDP-Gal*p*. The UGM from *M. tuberculosis* and *K. pneumoniae* also possess this arginine residue, R180 and R174, respectively. Molecular dynamics simulations and biophysical studies, including measuring changes in tryptophan and FAD fluorescence for various UGM mutants and STD NMR,[48] indicate that substrate binding induces closure of the flexible loop, which is necessary for the reaction.[49]

Since the first crystal structure of UGM was reported, there has been considerable progress towards elucidating its mechanism. Elegant isotope scrambling experiments demonstrated the anomeric carbon–OUDP bond is broken during the reaction.[50] Additionally, it was shown that 2- 3-, and 6-fluoro-galactose analogs, both in the pyranose and furanose form, can act as substrates for UGM.[51-54] The experiments with the fluorinated derivatives establish both that the UDP is not transferred to O2 during the reaction and that neither C2 nor C3 are oxidized during ring contraction. The catalytic efficiencies (k_{cat}/K_m) of the 2-deoxy-2-fluoro- and 3-deoxy-3-fluoro- analogs are decreased by four and three orders of magnitude, respectively, from UDP-Gal*f*,[52] while the 6-deoxy-6-fluoro-analog is only ten times less efficient.[54] These data support an oxocarbenium ion intermediate or transition state. Also, because the 2-deoxy-2-fluoro compound is dramatically less active than UDP-Gal*f*, there could be strong stabilizing interactions between the C2 hydroxyl and amino acid side chains in the active

site. Furthermore, neither talose, the C2 epimer of galactose, nor 2-deoxy-2-fluoro-talose serve as substrates for UGM.[54]

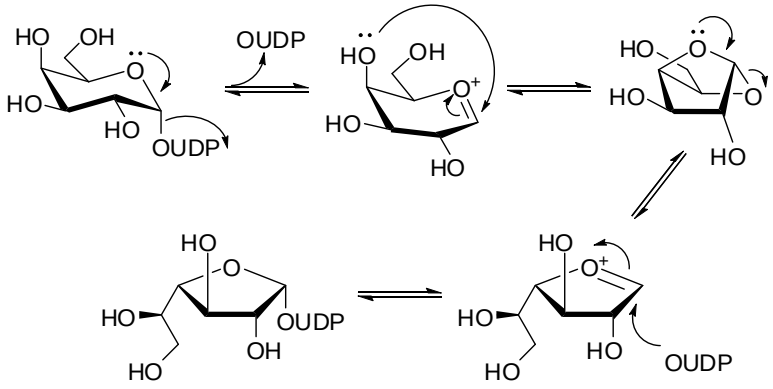

Figure 1.4. One of several proposed mechanisms for UGM.

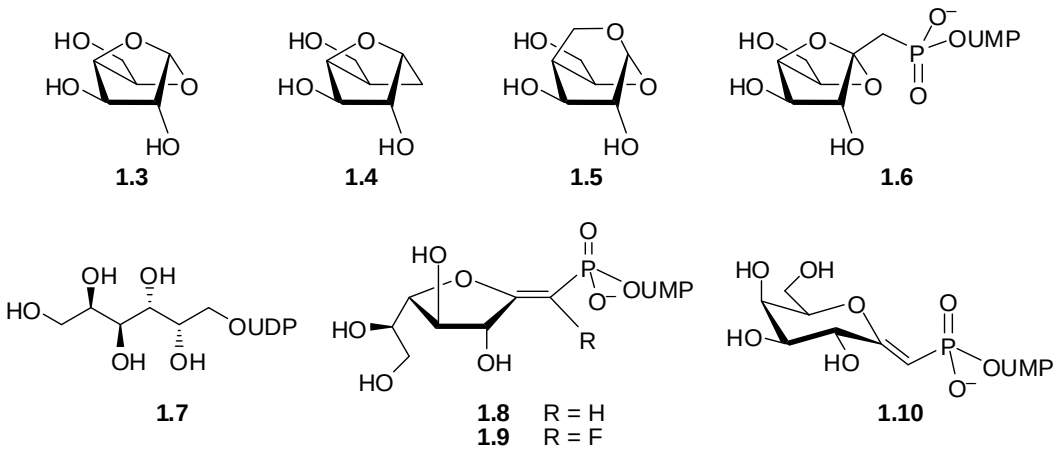

Figure 1.5. Several compounds designed to test the mechanism of UGM.

The isotope exchange data support a bicyclic intermediate in the ring contraction,[50] as is shown in Figure 1.4. This proposed mechanism would also be consistent with the fluorinated analogs serving as substrates. To test various proposed mechanisms, several groups have designed compounds to serve as substrates, transition state mimics, or inhibitors (Figure 1.5). Caravano et al. made the proposed bicyclic intermediate itself, 1,4-anhydrogalactopyranose (**1.3**),

and it was not a substrate for UGM in 0.5–5 mM concentration range.[55] The carbasugar analog **1.4** and methylene homologue **1.5** were synthesized by Sadeghi-Khomami et al. as potential inhibitors of UGM.[56-58] For **1.4**, no inhibition was seen at concentrations up to 100 μM, and **1.5** showed only 17% inhibition at 4 mM. In contrast, phosphonate **1.6** was designed as conformational probe,[59] and it is a weak inhibitor of the UGM, with ~30% inhibition at 1 mM. Compound **1.6** inhibits UGM, whereas **1.3** and **1.4** do not; this difference can be attributed to the presence of uridine. UDP itself is a competitive inhibitor of UGM with a K_i of 37 μM.[56] Itoh et al. synthesized UDP-galactitol (**1.7**) to test if the conversion of UDP-Gal*p* to UDP-Gal*f* goes through an oxocarbenium intermediate.[60] The rationale for the design of this compound is if the reaction undergoes a direct nucleophilic attack (S_N2), then **1.7** should be a substrate for UGM; if, on the other hand, the reaction goes through an oxocarbenium intermediate (either S_N1 or radical mechanisms), then UDP-galactitol should remain intact. UDP-galactitol is not a substrate for UGM; in fact, it is a weak inhibitor with comparable inhibition to UDP itself. Caravano et al. synthesized UDP-*exo*-galactofuranosyl glycal (**1.8**),[61] a fluorinated *exo*-glycal (**1.9**),[62] and UDP-*exo*-galactopyranosyl glycal (**1.10**)[63] as conformational mimics of an oxocarbenium transition state. The furanose compounds **1.8** and **1.9** showed time-dependent inactivation when assayed against oxidized (i.e. inactive) UGM; however, when a reducing agent was added the compounds were weak inhibitors (<10% inhibition at 1 mM). In contrast, **1.10** was a competitive inhibitor with 42% inhibition at 1 mM under non-reducing conditions.

UGM is a flavin-dependant enzyme; however, the conversion of Gal*p* to Gal*f* is not a redox process. Thus, the precise role of flavin adenosine dinucleotide (FAD) in the reaction has elicited much interest. Despite early reports to the contrary,[52,64] only the reduced form of the enzyme is active.[45,65-69] Potentiometric studies determined that the reduced form of the flavin in UGM is the anionic $FADH^-$, rather than the neutral $FADH_2$.[65] Further EPR experiments showed that binding of the sugar nucleotide stabilized the radical $FADH^{\bullet}$.[65] These data support a radical mechanism for the ring contraction catalyzed by UGM. Additional support comes from activity studies using enzymes reconstituted with deaza-analogs of FAD:[66] UGM is active with FAD or 1-deaza-FAD (Figure 1.6) but not with 5-deaza-FAD. Both FAD and 1-deaza-FAD can participate in one- or two-electron processes. However, 5-deaza-FAD is limited solely to two-electron processes. Interestingly, there are other enzymes, such as chorismate synthase, that also require reduced FAD to catalyze reactions that are not redox processes. In the case of chorismate synthase, the enzyme has been shown to proceed through a radical mechanism.[64]

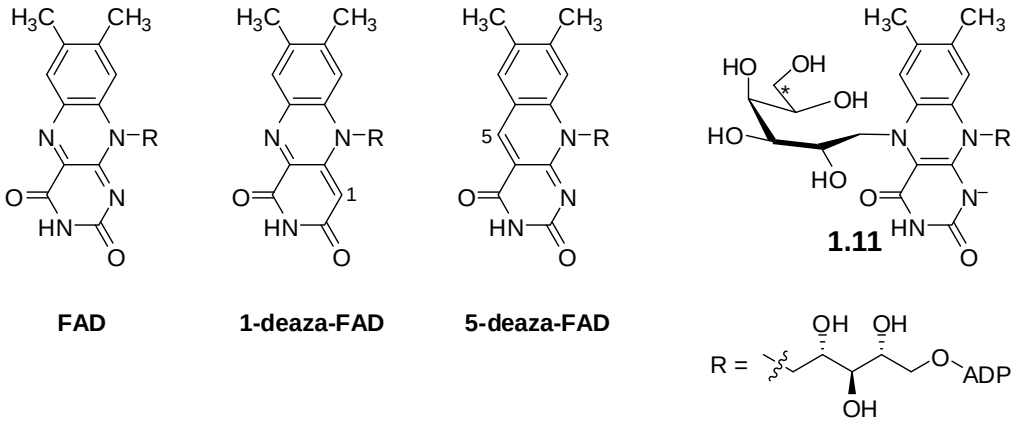

Figure 1.6. FAD-containing compounds to probe whether UGM uses a radical or nucleophilic mechanism.

Kiessling and coworkers put forth another possible mechanism for UGM, that N5 of $FADH^-$ acts as a nucleophile and attacks the anomeric carbon of the oxocarbenium intermediate, forming an iminium ion intermediate.[67] UGM was incubated with UDP-Gal*p* tritiated at C6 then treated with the reducing agent sodium cyanoborohydride, and a radiolabeled flavin–galactose adduct **1.11** was isolated (Figure 1.6), supporting the proposed nucleophilic mechanism. These results are also consistent with the reaction not being catalyzed with 5-deaza-FAD, as there is no nucleophilic nitrogen at the 5-position.[70]

Further support for $FADH^-$ as a nucleophile in an S_N2 reaction comes from positional isotope exchange (PIX) experiments and linear free energy relationships carried out by the Liu group.[71] UDP-Gal*p* was doubly labelled to have ^{13}C at C1 and ^{18}O at the anomeric oxygen. When UGM was reconstituted with 5-deaza-FAD, it could not catalyze the PIX of the doubly labelled substrate, implying that N5 is necessary to break the anomeric bond. UGM was also reconstituted with 7- or 8-substitued FAD analogs. When the nucleophilicity of

the FAD analogs was plotted against log(k_{cat}) of the reaction, the slope of the resulting Hammett plot is negative, as would be expected for an S_N2 reaction as the rate-limiting step. If the C1-O5 (or C1-O4) bond cleavage were the rate-limiting step, UDP-galactitol **1.7** should be a substrate for the reaction, and it is not, as discussed above. The current proposed mechanisms for UGM are summarized in Figure 1.7.[69]

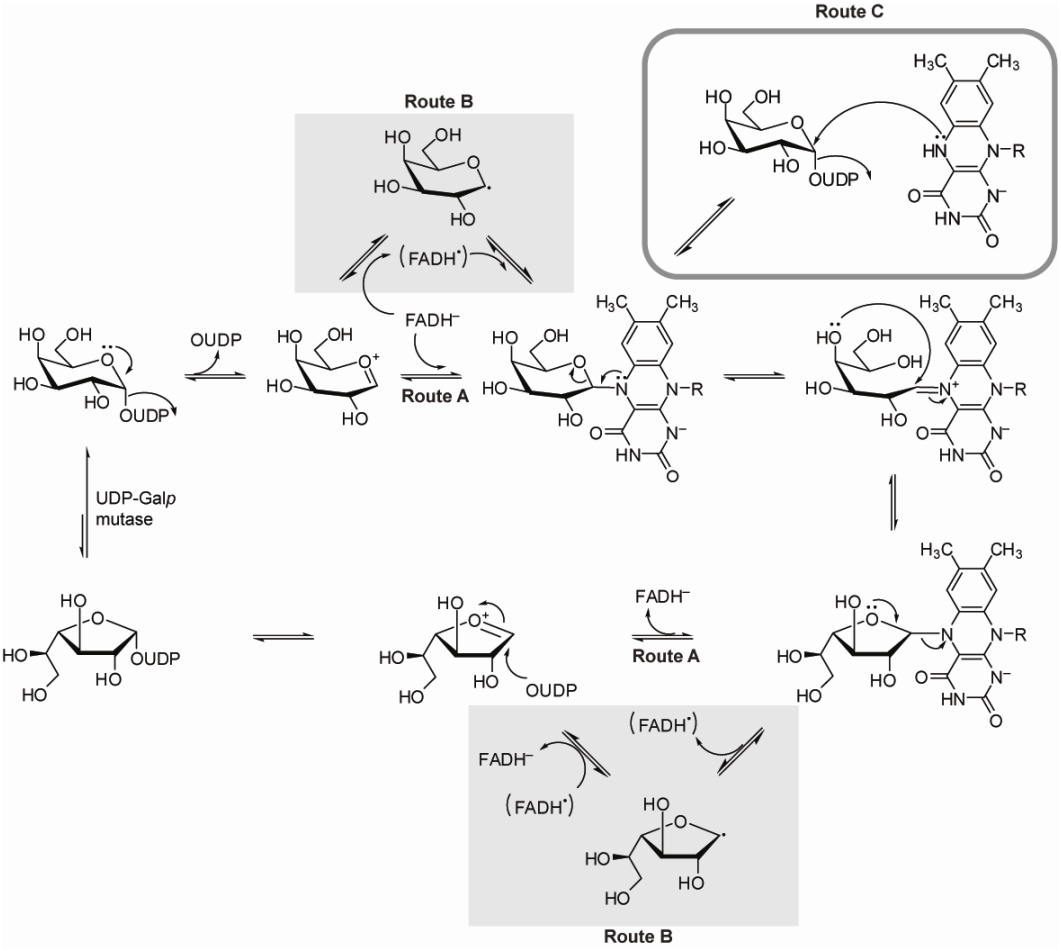

Figure 1.7. Currently proposed mechanisms for UGM. Route A involves nucleophilic attack by the FAD cofactor in an S_N1 manner, Route B involves a single electron transfer to the galactose, and Route C involves nucleophilic attack by the FAD cofactor in an S_N2 reaction.

Sanders and coworkers crystallized UGM from *Deinococcus radiodurans*, which has only ~40% sequence homology to the other crystallized enzymes, to facilitate substrate–enzyme crystallization studies.[72] This strategy was successful, and they were able to obtain X-ray crystal structures of UDP-Gal*p* and UDP bound to reduced UGM at 2.50 Å and 2.55 Å resolution, respectively.[73] Earlier studies suggested that W184 (or W156 in *E. coli*) stacked against uracil (see above); however, in the crystal structure, W184 forms a hydrogen bond with C3 hydroxyl group of ribose. The crystal structure does confirm that the arginine residue on the mobile loop (R198 in *D. radiodurans*) interacts with the diphosphate of UDP-Gal*p*. There is also significant electron density between N5 of FAD and the anomeric carbon of Gal*p*, supporting the existence of a substrate–cofactor intermediate. The 2- and 3-hydroxyl groups of Gal*p* form water-mediated hydrogen bonds within the active site, consistent with the fluorinated analogs described above. Finally, the conformation of UDP-Gal*p* bound to UGM is quite different to those of the inhibitors UDP-Glc*p*[74] or UDP-*C*-D-Gal*f*[75] (**1.19**, Figure 1.11) bound to UGM. Neither UDP-Glc*p* nor **1.19** interact with R198, and the anomeric carbon of Glc*p* is too far (6.0 Å) to form a bond with N5 of FAD.

Quite recently, the crystal structure of UGM from *A. fumigatus* bound with UDP-Gal*p* has been published.[76,77] The eukaryotic enzyme has low sequence identity to the bacterial enzymes (<20%), and small angle X-ray scattering shows that it forms a tetramer in solution, whereas the bacterial enzymes often form dimers.[76] Despite these differences, there is only 3.0 Å rmsd between 351 residues of the *A. fumigatus* and *D. radiodurans* structures.[77] Also,

the key contacts in the active site are similar between the eukaryotic and prokaryotic enzymes.

1.2.3. Assessing UGM activity

Effective assays are necessary to screen for inhibitors of UGM activity. The most commonly used assay, developed by Lee et al.,[78] is HPLC-based and relies on UDP-Gal*p* and UDP-Gal*f* having significantly different retention times (23 min versus 31 min). Although readily reproducible, it is not high-throughput. Also, because the reaction equilibrium heavily favors the pyranose product, this HPLC assay is best run using UDP-Gal*f* as a starting material; however, UDP-Gal*f* is not commercially available and can be difficult to synthesize (see below).

A radioactivity-based assay reported by Scherman et al. relies on $NaIO_4$ oxidation, which will cleave the C5–C6 bond of Gal*f* but not of Gal*p* (Figure 1.8).[79] This assay requires the preparation of C6 radiolabelled UDP-Gal*p,* and the release of tritiated formaldehyde from the product UDP-Gal*f* is monitored. After screening a 1300-member library of uridine-based compounds with this assay, a weak inhibitor of UGM was found; see Section 1.2.4 for details.

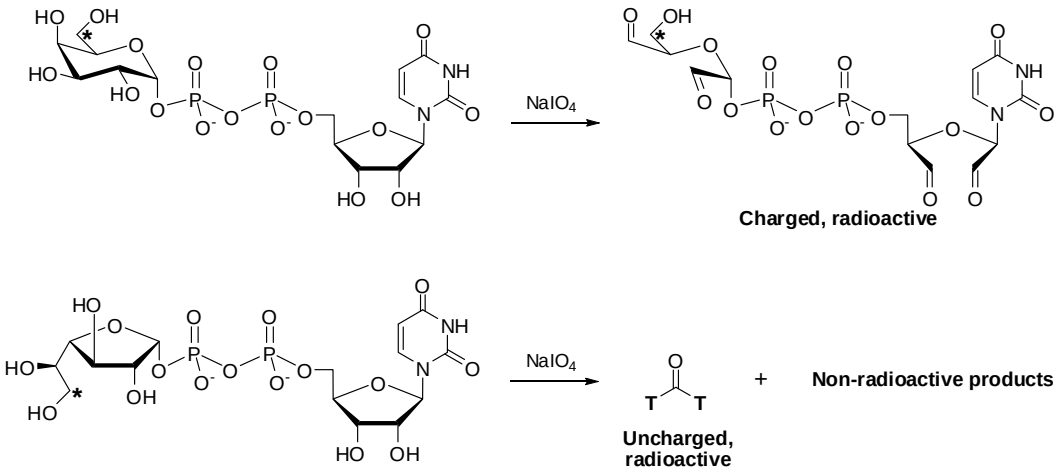

Figure 1.8. Gal*f* assay that relies on formation of tritiated formaldehyde.

Kiessling and coworkers developed a fluorescence polarization assay for UGM, which uses a fluorescent UDP analog (Figure 1.9, **1.12**).[80] The Kiessling group then screened a 16,000-member library and identified seven compounds with K_d values less than 10 μM that served as lead compounds for further development of inhibitors (Section 1.2.4).

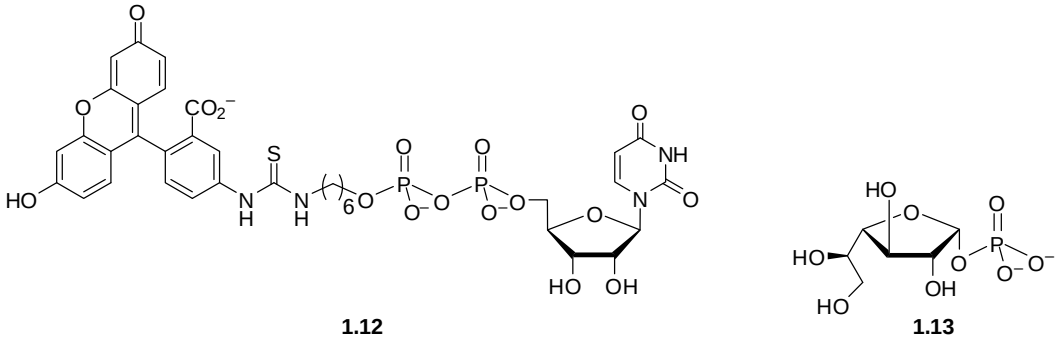

Figure 1.9. Compounds used in assays of UGM activity.

One barrier to enzymatic studies of UGM or enzymes that use UDP-Gal*f* is the limited access to this sugar nucleotide.[10] One approach to overcome these limitations is a chemoenzymatic synthesis described by Rose et al.,[81] and

originally reported by Field and coworkers[82] (Figure 1.10). In this process, α-Gal*f* 1-phosphate (Figure 1.10, **1.13**)[83] is converted to UDP-Gal*f* by the enzyme galactose-1-phosphate uridinyltransferase (GalPUT); 30 mg of UDP-Gal*f* can be obtained from **1.13** after HPLC purification. Peltier et al. probed the specificity of GalPUT.[84] The enzyme accepts a variety of furanoside phosphates, including D-galactose, 6-deoxy-6-fluoro-D-galactose, D-fucose, and L-arabinose but neither D-glucofuranose nor D-mannofuranose serve as substrates. Additionally, when an anomeric phosphate mixture is used, only the 1,2-*cis* anomer reacts. UDP-Gal*f* has been synthesized chemically,[64,85-88] but the various strategies are not detailed here. It is also possible to use UGM itself to produce UDP-Gal*f*;[17] however, this is not practical due to the ~9:1 ratio of UDP-Gal*p* to UDP-Gal*f* at equilibrium.[78]

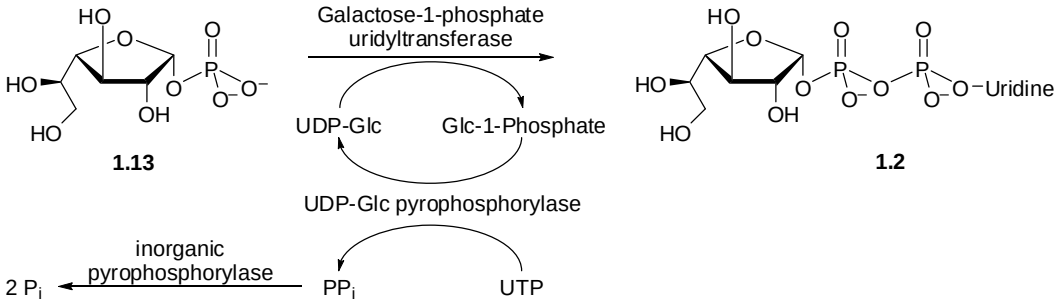

Figure 1.10. Chemoenzymatic synthesis of UDP-Gal*f*.

1.2.4. Inhibitors of UGM

The majority of compounds screened as potential inhibitors of UGM have been designed as substrate mimics. In fact, the first reported inhibitor from Fleet and coworkers was a pyrrolidine analog of Gal*f* (Figure 1.11, **1.14**);[89] this compound showed weak inhibition of UGM and prevented Gal*f* incorporation into the mycobacterial galactan chain in vitro. Building upon this result, they also

synthesized a pyrrolidine UDP-Gal*f* mimic (**1.15**),[90] though evaluation of this compound as an inhibitor of UGM was not reported. Liautard et al. designed and tested another pyrrolidine Gal*f* analog linked to UMP by a non-hydrolyzable, three carbon chain (**1.16**).[91,92] This compound showed low micromolar inhibition in the HPLC assay described previously.[78] Additionally, the same group used a [3+2] dipolar cycloaddition to synthesize a pyrrolidine- and phosphonate-containing UDP-Gal*f* mimic (**1.17**),[93] though no biological data were reported for this compound. Similarly, several other pyrrolidine analogs were synthesized by Desvergnes et al.,[94] and the best of these compounds (**1.18**) displayed <35% inhibition of UGM at 25 mM.

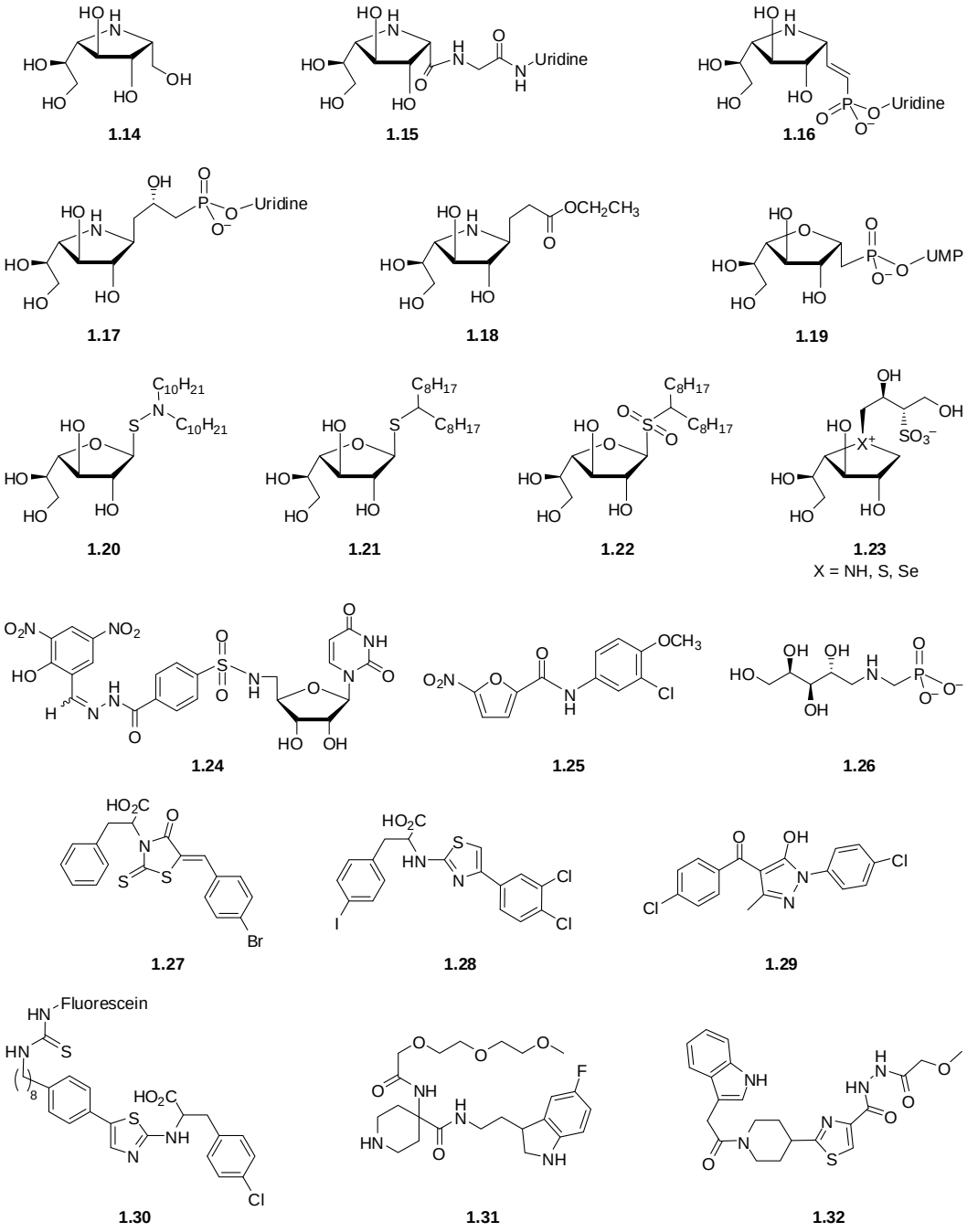

Figure 1.11. Compounds synthesized as inhibitors of UGM.

In addition to changes to the carbohydrate ring, other potential inhibitors have been synthesized with changes to the diphosphate linkage. Sinaÿ and coworkers synthesized UDP-*C*-D-Gal*f* (**1.19**), which is weak inhibitor of the *E.*

coli UGM.[95] A chemoenzymatic synthesis of **1.19** provided higher yields, and the compound showed >50% inhibition at 1 mM concentration against four bacterial UGM enzymes.[75] Following a similar strategy, Owen et al. replaced the uridine diphosphate of UDP-Gal*f* with sulfenamides and sulfonamides,[96,97] and the most potent of these analogs, the Gal*f* *N*,*N*-didecyl sulfenamide **1.20**, had a 1 μg/mL inhibitory concentration (MIC) against *M. smegmatis* in a cell-based assay. The same group also tested several thioglycosides and sulfones of Gal*f*,[98] and the best of these compounds, the Gal*f* 9-heptadecyl thioglycoside (**1.21**) and Gal*f* 9-heptadecyl sulfone (**1.22**), had comparable MIC values. None of the compounds were screened against UGM itself.

Pinto and coworkers designed ammonium, selenonium, and sulfonium ion mimics of Gal*f* phosphate, with a sulfate ion side chain (**1.23**).[99,100] The sulfate ion was chosen for stability and because it is present in known glycosidase inhibitors, salacinol and kotalanol.[101] The compounds were designed as transition state mimics for UGM but are only weak inhibitors (<45% inhibition at 10 mM).

A weak inhibitor (**1.24**) was found using the assay designed by Scherman et al.[79] (described in Section 1.2.3), but it was not active against whole cells. Using a different commercial library with the same assay, Tagallapally et al.[102] identified nitrofuranylamide **1.25** as an inhibitor of UGM (IC_{50} = 12 μg/mL) that was also active against *M. tuberculosis* H37Ra (MIC = 1.6 μg/mL). They went on to synthesize a panel of nitrofuranylamides and screened them against UGM, but none displayed significant improvement over the lead. Four compounds were

also tested in vivo, and although they displayed some anti-mycobacterial activity, it appears that UGM is not their target.[102]

Open-chain aminophosphonate mimics of L-arabinose have also been synthesized as potential inhibitors (**1.26**).[103] While these compounds are similar to UDP-galactitol **1.7** (Figure 1.5) synthesized as a mechanistic probe,[60] these aminophosphonates lack uridine, which appears necessary for binding, and they only showed weak inhibition of UGM at 2 M (< 11%).

Using the fluorescence polarization assay described in Section 1.2.3,[80] Kiessling and coworkers identified several thiazolidinone-based compounds that inhibit UGM with K_d values less than that of UDP. One of these also showed selectivity for UGM with low micromolar IC_{50} values (**1.27**);[104] however, the thiazolidinone reacts with free thiols present under biological conditions. Kiessling and coworkers subsequently reported aminothiazoles (**1.28**) that inhibit *M. smegmatis* growth at MICs comparable to ethambutol and rifampicin (50 μM).[105] An additional 20,000 compounds were screened, and 11 had K_d's of 10 μM or below. These were used as lead compounds for further SAR studies. The Pinto group later assayed both **1.28** and **1.29**,[106] a compound that inhibits *M. tuberculosis* but whose biological target was initially unknown.[107] Both **1.28** and **1.29** were active against UGM with low micromolar IC_{50} values, inhibit the growth of *M. smegmatis*, and are inactive against Gram-positive bacteria. However, only **1.29** inhibits the growth of *M. tuberculosis*. Following up on the fluorescence polarization assay itself, Dykhuizen et al.[108] identified an additional site on UGM with apparent affinity for an aromatic moiety. By varying the

number of carbons connecting UDP and fluorescein, they determined the optimal linker length was eight carbons. Furthermore, by attaching fluorescein to a known inhibitor, they identified an even more potent inhibitor against UGM with a K_d of 0.30 μM and an IC_{50} of 3.5 μM (**1.30**).

Once the crystal structure of substrate bound to UGM was available (Section 1.2.2), Sanders and coworkers used this structure as part of a virtual screening study.[109] Thirteen inhibitors were identified from an initial screen of 84,000 compounds. Of these, two had very low IC_{50} values against the UGM from *M. tuberculosis*, 0.8 μM for **1.31** and 1.0 μM for **1.32**. Compound **1.32** includes an aminothiazole ring, as does **1.28** identified by Kiessling and coworkers, and docking simulations indicated that this moiety is involved in a cation-π interaction with the arginine residues that engage the diphosphate of UDP.

1.2.5. Galactofuranosyltransferases

Mycobacterial galactan contains a chain of 30–35 Gal*f* residues attached via alternating β-(1→5) and β-(1→6) linkages. This motif is attached to a disaccharide consisting of a *N*-acetyl-D-glucosamine and L-rhamnose as illustrated in Figure 1.12. In 2001, Pan et al. determined that two genes involved in mycobacterial galactan biosynthesis (Rv3809c and Rv3808c) are necessary for mycobacterial growth,[16] highlighting that their protein products might make good therapeutic targets. The Rv3809c gene, also known as glf, encodes for UGM. The other gene, Rv3808c, was identified as a potential galactosyltransferase after it was cloned into *M. smegmatis*.[110] This gene encodes for GlfT2, a bifunctional

enzyme that creates both the β-(1→5) and β-(1→6) linkages found in mycobacterial galactan. GlfT2 was expressed, purified, and characterized in *E. coli* by Besra and coworkers.[111] They reported that earlier attempts at purification had been hampered due to the formation of insoluble inclusion bodies; the insolubility was overcome by adding chaperones to the plasmid containing Rv3808c. However, Palcic, Lowary and coworkers had earlier succeeded in isolating multi-milligram quantities of recombinant GlfT2 without the need for chaperones.[112] To aid in the identification of galactofuranosyltransferase inhibitors, Rose et al.[81] reported a coupled spectrophotometric assay for GlfT2 that requires α-UDP-Gal*f* and can be done in a 384-well plate (Figure 1.13).

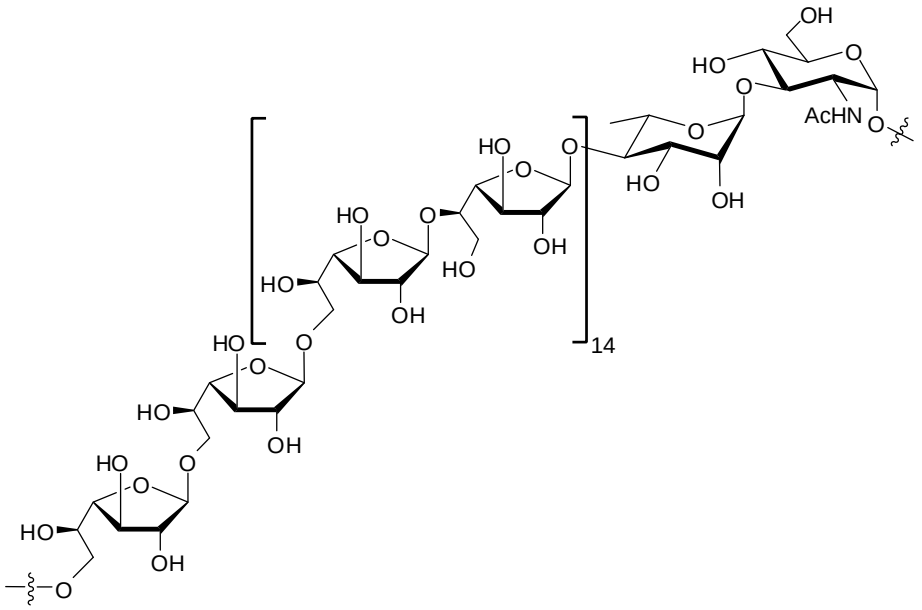

Figure 1.12. Mycobacterial galactan chain attached to the linker disaccharide.

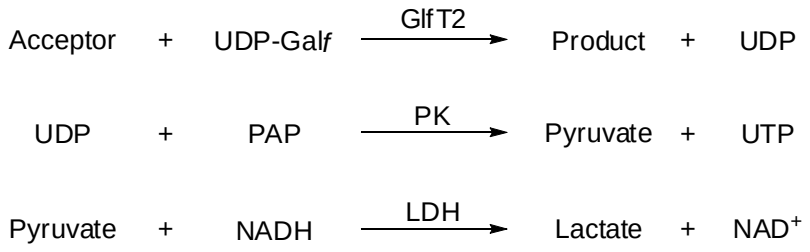

Figure 1.13. Basis of spectrophotometric assay for GlfT2.

Several groups have studied the mechanism of the GlfT2. STD NMR experiments demonstrated that synthetic trisaccharide acceptors (**1.33** and **1.34**, Figure 1.14) bind competitively to the same active site of GlfT2 and have similar K_d values, 85 ± 15 μM for **1.33** and 50 ± 10 μM for **1.34**.[113] Further STD NMR experiments with **1.33** and **1.34** indicated that the residue at the reducing end and the aglycone bind more tightly to the active site than non-reducing end, where the glycosylation takes place.[114] Weaker binding near the site of the reaction would allow the substrate to adopt the necessary transition state conformation. Mass spectrometry assays supported that the enzyme is processive rather than distributive.[115] In other words, once the acceptor binds to GlfT2, the Gal*f* moieties are added until chain termination occurs. Site-directed mutagenesis of GlfT2 indicated that the Asp372 acts as a catalytic base in the formation of both β-(1→5) and β-(1→6) linkages.[116] The X-ray crystal structure of GlfT2 as a homotetramer with UDP-Gal*f* bound was recently solved,[117] and the position of the sugar donor supports that Asp372 is the catalytic base. There is also a region of hydrophobic residues in the putative acceptor binding site, similar to other glycosyl transferases in the same enzyme family. The acceptors **1.33** and **1.34** were both modeled into this site, and the hydrophobic pocket can accept both β-

(1→5) and β-(1→6) linkages. When the non-reducing residue has a β-(1→5) linkage, the acceptor is more exposed than when the terminal residue has a β-(1→6) linkage, leaving the 6-OH is positioned appropriately for reaction. When the terminal residue is has a β-(1→6) linkage, then the terminal residue is positioned deeper in the active site, and the 5-OH is held in the correct orientation to react. GlfT2 can use 5- or 6-deoxy-UDF-Gal*f* , as well as UDP-β-L-Ara*f*, with both acceptors **1.33** and **1.34**.[118] However, the resulting oligosaccharides are dead-end products, indicating that both the 5- and 6-hydroxyl groups are necessary for substrate specificity.

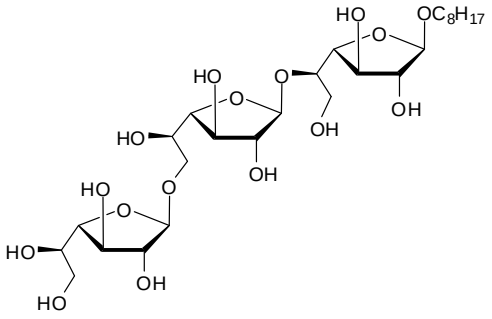

1.33

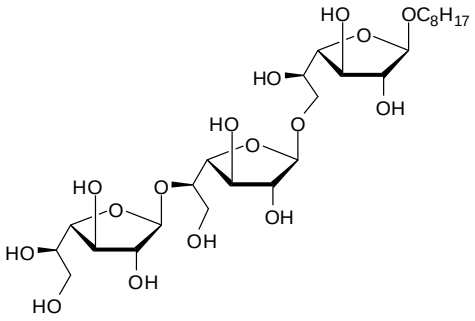

1.34

Figure 1.14. Synthetic trisaccharide donors used in STD NMR experiments of GlfT2

The gene for another galactosyltransferase involved in mycobacterial galactan biosynthesis was tentatively identified in 2006 by Brennan and coworkers as Rv3782.[119] This gene was overexpressed in *M. smegmatis*, and when decaprenyl pyrophosphate α-L-rhamnopyranosyl-(1→3)-*N*-acetyl-α-D-glucosamine was added to the membrane fraction, the production of the oligosaccharide with two Gal*f* residues increased, indicating that the enzyme has dual β-(1→5) and β-(1→6) transferase activity. Later, the enzyme encoded by

Rv3782 (GlfT1) was expressed in *M. smegmatis* and characterized.[120] In vitro assays, in which both GlfT1 and GlfT2 were probed with natural and synthetic substrates, demonstrated that GlfT1 puts the first two Gal*f* residues on the linker disaccharide, and GlfT2 adds the remainder.[120] As with GlfT2, UDP-β-L-Ara*f* and UDP-5-deoxy-α-D-Gal*f* serve as sugar donors for GlfT1, forming dead-end products that inhibit galactan biosynthesis in a cell-free reaction.[121] The current model for the assembly of mycobacterial galactan involves two bifunctional glycosyltranserases that are responsible for the polymerization of UDP-Gal*f* into the full-length structure. It remains to be established how the process is terminated; therefore, it is possible that additional galactofuranosyltransferases are involved in the later stages of biosynthesis. However, Kiessling and coworkers put forth the hypothesis that there is an additional binding site on GlfT2 for the lipid aglycone.[74] Once the galactan chain reaches the desired length, the lipid could fold back and interact with the second site to signal chain termination. However, there is no evidence of a lipid binding site in the crystal structure of GlfT2.[117]

Few other galactofuranosyltransferases have been well characterized. WbbO is another bifunctional galactosyltransferase from *K. pneumoniae*.[122] By expressing this enzyme in *E. coli*, Whitfield and coworkers demonstrated that it adds both Gal*f* and Gal*p* to synthesize galactan I, which is part of the O-antigen for *K. pneumoniae.* WbbI from *E. coli* K-12 was expressed and purified as a maltose binding protein conjugate.[123] In vitro assays confirmed this enzyme is a β-galactofuranosyltransferase that catalyzes the addition of Gal*f* to an α-

glucopyranose acceptor. Octyl α-Glc*p* gave octyl β-Gal*f*-(1→6)-α-Glc*p*, the structure of which was verified by comparison with the NMR spectrum of an authentic sample; however, octyl β-Glc*p* was not a substrate for the enzyme. In another investigation, the activity of a galactofuranosyltransferase in a membrane preparation from *Penicillium fellutanum* was demonstrated through incorporation of radiolabeled Gal*f* into the peptidophosphogalactomannan produced by this organism.[85] Galactofuranosyltransferase genes have also been identified in *Streptococcus anginosus*,[124] *T. cruzi*,[125] *T. rangeli*,[126] and *L. major*;[127-129] however, only the enzyme for *T. rangeli* has been expressed and purified.[126] The *L. major* genes were knocked out, and Gal*f* was no longer present in the lipophosphoglycan of the mutants.[127] Gal*f* incorporation in glycosylinositolphopholipids was unaffected.[128]

1.2.6. Galactofuranosyltransferase inhibitors

There have been fewer potential inhibitors synthesized for the galactofuranosyltransferases than for UGM. Pathak et al. demonstrated that the disaccharide octyl β-D-Gal*f*-(1→4)-α-L-Rha*p* is a substrate for the galactofuranosyltransferases in *M. smegmatis* membranes.[130] Additionally, two protected synthetic intermediates – octyl β-D-galactofuranosyl-(1→4)-2,3-*O*-isopropylidene-α-L-rhamnopyranoside (Figure 1.15, **1.35**) and octyl 2,3,5,6-tetra-*O*-acetyl-β-D-galactofuranosyl-(1→4)-α-L-rhamnopyranoside (**1.36**) – were modest inhibitors of the growth of *M. tuberculosis* and three clinical strains of *M. avium* complex.

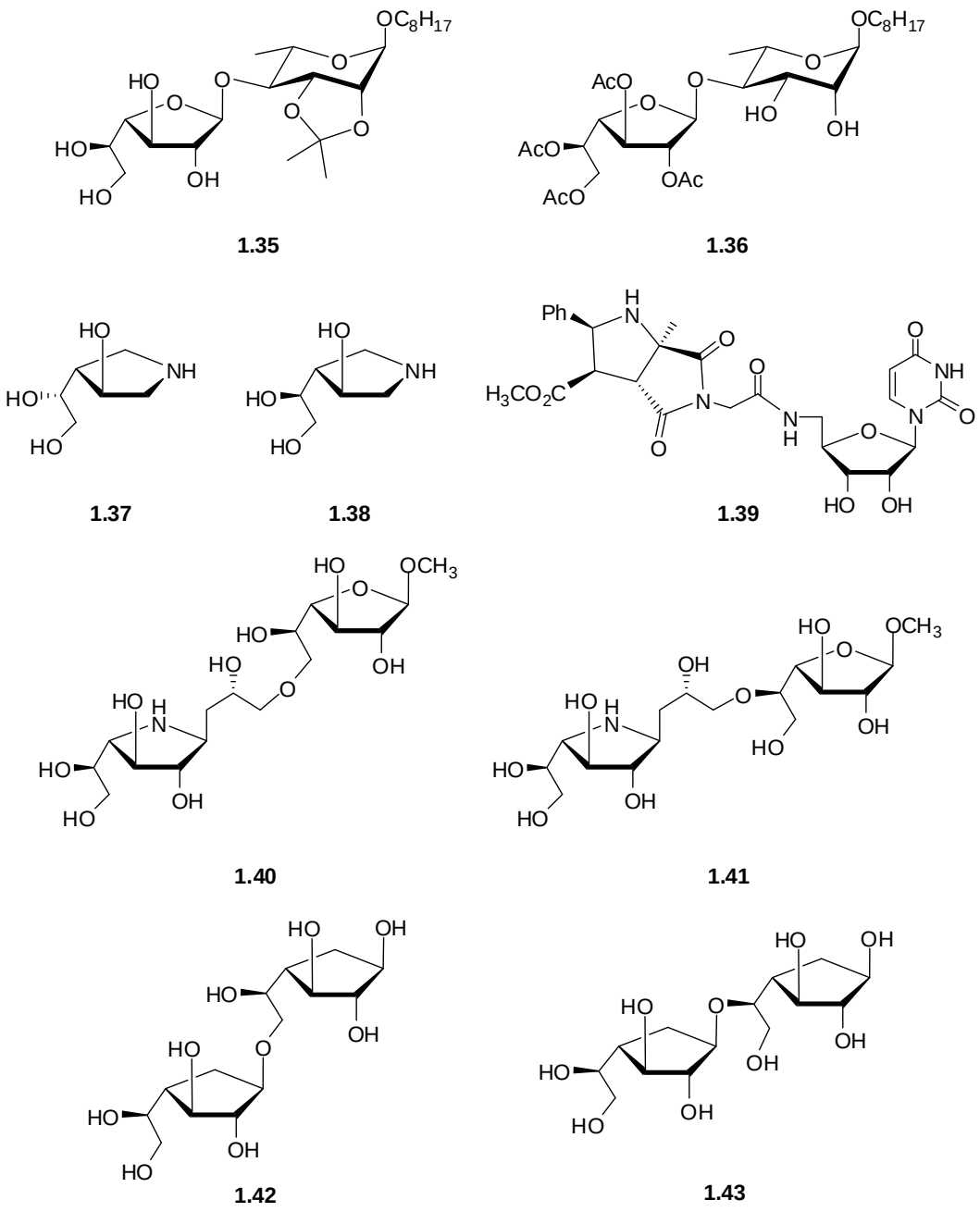

Figure 1.15. Compounds designed as inhibitors of galactofuranosyltransferases.

Presumably, the reaction catalyzed by GlfT2 involves a transition state with some oxocarbenium ion character. This rationale led to the design synthesis of the pyrrolidine **1.37**,[131] which is a weak inhibitor of GlfT2 (IC_{50} = 4.8 mM). It

is interesting to note that compound **1.38**, with the same absolute stereochemistry as C5 of Gal*f*, showed no activity. Another pyrrolidine containing compound **1.39** that was originally designed as a transition-state mimic for the *E. coli* glycosyltransferase MurG, is a weak inhibitor of GlfT2, showing 80% inhibition at 1 mM.[132] Liautard et al. synthesized two Gal*f* disaccharide mimics with iminogalactitol moieties (**1.40**, **1.41**),[133] using the same 1,3-dipolar cycloaddition methodology discussed earlier.[93] These compounds were designed as potential galactofuranosyltransferase inhibitors; however, no biological data have been reported. Carbasugar disaccharide analogs **1.42** and **1.43** were are similar to **1.40** and **1.41** and were designed as GlfT2 inhibitors.[134] Only **1.43** showed activity of 53% inhibition at 2 mM; **1.42** was showed no inhibition.

1.2.7. Galactofuranosidases

Early synthetic methodology for Gal*f*-containing mono- and oligosaccharides was directed toward understanding the substrate specificity of *exo*-β-D-galactofuranosidase,[135,136] an enzyme that cleaves Gal*f* residues from glycoconjugates as fungal colonies increase in age.[137] Galactofuranosidases have been identified in several species of fungi, including *Aspergillus* sp., *Penicillium* sp., and *Helminthosporium sacchari*.[138] de Lederkremer and coworkers synthesized and evaluated a panel of alkyl and aryl β-thioglycosides of Gal*f* as inhibitors of this enzyme and found the 4-aminophenyl-thioglycoside (Figure 1.16, **1.44**) was a moderate inhibitor (IC_{50} = 0.08 mM).[137] Additionally, D-galactono-1,4-lactone **1.45** was a more potent inhibitor (IC_{50} = 0.02 mM). The authors proposed that compound **1.44** might be usable in affinity chromatography

to "pull down" galactofuranosidases, and that **1.45** might then elute the enzymes off the column. Later, they used this approach to identify an *exo*-galactofuranosidase from *T. cruzi*.[138] Varela and coworkers later evaluated three thiodisaccharides with β-D-Gal*f* as the terminal moiety for inhibitory activity against the *P. fellutanum exo*-β-D-galactofuranosidase.[139] All of these compounds were worse inhibitors than **1.45**, with <60% inhibition at 1 mM.

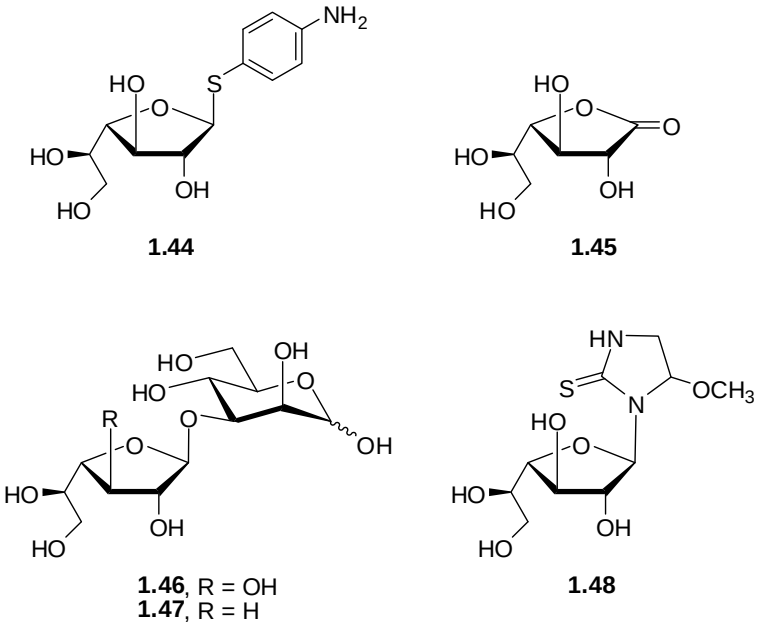

Figure 1.16. Compounds used for studying *exo*-galactofuranosidase.

To probe galactofuranosidase substrate specificity, a portion of the repeating unit of lipophosphoglycan of *Leishmania,* β-D-Gal*f*-(1→3)-α-D-Man*p* **1.46**, was synthesized.[140] Because the repeating unit also contains the α-D-Gal*p*-(1→3)-β-D-Gal*f* motif, the same disaccharide lacking the 3-OH of Gal*f* (**1.47**) was also synthesized. Compound **1.46** was a substrate for the galactofuranosidase while **1.47** was not, demonstrating that the 3-OH is necessary for enzyme recognition. Additional, deoxygenated analogs have also been evaluated as

substrates. The 6-deoxy analog, 4-nitrophenyl β-D-fucofuranoside, was synthesized in four steps from 2,3,5-tri-*O*-benzoyl-6-bromo-6-deoxy-D-galactono-1,4-lactone,[141] and this compound was also not a substrate for the galactofuranosidase. Using a photoinduced electron-transfer strategy, the 2-deoxy-[142] and 5-deoxy-analogs[143] were both synthesized from D-galacturonic acid. The 2-deoxy-Gal*f* was not a substrate for galactofuranosidase, while the 5-deoxy compound had not been assayed. Much is know about the substrate specificity of the *exo*-galactofuranosidase, but only one inhibitor has been synthesized, the imidazolidine-2-thione **1.48**.[21]

1.3. Conformation of galactofuranosides

While crystal structure for UGM and GlfT2 with UDP bound have both been solved, no enzyme structures with UDP-Gal*f* bound exist. Additional knowledge of the conformation of Gal*f* in active sites, as well as in solution, would help in the design of inhibitors; however, there are few reports on the conformation of Gal*f*. Weller, et al. used nuclear Overhauser effect (NOE) data in combination with restrained molecular dynamics (MD) simulations to determine the solution conformation of the glycoinositol phospholipid **1.49** from *L. major* (Figure 1.17).[144] The MD simulations indicated that **1.49** has a hairpin structure in solution, and the bend in the glycan occurs at the Gal*f* residue. Lichtenthaler and coworkers used Monte Carlo searches to find low energy conformations of cyclic β-(1→3)- and β-(1→6)-linked oligogalactofuranosides of three to five Gal*f* residues.[145] Unlike cyclodextrins (cyclic α-(1→4)-linked glucopyranosides), the

conformations of the cyclic oligogalactofuranosides were not symmetric and had small central cavities. The small cyclic structures also forced the ring conformations of the Gal*f* residues into higher energy conformations than the monosaccharide. Other reports of Gal*f* conformation describe protected synthetic intermediates, such as the bicyclic thiocarbamate, **1.50** (Figure 1.17).[146]

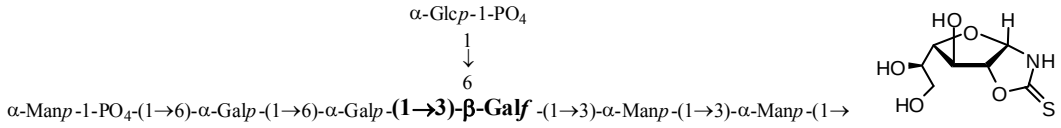

1.49 **1.50**

Figure 1.17. Compounds evaluated for the conformation of Gal*f*. Only the non-reducing end residues of **1.49** are shown.

1.4. Summary and thesis research goals

Gal*f*-containing glycans are essential components of a host of bacterial, fungal, and parasitical organisms, and the biochemical pathways by which these molecules are assembled and catabolized are attractive sites for drug action. This potential has led to increasing interest in the synthesis of molecules containing Gal*f* residues, their subsequent use in studies directed at understanding the enzymes that processes these residues, and the identification of potential inhibitors of these pathways.

Among the major achievements of the past several years has been an in-depth understanding of the mechanism of the UDP-galactopyranose mutase (UGM), the enzyme that produces the donor species for galactofuranosyltransferases, UDP-Gal*f*, and crystal structures of UGM with substrates and inhibitors bound in the active site. There has already been success

in identifying inhibitors with in vivo anti-bacterial activity, as well as lead compounds, which will serve as the basis for future analog synthesis. Future work in this area would involve docking known inhibitors in the active site, which would provide additional key insights into the UGM mechanism, and would, in turn, guide further efforts to design inhibitors. Additionally, having the structure of UDP-Gal*p* bound to UGM would provide a starting point for quantum mechanics/molecular mechanics (QM/MM) calculations to study the reaction mechanism.

Other achievements of note are reported in papers that have studied galactofuranosyltransferases. Those receiving the most intense scrutiny are the enzymes involved in mycobacterial cell wall assembly, and the current model for galactan synthesis in mycobacteria involves two bifunctional enzymes, GlfT1 and GlfT2. Future mechanistic work in this area, including X-ray crystallographic investigations of GlfT1, is essential to develop high-affinity inhibitors of galactan biosynthesis. In particular, the known essentiality of galactan formation for mycobacterial viability suggests that potent inhibitors of GlfT1 and GlfT2 have significant clinical potential. A crystal structure of GlfT2 was recently reported with **1.33** and **1.34** modelled into the active site; these docked structures could provide initial structures for MD simulations of the enzyme–substrate complex, which would highlight key interactions for substrate recognition that are not readily apparent. Docking simulations of the natural substrate or of galactan chains of varying lengths could lead to understanding of substrate recognition and

how chain termination occurs. Furthermore, docking of known inhibitors could allow for virtual screening or aide in the design of new inhibitors of the enzyme.

The experiments and calculations presented in this thesis lay the foundation for future docking, MD, or QM/MM simulations. All of these techniques rely on accurate models of Gal*f* behaviour in aqueous solution. We set out to develop these models. Chapter 2 describes the potential energy surface (PES) of methyl α- and β-D-Gal*f* (**1.51** and **1.52**, respectively, Figure 1.18) in the gas phase, calculated with density functional theory (DFT) methods. We then compare the low energy conformations on the PES with those predicted using the proton nuclear magnetic resonance (NMR) spectra and the program PSEUROT.[147,148] We also used the conformations from the PES to develop Gal*f*-specific Karplus relationships,[149,150] which are described in Chapter 3. The new equations allowed us to interpret the results of MD simulations of **1.51** and **1.52** in solution, by comparing the coupling constants averaged of the calculations with those from the proton NMR spectra. These calculations highlighted problems with the chosen force field, and we addressed these shortcomings in Chapter 4. Our changes to the force field improved agreement between the simulation results and experiment. We calculated the solution conformations of **1.33** and **1.34** using both the original and improved force field, and the results are summarized in Chapter 5.

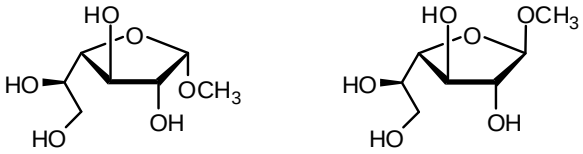

1.51 **1.52**

Figure 1.18. The conformations of methyl α- and β-D-Gal*f* are the focus of Chapters 2 through 4.

1.5. References

1. Richards, M. R.; Lowary, T. L. *ChemBioChem* **2009**, *10*, 1920–1938.

2. Taylor, M. E.; Drickamer, K. *Introduction to Glycobiology*. 2nd ed.; Oxford University Press: Oxford, 2006.

3. Ho, M. C.; Shi, W. X.; Rinaldo-Matthis, A.; Tyler, P. C.; Evans, G. B.; Clinch, K.; Almo, S. C.; Schramm, V. L. *Proc. Natl. Acad. Sci. U.S.A.* **2010**, *107*, 4805–4812.

4. Nagar, B.; Bornmann, W. G.; Pellicena, P.; Schindler, T.; Veach, D. R.; Miller, W. T.; Clarkson, B.; Kuriyan, J. *Cancer Research* **2002**, *62*, 4236–4243.

5. Cremer, D.; Pople, J. A. *J. Am. Chem. Soc.* **1975**, *97*, 1358–1367.

6. Altona, C.; Sundaralingam, M. *J. Am. Chem. Soc.* **1972**, *94*, 8205–8212.

7. Napolitano, J. G.; Gavin, J. A.; Garcia, C.; Norte, M.; Fernandez, J. J.; Daranas, A. H. *Chem.-Eur. J.* **2011**, *17*, 6338–6347.

8. Beis, K.; Srikannathasan, V.; Liu, H.; Fullerton, S. W. B.; Bamford, V. A.; Sanders, D. A. R.; Whitfield, C.; McNeil, M. R.; Naismith, J. H. *J. Mol. Biol.* **2005**, *348*, 971–982.

9. Nassau, P. M.; Martin, S. L.; Brown, R. E.; Weston, A.; Monsey, D.; McNeil, M. R.; Duncan, K. *J. Bacteriol.* **1996**, *178*, 1047–1052.

10. Houseknecht, J. B.; Lowary, T. L. *Curr. Opin. Chem. Biol.* **2001**, *5*, 677–682.

11. Pedersen, L. L.; Turco, S. J. *Cell. Mol. Life Sci.* **2003**, *60*, 259–266.

12. Peltier, P.; Euzen, R.; Daniellou, R.; Nugier-Chauvin, C.; Ferrières, V. *Carbohydr. Res.* **2008**, *343*, 1897–1923.

13. von Itzstein, M. *Curr. Opin. Struct. Biol.* **2008**, *18*, 558–566.

14. Tefsen, B.; Ram, A. F. J.; van Die, I.; Routier, F. H. *Glycobiology* **2012**, *22*, 456–469.

15. Brennan, P. J. *Tuberculosis* **2003**, *83*, 91–97.

16. Pan, F.; Jackson, M.; Ma, Y. F.; McNeil, M. *J. Bacteriol.* **2001**, *183*, 3991–3998.

17. Köplin, R.; Brisson, J. R.; Whitfield, C. *J. Biol. Chem.* **1997**, *272*, 4121–4128.

18. de Lederkremer, R. M.; Bertello, L. E. *Curr. Pharm. Des.* **2001**, *7*, 1165–1179.

19. Salto, M. L.; Kuhlenschmidt, T.; Kuhlenschmidt, M.; de Lederkremer, R. M.; Docampo, R. *Mol. Biochem. Parasitol.* **2008**, *158*, 120–130.

20. de Lederkremer, R. M.; Colli, W. *Glycobiology* **1995**, *5*, 547–552.

21. Marino, C.; Herczegh, P.; de Lederkremer, R. M. *Carbohydr. Res.* **2001**, *333*, 123–128.

22. Leitão, E. A.; Bittencourt, V. C. B.; Haido, R. M. T.; Valente, A. P.; Peter-Katalinic, J.; Letzel, M.; de Souza, L. M.; Barreto-Bergter, E. *Glycobiology* **2003**, *13*, 681–692.

23. Bernard, M.; Latge, J. P. *Med. Mycol.* **2001**, *39*, 9–17.

24. Heesemann, L.; Kotz, A.; Echtenacher, B.; Broniszewska, M.; Routier, F.; Hoffmann, P.; Ebel, F. *Int. J. Med. Microbiol.* **2011**, *301*, 523–530.

25. El-Ganiny, A. M.; Sanders, D. A. R.; Kaminskyj, S. G. W. *Fungal Genet. Biol.* **2008**, *45*, 1533–1542.

26. Bollig, K.; Lamshöft, M.; Schweimer, K.; Marner, F. J.; Budzikiewicz, H.; Waffenschmidt, S. *Carbohydr. Res.* **2007**, *342*, 2557–2566.

27. van Holst, G.-J.; Varner, J. E. *Plant Physiol.* **1984**, *74*, 247–251.

28. Katzenellenbogen, E.; Toukach, P. V.; Kocharova, N. A.; Korzeniowska-Kowal, A.; Gamian, A.; Shashkov, A. S.; Knirel, Y. A. *FEMS Immunol. Med. Microbiol.* **2008**, *53*, 60–64.

29. Wieneke, R.; Klein, S.; Geyer, A.; Loos, E. *Carbohydr. Res.* **2007**, *342*, 2757–2765.

30. Leal, J. A.; Giménez-Abián, M. I.; Canales, A.; Jiménez-Barbero, J.; Bernabé, M.; Prieto, A. *Glycoconjugate J.* **2009**, *26*, 1047–1054.

31. Prieto, A.; Leal, J. A.; Bernabé, M.; Hawksworth, D. L. *Mycol. Res.* **2008**, *112*, 381–388.

32. Costantino, V.; Fattorusso, E.; Imperatore, C.; Mangoni, A. *J. Org. Chem.* **2008**, *73*, 6158–6165.

33. Leivers, S.; Hidalgo-Cantabrana, C.; Robinson, G.; Margolles, A.; Ruas-Madiedo, P.; Laws, A. P. *Carbohydr. Res.* **2011**, *346*, 2710–2717.

34. Bernabé, M.; Salvachúa, D.; Jiménez-Barbero, J.; Leal, J. A.; Prieto, A. *Fungal Biol.* **2011**, *115*, 862–870.

35. Weston, A.; Stern, R. J.; Lee, R. E.; Nassau, P. M.; Monsey, D.; Martin, S. L.; Scherman, M. S.; Besra, G. S.; Duncan, K.; McNeil, M. R. *Tubercule Lung Dis.* **1998**, *78*, 123–131.

36. Beverley, S. M.; Owens, K. L.; Showalter, M.; Griffith, C. L.; Doering, T. L.; Jones, V. C.; McNeil, M. R. *Eukaryotic Cell* **2005**, *4*, 1147–1154.

37. Oppenheimer, M.; Poulin, M. B.; Lowary, T. L.; Helm, R. F.; Sobrado, P. *Arch. Biochem. Biophys.* **2010**, *502*, 31–38.

38. Oppenheimer, M.; Valenciano, A. L.; Sobrado, P. *Biochem. Biophys. Res. Commun.* **2011**, *407*, 552–556.

39. Bakker, H.; Kleczka, B.; Gerardy-Schahn, R.; Routier, F. H. *Biol. Chem.* **2005**, *386*, 657–661.

40. Novelli, J. F.; Chaudhary, K.; Canovas, J.; Benner, J. S.; Madinger, C. L.; Kelly, P.; Hodgkin, J.; Carlow, C. K. S. *Dev. Biol.* **2009**, *335*, 340–355.

41. Poulin, M. B.; Nothaft, H.; Hug, I.; Feldman, M. F.; Szymanski, C. M.; Lowary, T. L. *J. Biol. Chem.* **2010**, *285*, 493–501.

42. Kleczka, B.; Lamerz, A. C.; Van Zandbergen, G.; Wenzel, A.; Gerardy-Schahn, R.; Wiese, M.; Routier, F. H. *J. Biol. Chem.* **2007**, *282*, 10498–10505.

43. Schmalhorst, P. S.; Krappmann, S.; Vervecken, W.; Rohde, M.; Muller, M.; Braus, G. H.; Contreras, R.; Braun, A.; Bakker, H.; Routier, F. H. *Eukaryotic Cell* **2008**, *7*, 1268–1277.

44. Chen, P.; Bishai, W. R. *Infect. Immun.* **1998**, *66*, 5099–5106.

45. Sanders, D. A. R.; Staines, A. G.; McMahon, S. A.; McNeil, M. R.; Whitfield, C.; Naismith, J. H. *Nature Struct. Biol.* **2001**, *8*, 858–863.

46. Sanders, D. A. R.; McMahon, S. A.; Leonard, G. L.; Naismith, J. H. *Acta Crystallogr., Sect D: Biol. Crystallogr.* **2001**, *57*, 1415–1420.

47. Chad, J. M.; Sarathy, K. P.; Gruber, T. D.; Addala, E.; Kiessling, L. L.; Sanders, D. A. R. *Biochemistry* **2007**, *46*, 6723–6732.

48. Mayer, M.; Meyer, B. *Angew. Chem. Int. Ed.* **1999**, *38*, 1784–1788.

49. Yao, X.; Bleile, D. W.; Yuan, Y.; Chao, J.; Sarathy, K. P.; Sanders, D. A. R.; Pinto, B. M.; O'Neill, M. A. *Proteins: Struct., Funct., Bioinf.* **2009**, *74*, 972–979.

50. Barlow, J. N.; Girvin, M. E.; Blanchard, J. S. *J. Am. Chem. Soc.* **1999**, *121*, 6968–6969.

51. Barlow, J. N.; Blanchard, J. S. *Carbohydr. Res.* **2000**, *328*, 473–480.

52. Zhang, Q.; Liu, H.-w. *J. Am. Chem. Soc.* **2001**, *123*, 6756–6766.

53. Burton, A.; Wyatt, P.; Boons, G.-J. *J. Chem. Soc., Perkin Trans. 1* **1997**, 2375–2382.

54. Errey, J. C.; Mann, M. C.; Fairhurst, S. A.; Hill, L.; McNeil, M. R.; Naismith, J. H.; Percy, J. M.; Whitfield, C.; Field, R. A. *Org. Biomol. Chem.* **2009**, *7*, 1009–1016.

55. Caravano, A.; Sinaÿ, P.; Vincent, S. P. *Bioorg. Med. Chem. Lett.* **2006**, *16*, 1123–1125.

56. Sadeghi-Khomami, A.; Blake, A. J.; Wilson, C.; Thomas, N. R. *Org. Lett.* **2005**, *7*, 4891–4894.

57. Sadeghi-Khomami, A.; Thomas, N. R.; Wilson, C. *Acta Crystallogr. Sect. E: Struct. Rep. Online* **2006**, *62*, o3759–o3761.

58. Sadeghi-Khomami, A.; Forcada, T. J.; Wilson, C.; Sanders, D. A. R.; Thomas, N. R. *Org. Biomol. Chem.* **2010**, *8*, 1596–1602.

59. Caravano, A.; Mengin-Lecreulx, D.; Brondello, J. M.; Vincent, S. P.; Sinaÿ, P. *Chem. Eur. J.* **2003**, *9*, 5888–5898.

60. Itoh, K.; Huang, Z.; Liu, H.-w. *Org. Lett.* **2007**, *9*, 879–882.

61. Caravano, A.; Vincent, S. P.; Sinaÿ, P. *Chem. Commun.* **2004**, *10*, 1216–1217.

62. Caravano, A.; Dohi, H.; Sinaÿ, P.; Vincent, S. P. *Chem. Eur. J.* **2006**, *12*, 3114–3123.

63. Caravano, A.; Vincent, S. P. *Eur. J. Org. Chem.* **2009**, 1771–1780.

64. Zhang, Q.; Liu, H.-w. *J. Am. Chem. Soc.* **2000**, *122*, 9065–9070.

65. Fullerton, S. W. B.; Daft, S.; Sanders, D. A. R.; Ingledew, W. J.; Whitfield, C.; Chapman, S. K.; Naismith, J. H. *Biochemistry* **2003**, *42*, 2104–2109.

66. Huang, Z.; Zhang, Q.; Liu, H.-w. *Bioorg. Chem.* **2003**, *31*, 494–502.

67. Soltero-Higgin, M.; Carlson, E. E.; Gruber, T. D.; Kiessling, L. L. *Nature Struct. Mol. Biol.* **2004**, *11*, 539–543.

68. Yuan, Y.; Bleile, D. W.; Wen, X.; Sanders, D. A. R.; Itoh, K.; Liu, H. W.; Pinto, B. M. *J. Am. Chem. Soc.* **2008**, *130*, 3157–3168.

69. Yuan, Y.; Wen, X.; Sanders, D. A. R.; Pinto, B. M. *Biochemistry* **2005**, *44*, 14080–14089.

70. Miller, S. M. *Nature Struct. Mol. Biol.* **2004**, *11*, 497–498.

71. Sun, H. G.; Ruszczycky, M. W.; Chang, W. C.; Thibodeaux, C. J.; Liu, H. W. *J. Biol. Chem.* **2012**, *287*, 4602–4608.

72. Partha, S. K.; Bonderoff, S. A.; Van Straaten, K. E.; Sanders, D. A. R. *Acta Crystallogr., Sect. F: Struct. Biol. Cryst. Commun.* **2009**, *65*, 843–845.

73. Partha, S. K.; van Straaten, K. E.; Sanders, D. A. R. *J. Mol. Biol.* **2009**, *394*, 864–877.

74. Gruber, T. D.; Borrok, M. J.; Westler, W. M.; Forest, K. T.; Kiessling, L. L. *J. Mol. Biol.* **2009**, *391*, 327–340.

75. Partha, S. K.; Sadeghi-Khomami, A.; Slowski, K.; Kotake, T.; Thomas, N. R.; Jakeman, D. L.; Sanders, D. A. R. *J. Mol. Biol.* **2010**, *403*, 578–590.

76. Dhatwalia, R.; Singh, H.; Oppenheimer, M.; Karr, D. B.; Nix, J. C.; Sobrado, P.; Tanner, J. J. *J. Biol. Chem.* **2012**, *287*, 9041–9051.

77. van Straaten, K. E.; Routier, F. H.; Sanders, D. A. R. *J. Biol. Chem.* **2012**, doi:10.1074/jbc.M111.322974

78. Lee, R.; Monsey, D.; Weston, A.; Duncan, K.; Rithner, C.; McNeil, M. *Anal. Biochem.* **1996**, *242*, 1–7.

79. Scherman, M. S.; Winans, K. A.; Stern, R. J.; Jones, V.; Bertozzi, C. R.; McNeil, M. R. *Antimicrob. Agents Chemother.* **2003**, *47*, 378–382.

80. Soltero-Higgin, M.; Carlson, E. E.; Phillips, J. H.; Kiessling, L. L. *J. Am. Chem. Soc.* **2004**, *126*, 10532–10533.

81. Rose, N. L.; Zheng, R. B.; Pearcey, J.; Zhou, R.; Completo, G. C.; Lowary, T. L. *Carbohydr. Res.* **2008**, *343*, 2130–2139.

82. Errey, J. C.; Mukhopadhyay, B.; Kartha, K. P. R.; Field, R. A. *Chem. Commun.* **2004**, 2706–2707.

83. de Lederkremer, R. M.; Nahmad, V. B.; Varela, O. *J. Org. Chem.* **1994**, *59*, 690–692.

84. Peltier, P.; Guégan, J. P.; Daniellou, R.; Nugier-Chauvin, C.; Ferrières, V. *Eur. J. Org. Chem.* **2008**, 5988–5994.

85. Mariño, K.; Marino, C.; Lima, C.; Baldoni, L.; de Lederkremer, R. M. *Eur. J. Org. Chem.* **2005**, 2958–2964.

86. Tsvetkov, Y. E.; Nikolaev, A. V. *J. Chem. Soc., Perkin Trans. 1* **2000**, 889–891.

87. Marlow, A. L.; Kiessling, L. L. *Org. Lett.* **2001**, *3*, 2517–2519.

88. Peltier, P.; Daniellou, R.; Nugier-Chauvin, C.; Ferrières, V. *Org. Lett.* **2007**, *9*, 5227–5230.

89. Lee, R. E.; Smith, M. D.; Nash, R. J.; Griffiths, R. C.; McNeil, M.; Grewal, R. K.; Yan, W.; Besra, G. S.; Brennan, P. J.; Fleet, G. W. J. *Tetrahedron Lett.* **1997**, *38*, 6733–6736.

90. Lee, R. E.; Smith, M. D.; Pickering, L.; Fleet, G. W. J. *Tetrahedron Lett.* **1999**, *40*, 8689–8692.

91. Liautard, V.; Desvergnes, V.; Martin, O. R. *Org. Lett.* **2006**, *8*, 1299–1302.

92. Liautard, V.; Desvergnes, V.; Itoh, K.; Liu, H.-w.; Martin, O. R. *J. Org. Chem.* **2008**, *73*, 3103–3115.

93. Liautard, V.; Christina, A. E.; Desvergnes, V.; Martin, O. R. *J. Org. Chem.* **2006**, *71*, 7337–7345.

94. Desvergnes, S.; Desvergnes, V.; Martin, O. R.; Itoh, K.; Liu, H.-w.; Py, S. *Bioorg. Med. Chem.* **2007**, *15*, 6443–6449.

95. Kovensky, J.; McNeil, M.; Sinaÿ, P. *J. Org. Chem.* **1999**, *64*, 6202–6205.

96. Owen, D. J.; Davis, C. B.; Hartnell, R. D.; Madge, P. D.; Thomson, R. J.; Chong, A. K. J.; Coppel, R. L.; von Itzstein, M. *Bioorg. Med. Chem. Lett.* **2007**, *17*, 2274–2277.

97. Owen, D. J.; von Itzstein, M. *Carbohydr. Res.* **2000**, *328*, 287–292.

98. Davis, C. B.; Hartnell, R. D.; Madge, P. D.; Owen, D. J.; Thomson, R. J.; Chong, A. K. J.; Coppel, R. L.; von Itzstein, M. *Carbohydr. Res.* **2007**, *342*, 1773–1780.

99. Veerapen, N.; Yuan, Y.; Sanders, D. A. R.; Pinto, B. M. *Carbohydr. Res.* **2004**, *339*, 2205–2217.

100. Ghavami, A.; Chen, J. J. W.; Pinto, B. M. *Carbohydr. Res.* **2004**, *339*, 401–407.

101. Mohan, S.; Pinto, B. M. *Carbohydr. Res.* **2007**, *342*, 1551–1580.

102. Tangallapally, R. P.; Yendapally, R.; Lee, R. E.; Hevener, K.; Jones, V. C.; Lenaerts, A. J. M.; McNeil, M. R.; Wang, Y.; Franzblau, S.; Lee, R. E. *J. Med. Chem.* **2004**, *47*, 5276–5283.

103. Pan, W.; Ansiaux, C.; Vincent, S. P. *Tetrahedron Lett.* **2007**, *48*, 4353–4356.

104. Carlson, E. E.; May, J. F.; Kiessling, L. L. *Chem. Biol.* **2006**, *13*, 825–837.

105. Dykhuizen, E. C.; May, J. F.; Tongpenyai, A.; Kiessling, L. L. *J. Am. Chem. Soc.* **2008**, *130*, 6706–6707.

106. Borrelli, S.; Zandberg, W. F.; Mohan, S.; Ko, M.; Martinez-Gutierrez, F.; Partha, S. K.; Sanders, D. A. R.; Av-Gay, Y.; Pinto, B. M. *Int. J. Antimicro. Ag.* **2010**, *36*, 364–368.

107. Castagnolo, D.; De Logu, A.; Radi, M.; Bechi, B.; Manetti, F.; Magnani, M.; Supino, S.; Meleddu, R.; Chisu, L.; Botta, M. *Bioorg. Med. Chem.* **2008**, *16*, 8587–8591.

108. Dykhuizen, E. C.; Kiessling, L. L. *Org. Lett.* **2009**, *11*, 193–196.

109. Partha, S. K.; Sadeghi-Khomami, A.; Cren, S.; Robinson, R. I.; Woodward, S.; Slowski, K.; Berast, L.; Zheng, B.; Thomas, N. R.; Sanders, D. A. R. *Mol. Inf.* **2011**, *30*, 873–883.

110. Mikušová, K.; Yagi, T.; Stern, R.; McNeil, M. R.; Besra, G. S.; Crick, D. C.; Brennan, P. J. *J. Biol. Chem.* **2000**, *275*, 33890–33897.

111. Alderwick, L. J.; Dover, L. G.; Veerapen, N.; Gurcha, S. S.; Kremer, L.; Roper, D. L.; Pathak, A. K.; Reynolds, R. C.; Besra, G. S. *Protein Expression Purif.* **2008**, *58*, 332–341.

112. Rose, N. L.; Completo, G. C.; Lin, S. J.; McNeil, M.; Palcic, M. M.; Lowary, T. L. *J. Am. Chem. Soc.* **2006**, *128*, 6721–6729.

113. Szczepina, M. G.; Zheng, R. B.; Completo, G. C.; Lowary, T. L.; Pinto, B. M. *ChemBioChem* **2009**, *10*, 2052–2059.

114. Szczepina, M. G.; Zheng, R. X. B.; Completo, G. C.; Lowary, T. L.; Pinto, B. M. *Bioorg. Med. Chem.* **2010**, *18*, 5123–5128.

115. Levengood, M. R.; Splain, R. A.; Kiessling, L. L. *J. Am. Chem. Soc.* **2011**, *133*, 12758–12766.

116. May, J. F.; Levengood, M. R.; Splain, R. A.; Brown, C. D.; Kiessling, L. L. *Biochemistry* **2012**, *51*, 1148–1159.

117. Wheatley, R. W.; Zheng, R. B.; Richards, M. R.; Lowary, T. L.; Ng, K. K. S. *J. Biol. Chem. In press*, doi: 10.1074/jbc.M112.347484

118. Lowary, T. L.; Poulin, M. B.; Zhou, R. *Org. Biomol. Chem.* **2012**, doi: 10.1039/c2ob25159k.

119. Mikušová, K.; Beláňová, M.; Korduláková, J.; Honda, K.; McNeil, M. R.; Mahapatra, S.; Crick, D. C.; Brennan, P. J. *J. Bacteriol.* **2006**, *188*, 6592–6598.

120. Beláňová, M.; Dianišková, P.; Brennan, P. J.; Completo, G. C.; Rose, N. L.; Lowary, T. L.; Mikušová, K. *J. Bacteriol.* **2008**, *190*, 1141–1145.

121. Peltier, P.; Belanova, M.; Dianiskova, P.; Zhou, R.; Zheng, R. B.; Pearcey, J. A.; Joe, M.; Brennan, P. J.; Nugier-Chauvin, C.; Ferrieres, V.; Lowary, T. L.; Daniellou, R.; Mikusova, K. *Chem. Biol.* **2010**, *17*, 1356–1366.

122. Guan, S.; Clarke, A. J.; Whitfield, C. *J. Bacteriol.* **2001**, *183*, 3318–3327.

123. Wing, C.; Errey, J. C.; Mukhopadhyay, B.; Blanchard, J. S.; Field, R. A. *Org. Biomol. Chem.* **2006**, *4*, 3945–3950.

124. Tsunashima, H.; Miyake, K.; Motono, M.; Iijima, S. *J. Biosci. Bioeng.* **2012**, *113*, 271–278.

125. El-Sayed, N. M.; Myler, P. J.; Bartholomeu, D. C.; Nilsson, D.; Aggarwal, G.; Tran, A.-N.; Ghedin, E.; Worthey, E. A.; Delcher, A. L.; Blandin, G.; Westenberger, S. J.; Caler, E.; Cerqueira, G. C.; Branche, C.; Haas, B.; Anupama, A.; Arner, E.; Åslund, L.; Attipoe, P.; Bontempi, E.; Bringaud,

F.; Burton, P.; Cadag, E.; Campbell, D. A.; Carrington, M.; Crabtree, J.; Darban, H.; da Silveira, J. F.; de Jong, P.; Edwards, K.; Englund, P. T.; Fazelina, G.; Feldblyum, T.; Ferella, M.; Frasch, A. C.; Gull, K.; Horn, D.; Hou, L.; Huang, Y.; Kindlund, E.; Klingbeil, M.; Kluge, S.; Koo, H.; Lacerda, D.; Levin, M. J.; Lorenzi, H.; Louie, T.; Machado, C. R.; McCulloch, R.; McKenna, A.; Mizuno, Y.; Mottram, J. C.; Nelson, S.; Ochaya, S.; Osoegawa, K.; Pai, G.; Parsons, M.; Pentony, M.; Pettersson, U.; Pop, M.; Ramirez, J. L.; Rinta, J.; Robertson, L.; Salzberg, S. L.; Sanchez, D. O.; Seyler, A.; Sharma, R.; Shetty, J.; Simpson, A. J.; Sisk, E.; Tammi, M. T.; Tarleton, R.; Teixeira, S.; Van Aken, S.; Vogt, C.; Ward, P. N.; Wickstead, B.; Wortman, J.; White, O.; Fraser, C. M.; Stuart, K. D.; Andersson, B. *Science* **2005**, *309*, 409–415.

126. Stoco, P. H.; Aresi, C.; Lückemeyer, D. D.; Sperandio, M. M.; Sincero, T. C. M.; Steindel, M.; Miletti, L. C.; Grisard, E. C. *Exp. Parasitol.* **2012**, *130*, 246–252.

127. Späth, G. F.; Epstein, L.; Leader, B.; Singer, S. M.; Avila, H. A.; Turco, S. J.; Beverley, S. M. *Proc. Natl. Acad. Sci. U.S.A.* **2000**, *97*, 9258–9263.

128. Zhang, K.; Barron, T.; Turco, S. J.; Beverley, S. M. *Mol. Biochem. Parasitol.* **2004**, *136*, 11–23.

129. Ivens, A. C.; Peacock, C. S.; Worthey, E. A.; Murphy, L.; Aggarwal, G.; Berriman, M.; Sisk, E.; Rajandream, M.-A.; Adlem, E.; Aert, R.; Anupama, A.; Apostolou, Z.; Attipoe, P.; Bason, N.; Bauser, C.; Beck, A.; Beverley, S. M.; Bianchettin, G.; Borzym, K.; Bothe, G.; Bruschi, C. V.; Collins, M.; Cadag, E.; Ciarloni, L.; Clayton, C.; Coulson, R. M. R.; Cronin, A.; Cruz, A. K.; Davies, R. M.; De Gaudenzi, J.; Dobson, D. E.; Duesterhoeft, A.; Fazelina, G.; Fosker, N.; Frasch, A. C.; Fraser, A.; Fuchs, M.; Gabel, C.; Goble, A.; Goffeau, A.; Harris, D.; Hertz-Fowler, C.; Hilbert, H.; Horn, D.; Huang, Y.; Klages, S.; Knights, A.; Kube, M.; Larke, N.; Litvin, L.; Lord, A.; Louie, T.; Marra, M.; Masuy, D.; Matthews, K.; Michaeli, S.; Mottram, J. C.; Müller-Auer, S.; Munden, H.; Nelson, S.; Norbertczak, H.; Oliver, K.; O'Neil, S.; Pentony, M.; Pohl, T. M.; Price, C.; Purnelle, B.; Quail, M. A.; Rabbinowitsch, E.; Reinhardt, R.; Rieger, M.; Rinta, J.; Robben, J.; Robertson, L.; Ruiz, J. C.; Rutter, S.; Saunders, D.; Schäfer, M.; Schein, J.; Schwartz, D. C.; Seeger, K.; Seyler, A.; Sharp, S.; Shin, H.; Sivam, D.; Squares, R.; Squares, S.; Tosato, V.; Vogt, C.; Volckaert, G.; Wambutt, R.; Warren, T.; Wedler, H.; Woodward, J.; Zhou, S.; Zimmermann, W.; Smith, D. F.; Blackwell, J. M.; Stuart, K. D.; Barrell, B.; Myler, P. J. *Science* **2005**, *309*, 436–442.

130. Pathak, A. K.; Besra, G. S.; Crick, D.; Maddry, J. A.; Morehouse, C. B.; Suling, W. J.; Reynolds, R. C. *Bioorg. Med. Chem.* **1999**, *7*, 2407–2413.

131. Cren, S.; Gurcha, S. S.; Blake, A. J.; Besra, G. S.; Thomas, N. R. *Org. Biomol. Chem.* **2004**, *2*, 2418–2420.

132. Trunkfield, A. E.; Gurcha, S. S.; Besra, G. S.; Bugg, T. D. H. *Bioorg. Med. Chem.* **2010**, *18*, 2651–2663.

133. Liautard, V.; Desvergnes, V.; Martin, O. R. *Tetrahedron: Asymmetry* **2008**, *19*, 1999–2002.

134. Frigell, J.; Pearcey, J. A.; Lowary, T. L.; Cumpstey, I. *Eur. J. Org. Chem.* **2011**, 1367–1375.

135. Varela, O.; Marino, C.; de Lederkremer, R. M. *Carbohydr. Res.* **1986**, *155*, 247–251.

136. Mariño, K.; Baldoni, L.; Marino, C. *Carbohydr. Res.* **2006**, *341*, 2286–2289.

137. Marino, C.; Mariño, K.; Miletti, L.; Alves, M. J. M.; Colli, W.; de Lederkremer, R. M. *Glycobiology* **1998**, *8*, 901–904.

138. Miletti, L. C.; Mariño, K.; Marino, C.; Colli, W.; Manso Alves, M. J.; de Lederkremer, R. M. *Mol. Biochem. Parasitol.* **2003**, *127*, 85–88.

139. Repetto, E.; Marino, C.; Laura Uhrig, M.; Varela, O. *Bioorg. Med. Chem.* **2009**, *17*, 2703–2711.

140. Marino, C.; Chiocconi, A.; Varela, O.; de Lederkremer, R. M. *Carbohydr. Res.* **1998**, *311*, 183–189.

141. Chiocconi, A.; Marino, C.; de Lederkremer, R. M. *Carbohydr. Res.* **2000**, *323*, 7–13.

142. Chiocconi, A.; Marino, C.; Otal, E.; de Lederkremer, R. M. *Carbohydr. Res.* **2002**, *337*, 2119–2126.

143. Bordoni, A.; de Lederkremer, R. M.; Marino, C. *Tetrahedron* **2008**, *64*, 1703–1710.

144. Weller, C. T.; McConville, M.; Homans, S. W. *Biopolymers* **1994**, *34*, 1155–1163.

145. Gohlke, H.; Immel, S.; Lichtenthaler, F. W. *Carbohydr. Res.* **1999**, *321*, 96–104.

146. Baldoni, L.; Stortz, C. A.; Marino, C. *Carbohydr. Res.* **2011**, *346*, 191–196.

147. de Leeuw, F. A. A. M.; Altona, C. *J. Comput. Chem.* **1983**, *4*, 428–437.

148. van Wijk, J.; Haasnoot, C. A. G.; de Leeuw, F. A. A. M.; Huckriede, B. D.; Westra Hoekzema, A.; Altona, C. *PSEUROT 6.3*, Leiden Institute of Chemistry, Leiden University: Leiden, 1999.

149. Karplus, M. *J. Chem. Phys.* **1959**, *30*, 11–15.

150. Karplus, M. *J. Am. Chem. Soc.* **1963**, *85*, 2870–2871.

Chapter 2:

A comparison between the gas-phase potential energy surfaces of methyl α- and β-D-galactofuranosides and solution conformations predicted by PSEUROT

Compounds **2.1** and **2.2** discussed in this chapter were synthesized by Mr. Yu Bai, using published protocols.[1,2]

2.1. Introduction

Pyranose rings typically exist in one chair conformation that is much lower in energy than the corresponding ring-flipped form. Furanose rings, however, often exist in a variety of envelope and twist conformations that are similar in energy, and these conformers interconvert through a process known as pseudorotation.[3] For example, Kilpatrick, et al.[3] first calculated that the envelope and twist conformations of cyclopentane had the same energy. The planar form was calculated to be 4 kcal/mol higher in energy. The dynamic structure of the furanose ring makes its conformational analysis an area of active research.[4]

Galactose is present in the furanose form in several species of bacteria, fungi, protozoa,[5,6] and metaozoans,[7] although galactofuranose (Gal*f*) is absent in mammals (Chapter 1). An example of a glycoconjugate containing Gal*f* is the mycolyl arabinogalactan (mAG) complex that forms part of the cellular envelope of *Mycobacterium tuberculosis* and other mycobacteria species.[8] The mAG complex is composed of a linear chain of 30–35 Gal*f* residues connected through alternating β-(1→5) and β-(1→6) linkages (Figure 2.1). At three points on the galactan chain – residues 8, 10, and 12 – branched arabinan chains are attached.[9] The arabinan chains are capped with mycolic acids, complex lipids containing 60–90 carbon atoms.[10,11]

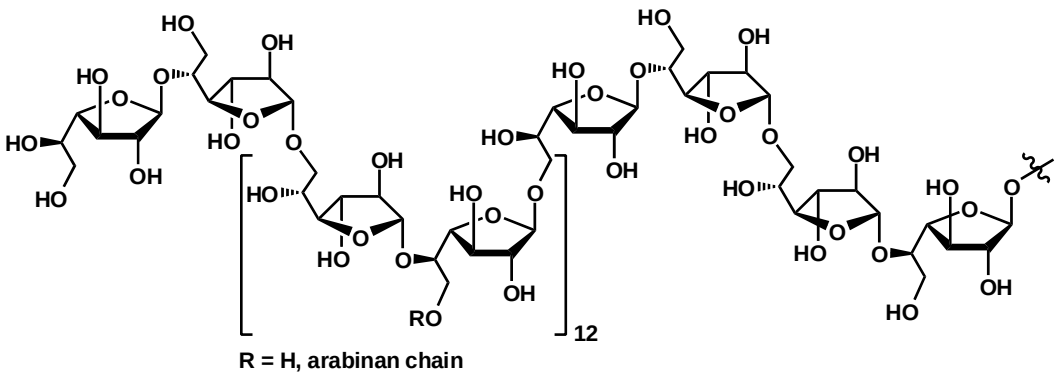

Figure 2.1. The galactan portion of the mycolyl arabinogalactan (mAG) complex.

The arabinose and galactose moieties of the mAG complex are in their furanose forms. For both carbohydrates, the furanose form is less thermodynamically stable than the pyranose form, as illustrated by the proportion of each found at equilibrium in aqueous solution.[12] Thus, it is unclear why mycobacteria produce these configurations. One proposed rationale is the "flexible scaffold hypothesis",[13,14] which suggests that the inherent flexibility of the furanose ring allows the mycolic acids to tightly pack against one another to form a protective barrier at the outer surface of the cell wall (Figure 2.2). There has been little experimental evidence to support this hypothesis, however.[15,16]

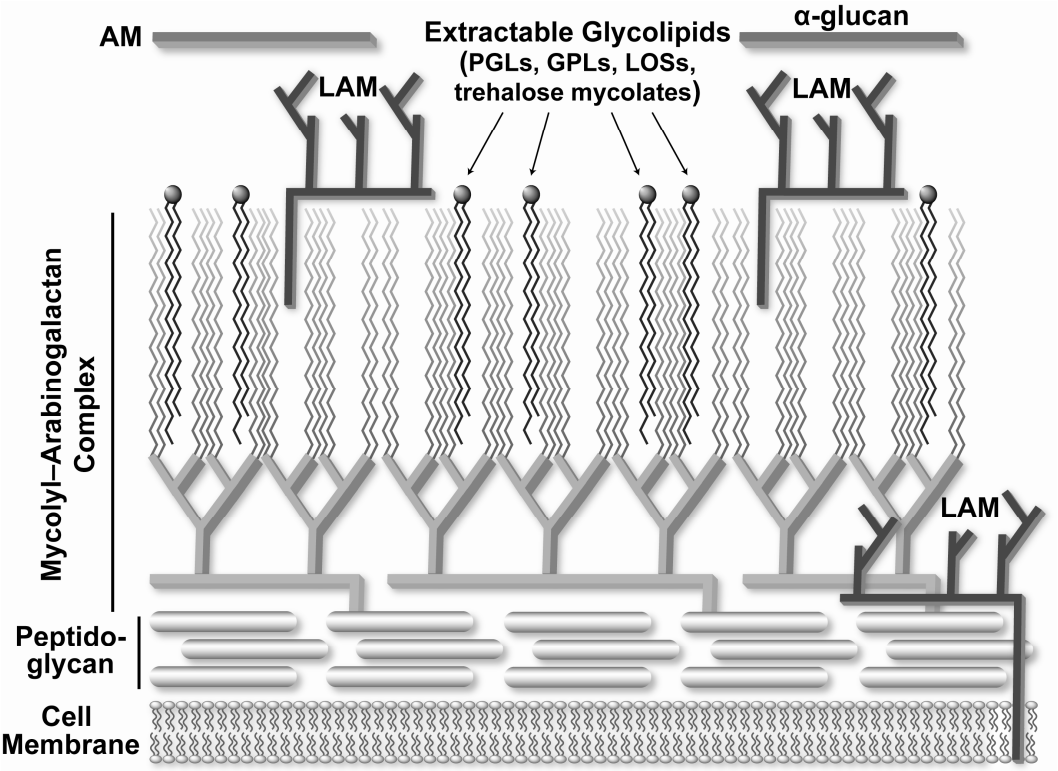

Figure 2.2. The mycobacterial cell wall, showing the mAG complex.

As part of our on-going study of furanosides present in the mAG complex, we present here partial potential energy surfaces (PES) of methyl α- and β-D-galactofuranosides (**2.1** and **2.2**, Figure 2.3) in the gas-phase derived from density functional theory (DFT) calculations. Ninety conformations for both **2.1** and **2.2** are described, as a full scan of conformational space would require 21,870 conformations (10×3^7) to include every C–C–O–H rotamer for each anomer. We limited our conformers to those without intramolecular hydrogen bonds, which are not expected to form in aqueous solution. Our group has already discussed in detail the structural parameters for both anomers of D-arabinofuranose (D-Ara*f*) from quantum mechanical calculations.[17-19] The configuration of the furanose ring is the same for D-Gal*f* and L-Ara*f* (Figure 2.3); however, Gal*f* is a hexose,

while Ara*f* is a pentose. Because there should no difference in geometries between the enantiomers D-Ara*f* and L-Ara*f*, we have focused on the exocyclic portions of **2.1** and **2.2** in our discussion of the conformations below. Finally, a comparison is presented between the gas-phase PES for **2.1** and **2.2** and the solution conformations.

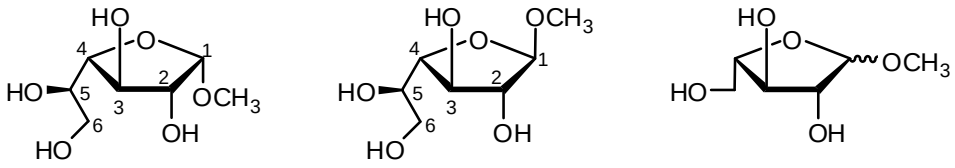

Figure 2.3 The structures of methyl α-D-galactofuranoside (**2.1**) and methyl β-D-galactofuranoside (**2.2**) with the carbon atoms numbered. Methyl L-Ara*f* is also shown for comparison.

2.2. Methods

2.2.1. Nomenclature

Envelope (E) ring conformations have one atom above or below the plane of the ring formed by the remaining four atoms. If the atom is above the plane, it is designated by a superscript preceding E; if the atom is below the plane, it is designated by a subscript following E. For example, the ^{1}E conformation corresponds to the envelope with C1 above the plane of the ring. Twist (T) conformations have one atom above and one atom below the plane of the ring formed by the remaining three ring atoms. The atoms displaced from the plane are similarly designated by superscripts and subscripts. For example, the $^{3}T_{2}$ conformation would indicate the twist conformer with C3 above and C2 below the plane of the ring.

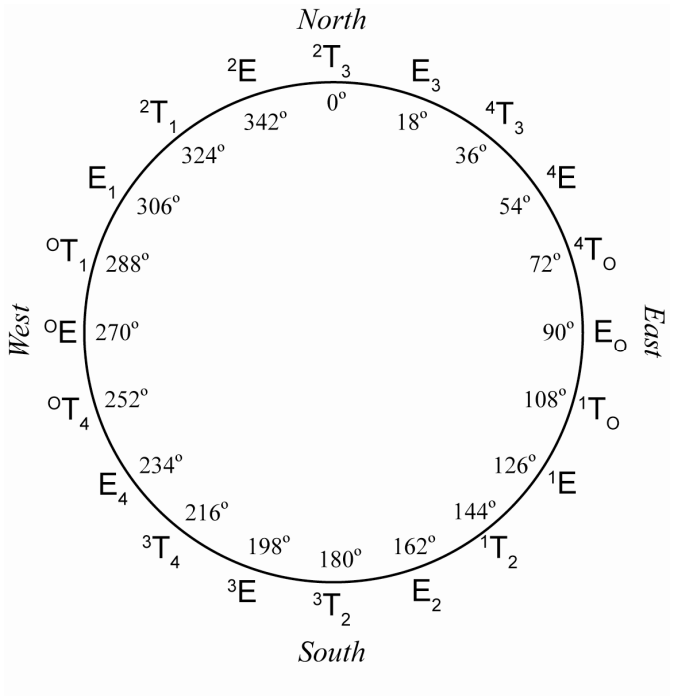

Figure 2.4. The pseudorotational itinerary, showing the value of *P* in degrees along the inside of the circle and the corresponding envelope or twist conformation along the outside.

The conformation of a furanose ring can also be defined by two parameters, *P* and ϕ_m. *P* refers to the Altona–Sundaralingam pseudorotational phase angle.[20] Values of *P* = 18°, 54°, 90°, etc. correspond to envelope conformations, and values of *P* = 0°, 36°, 72°, etc. correspond to twist conformations, as shown in Figure 2.4. The value of *P* can be calculated from the endocyclic torsion angles ϕ_0–ϕ_4 (Figure 2.5) using eq. 2.1. The value of ϕ_m describes the puckering of the five-membered ring or the displacement from planarity. The value of ϕ_m can be calculated from eq. 2.2.

$$\tan P = \frac{(\phi_2 + \phi_4) - (\phi_1 + \phi_3)}{2\phi_0 (\sin 36° + \sin 72°)} \qquad 2.1$$

$$\phi_m = \frac{\phi_0}{\cos P} \qquad 2.2$$

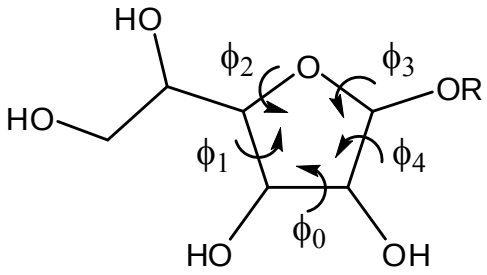

Figure 2.5. Definition of the endocyclic ring torsion angles ϕ_0–ϕ_4.

In addition to ring conformation, Gal*f* has additional sites of conformational variation, including the exocyclic C4–C5 and C5–C6 bonds. These bonds have three possible staggered rotamers (Figure 2.6), and each rotamer is named according to the *gauche* or *trans* relationships of the O–C–C–O and O–C–C–C dihedral angles – *gg*, *gt*, or *tg*. For example, when the O4–C4–C5–O5 is 60° and C3–C4–C5–O5 is 300°, both torsions are in a *gauche* relationship, and the rotamer is termed *gg*. The angles for each rotamer about the C4–C5 and C5–C6 bonds of Gal*f* in the ideal staggered conformation are also shown in Figure 2.6.

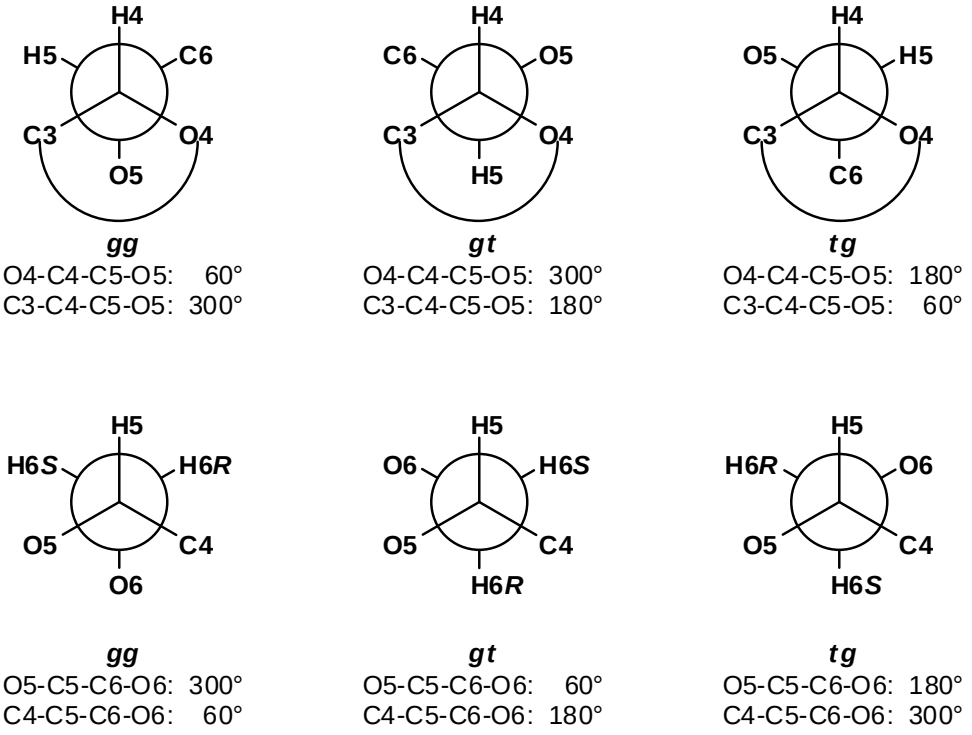

Figure 2.6. (*top*) The three staggered rotamers about the C4–C5 bond, viewing down the C4–C5 bond axis. (*bottom*) The three staggered rotamers about the C5–C6 bond, viewing down the C5–C6 bond axis.

Throughout the discussion in this thesis, the individual conformations of **2.1** and **2.2** are named according to their ring conformation, followed by the orientations about the C4–C5 bond and the C5–C6 bond (*gg*, *gt*, or *tg*). For example, E_4-*gg*-*gt* refers to an envelope ring conformer with C4 below the plane, the C4–C5 bond in the *gg* orientation, and the C5–C6 bond in the *gt* orientation. Additionally, hydrogens in the hydroxyl groups are referred to by the oxygen to which they are attached; for example, O5H refers to the hydrogen attached to O5.

2.2.2. Computational methodology

All calculations were performed in the Gaussian 03 program.[21] For the PES, the ten envelopes of both **2.1** and **2.2** were constructed, then each of the

three staggered rotamers for the C4–C5 and C5–C6 bonds (Figure 2.6) were generated for every envelope, giving a total of 90 conformations for both **2.1** and **2.2**. The geometries of all 180 conformations were optimized using DFT, specifically B3LYP/6-31G*.[22,23] Previous studies in our group[17-19] and others[24] demonstrated that this level of theory provides structural parameters in good agreement with experimental crystal structures for carbohydrates. During the optimization, the endocyclic ring torsion angle corresponding to the four atoms in the plane of the ring was fixed at 0° to maintain the envelope structure. For example, the C1–C2–C3–C4 dihedral angle was constrained at 0° in the E_O and ^OE conformations. Additionally, the C–C–O–H torsion angles were fixed to preclude the development of any intramolecular hydrogen bonds during geometry optimization. The values of these dihedral angles varied, depending on the overall conformation of the molecule. The C2–C1–O1–CH_3 dihedral angle was initially set at 180° (i.e. in the *exo*-anomeric preferred configuration) but was not fixed during geometry optimization. All other parameters – bond lengths, bond angles, and dihedral angles – were allowed to vary freely during geometry optimization. Single point energies were then calculated using both B3LYP/6-31+G**[22,23,25,26] and MP2/6-311+G**.[27]

The Cartesian coordinates for all optimized conformations of **2.1** and **2.2** are listed in the Appendix A. All 3D images were created using the program PyMol.[28]

2.2.3. NMR spectroscopy and PSEUROT

One-dimensional solution-state ^{1}H nuclear magnetic resonance (NMR) spectra were obtained for **2.1** and **2.2** in D_2O at 300 K on a 600 MHz spectrometer. For both compounds, the three-bond proton–proton coupling constants ($^3J_{H,H}$) were determined and are discussed in Section 2.3.4. A presaturation pulse sequence was used to reduce the intensity of the residual HOD signals (4.78 ppm at 300 K).

The magnitude of the coupling constant between vicinal protons is dictated by the dihedral angle ϕ_i^{HH} between them, as described by the Karplus relationship (eq. 2.3).[29,30] In addition, the dihedral angle ϕ_i^{HH} can be related to the corresponding ring dihedral angle ϕ_i by eq. 2.4.[31] (See Figure 2.5) for the definition of ϕ_0 through ϕ_4.) For a system with ideal tetrahedral geometry at each atom, the dihedral angle ϕ_i^{HH} between *cis* protons would be equivalent to the ring dihedral angle ϕ_i. Therefore, the coefficient a_i would be 1, and b_i would be 0°. The dihedral angle ϕ_i^{HH} between *trans* protons would differ from the ring torsion ϕ_i by ± 120°; thus, the coefficient a_i would still be 1, but b_i would be ± 120°. Most atoms in furanosides do not have ideal tetrahedral geometries; therefore, the values of a_i and b_i come from crystal structure data or from quantum mechanical calculations. Plotting the ring dihedral angle ϕ_i (*x*-axis) vs. the proton–proton dihedral angle ϕ_i^{HH} (*y*-axis) should give a linear relationship, where the slope of the line is a_i and the *y*-intercept is b_i.[32] Also, D-Gal*f* has the same relative configuration of the ring as D-Ara*f*, but the two rings are mirror images. Thus, the

opposite of slope of the line a_i should be used in PSEUROT calculations of D-Gal*f*.[20,33]

$$^3J_{H,H} = A + B\cos\phi^{HH} + C\cos 2\phi^{HH} \quad 2.3$$

$$\phi_i = a_i\phi_i^{HH} + b_i, \quad i = 0,1,2,3,4 \quad 2.4$$

The program PSEUROT[31,34] was developed by Altona and coworkers to determine the ring conformation of furanosides based on vicinal proton–proton coupling constants, as well as eq. 2.3 and eq. 2.4. PSEUROT assumes that the observed coupling constants represent equilibrium values between two conformations – one in the northern part of the pseudorotational wheel (Figure 2.4) and one in the southern part. This assumption means the program has five unknowns to solve for: P and ϕ_m for the northern conformation, P and ϕ_m for the southern conformation, and the ratio between the two conformers. However, Gal*f* only has three vicinal proton coupling constants for the ring. Thus, in PSEUROT calculations of **2.1** and **2.2**, the value of ϕ_m for both conformers was held constant at 39°, leaving only three unknowns. The value ϕ_m = 39° was used because it was observed in crystal structures of methyl α- and β-D-Ara*f*, which has the same substitution pattern on the ring as Gal*f*.[32] PSEUROT also requires initial values of P for both conformers. For both **2.1** and **2.2**, four different calculations were run with the following starting values – run A: P_N = 50°, P_S = 150°; run B: P_N = 50°, P_S = 250°; run C: P_N = 320°, P_S = 250°; and run D: P_N = 320°, P_S = 50°.[35] The program then takes the initial values of P and ϕ_m and obtains the best fit to the observed coupling constants through Newton–Raphson minimization.[36]

2.3. Results and discussion

2.3.1. Optimized conformations for 2.1

2.3.1.1. Pseudorotational phase angle and puckering

Each individual envelope conformation of **2.1** started from the same initial ring geometry prior to geometry optimization, i.e., the furanose ring was the same for the E_3-*gg*-*gg* conformer as for the E_3-*tg*-*tg* conformer. After geometry optimization, however, a range of ring conformations were present, as illustrated in Figure 2.7. All of the conformers maintained near ideal values of *P* because one endocyclic torsion angle was fixed during the optimization process, but the ring puckering varied. In particular, the northeast – E_3, ^4E, and E_O geometries – showed a larger range of puckering than the remaining conformations. The ϕ_m values for these three rings ranged from 17° to 39°. In contrast, the puckering for the E_1 conformers was much narrower, ϕ_m = 39–42°. For all 90 optimized conformations of **2.1**, the average ϕ_m was 34.8°, with the total range ϕ_m = 17–43°.

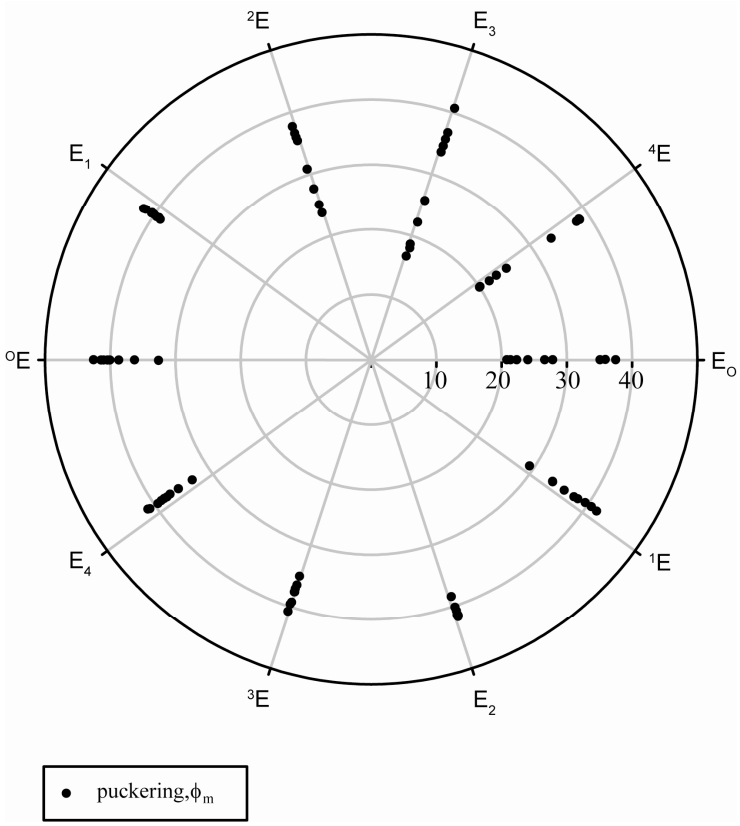

Figure 2.7. Ring conformations for the optimized geometries of **2.1**. Each spoke on the wheel represents a phase angle *P*, and the distance from the center of the wheel represents the ring puckering, ϕ_m, in degrees.

2.3.1.2. Orientation about the C4–C5 bond for the gg rotamers

As with the ring geometries, each of the exocyclic torsions of **2.1** started from the same point, but over the course of geometry optimization, the values of O4–C4–C5–O5 dihedral angles diverged. The ideal angles for the O4–C4–C5–O5 torsion in each of the three staggered rotamers is shown in Figure 2.6; i.e., *gg* is 60°, *gt* is 300°, and *tg* is 180°. The value of this torsion was close to the ideal value of 60° for all ring conformations when the C4–C5 bond was in the *gg* orientation and the C5–C6 bond was in either the *gg* or *tg* conformation (Figure 2.8a). For these 20 conformers, the O4–C4–C5–O5 torsion was between 60° and

69°, with an average of 66°. A larger range of values was seen when the C5–C6 bond was in the *gt* orientation; the O4–C4–C5–O5 torsion was lower than the ideal, with an average value of 50°. The lowest extreme was seen in the E_2-*gg*-*gt* conformer, which had a 39° O4–C4–C5–O5 dihedral angle. The E_2-*gg*-*gt* conformer contained an intramolecular hydrogen bond from O5H to O2, which may account for the small O4–C4–C5–O5 torsion angle.

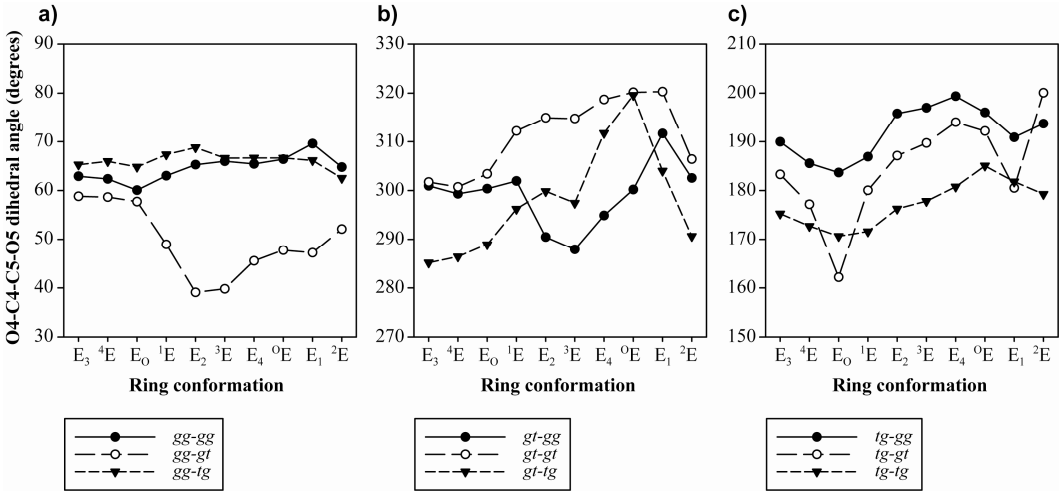

Figure 2.8. O4–C4–C5–O5 dihedral angles for optimized geometries of **2.1**. Graph *a*) shows the O4–O5 torsion for each envelope when the C4–C5 bond is in the *gg* orientation, *b*) shows the O4–O5 torsion for each envelope when the C4–C5 bond is in the *gt* orientation, and *c*) shows the O4–O5 torsion for each envelope when the C4–C5 bond is in the *tg* orientation. For all three graphs, each line represents a different rotamer about the C5–C6 bond: *gg* is the filled circles and solid line, *gt* is the open circles and long dashed line, and *tg* is the filled triangle and short dashed line.

We tried to exclude intramolecular hydrogen bonds in our sampling of the PES; however, for some ring conformations, this was impossible. In particular, with the C4–C5 bond in the *gg* orientation and the C5–C6 bond in the *gt* conformation, the E_2, ^3E, and E_4 conformers all contained a hydrogen bond from O5H to O2 (Figure 2.9a). These conformations all had the C4–C5–O5–H

dihedral angle at 55° (or the *g*+ orientation), which was consistent with the remaining conformers in the series. When the C4–C5–O5–H was set to the *t* or *g*– orientations and the conformer was optimized, other intramolecular hydrogen bonds developed, between O5H and O6 or O5H and O4, respectively. Finally, the E_1-*gg*-*gt* conformer had an intramolecular hydrogen bond between O5H and O1, though the geometry for this hydrogen bond was not ideal, having an O5–O1 distance of 2.8 Å and an O5–H–O1 angle of 108° (Figure 2.9b).

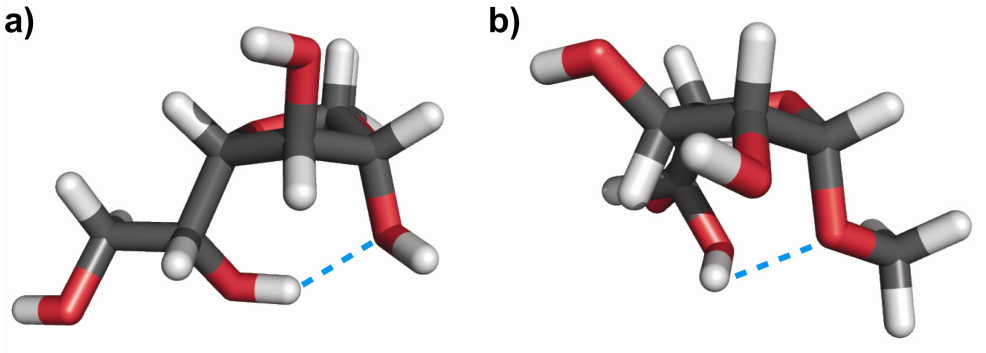

Figure 2.9. Examples of hydrogen bonds (blue dashed lines) in optimized conformations of **2.1**. *a*) E_2-*gg*-*gt* has a hydrogen bond from O5H to O2. *b*) E_1-*gg*-*gt* has a hydrogen bond from O5H to O1.

2.3.1.3. Orientation about the C4–C5 bond for the gt rotamers

For the conformers of **2.1** with the O4–C4–C5–O5 dihedral angle in the *gt* conformation, the average value for this torsion was 303°, with a range of 285–320° (Figure 2.8b). When the C5–C6 bond was in the *gt* orientation, the O4–C4–C5–O5 dihedral angle took on the largest values from 285° to 320°. Specifically, in the northeast section from ^1E to E_1, O4–C4–C5–O5 averaged 317°, presumably to reduce steric clashes between H3 and H6*S*. For example, the O4–C4–C5–O5

torsion angle in E_1-*gt*-*gt* took on the largest value at 320°, and the distance between H3 and H6*S* is 2.5 Å (Figure 2.10a). If this angle is decreased to 300°, the distance between the two protons decreases to 1.9 Å, which is smaller than twice the van der Waals radius for two hydrogens (2.4 Å).[37] Conformers in the southwest section from ^2E to E_O averaged values closer to the ideal angle at 303°.

There was similar trend for conformations with the C5–C6 bond in the *tg* conformation: the northeast section from ^1E to E_1, O4–C4–C5–O5 averaged 305°, while the southwest section from ^2E to E_O had a lower average of 288°. The lower than ideal values for the southwest region was due to relieving steric strain between O4 and O5. For example, the E_3-*gt*-*tg* conformation has the lowest value for the O4–C4–C5–O5 dihedral angle at 285°, and the O4–O5 distance is 2.9 Å in this conformation, which is quite close to twice the van der Waals radius for two oxygens (3.0 Å, Figure 2.10b).[37] If the angle is increased to 300°, this distance drops to 2.7 Å. Finally, the trend is different for conformations with C5–C6 in the *gg* conformation. For these structures, the northeast region from E_1 to ^1E has an average O4–C4–C5–O5 value of 303°, and the southwest from E_2 to ^OE had an average of 293°. The lower than ideal values for the southern conformations were due to steric repulsion between O4 and O5.

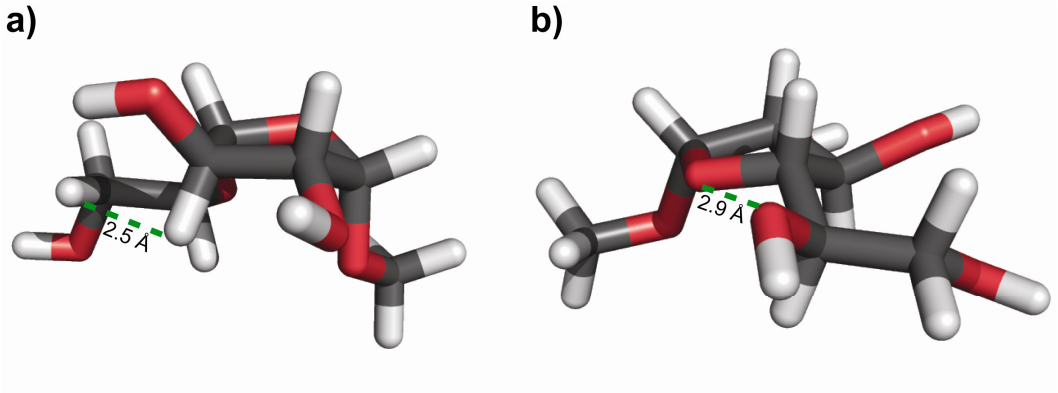

Figure 2.10. Examples of close contacts (green dashed lines) in optimized conformations of **2.1**. *a*) The distance between H3 and H6*S* is 2.5 Å in E_1-*gt*-*gt*. *b*) The distance between O4 and O5 is 2.9 Å in E_3-*gt*-*tg*.

2.3.1.4. Orientation about the C4–C5 bond for the tg rotamers

The conformations of **2.1** with the O4–C4–C5–O5 dihedral angle in the *tg* conformation showed a consistent trend among the three conformations about the C5–C6 bond (Figure 2.8c). The average value for the O4–C4–C5–O5 torsion was close to 185°, ranging from 162° to 200°. The conformers with the C5–C6 bond in the *gg* and *tg* orientations show the same pattern, with *gg* offset 15° higher than *tg*, with the southern conformations E_2 to ^{O}E having higher values than the rest of the pseudorotational itinerary. Additionally, both *tg*-*gg* and *tg*-*tg* exhibited a narrow range of values – the range for *tg*-*gg* is 14° with an average O4–C4–C5–O5 dihedral angle of 192°, and the range for *tg*-*tg* is 16° with an average O4–C4–C5–O5 dihedral angle of 185°. The trend for the structures with C5–C6 in the *gt* orientation also follow the same overall trend as the other conformations with two outliers. The O4–C4–C5–O5 dihedral angle of E_O-*tg*-*gt* conformation is the lowest value of the series at 162°, which increases the distance between the partial positive charges on O3H and O5H, relieving some electrostatic repulsion (Figure

2.11a). The distance between O3H and O5H is significantly shorter in E_O-*tg*-*gt* (2.3 Å) than for its neighbor ^{1}E-*tg*-*gt* (2.9 Å). The ^{2}E-*tg*-*gt* conformation has the highest value of the series at 200°, and its deviation from ideal is to accommodate electrostatic repulsion between O3 and O5. With the angle at 200°, the distance between O3 and O5 is 3.2 Å; whereas, closer to the ideal value of 180°, the distance drops to 3.1 Å (Figure 2.11b). Additionally, O5H and O3 are closer to the proper orientation for a weak hydrogen bond when the angle is 200°.[38]

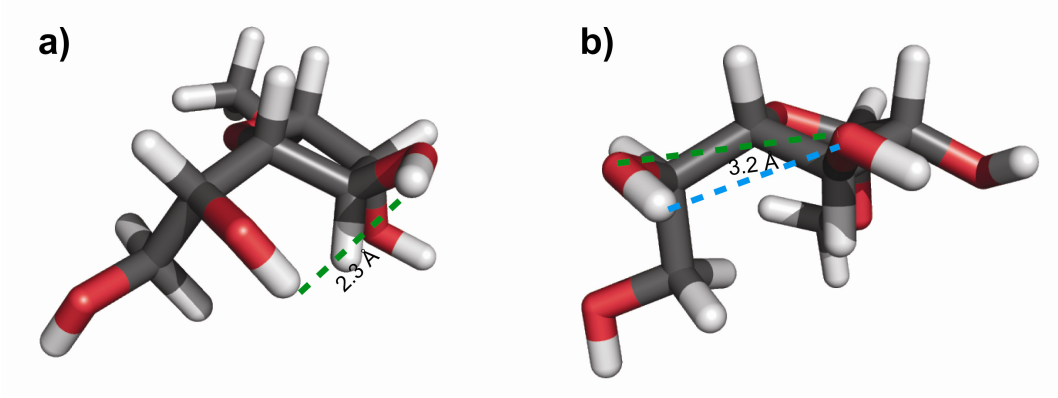

Figure 2.11. Examples of close contacts (green dashed lines) in optimized conformations of **2.1**. *a*) The distance between O3H and O5H is 2.3 Å in E_O-*tg*-*gt*. *b*) The distance between O3 and O5 is 3.1 Å in ^{2}E-*tg*-*gt*. When the O4–C4–C5–O5 dihedral angle is 200º there is also a favorable interaction between O5H and O3 (blue dashed line).

2.3.1.5. Orientation about the C5–C6 bond for the gg rotamers

For the C5–C6 bond, the ideal angles for the O5–C5–C6–O6 torsion are shown in Figure 2.12; i.e. *gg* is 300°, *gt* is 60°, and *tg* is 180°. Structures of **2.1** with *gg* orientation about the C5–C6 bond have O5–C5–C6–O6 dihedral angles ranging from 280° to 319°, with an average value of 304° (Figure 2.12a). When the C4–C5 bond is also in the *gg* conformation, the values for the O5–C5–C6–O6 torsion angle have a narrow range very close to ideal, 302–306°. The largest

variation is seen for *gt-gg* conformations with a range from 280° to 302° and an average of 294°. The southwest region from E_2 to ^{O}E has lower than ideal values averaging 283°, while the conformations from E_1 to ^{1}E average near ideal at 301°. The low values for the O5–C5–C6–O6 torsion of E_2-*gt-gg*, ^{3}E-*gt-gg*, E_1-*gt-gg*, and ^{O}E-*gt-gg* can be explained by the presence of a hydrogen bond between O3H and O6 (Figure 2.13a). The average O3 to O6 distance is 3.8 Å, and the average O3–H···O6 angle is 114°. Taken together, these two values are within the range of a weak hydrogen bond.[38] The average value for the O5–C5–C6–O6 torsion of the *tg-gg* conformers is above the ideal angle at 314°, with a range from 306° to 319°. The deviation from the ideal 300° reduces the potential *syn*-pentane strain along O6–C6–C5–C4–C3 motif (Figure 2.13b).[39]

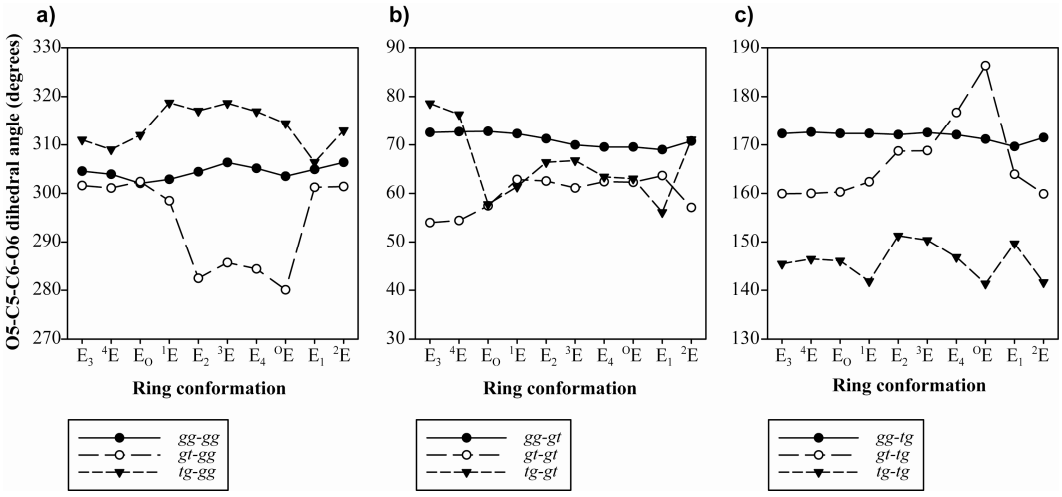

Figure 2.12. O5–C5–C6–O6 dihedral angles for optimized geometries of **2.1**. Graph *a*) shows the O5–O6 torsion for each envelope when the C5–C6 bond is in the *gg* orientation, *b*) shows the O5–O6 torsion for each envelope when the C5–C6 bond is in the *gt* orientation, and *c*) shows the O5–O6 torsion for each envelope when the C5–C6 bond is in the *tg* orientation. For all three graphs, each line represents a different rotamer about the C4–C5 bond: *gg* is the filled circles and solid line, *gt* is the open circles and long dashed line, and *tg* is the filled triangle and short dashed line.

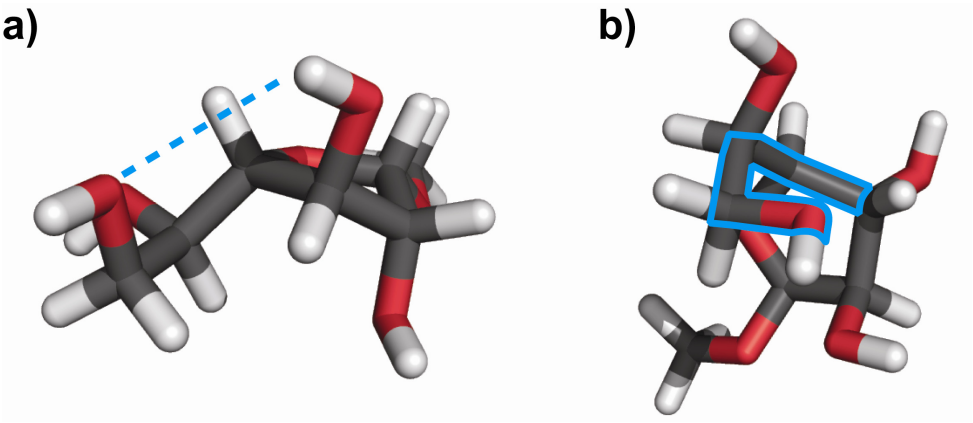

Figure 2.13. Optimized conformations of **2.1**. *a*) Example hydrogen bond (blue dashed line) between O3H and O6 in E_2-*gt*-*gg*. *b*) The O6–C6–C5–C5–C3 motif is highlighted (blue solid line) in E_2-*tg*-*gg*.

2.3.1.6. Orientation about the C5–C6 bond for the gt rotamers

Conformations of **2.1** with the C5–C6 angle in the *gt* orientation have the smallest variation in the O5–C5–C6–O6 angle (Figure 2.12b), with an average value close to ideal at 65°. The structures in the *gg*-*gt* orientation have a narrow range of values for the O5–C5–C6–O6 dihedral angle between 69° and 73° with an average of 71°, reducing the distance between the partial electron-rich substituents on O5 and O6. While the range for the conformers in the *gt*-*gt* orientation is larger than those for the *gg*-*gt* orientation (54°–64°), the average is 60°. Finally, several values for the O5–C5–C6–O6 torsion in *tg*-*gt* are similar to those for the *gg*-*gt* orientation, with the exception of the northern conformations E_2, ^3E, and E_4. In these three conformations, the O5–C5–C6–O6 torsion ranges from 71° to 79°. These conformers also have the C4–C3–O3–H dihedral angle in the *g*+ conformation (Figure 2.14a) to prevent a hydrogen bond between O5H and

O3, while the remaining structures in the series have the C4–C3–O3–H dihedral angle in the *g*– orientation (Figure 2.14b).

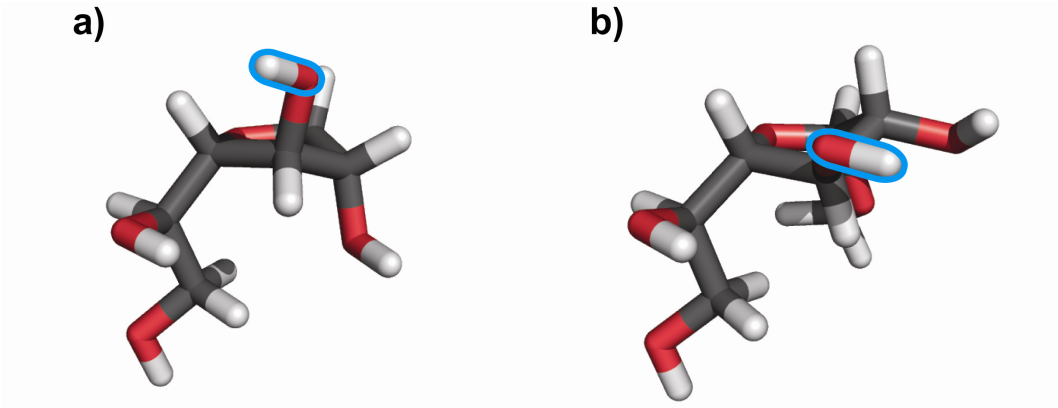

Figure 2.14. Variations in the C4–C3–O3–H dihedral angle (blue solid line) of **2.1**. *a*) This torsion is *g*+ in E_2-*tg*-*gt*. *b*) This torsion is *g*– in ^{2}E-*tg*-*gt*.

2.3.1.7. Orientation about the C5–C6 bond for the tg rotamers

For *tg* orientations about the C5–C6 bond of **2.1**, the range of values of O5–C5–C6–O6 is fairly large, from 141° to 186°, with an average value well below the ideal, at 162° (Figure 2.12c). Once again, when the C4–C5 bond is in the *gg* conformation, the range of values for the O5–C5–C6–O6 dihedral angle is narrow, 170–173°. The largest range of values is seen for the structures with the C4–C5 bond in the *gt* conformation from 160° to 186°. The E_4-*gt*-*tg* and the ^{O}E-*gt*-*tg* conformations are closest to the ideal 180°, while the remainder range between 160° and 170°. In both E_4-*gt*-*tg* and ^{O}E-*gt*-*tg*, the C3 and C4 substituents are pseudoaxial; therefore, when the O5–C5–C6–O6 dihedral angle is close to 180°, O3 and O6 are not close to one another (Figure 2.15a). However, in other conformers, when this torsion is close to its ideal value, *syn*-pentane strain would arise along the O6–C6–C5–C4–C3 structural domain.[39] By reducing this angle to

below 170°, the steric strain is removed. The largest deviations from ideal are seen for the values of the O5–C5–C6–O6 dihedral angle when C4–C5 is in the *tg* conformation. The range for these structures is 141–151° with an average value of 146°. Conformers of **2.1** with the *tg*-*tg* orientation bring the O6 and O1 atoms close to one another, and if the O5–C5–C6–O6 angle is closer to 180°, these atoms are within twice the distance of the van der Waals radius for oxygen (3.0 Å, Figure 2.15b).[37]

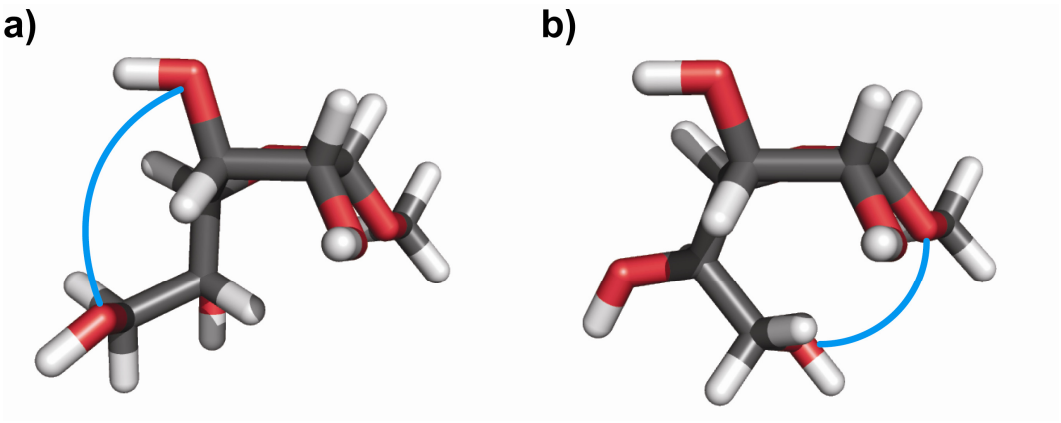

Figure 2.15. Optimized conformations of **2.1**. *a*) In E_4-*gt*-*tg*, the distance between O3 and O6 (connected by a blue solid line) is large due to the pseudoaxial substituents. *b*) In E_4-*tg*-*tg*, O5–C5–C6–O6 is 147°, keeping the distance between O1 and O6 (connected by a blue solid line) larger than their combined van der Waals radii.

2.3.2. Optimized conformations for 2.2

2.3.2.1. Pseudorotational phase angle and puckering

Just as with the α-anomer **2.1**, a range of ring conformations were present for the β-anomer **2.2** after geometry optimization (Figure 2.16). Because the torsion angle in the plane of the ring was constrained during the optimization process, only near ideal values of *P* are observed. However, the puckering amplitude ϕ_m varies from 16°–44°, a slightly larger range than was observed for

2.1. Also similar to **2.1**, the northeast region – ^{2}E through E_O – have the largest spread of values, with an average range of ϕ_m of 16°. The remaining envelope conformations have an average range of ϕ_m of 8°.

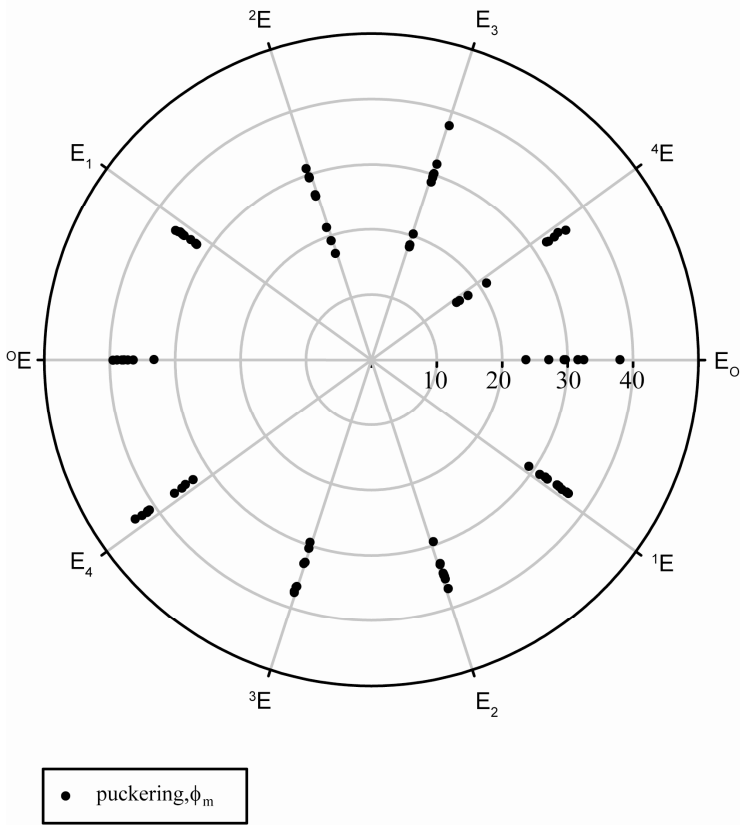

Figure 2.16. Ring conformations for the optimized geometries of **2.2**. Each spoke on the wheel represents a value of the phase angle, P/π in radians, and the distance from the center of the wheel represents the ring puckering, ϕ_m in degrees.

2.3.2.2. Orientation about the C4–C5 bond for the gg rotamers

While the graphs for O4–C4–C5–O5 dihedral angles for **2.1** and **2.2** are not identical (Figure 2.8 and Figure 2.17, respectively), the trends are similar. Specifically, for the conformations with C4–C5 in the *gg* orientation (Figure 2.17a), the average value for the O4–C4–C5–O5 torsion is exactly the ideal at 60°, with a large range of 42–69°. Among the three possible orientations about

the C5–C6 bond, the *gg-tg* conformers of **2.2** have the narrowest range, 60–66°, which is similar to what was seen for **2.1**. The *gg-gt* structures also follow a similar trend as described above, with the northern conformations ^{O}E to E_O close to the ideal value with an average of 61°. The southern conformations ^{1}E to E_4, however, have O4–C4–C5–O5 dihedral angles much lower than the idea value, averaging 48°. These conformations also all have a hydrogen bond between O5H and O2 (Figure 2.18a), and the C4–C5–O5–H torsion is in the *g*+ orientation, consistent with the remaining conformers in the series. We attempted to eliminate this hydrogen bonding by introducing additional constraints. However, constraining C4–C5–O5–H to one of the other rotamers led to the development of other intramolecular hydrogen bonds, as described above. The ^{3}E-*gg-gg* conformation is a major outlier with a 42° O4–C4–C5–O5 torsion angle. The deviation from the ideal can be accounted for by the electrostatic repulsion between O6 and O4 in this rotamer (Figure 2.18b). If the dihedral angle is closer to 60°, then the oxygen–oxygen distance drops to 2.7 Å. Despite this conformation, the average for *gg-gg* is 60°.

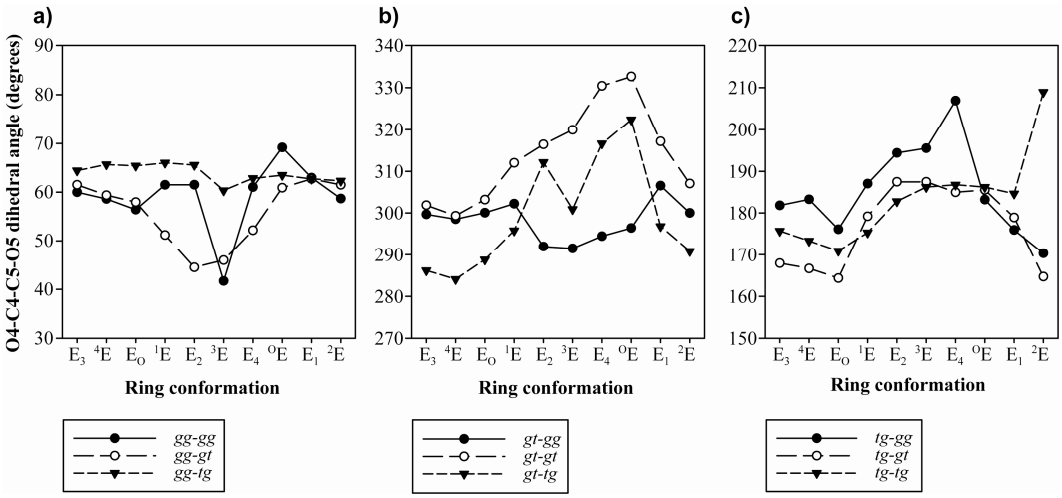

Figure 2.17. O4–C4–C5–O5 dihedral angles for optimized geometries of **2.2**. Graph *a*) shows the O4–O5 torsion for each envelope when the C4–C5 bond is in the *gg* orientation, *b*) shows the O4–O5 torsion for each envelope when the C4–C5 bond is in the *gt* orientation, and *c*) shows the O4–O5 torsion for each envelope when the C4–C5 bond is in the *tg* orientation. For all three graphs, each line represents a different rotamer about the C5–C6 bond: *gg* is the filled circles and solid line, *gt* is the open circles and long dashed line, and *tg* is the filled triangle and short dashed line.

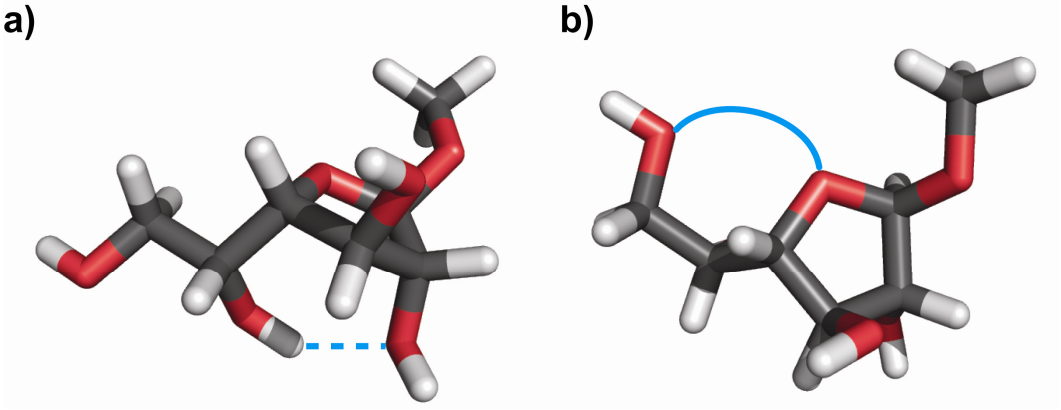

Figure 2.18. Optimized conformations of **2.2**. *a*) An example of the hydrogen bond (blue dashed line) between O2 and O5H in E_3-*gg*-*gt*. *b*) The smaller than ideal value for the O4–C4–C5–O5 dihedral angle in E_3-*gg*-*gg* decreases the electrostatic repulsion between O4 and O6 (blue solid line).

2.3.2.3. Orientation about the C4–C5 bond for the gt rotamers

The conformations of **2.2** with the C4–C5 bond in the *gt* orientation all show similar trends to the same conformations of **2.1**. Briefly, the overall range for the O4–C4–C5–O5 dihedrals angle is 284–333°, and the average is 303° (Figure 2.17b). When the C5–C6 bond is in the *gg* orientation, the southwest conformers E_2 through ^{O}E have lower values than the remainder of the series. This trend is reversed for the structures with the C5–C6 bond is in either *gt* or *tg*.

2.3.2.4. Orientation about the C4–C5 bond for the tg rotamers

When the C4–C5 bond is in the *tg* orientation, conformations of **2.2** show the least similarity to those of **2.1**. The range of the O4–C4–C5–O5 dihedral angle for the *tg* conformers is 45°, with an average close to the ideal at 182° (Figure 2.17c). The overall trend in the values of O4–C4–C5–O5 for **2.2** is *tg-gt* < *tg-tg* < *tg-tg*, with average values of 177°, 183°, and 185°, respectively. The trend for **2.1**, however, is *tg-tg* < *tg-gt* < *tg-gg*. For all the structures of **2.2**, the southern conformations ^{1}E to ^{O}E have higher values for the O4–C4–C5–O5 dihedral angle, with an average of 187°, than the northern ones E_1 to E_O, which average 175°. The exception to this is the ^{2}E-*tg-tg* conformer with a O4–C4–C5–O5 torsion of 209°, the highest of all 30 structures. This conformation puts O5 and O3 at a distance of 3.1 Å when O4–C4–C5–O5 is close to 180°; when the dihedral angle is at 209°, these atoms are 3.4 Å apart (Figure 2.19a). Despite the magnitudes of the O4–C4–C5–O5 torsions having different trends between **2.1** and **2.2**, the curves themselves are quite similar. For the *tg-gg* curve, the exception is the outlier E_4-*tg-gg*, possessing an O4–C4–C5–O5 torsion of 207°.

The adoption of a larger than ideal angle prevents a steric clash between O5 and H3 (Figure 2.19b). A value of 180° puts these atoms within 2.6 Å of each other, while at 207°, they are 3.0 Å apart. For the *tg-gt* curve, the values for the northern conformation ^{2}E through ^{4}E have lower values for O4–C4–C5–O5 in the β-anomer than the α-anomer. The trend for *tg-tg* is the same between **2.1** and **2.2**, except for ^{2}E-*tg-tg* conformer, discussed above.

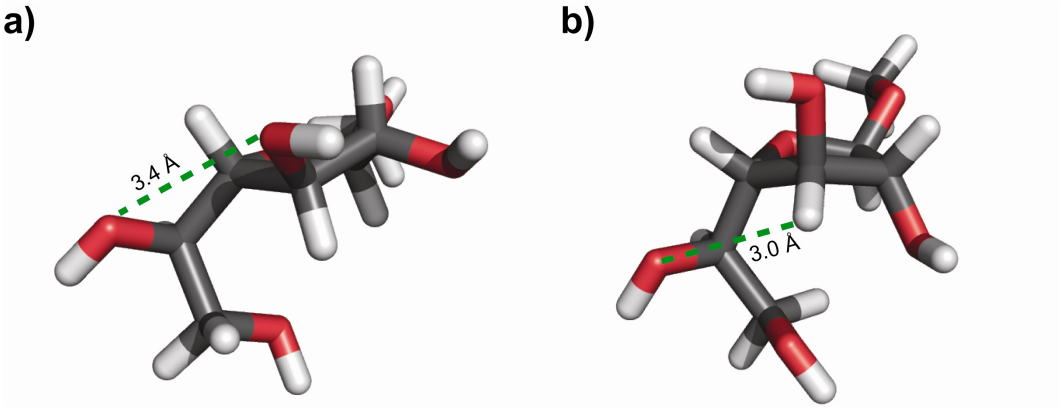

Figure 2.19. Examples of close contacts (green dashed lines) in optimized conformations of **2.2**. *a*) The distance between O3 and O5 is 3.4 Å in ^{2}E-*tg-tg*. *b*) The distance between H3 and O5 is 3.0 Å in E_4-*tg-gg*.

2.3.2.5. Orientation about the C5–C6 bond for the gg rotamers

The graphs for the O5–C5–C6–O6 dihedral angles for **2.2** (Figure 2.20) are quite similar to those for **2.1** (Figure 2.12). For conformations with the C5–C6 bond in the *gg* orientation (Figure 2.20a), the trend *gt-gg* < *gg-gg* < *tg-gg* holds for both the α- and β-anomers. Specifically, the curve for *gt-gg* is the same between the two, with a range from 280–303° and an average value of 293°. The *gg-gg* conformers for **2.2** show more variation than in **2.1**, with a range of O5–C5–C6–O6 values spanning 38°. While structures with the *tg-gg* conformation also show a similar overall trend between the anomers, there are larger values for

2.2 with a maximum at 318° for the southeastern conformations ^{1}E through ^{3}E. These larger than ideal values for the O5–C5–C6–O6 dihedral put the O6 and H3 atoms 2.3–2.4 Å apart, whereas if the angle were closer to 300°, this distance decreases to 2.1–2.2 Å (Figure 2.21).

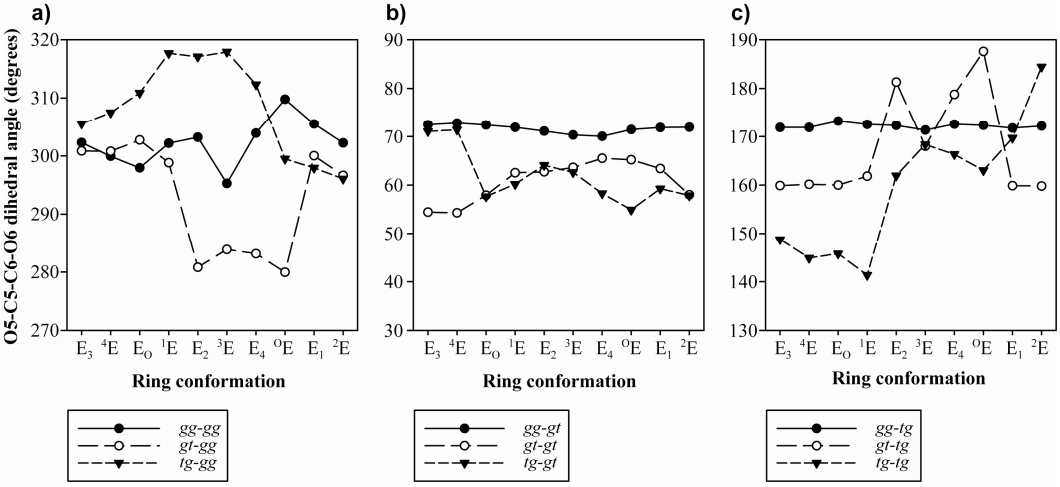

Figure 2.20. O5–C5–C6–O6 dihedral angles for optimized geometries of **2.2**. Graph *a*) shows the O5–O6 torsion for each envelope when the C5–C6 bond is in the *gg* orientation, *b*) shows the O5–O6 torsion for each envelope when the C5–C6 bond is in the *gt* orientation, and *c*) shows the O5–O6 torsion for each envelope when the C5–C6 bond is in the *tg* orientation. For all three graphs, each line represents a different rotamer about the C4–C5 bond: *gg* is the filled circles and solid line, *gt* is the open circles and long dashed line, and *tg* is the filled triangle and short dashed line.

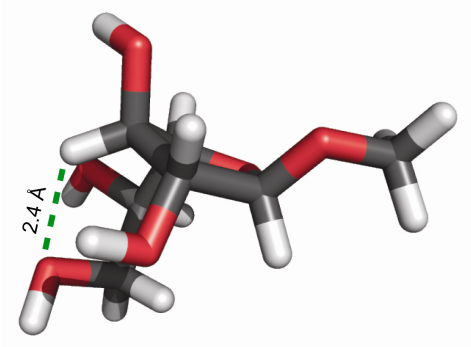

Figure 2.21. The ^{3}E-*tg-gg* conformation of **2.2**, showing the distance between H3 and O6 (green dashed line).

2.3.2.6. Orientation about the C5–C6 bond for the gt rotamers

The conformations of **2.2** with the C5–C6 bond in the *gt* orientation (Figure 2.20b) all show similar trends to the same conformations of **2.1** with an average value close to ideal at 65°. The structures of **2.2** in the *gg-gt* orientation have an even narrower range of values for the O5–C5–C6–O6 dihedral angle than for **2.1**: 70° to 73°, with an average of 72°. The range for the conformers in the *gt-gt* orientation is larger than those for the *gg-gt* orientation (54°–66°), but the average is very close to ideal at 61°. Finally, many of the conformations with the *tg-gt* conformation are close to those in the *gg-gt* orientation, with the exception of the northern conformations ^{3}E and E_4. In these two conformations, O5–C5–C6–O6 is 71°, and if the O5–C5–C6–O6 dihedral angle is closer to the ideal value, the O5 and O6 atoms would be only 2.7 Å apart. Increasing the angle to 71° also increases the distance between O5 and O6 to 2.8 Å (Figure 2.22).

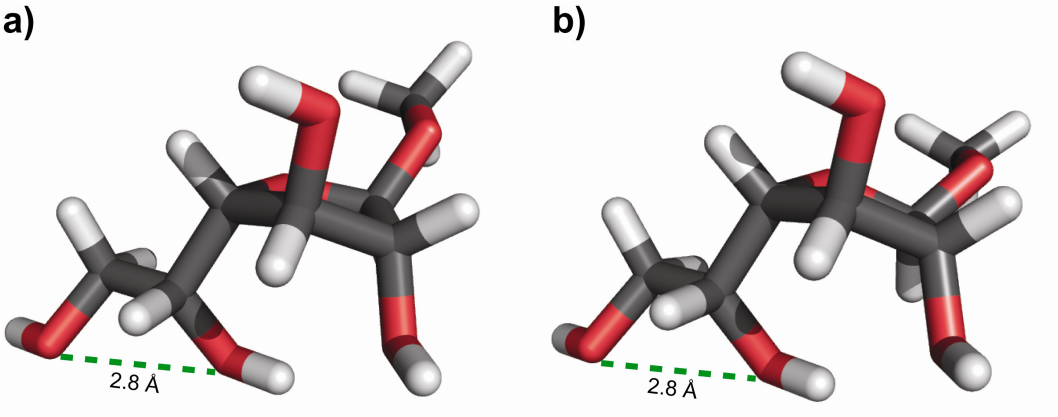

Figure 2.22. Optimized conformations of **2.2**, showing the distance between O5 and O6 (green dashed line). *a*) ^{3}E-*gg-gt* conformation. *b*) E_4-*gg-gt* conformation.

2.3.2.7. Orientation about the C5–C6 bond for the tg rotamers

For *tg* orientations about the C5–C6 bond of **2.2**, the range of values of O5–C5–C6–O6 is fairly large, from 141° to 188°, with an average value well below the ideal at 166° (Figure 2.20c). The β-anomer **2.2** shows similar trends as the α-anomer **2.1** when the exocyclic bonds are in the *gg*-*tg* or *gt*-*tg* conformation. Specifically, when the C4–C5 bond is in the *gg* conformation, the range of values for the O5–C5–C6–O6 dihedral angle of **2.2** is narrow, 171–173°. When the C4–C5 bond is in the *gt* conformation, the range of values for the O5–C5–C6–O6 dihedral angle is larger, 160–180°, with an average value of 168°. For the western and southern conformations E_1 through ^1E, the values are between 160° and 162°, while the average of the remaining conformations is 179°. The value of the O5–C5–C6–O6 dihedral angle in ^OE-*gt*-*tg* is the largest at 187°, due to a favorable electrostatic interaction between O3H and O6 (Figure 2.23a). The heavy atoms are 3.4 Å apart, and the angle between O3H and O6 is 117°. For conformations with the C4–C5 bond in the *tg* conformation, the values of the O5–C5–C6–O6 dihedral angle range from 141° to 184°, with an average of 159°. In particular, the eastern ring conformations from E_3 to ^1E have O4–O5 torsion angles between 141° and 149°, similar to what is seen for the α-anomer. For all of these ring conformations, the bringing the O5–C5–C6–O6 dihedral angle closer to the ideal value of 180° would lead to *syn*-pentane strain along O3–C3–C4–C5–O5 (Figure 2.23b).[39] In the remaining ring conformations, the range of values for O5–O6 torsion is closer to the ideal, 161–184°, with an average value of 169°.

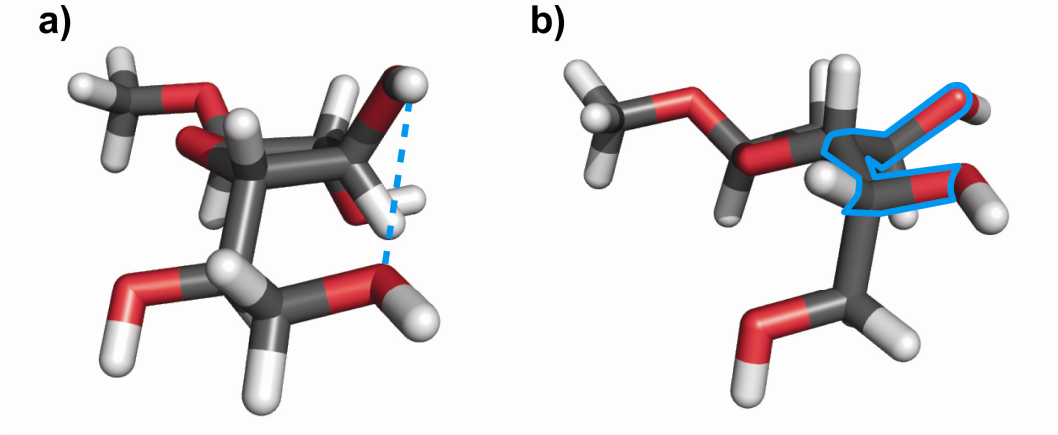

Figure 2.23. Optimized conformations of **2.2**. *a*) There is a favorable electrostatic interaction (blue dashed line) between O3H and O6 in ^{O}E-*gt*-*tg*. *b*) The O3–C3–C4–C5–O5 motif is highlighted (blue solid line) in E_3-*tg*-*tg*.

2.3.3. Relative energies calculated for 2.1 and 2.2

*2.3.3.1. Relative energies for 2.1 at B3LYP/6-31+G***

Once all of the conformations were optimized, single point energies were calculated at the B3LYP/6-31+G** level of theory. The resulting smoothed[40] PES for methyl α-D-Gal*f* is shown in Figure 2.24, and the energies have been scaled relative to the lowest energy conformation, ^{2}E-*gg*-*tg*, which was arbitrarily set at 0.0 kcal/mol. All but three conformations have single point energies less than 14 kcal/mol. The outliers are ^{2}E-*gt*-*tg* (34.6 kcal/mol), E_3-*gt*-*tg* (38.2 kcal/mol), and ^{4}E-*gt*-*tg* (39.2 kcal/mol). The ring geometry of these conformers forces O1, O2, O3, and O6 all close together, as shown in Table 2.1 and Figure 2.25. As mentioned above, twice the van der Waals radius for oxygen is 3.0 Å,[37] and the distance between O1 and O2 is 2.6–2.7 for all three conformations. The O2–O3 and O3–O6 distances vary between 3.1 and 3.4 Å, only slightly larger than two van der Waals radii. For the ^{4}E-*gt*-*tg* conformation, the O2–O3 distance

is the largest at 3.4 Å, but this conformer also has a high-energy eclipsing interaction due to the small O1–C1–C2–O2 dihedral angle (4°, Table 2.1).

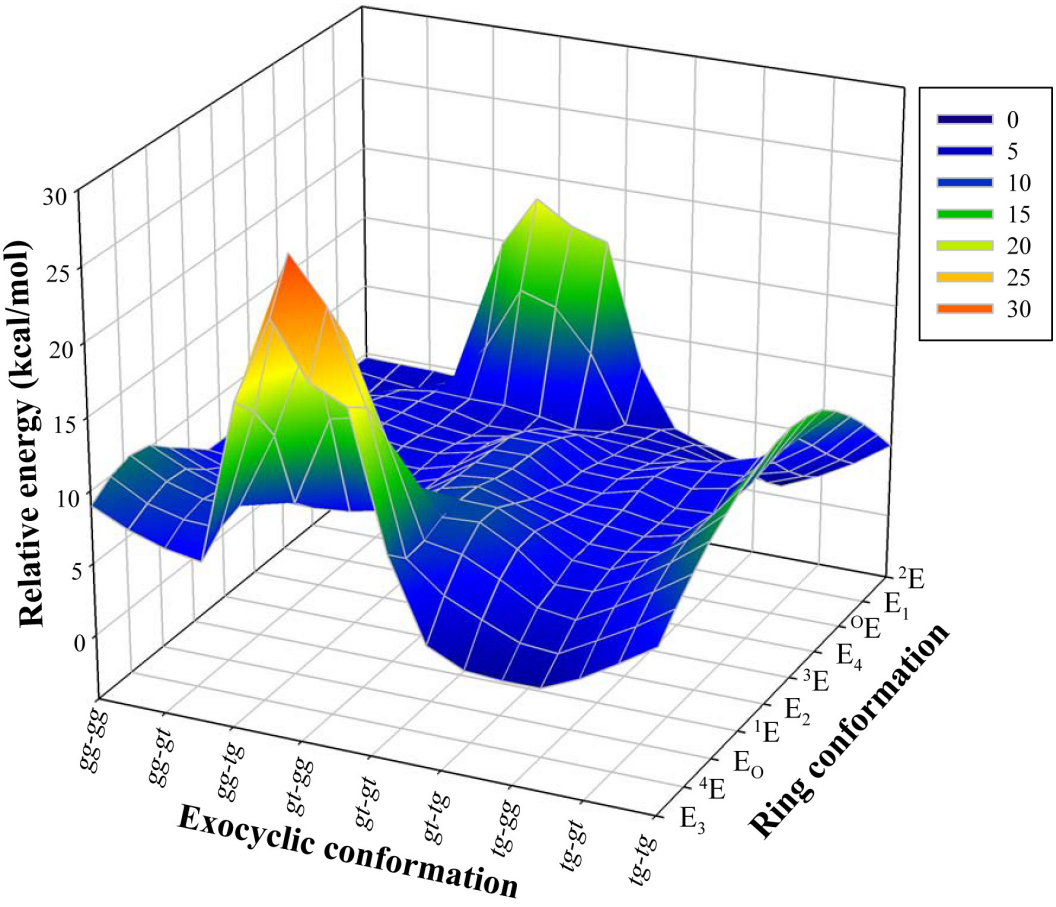

Figure 2.24. Potential energy surface (PES) for **2.1**. The surface was calculated with B3LYP/6-31+G**, and a Loess smoothing algorithm[40] with a polynomial of one was applied in SigmaPlot.[41]

Table 2.1. Oxygen-oxygen distances and O1–C1–C2–O2 dihedral angles for select conformations of **2.1**.

Conformer	O1–O2 dist. (Å)	O2–O3 dist. (Å)	O3–O6 dist. (Å)	O1–C1–C2–O2 (degrees)
^{2}E-*gt-tg*	2.7	3.2	3.2	44
E_3-*gt-tg*	2.6	3.2	3.1	29
^{4}E-*gt-tg*	2.6	3.4	3.1	4

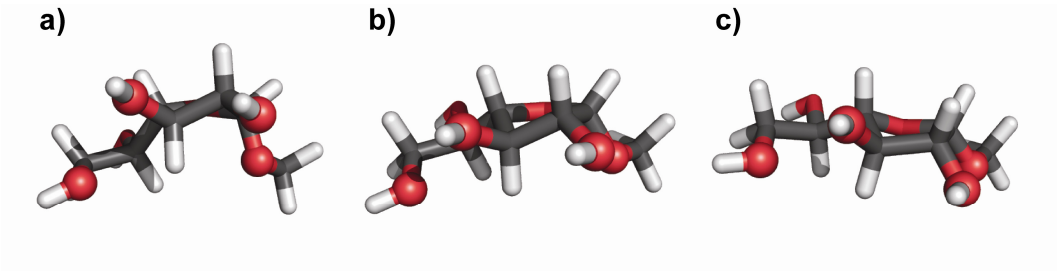

Figure 2.25. High energy conformations of **2.1** with O1, O2, O3, and O6 represented as spheres: *a*) ^{2}E-*gt-tg, b*) E_3-*gt-tg, c*) ^{4}E-*gt-tg*.

The relative energies of **2.1** broken down by exocyclic geometries are shown in Figure 2.26. To keep the y-axis the same in all three graphs, three points are not shown in Figure 2.26b; however, the entire graph is shown in Figure 2.27. As stated above, the lowest energy conformation is ^{2}E-*gg-tg*, which is in the northern portion of the pseudorotational itinerary (Figure 2.4). The lowest energy conformation in the southern part of the pseudorotational wheel is ^{1}E-*tg-gg*, which is 4.0 kcal/mol higher in energy than the global minimum.

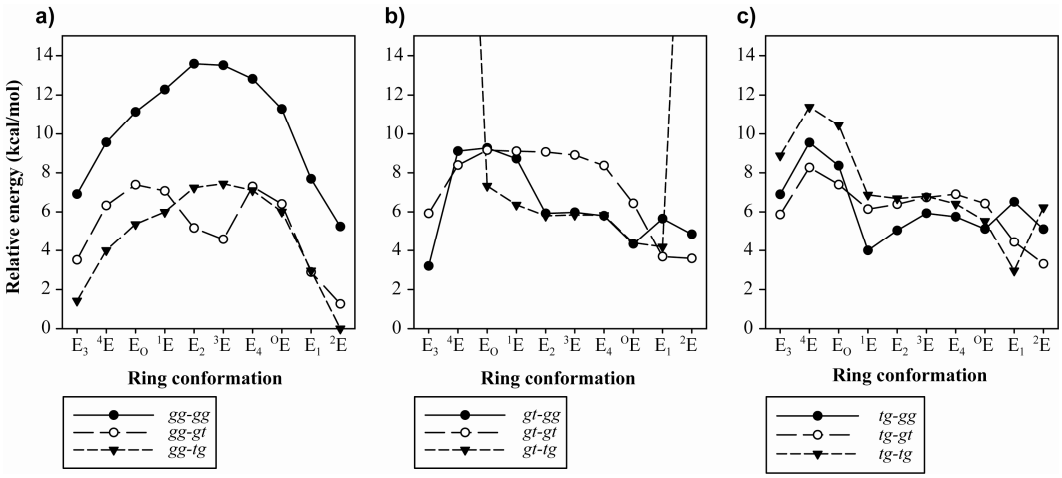

Figure 2.26. Relative energies for **2.1** calculated with B3LYP/6-31+G**. Graph *a*) shows the relative energies for each envelope when the C4–C5 bond is in the *gg* orientation, *b*) shows the relative energies for each envelope when the C4–C5 bond is in the *gt* orientation, and *c*) shows the relative energies for each envelope when the C4–C5 bond is in the *tg* orientation. Note that the full graph for *b*) can be seen in Figure 2.27. For all three graphs, each line represents a different rotamer about the C5–C6 bond: *gg* is the filled circles and solid line, *gt* is the open circles and long dashed line, and *tg* is the filled triangle and short dashed line.

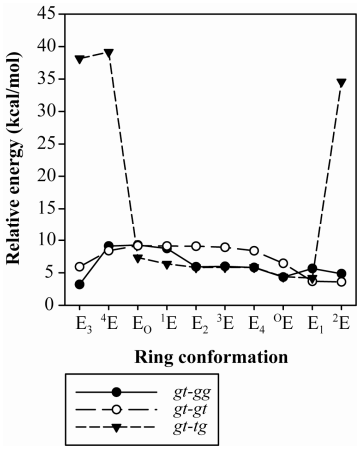

Figure 2.27. Full graph of Figure 2.26b showing the entire range of data points.

The relative energies of **2.1** when the C4–C5 bond is in the *gg* orientation follow an inverted U shape if the C5–C6 bond is in either the *gg* or *tg* (Figure 2.26a). That is, for the *gg-gg* and *gg-tg* conformations, the northern ^{2}E and E_3

conformers are approximately 6 kcal/mol lower in energy than the southern conformers, E_2, ^3E and E_4. The northern conformations have the C1–O1 bond in the pseudoaxial position; therefore, these geometries have some stabilization due to the *endo*-anomeric effect. Also, the *gg-tg* conformers are approximately 6 kcal/mol lower in energy than the *gg-gg* conformers (Figure 2.28). By rotating the C5–C6 bond into the *tg* orientation, O6 is moved away from O4, relieving strain caused by having two electronegative atoms close together (~3.0 Å). The trend for the *gg-gt* conformations is different, having an M shape. The ^2E and E_1 conformers are still lower in energy than the remainder, but the E_2 and ^3E conformers only slightly higher in energy. As noted above (Sections 2.3.1.2–2.3.1.4), the E_2-*gg-gt* and ^3E-*gg-gt* structures are stabilized by a hydrogen bond from O5H to O2 (Figure 2.9a).

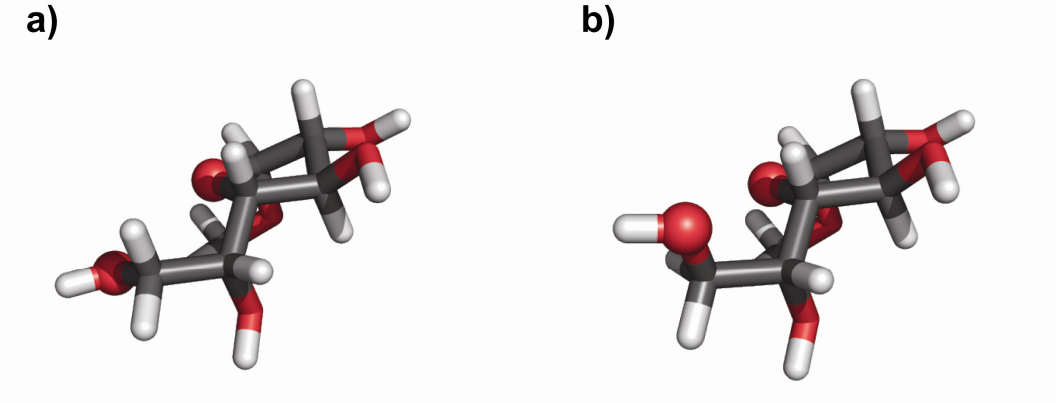

Figure 2.28. Optimized conformations of **2.1** with O4 and O6 shown as spheres. In ^2E-*gg-gg* (*a*) O4 and O6 are closer than in ^2E-*gg-tg* (*b*), and ^2E-*gg-gg* is also approximately 6 kcal/mol higher in energy than global minimum, ^2E-*gg-tg*.

When the C4–C5 bond is in the *gt* orientation, the E_3-*gt-gg* structure is the lowest in energy (Figure 2.26b). The other *gt-gg* conformers are all between 1 and 6 kcal/mol higher in energy. For conformations with the *gt-gt* orientation,

trend is again an inverted U shape, with the southern conformations (^{1}E through ^{3}E) having higher energies than those in the north (E_1 through E_3). As mentioned earlier, the relative energies when the exocyclic portion is *gt-tg* are the highest for all the calculated conformations of **2.1** when the ring is in the ^{2}E, E_3, or ^{4}E envelope (Figure 2.27, Table 2.1). The remaining *gt-tg* conformations similar in energy to the corresponding *gt-gg* geometries.

The trend in the relatives energies for all three rotamers about the C5–C6 bond is similar, when the C4–C5 bond is in the *tg* orientation. Approximately 3 kcal/mol separate the three geometries (Figure 2.26c). The southern ring conformations E_2 through ^{O}E are lower in energy than the northern conformations E_3 through E_O. The northern conformers also have *syn*-pentane strain[39] along O5–C5–C4–C3–O3 when the C3–O3 bond is pseudoequatorial (shown above in Figure 2.23b). This strain is relieved in the southern conformer when the C3–O3 bond is pseudoaxial.

*2.3.3.2. Relative energies for 2.2 at B3LYP/6-31+G***

The smoothed[40] PES for methyl β-D-Gal*f* is shown in Figure 2.29, and the energies have been scaled to the lowest energy conformation, ^{4}E-*gg*-*tg*, which is a northern conformation. Unlike the α-anomer, all of the conformations of **2.2** are within 13 kcal/mol of the global minimum. The lowest energy southern conformation ^{1}E-*tg*-*gg* is only 2.3 kcal/mol higher in energy than the global minimum. This is also the same low energy southern conformer that is seen for **2.1**.

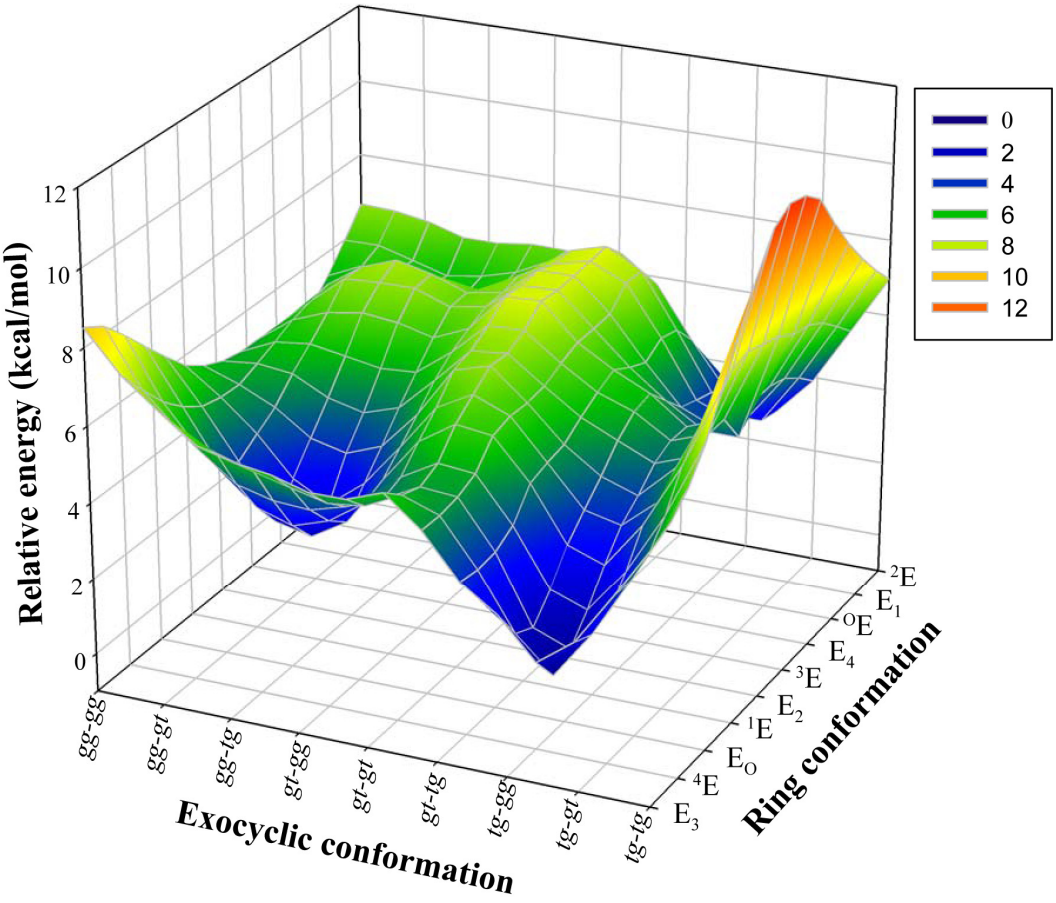

Figure 2.29. Potential energy surface (PES) for **2.2**. The surface was calculated with B3LYP/6-31+G**, and a Loess smoothing algorithm[40] with a polynomial of one was applied in SigmaPlot.[41]

The relative energies of **2.2** broken down by exocyclic geometry are shown in Figure 2.30. When the C4–C5 bond is in the *gg* orientation, the relative energies follow an inverted U shape if the C5–C6 bond is in either the *gg* or *tg* rotamer (Figure 2.30a). Specifically, the ^{3}E-*gg*-*gg* and ^{3}E-*gg*-*tg* conformations are approximately 7 kcal/mol higher in energy than E_3-*gg*-*gg* and E_3-*gg*-*tg*. The ^{3}E-*gg*-*gg* structure is also the global maximum for **2.2**. When the β-D-Gal*f* ring is

in the ^{3}E conformation, all the substituents are pseudoaxial, which forces O2 and O5 close to one another (2.8–2.9 Å) in E_3-*gg*-*gg* and E_3-*gg*-*tg* (Figure 2.31a). However, in the E_3 conformation, all the substituents are pseudoequatorial, and the O2–O5 distance is 4.9 Å in E_3-*gg*-*gg* and E_3-*gg*-*tg* (Figure 2.31b). Additionally, when the C1–O1 bond is pseudoaxial in **2.2**, the *endo*-anomeric effect is diminished because the lone pairs on oxygen are eclipsed with the C1–O1 and C1–H1 bonds. The relative energies do no follow the same trend for the *gg*-*gt* conformation. As mentioned in Section 2.3.2.2, the ring geometries ^{1}E to E_4 all have a hydrogen bond between O5H and O2, which would stabilize these conformers and lower their relative energies.

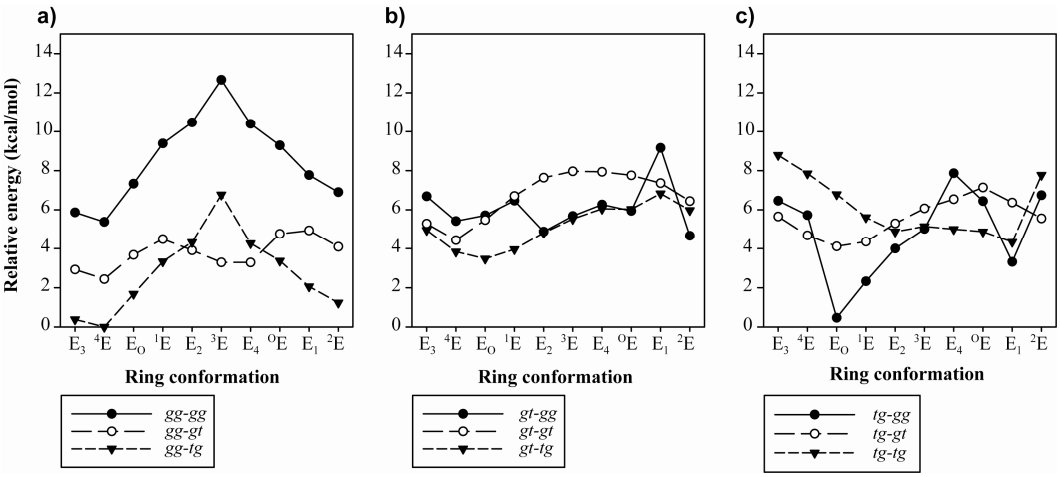

Figure 2.30. Relative energies for **2.2** calculated with B3LYP/6-31+G**. Graph *a*) shows the relative energies for each envelope when the C4–C5 bond is in the *gg* orientation, *b*) shows the relative energies for each envelope when the C4–C5 bond is in the *gt* orientation, and *c*) shows the relative energies for each envelope when the C4–C5 bond is in the *tg* orientation. For all three graphs, each line represents a different rotamer about the C5–C6 bond: *gg* is the filled circles and solid line, *gt* is the open circles and long dashed line, and *tg* is the filled triangle and short dashed line.

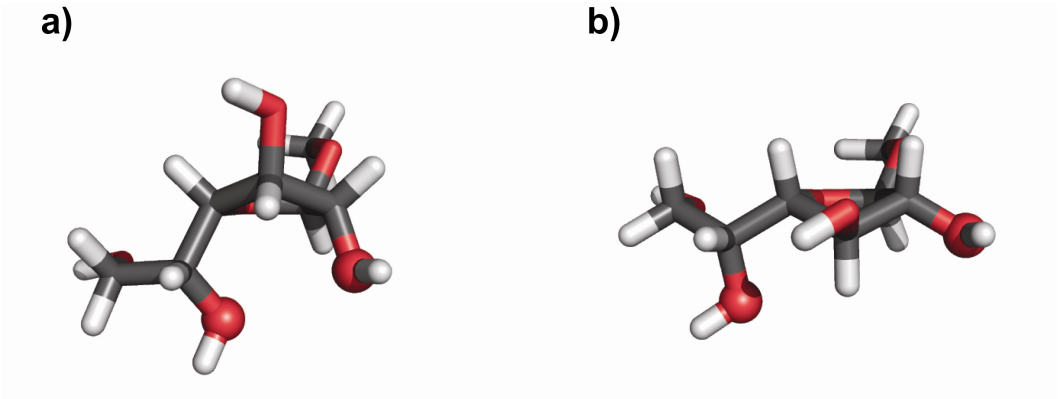

Figure 2.31. Optimized conformations of **2.2** with O2 and O5 shown as spheres. *a*) In ^{3}E-*gg*-*gg*, the pseudoaxial substituents force O2 and O5 close together, resulting in higher relative energy. *b*) In E_3-*gg*-*gg*, the substituents are pseudoequatorial, thus O2 and O5 are farther apart.

For structures with the C4–C5 bond in the *gt* orientation (Figure 2.30b), the trends in relative energies are the similar for *gt*-*gt* and *gt*-*tg*. For both, the

energies for eastern E_3 through ^1E conformations are ~2.0 kcal/mol lower in energy than the remaining conformations E_2 through ^2E, with minima at ^4E-*gt*-*gt* (4.4 kcal/mol) and E_O-*gt*-*tg* (3.5 kcal/mol). Also for the E_O through ^OE conformations, the *gt*-*gt* geometries are approximately 2 kcal/mol higher in energy than *gt*-*tg*. The energies for structures with the *gt*-*gg* geometry overlay with *gt*-*tg* conformations when the ring is in the southern orientations E_2 through ^OE, while the remaining *gt*-*gg* conformations do not follow any obvious trend.

The E_O-*tg*-*gg* structure is only 0.5 kcal/mol higher in energy than the global minimum (Figure 2.30c). The low energy may be due to a weak hydrogen bond between O3H and O5 (Figure 2.32). The heavy atoms are 3.1 Å apart, and the angle between O3H and O5 is 120°.[38] All of the remaining conformations with the *tg* orientation about C4–C5 bond are at least 2.3 kcal/mol higher in energy than the global minimum. The *tg*-*gg* conformers show the greatest variation, 0.5 to 7.9 kcal/mol, while conformations with the *tg*-*gt* orientation show the smallest spread from 4.1 to 7.2 kcal/mol. For the *tg*-*tg* exocyclic orientation, the energies for the E_2 through E_1 ring geometries are all very close in energy, 4.3 to 5.0 kcal/mol, and the remaining envelope conformations are all at least 1.7 kcal/mol higher.

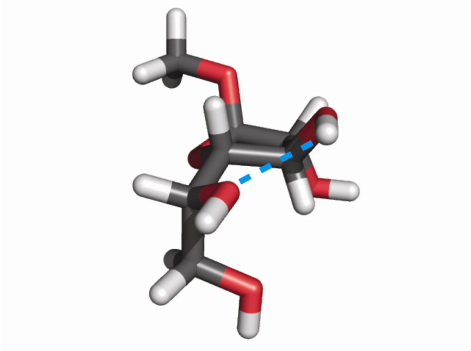

Figure 2.32. Optimized conformation of **2.2** in E_O-*tg*-*gg*, showing the weak hydrogen bond between O3H and O5 as a blue dashed line.

2.3.3.3. A comparison between B3LYP and MP2

Recently, Csonka and coworkers evaluated several common basis sets and density functionals for the relative energies of carbohydrate conformations.[24] For basis sets, they concluded that polarization functions on both the hydrogens and heavy atoms were necessary for relative energies that closely matched their reference values, which were calculated using MP2/aug-cc-pVTZ. Additionally, diffuse functions were needed on the heavy atoms but not on the hydrogens. Various conformations of four different carbohydrates were evaluated, and they used 15 conformations of 3,6-anhydro-4-*O*-methyl-D-galactitol (**2.3**, Figure 2.33) as a reference for furanosides. Of the functionals used, M05-2X/6-311+G** gave relative energies closest to the reference. The values calculated for **2.3** using MP2 and the same basis differed from M05-2X by 0.5 kcal/mol or less. While the authors did not recommend using the B3LYP functional, the average difference in relative energies between B3LYP and M05-2X was 0.8 ± 0.6 kcal/mol.

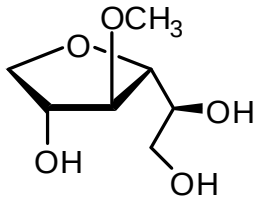

2.3

Figure 2.33. The structure of 3,6-anhydro-4-*O*-methyl-D-galactitol (**2.3**).

To determine if the observations for **2.3** are similar for the conformations of Gal*f*, the single point energies for **2.1** and **2.2** were calculated using MP2/6-311+G** and the optimized geometries described above (Sections 2.3.1 and 2.3.2). A comparison between the relative energies for **2.1** calculated at B3LYP/6-31+G** and MP2/6-311+G** are shown in Figure 2.34, and the conformations are sorted according to their relative energies. Both methods found the same overall minimum conformation, ^{2}E-*gg*-*tg*. On average, the values calculated at MP2/6-311+G** are 1.1 ± 0.5 kcal/mol higher in energy than those calculated at B3LYP/6-31+G**, which is the same as the differences seen by Csonka, et al within error.[24] Although for the three lowest energy conformations of **2.1** – all under 1.5 kcal/mol – the relative energies calculated with MP2 are only 0.2 ± 0.3 kcal/mol higher in energy than those calculated with B3LYP. The maximum difference seen between the two methods is 2.5 kcal/mol, and this conformation is 6.4 kcal/mol higher in energy than the global minimum (B3LYP/6-31+G**).

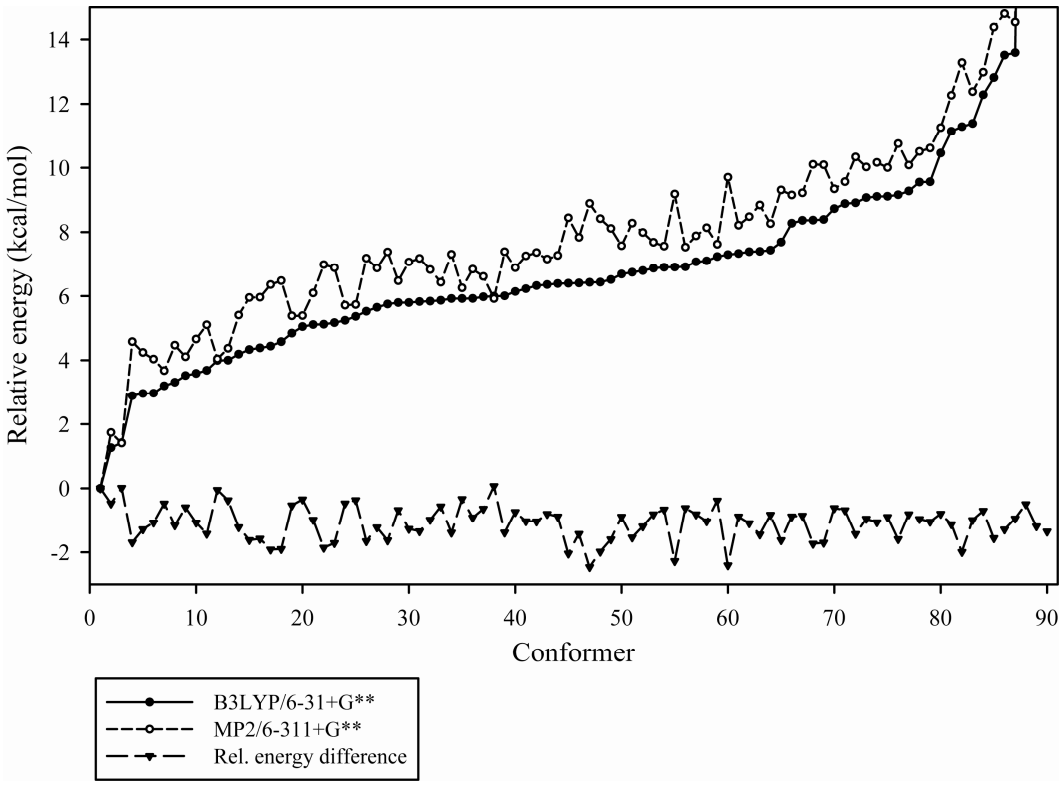

Figure 2.34. Relative energies for **2.1** calculated with B3LYP/6-31+G**[22,23,25,26] (filled circles, solid line) and MP2/6-311+G**[27] (open circles, short dashed line). The difference between the two methods is also shown (filled triangles, long dashed line).

The energy differences between the two methods are lower for **2.2** (Figure 2.35), but the methods also predict different low energy conformations. For B3LYP/6-31+G**, the lowest energy conformation is ^{4}E-*gg*-*gt*, and ^{3}E-*gg*-*tg* is 0.4 kcal/mol higher in energy (Figure 2.30). For MP2/6-311+G**, these conformers are reversed, but ^{4}E-*gg*-*gt* is only slightly higher in energy than ^{3}E-*gg*-*tg* (0.04 kcal/mol). On average, the MP2/6-311+G** relative energies are 0.6 ± 0.4 kcal/mol higher than B3LYP/6-31+G**, which is the same as Csonka, et al.[24] For energies under 2.4 kcal/mol – the first seven points on the graph – the MP2 values are only 0.1 ± 0.3 kcal/mol higher than B3LYP. The largest energy

difference seen for conformations of **2.2** is 1.9 kcal/mol, and this conformer is 3.3 kcal/mol higher in energy than the global minimum (B3LYP). As a compromise between speed of calculations and accuracy, B3LYP/6-31+G** seems to give reasonable results for conformations of Gal*f*. Csonka and coworkers also suggest that the quickest methods for "useful results" are B3LYP/6-31+G** or B3PW91/6-31+G**.[24]

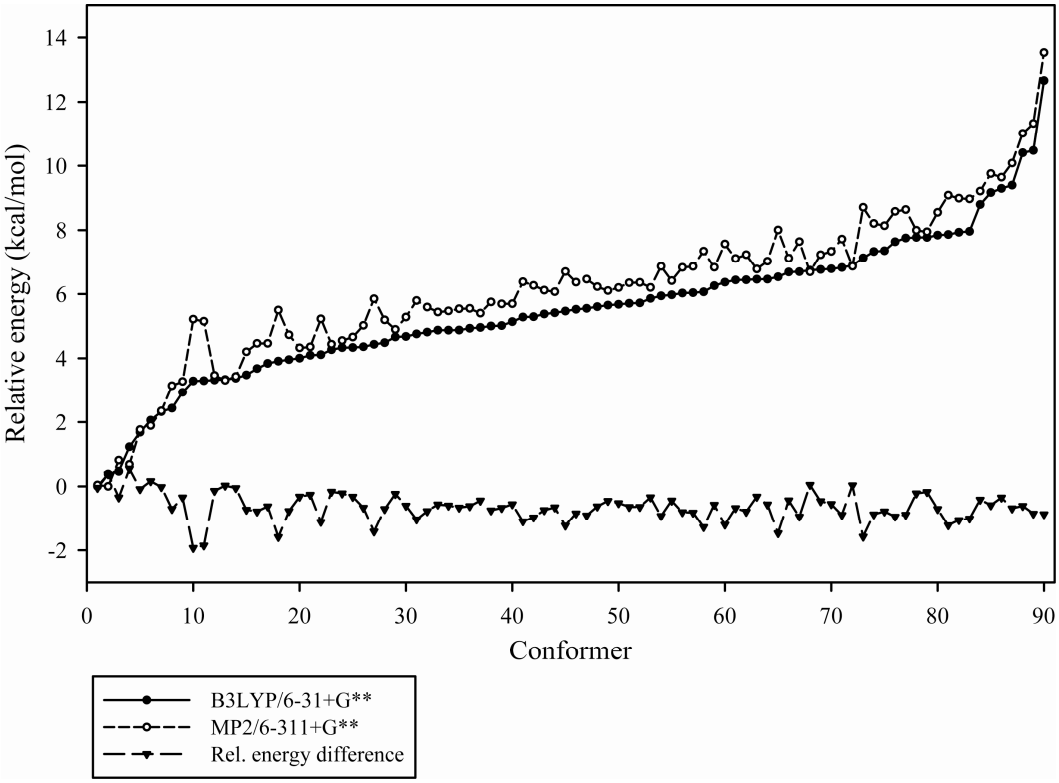

Figure 2.35. Relative energies for **2.2** calculated with B3LYP/6-31+G**[22,23,25,26] (filled circles, solid line) and MP2/6-311+G**[27] (open circles, short dashed line). The difference between the two methods is also shown (filled triangles, long dashed line).

2.3.4. NMR spectra and coupling constants for 2.1 and 2.2

The 1D ^{1}H NMR spectra for **2.1** and **2.2** are shown in Figure 2.36 with the proton resonances labeled above each signal. The chemical shifts and $^{3}J_{H,H}$ values

for methyl β-D-Gal*f* were easily determined from the first-order spectrum (Figure 2.36b) and are listed in Table 2.2. However, the spectrum for methyl α-D-Gal*f* (Figure 2.36a) is a seven-spin virtually coupled[42] spectrum, due to the small differences in chemical shifts between H2 and H3, as well as between H5 and H6. Simulation of the spectrum for **2.1** was necessary in order to determine accurate $^{3}J_{H,H}$ values. The program SpinWorks[43] can determine the coupling constants and chemical shifts for up to ten spins using the NUMARIT algorithm.[44] This program was used to simulate the spectrum of **2.1** until the RMS difference between the simulation and the actual spectrum was less than the digital resolution of the spectrum (RMS difference = 0.021 Hz, digital resolution = 0.1 Hz). A comparison between the simulated and actual spectra can be seen in Figure 2.37. The chemical shifts and $^{3}J_{H,H}$ values for **2.1** were taken from this simulation and are listed in Table 2.2. As further validation of the coupling constants derived from SpinWorks,[43] the spectrum of **2.1** taken in D_2O at 300 MHz was also simulated. The $^{3}J_{H,H}$ values from this simulation were within ± 0.1 Hz of the simulation at 600 MHz (data not shown).

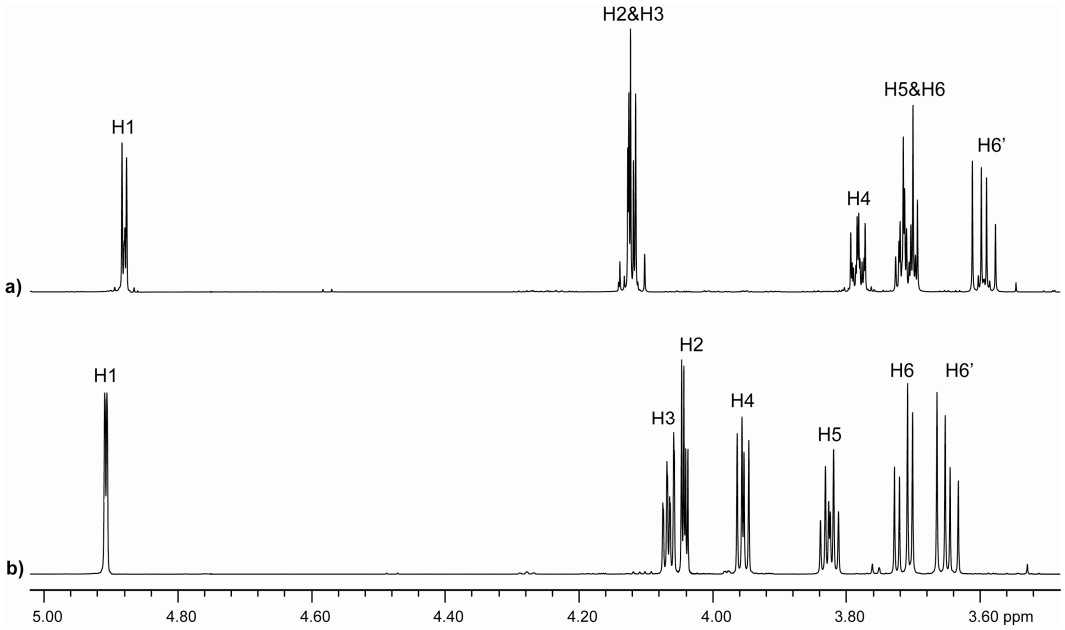

Figure 2.36. a) The ^{1}H NMR spectrum for **2.1**. b) The ^{1}H NMR spectrum of **2.2**. Both spectra were acquired in D_2O at 300 K on a 600 MHz spectrometer.

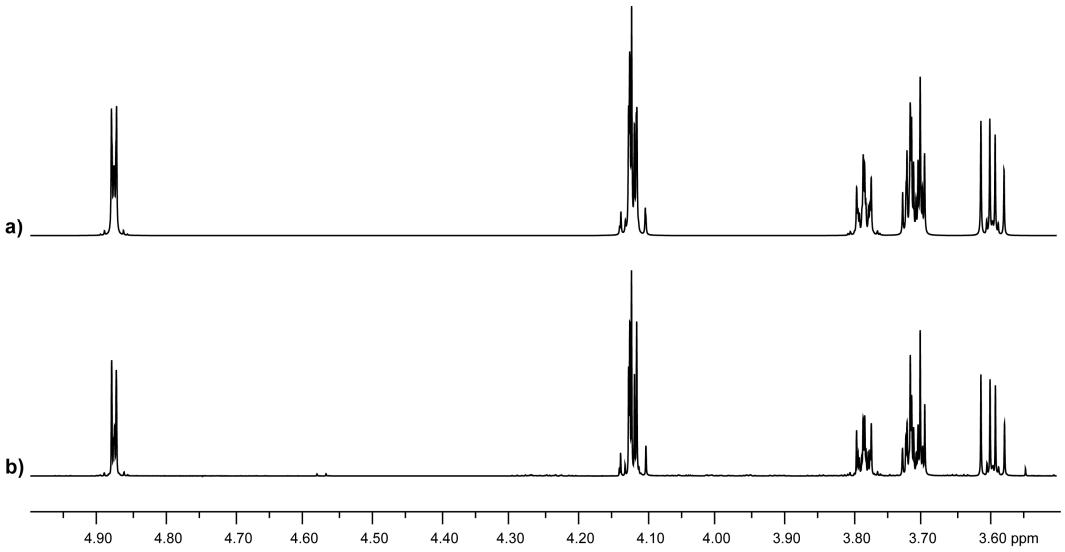

Figure 2.37. a) The ^{1}H NMR spectrum for **2.1** simulated in SpinWorks. b) The experimental ^{1}H NMR spectrum for **2.1**, which is also shown in Figure 2.36a. The RMS difference between the simulated and actual spectra is 0.021 Hz.

Table 2.2. Chemical shifts and three-bond coupling constants for **2.1** and **2.2**.

	2.1	**2.2**		**2.1**	**2.2**
δ_{H1} **(ppm)**	4.88	4.91	$^{3}J_{H1,H2}$ **(Hz)**	4.5	2.0
δ_{H2} **(ppm)**	4.13	4.04	$^{4}J_{H1,H3}$ **(Hz)**	– [a]	0.6
δ_{H3} **(ppm)**	4.12	4.06	$^{3}J_{H2,H3}$ **(Hz)**	8.0	3.6
δ_{H4} **(ppm)**	3.78	3.95	$^{3}J_{H3,H4}$ **(Hz)**	7.1	6.2
δ_{H5} **(ppm)**	3.71	3.82	$^{3}J_{H4,H5}$ **(Hz)**	6.0	4.4
δ_{H6} **(ppm)**	3.71	3.71	$^{3}J_{H5,H6}$ **(Hz)**	3.9	4.4
$\delta_{H6'}$ **(ppm)**	3.60	3.65	$^{3}J_{H5,H6'}$ **(Hz)**	7.0	7.4
			$^{2}J_{H6,H6'}$ **(Hz)**	–11.7	–11.8

[a] Not observed.

As mentioned above, the spectrum for methyl α-D-Gal*f* is virtually coupled.[42] In other words, all seven spins behave as if they are each coupled to the other six spins, leading to more complex splitting patterns than expected for each signal. For example, based on the structure of **2.1**, H4 should only be coupled to H3 and H5 and is expected to give a doublet of doublets in the 1D ^{1}H NMR spectrum. The multiplet that is actually observed for H4 (Figure 2.36a) is clearly more complex than a doublet of doublets. Virtual coupling between two protons occurs when the difference in chemical shifts in Hz, Δν, is smaller than or about the same size as the coupling constant in Hz, *J*. For **2.1**, this ratio Δν/*J* is 0.65 for H2 and H3 and 0.74 for H5 and H6 at 600 MHz. Because the frequency difference between two chemical shifts changes with spectrometer frequency,

$\Delta\nu/J$ decreases for both sets of spins at 300 MHz: 0.35 for H2 and H3 and 0.36 for H5 and H6.

2.3.5. Ring conformations of 2.1 and 2.2 from PSEUROT

As discussed in section 2.2.3, the program PSEUROT takes vicinal proton coupling constants and relates them to ring conformation dihedrals ϕ_i through eqs. 2.3 and 2.4. Only three values of ϕ_i^{HH} are available in either anomer of Gal*f* – ϕ_0^{HH}, ϕ_1^{HH}, and ϕ_4^{HH}. These dihedral angles, along with the corresponding values for ϕ_0, ϕ_1, and ϕ_4, were determined from the optimized geometries of **2.1** or **2.2** (described in Sections 2.3.1 and 2.3.2). Then the relationship between ring dihedral angles ϕ_i and the proton–proton dihedral angles ϕ_i^{HH} were calculated. The resulting graphs are shown in Figure 2.38 for **2.1** and Figure 2.39 for **2.2**.

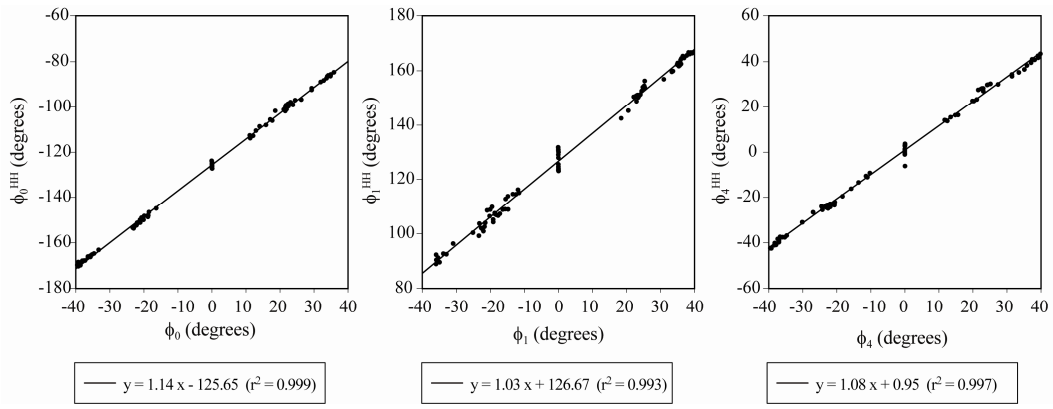

Figure 2.38. Graphs of ϕ_i vs. ϕ_i^{HH} for **2.1**. The slope of the line is $-a_i$ and the *y*-intercept is b_i described in eq. 2.4.

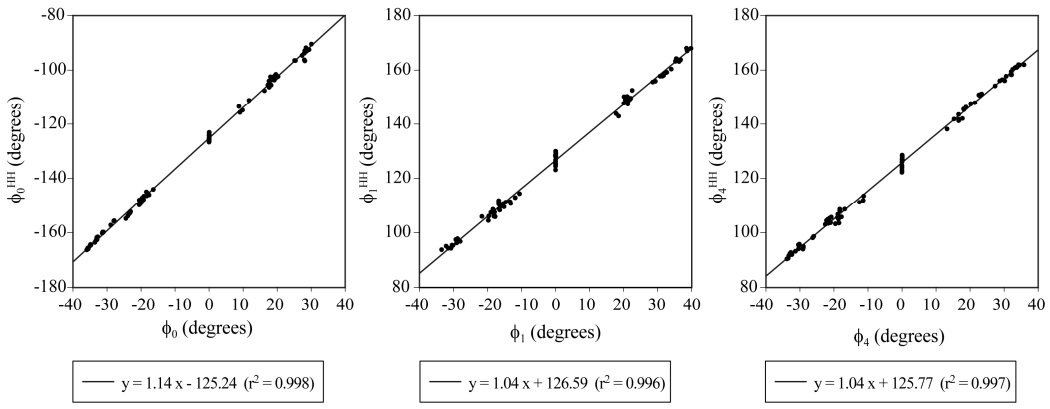

Figure 2.39. Graphs of ϕ_i vs. ϕ_i^{HH} for **2.2**. The slope of the line is $-a_i$ and the intercept is b_i described in eq. 2.4.

The newly determined values of a_i and b_i were used in four PSEUROT calculations on **2.1** (Table 2.3); all four runs gave the same results. (The initial values of P_N and P_S are detailed in Section 2.2.3.) Additionally, using the new a_i and b_i values instead of those determined for Ara*f*,[32] improved the RMS difference in PSEUROT from 0.112 Hz to 0.008 Hz (data not shown), though the conformations and populations predicted were the same. The northern conformation ^{2}E is predicted to be present 88% of the time, while the southern conformation ^{1}E will be present only 12% of the time. The PSEUROT results agree nicely with the relative energies predicted from the DFT calculations (Section 2.3.3.1). In fact, the identity of the ring conformations are the same, but the relative populations differ. DFT gave the lowest energy for the northern ^{2}E-*gg-tg* structure. The lowest energy southern conformation ^{1}E-*tg-gg* was 4.0 kcal/mol higher in energy. Assuming a two-state model, the ratio between ^{2}E-*gg-tg* and ^{1}E-*tg-gg* at 300 K is would be 823:1. Thus at room temperature almost none of the ^{1}E-*tg-gg* would be observed.

Table 2.3. Results of PSEUROT calculations for **2.1**.

	P_N	%N	P_S	%S	RMS (Hz)
run A	345.9° (^{2}E)	88	125.1° (^{1}E)	12	0.008
run B	345.9° (^{2}E)	88	125.2° (^{1}E)	12	0.008
run C	346.0° (^{2}E)	88	125.4° (^{1}E)	12	0.008
run D	345.9° (^{2}E)	88	124.9° (^{1}E)	12	0.008

The four runs in PSEUROT for **2.2** using the new values of a_i and b_i gave three different solutions (Table 2.4). Unlike for **2.1**, the new a_i and b_i values gave different results than the values from Ara*f* (data not shown).[32] Runs A and B predicted a 68:32 ratio between the northern ^{4}E and southern E_4 conformations. For runs C and D, the southern conformations are preferred. Run C predicted a 56:44 ratio between the northern E_1 conformation and the southern conformation $^3T_4$. Run D had the largest RMS difference at 0.415 Hz, and it predicted a 72:28 ratio between ^{O}E/^{O}T$_1$ in the north and E_2 in the south. None of the PSEUROT results predict the same lowest energy conformations from the DFT calculations (Section 2.3.3.2). The DFT gave the lowest energy for the northern ^{4}E-*gg*-*tg* structure, and the southern ^{1}E-*tg*-*gg* is 2.3 kcal/mol higher in energy. Thus, PSEUROT runs A and B predicted the same northern geometry as DFT, but the southern conformers and the ratio between the two was different.

Table 2.4. Results of PSEUROT calculations for **2.2**.

	P_N	%N	P_S	%S	RMS (Hz)
Run A	62.3° (^{4}E)	68	242.7° (E_4)	32	0.001
Run B	62.3° (^{4}E)	68	242.7° (E_4)	32	0.001
Run C	303.3° (E_1)	56	218.3° ($^3T_4$)	44	0.001
Run D	281.1° (^{O}E/$^O T_1$)	72	161.2° (E_2)	28	0.415

2.4. Conclusions

In this chapter, we presented a gas-phase, partial PES for both anomers of methyl D-Gal*f*. We focused on the exocyclic portion of Gal*f* in our discussion of conformations optimized using B3LYP/6-31G*, as the ring conformations of Ara*f* have already been discussed.[17-19] While all conformations started from the ideal values of 60°, 180°, or 300°, deviations from the ideal value of the O4–C4–C5–O5 torsions occurred because of intramolecular hydrogen bonds or to relieve steric interactions. The O5–C5–C6–O6 torsions also deviated from ideal values to relieve strain between electronegative groups. Compared to the O4–C4–C5–O5 torsion, the O5–C5–C6–O6 dihedral was more prone to develop *syn*-pentane interactions, which were alleviated by rotation about the C5–C6 bond.

Single-point energies were calculated from the optimized geometries using two different levels of theory, B3LYP/6-31+G** and MP2/6-311+G**. In general, the energies from B3LYP are lower than those from MP2 by 0.9 ± 0.5 kcal/mol for both anomers. The northern ring conformations ^{2}E, E_3, and ^{4}E of **2.1** all have the C1–O1 bond in the pseudoaxial position and would have some stabilization from the *endo*-anomeric effect. As expected, the ^{2}E ring

conformation of **2.1** is the lowest energy conformation for all but one of the exocyclic geometries calculated (Figure 2.26). For **2.2**, the southern conformations E_2, ^3E, and E_4 have the bond in the pseudoaxial position, but the *endo*-anomeric effect would provide less stabilization because neither of the lone-pair electrons are antiperiplanar to the C1–O1 bond. Correspondingly, the relatives energies for E_2, ^3E, and E_4 of **2.2** are neither the highest nor lowest energy conformations.

The 1D ^1H NMR spectra of **2.1** and **2.2** are presented, along with the $^3J_{H,H}$ values determined from these spectra. The coupling constants $^3J_{H1,H2}$, $^3J_{H2,H3}$, and $^3J_{H3,H4}$ were used with the program PSEUROT to determine the solution state ring conformations. For both **2.1** and **2.2**, the conformations predicted by PSEUROT are similar to the lowest energy conformations determined by gas-phase calculations. PSEUROT favors northern conformations in an 88:12 ratio to the southern conformers for all calculations on **2.1**, but DFT predicts the southern conformations are substantially higher in energy. The relative energy difference between the lowest energy northern conformation for **2.1** (^2E-*gg*-*tg*) and the lowest energy southern conformation (^1E-*tg*-*gg*) is 4.0 kcal/mol. At 300 K, the ratio between north and south would be 824:1. For **2.2**, PSEUROT predicts that the northern conformation is favored in only two of the four runs, and three different solutions are returned from PSEUROT.

The differences in preferred conformations predicted by DFT and PSEUROT can be explained because the DFT calculations are in the gas-phase. PSEUROT predicts solution-state conformations from NMR data, and the solvent

can stabilize different conformations due to the presence of intermolecular interactions, such as hydrogen bonds. However, PSEUROT is also a purely mathematical solution that is based on the assumption that there are two equilibrating populations, and a two-state model is most likely not appropriate for this system. As such, PSEUROT can predict chemically unreasonable structures.[35] Or, as in the case with **2.2**, PSEUROT can give two or more solutions with the same average coupling constants. Also, all of the northern conformations predicted by PSEUROT (Figure 2.40) have the substituents in pseudoaxial positions; therefore, it is not obvious which conformation is expected to be lower in energy. A model that predicts solution-phase conformations from chemical principles would be preferred over one that relies solely on math. Such a model will be discussed in the remaining chapters.

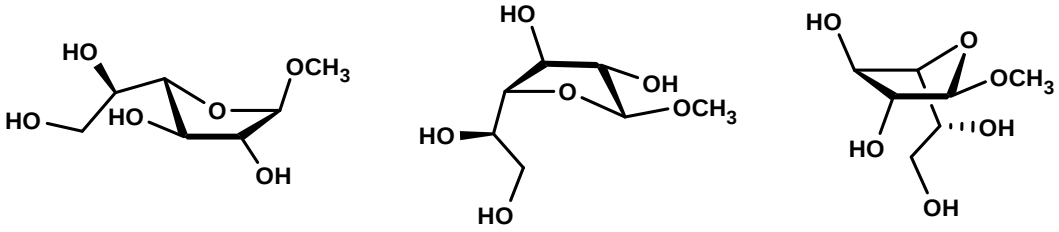

2.2 in ^{4}E **2.2** in E_1 **2.2** in ^{O}E

Figure 2.40. Northern conformations of **2.2** predicted by PSEUROT. The ^{4}E conformation was found in runs A and B, E_1 was found in run C, and ^{O}E was found in run D (Table 2.4).

2.5. References

1. Completo, G. C.; Lowary, T. L. *J. Org. Chem.* **2008**, *73*, 4513–4525.

2. Szarek, W. A.; Zamojski, A.; Tiwari, K. N.; Ison, E. R. *Tetrahedron Lett.* **1986**, *27*, 3827–3830.

3. Kilpatrick, J. E.; Pitzer, K. S.; Spitzer, R. *J. Am. Chem. Soc.* **1947**, *69*, 2483–2488.

4. Taha, H. A. Conformational Analysis of D-Arabinofuranosides using NMR Spectroscopy and Computational Chemistry. Ph.D. Thesis, University of Alberta, Edmonton, AB, 2010.

5. Richards, M. R.; Lowary, T. L. *ChemBioChem* **2009**, *10*, 1920–1938.

6. Peltier, P.; Guégan, J. P.; Daniellou, R.; Nugier-Chauvin, C.; Ferrières, V. *Eur. J. Org. Chem.* **2008**, 5988–5994.

7. Novelli, J. F.; Chaudhary, K.; Canovas, J.; Benner, J. S.; Madinger, C. L.; Kelly, P.; Hodgkin, J.; Carlow, C. K. S. *Dev. Biol.* **2009**, *335*, 340–355.

8. Jarlier, V.; Nikaido, H. *FEMS Microbiol. Lett.* **1994**, *123*, 11–18.

9. Alderwick, L. J.; Radmacher, E.; Seidel, M.; Gande, R.; Hitchen, P. G.; Morris, H. R.; Dell, A.; Sahm, H.; Eggeling, L.; Besra, G. S. *J. Biol. Chem.* **2005**, *280*, 32362–32371.

10. Bhowruth, V.; Alderwick, L. J.; Brown, A. K.; Bhatt, A.; Besra, G. S. *Biochem. Soc. Trans.* **2008**, *36*, 555–565.

11. Takayama, K.; Wang, C.; Besra, G. S. *Clin. Microbiol. Rev.* **2005**, *18*, 81–101.

12. Angyal, S. J.; Pickles, V. A. *Aust. J. Chem.* **1972**, *25*, 1695–1710.

13. Nikaido, H.; Kim, S.-H.; Rosenberg, E. Y. *Mol. Microbiol.* **1993**, *8*, 1025–1030.

14. Brennan, P. J.; Nikaido, H. *Annu. Rev. Biochem* **1995**, *64*, 29–63.

15. Liu, C.; Richards, M. R.; Lowary, T. L. *J. Org. Chem.* **2010**, *75*, 4992–5007.

16. Liu, C.; Richards, M. R.; Lowary, T. L. *Org. Biomol. Chem.* **2011**, *9*, 165–176.

17. Gordon, M. T.; Lowary, T. L.; Hadad, C. M. *J. Am. Chem. Soc.* **1999**, *121*, 9682–9692.

18. Gordon, M. T.; Lowary, T. L.; Hadad, C. M. *J. Org. Chem.* **2000**, *65*, 4954–4963.

19. McCarren, P. R.; Gordon, M. T.; Lowary, T. L.; Hadad, C. M. *J. Phys. Chem. A* **2001**, *105*, 5911–5922.

20. Altona, C.; Sundaralingam, M. *J. Am. Chem. Soc.* **1972**, *94*, 8205–8212.

21. Frisch, M. J.; Trucks, G. W.; Schlegel, H. B.; Scuseria, G. E.; Robb, M. A.; Cheeseman, J. R.; Montgomery, J. A., Jr.; Vreven, T.; Kudin, K. N.; Burant, J. C.; Millam, J. M.; Iyengar, S. S.; Tomasi, J.; Barone, V.; Mennucci, B.; Cossi, M.; Scalmani, G.; Rega, N.; Petersson, G. A.; Nakatsuji, H.; Hada, M.; Ehara, M.; Toyota, K.; Fukuda, R.; Hasegawa, J.; Ishida, M.; Nakajima, T.; Honda, Y.; Kitao, O.; Nakai, H.; Klene, M.; Li, X.; Knox, J. E.; Hratchian, H. P.; Cross, J. B.; Bakken, V.; Adamo, C.; Jaramillo, J.; Gomperts, R.; Stratmann, R. E.; Yazyev, O.; Austin, A. J.; Cammi, R.; Pomelli, C.; Ochterski, J. W.; Ayala, P. Y.; Morokuma, K.; Voth, G. A.; Salvador, P.; Dannenberg, J. J.; Zakrzewski, V. G.; Dapprich, S.; Daniels, A. D.; Strain, M. C.; Farkas, O.; Malick, D. K.; Rabuck, A. D.; Raghavachari, K.; Foresman, J. B.; Ortiz, J. V.; Cui, Q.; Baboul, A. G.; Clifford, S.; Cioslowski, J.; Stefanov, B. B.; Liu, G.; Liashenko, A.; Piskorz, P.; Komaromi, I.; Martin, R. L.; Fox, D. J.; Keith, T.; Al-Laham, M. A.; Peng, C. Y.; Nanayakkara, A.; Challacombe, M.; Gill, P. M. W.; Johnson, B.; Chen, W.; Wong, M. W.; Gonzalez, C.; Pople, J. A. *Gaussian 03* Revision C.02; Gaussian, Inc.: Wallingford, CT, 2004.

22. Becke, A. D. *J. Chem. Phys.* **1993**, *98*, 5648–5652.

23. Rassolov, V. A.; Ratner, M. A.; Pople, J. A.; Redfern, P. C.; Curtiss, L. A. *J. Comput. Chem.* **2001**, *22*, 976–984.

24. Csonka, G. I.; French, A. D.; Johnson, G. P.; Stortz, C. A. *J. Chem. Theory Comput.* **2009**, *5*, 679–692.

25. Clark, T.; Chandrasekhar, J.; Spitznagel, G. W.; Schleyer, P. V. *J. Comput. Chem.* **1983**, *4*, 294–301.

26. Frisch, M. J.; Pople, J. A.; Binkley, J. S. *J. Chem. Phys.* **1984**, *80*, 3265–3269.

27. Head-Gordon, M.; Pople, J. A.; Frisch, M. J. *Chem. Phys. Lett.* **1988**, *153*, 503–506.

28. DeLano, W. L. *The PyMol Molecular Graphics System*, version 1.5.0.3; Schrödinger, LLC: San Diego, CA, USA, 2012.

29. Karplus, M. *J. Chem. Phys.* **1959**, *30*, 11–15.

30. Karplus, M. *J. Am. Chem. Soc.* **1963**, *85*, 2870–2871.

31. de Leeuw, F. A. A. M.; Altona, C. *J. Comput. Chem.* **1983**, *4*, 428–437.

32. Houseknecht, J. B.; Altona, C.; Hadad, C. M.; Lowary, T. L. *J. Org. Chem.* **2002**, *67*, 4647–4651.

33. Hoffmann, R. A.; Van Wijk, J.; Leeflang, B. R.; Kamerling, J. P.; Altona, C.; Vliegenthart, J. F. G. *J. Am. Chem. Soc.* **1992**, *114*, 3710–3714.

34. van Wijk, J.; Haasnoot, C. A. G.; de Leeuw, F. A. A. M.; Huckriede, B. D.; Westra Hoekzema, A.; Altona, C. *PSEUROT 6.3*, Leiden Institute of Chemistry, Leiden University: Leiden, 1999.

35. Houseknecht, J. B.; Lowary, T. L.; Hadad, C. M. *J. Phys. Chem. A* **2003**, *107*, 372–378.

36. Leach, A. R. Second Derivative Methods: The Newton–Raphson Method. In *Molecular Modelling: Principles and Applications*, 2nd ed.; Prentice Hall: Harlow, England, 2001; pp 267–268.

37. Bondi, A. *J. Phys. Chem.* **1964**, *68*, 441–451.

38. Jeffrey, G. A. *An Introduction to Hydrogen Bonding*. Oxford University Press, Inc.: New York, 1997.

39. Anslyn, E. V.; Dougherty, D. A. In *Modern Physical Organic Chemistry*, University Science Books: Sausalito, CA, 2006; p 99.

40. Cleveland, W. S. *J. Am. Stat. Assoc.* **1979**, *74*, 829–836.

41. *SigmaPlot 11*, Systat Software, Inc.: San Jose, CA, 2010.

42. Musher, J. I.; Corey, E. J. *Tetrahedron* **1962**, *18*, 791–809.

43. Marat, K. *SpinWorks 3.1.3*, University of Manitoba: Winnipeg, 2009.

44. Quirt, A. R.; Martin, J. S. *J. Magn. Reson.* **1971**, *5*, 318–327.

Chapter 3:

Solution-state conformation of methyl α- and β-D-galactofuranosides from AMBER/GLYCAM simulations: Advantages and limitations

Compounds **3.1** and **3.2** discussed in this chapter were synthesized by Mr. Yu Bai, using published protocols.[1,2]

3.1. Introduction

Karplus developed the familiar equation to describe the dependence of vicinal proton-proton coupling constants ($^3J_{H,H}$) on the dihedral angle between the protons.[3,4] His theoretical work was based on the empirical data of Lemieux,[5] among others. The relationship between $^3J_{H,H}$ values and the torsions follows a Fourier series (eq. 3.1) with maxima when the H–C–C–H angle is eclipsed (0°) or antiperiplanar (180°) and minima when the H–C–C–H angle is perpendicular (±90°). Later, Pachler determined the Karplus-like relationships for mono- and disubstituted fluoroethanes using extended Hückel theory.[6,7] He found that one of the curves was phase-shifted relative to unsubstituted ethane (Figure 3.1) and that the addition of sine terms were necessary to describe the data (eq. 3.2). Another way of incorporating this phase-shift is to rewrite eq. 3.2 as shown in eq. 3.3. The advantage of the new equation is that the ε_X term correlates with the electronegativity difference between hydrogen and the other substituents on the C–C bond. Pachler went on to determine an empirical expression for $A_{X'}$, $B_{X'}$, and $C_{X'}$ for ethane fragments mono- or di-substituted with electronegative groups.

$$^3J_{H,H} = A + B\cos\phi + C\cos 2\phi \qquad 3.1$$

$$^3J_{H,H} = A + B\cos\phi + C\cos 2\phi + D\sin\phi + E\sin 2\phi \qquad 3.2$$

$$^3J_{H,H} = A_{X'} + B_{X'}\cos(\phi + \varepsilon_X) + C_{X'}\cos 2(\phi + \varepsilon_X) \qquad 3.3$$

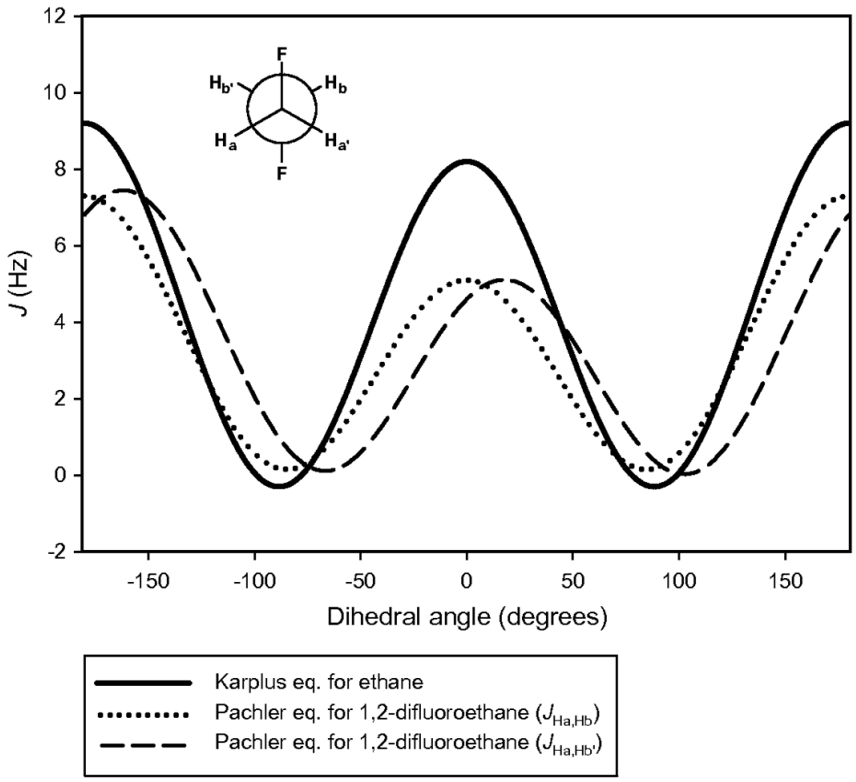

Figure 3.1. A comparison between the original Karplus equation (eq. 3.1) and the extended equation developed by Pachler (eq. 3.2). The solid line is the original Karplus equation, the dotted line is Pachler's equation for $^3J_{Ha,Hb}$ for 1,2-difluoroethane, and the dashed line is Pachler's equation for $^3J_{Ha,Hb'}$ for 1,2-difluoroethane. See the inset Newman projection for the relationship between $H_a/H_{a'}$ and $H_b/H_{b'}$.

Haasnoot et al.[8] extended Pachler's ideas further to develop a generalized Karplus-like equation (eq. 3.4) that takes into account the electronegativity and orientation of the substituents on the C–C bond. In the eq. 3.4, P_1 through P_6 were empirically determined from a set of 315 experimental coupling constants and molecular mechanics calculations using the MM1 force field.[9] The $\Delta\chi_i$ term is the electronegativity difference between the substituent and hydrogen, and the ξ_i term refers to the orientation about the C–C bond, as illustrated in Figure 3.2. The generalized Karplus equation was then extended by Donders, et al.[10,11] (eq. 3.5) to

use a new empirical electronegativity scale (λ) that also incorporates solvent effects. This is the equation used in the program PSEUROT (Chapter 2).[12,13]

$$^3J_{H,H} = P_1 \cos^2\phi + P_2 \cos\phi + P_3 + \sum_{i=1}^{4} \Delta\chi_i \{P_4 + P_5 \cos^2(\xi_i\phi + P_6 \,|\, \Delta\chi_i \,|)\} \qquad 3.4$$

$$^3J_{H,H} = \sum_{m=0}^{3} C_m \cos m\phi + \sum_{n=1}^{3} S_n \sin n\phi \qquad 3.5$$

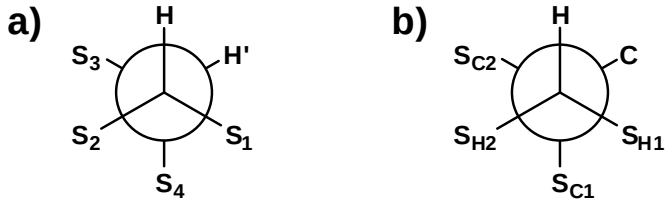

Figure 3.2. Newman projections to describe the ξ_i terms in eq. 3.4 and 3.6. a) For substituents S_1 and S_3, ξ_i is +1; for S_2 and S_4, ξ_i is –1. b) For substituents S_{H1} and S_{C1}, ξ_i is +1; for S_{H2} and S_{C2}, ξ_i is –1.

Eqs. 3.1 through 3.5 discussed above, all relate proton–proton coupling constants to the H–C–C–H dihedral angle. Carbon–proton coupling constants and the C_α–C_β–C_γ–H dihedral angle can also be described by a similar Karplus-like relationship. Recently, Palermo et al. developed such an equation that includes electronegativity terms (eq. 3.6) using density functional theory (DFT) calculations of 2157 conformations of butane fragments with amine, halide, hydroxyl, and thiol substiuents.[14] They used the Haasnoot equation (eq. 3.4) as a starting point, and, like that equation, there are terms for the electronegativity difference between the substituent and hydrogen ($\Delta\chi_{Hi}$) or carbon ($\Delta\chi_{Ci}$), as well as for the orientation about the central C–C bond (ξ_i, Figure 3.2). The new equation also includes more coefficients to account for the different effects of electronegative substituents on the β- or γ-carbons. The root mean square (RMS)

difference between the generalized equation and the calculated couplings is 0.66Hz, which is comparable to the 0.52 Hz RMS difference observed by Haasnoot, et al.[8] It should be noted that only a few examples of Karplus-type relationships have been discussed here; for a more in depth discussion, the reader is referred to a recent review by Coxon.[15]

$$
\begin{aligned}
{}^3J_{H,C} = P_1\cos^2\phi + P_2\cos\phi + P_3 + \sum_{i=1}^{2}\Delta\chi_{Hi}\{P_4 + P_5\cos^2(\xi_i\phi + P_6\,|\,\Delta\chi_{Hi}\,|)\} \\
\ldots + \sum_{i=1}^{2}\Delta\chi_{Ci}\{P'_4 + P'_5\cos^2(\xi_i\phi + P'_6\,|\,\Delta\chi_{Ci}\,|)\}
\end{aligned}
\qquad 3.6
$$

The observed value of ${}^3J_{\mathrm{H,H}}$ or ${}^3J_{\mathrm{H,C}}$ can be easily related to the corresponding dihedral angle via the Karplus relationship when that angle is conformationally restricted. When the H–C–C–H or H–C–C–C fragment can freely rotate – like the C4–C5 or C5–C6 bonds of methyl α- and β-D-galactofuranosides (**3.1** and **3.2**, Figure 3.3) – the observed vicinal coupling constants represent a weighted average of several states. A common approach to determine the conformation of freely rotating bonds in carbohydrates is to assume the three staggered rotamers – *gg*, *gt*, and *tg* – represent "limiting values" for the observed ${}^3J_{\mathrm{H,H}}$ or ${}^3J_{\mathrm{H,C}}$, as shown in eq. 3.7.[16] The variable X represents the mole fraction of each rotamer; thus, the sum of X_{gg}, X_{gt}, and X_{tg} must be one. With two known coupling constants for each rotatable bond, there are three equations and three unknowns; therefore, the populations for each rotamer can be determined.

$$
{}^3J_{observed} = {}^3J_{gg}X_{gg} + {}^3J_{gt}X_{gt} + {}^3J_{tg}X_{tg} \qquad 3.7
$$

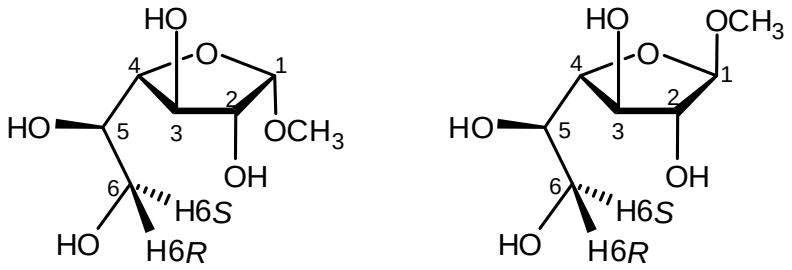

3.1 **3.2**

Figure 3.3. The structures of methyl α-D-galactofuranoside (**3.1**) and methyl β-D-galactofuranoside (**3.2**) with the carbon atoms numbered. The pro-*R* and pro-*S* hydrogens on C6 are also labeled as H6*R* and H6*S*, respectively.

The limiting values method for determining rotamer populations has drawbacks. To determine the value of $^3J_{gg}$, $^3J_{gt}$, and $^3J_{tg}$ to be used in eq. 3.7, some knowledge of the H–C–C–H or H–C–C–C dihedrals is required. The ideal values of –60°, 60°, and 180° can be used, but they may not be appropriate for the system of interest (see Section 3.3.3). The limiting values approach also neglects contributions from small populations that may have large values of $^3J_{H,H}$ or $^3J_{H,C}$. Markley and coworkers introduced a new technique to overcome these limitations, the Continuous Probability Distribution (CUPID) method.[16] In CUPID, the probability for the dihedral angle ϕ is treated as a periodic Fourier series, eq. 3.8. The coefficients ρ_0, ρ_n, and σ_n are fit to the data for each system using linear regression. CUPID does not require any knowledge of the values of dihedral angle ϕ; however, it does rely on having accurate Karplus equations for the system of interest.

$$\rho(\phi) = \rho_0 + \sum_{n=1}^{\infty} \rho_n \cos(n\phi) + \sum_{n=1}^{\infty} \sigma_n \sin(n\phi) \qquad 3.8$$

Our group[17-19] and others[20-26] have used molecular dynamics (MD) simulations as another way for determining the probabilities for dihedral angles. Rather than using discrete values for dihedral angles (eq. 3.7), the observed vicinal coupling constant can also be represented an average over all 360° (eq. 3.9).[16] In this equation, $J(\phi)$ is the appropriate Karplus-like relationship, and $\rho(\phi)$ is the probability distribution of dihedral angles. In this chapter, we present newly determined equations for $J(\phi)$ that are specific to methyl α- and β-D-galactofuranosides (**3.1** and **3.2**, Figure 3.3). These new equations are then used in conjunction with MD simulations to evaluate the solution conformations of **3.1** and **3.2**. In particular, the distribution of H–C–C–H and H–C–C–C, or $\rho(\phi)$, come from the simulations. Limitations of the MD simulations will also be discussed.

$$\langle J \rangle = \int_0^{360} J(\phi)\rho(\phi)d(\phi) \qquad 3.9$$

3.2. Methods

3.2.1. Coupling constant calculations and determination of Karplus-like relationships

The spin–spin coupling constants were calculated in Gaussian 03[27] using the 180 optimized envelope geometries of **3.1** and **3.2** described in Chapter 2. A basis set developed by the Serianni and Carmichael groups specifically for coupling constant calculations ([5s2p1d|3s1p])[28] was used for the DFT calculations with the B3LYP functional.[29] This level of theory has been

successfully used by our group for similar arabinofuranose systems.[17-19] Calculations were also run with Dunning's triple-zeta basis set (cc-pVTZ),[30] but the calculated $^{3}J_{H2,H3}$ and $^{3}J_{H3,H4}$ values were all lower than the experimental values (data not shown). The coupling constants and associated dihedral angles were extracted for all conformations and are listed in Appendix B. The resulting coupling constants were fit to the Karplus-like relationship[6,7] in eq. 3.2, using the Marquardt-Levenberg algorithm,[31] as implemented in SigmaPlot.

While fitting the data, we noticed that none of the conformers for **3.1** had H2–C2–C3–H3 or H3–C3–C4–H4 values of ±180°, leaving these regions of the curve undefined. Similarly, none of the conformers for **3.2** had H2–C2–C3–H3 or H3–C3–C4–H4 values of ±180°, nor were any of the H1–C1–C2–H2 at ±180°. Because these regions represent local maxima in the Karplus-like equations, an additional six conformations of **3.1** and an additional nine conformations of **3.2** were optimized in Gaussian 03 using B3LYP/6-31G*,[29,32] and their coupling constants were calculated as described above (B3LYP/[5s2p1d|3s1p]).[28] During geometry optimization for **3.1**, H2–C2–C3–H3 was frozen at 180° for ^{2}E-*gg-gt*, ^{2}E-*gt-gt*, and ^{2}T$_{3}$-*tg-gt*; and H3–C3–C4–H4 was frozen at 180° for E$_{3}$-*gg-gt*, E$_{3}$-*gt-gt*, and E$_{3}$-*tg-gt*. During geometry optimization for **3.2**, H1–C1–C2–H2 was frozen at 180° for ^{2}T$_{1}$-*gg-tg*, ^{2}T$_{1}$-*gt-tg*, and ^{2}E-*tg-tg*; H2–C2–C3–H3 was frozen at 180° E$_{3}$-*gg-tg*, E$_{3}$-*gt-tg*, and E$_{3}$-*tg-tg*; and H3–C3–C4–H4 was frozen at 180° for ^{4}T$_{3}$-*gg-tg*, ^{4}T$_{3}$-*gt-tg*, and ^{4}T$_{3}$-*tg-tg*. The ^{2}T$_{1}$ and ^{4}T$_{3}$ conformations were included because they were the low energy conformations resulting from holding the H1–C1–C2–H2 or H3–C3–C4–H4 torsion at 180°. For both compounds, all of the

C–C–O–H were also fixed during geometry optimization to prevent formation of intramolecular hydrogen bonds. The coupling constants and associated dihedral angles for these 15 additional conformations are also listed in Appendix B.

3.2.2. NMR spectroscopy

All spectra were acquired at 600 MHz, in D_2O, and at 300 K. The values for $^{3}J_{H,H}$ were determined from the 1D ^{1}H NMR spectra that were described in Section 2.3.4. The $^{3}J_{H4,C6}$ values for **3.1** and **3.2** were determined from an average of three Excitation-Sculptured Indirect-Detection Experiments (EXSIDE).[33,34] A sculpted pulse selectively inverted proton H4 and was generated through Agilent's "Pandora's Box" module of the VNMRJ software package; specifically, a Q3 inversion pulse was used. For **3.1**, three different widths of selective pulses were used – 25, 35, and 40 Hz. For **3.2**, only two widths were used, 50 and 55 Hz. The spectra were acquired with a small sweep width (500 Hz) in the ^{13}C dimension to increase resolution. Also, in the indirect dimension, 64 or 128 increments were acquired, resulting in 12 or 24 h experiments. In all experiments, 96 transients were acquired in the directly-detected dimension. A 5 Hz $^{3}J_{C,H}$ value for the refocusing delay and a *J*-scaling factor of 10 were used for all EXSIDE spectra. Sine-bell functions were applied interactively during processing to improve the signal-to-noise in the spectra.

3.2.3. MD simulations

All MD simulations were performed using the PMEMD module of the AMBER 10[35] software package and the GLYCAM06[36] force field. Partial

charges were calculated using our previously reported approach for restrained electrostatic potential (RESP) charge fitting.[37-39] Briefly, a 50 ns MD simulation was run as described below, and 200 conformations were selected over the entire trajectory. Geometry optimizations (HF/6-31G*) were run in Gaussian 03,[27] and the C–C–O–H bonds were all frozen during optimization. Single point energies were calculated at the same level of theory, fit using RESP, and averaged over all conformations. The charges for C1–C4 and O1–O4 for **3.1** and **3.2** were taken from our earlier calculations on β-D-Ara*f*[38] and α-D-Ara*f*,[37] respectively. In the GLYCAM06 force field, aliphatic hydrogens have a partial charge of zero to reduce artifactual fluctuations.[40] Therefore, we did not include the aliphatic hydrogens in the fitting process. The calculated charges for all the monosaccharides discussed in this chapter are listed in Appendix B.

For all production runs, 250 ns MD simulations were performed with a 2 fs timestep in a box of approximately 300 TIP3P[41] water molecules, under periodic boundary conditions and using particle mesh Ewald summation for long-range interactions. Specifically, 312 water molecules were included in a 27.9 x 26.3 x 23.3 Å box for **3.1**, and 292 water molecules were included in a 26.5 x 25.0 x 24.1 Å box for **3.2**. The simulations were run under NPT conditions at 1 atm and 300 K. The temperature was maintained with either the Berendsen[42] (*ntt = 1*) or Langevin[43] (*ntt = 3*) thermostat. With the Berendsen thermostat, the velocities were rescaled every 1 ps, and with the Langevin thermostat, the collision frequency γ was 2 ps^{-1}. All bonds containing hydrogens were fixed using the

SHAKE[44] algorithm. The cutoff for nonbonding interactions was 8 Å, and nonbonded and electrostatic interactions were unscaled.

To prepare the system for dynamics, the water molecules were minimized to remove any high-energy contacts, via 50 steps of steepest descent followed by 950 steps of conjugate gradient minimization. The entire system was then minimized similarly. An equilibration period was carried out that included heating the system from 5 K to 300 K over 50 ps, then cooling to 5 K over 50 ps. This simulated annealing step was followed by a second, slower heating from 5 K to 300 K over 100 ps. After an additional equilibration at 300 K for 100 ps, the production simulation began.

3.3. Results and discussion

3.3.1. Karplus-like relationships for vicinal couplings in galactofuranosides

Because the single point energies (B3LYP/6-31+G**, Chapter 2) of the ^{2}E-*gt-tg*, E$_{3}$-*gt-tg*, and ^{4}E-*gt-tg* conformation of **3.1** were all more than 34 kcal/mol higher than the global minimum, these conformations are all excluded from the data presented below. These conformations are also not included in the tables in Appendix B.

3.3.1.1. Equations for ring couplings in 3.1 and 3.2

The values of $^{3}J_{H1,H2}$, $^{3}J_{H2,H3}$, and $^{3}J_{H3,H4}$ for **3.1** and **3.2** from the DFT calculations were plotted as a function of their respective H–C–C–H dihedral angle and fit to eq. 3.2 (Figure 3.4). The H1–C1–C2–H2 angles for

conformations of the α-anomer **3.1** have values between –50° and +50°, while for the β-anomer **3.2**, the same angles have a range between 75° and 180° (Figure 3.4a). When the data were fit separately for each anomer, the resulting equations were quite similar (data not shown); therefore, we combined the data for both anomers and fit to one Karplus-like equation, eq. 3.10 (Figure 3.4a, solid grey line) that had an overall $r^2 = 0.985$. The resulting equation differs from the empirical equation 3.5 for $^3J_{H1,H2}$ (Figure 3.4a, dashed line), especially for values of H1–C1–C2–H2 near 0° ± 30°. The empirical equation predicts $^3J_{H1,H2}$ values that are about 2 Hz lower than the calculated values near 0°. Near ±180°, the empirical equation overestimates $^3J_{H1,H2}$ by 1 Hz.

$$^3J_{H1,H2} = 4.03 - 0.54\cos\phi + 3.55\cos 2\phi - 0.34\sin\phi + 1.27\sin 2\phi \qquad 3.10$$

For the couplings along the C2–C3 and C3–C4 bond, the H–C–C–H torsion are constrained by the ring and take on a narrow range of values, ~90°. Specifically, the values of H2–C2–C3–H3 are between –80° and –180° (Figure 3.4b), and the values of H3–C3–C4–H4 are between +85° and +180° (Figure 3.4c) for both **3.1** and **3.2**. Because a large region of the curve is not defined, constraints were used for coefficients B and D when fitting the data to eq. 3.2. Without the constraints, the equations took on unreasonable values in the undefined region of the function, e.g. $^3J_{H3,H4}$ was less than –30 Hz for H3–C3–C4–H4 of –90°. For $^3J_{H2,H3}$, the constraints were 2*B < –0.5 and 2*D > –1, and the constraints for $^3J_{H3,H4}$ were 2*B < –1.2 and 2*D < 1, as suggested by Schmidt.[45] Adding the constraints did not significantly affect the fit to the data.

For $^3J_{H2,H3}$, the unconstrained fit had an r^2 value of 0.991, and the constrained fit had $r^2 = 0.988$. For $^3J_{H3,H4}$, both the unconstrained and constrained fits had $r^2 = 0.990$.

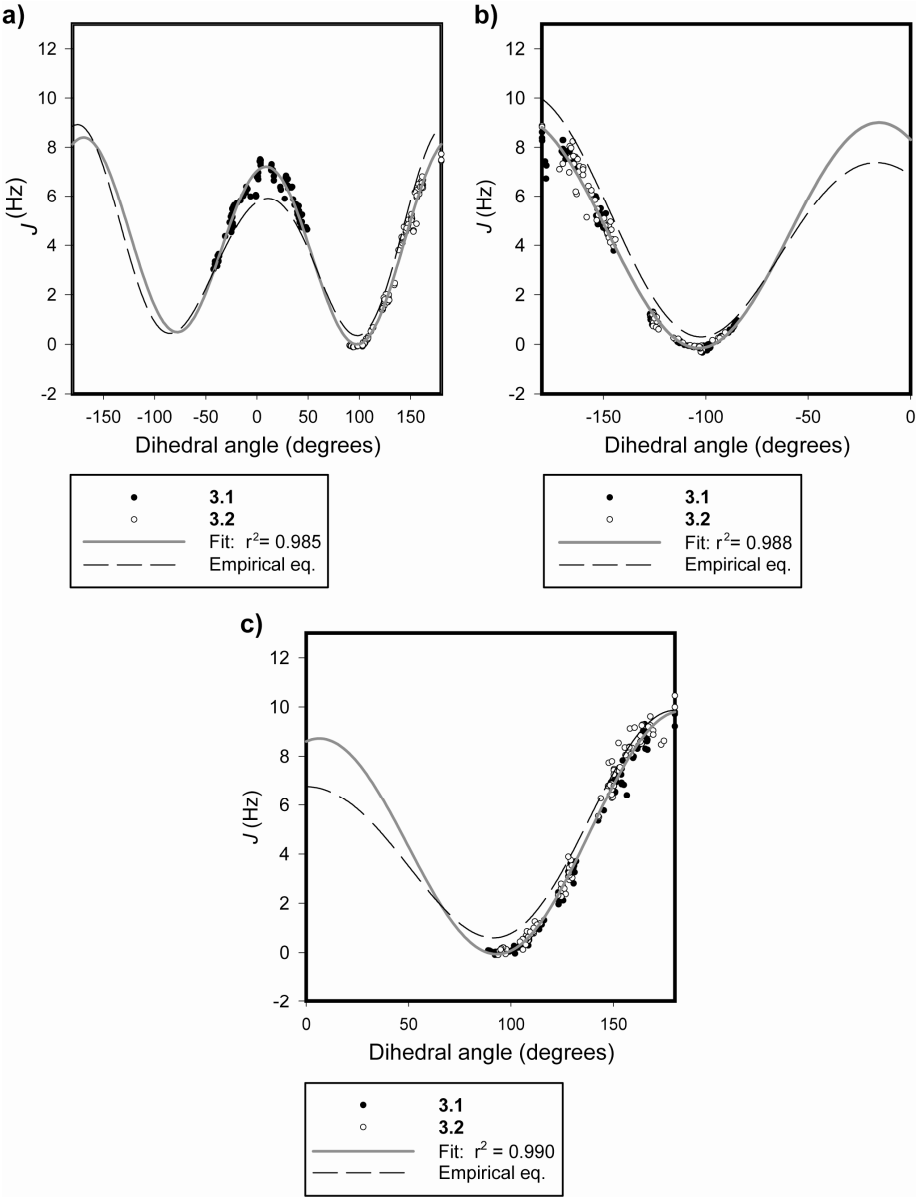

Figure 3.4. Karplus-like relationships for the ring dihedral angles. Graph *a*) shows H1–C1–C2–H2 versus $^3J_{H1,H2}$. Graph *b*) shows H2–C2–C3–H3 versus $^3J_{H2,H3}$. Graph *c*) shows H3–C3–C4–H4 versus $^3J_{H3,H4}$. For all three graphs, the filled circles are conformations of **3.1** and open circles are conformations of **3.2**. The solid grey line represents the fit to eq. 3.2 and the dashed black line represents the empirical eq. 3.5.

The resulting equation for $^3J_{H2,H3}$ as a function of H2–C2–C3–H3 is shown in Figure 3.4b as a solid grey line (eq. 3.11). The empirical equation for $^3J_{H2,H3}$ is shown as a dashed line. The two equations are quite similar for the values of H2–C2–C3–H3 for values from –90° to –150°, though the empirical equation overestimates the value of $^3J_{H2,H3}$ near –180° by about 1 Hz. Larger deviations are seen for dihedral angles near –15° where the calculated equation predicts larger coupling constants than the empirical one. Only –180º to 0º is shown in Figure 3.4b, as the constraints of the ring precludes the H2–C2–C3–H3 torsion angle from the region not pictured.

Figure 3.4c shows the equation for $^3J_{H3,H4}$ as a function of the H3–C3–C4–H4 dihedral angle (solid grey line, eq. 3.12), as well as the empirical equation for $^3J_{H3,H4}$ (dashed line). Both equations are similar for torsion angles from 85° to 180°, though the empirical equation underestimates the value of $^3J_{H3,H4}$ near 90° by about 0.7 Hz. As with Figure 3.4b, the portion of the graph shown in Figure 3.4c is limited to the angles accessible to the H3–C3–C4–H4 torsion in the furanose ring (i.e. 0° to 180°).

$$^3J_{H2,H3} = 4.21 - 0.25\cos\phi + 4.35\cos 2\phi - 0.50\sin\phi - 2.27\sin 2\phi \qquad 3.11$$

$$^3J_{H3,H4} = 4.33 - 0.60\cos\phi + 4.87\cos 2\phi + 0.50\sin\phi + 0.82\sin 2\phi \qquad 3.12$$

3.3.1.2. Equations for couplings along the C4–C5 bond in 3.1 and 3.2

For the couplings along the ring, the empirical equations agreed well with the newly determined Karplus-like relationships. However, for the couplings along the C4–C5 bond, this was not the case. The relationship between H4–C4–

C5–H5 dihedral angle and $^3J_{H4,H5}$ for both **3.1** and **3.2** was plotted (Figure 3.5a), and the data were fit to eq. 3.2 (solid grey line, eq. 3.13). Because we selected conformations for all three staggered rotamers about the C4–C5 bond (see Chapter 2), the entire curve is well defined, and no constraints were used during the fitting procedure. A good correlation between the fit and the data is observed ($r^2 = 0.983$). The values for $^3J_{H4,H5}$ calculated for the *tg* rotamer (H4–C4–C5–H5 near 55° ± 20°, Figure 3.8) differ significantly from those predicted by the empirical equation (eq. 3.5, Figure 3.5a, dashed line). Eq. 3.13 predicts that $^3J_{H4,H5}$ is 9.3 Hz at H4–C4–C5–H5 = 35°, but the empirical equation predicts a value that is 3 Hz less. For the *gt* and *tg* rotamers, the agreement between the two equations is better, though the maximum near –180° is larger in eq. 3.13.

$$^3J_{H4,H5} = 5.56 + 0.15\cos\phi + 4.18\cos 2\phi - 0.21\sin\phi + 2.54\sin 2\phi \qquad 3.13$$

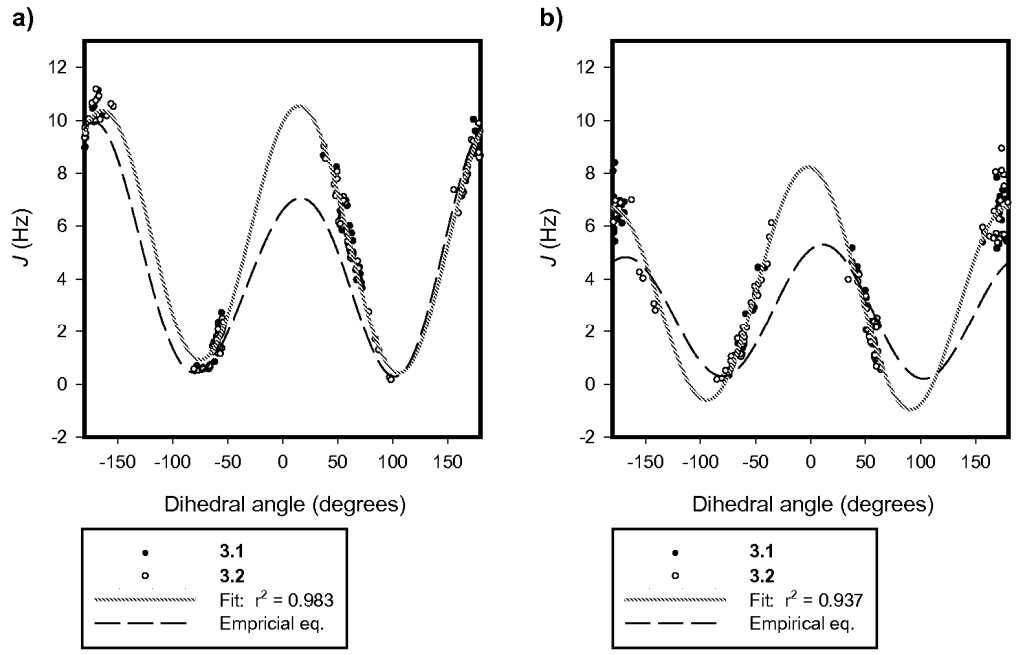

Figure 3.5. Karplus-like relationships for the couplings about the C4–C5 bond. Graph *a*) shows H4–C4–C5–H5 versus $^{3}J_{H4,H5}$. Graph *b*) shows H4–C4–C5–C6 versus $^{3}J_{H4,C6}$. For both graphs, the filled circles are conformations of **3.1** and open circles are conformations of **3.2**. The solid grey line represents the fit to eq. 3.2 and the dashed black line represents the empirical eq. 3.5 or eq. 3.6.

The proton–carbon coupling constants $^{3}J_{H4,C6}$ for **3.1** and **3.2** were plotted against the H4–C4–C5–C6 dihedral angles (Figure 3.5b) and fit to eq. 3.2 (eq. 3.14, solid grey line). The ranges of $^{3}J_{H4,C6}$ values near ±180° is large – from 5.5 to 9.0 Hz – and, as a result, the fit for eq. 3.14 is the lowest of all the new equations, $r^2 = 0.937$. Also, there is poor agreement between eq. 3.14 and the empirical equation (eq. 3.6, Figure 3.5b, dashed line). The empirical equation is asymmetric about 0°, with a maximum at 15°. However, eq. 3.14, has a maximum much closer to 0°. Similarly, eq. 3.14 has minima near the expected ±90°, but the empirical equation has minima at –80° and 100°. Also, the largest

values for $^3J_{H4,C6}$ predicted by eq. 3.14 are 2–3 Hz larger than those predicted by the empirical equation.

$$^3J_{H4,C6} = 3.36 + 0.76\cos\phi + 4.12\cos 2\phi - 0.20\sin\phi - 0.21\sin 2\phi \quad 3.14$$

3.3.1.3. Equations for couplings along the C5–C6 bond in 3.1 and 3.2

As with the C4–C5 bond, we selected conformations that included all three staggered rotamers about the C5–C6 bond. Thus, the curves for both $^3J_{H5,H6R}$ and $^3J_{H5,H6S}$ are well defined (eq. 3.15 and eq. 3.16, respectively), and no constraints were necessary in the fitting process. Eq. 3.15 is shown in Figure 3.6a (solid grey line), along with the values $^3J_{H5,H6R}$ and H5–C5–C6–H6*R* for **3.1** and **3.2**. The empirical eq. 3.5 is also shown as a dashed line. Both equations show good agreement in regions of the curve that contain data points for the staggered rotamers (Figure 3.8), i.e. –180° to –160° for the *gt* rotamer, –100 to –55° for the *gg* rotamer, and 35° to 75° for the *tg* rotamer. Neither the calculated nor the empirical equations are symmetric about 0°, rather both have a maximum at –18°. At this maximum, the empirical equation predicts a value of $^3J_{H5,H6R}$ that is 2 Hz lower than the one predicted by eq. 3.15. Similarly, for the maximum near 180°, the empirical equation also predicts a lower value than eq. 3.15.

$$^3J_{H5,H6R} = 5.75 - 0.69\cos\phi + 4.08\cos 2\phi - 0.53\sin\phi - 3.34\sin 2\phi \quad 3.15$$

$$^3J_{H5,H6S} = 5.64 - 0.36\cos\phi + 5.08\cos 2\phi + 0.20\sin\phi - 0.05\sin 2\phi \quad 3.16$$

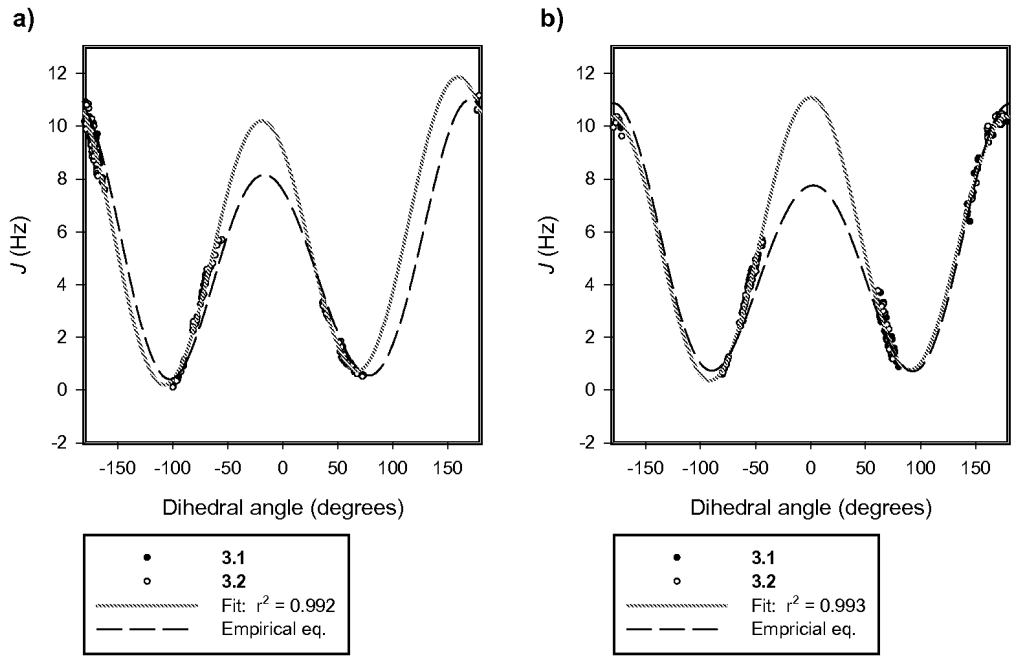

Figure 3.6. Karplus-like relationships for the couplings about the C5–C6 bond. Graph *a*) shows H5–C5–C6–H6*R* versus $^3J_{H5,H6R}$. Graph *b*) shows H5–C5–C6–H6*S* versus $^3J_{H5,H6S}$. For both graphs, the filled circles are conformations of **3.1** and open circles are conformations of **3.2**. The solid grey line represents the fit to eq. 3.2 and the dashed black line represents the empirical eq. 3.5.

Unlike eq. 3.15, the equation for $^3J_{H5,H6S}$ as a function of H5–C5–C6–H6*S* (eq. 3.16, Figure 3.6b, solid grey line) is symmetric about 0°. A similar observation was made by Pachler for 1,2-difluoroethane – one of the curves for $^3J_{H,H}$ was symmetric about 0°, while the other was phase shifted by 20° (Figure 3.1).[7] As observed for eq. 3.15 for $^3J_{H5,H6R}$, the empirical equation (Figure 3.6b, dashed line) and eq. 3.16 for $^3J_{H5,H6S}$ agree well for the regions of the curve with data points for the staggered rotamers (Figure 3.8), i.e. –85° to –40° for the *gt* rotamer, 55° to 80° for the *gg* rotamer and 140° to –165° for the *tg* rotamer. The area of the curve near 0° differs between the two equations; eq. 3.16 predicts a coupling constant that is more than 3 Hz larger than the empirical equation.

3.3.2. $^3J_{H4,C6}$ values from EXSIDE experiments

To determine the rotamer populations about the C4–C5 bond, two coupling constants that relate to the C4–C5 bond are needed (Section 3.1). However, there is only one H–C–C–H torsion angle for this bond. Three-bond proton–carbon coupling constants follow the same Karplus-type relationship as vicinal proton–proton coupling constants, so a $^3J_{C,H}$ value could also be used. There are two options for the C4–C5 bond of **3.1** and **3.2**, H4–C4–C5–C6 or H5–C5–C4–C3. We chose to determine $^3J_{H4,C6}$ for both compounds because H4 was isolated in both 1D ^{1}H NMR spectra, and the signal for H5 in **3.1** overlapped with the resonance for one of the H6 protons (Figure 2.21, Chapter 2). Two examples of the EXSIDE[33,34] spectra are shown in Figure 3.7. The value of $^3J_{H4,C6}$ for **3.1** is 3.0 ± 0.1 Hz, which is the average for the three spectra that were acquired. For **3.2**, the average value of $^3J_{H4,C6}$ is 1.6 ± 0.1 Hz.

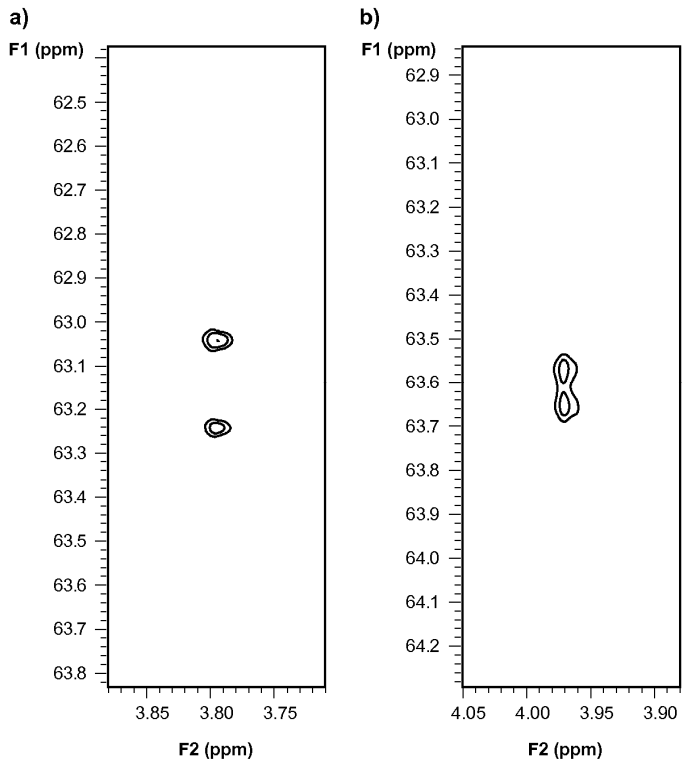

Figure 3.7. a) The EXSIDE spectrum of **3.1**. H4 was selectively inverted with a 40 Hz Q3 pulse. b) The EXSIDE spectrum of **3.2**. H4 was selectively inverted with a 50 Hz Q3 pulse. For both spectra, the splitting along the F1 dimension is equal to ten times the value of $^{3}J_{H4,C6}$.

3.3.3. Rotamer populations for 3.1 and 3.2 using the limiting value method

3.3.3.1. Rotamer populations for the C4–C5 bond

The three staggered rotamers for **3.1** and **3.2** are shown in Figure 3.8, along with the ideal values for the H4–C4–C5–H5 and H4–C4–C5–C6. As Figure 3.5 shows, these two dihedral angles clustered near the ideal values during the geometry optimization process; therefore, we used the ideal values in eq. 3.13 and 3.14 to determine the values of $^{3}J_{gg}$, $^{3}J_{gt}$, and $^{3}J_{tg}$ for both H4–C4–C5–H5 and H4–C4–C5–C6. The limiting values (Table 3.1) were then used with eq. 3.7 to determine the rotamer populations for **3.1** and **3.2**.

Table 3.1. Limiting values of $^3J_{gg}$, $^3J_{gt}$, and $^3J_{tg}$ for the C4–C5 bond.

	$^3J_{gg}$ (Hz)	$^3J_{gt}$ (Hz)	$^3J_{tg}$ (Hz)
H4–C4–C5–H5	1.5	9.6	5.6
H4–C4–C5–C6	1.3	2.0	6.7

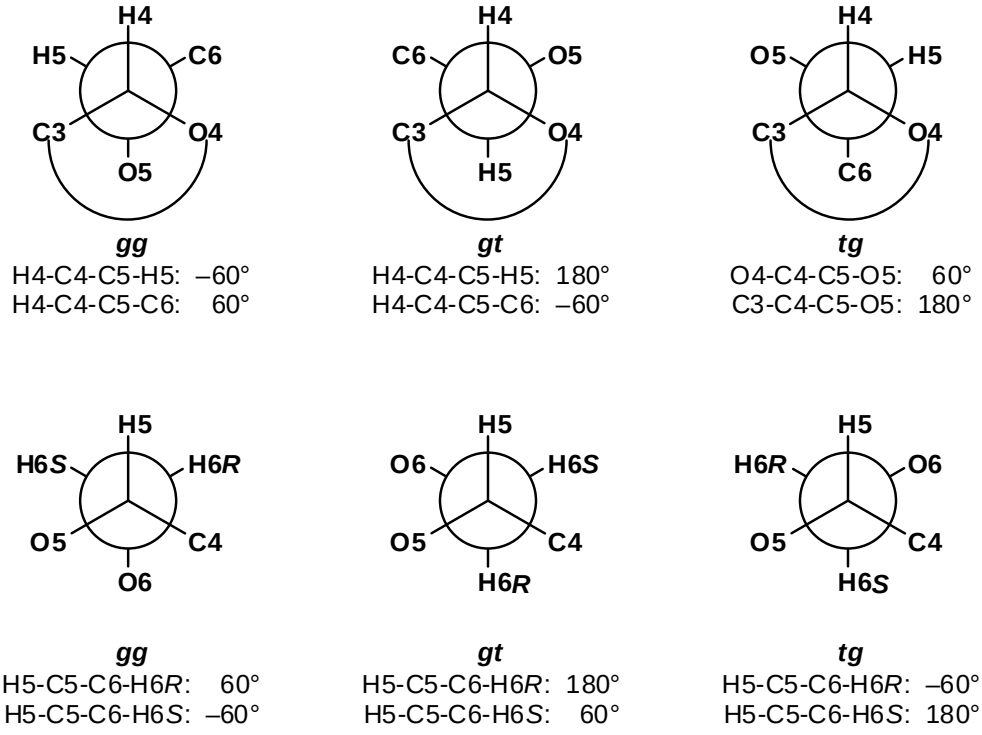

Figure 3.8. (*top*) The three staggered rotamers about the C4–C5 bond, viewing down the C4–C5 bond axis. (*bottom*) The three staggered rotamers about the C5–C6 bond, viewing down the C5–C6 bond axis. The ideal values for the dihedral angles associated with the measured coupling constants are shown.

The observed values of $^3J_{H4,H5}$ and $^3J_{H4,C6}$ for **3.1** are 6.0 and 3.0 Hz, respectively (see also Table 2.6, Chapter 2). Using eq. 3.7, the rotamers for the C4–C5 bond are 32 ± 4% *gg* : 42 ± 1% *gt* : 26 ± 4% *tg*. The *gt* rotamer is slightly more preferred than the others, but it is present less than half the time. The small

differences in populations indicate that the energy differences among all the rotamers are also small.

For **3.2**, the observed values for $^3J_{H4,H5}$ and $^3J_{H4,C6}$ are 4.4 and 1.6 Hz, respectively (see also Table 2.6, Chapter 2). The rotamer populations calculated using eq. 3.7 are 64 ± 3% *gg* : 35 ± 2% *gt* : 1 ± 2% *tg*. The rotamers with the oxygen substituents in the gauche orientation dominate, which is expected due to the gauche effect.[46] Also, the *tg* rotamer is a minor component of the population, indicating that it is significantly higher in energy than the other two conformations.

3.3.3.2. Rotamer populations for the C5–C6 bond

Unlike for the C4–C5 bond, the H5–C5–C6–H6*R* and H5–C5–C6–H6*S* dihedral angles did not cluster about the ideal values (Figure 3.8) after the geometry optimization, as shown in the graphs in Figure 3.6. Instead, they took on the values shown in Table 3.2. The H5–C5–C6–H6*S* and the O5–C5–C6–O6 dihedral angles have the same relative orientation, i.e., for the *gg* rotamer both have average values near 300°. After geometry optimization, the average values for the O5–C5–C6–O6 were 303° for *gg*, 65° for *gt*, and 164° for *tg* for both **3.1** and **3.2** (see also Sections 2.3.1 and 2.3.2). These deviations from the ideal values are reflected in the average values for the H5–C5–C6–H6*R* and H5–C5–C6–H6*S* torsions. The non-ideal values in Table 3.2 were used in eq. 3.15 and 3.16 to determine the values of $^3J_{gg}$, $^3J_{gt}$, and $^3J_{tg}$ for both H4–C4–C5–H5 and H4–C4–C5–C6. The limiting values (Table 3.2) were then used with eq. 3.7 to determine the rotamer populations for **3.1** and **3.2**.

Table 3.2. The dihedral angles ϕ_{gg}, ϕ_{gt}, ϕ_{tg}, and limiting values of $^3J_{gg}$, $^3J_{gt}$, and $^3J_{tg}$ for the C5–C6 bond.

	ϕ_{gg} (°)	$^3J_{gg}$ (Hz)	ϕ_{gt} (°)	$^3J_{gt}$ (Hz)	ϕ_{tg} (°)	$^3J_{tg}$ (Hz)
H5–C5–C6–H6*R*	58.2	1.0	187.3	9.5	283.4	2.9
H5–C5–C6–H6*S*	302.3	3.5	70.1	2.0	166.3	9.9

The experimental values for $^3J_{H5,H6R}$ and $^3J_{H5,H6S}$ for **3.1** are 7.0 and 3.9 Hz, respectively(see also Table 2.6, Chapter 2). These coupling constants lead to rotamer populations of 12 ± 5% *gg* : 66 ± 2% *gt* : 22 ± 4% *tg*. The *gt* rotamer occurs more than twice as often as either of the other rotamers. The same trend is seen for **3.2**, which has $^3J_{H5,H6R}$ of 7.4 Hz, and $^3J_{H5,H6S}$ of 4.4 Hz(see also Table 2.6, Chapter 2). Using eq. 3.7, the rotamer populations for the C5–C6 bond of **3.2** are 1 ± 5% *gg* : 69 ± 2% *gt* : 30 ± 4% *tg*.

3.3.4. Results from MD simulations

Because β-D-galactofuranosides are more common in nature,[47] we began our simulations with **3.2**. The discussion in Sections 3.3.4.1 though 3.3.4.3 below will also start with **3.2**.

3.3.4.1. Ring conformation

We observe mainly one broad distribution of ring conformations in the MD simulation of **3.2** (Figure 3.9). The population is centered at a pseudorotational phase angle *P* of 16°, which corresponds to the E_3 ring conformation. Upon closer inspection of the histogram, there appears to be a minor population around *P* = 125–135°. When the MD data are fit to two

Gaussian functions (eq. 3.17) with the same width, 90% of the population is centered at P = 16° and 10% is centered at P = 132°, which is the ^{1}E conformation. The furanose ring spends very little time in the regions of a P of 200° to 220° or a P of –140° to –100°. In contrast, the program PSEUROT had predicted that 32% of the population of **3.2** had a conformation of P = 242°, the E_4 conformation (Section 2.3.5). For cases like this with a broad distribution of conformers, PSEUROT fails, which may be one reason the four separate PSEUROT calculations for **3.2** gave three different answers.

$$f(x) = w * ae^{-\left(\frac{x-x_0}{2b}\right)^2} + (1-w) * ce^{-\left(\frac{x-x_1}{2b}\right)^2} \qquad 3.17$$

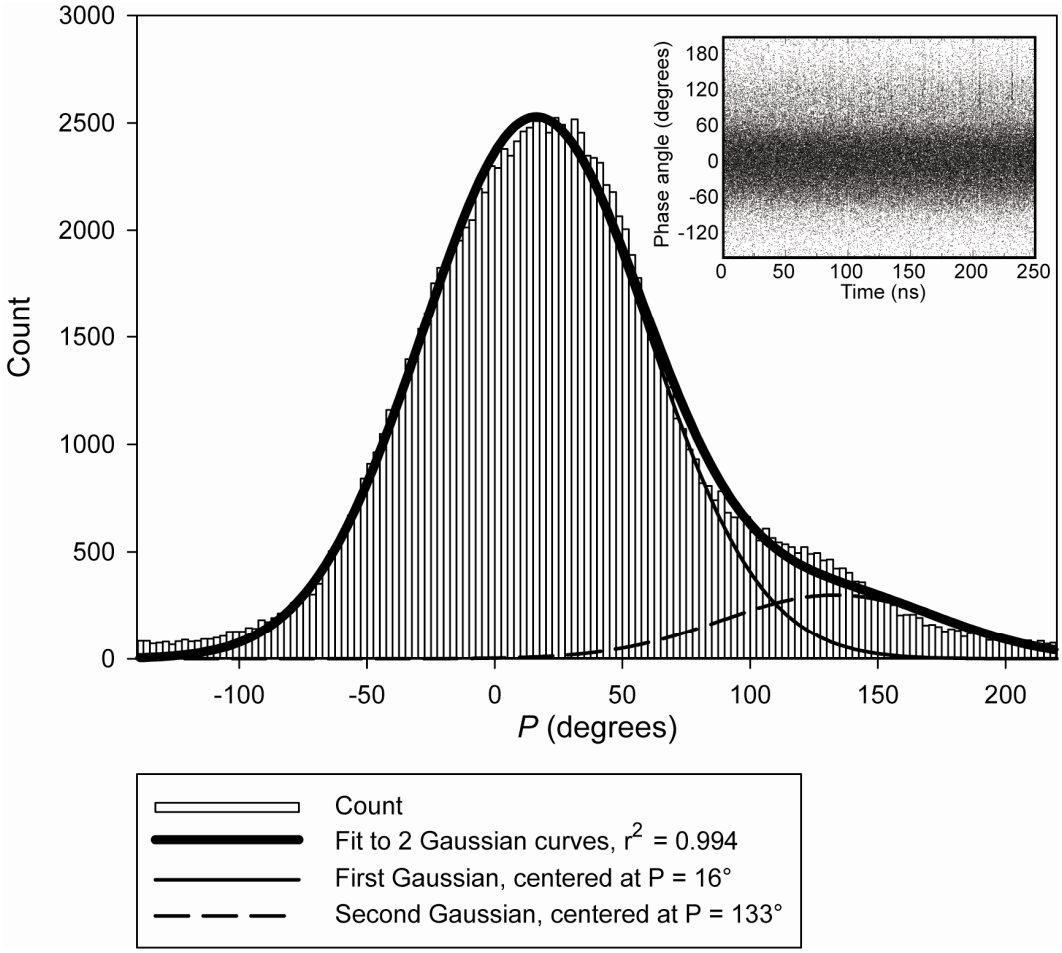

Figure 3.9. Histogram of pseudorotational phase angle *P* for **3.2** fit to two Gaussian functions (thick solid black line). The major population is centered at *P* = 16° (thin solid black line), and the minor population is centered at *P* = 133° (thin dashed line). The inset shows *P* versus time of the simulation.

The minor population for **3.2** is more apparent in two of the individual distributions of the H–C–C–H dihedral angles along the ring (Figure 3.10). For H1–C1–C2–H2, the major population occurs around 145° and the minor population occurs near 100°. For H2–C2–C3–H3, the major population is near –154°, and the minor one is near –106°. However, the H3–C3–C4–H4 dihedral angle does not have an apparent peak for the minor population. Its distribution is centered near 155°. We have observed similar distributions for oligosaccharides

containing α-L-Ara*f*,[19] which is a pentose with the same configuration of substituents on the furanose ring.

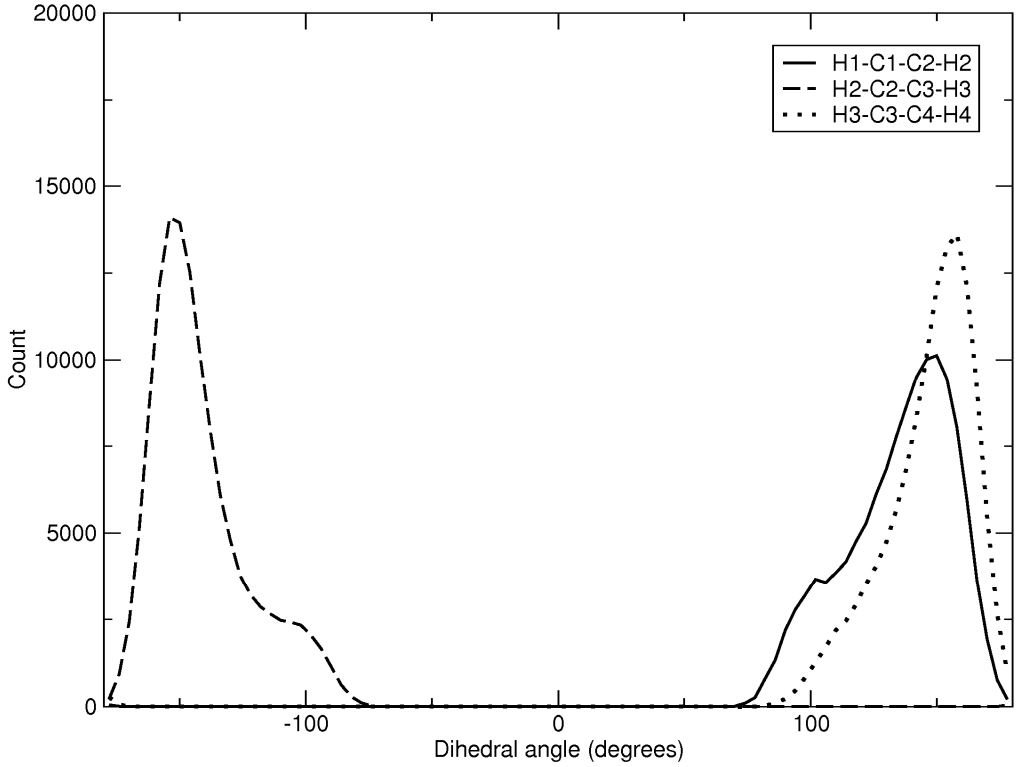

Figure 3.10. Histograms for the ring dihedral angles for **3.2**. The solid line is for H1–C1–C2–H2, the long dashed line is for H2–C2–C3–H3, and the dotted line is for H3–C3–C4–H4.

Unlike for **3.2**, we observe two distinct distributions of ring conformation in the MD simulation of **3.1** (Figure 3.11). The major population is centered near $P = -12°$, which is the ^{2}E conformation. The minor population, like that of **3.2**, is centered near $P = 135°$, which is between the ^{1}E and $^1T_2$ conformations. When the MD distribution is fit to two Gaussian functions (eq. 3.17), the resulting equation does not correspond to the data as nicely as it does with **3.2**. For **3.1**, the fit has an $r^2 = 0.943$, but the fit was almost perfect for **3.2** ($r^2 = 0.994$). One

reason for the worse fit for **3.1** is because the major distribution does not have a perfect Gaussian curve; rather, it has a long tail on the positive side of the peak. Despite the lower value for r^2, we can determine the ratio between the two populations by fitting the data to two Gaussian curves. The major population is present 78% of the time, and the minor population is present 22% of the time. The MD results also agree favorably with the PSEUROT results (Section 2.3.5). PSEUROT predicts an 88:12 ^{2}E–^{1}E conformational equilibrium.

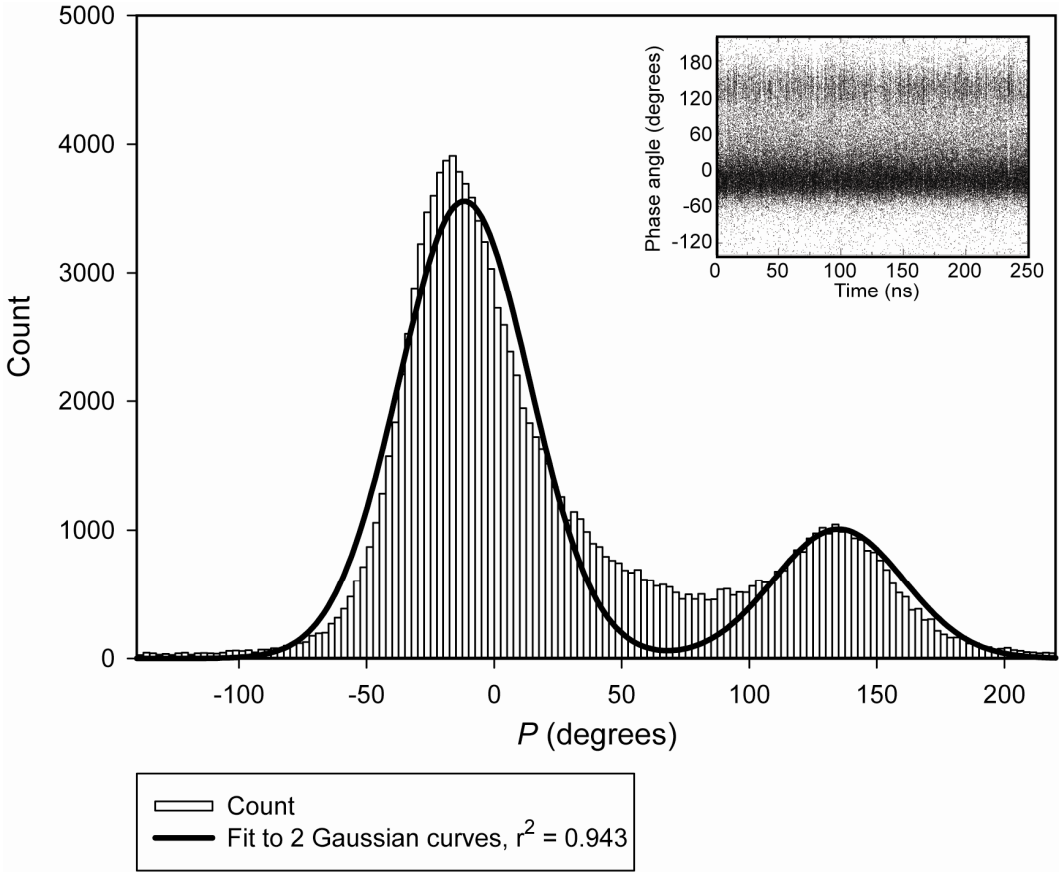

Figure 3.11. Histogram of pseudorotational phase angle *P* for **3.1** fit to two Gaussian functions (thick solid black line). The one population is centered at *P* = –11°, and the other is centered at *P* = 135°. The inset shows *P* versus time of the simulation.

The H2–C2–C3–H3 and H3–C3–C4–H4 dihedral angles for **3.1** (Figure 3.12) look very similar to those from **3.2**. For H2–C2–C3–H3, the major population is centered at –158°, and the minor population is centered near –94°. The H3–C3–C4–H4 torsion appears to have only a shoulder for the minor population, near 118°, and the major population is centered at 154°. Unsurprisingly, the two populations for the H1–C1–C2–H2 dihedral angle are near 0°, reflecting the *cis* orientation of H1 and H2 in **3.1**. The major conformation is centered near 34°, and the minor one is near –34°. We also observed similar distributions for the ring dihedrals of β-D-Ara*f*[18] – a pentose with the enantiomeric configuration for the furanose ring.

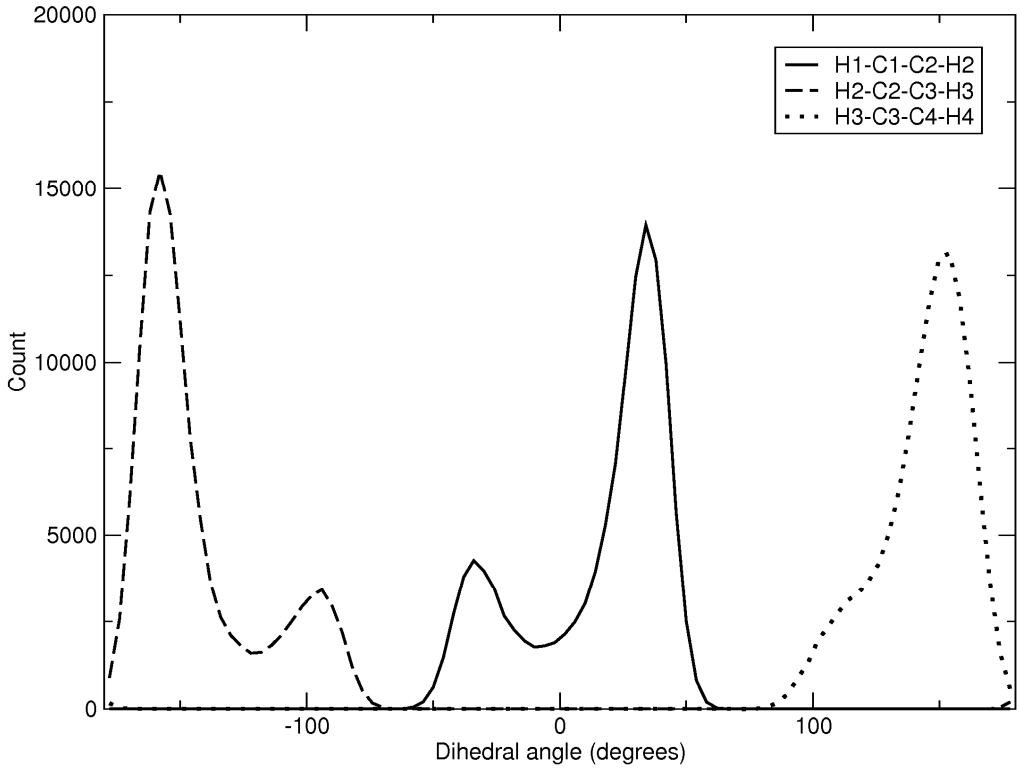

Figure 3.12. Histograms for the ring dihedral angles for **3.1**. The solid line is for H1–C1–C2–H2, the long dashed line is for H2–C2–C3–H3, and the dotted line is for H3–C3–C4–H4.

3.3.4.2. Conformation about the C4–C5 bond

In previous MD studies on arabinofuranoside systems,[37,38] we found simulations of 200 ns were necessary to achieve convergence of the C4–C5 rotamer populations. We observed convergence of the C4–C5 rotamers of **3.2** in 250 ns simulations, as shown in Figure 3.13. Although the distribution changes little throughout the simulation, the variation in the mean[48] is not 3% or less until after 220 ns. Integrating the area under the curves in the histogram shown in Figure 3.14 give us the overall distribution for each rotamer, which 97 ± 3% *gg*, 1 ± 1% *tg*, and 2 ± 1% *gt*. The dominant conformation is *gg*, which is also the major conformer predicted using the limiting values approach (Section 3.3.3.1). However, neither of the other rotamers are substantially populated over the course of the simulation, in contrast with the results presented earlier.

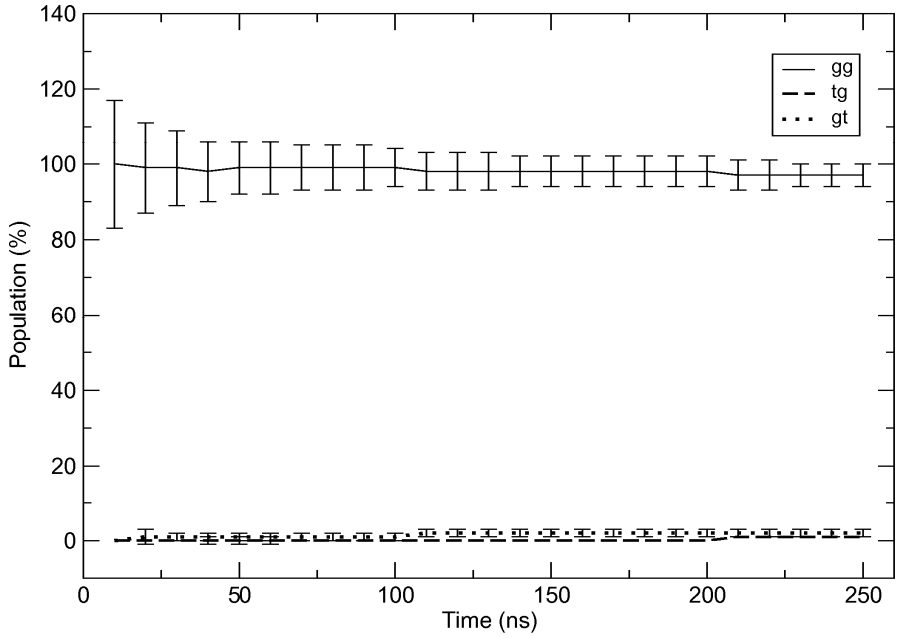

Figure 3.13. Convergence of the C4–C5 rotamer distribution of **3.2** as a function of simulation time.

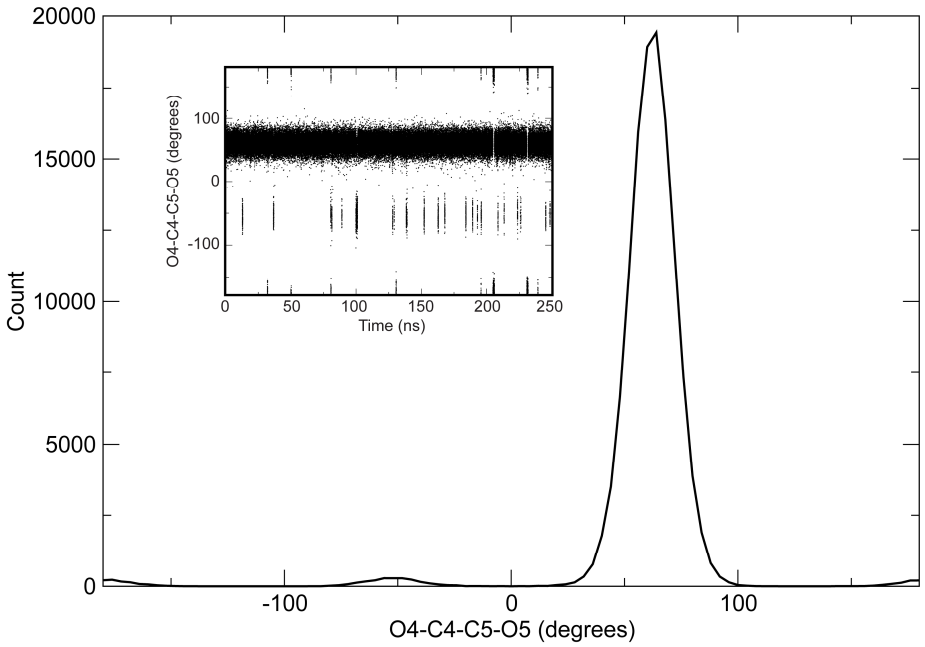

Figure 3.14. Histogram of the O4–C4–C5–O5 dihedral angle for **3.2**. The inset shows the same angle over the time of the simulation.

We tried altering the simulation conditions because the results from the MD simulation of **3.2** differed quite substantially from what we calculated using the limiting values approach. However, none of the parameters we varied in the solution simulations significantly altered the rotamers populations along the C4–C5 bond. The results discussed above were run with the Berendsen[42] thermostat; changing to the Langevin[43] thermostat gave exactly the same rotamer distribution. Raising the simulation temperature to 370 K, with either thermostat, resulted in a small increase in the *gt* rotamer to 5%. Altering the initial conformation of **3.2** had no effect, so it did not appear that the molecule was trapped in one conformation. Using either the TIP4P[41] or TIP5P[49] water models led to 100% of the population in the *gg* rotamer. We constrained the furanose ring into either the E_3 or ^1E conformation, which are the centers of the populations of ring

conformations (Figure 3.9). Neither ring conformation affected the C4–C5 rotamers. We biased the partial charges used in the simulations to those from only the *gt* or *tg* rotamers, and the new charges had no effect on the rotamer distribution. Finally, we ran a short 50 ns simulation in the gas phase. While this calculation did not converge, it was the only one to produce different C4–C5 rotamer populations: 74 ± 7% *gg*, 2 ± 1% *tg*, and 24 ± 4% *gt*.

Despite the unsatisfying results for the C4–C5 rotamers of **3.2**, we proceeded with simulations on **3.1**. Similar to **3.2**, the rotamer populations for **3.1** did not show variations in the mean of 3% or less until after 220 ns (Figure 3.15). However, the final converged values were similar to those observed at 50 ns. The rotamer distribution over the course of the simulation was 94 ± 3% *gg*, 3 ± 1% *tg*, and 3 ± 1% *gt* (Figure 3.16), very similar to that observed for **3.2**. For **3.1**, the major conformer populated in the MD simulation is not even the same one that was predicted using the limiting values approach (Section 3.3.3.1). Also, the anomeric configuration clearly has little effect on the distribution of rotamers about the C4–C5 bond in MD simulations using GLYCAM06.

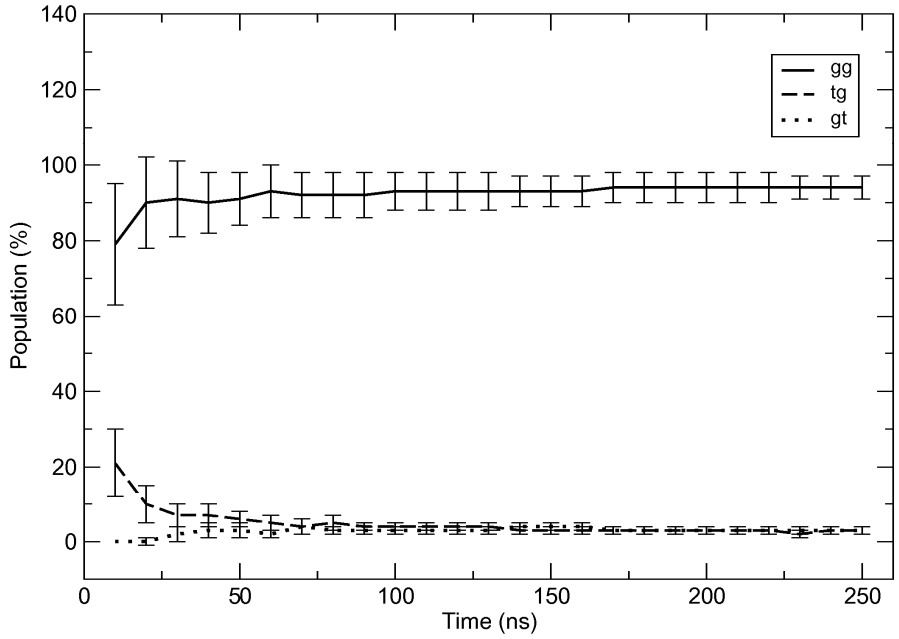

Figure 3.15. Convergence of the C4–C5 rotamer distribution of **3.1** as a function of simulation time.

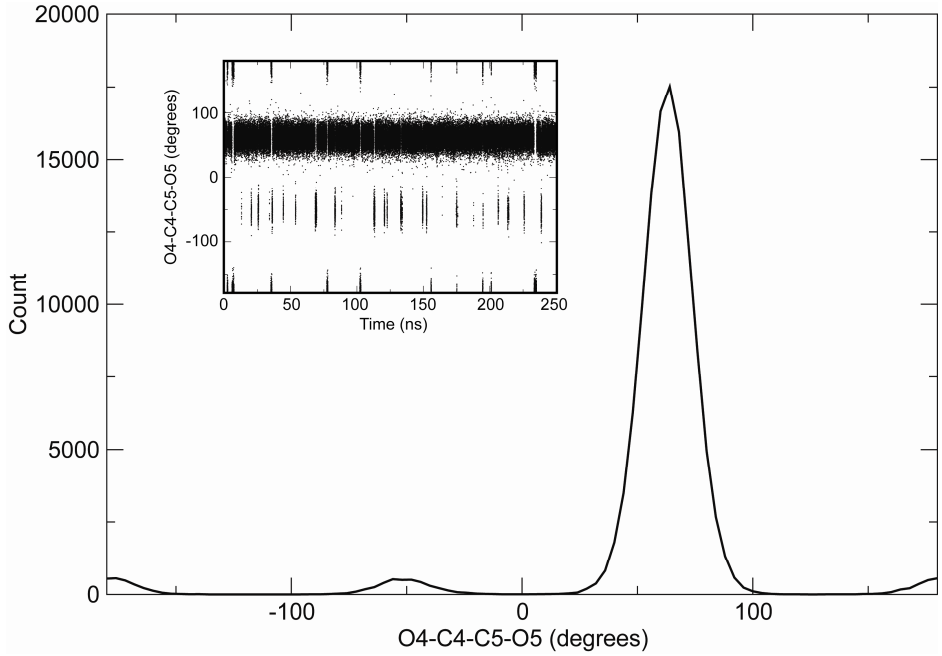

Figure 3.16. Histogram of the O4–C4–C5–O5 dihedral angle for **3.1**. The inset shows the same angle over the time of the simulation.

Because **3.1** and **3.2** both showed similar rotamer distributions about the C4–C5 bond (Figure 3.14 and Figure 3.16), we were curious if other hexofuranosides would behave the same way in MD simulations with GLYCAM06. Simulations were performed as described in Section 3.2.3 on the α- and β-methyl glycosides of glucofuranose (Glc*f*, **3.3** and **3.4**, Figure 3.17), allofuranose (All*f*, **3.5** and **3.6**, Figure 3.17), and gulofuranose (Gul*f*, **3.7** and **3.8**, Figure 3.17). Both Glc*f* and Gul*f* have *cis* orientation of the C3 and C4 substituents, and both Gal*f* and All*f* have *trans* orientation of the C3 and C4 substituents. Thus, if the C3 hydroxyl influences the rotamers about the C4–C5 bond, one might expect MD simulations on Glc*f* and Gul*f* to result in the same rotamer distributions, and simulations of Gal*f* and All*f* to also yield the same results.

The populations of the C4–C5 rotamers of **3.3** through **3.8** from 250 ns MD simulations with TIP3P water are shown in Table 3.3. None of the rotamer distributions are similar to those of **3.1** or **3.2**. All have at least two rotamers significantly populated during the simulation. For the glucofuranosides **3.3** and **3.4**, the *tg* rotamer is occupied about three times as often as the *gg* rotamer, and the *gt* rotamer does not occur very frequently. The allofuranosides **3.5** and **3.6** differ the most between anomers. For the α-anomer **3.5**, the *gt* rotamer dominates, but for the β-anomer **3.6**, all three rotamers occur in similar amounts. While Gul*f* and Glc*f* have the same relative orientation between the C3 and C4 substituents, both have a different dominant rotamer. For both **3.7** and **3.8**, the *gg* orientation occurs most frequently, followed by *gt* then the sparsely populated *tg*.

Based on these results, **3.1** and **3.2** are unique in their behavior in GLYCAM06. However, we cannot say if the rotamer populations that GLYCAM06 predicts for **3.3–3.8** are accurate due to the lack of experimental vicinal coupling constants, especially $^{3}J_{H4,C6}$.

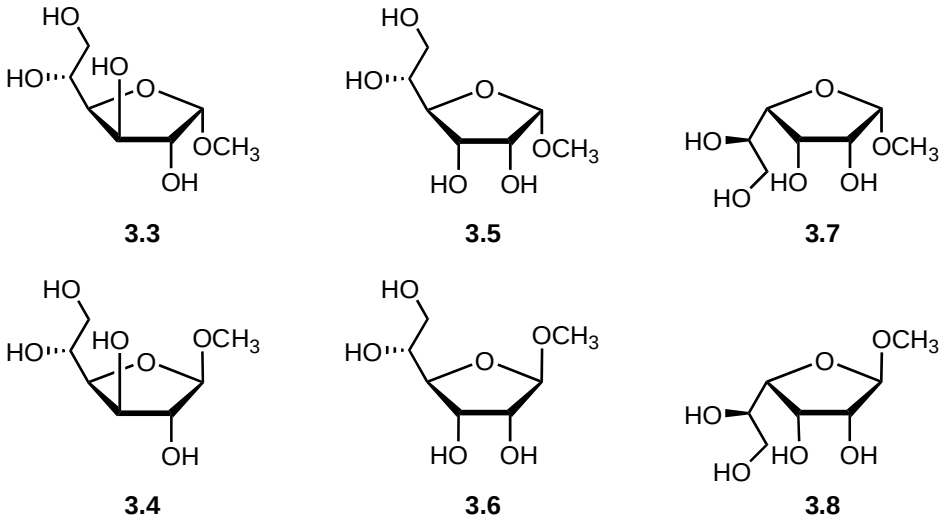

Figure 3.17. Other methyl furanosides studied in AMBER/GLYCAM06 simulations.

Table 3.3. C4–C5 rotamer populations from 250 ns MD simulations of **3.3**–**3.8**.

	C4–C5 rotamer populations
3.3	21 ± 2% *gg* : 76 ± 3% *tg* : 3 ± 1% *gt*
3.4	26 ± 2% *gg* : 68 ± 3% *tg* : 6 ± 1% *gt*
3.5	11 ± 1% *gg* : 31 ± 2% *tg* : 58 ± 3% *gt*
3.6	31 ± 2% *gg* : 42 ± 3% *tg* : 27 ± 2% *gt*
3.7	68 ± 3% *gg* : 2 ± 1% *tg* : 31 ± 2% *gt*
3.8	61 ± 3% *gg* : 3 ± 1% *tg* : 36 ± 2% *gt*

We also wanted to determine if ring size played a role in the in the rotamers observed for the C4–C5 bond. Thus, we ran AMBER/GLYCAM06 simulations on methyl β-D-*glycero*-D-*galacto*-heptopyranoside **3.9** and methyl β-D-*glycero*-D-*gluco*-heptopyranoside **3.10** (Figure 3.18) using the same methods described in Section 3.2.3. The relative orientation for the C4 and C5 substitutents on **3.9** is *trans*, and it is opposite for **3.10**. Thus, we might expect that the C5–C6 rotamers of **3.10** would behave the same way as **3.1** or **3.2**, if the C4 substituent on the heptopyranosides influences the rotamers about the C5–C6 bond. (Note that the C5–C6 bond is the first exocyclic bond for the heptopyranoside, and is equivalent to the C4–C5 bond in **3.1** or **3.2**.) Neither **3.9** nor **3.10** has only one C5–C6 rotamer populated in the MD simulations. For **3.9**, the C5–C6 rotamer distribution is 16 ± 2% *gg* : 83 ± 3% *tg* : 1 ± 1% *gt*. For **3.10**, the C5–C6 rotamer distribution is 65 ± 3% *gg* : 15 ± 2% *tg* : 20 ± 2% *gt*. As is the case for **3.3–3.8**, there are no experimental vicinal coupling constants for **3.9** and **3.10** to compare to.

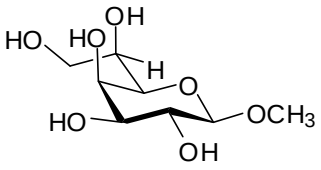

3.9

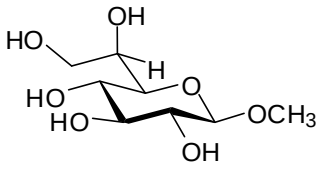

3.10

Figure 3.18. Heptopyranosides studied in AMBER/GLYCAM06 simulations.

3.3.4.3. Conformation about the C5–C6 bond

For **3.2**, the rotamers about the C5–C6 bond converged, i.e., the variation in the mean was 3% or less for each population (Figure 3.19) after 180 ns. Unlike

the C4–C5 bond, each rotamer about C5–C6 is populated, and the distribution seen at 50 ns is similar to the distribution seen after 250 ns. The final distribution after a 250 ns simulation is 65 ± 3% *gt*, 28 ± 2% *tg*, and 7 ± 1% *gg* (Figure 3.20), which is remarkably similar to the populations that the limiting values method predicted (Section 3.3.3.2).

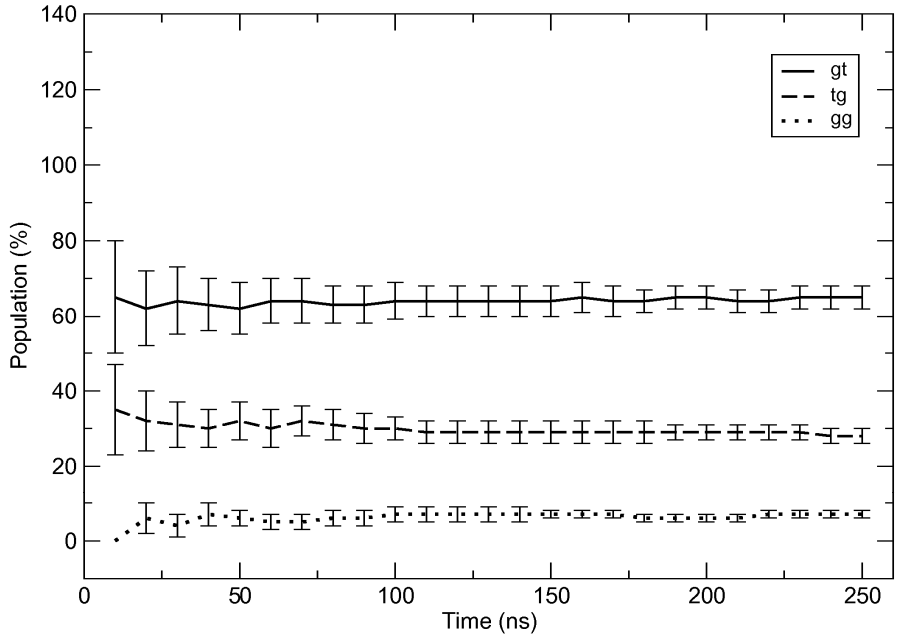

Figure 3.19. Convergence of the C5–C6 rotamer distribution of **3.2** as a function of simulation time.

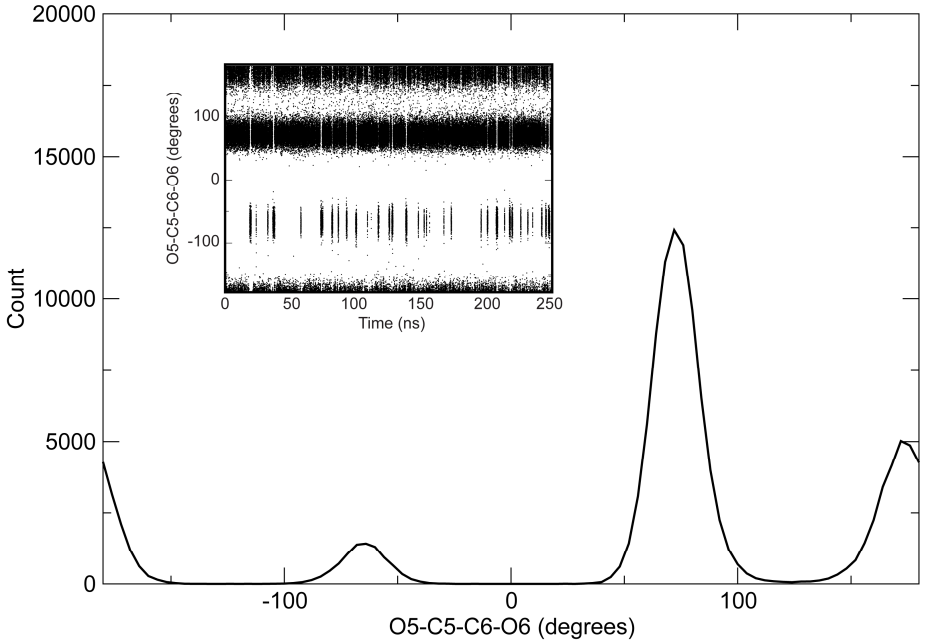

Figure 3.20. Histogram of the O5–C5–C6–O6 dihedral angle for **3.2**. The inset shows the same angle over the time of the simulation.

Just as we saw for the C4–C5 bond, rotamers about the C5–C6 bond take on similar values for both **3.1** and **3.2**. The rotamers for **3.1** also converged after 180 ns, showing variations in the mean of 3% or less for each conformation (Figure 3.21). The populations seen in the first 50 ns of the simulation differ significantly from the final distribution seen after 250 ns. After integrating the histogram shown in Figure 3.22, the rotamer distribution for **3.1** is 64 ± 3% *gt*, 29 ± 2% *tg*, and 7 ± 1% *gg* – the same distribution (within error) as we saw for **3.2**. Also, the populations obtained from MD simulation agree nicely with those determined using the limiting values approach (Section 3.3.3.2).

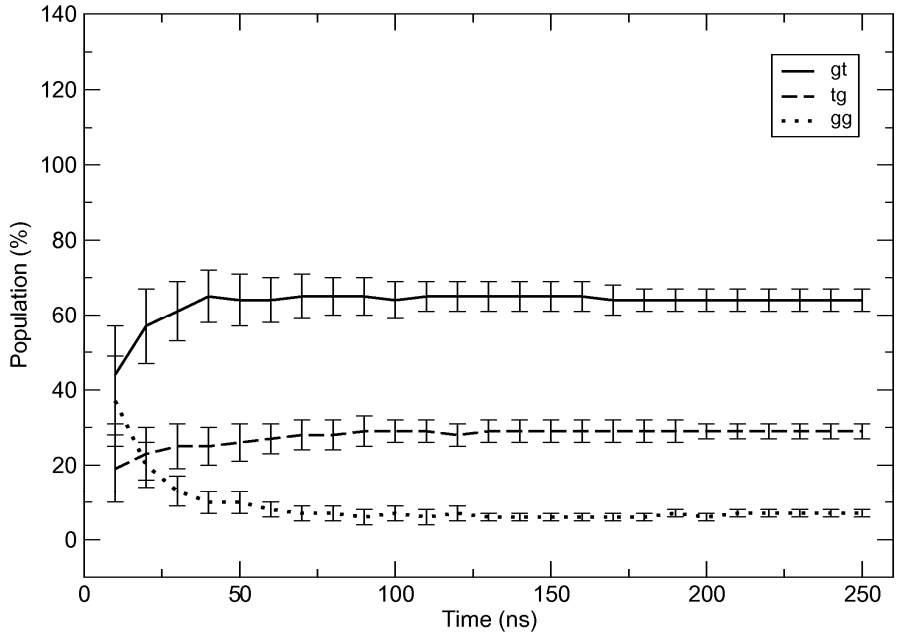

Figure 3.21. Convergence of the C5–C6 rotamer distribution of **3.1** as a function of simulation time.

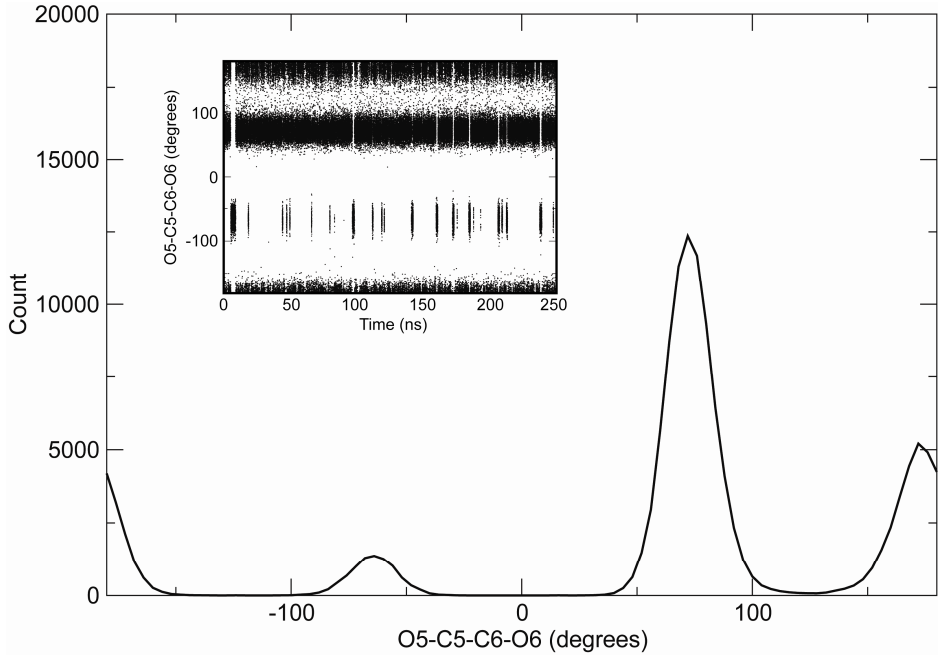

Figure 3.22. Histogram of the O5–C5–C6–O6 dihedral angle for **3.1**. The inset shows the same angle over the time of the simulation.

As with the C4–C5 rotamers, we wanted to see if the C5–C6 rotamers for **3.3** through **3.8** showed similar distributions to **3.1** and **3.2** (Table 3.4). The populations for the C5–C6 rotamer differed among all the hexofuranosides. For the glucofuranosides **3.3** and **3.4**, the *gt* rotamer dominates, just as it does for the galactofuranosides **3.1** and **3.2**. However, for **3.3** and **3.4**, the *gg* rotamer is also significantly populated, not the *tg* rotamer like **3.1** and **3.2**. For the allo- and gulofuranosides **3.5** through **3.8**, all three rotamers are significantly populated. From these results, it appears that relative orientation of the C3 and C4 substituents alone does not determine the configuration about the C5–C6 bond, because all four saccharides yield different results in the MD simulations. Instead, it appears that the overall configuration of the furanoside affects the rotamers about both exocyclic bonds.

Table 3.4. C5–C6 rotamer populations from 250 ns MD simulations of **3.3**–**3.8**.

	C5–C6 rotamer populations
3.3	55 ± 3% *gt* : 7 ± 1% *tg* : 38 ± 2% *gg*
3.4	59 ± 3% *gt* : 9 ± 1% *tg* : 32 ± 2% *gg*
3.5	30 ± 2% *gt* : 41 ± 3% *tg* : 30 ± 2% *gg*
3.6	42 ± 3% *gt* : 28 ± 2% *tg* : 30 ± 2% *gg*
3.7	39 ± 2% *gt* : 39 ± 2% *tg* : 23 ± 2% *gg*
3.8	43 ± 3% *gt* : 32 ± 2% *tg* : 25 ± 2% *gg*

For the C6–C7 bond in heptopyranosides **3.9** and **3.10**, the *gt* rotamer is dominant for both. For **3.9**, the C6–C7 rotamers are 56 ± 3% *gt* : 5 ± 1% *tg* : 39 ± 2% *gg*, and for **3.10**, they are 57 ± 3% *gt* : 28 ± 2% *tg* : 15 ± 2% *gg*. Like **3.3** and

3.4, the *gt* rotamer is present about twice as often as the *gg* rotamer in **3.9**, while the *tg* rotamer is sparsely populated. The glucofuranosides have a *cis* relationship between the C3 and C4 substituents; similarly, **3.9** has a *cis* relationship between the C4 and C5 substituents. Likewise, the rotamer distribution seen for **3.10** is similar to those seen for **3.1** and **3.2**. The C4 and C5 substituents in **3.10** are in a *trans* relationship, just as the C3 and C4 substituents are in the galactofuranosides. Based on the C5–C6 rotamers for **3.1** through **3.8**, and the C6–C7 rotamers for **3.9** and **3.10**, the relative orientation of the hydroxyl group three bonds away appears to affect the rotamers along both the C5–C6 and C6–C7 bonds.

3.3.4.4. Coupling constants from MD simulations

In Sections 3.3.4.1 though 3.3.4.3, we compared the results from MD simulations to those from PSEUROT or from the limiting values method. Both the program PSEUROT and the limiting values method have built in assumptions that may not be applicable to every system. PSEUROT is a purely mathematical algorithm; thus, it may return chemically unreasonably conformations. The limiting values approach for determining rotamer populations requires some knowledge of the dihedral angles associated with each of the staggered rotamers. Obtaining average coupling constants from an MD simulation provides a *direct comparison* between experiment and calculation.[17-19]

Table 3.5 lists the experimental vicinal coupling constants for **3.1** and **3.2**, as well as those determined from MD simulations. The $^{3}J_{H,H}$ or $^{3}J_{H,C}$ values from the MD simulations were calculated using the Karplus-like relationships described in Section 3.3.1 (eq. 3.10–3.16) and averaged over the entire

simulation, as described in eq. 3.9 in the introduction. The errors in the MD-derived coupling constants are simply the standard deviation for the ring couplings $^3J_{H1,H2}$, $^3J_{H2,H3}$, and $^3J_{H3,H4}$. For the exocyclic couplings – $^3J_{H4,H5}$, $^3J_{H4,C6}$, $^3J_{H5,H6R}$, and $^3J_{H5,H6S}$ – the average and standard deviation was determined for each rotamer, then the three populations and their standard deviations were averaged.

Table 3.5. Comparison between the coupling constants from experiment and from MD simulations in **3.1** and **3.2**.

	Experimental[a] 3.1 (Hz)	**MD-derived 3.1 (Hz)**	**Experimental[a] 3.2 (Hz)**	**MD-derived 3.2 (Hz)**
$^3J_{H1,H2}$ (Hz)	4.5	5.6 ± 1.1	2.0	3.3 ± 2.3
$^3J_{H2,H3}$ (Hz)	8.0	4.5 ± 2.7	3.6	4.0 ± 2.3
$^3J_{H3,H4}$ (Hz)	7.1	5.7 ± 2.6	6.2	6.2 ± 2.6
$^3J_{H4,H5}$ (Hz)	6.0	2.0 ± 0.8	4.4	1.7 ± 0.7
$^3J_{H4,C6}$ (Hz)	3.0	2.2 ± 1.4	1.6	2.1 ± 1.3
$^3J_{H5,H6}$ (Hz)	7.0	7.0 ± 1.9	7.4	7.0 ± 1.9
$^3J_{H5,H6'}$ (Hz)	3.9	4.4 ± 1.1	4.4	4.3 ± 1.1

[a] From 1D ^{1}H NMR or EXSIDE spectra at 600 MHz in D_2O (Sections 2.3.4 and 3.3.2). The error in the experimental values is estimated to be ± 0.2 Hz.

For **3.1**, the MD value for $^3J_{H1,H2}$ is within error of the experimental value. However, the MD values for $^3J_{H2,H3}$ and $^3J_{H3,H4}$ do not agree with the experimental values, indicating that the ring conformations from the MD simulations do not reflect the actual solution conformation of **3.1**. Similarly, the values for $^3J_{H4,H5}$ and $^3J_{H4,C6}$ obtained in the AMBER/GLYCAM06 simulations vary substantially from experiment. Presumably, the C4–C5 is not locked into the one conformation

observed in the MD simulation. Very good agreement is seen between experiment and simulation for $^3J_{H5,H6R}$, and the value for $^3J_{H5,H6S}$ obtained from MD is also within error of the experimental value.

All of the ring couplings for **3.2** agree nicely between experiment and simulation, especially $^3J_{H3,H4}$. Thus the ring conformation that is present in solution is well represented by the distribution seen in Figure 3.9. As with **3.1**, the values for $^3J_{H4,H5}$ and $^3J_{H4,C6}$ from the simulation vary substantially from the experimental values for **3.2**. Also, while the MD simulations for **3.1** and **3.2** predict similar rotamer distributions for the C4–C5 bond, the experimental values for $^3J_{H4,H5}$ and $^3J_{H4,C6}$ are not the same. Therefore, the anomeric configuration of the galactofuranose ring has some effect on the conformation about the C4–C5 bond, in addition to ring conformation. The anomeric configuration seems to have little effect on the C5–C6 conformation, as the experimental values for $^3J_{H5,H6R}$ and $^3J_{H5,H6S}$ are quite similar between **3.1** and **3.2**. The calculated values for $^3J_{H5,H6R}$ and $^3J_{H5,H6S}$ are also similar between **3.1** and **3.2**, which is not surprising as the distributions seen in Figure 3.20 and Figure 3.22 are the same within error. MD simulations on **3.2** seem to accurately represent the solution conformation for the C5–C6 bond.

3.4. Conclusions

In this chapter, we present new Karplus-like equations (eq. 3.10–3.16) that are specific for galactofuranosides. The new equations for the ring couplings $^3J_{H1,H2}$, $^3J_{H2,H3}$, and $^3J_{H3,H4}$ all agree well with the empirical equation used in in the

program PSEUROT (eq. 3.5), especially for the range of $^3J_{H,H}$ that are allowed by the ring. For the exocyclic bonds, we observed better agreement between the empirical equation and the equations for the C5–C6 bond. For the C4–C5 bond, the poor agreement between the empirical equation and the equation for $^3J_{H4,H5}$ is pronounced for the *tg* conformations (50–100°). Moreover, for $^3J_{H4,C6}$, the empirical equation is not symmetric about zero, which is a feature of our calculated equation.

We used the new Karplus-like relationships to evaluate the conformation about the exocyclic bonds of **3.1** and **3.2** using the limiting values approach. They were also used to calculate average coupling constants from MD simulations. For the α-anomer **3.1**, we saw poor agreement between the experimental and calculated coupling constants along the ring and along the C4–C5 bond; however, the MD values agreed well for the couplings along the C5–C6 bond. Previously, we had seen similarly poor agreement for the ring couplings of β-D-arabinofuranosides with the GLYCAM06 force field,[18] which implies that this force field is not an appropriate model for either β-D-arabinofuranosides or α-D-galactofuranosides. With the β-anomer **3.2**, we also saw good agreement for the C5–C6 couplings, and additionally, the ring couplings were similar between experiment and calculations. The C4–C5 couplings still show poor agreement for **3.2**.

The limiting values approach for the C5–C6 bond give similar rotamer distributions as the MD simulations, while the C4–C5 populations differ significantly between the two methods. There is essentially one rotamer for the

C4–C5 bond for both **3.1** and **3.2** during the entire MD simulation. Varying the thermostat, temperature, water model, and partial charges all have no effect on the rotamers about this bond. We previously saw distorted populations along the C4–C5 bond of oligosaccharides of α-L-Ara*f*; that is, the calculated coupling constants for the trisaccharide and hexasaccharide show worse agreement with experiment than the monosaccharide.[17,19] Furthermore, the C4–C5 bond behaves differently in AMBER/GLYCAM06 simulations of Gal*f* than simulations of other hexofuranosides. All these results indicate that the GLYCAM06 parameters for the C4–C5 bond in Gal*f* are not appropriate. We will address this, along with the ring conformation of **3.1**, in the next chapter.

3.5. References

1. Completo, G. C.; Lowary, T. L. *J. Org. Chem.* **2008**, *73*, 4513–4525.
2. Szarek, W. A.; Zamojski, A.; Tiwari, K. N.; Ison, E. R. *Tetrahedron Lett.* **1986**, *27*, 3827–3830.
3. Karplus, M. *J. Chem. Phys.* **1959**, *30*, 11–15.
4. Karplus, M. *J. Am. Chem. Soc.* **1963**, *85*, 2870–2871.
5. Lemieux, R. U.; Kullnig, R. K.; Moir, R. Y. *J. Am. Chem. Soc.* **1958**, *80*, 2237–2242.
6. Pachler, K. G. R. *Tetrahedron* **1971**, *27*, 187–199.
7. Pachler, K. G. R. *J. Chem. Soc., Perkin Trans. 2* **1972**, 1936–1940.
8. Haasnoot, C. A. G.; Deleeuw, F.; Altona, C. *Tetrahedron* **1980**, *36*, 2783–2792.
9. Allinger, N. L. Calculation of Molecular Structure and Energy by Force-Field Methods. In *Advances in Physical Organic Chemistry*, Gold, V.; Bethell, D., Eds. Academic Press: 1976; Vol. Volume 13, pp 1–82.

10. Donders, L. A.; Leeuw, F. A. A. M. D.; Altona, C. *Magn. Reson. Chem.* **1989**, *27*, 556–563.

11. Altona, C.; Ippel, J. H.; Hoekzema, A. J. A. W.; Erkelens, C.; Groesbeek, M.; Donders, L. A. *Magn. Reson. Chem.* **1989**, *27*, 564–576.

12. de Leeuw, F. A. A. M.; Altona, C. *J. Comput. Chem.* **1983**, *4*, 428–437.

13. van Wijk, J.; Haasnoot, C. A. G.; de Leeuw, F. A. A. M.; Huckriede, B. D.; Westra Hoekzema, A.; Altona, C. *PSEUROT 6.3*, Leiden Institute of Chemistry, Leiden University: Leiden, 1999.

14. Palermo, G.; Riccio, R.; Bifulco, G. *J. Org. Chem.* **2010**, *75*, 1982–1991.

15. Coxon, B. *Adv. Carbohydr. Chem. Biochem.* **2009**, *62*, 17–82.

16. Džakula, Ž.; Westler, W. M.; Edison, A. S.; Markley, J. L. *J. Am. Chem. Soc.* **1992**, *114*, 6195–6199.

17. Taha, H. A.; Castillo, N.; Sears, D. N.; Wasylishen, R. E.; Lowary, T. L. *J. Chem. Theory Comput.* **2010**, *6*, 212–222.

18. Taha, H. A.; Roy, P.-N.; Lowary, T. L. *J. Chem. Theory Comput.* **2011**, *7*, 420–432.

19. Islam, S. M.; Richards, M. R.; Taha, H. A.; Byrns, S. C.; Lowary, T. L.; Roy, P.-N. *J. Chem. Theory Comput.* **2011**, *7*, 2989–3000.

20. Yongye, A. B.; Foley, B. L.; Woods, R. J. *J. Phys. Chem. A* **2008**, *112*, 2634–2639.

21. Christensen, N. J.; Hansen, P. I.; Larsen, F. H.; Folkerman, T.; Motawia, M. S.; Engelsen, S. B. *Carbohydr. Res.* **2010**, *345*, 474–486.

22. Sattelle, B. M.; Almond, A. *J. Comput. Chem.* **2010**, *31*, 2932–2947.

23. Raman, E. P.; Guvench, O.; MacKerell, A. D. *J. Phys. Chem. B* **2010**, *114*, 12981–12994.

24. Hatcher, E.; Säwén, E.; Widmalm, G.; MacKerell, A. D. *J. Phys. Chem. B* **2011**, *115*, 597–608.

25. Guvench, O.; Mallajosyula, S. S.; Raman, E. P.; Hatcher, E.; Vanommeslaeghe, K.; Foster, T. J.; Jamison, F. W.; MacKerell, A. D. *J. Chem. Theory Comput.* **2011**, 3162–3180.

26. Mallajosyula, S. S.; MacKerell, A. D. *J. Phys. Chem. B* **2011**, 11215–11229.

27. Frisch, M. J.; Trucks, G. W.; Schlegel, H. B.; Scuseria, G. E.; Robb, M. A.; Cheeseman, J. R.; Montgomery, J. A., Jr.; Vreven, T.; Kudin, K. N.; Burant, J. C.; Millam, J. M.; Iyengar, S. S.; Tomasi, J.; Barone, V.; Mennucci, B.; Cossi, M.; Scalmani, G.; Rega, N.; Petersson, G. A.; Nakatsuji, H.; Hada, M.; Ehara, M.; Toyota, K.; Fukuda, R.; Hasegawa, J.; Ishida, M.; Nakajima, T.; Honda, Y.; Kitao, O.; Nakai, H.; Klene, M.; Li, X.; Knox, J. E.; Hratchian, H. P.; Cross, J. B.; Bakken, V.; Adamo, C.; Jaramillo, J.; Gomperts, R.; Stratmann, R. E.; Yazyev, O.; Austin, A. J.; Cammi, R.; Pomelli, C.; Ochterski, J. W.; Ayala, P. Y.; Morokuma, K.; Voth, G. A.; Salvador, P.; Dannenberg, J. J.; Zakrzewski, V. G.; Dapprich, S.; Daniels, A. D.; Strain, M. C.; Farkas, O.; Malick, D. K.; Rabuck, A. D.; Raghavachari, K.; Foresman, J. B.; Ortiz, J. V.; Cui, Q.; Baboul, A. G.; Clifford, S.; Cioslowski, J.; Stefanov, B. B.; Liu, G.; Liashenko, A.; Piskorz, P.; Komaromi, I.; Martin, R. L.; Fox, D. J.; Keith, T.; Al-Laham, M. A.; Peng, C. Y.; Nanayakkara, A.; Challacombe, M.; Gill, P. M. W.; Johnson, B.; Chen, W.; Wong, M. W.; Gonzalez, C.; Pople, J. A. *Gaussian 03* Revision C.02; Gaussian, Inc.: Wallingford, CT, 2004.

28. Stenutz, R.; Carmichael, I.; Widmalm, G.; Serianni, A. S. *J. Org. Chem.* **2002**, *67*, 949–958.

29. Becke, A. D. *J. Chem. Phys.* **1993**, *98*, 5648–5652.

30. Kendall, R. A.; Dunning, T. H.; Harrison, R. J. *J. Chem. Phys.* **1992**, *96*, 6796–6806.

31. Marquardt, D. W. *J. Soc. Indust. Appl. Math.* **1963**, *11*, 431–441.

32. Rassolov, V. A.; Ratner, M. A.; Pople, J. A.; Redfern, P. C.; Curtiss, L. A. *J. Comput. Chem.* **2001**, *22*, 976–984.

33. Krishnamurthy, V. V. *J. Magn. Reson., Ser A* **1996**, *121*, 33–41.

34. Otter, A.; Lemieux, R. U.; Ball, R. G.; Venot, A. P.; Hindsgaul, O.; Bundle, D. R. *Eur. J. Biochem.* **1999**, *259*, 295–303.

35. Case, D. A.; Darden, T. A.; T.E. Cheatham, I.; Simmerling, C. L.; Wang, J.; Duke, R. E.; Luo, R.; Crowley, M.; Walker, R. C.; Zhang, W.; Merz, K. M.; Wang, B.; Hayik, S.; Roitberg, A.; Seabra, G.; Kolossváry, I.; Wong, K. F.; Paesani, F.; Vanicek, J.; Wu, X.; Brozell, S. R.; Steinbrecher, T.; Golke, H.; Yang, L.; Tan, C.; Mongan, J.; Hornak, V.; Cui, G.; Mathews, D. H.; Seetin, M. G.; Saugi, C.; Babin, V.; Kollman, P. A. *AMBER 10*, Univeristy of California, San Francisco: 2008.

36. Kirschner, K. N.; Yongye, A. B.; Tschampel, S. M.; González-Outeiriño, J.; Daniels, C. R.; Lachele Foley, B.; Woods, R. J. *J. Comput. Chem.* **2008**, *29*, 622–655.

37. Seo, M.; Castillo, N.; Ganzynkowicz, R.; Daniels, C. R.; Woods, R. J.; Lowary, T. L.; Roy, P. N. *J. Chem. Theory Comput.* **2008**, *4*, 184–191.

38. Taha, H. A.; Castillo, N.; Roy, P.-N.; Lowary, T. L. *J. Chem. Theory Comput.* **2009**, *5*, 430–438.

39. Bayly, C. I.; Cieplak, P.; Cornell, W.; Kollman, P. A. *J. Phys. Chem.* **1993**, *97*, 10269–10280.

40. Macke, T. J.; Svrcek-Seiler, W. A.; Brown, R. A.; Kolossváry, I.; Bomble, Y. J.; Case, D. A.; Zhang, W.; Hou, T.; Schafmeister, C.; Ross, W. S.; Wang, J.; Cheatham, T. E. AmberTools Users' Manual. In The Scripps Research Institute: La Jolla, CA, 2008; p 19.

41. Jorgensen, W. L.; Chandrasekhar, J.; Madura, J. D.; Impey, R. W.; Klein, M. L. *J. Chem. Phys.* **1983**, *79*, 926–935.

42. Berendsen, H. J. C.; Postma, J. P. M.; Gunsteren, W. F. v.; DiNola, A.; Haak, J. R. *J. Chem. Phys.* **1984**, *81*, 3684–3690.

43. Adelman, S. A.; Doll, J. D. *J. Chem. Phys.* **1976**, *64*, 2375–2388.

44. Ryckaert, J.-P.; Ciccotti, G.; Berendsen, H. J. C. *J. Comput. Phys.* **1977**, *23*, 327–341.

45. Schmidt, J. M. *J. Biomol. NMR* **2007**, *37*, 287–301.

46. Wolfe, S. *Acc. Chem. Res.* **1972**, *5*, 102–111.

47. Bai, Y.; Lowary, T. L. *J. Org. Chem.* **2006**, *71*, 9658–9671.

48. Allen, M. P.; Tildesley, D. J. Errors in equilibrium averages. In *Computer Simulation of Liquids*, Calrendon Press: Oxford, UK, 1987; pp 192–195.

49. Mahoney, M. W.; Jorgensen, W. L. *J. Chem. Phys.* **2000**, *112*, 8910–8922.

Chapter 4:

Overcoming limitations in AMBER/GLYCAM simulations of methyl α- and β-D-galactofuranosides: Umbrella sampling and new torsion parameters

4.1. Introduction

In the previous chapter, molecular dynamics (MD) simulations on methyl α- and β-galactofuranosides (**4.1** and **4.2**, respectively, Figure 4.1) gave effectively one conformation about the C4–C5 bond (see Section 3.3.4.2). Furthermore, the $^{3}J_{H4,H5}$ values derived from the MD simulations show poor agreement with the experimental values (Table 3.5). Several attempts to overcome this disparity were unsuccessful. However, it is unclear whether the energy barriers separating the rotamers about the C4–C5 bond are too high to show adequate sampling. Calculating the potential of mean force (PMF, $W(\chi)$, eq. 4.1),[1-3] which is the free energy change along a reaction coordinate χ, will reveal the energy barriers for rotation about this bond in GLYCAM06.[4] In eq. 4.1, the $\rho(\chi)$ function is the Boltzmann weighted average for the reaction coordinate (eq. 4.2). The functions $V(q)$ and $\chi'(q)$ in eq. 4.2 are both dependent on the conformation q: $V(q)$ is the total energy of the system, and $\chi'(q)$ describes the reaction coordinate in terms of conformation. It should be noted that the reaction coordinate χ is not limited to rotation about a bond; rather, it can be any conformational change, including the separation between two atoms or pseudorotation about a five membered ring.[3,5]

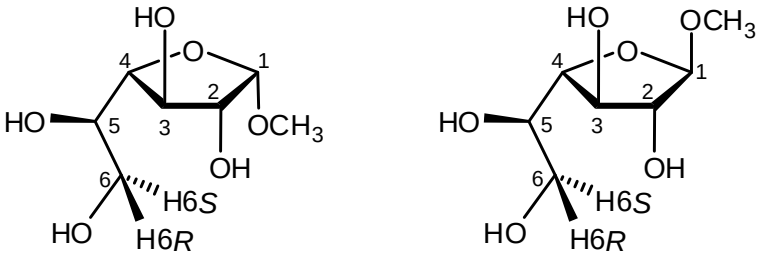

4.1 **4.2**

Figure 4.1. The structures of methyl α-D-galactofuranoside (**4.1**) and methyl β-D-galactofuranoside (**4.2**) with the carbon atoms numbered. The pro-*R* and pro-*S* hydrogens on C6 are labeled as H6*R* and H6*S*, respectively.

$$W(\chi) = -k_b T \ln\langle \rho(\chi) \rangle \qquad 4.1$$

$$\langle \rho(\chi) \rangle = \frac{\int dq\ \delta(\chi'(q) - \chi)\ e^{-V(q)/k_b T}}{\int dq\ e^{-V(q)/k_b T}} \qquad 4.2$$

If large energy barriers separate the C4–C5 rotamers of **4.1** and **4.2**, then determining the PMF from long MD simulations can give inaccurate results.[1,2] Umbrella sampling[6] techniques can overcome large energy barriers by artificially smoothing the potential energy surface (PES) through the application of a weighting function over a series of simulations. Each simulation restrains the system to a particular value of χ through a weighting function. An example of a harmonic weighting potential is shown in eq. 4.3, where k is a force constant and χ_r is the restrained value. Once all the individual simulations are complete, they can be combined to reveal the unbiased Boltzmann weighted average.

One popular technique to combine the simulations is the weighted histogram analysis method (WHAM),[3,5,7] introduced by Kumar and Kollman. An advantage of this algorithm is that it uses all the information in the individual

histograms, preventing the need for significant overlap between restrained simulations. WHAM involves two equations (eq. 4.4 and 4.5) with two unknowns – the Boltzmann weighted average $\rho(\chi)$ and the free energy constants f_j. Therefore, the WHAM equations must be solved iteratively and self-consistently. In eq. 4.4, n_j is the number of points in histogram h_j, and eq. 4.5 relates free energy constants f_j to the Boltzmann weighted average. Roux has written an excellent review of the method.[3]

$$V_b(\chi) = \frac{1}{2} k\,(\chi - \chi_r)^2 \qquad 4.3$$

$$\left\langle \rho(\chi) \right\rangle = \frac{\sum_{i=1}^{N} h_i(\chi)}{\sum_{j=1}^{N} n_i\, e^{-[V_b(\chi) - f_j]/k_b T}} \qquad 4.4$$

$$e^{-f_j / k_b T} = \int d\chi\; e^{-V_b(\chi)/k_b T} \left\langle \rho(\chi) \right\rangle \qquad 4.5$$

The energy barriers associated with rotation about a dihedral angle are determined by the force field used in the simulation. The form of the force field equation used by the AMBER 10[8] software package is shown in eq. 4.6.[9,10] There are bonding terms to describe bond stretching, angle bending, and dihedral angle rotation, all of which are in the form of harmonic potentials. There are also non-bonding terms to describe van der Waals and electrostatic interactions. The van der Waals forces are in the form of the Lennard–Jones 12-6 function, and the electrostatic term is a Coulomb potential. The bonding and non-bonding terms are summed over all N atoms in the system at each time step to give the potential energy of the system, $V(r^N)$. Other molecular mechanics (MM) software packages

may include additional terms in their force field equations, such as improper torsions, out-of-plane bending, and cross terms.[10-16]

$$V(r^N) = \overbrace{\sum_{bonds} \frac{K_r}{2}\left(r - r_{eq}\right)^2 + \sum_{angles} \frac{K_\theta}{2}\left(\theta - \theta_{eq}\right)^2 + \sum_{torsions} \frac{V_n}{2}\left(1 + \cos(n\phi - \gamma)\right)}^{bonding\ terms}$$
$$\underbrace{\cdots + \sum_{i=1}^{N} \sum_{j=i+1}^{N} \left(4\varepsilon_{ij}\left[\left(\frac{\sigma_{ij}}{r_{ij}}\right)^{12} - \left(\frac{\sigma_{ij}}{r_{ij}}\right)^{6}\right] + \frac{q_i q_j}{4\pi\varepsilon_o r_{ij}} \right)}_{non\text{-}bonding\ terms} \qquad 4.6$$

Guvench and MacKerell[17] have developed a Metropolis Monte Carlo[18] simulated annealing (MMCSA) procedure to determine force field parameters using two PES – one from quantum mechanical (QM) calculations and one from force field calculations. The MM PES is determined by setting the torsion parameters to be fit to zero then new force field terms are calculated to give the lowest root mean squared error (RMSE) to the QM PES (eq. 4.7). The difference between the QM energies, E_i^{QM}, and MM energies, E_i^{MM}, is minimized over all i conformations. An optional weighting factor w_i is included during the fitting processes to favor lower energy conformers, and a constant c is included to align the relative energies of the two PES.

$$RMSE = \sqrt{\frac{\sum_i w_i \left(E_i^{QM} - E_i^{MM} + c\right)^2}{\sum_i w_i}} \qquad 4.7$$

In this chapter, we present the use of WHAM to determine the free energy of rotation about the C4–C5 bonds of **4.1** and **4.2**. This information prompted us to examine new terms for the GLYCAM06 force field. The new terms were used in subsequent MD simulations to evaluate the solution-state conformation of **4.1** and **4.2** in conjunction with the new Karplus-like equations discussed in the previous chapter (eq. 3.10–3.16).

4.2. Methods

4.2.1. Umbrella sampling

The umbrella sampling simulations of **4.1** and **4.2** were run using the PMEMD module of AMBER 10[8] and the GLYCAM06 force field[4] with either the original or new torsion parameters for the O4–C4–C5–C6 and C3–C4–C5–C6 bonds. The O4–C4–C5–O5 dihedral angle was chosen as the reaction coordinate χ. This dihedral angle was restrained every 5° from –180° to 180° (for a total of 73 simulations), using a harmonic restraining potential (eq. 4.3) of 30 kcal (mol $rad^2)^{-1}$, and each simulation was run for 200 ps. These conditions were appropriate in previous studies in our group on arabinofuranoside monomers.[2]

Each simulation started from the same equilibrated structure. The equilibration phase started by minimizing the water molecules, while holding **4.1** or **4.2** fixed, then the entire system was minimized. Minimization was followed by simulated annealing, heating the system from 5 K to 300 K over 50 ps, then cooling back to 5 K over 50 ps. A final simulation was run, heating the system back to 300 K over 100 ps, then kept at a constant 300 K for 100 ps. All

simulations were performed under NPT conditions, used a 2 fs timestep, and included approximately 300 molecules of explicit TIP3P[19] water. The temperature was maintained using the Langevin thermostat,[20] with a collision frequency of 2.0 ps^{-1}, and the pressure was a constant 1 atm. All bonds to hydrogen were constrained using the SHAKE algorithm,[21] and 8 Å was the cutoff for non-bonding interactions. The PMF and Boltzmann weighted average were calculated using the WHAM software package of Grossfield.[22-24]

4.2.2. Development of new C4–C5 torsion parameters

Following the procedure of Guvench and MacKerell,[17] we calculated two gas-phase QM PES for both **4.1** and **4.2**, using a relaxed PES scan in Gaussian 03.[25] Geometries were optimized using HF/6-31G*,[26,27] and single-point energies were calculated using B3LYP/6-31++G(2d,2p)[28-30] for consistency with the GLYCAM06 force field.[4] Each PES for **4.1** or **4.2** constrained the furanose ring into one conformation, and the ring conformers chosen were the center of the populations observed in AMBER/GLYCAM06 simulations (Section 3.3.4.1). The first conformation for **4.1** was ^{2}E, and the C3–C4–O4–C1 dihedral angle was frozen at 0° to maintain the desired ring conformation. For **4.2**, the first conformation was E_3, and the C4–O4–C1–C2 dihedral angle was fixed at 0°. Both **4.1** and **4.2** had minor populations centered at the ^{1}E conformation, so a PES was calculated with this ring conformation for both, freezing the C2–C3–C4–O4 torsion at 0°.

For all of the PES, the O4–C4–C5–O5 and O5–C5–C6–O6 dihedral angles were varied separately from 0º to 360º in 15º increments, yielding 625 points for

each surface. When the O4–C4–C5–O5 was rotated, the O5–C5–C6–O6 angle was fixed, and vice versa. The C–C–O–H torsions were also fixed during geometry optimization to prevent the formation of intramolecular hydrogen bonds. The angles at which these bonds were fixed varied as a function of ring and C4–C5 and C5–C6 conformation.

The optimized geometries from the QM PES were used to calculate the gas-phase MM PES in the Sander module of the AMBER 10 program suite and using the GLYCAM06 force field. To not conflict with existing GLYCAM06 force field parameters, a new atom type, CF, was created and assigned to C6 in **4.1** and **4.2**. The torsion parameters for C6–C5–C4–C3 and C6–C5–C4–O4 were set to zero (see below) when calculating the MM surfaces to be used in the fitting procedure described in Section 4.1.

Figure 4.2 shows the Newman projection along the C4–C5 bond of **4.1** and **4.2**, with the O4–C4–C5–O5 dihedral angle labeled θ. There are nine separate equations in GLYCAM06 to define the potential energy V for rotation about the C4–C5 bond (Table 4.1, eq. 4.8–4.16). When these equations are all graphed, only the equations for O4–C4–C5–C6 and C3–C4–C5–C6 (eq. 4.14 and 4.15, respectively) lead to asymmetry in the overall equation for V. Therefore, these were the parameters that were fit using the MMCSA protocol.

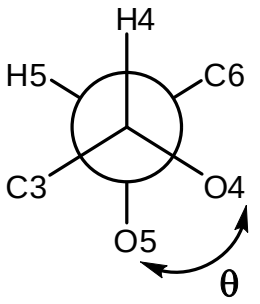

Figure 4.2. The O4–C4–C5–O5 dihedral angle, or θ, for **4.1** and **4.2**.

Table 4.1. Separate equations from GLYCAM06 to define the potential energy *V* about the C4–C5 bond.

Torsion	Value of torsion (in terms of θ)[a]	Eq. for *V*	
O4–C4–C5–O5	θ	$V = 0.45[1 + \cos(2\theta)] - 1.10[1 + \cos(\theta)]$	4.8
C3–C4–C5–O5	θ – 120º	$V = 0.10\{1 + \cos[3(\theta - 120)]\}$	4.9
H4–C4–C5–O5	θ + 120º	$V = 0.05\{1 + \cos[3(\theta + 120)]\}$	4.10
O4–C4–C5–H5	θ + 120º	$V = 0.05\{1 + \cos[3(\theta + 120)]\}$	4.11
C3–C4–C5–H5	θ	$V = 0.15[1 + \cos(3\theta)]$	4.12
H4–C4–C5–H5	θ – 120º	$V = 0.17\{1 + \cos[3(\theta - 120)]\}$	4.13
O4–C4–C5–C6	θ – 120º	$V = -0.27[1 + \cos(\theta - 120)]$	4.14
C3–C4–C5–C6	θ + 120º	$V = 0.45[1 + \cos(\theta + 120)]$	4.15
H4–C4–C5–C6	θ	$V = 0.15[1 + \cos(3\theta)]$	4.16

[a] The dihedral angle θ, O4–C4–C5–O5, is shown in Figure 4.2.

4.2.3. MD simulations with new torsion parameters

MD simulations of **4.1** and **4.2** were run using the PMEMD module of AMBER 10 and the GLYCAM06 force field with new torsion parameters for the

O4–C4–C5–C6 and C3–C4–C5–C6 bonds. All simulations were carried out for 250 ns with a 2 fs timestep in a box of approximately 300 TIP3P water molecules under periodic boundary conditions and using particle mesh Ewald summation for long-range interactions. The simulations were run under NPT conditions at 1 atm and 300 K. The temperature was maintained by the Berendsen[31] thermostat, and velocities were rescaled every 1 ps. All bonds containing hydrogens were fixed using the SHAKE[21] algorithm, and 8 Å was the cutoff for nonbonding interactions. Both the non-bonding and electrostatic interactions were not scaled over the course of the simulations.

The systems were first equilibrated by minimizing only the water molecules with 50 steps of steepest decent followed by 950 steps conjugate gradient minimization. Then the entire system, including **4.1** or **4.2**, was minimized in the same fashion. Minimization was followed by simulated annealing, heating the system from 5 K to 300 K over 50 ps, then cooling back to 5 K for 50 ps. Finally, the system was again heated from 5 K to 300 K over 100 ps and allowed to run at a constant 300 K for an additional 100 ps before the production period began.

4.3. Results and discussion

4.3.1. Umbrella sampling and WHAM for 4.1 and 4.2 with the original GLYCAM06 parameters

With the umbrella sampling simulations of **4.1** and **4.2**, we wanted to determine the free energy of rotation about the C4–C5 bond in solution. As the histograms in Figure 4.3 and Figure 4.4 show, the O4–C4–C5–O5 dihedral angle

was restrained to the desired values in all 73 windows along the reaction coordinate, indicating that the choice of restraining potential was appropriate. There are no deviations from the expected values, nor any gaps in the individual distributions. Overlap of the histograms is necessary for the WHAM analysis.[32]

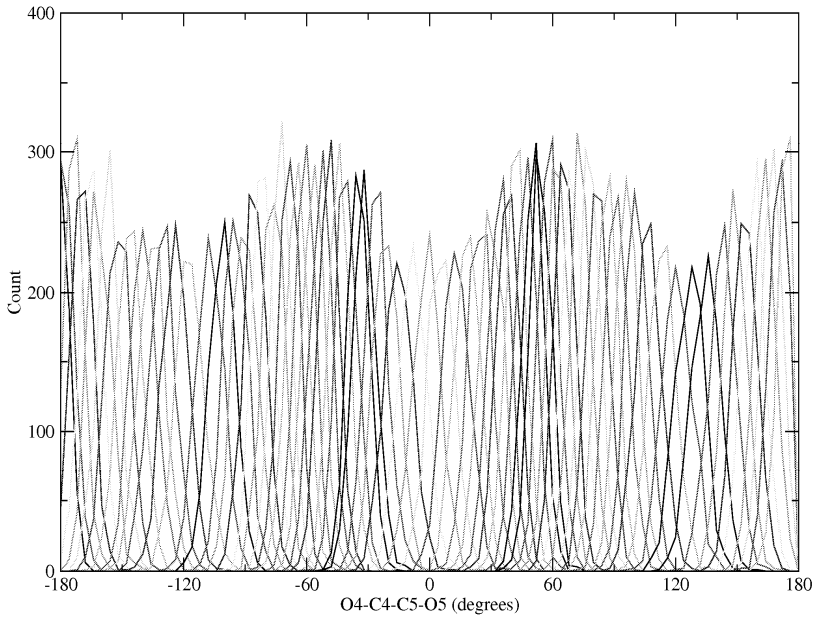

Figure 4.3. Histograms showing the O4–C4–C5–O5 dihedral angle distributions from each 5° window for **4.1**.

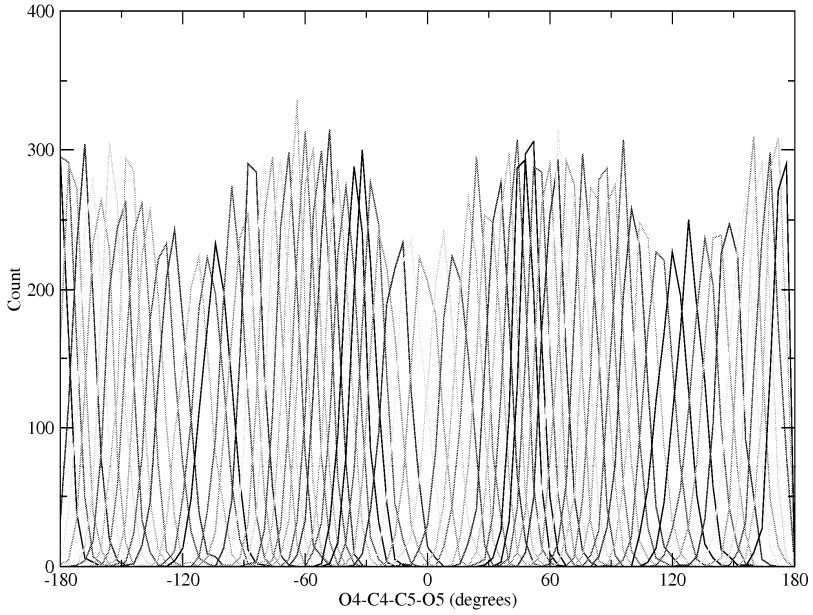

Figure 4.4. Histograms the O4–C4–C5–O5 dihedral angle distributions from each 5° window for **4.2**.

Once we confirmed that the individual windows gave the expected distributions, all the windows were combined to determine the rotamer populations and free energy of rotation using the WHAM equations, eq. 4.4 and 4.5. The rotamer distribution for **4.1** is shown in Figure 4.5. The distribution from the umbrella sampling calculations is very similar to that from long MD simulations (see also Figure 3.16). Long, unbiased MD simulations gave a ratio of 94 ± 3% *gg*, 3 ± 1% *tg*, and 3 ± 1% *gt*, while the WHAM analysis gave 93 ± 1% *gg*, 1 ± 1% *tg*, and 6 ± 3% *gt*.

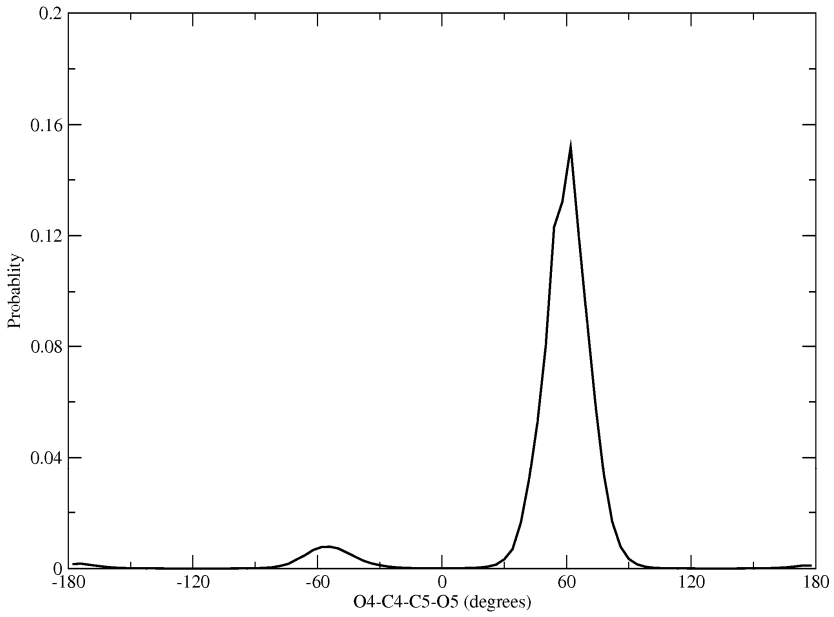

Figure 4.5. Rotamer distribution about the C4–C5 bond of **4.1**.

The free energy for rotation about the C4–C5 bond of **4.1** is shown in Figure 4.6. The global minimum occurs at an O4–C4–C5–O5 torsion of 58°, which is the *gg* conformation. There are two other minima – one for the *gt* conformation at –54° and one for the *tg* conformation at –174°. The energy difference between the *gg* and *gt* conformations is 1.8 kcal mol^{-1}. Assuming a two-state model, eq. 4.17 predicts a 95:5 ratio of *gg:gt* with the calculated energy difference, which is observed in the long MD simulations. Therefore, the energy barriers between the rotamers along the C4–C5 bond are not too high to prevent adequate sampling in the long MD simulations. Rather, the calculated population reflects the energy differences between the rotamers.

$$\Delta G = RT \ln K \qquad 4.17$$

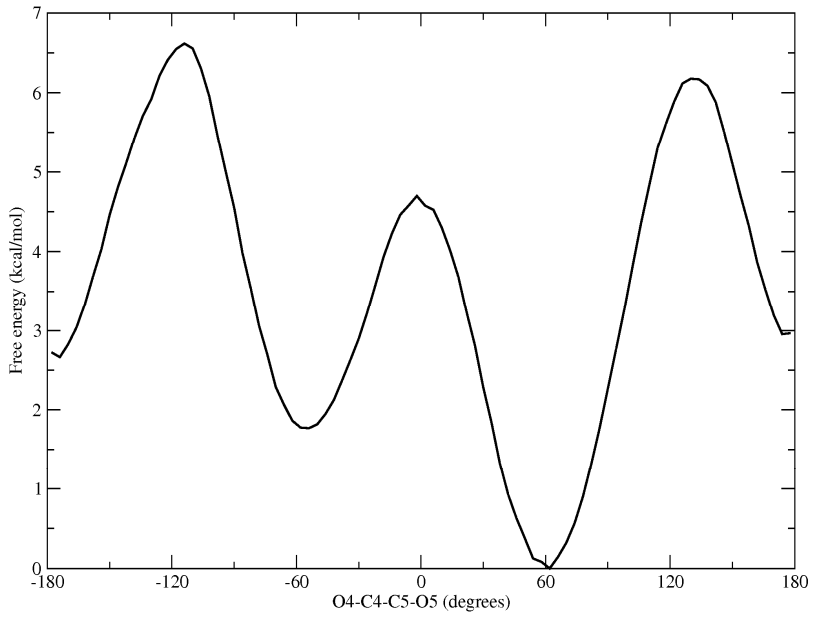

Figure 4.6. Free energy for rotation about the C4–C5 bond of **4.1**.

A similar rotamer distribution is seen after the WHAM analysis of **4.2** (Figure 4.7). The *gg* rotamer is heavily favored, while the other rotamers are sparsely populated. The WHAM equations gave 96 ± 1% *gg*, 1 ± 1% *tg*, and 3 ± 3% *gt*, which is similar to results above and from the long MD simulations of **4.2**: 97 ± 3% *gg*, 1 ± 1% *tg*, and 2 ± 1% *gt* (see also Figure 3.14).

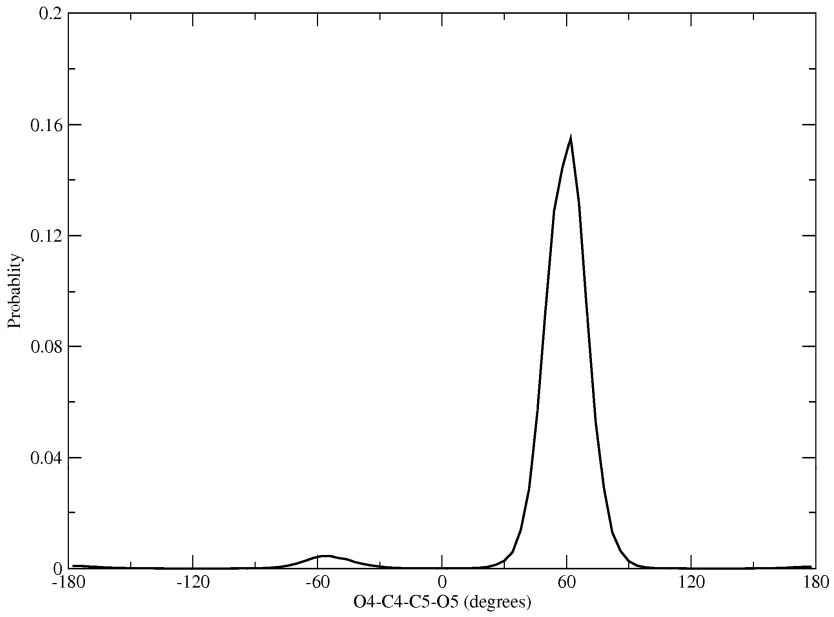

Figure 4.7. Rotamer distribution about the C4–C5 bond of **4.2**.

As with **4.1**, the global minimum for rotation about the C4–C5 bond of **4.2** is corresponds to the *gg* rotamer at 62° (Figure 4.8). The minimum for the *gt* rotamer at –54° is 2.1 kcal mol^{-1} higher in energy, and the one for the *tg* rotamer at –174° is 3.1 kcal mol^{-1} higher in energy. With a two-state model, eq. 4.17 predicts a 97:3 ratio between the *gg* and *gt* rotamers. Once again, the relative energies between the rotamers governs the distribution observed from the long MD simulations. The energy barriers between the rotamers have little effect.

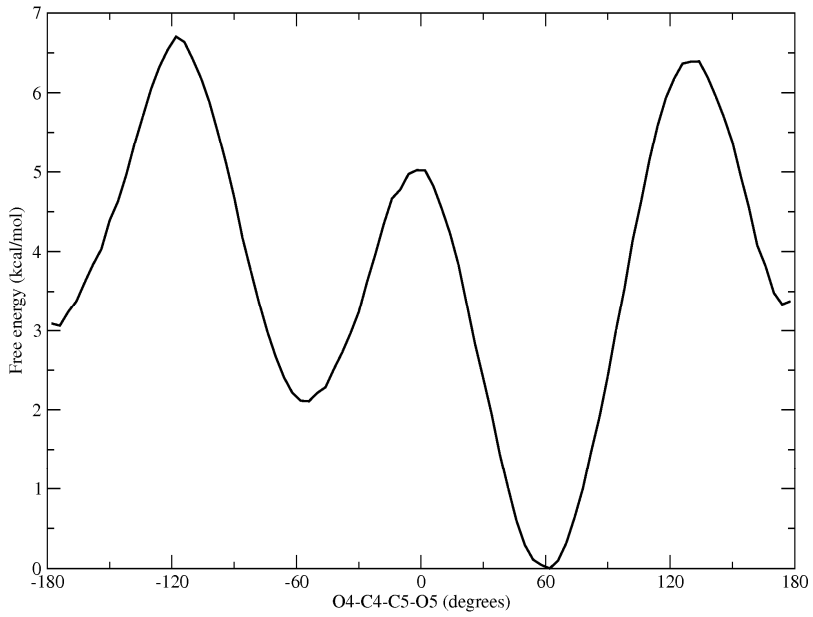

Figure 4.8. Free energy for rotation about the C4–C5 bond of **4.2**.

4.3.2. New torsion parameters for the C4–C5 bond of galactofuranosides

4.3.2.1. Potential energy surfaces for 4.1 and 4.2

The O4–C4–C5–O5 and O5–C5–C6–O6 dihedral angles and the relative QM and MM energies for **4.1** and **4.2** in both ring conformations are listed in Appendix C. These values were used to produce the PES shown in Figure 4.10. The energies for all of the PES were scaled such that the lowest energy for each was set to 0.0 kcal mol^{-1}. Also similar to Guvench and MacKerell,[17] any relative energies above 12 kcal mol^{-1} are not shown and were not used in the fitting process. To aide in the discussion below, the staggered rotamers about the C4–C5 and C5–C6 bonds are shown in Figure 4.9, along with the ideal values for the O4–C4–C5–O5 and O5–C5–C6–O6 dihedral angles.

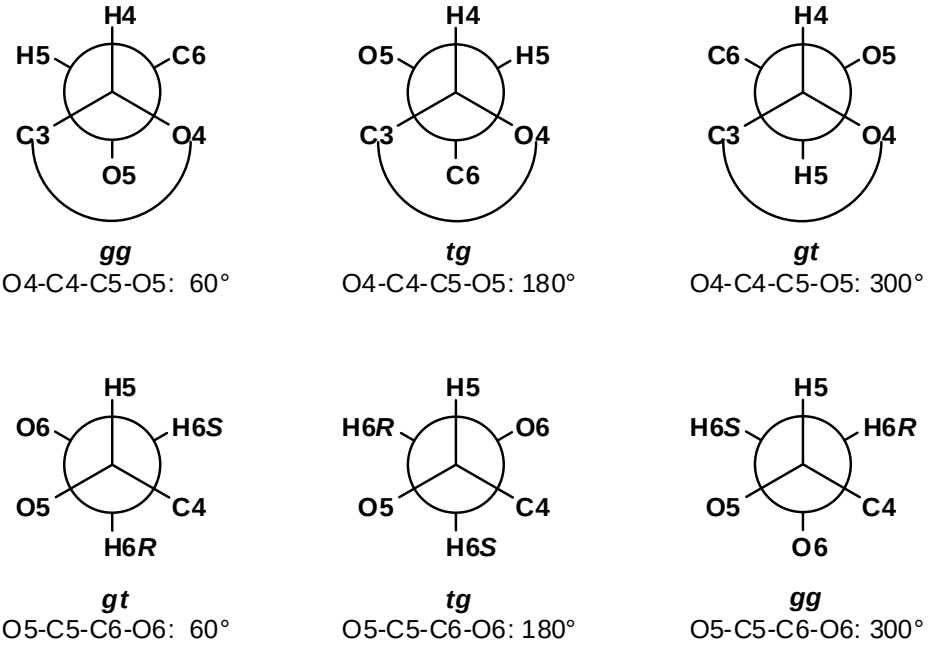

Figure 4.9. (*top*) Three staggered rotamers about the C4–C5 bond, viewing down the C4–C5 bond axis. (*bottom*) Three staggered rotamers about the C5–C6 bond, viewing down the C5–C6 bond axis.

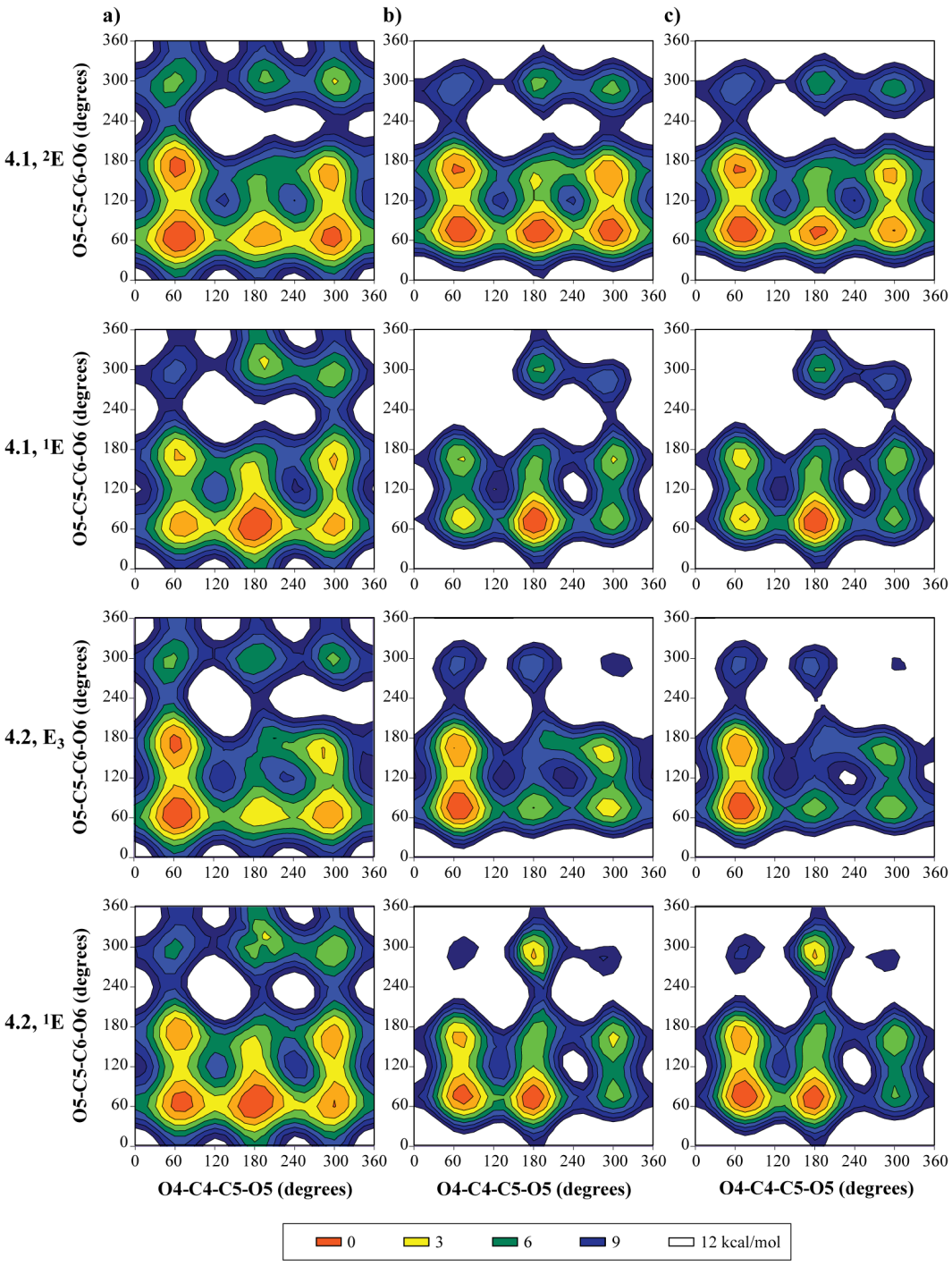

Figure 4.10. PES surfaces calculated for **4.1** and **4.2**. Each row represents a different ring conformation, labeled on the left. The graphs in column *a*) show QM surfaces, column *b*) are the GLYCAM06 surfaces with the O4–C4–C5–C6 and C3–C4–C5–C6 terms removed, and column *c*) are the surfaces from the original GLYCAM06 parameters.

For all four sets of graphs, the PES with the O4–C4–C5–C6 and C3–C4–C5–C6 terms removed (Figure 4.10, center column) bears a close resemblance to the PES with the original GLYCAM parameters (right column). Also, the ring conformation affects the relative energies of the conformations about the C4–C5 and C5–C6 bonds. The QM PES for **4.1** with the ring in the ^{2}E conformation looks quite similar to both MM PES (top row). All three surfaces show three regions of low energy when the O5–C5–C6–O6 dihedral angle is in the *gt* conformation; although in the QM PES, the energies are lower when C4–C5 is in the *gg* or *gt* orientation. Similarly, when O5–C5–C6–O6 is in the *tg* conformation, all three surfaces show lower energies when C4–C5 bonds is *gg* or *gt*. The relative energies when the C5–C6 bond is in the *gg* orientation are all over 3 kcal mol^{-1} higher in energy than the other two orientations; thus, this rotamer would be sparsely populated compared with the others, regardless of the C4–C5 orientation.

The two MM PES for **4.1** with the ring in the ^{1}E conformation differ more from the QM PES than in the previous example (Figure 4.10, second row). For both MM surfaces, the lowest energy conformation occurs with the C4–C5 bond in the *tg* orientation and the C5–C6 bond in the *gt* orientation. All the other staggered rotamers are at least 3 kcal mol^{-1} higher in energy. In the QM PES, all three staggered rotamers of C4–C5 have energies of 3 kcal mol^{-1} or less when the O5–C5–C6–O6 torsion is *gt*, though the *tg*-*gt* conformer is the lowest in energy, as it is for the MM surfaces. When both the O4–C4–C5–O5 and O5–C5–C6–O6 dihedrals angles are *gg*, the relative energy is over 12 kcal mol^{-1} higher in energy

than the global minimum on both MM surfaces. For the QM surface, however, this orientation is still within 6 kcal mol^{-1} of the minimum.

For both ring conformations of **4.2**, the QM PES differs from both the MM PES. When the ring is in the E_3 conformation, there are four regions that are within 3 kcal mol^{-1} of the global minimum (Figure 4.10, third row). These regions occur when the C4–C5 bond is in either the *gg* or *gt* orientation and when the C5–C6 rotamer is either *gt* or *tg*. In both the MM PES, the conformations within 3 kcal mol^{-1} of the global minimum only occur with C4–C5 is in the *gg* orientation, though the C5–C6 rotamer can be either *gt* or *tg*. Also, the *gg* rotamers for the O5–C5–C6–O6 dihedral angle are all 9 kcal mol^{-1} or higher in energy for the MM PES but are 6 kcal mol^{-1} or higher in the QM PES.

The QM PES for **4.2** with the ring in the ^1E conformation (Figure 4.10, bottom row) is quite similar to **4.1** in the same ring conformation. The largest region of low energy conformation occurs for the *tg-gt* rotamer, but all three staggered rotamers of C4–C5 have energies of 3 kcal mol^{-1} or less when the O5–C5–C6–O6 torsion is *gt*. In both of the MM PES, the *tg-gt*, *gg-gt*, and *gg-tg* rotamers all have energies within 3 kcal mol^{-1} of the global minimum, but the *gt-gt* conformer is higher in energy. The *gg-gg* and *gt-gg* conformations on the MM surfaces are both significantly higher in energy than the same regions on the QM surface.

4.3.2.2. Metropolis Monte Carlo simulated annealing fitting procedure and new torsion parameters

The contribution to the overall potential energy due to rotation about a bond is given by eq. 4.18, where V_n is the barrier to rotation, n is the n^{th} term in a Fourier expansion or the periodicity, and γ is a phase factor.[4] The PES shown in Figure 4.10 were used in the MMCSA procedure described in Section 4.2.2 with a up to three or four Fourier terms. Specifically, the surfaces without the O4–C4–C5–C6 and C3–C4–C5–C6 terms (center column) were fit to the QM surfaces (left column). Relative energies within 6 kca mol^{-1} of the global minimum were weighted five times higher than energies from 6–12 kcal mol^{-1} higher than the global minimum (refer to eq. 4.7).[17] Energies above 12 kcal mol^{-1} were not used for fitting. Each fitting procedure was run five times, using 5000 Monte Carlo steps. For three Fourier terms, the RMSE ranged from 2.195 to 2.204 kcal mol^{-1} for the five runs; with four Fourier terms, the RMSE range was similar, from 2.188 to 2.203 kcal mol^{-1}. The parameters with the lowest RMSE from each are shown in Table 4.2 and were tested in MD simulations.

$$V(r^N)_{torsion} = \sum_{1}^{n} \frac{V_n}{2}\left(1 + (\cos n\phi - \gamma)\right) \qquad 4.18$$

Table 4.2. New torsion parameters for the C4–C5 bond of **4.1** and **4.2** obtained from the MMCSA fitting procedure.

Fourier terms	Dihedral angle	$\frac{V_n}{2}$ (kcal mol^{-1})	n	γ (degrees)
3	C3–C4–C5–C6	0.24	1	0
		0.20	2	180
		0.04	3	180
3	O4–C4–C5–C6	0.74	1	0
		0.20	2	180
		0.47	3	180
4	C3–C4–C5–C6	0.01	1	0
		0.05	2	0
		1.68	3	180
		0.44	4	180
4	O4–C4–C5–C6	0.64	1	0
		0.08	2	180
		1.01	3	0
		0.54	4	180

Because the parameters with three Fourier terms gave better results in MD simulations (Section 4.3.3), we will limit our discussion to these for the rest of this section. Figure 4.11 shows the PES for two different ring conformations of **4.1** and **4.2** using these torsion parameters, along with the surfaces from the QM calculations and the GLYCAM06 parameters. The relative energies to create the graphs are included in the tables in Appendix C. As before, the energies for each PES were scaled independently to set the lowest energy to 0.0 kcal mol^{-1}, and relative energies above 12 kcal mol^{-1} are not shown.

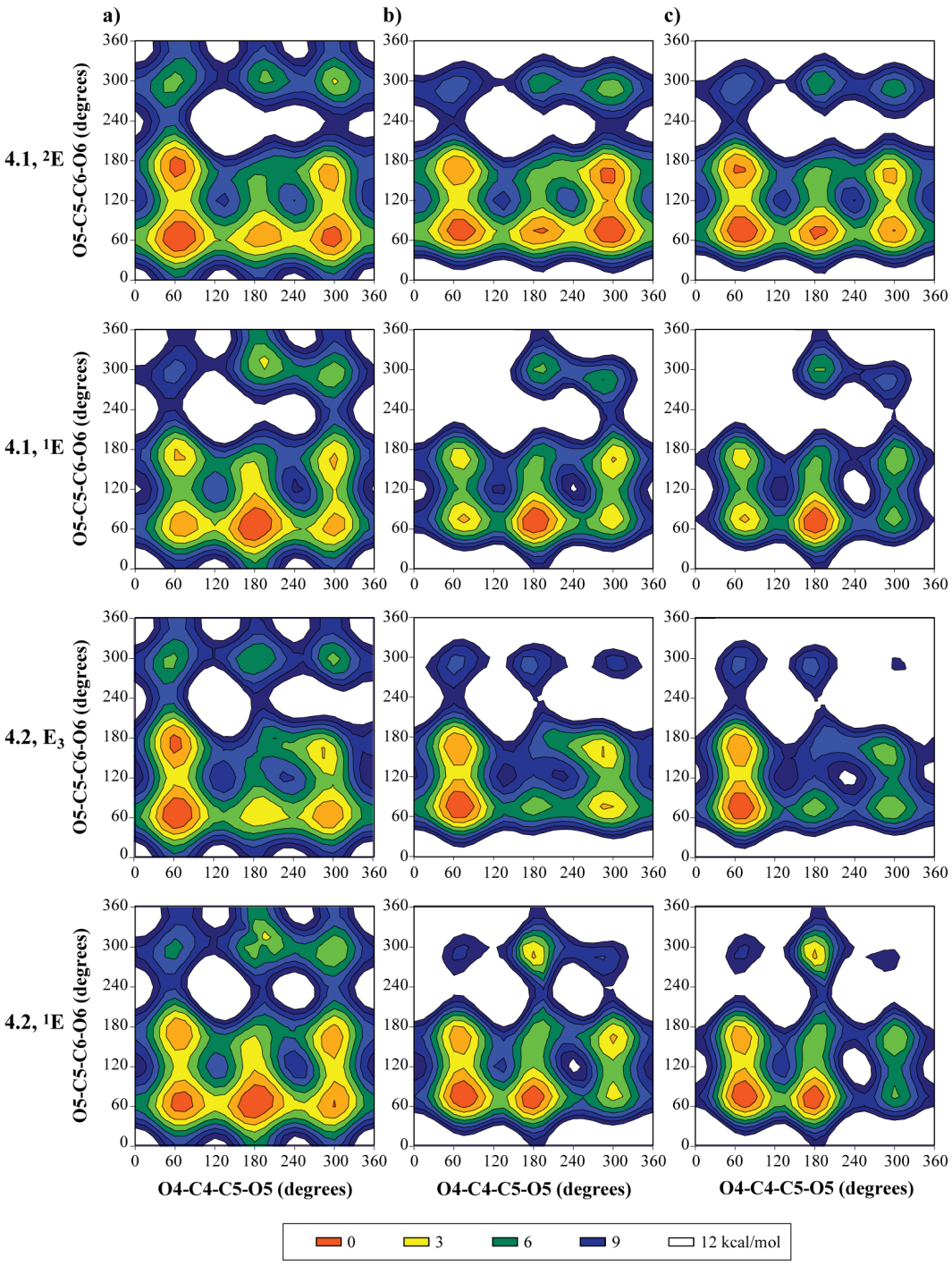

Figure 4.11. PES surfaces calculated for **4.1** and **4.2**. Each row represents a different ring conformation, labeled on the left. The graphs in column *a*) show QM surfaces, column *b*) are the GLYCAM06 surfaces with the new terms for O4–C4–C5–C6 and C3–C4–C5–C6, and column *c*) are the surfaces from the original GLYCAM06 parameters. It should be noted that the columns *a* and *c* are the same as in Figure 4.10.

For all ring conformations shown, the PES with the new torsion parameters are quite similar to those with the original GLYCAM parameters (Figure 4.11, columns *b* and *c*). As we saw in Section 4.3.2.1, the ring conformation of **4.1** and **4.2** affect the overall PES. For **4.1** in the ^{2}E conformation (top row), the new torsion parameters favor the C4–C5 *gt* conformation over the *gg* conformation when O5–C5–C6–O6 is 180°, which is the opposite of the QM PES and the original GLYCAM06 parameters. Also, the area of the minimum when the C4–C5 bond is *tg* and C5–C6 is *gt* is smaller with the new parameters, which is similar to the QM PES. When **4.1** is in the ^{1}E conformation (Figure 4.11, second row), the major difference with the new torsion parameters is to lower the energies for the conformations when the C4–C5 bond is in the *gt* orientation. If the C5–C6 bond is in either the *gt* or *tg* conformation, the relative energies are within 3 kcal mol^{-1} of the global minimum. Otherwise, there is little difference to the PES with the O4–C4–C5–C6 and C3–C4–C5–C6 terms removed (Figure 4.10) for both ring conformations of **4.1**

For **4.2** with the ring in the E_3 conformation (Figure 4.11, third row), the new parameters reduced the relative energies for conformations with the C4–C5 bond in the *gt* orientation and C5–C6 in either *gt* or *tg*. For ^{1}E ring conformations (Figure 4.11, bottom row), the energies when the C4–C5 is *gt* and the C5–C6 is *gt* or *tg* are similarly reduced. The area for the minimum with O4–C4–C5–O5 at 60° and O5–C5–C6–O6 at 180° is larger with the new torsion parameters than when the terms are removed (Figure 4.10). The new parameters put these conformers within 3 kcal mol^{-1} of the global minimum. Other than the changes noted here,

the PES for **4.2** with the new parameters look similar to the ones with the torsion terms removed in Figure 4.10.

4.3.3. MD simulations with new torsion parameters

We ran 250 ns MD simulations on **4.1** and **4.2** with the new parameters described above. Simulations with both sets of new parameters shown in Table 4.2 were run; however, the C4–C5 rotamer population of **4.2** from the simulations with a periodicity up to $n = 4$ was split almost evenly between *gg* and *gt* (51 ± 3% *gg*: 1 ± 1% *tg*: 49 ± 3% *gt*). Thus, we focused on simulations using the parameters with a periodicity up to $n = 3$.

4.3.3.1. Conformation about the C4–C5 bond

In the previous chapter, we showed that a 250 ns simulation with the original GLYCAM06 parameters was long enough for the populations of the C4–C5 rotamers to converge. The same length simulation with the new torsion terms also allows the C4–C5 populations to converge, as measured by a variance in the mean of 3% or less.[33] For **4.1**, the C4–C5 rotamer distribution over time is shown in Figure 4.12. The populations change little from the values at 140 ns, while the variances are all 3% or less by 170 ns. Thus, in terms of the rotamers about the C4–C5 bond, a 250 ns simulation is sufficently long. The histogram of the C4–C5 populations is shown in Figure 4.13. Integrating the area under the curves gives the overall population for each conformation: 44 ± 3% *gg*, 1 ± 1% *tg*, and 55 ± 3% *gt*. The *gt* rotamer is favored over the *gg* rotamer, while the *tg* rotamer is hardly populated during the simulation.

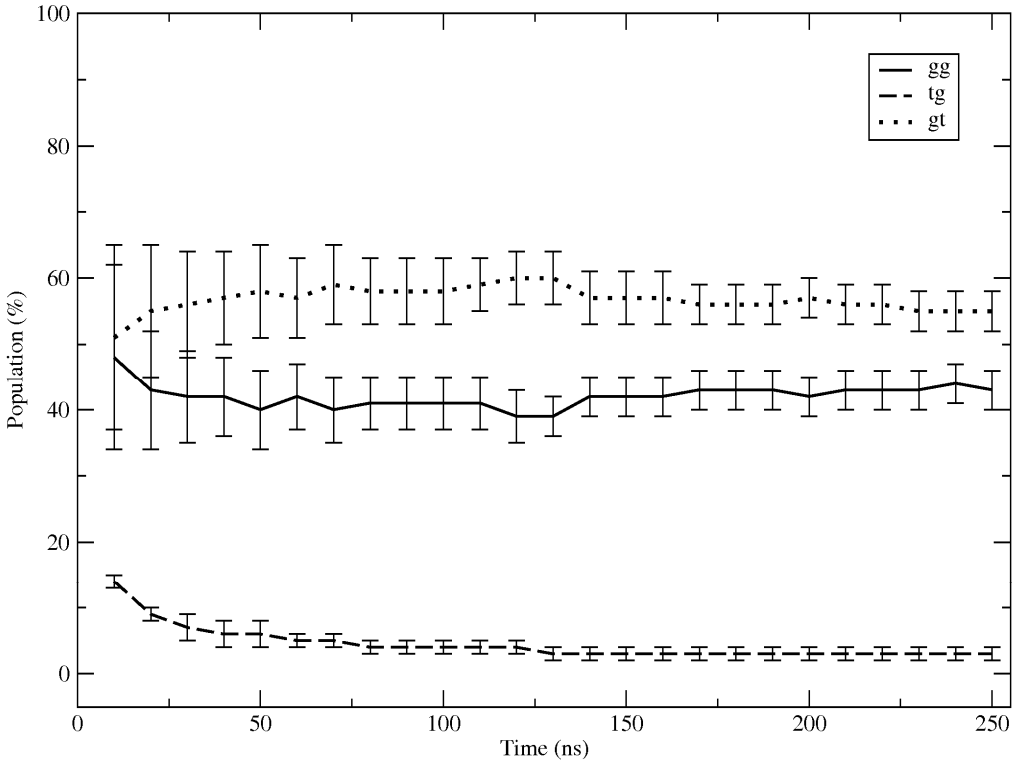

Figure 4.12. Convergence of the C4–C5 rotamer distribution of **4.1** with new torsion parameters as a function of simulation time.

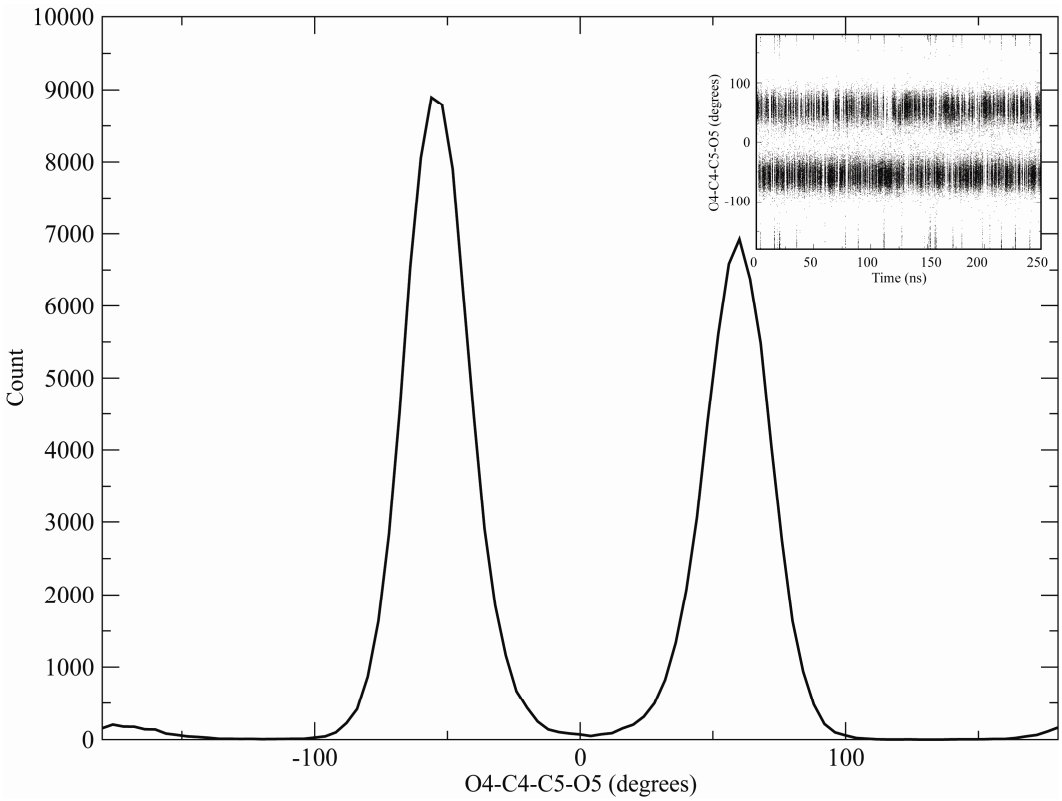

Figure 4.13. Histogram of the O4–C4–C5–O5 dihedral angle for **4.1** with new torsion parameters. The inset shows the same angle over the time of the simulation.

The C4–C5 rotamers of **4.2** took longer to converge (Figure 4.14) than the ones for **4.1** in the simulation with the new torsion parameters. The variances were not 3% or less until after 200 ns, though the populations did not change appreciably from the values at 100 ns. The rotamer population over the course of the simulation was 68 ± 3% *gg*, 1 ± 1% *tg*, and 31 ± 3% *gt*. Unlike with the original GLYCAM06 parameters, the different anomers have different populations about the C4–C5 bond during MD simulations. Furthermore, the values for **4.2** are quite similar to what was calculated using the limiting values approach (Section 3.3.3.1), which was 64% *gg*, 1% *tg*, and 35% *gt*. However, the

values for **4.1** differ from those determined using the limiting values, 32% *gg*, 26% *tg*, and 42% *gt*.

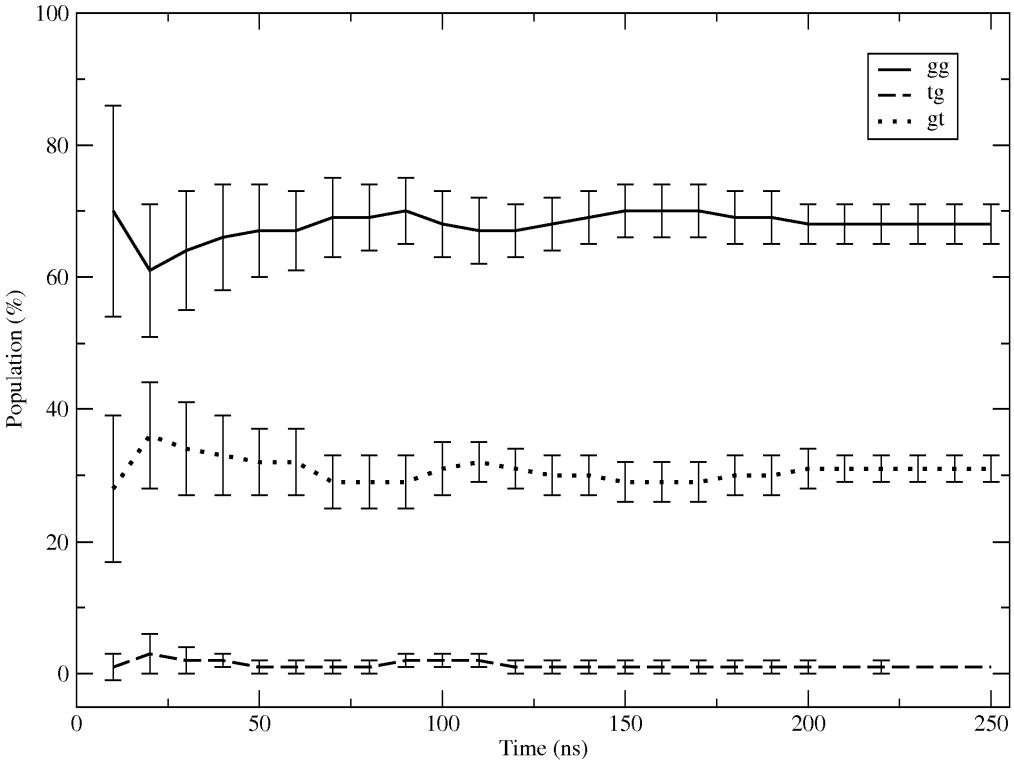

Figure 4.14. Convergence of the C4–C5 rotamer distribution of **4.2** with new torsion parameters as a function of simulation time.

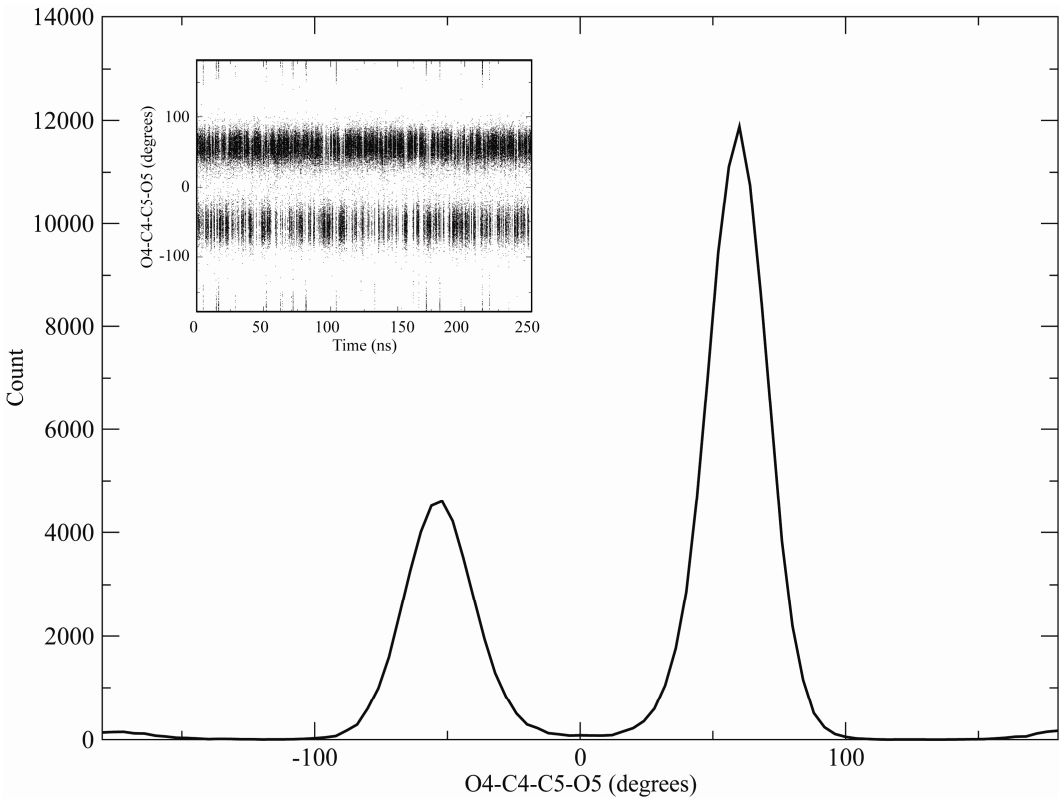

Figure 4.15. Histogram of the O4–C4–C5–O5 dihedral angle of **4.2** with new torsion parameters. The inset shows the same angle over the time of the simulation.

4.3.3.2. Conformation about the C5–C6 bond

The new torsion parameters altered the rotamer populations for the C4–C5 bond, as they were designed to do. The next thing we wanted to determine was their effect on the C5–C6 rotamers. For **4.1**, the C5–C6 rotamers converged within 150 ns, as shown in Figure 4.16. The distribution of the rotamers seen at 120 ns is similar to the final values. After the simulation, the final populations were 47 ± 3% *gt*, 24 ± 2% *tg*, and 29 ± 3% *gg* (Figure 4.17). The populations for the *gt* and *gg* rotamers both differed by about 20% from the values obtained with

the original GLYCAM06 parameters, which were 68% *gt*, 28% *tg*, and 7% *gg* (Section 3.3.4.3).

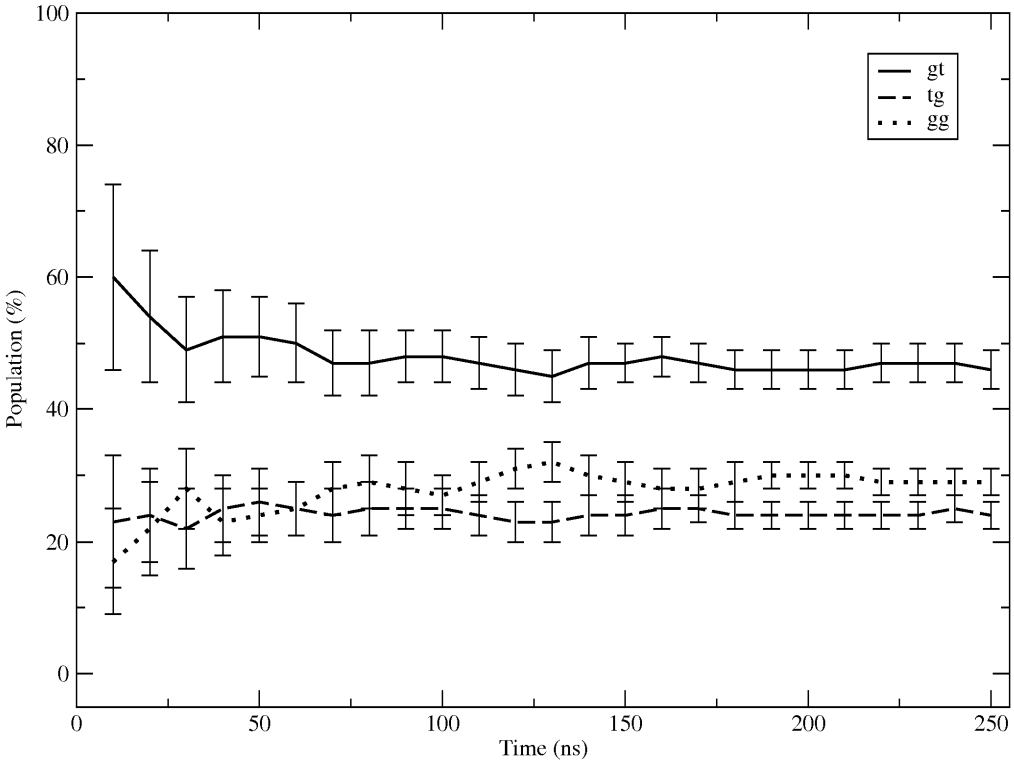

Figure 4.16. Convergence of the C5–C6 rotamer distribution of **4.1** with new torsion parameters as a function of simulation time.

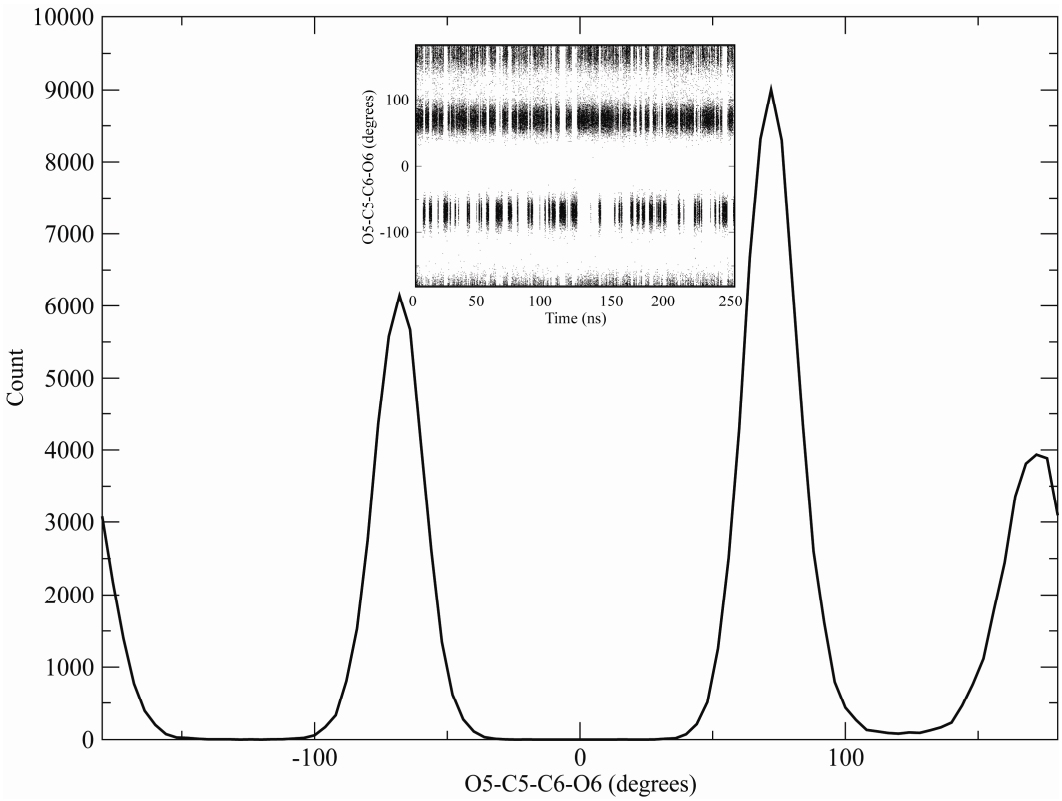

Figure 4.17. Histogram of the O5–C5–C6–O6 dihedral angle of **4.1** with new torsion parameters. The inset shows the same angle over the time of the simulation.

Like with **4.1**, the C5–C6 rotamer population from an MD simulation of **4.2** with the new torsion parameters converged within 150 ns. The population of the three rotamers at 100 ns was also similar to the final distribution. The final populations are 49 ± 3% *gt*, 26 ± 2% *tg*, and 25 ± 2% *gg*, which are all within 4% of the values obtained for **4.1**. As above, the populations for the *gt* and *gg* rotamers of **4.2** differ substantially from those observed with the original GLYCAM06 parameters: 69% *gt*, 22% *tg*, and 12% *gg*. For both anomers, the population of the *tg* conformation remains essentially unchanged with the new torsion parameters. Not only do the new parameters change the conformation of

the C4–C5 bond, they also affect the conformation of the C5–C6 bond. The rotamer populations themselves cannot be directly compared to experiment, however. One way to assess the significance of the changes in the C5–C6 rotamers is to evaluate proton–proton coupling constants obtained from the MD simulations.

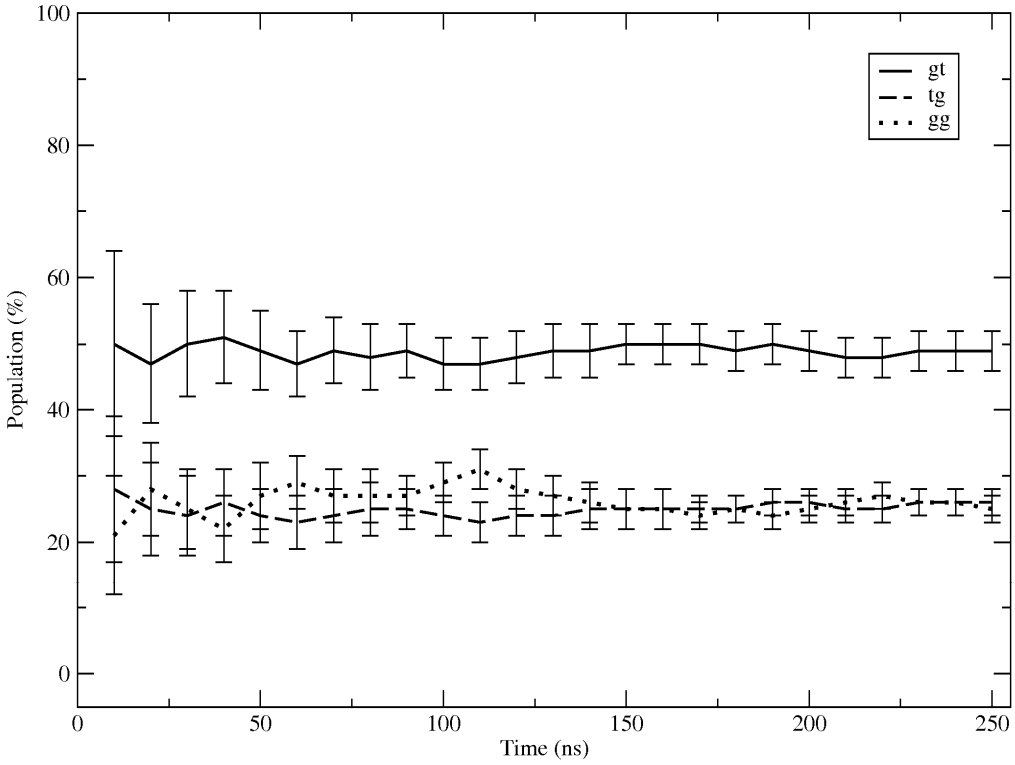

Figure 4.18 Convergence of the C5–C6 rotamer distribution of **4.2** with new torsion parameters as a function of simulation time.

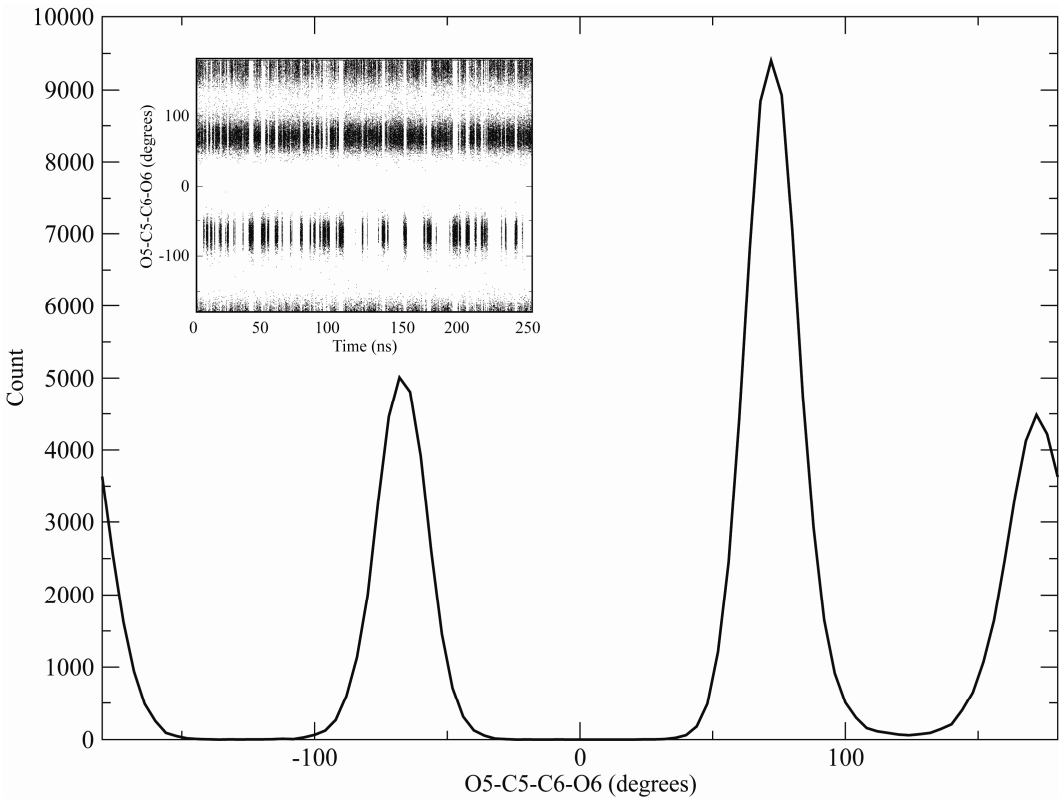

Figure 4.19. Histogram of the O5–C5–C6–O6 dihedral angle of **4.2** with new torsion parameters. The inset shows the same angle over the time of the simulation.

4.3.3.3. Coupling constants from MD simulations

The new torsion parameters improve the agreement between the experimental and MD-derived $^{3}J_{H4,H5}$ values. Table 4.3 lists the experimental vicinal coupling constants for **4.1**, as well as those determined from MD simulations with the original and new GLYCAM06 torsion parameters. Table 4.4 lists the same values for **4.2**. As described in Section 3.3.4.4, the values for $^{3}J_{H,H}$ or $^{3}J_{H,C}$ from the MD simulations were determined with the Karplus-like relationships of equations 3.10–3.16 then averaged over the entire simulation.

Table 4.3. Comparison between the coupling constants from experiment and from MD simulations of **4.1** with the new and original GLYCAM06 torsion parameters.

	Experimental[a]	**New parameters**[b]	**Original parameters**[b]
$^3J_{H1,H2}$ **(Hz)**	4.5	5.5 ± 1.3	5.6 ± 1.1
$^3J_{H2,H3}$ **(Hz)**	7.9	4.3 ± 2.7	4.5 ± 2.7
$^3J_{H3,H4}$ **(Hz)**	7.1	5.3 ± 2.8	5.7 ± 2.6
$^3J_{H4,H5}$ **(Hz)**	6.0	5.7 ± 1.1	2.0 ± 0.8
$^3J_{H4,C6}$ **(Hz)**	3.0	2.5 ± 1.8	2.2 ± 1.4
$^3J_{H5,H6R}$ **(Hz)**	7.0	5.6 ± 1.7	7.0 ± 1.9
$^3J_{H5,H6S}$ **(Hz)**	3.9	4.1 ± 1.2	4.4 ± 1.1

[a] From 1D ^{1}H NMR or EXSIDE spectra at 600 MHz in D_2O (Sections 2.3.4 and 3.3.2). The error in the experimental values is estimated to be ± 0.2 Hz.
[b] The error analysis for the MD simulations is described in Section 3.3.4.4.

Table 4.4. Comparison between the coupling constants from experiment and from MD simulations of **4.2** with the new and original GLYCAM06 torsion parameters.

	Experimental[a]	**New parameters**[b]	**Original parameters**[b]
$^3J_{H1,H2}$ **(Hz)**	2.0	3.2 ± 2.2	3.3 ± 2.3
$^3J_{H2,H3}$ **(Hz)**	3.2	4.0 ± 2.3	4.0 ± 2.3
$^3J_{H3,H4}$ **(Hz)**	6.2	6.3 ± 2.6	6.2 ± 2.6
$^3J_{H4,H5}$ **(Hz)**	4.4	3.8 ± 0.9	1.7 ± 0.7
$^3J_{H4,C6}$ **(Hz)**	1.6	2.6 ± 1.8	2.1 ± 1.3
$^3J_{H5,H6R}$ **(Hz)**	7.4	5.8 ± 1.7	7.0 ± 1.9
$^3J_{H5,H6S}$ **(Hz)**	4.4	4.3 ± 1.2	4.3 ± 1.1

[a] From 1D ^{1}H NMR or EXSIDE spectra at 600 MHz in D_2O (Sections 2.3.4 and 3.3.2). The error in the experimental values is ±0.2 Hz.
[b] The error analysis for the MD simulations is described in Section 3.3.4.4.

For **4.1,** the value of $^3J_{H4,H5}$ with the new torsion parameters is 5.7 ± 1.1 Hz, which compares favorably with the experimental value of 6.0 ± 0.2 Hz. With the original GLYCAM06 parameters, this coupling from MD simulations is 2.0 ± 0.8 Hz. The other coupling constant determined for the C4–C5 bond, $^3J_{H4,C6}$, has an experimental value of 3.0 ± 0.2 Hz, and both simulations produce similar values for this coupling constant. The original parameters give 2.2 ± 1.4 Hz, and the new parameters give 2.5 ± 1.8 Hz.

Similar improvement is seen for **4.2**. The value of $^3J_{H4,H5}$ from MD simulations with the new parameters is 3.8 ± 0.9 Hz, and the experimental value is 4.4 ± 0.2 Hz. Because the simulation with the original parameter gives essentially one conformation, $^3J_{H4,H5}$ from that simulation is 1.7 ± 0.7 Hz. The values for $^3J_{H4,C6}$ change little between the old and new parameters, 2.1 ± 1.3 and 2.6 ± 1.8 Hz, respectively. Both values are within error of the experimental value, 1.6 ± 0.2 Hz.

In the *gt* conformation, the H4–C4–C5–H5 dihedral angle is close to 180° (Figure 4.9), which is a maximum in the Karplus curve. This torsion is close to –60º in the *gg* conformation and, consequently, has a small value in the Karplus curve. Therefore, by increasing the population of the *gt* rotamer, the value of $^3J_{H4,H5}$ also increases. In contrast, the H4–C4–C5–C6 dihedral angle is close to 60° in the *gg* conformation and close to –60° in the *gt* conformation. Both angles would have small *J* values in the Karplus curve. The H4–C4–C5–C6 torsion is less sensitive to the conformation about the C4–C5 bond than the H4–C4–C5–H5 dihedral angle.

With the original GLYCAM06 parameters, there was excellent agreement between the experimental and calculated values of both $^3J_{H5,H6R}$ and $^3J_{H5,H6S}$ for both anomers. With the new parameters, the MD-derived values for $^3J_{H5,H6S}$ are unchanged from the original parameters. However, the agreement for $^3J_{H5,H6R}$ is not as good. This vicinal coupling is 5.6 ± 1.7 Hz for **4.1**, compared with 7.0 ± 0.2 Hz experimentally, and for **4.2**, the calculated coupling is 5.8 ± 1.7 Hz, compared with 7.4 ± 0.2 Hz experimentally. Both calculated values are within error of the experimental value. The value for $^3J_{H5,H6R}$ is more sensitive to the populations of the *gt* and *gg* rotamers than the value for $^3J_{H5,H6S}$. The H5–C5–C6–H6*R* dihedral angle is close to 180° for *gt* and close to 60° for *gg*, whereas the H5–C5–C6–H6*S* dihedral angle is close to 60° for *gt* and close to –60° for *gg*.

The new torsion parameters for the C4–C5 bond have little effect on the ring conformation. The values for the three ring couplings – $^3J_{H1,H2}$, $^3J_{H2,H3}$, and $^3J_{H3,H4}$ – show little difference between simulations with the original and new GLYCAM06 parameters. Specifically, both simulation conditions give good agreement between experiment and calculations for $^3J_{H1,H2}$ of **4.1**, though the agreement for $^3J_{H2,H3}$, and $^3J_{H3,H4}$ is poor. For **4.2**, the all three values show good agreement to the experimental values. The ring conformation will be discussed in the next section.

4.3.3.4. Ring conformation

We observe two distinct ring populations for **4.1** in MD simulations with the new torsion parameters (Figure 4.20). The populations are similar to those observed with the original parameters. When the overall distribution is fit to two

Gaussian functions with the same width, using eq. 3.17, the major population is centered at P = –18°, which is the ^{2}E conformation. This is the same major conformer given by the original GLYCAM06 parameters (Section 3.3.4.1). The minor population is centered at P = 140°, which is the $^1T_2$ conformation. The minor population is similar to the one from the original parameters, centered at 135° and between ^{1}E and $^1T_2$. The major conformation is present 75% of the time, which is also comparable to the originally observed value of 78%. Similarly, the distributions of the ring dihedral angles (Figure 4.21) are quite similar to those obtained with the original parameters (Figure 3.12).

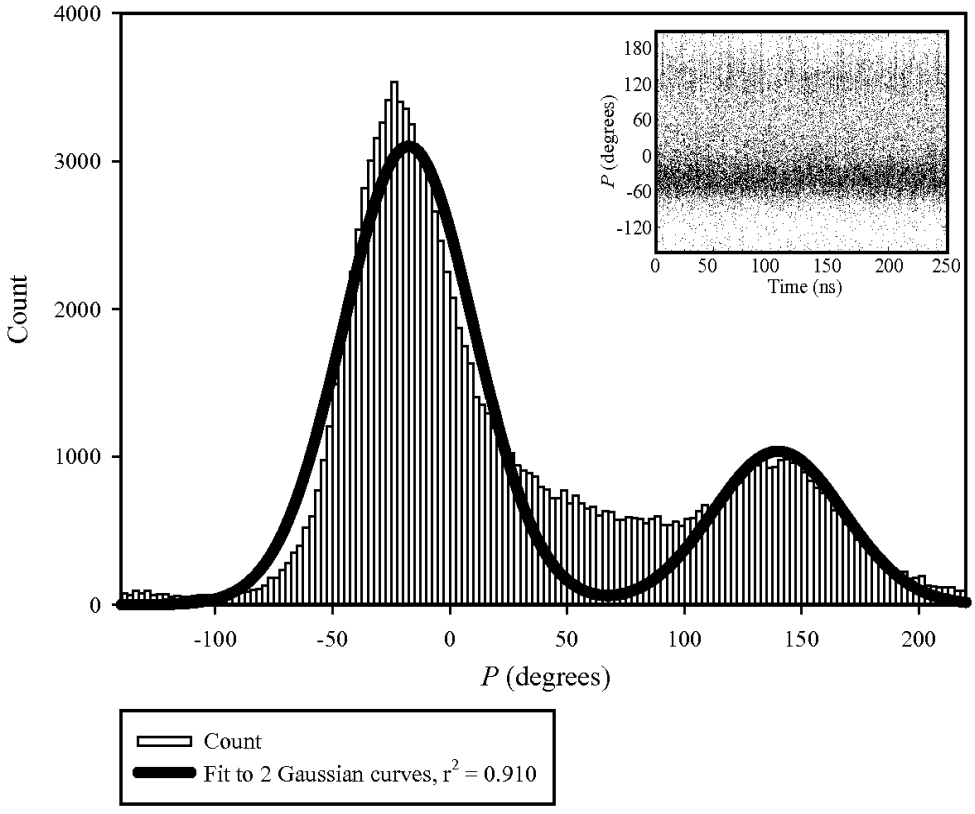

Figure 4.20. Histogram of pseudorotational phase angle P for **4.1** fit to two Gaussian functions (thick solid black line). One population is centered at P = –18°, and the other is centered at P = 140º. The inset shows P versus time of the simulation.

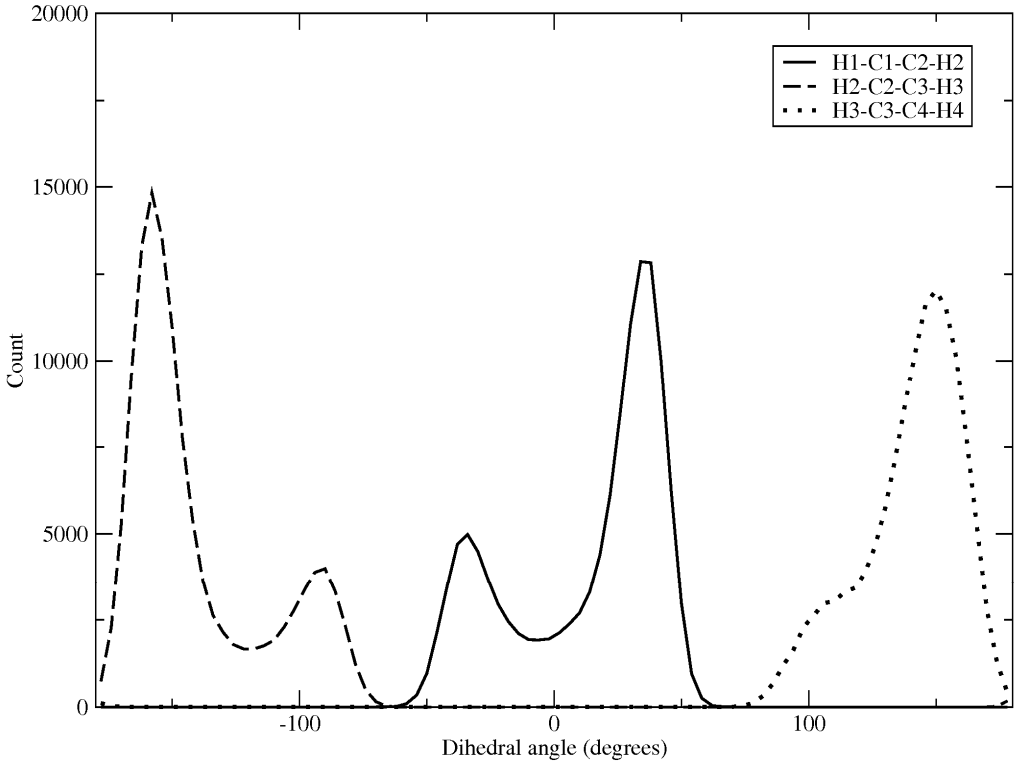

Figure 4.21. Histograms for the ring dihedral angles of **4.1**. The solid line is for H1–C1–C2–H2, the long dashed line is for H2–C2–C3–H3, and the dotted line is for H3–C3–C4–H4.

Unlike with **4.1**, we observed one broad distribution of ring conformation for **4.2** in simulations with the new torsion parameters (Figure 4.22). The population is centered at P = 22°, which is the E_3 conformer. This is the same major conformation observed with the original parameters. Upon closer inspection of the data, there is a shoulder around P = 140–150°. When the distribution is fit to two Gaussian functions, using eq. 3.17, there is a minor population at P = 148°, the $^1T_2$ conformer. The original GLYCAM06 parameters gave a minor conformation of P = 132° (^1E); therefore, the new C4–C5 torsion parameters do have small effect on the overall ring conformation. The major

population is present 91% of the time, which is similar to what we observed with the original parameters. As with **4.1**, the distributions of ring dihedral angles for **4.2** obtained with the new parameters (Figure 4.23) looks very similar to those from the original parameters (Figure 3.10).

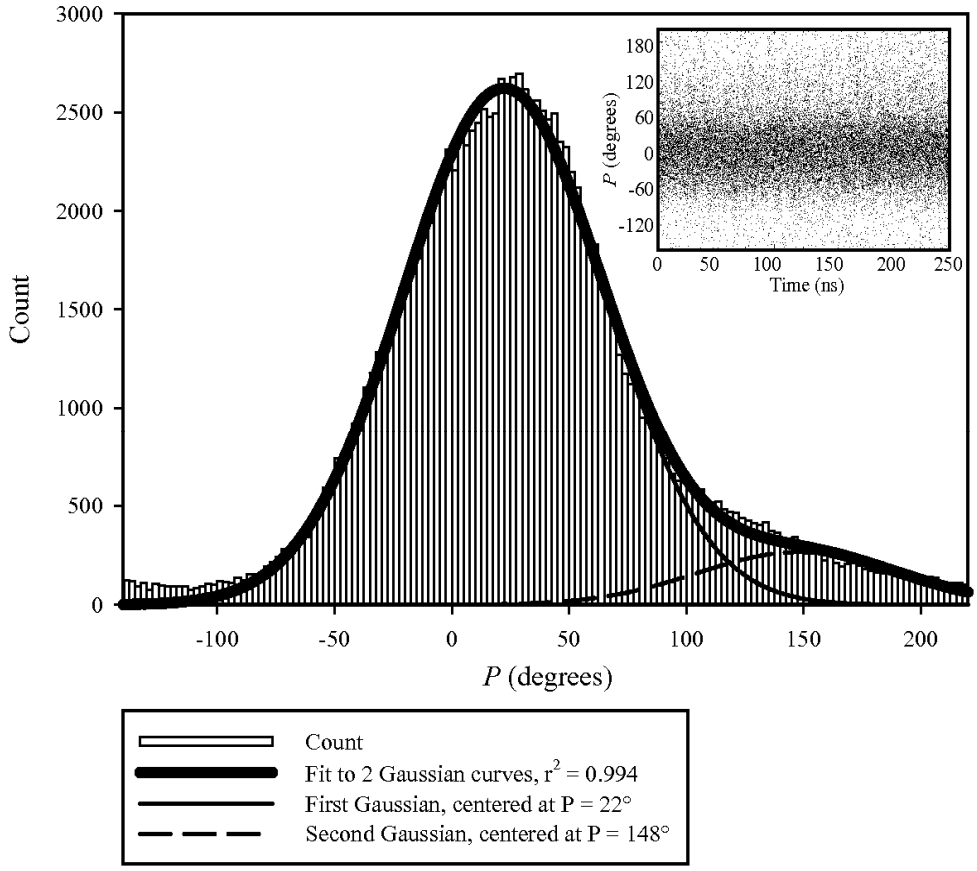

Figure 4.22. Histogram of pseudorotational phase angle *P* for **4.2** fit to two Gaussian functions (thick solid black line). One population is centered at *P* = 22° (thin solid black line), and the other is centered at *P* = 148º (thin dashed line). The inset shows *P* versus time of the simulation.

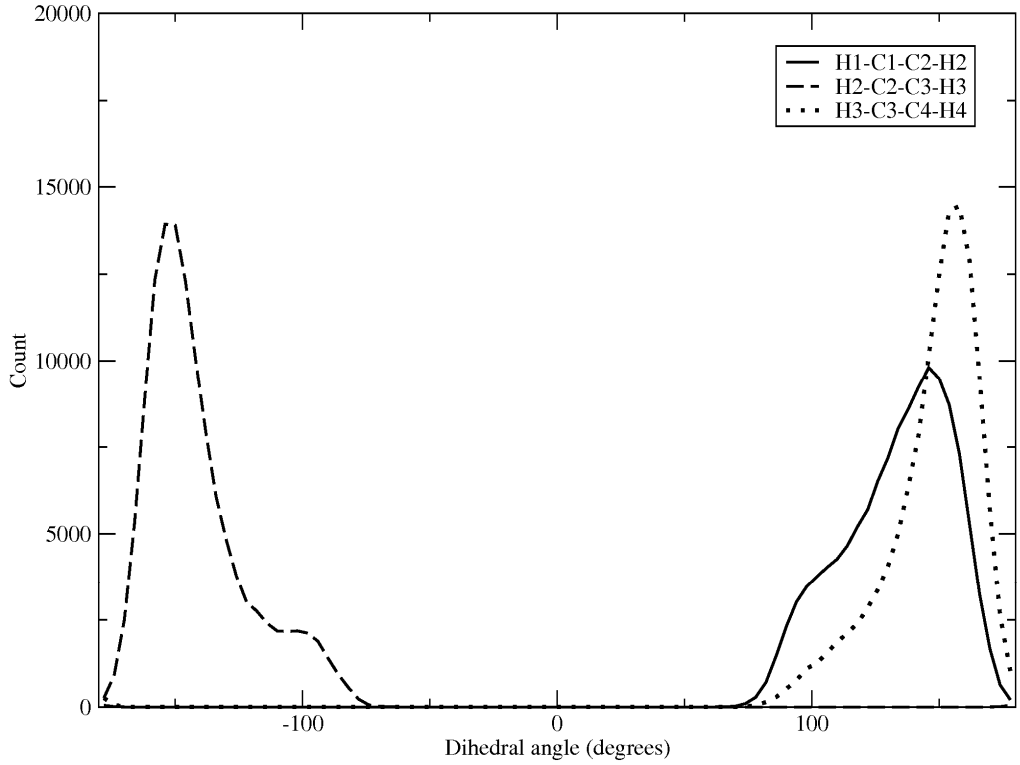

Figure 4.23. Histograms for the ring dihedral angles of **4.2**. The solid line is for H1–C1–C2–H2, the long dashed line is for H2–C2–C3–H3, and the dotted line is for H3–C3–C4–H4.

4.3.4. Umbrella sampling and WHAM for 4.1 and 4.2 with the new GLYCAM06 parameters

After the long MD simulations were complete, umbrella sampling simulations on **4.1** and **4.2** were run as described above to determine the free energy of rotation about the C4–C5 bond due to the newly determined torsion parameters. The histograms in Figure 4.24 and Figure 4.25 show that the O4–C4–C5–O5 dihedral angle was restrained to the desired values in all 73 windows along the reaction coordinate, as in the previous simulations. There were also no deviations from the expected values, nor any gaps in the individual distributions.

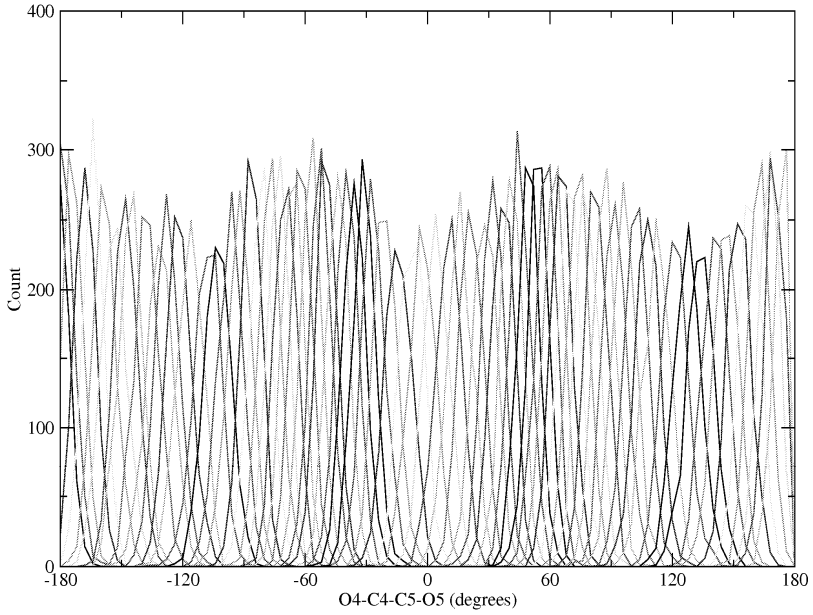

Figure 4.24. Histograms showing the O4–C4–C5–O5 dihedral angle distributions from each 5° window for **4.1**, calculated with the new torsion parameters.

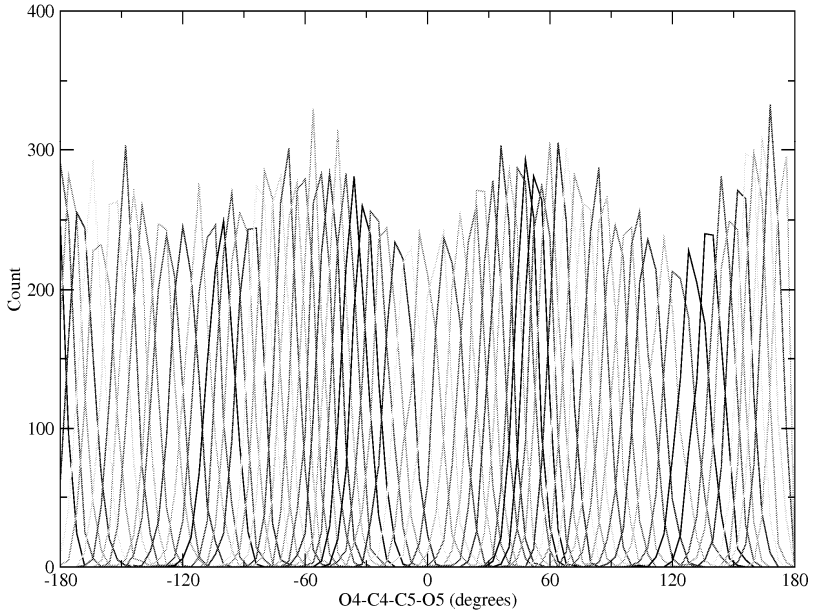

Figure 4.25. Histograms showing the O4–C4–C5–O5 dihedral angle distributions from each 5° window for **4.2**, calculated with the new torsion parameters.

The rotamer distribution for **4.1** from the WHAM calculations does not agree with the long MD simulations (Figure 4.26). In fact, the results from WHAM favor the *gg* rather than the *gt* rotamer. The WHAM equations gave 62 ± 3% *gg*, 1 ± 1% *tg*, and 37 ± 3% *gt*, which is in sharp contrast to the long MD results: 43 ± 3% *gg*, 1 ± 1% *tg*, and 55 ± 3% *gt*. The free energy for rotation about the C4–C5 (Figure 4.27) matches the rotamer distribution. That is, the global minimum is at 62°, corresponding to the *gt* rotamer. The minimum for the *gt* rotamer is at –62° and is 0.4 kcal mol^{-1} higher in energy. The minimum for the *tg* rotamer occurs at –174° and is 2.8 kcal mol^{-1} above the global minimum. The energy barriers separating each of the rotamers are lower than those from the original GLYCAM06 parameters (Figure 4.6).

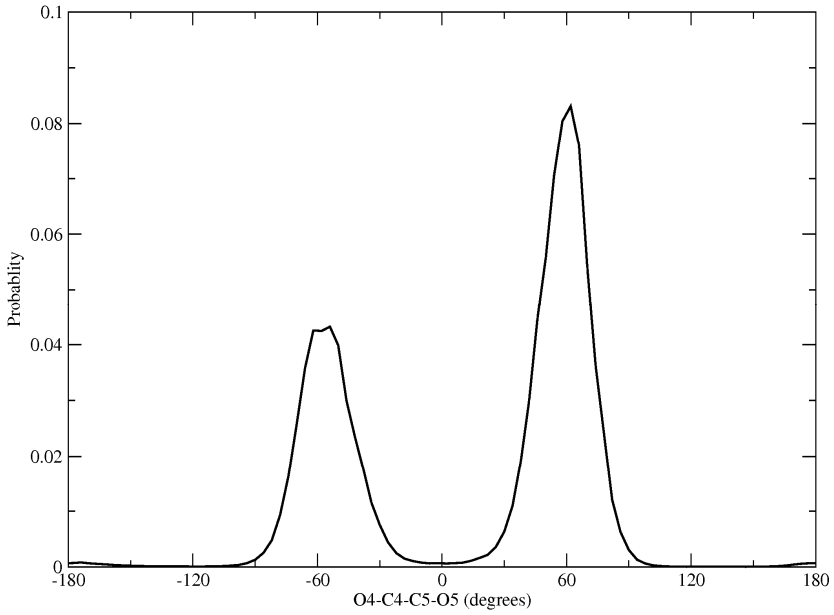

Figure 4.26. Rotamer distribution about the C4–C5 bond of **4.1**, calculated with the new torsion parameters.

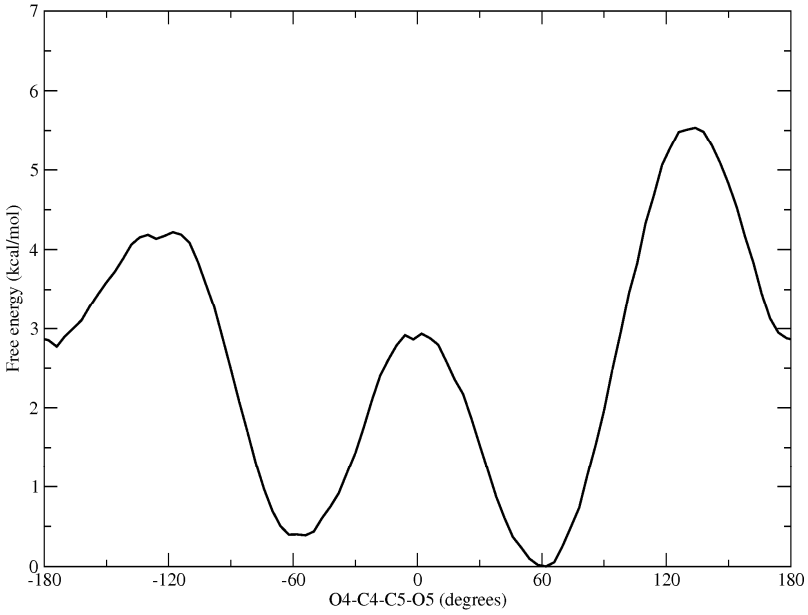

Figure 4.27. Free energy for rotation about the C4–C5 bond of **4.1**, calculated with the new torsion parameters.

As with **4.1**, the rotamer distribution for **4.2** determined from WHAM using the new torsion parameters does not match that of the long MD simulations. However, both WHAM and the long MD simulations favor the *gg* rotamer. The rotamer populations from WHAM are 53 ± 3% *gg*, 1 ± 1% *tg*, and 46 ± 3% *gt*, compared with 68 ± 3% *gg*, 1 ± 1% *tg*, and 31 ± 3% *gt*. The energy difference between the global minimum *gg* conformation at 54° and the *gt* conformation at –54° is quite small, 0.2 kcal mol^{-1}. The relative energy for the minimum corresponding to the *tg* rotamer at –174° is 2.8 kcal mol^{-1}, as it was for **4.1**. The energy barriers separating the rotamers are also lower with the new torsion parameters than those from the original GLYCAM06 values (Figure 4.8).

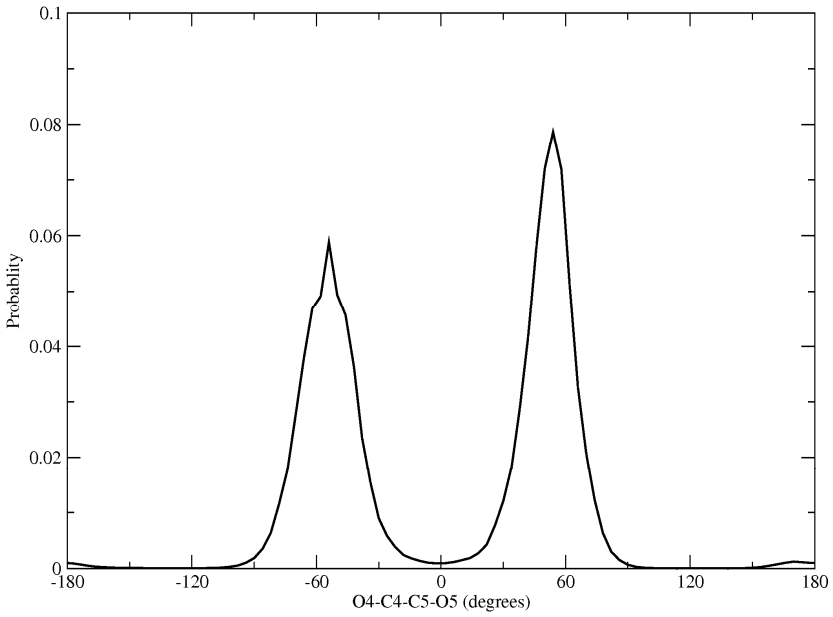

Figure 4.28. Rotamer distribution about the C4–C5 bond of **4.2**, calculated with the new torsion parameters.

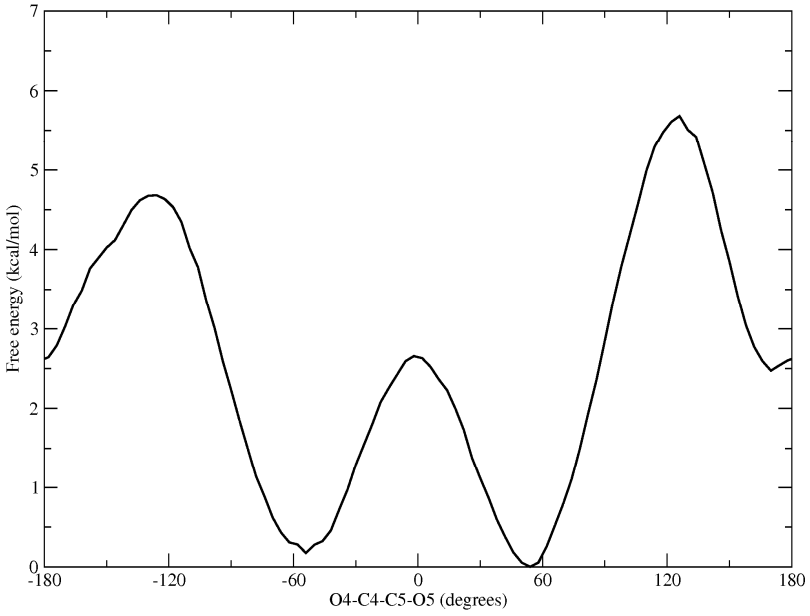

Figure 4.29. Free energy for rotation about the C4–C5 bond of **4.2**, calculated with the new torsion parameters.

Because the results of WHAM calculations did not match those obtained from the long MD simulations, the umbrella sampling simulations were repeated under different conditions. We increased the length of each window to 500 ps, used the Berendsen thermostat, or changed the restraint potential. Changing to the Berendsen thermostat had no effect. However, longer simulations did alter the rotamer ratios. For **4.1**, the ratio between *gg* and *gt* was 55:44; for **4.2**, the ratio was 33:66. Both ratios are flipped from what is observed in the long MD simulations. A restraining potential that is too large can bias the final distribution because higher energy conformations will dominate.[1,32] Thus, we tried smaller restraining potentials of 15 and 5 kcal (mol rad^2)$^{-1}$, and both gave the opposite results from the long MD simulations.

Finally, we also used fewer windows in the WHAM calculations. There is good overlap between the individual windows shown in Figure 4.24 and Figure 4.25. We used 19 of these windows, every 20° from –180° to 180°, and the ratio between *gg* and *gt* for **4.2** changed to 60:38, much closer to the long MD simulations. The energy difference between the two conformations increased to 0.3 kcal mol^{-1}. For **4.1**, using fewer windows did not affect the energy difference between *gg* and *gt*, thus the rotamer ratio was unchanged. However, for the umbrella sampling simulations with the 5 kcal (mol rad^2)$^{-1}$, the *gg*:*gt* ratio for **4.1** was 44:55 when 19 windows were used. This ratio matches the long MD simulations and was reversed when all 73 windows were used. For the simulations of **4.2** under the same conditions, both 73 and 19 windows gave 38:61 *gg:gt* – the reverse of the MD simulations.

4.4. Conclusions

In the previous chapter, AMBER/GLYCAM06 MD simulations of **4.1** and **4.2** gave effectively one rotamer population about the C4–C5 bond. The results in Section 4.3.1 show that the GLYCAM06 energy difference between the *gg* and *gt* rotamers is about 2 kcal mol^{-1}. This energy difference gives a 29:1 ratio between *gg* and *gt* rotamers (or 97% *gg*), which is the same result that GLYCAM06 yields in the MD simulations (Figures 3.14 and 3.16). Additionally, the vicinal coupling constants from MD simulations of **4.1** and **4.2** differ substantially from the observed experimental values. The original GLYCAM06 parameters for the C4–C5 bond clearly overestimate the energy different between these two rotamers.

We developed new force field parameters for the rotations about the C4–C5 bond. The new terms improved the MD results for $^{3}J_{H4,H5}$ without affecting the couplings for the galactofuranose ring. However, these new terms also negatively affected the rotamer distribution about the C5–C6 bond. Consequently, the MD values for $^{3}J_{H5H6R}$ do not show as good agreement to experiment as the values from simulations with the original parameters, though the new values are within error of the experimental values. Further improvements to the force field parameters may be necessary. The MMCSA procedure is not limited to a three dimensional PES; therefore, including the H4–C4–C5–C6 term might be one way to improve the fits.

The WHAM calculations for **4.1** and **4.2** with the new torsion parameters are unsatisfying. The first simulation conditions worked well for the original GLYCAM06 parameters. Specifically, the results from WHAM matched those

from long MD simulations, while taking significantly less time (14.6 ns vs. 250 ns). However, with the new torsion parameters, the same umbrella sampling conditions gave WHAM results that did not match the long MD simulations. Changing parameters, such as the restraining potential or the number of windows used in the WHAM equations, gave different results for each anomer. Relatively small changes in the relative energies between rotamers have larger effects on the rotamer distributions. For example, if the *gt* rotamer is 0.2 kcal mol^{-1} higher in energy than the *gg* rotamer, the ratio between the two will be 53:46 *gg:gt*. Increasing the energy difference to 0.4 kcal mol^{-1} changes the ratio to 62:37 *gg:gt*. These small energy differences may be at the limit of force-field based calculations.[34,35]

4.5. References

1. Leach, A. R. Potentials of Mean Force. In *Molecular Modelling: Principles and Applications*, 2nd ed.; Prentice Hall: New York, 2001; pp 580–585.

2. Islam, S. M.; Richards, M. R.; Taha, H. A.; Byrns, S. C.; Lowary, T. L.; Roy, P.-N. *J. Chem. Theory Comput.* **2011**, *7*, 2989–3000.

3. Roux, B. *Comput. Phys. Commun.* **1995**, *91*, 275–282.

4. Kirschner, K. N.; Yongye, A. B.; Tschampel, S. M.; González-Outeiriño, J.; Daniels, C. R.; Lachele Foley, B.; Woods, R. J. *J. Comput. Chem.* **2008**, *29*, 622–655.

5. Kumar, S.; Rosenberg, J. M.; Bouzida, D.; Swendsen, R. H.; Kollman, P. A. *J. Comput. Chem.* **1992**, *13*, 1011–1021.

6. Torrie, G. M.; Valleau, J. P. *J. Comput. Phys.* **1977**, *23*, 187–199.

7. Hub, J. S.; de Groot, B. L.; van der Spoel, D. *J. Chem. Theory Comput.* **2010**, *6*, 3713–3720.

8. Case, D. A.; Darden, T. A.; T.E. Cheatham, I.; Simmerling, C. L.; Wang, J.; Duke, R. E.; Luo, R.; Crowley, M.; Walker, R. C.; Zhang, W.; Merz, K. M.; Wang, B.; Hayik, S.; Roitberg, A.; Seabra, G.; Kolossváry, I.; Wong, K. F.; Paesani, F.; Vanicek, J.; Wu, X.; Brozell, S. R.; Steinbrecher, T.; Golke, H.; Yang, L.; Tan, C.; Mongan, J.; Hornak, V.; Cui, G.; Mathews, D. H.; Seetin, M. G.; Saugi, C.; Babin, V.; Kollman, P. A. *AMBER 10*, Univeristy of California, San Francisco: 2008.

9. Pearlman, D. A.; Case, D. A.; Caldwell, J. W.; Ross, W. S.; Cheatham, T. E.; DeBolt, S.; Ferguson, D.; Seibel, G.; Kollman, P. *Comput. Phys. Commun.* **1995**, *91*, 1–41.

10. Leach, A. R. Empirical Force Field Models: Molecular Mechanics. In *Molecular Modelling: Principles and Applications*, 2nd ed.; Prentice Hall: New York, 2001; pp 165–252.

11. Allinger, N. L. *J. Am. Chem. Soc.* **1977**, *99*, 8127–8134.

12. Allinger, N. L.; Li, F. B.; Yan, L. Q. *J. Comput. Chem.* **1990**, *11*, 848–867.

13. Allinger, N. L.; Li, F. B.; Yan, L. Q.; Tai, J. C. *J. Comput. Chem.* **1990**, *11*, 868–895.

14. Allinger, N. L.; Chen, K. S.; Lii, J. H. *J. Comput. Chem.* **1996**, *17*, 642–668.

15. Allinger, N. L.; Chen, K. S.; Katzenellenbogen, J. A.; Wilson, S. R.; Anstead, G. M. *J. Comput. Chem.* **1996**, *17*, 747–755.

16. Lii, J. H.; Allinger, N. L. *J. Phys. Chem. A* **2008**, *112*, 11903–11913.

17. Guvench, O.; MacKerell, A. D. *J. Mol. Model.* **2008**, *14*, 667–679.

18. Metropolis, N.; Rosenbluth, A. W.; Rosenbluth, M. N.; Teller, A. H.; Teller, E. *J. Chem. Phys.* **1953**, *21*, 1087–1092.

19. Jorgensen, W. L.; Chandrasekhar, J.; Madura, J. D.; Impey, R. W.; Klein, M. L. *J. Chem. Phys.* **1983**, *79*, 926–935.

20. Adelman, S. A.; Doll, J. D. *J. Chem. Phys.* **1976**, *64*, 2375–2388.

21. Ryckaert, J.-P.; Ciccotti, G.; Berendsen, H. J. C. *J. Comput. Phys.* **1977**, *23*, 327–341.

22. Grossfield, A. *An Implementaion of WHAM: the Weighted Histogram Analysis Method*, 2.0.2; 2008.

23. Grossfield, A. http://membrane.urmc.rochester.edu/Software/WHAM/WHAM.html (accessed March 22, 2010)

24. Wang, T. Potential of mean force (PMF) calculations with AMBER and WHAM. http://projects.eml.org/mcm/people/wang/PMF/tutorial.html (March 22, 2010)

25. Frisch, M. J.; Trucks, G. W.; Schlegel, H. B.; Scuseria, G. E.; Robb, M. A.; Cheeseman, J. R.; Montgomery, J. A., Jr.; Vreven, T.; Kudin, K. N.; Burant, J. C.; Millam, J. M.; Iyengar, S. S.; Tomasi, J.; Barone, V.; Mennucci, B.; Cossi, M.; Scalmani, G.; Rega, N.; Petersson, G. A.; Nakatsuji, H.; Hada, M.; Ehara, M.; Toyota, K.; Fukuda, R.; Hasegawa, J.; Ishida, M.; Nakajima, T.; Honda, Y.; Kitao, O.; Nakai, H.; Klene, M.; Li, X.; Knox, J. E.; Hratchian, H. P.; Cross, J. B.; Bakken, V.; Adamo, C.; Jaramillo, J.; Gomperts, R.; Stratmann, R. E.; Yazyev, O.; Austin, A. J.; Cammi, R.; Pomelli, C.; Ochterski, J. W.; Ayala, P. Y.; Morokuma, K.; Voth, G. A.; Salvador, P.; Dannenberg, J. J.; Zakrzewski, V. G.; Dapprich, S.; Daniels, A. D.; Strain, M. C.; Farkas, O.; Malick, D. K.; Rabuck, A. D.; Raghavachari, K.; Foresman, J. B.; Ortiz, J. V.; Cui, Q.; Baboul, A. G.; Clifford, S.; Cioslowski, J.; Stefanov, B. B.; Liu, G.; Liashenko, A.; Piskorz, P.; Komaromi, I.; Martin, R. L.; Fox, D. J.; Keith, T.; Al-Laham, M. A.; Peng, C. Y.; Nanayakkara, A.; Challacombe, M.; Gill, P. M. W.; Johnson, B.; Chen, W.; Wong, M. W.; Gonzalez, C.; Pople, J. A. *Gaussian 03* Revision C.02; Gaussian, Inc.: Wallingford, CT, 2004.

26. Roothaan, C. C. J. *Rev. Mod. Phys.* **1951**, *23*, 69–89.

27. Rassolov, V. A.; Ratner, M. A.; Pople, J. A.; Redfern, P. C.; Curtiss, L. A. *J. Comput. Chem.* **2001**, *22*, 976–984.

28. Becke, A. D. *J. Chem. Phys.* **1993**, *98*, 5648–5652.

29. Clark, T.; Chandrasekhar, J.; Spitznagel, G. W.; Schleyer, P. V. *J. Comput. Chem.* **1983**, *4*, 294–301.

30. Frisch, M. J.; Pople, J. A.; Binkley, J. S. *J. Chem. Phys.* **1984**, *80*, 3265–3269.

31. Berendsen, H. J. C.; Postma, J. P. M.; Gunsteren, W. F. v.; DiNola, A.; Haak, J. R. *J. Chem. Phys.* **1984**, *81*, 3684–3690.

32. Kästner, J. *WIREs Comput. Mol. Sci.* **2011**, *1*, 932–942.

33. Allen, M. P.; Tildesley, D. J. Errors in equilibrium averages. In *Computer Simulation of Liquids*, Calrendon Press: Oxford, UK, 1987; pp 192–195.

34. Yongye, A. B.; Foley, B. L.; Woods, R. J. *J. Phys. Chem. A* **2008**, *112*, 2634–2639.

35. Taha, H. A.; Castillo, N.; Sears, D. N.; Wasylishen, R. E.; Lowary, T. L. *J. Chem. Theory Comput.* **2010**, *6*, 212–222.

Chapter 5:

Solution-state conformation of β-D-galactofuranosyl trisaccharides from NMR experiments and AMBER/GLYCAM simulations

Compounds **5.1** and **5.2** discussed in this chapter were synthesized by Mr. Simon Byrns or Dr. Maju Joe, using published protocols.[1]

5.1. Introduction

In Chapters 3 and 4, we presented molecular dynamics (MD) simulations as a method to elucidate solution-state conformation of galactofuranose (Gal*f*) monosaccharides. Gal*f* residues are often components of oligosaccharides (Chapter 1);[2,3] therefore, we sought to extend our studies to trisaccharides **5.1** and **5.2** (Figure 5.1). Both **5.1** and **5.2** represent substructures of the galactan chain that forms part of the cell wall of mycobacteria. Information on the conformation of these trisaccharides may provide insight into their biosynthesis. For example, the octyl glycoside of **5.1** and **5.2** are known acceptors for GlfT2,[4] one of the enzymes responsible for the synthesis of the mycobacterial galactan. The X-ray crystal structure of GlfT2 has recently been solved,[5] and docking **5.1** and **5.2,** or the natural galactan acceptor, into this structure would provide information about important interactions in the active site.

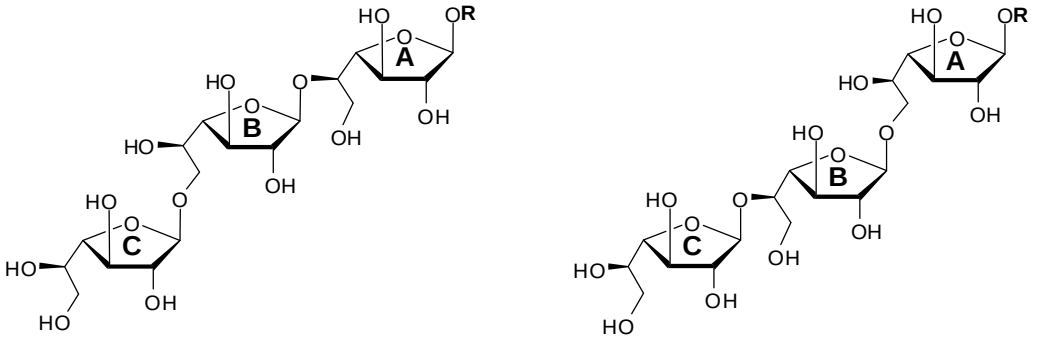

5.1 **5.2**

R = CH_3, C_8H_{17}

Figure 5.1. The trisaccharides discussed in this chapter, methyl or octyl β-D-galactofuranosyl-(1→6)-β-D-galactofuranosyl-(1→5)-β-D-galactofuranoside (**5.1**), and methyl or octyl β-D-galactofuranosyl-(1→5)-β-D-galactofuranosyl-(1→6)-β-D-galactofuranoside (**5.2**). The rings are labeled in each compound to facilitate discussion.

Outside the plasma membrane of *Mycobacterium tuberculosis*, there is a large glycolipid, the mycolyl–arabinogalactan (mAG) complex, which is attached to peptidoglycan through a linker disaccharide, phosphate α-L-rhamnopyranosyl-(1→3)-2-acetamido-2-deoxy-β-D-glucopyranoside.[6,7] The galactan of mAG is composed of 30–35 residues of alternating β-(1→5) and β-(1→6) linkages, as illustrated in Figure 5.2. Two bifunctional enzymes are responsible for the biosynthesis of the galactan chain, GlfT1 and GlfT2.[4,8,9] GlfT1 attaches the first two Gal*f* moieties, and GlfT2 adds the remaining residues.

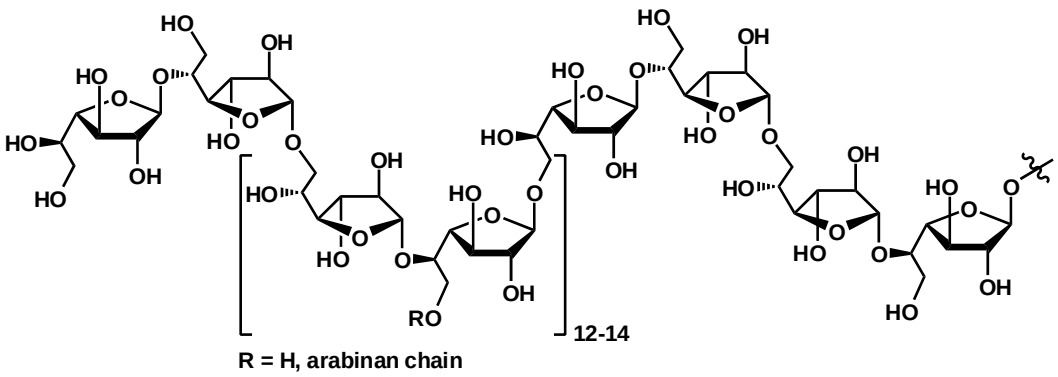

Figure 5.2. The galactan chain of the mAG complex.

Saturation transfer difference (STD) NMR experiments[10] have shown that the octyl glycosides of **5.1** and **5.2** bind competitively to GlfT2.[11] More recent STD NMR experiments, in combination with site-directed mutagenesis, demonstrate that both glycosidic linkages are formed in the same active site.[12] Additionally, the reducing end residue (ring A) of **5.1** or **5.2** show the strongest STD signals, indicating it is in closer contact with the enzyme than non-reducing residues involved in the reaction.[13] It is unclear whether the same would hold true for longer oligosaccharides. One rationale for the weaker STD signals at the non-reducing end of the trisaccharides is to allow for conformational changes to accommodate the glycosylation reaction. However, the details of such conformational changes are unknown. Computational models of the galactan could aid in our understanding of the specificity of GlfT2.[12]

The X-ray crystal structure of GlfT2, mentioned above, has a hydrophobic channel that can accept the growing galactan chain.[5] Neither acceptor **5.1** nor **5.2** has been able to crystallize with GlfT2 to day. However, the acceptors **5.1** and **5.2** were modeled into the active site, and their relative positions provide an

explanation for the alternating regiochemistry of the glycosidic linkages. When **5.1** is in the hydrophobic channel, the non-reducing residue has a β-(1→6) linkage, and the acceptor is deeper in the active site, leaving the 5-OH positioned appropriately for reaction. With **5.2**, the terminal residue has a β-(1→5) linkage and is more exposed; thus, the 6-OH is held in the correct orientation to react. This mechanism is still tentative, and MD simulations of the GlfT2-acceptor complex would provide more information on key contacts that are not apparent in the current model.

In this chapter, we present MD simulations on the methyl glycosides of **5.1** and **5.2**, which are simple models of the galactan present in the mAG complex. Both compounds contain a β-(1→5) and β-(1→6) glycosidic linkage; thus, they represent the smallest repeating units of the galactan. We compare the simulations with coupling constants from solution-state NMR experiments. Earlier, we described new parameters for the O4–C4–C5–C6 and C3–C4–C5–C6 terms to address the limitations of the original GLYCAM06[14] terms that held the C4–C5 bond in one conformation (Chapter 4). The new terms successfully altered the rotamer populations for the galactofuranose monosaccharides (Section 4.3.3.1). We also discuss the roles the new terms play on the conformation of the trisaccharides **5.1** and **5.2** in MD simulations.

5.2. Methods

5.2.1. NMR spectroscopy

^{1}H NMR spectra of the octyl glycosides **5.1** and **5.2** were acquired in D_2O on a 700 MHz spectrometer at 300 K. For the 1D spectra, a presaturation pulse sequence was used to eliminate the residual HOD signal. While the trisaccharides are both known compounds and spectral details have been reported,[1] there is significant overlap in the region for the ring protons. Thus, we ran a series of 1D gradient-enhanced chemical shift selective filtering (ge-CSSF) TOCSY spectra[15,16] to accurately determine the vicinal proton–proton coupling constants for comparison with our MD simulations. The spectra are shown in Section 5.3.1, and their captions indicate the conditions used to acquire each spectrum, including the mixing times (mix) and the frequency differences (Δ) between the irradiated peak and its nearest neighbor. Several of the galactofuranose rings were virtually coupled[17] spin systems, and we simulated these spectra using the SpinWorks[18] and WinDNMR[19] programs. No line broadening or window functions were applied during the data analysis.

5.2.2. MD simulations

All MD simulations of the methyl glycosides of **5.1** and **5.2** were carried out using the PMEMD module of the AMBER 10[20] suite of programs and the GLYCAM06[14] force field with either the original or new torsion parameters for the O4–C4–C5–C6 and C3–C4–C5–C6 dihedral angles (described in Chapter 4). The simulations were carried out under periodic boundary conditions and using particle mesh Ewald summation for long-range interactions. The trisaccharides

were built from multiple units of β-D-Gal*f* (described in Chapter 3), using additive atomic charges[21-24] and solvated in boxes of explicit TIP3P[25] water molecules. For **5.1**, the initial box was 35.0 x 34.3 x 30.1 Å and contained 724 water molecules. For **5.2**, the box was 32.3 x 30.5 x 34.2 Å and contained 669 water molecules. All simulations were run under NPT conditions at 300 K and 1 atm. The temperature was maintained with the Berendsen theromostat,[26] and velocities were rescaled every 1 ps. The SHAKE algorithm[27] was used to constrain bonds containing hydrogen. The cutoff for nonbonding interactions was 8 Å, and nonbonded and electrostatic inteactions were unscaled throughout the simulations.

The simulations were run for 250 ns with a 2 fs timestep, after an equilibration period. Equilibration began by holding the trisaccharides fixed and minimizing the water molecules with 50 steps of steepest decent followed by 950 steps conjugate gradient minimization. Then the entire system was minimized in the same manner. After minimization, a short period of simulated annealing was run, heating the system from 5 K to 300 K over 50 ps then cooling back to 5 K over 50 ps. The final step of equilibration heated the system back to 300 K over 100 ps and ran at constant temperature for 100 ps before the production period began.

5.3. Results and discussion

5.3.1. NMR spectroscopy

The 1D ^{1}H and CSSF-TOCSY spectra for the octyl glycoside **5.1** are shown in Figure 5.3. Figure 5.4 shows the same spectra for the octyl glycoside

5.2. For both trisaccharides, the 3.55–4.20 ppm region of the 1D spectrum is crowded, making a first-order interpretation of the spectrum difficult. The three anomeric signals are all distinct, however, and provide handles for selective NMR experiments. For **5.1**, the individual anomeric signals were selectively irradiated in 1D-ge-CSSF-TOCSY experiments to provide a separate spectrum for each ring system. Because $^{3}J_{H1,H2}$ is small (~2 Hz), the intensities of the signals for H5, H6, and H6' fall off sharply, though the multiplets can still be observed. For **5.2**, we obtained spectra that were difficult to interpret using the anomeric signals at 5.22 ppm (ring C) and 4.99 ppm (ring A). Instead, we irradiated the signals at 3.68 ppm (ring C) and 3.62 ppm (ring A). The signal intensities for the anomeric protons in these spectra are significantly reduced, but the remaining multiplets are still distinct.

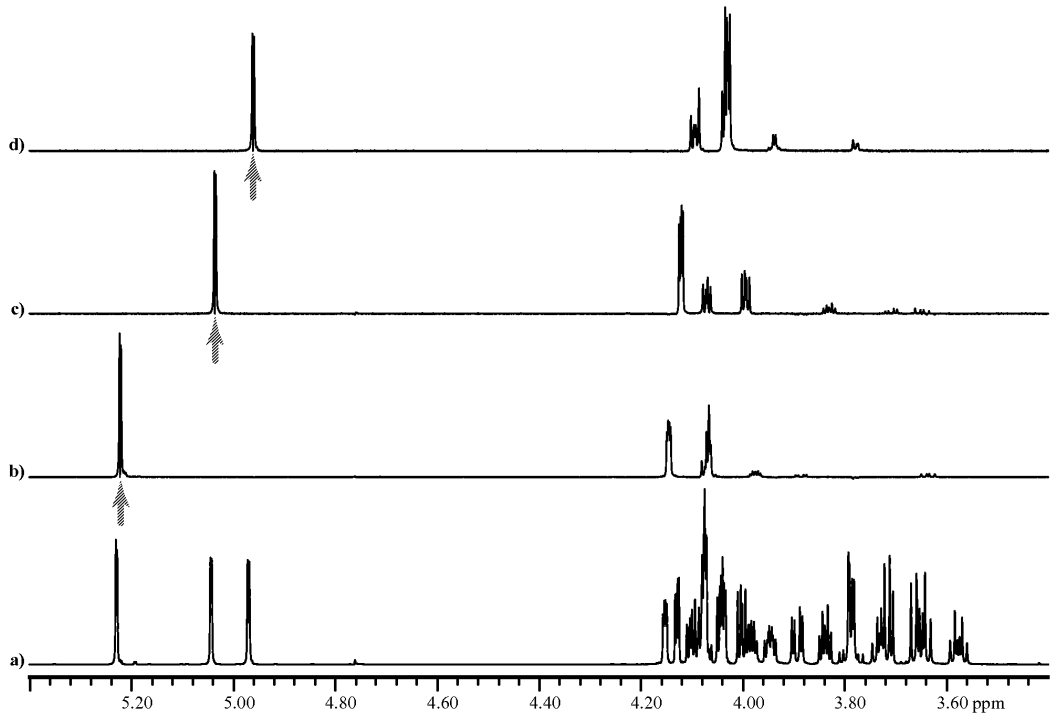

Figure 5.3. CSSF-TOCSY spectra for the octyl glycoside **5.1**. Spectrum *a* is an expansion of the 1D ^{1}H spectrum, spectra *b* through *d* show the 1D-ge-CSSF-TOCSY of each ring with an arrow indicating the irradiation frequency as follows: b) ring B, selectively irradiated at 5.15 ppm, mix = 0.2 s, Δ = 111 Hz; c) ring C, selectively irradiated at 5.04 ppm, mix = 0.2 s, Δ = 38 Hz; d) ring A, selectively irradiated at 5.97 ppm, mix = 0.2 s, Δ = 38 Hz.

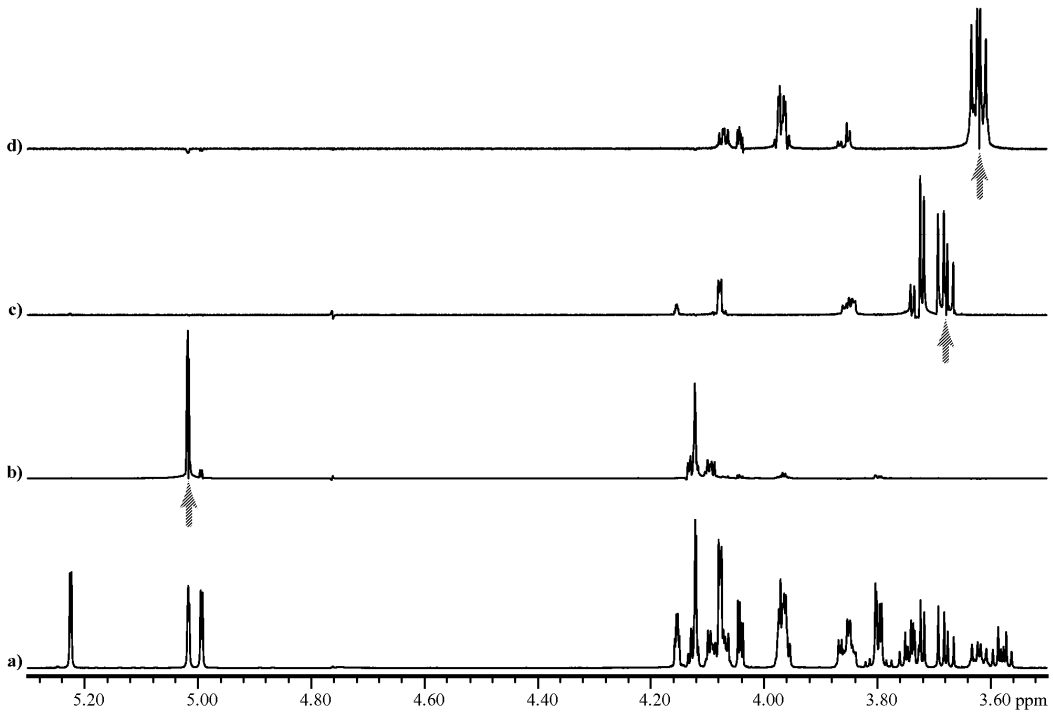

Figure 5.4. CSSF-TOCSY spectra for the octyl glycoside **5.2**. Spectrum *a* is an expansion of the 1D ^{1}H spectrum, spectra *b–d* show the 1D-ge-CSSF-TOCSY of each ring with an arrow indicating the irradiation frequency as follows: b) ring B, selectively irradiated at 5.02 ppm, mix = 0.2 s, Δ = 3.5 Hz; c) ring C, selectively irradiated at 3.68 ppm, mix = 0.12 s, Δ = 10 Hz; d) ring A, selectively irradiated at 3.62 ppm, mix = 0.12 s, Δ = 10 Hz.

The spin systems for rings A and B of **5.1** contain virtually coupled[17] multiplets (Figure 5.3, spectra *d* and *b*, respectively). Specifically, in ring A, H6 is separated from H6' by 7.3 Hz, $^{2}J_{H6,H6'}$ is –12.1 Hz, and the ratio Δν/*J* is 0.60. For ring B, H3 is separated from H4 by 6.6 Hz, $^{3}J_{H3,H4}$ is 6.4 Hz, and the ratio Δν/*J* is 1.0. For both rings, the ratio Δν/*J* is less than 2, which mean a first-order analysis of the spectra will give inaccurate values for the coupling constants and chemical shifts. (Virtual coupling was also discussed in Section 2.3.4.) The CSSF-TOCSY spectra for these rings were simulated in SpinWorks[18] until a good fit was obtained visually. Because the intensities of the CSFF-TOCSY spectra are

distorted, the root-mean square difference in SpinWorks between the experimental and simulated spectra was inadequate to judge the quality of the simulation. Therefore, the spectra for all three rings were also simulated in WinDNMR,[19] summed, and compared with the experimental 1D ^{1}H spectrum until a good correlation (i.e. Pearson's $r \geq 0.95$) was obtained (Figure 5.5), as we have described previously.[28] The chemical shifts and coupling constants from this interpretation are listed in Table 5.1 and Table 5.2, respectively.

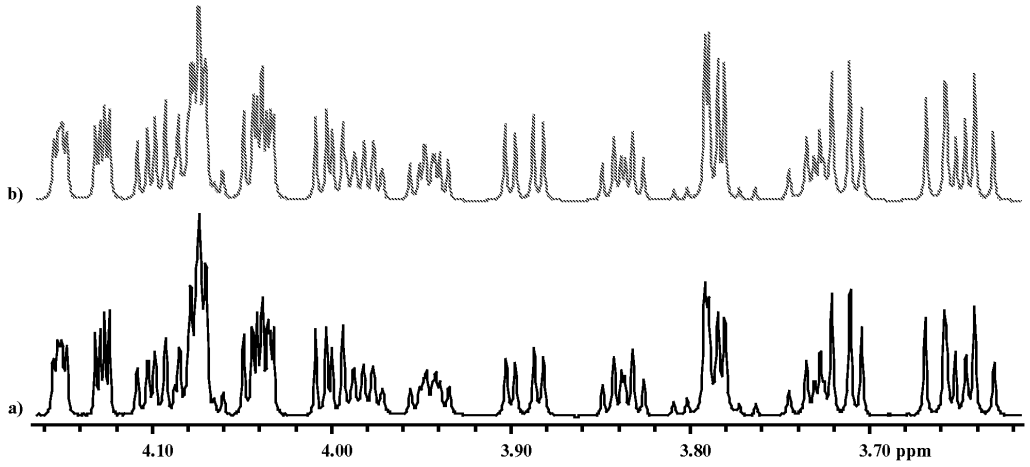

Figure 5.5. Simulated and experimental spectra for **5.1**. Spectrum *a* is an expansion of the 1D ^{1}H spectrum (also shown in Figure 5.3), and *b* is the simulated ^{1}H spectrum for the same region. The correlation coefficient (i.e. Pearson correlation) between the spectra in *a* and *b* is r = 0.967.

All three rings of **5.2** contain virtually coupled multiplets. In ring A, the chemical shifts of H4 and H5 differ by less than 1 Hz, and the ratio $\Delta\nu/J$ is quite small at 0.11. There are two virtually coupled multiplets in ring B, H2 and H3 are separated by 3.2 Hz, and H6 and H6' are separated by 7.0 Hz, giving $\Delta\nu/J$ ratios of 0.89 and 0.58, respectively. In ring C, the difference in the chemical shifts for H3 and H4 is only 2 Hz, leading to a ratio $\Delta\nu/J$ of 0.30. All three of these ring

systems were simulated in SpinWorks and WinDNMR, as described above, until we obtained a good correlation between the simulated and experimental spectra (Figure 5.6). The chemical shifts and coupling constants for **5.2**. are also listed in Table 5.1 and Table 5.2, respectively.

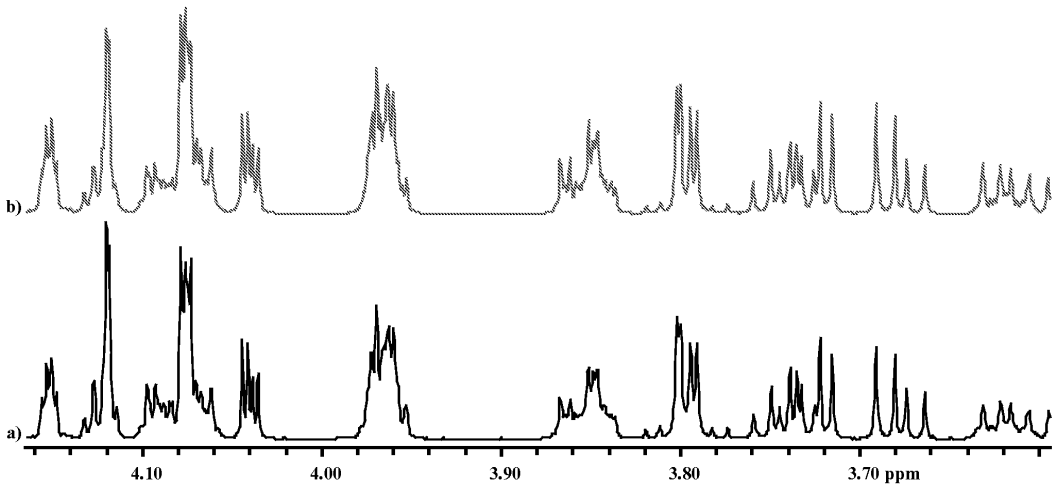

Figure 5.6. Simulated and experimental spectra for **5.2**. Spectrum *a* is an expansion of the 1D ^{1}H spectrum (also shown in Figure 5.4), and *b* is the simulated ^{1}H spectrum for the same region. The correlation coefficient (i.e. Pearson correlation) between the spectra in *a* and *b* is r = 0.984.

Table 5.1. Chemical shifts for the carbohydrate portion of the octyl glycosides **5.1** and **5.2**.

	5.1	**5.1**	**5.1**	**5.2**	**5.2**	**5.2**
	Ring A	**Ring B**	**Ring C**	**Ring A**	**Ring B**	**Ring C**
δ_{H1} (ppm)	4.97	5.23	5.04	4.99	5.02	5.22
δ_{H2} (ppm)	4.04	4.15	4.13	4.04	4.12	4.15
δ_{H3} (ppm)	4.10	4.08	4.08	4.07	4.12	4.08
δ_{H4} (ppm)	4.04	4.07	4.00	3.97	4.09	4.07
δ_{H5} (ppm)	3.95	3.98	3.84	3.97	3.96	3.85
δ_{H6} (ppm)	3.79	3.89	3.72	3.86	3.80	3.73
$\delta_{H6'}$ (ppm)	3.78	3.64	3.66	3.62	3.79	3.68

Table 5.2. Proton–proton coupling constants for the carbohydrate portion of the octyl glycosides **5.1** and **5.2**.

	5.1 Ring A	**5.1 Ring B**	**5.1 Ring C**	**5.2 Ring A**	**5.2 Ring B**	**5.2 Ring C**
$^{3}J_{H1,H2}$ **(Hz)**	2.3	1.9	1.9	2.2	1.9	2.0
$^{4}J_{H1,H3}$ **(Hz)**	0.0	0.0	0.0	0.0	0.5	0.0
$^{3}J_{H2,H3}$ **(Hz)**	4.2	3.6	3.6	4.1	3.6	4.1
$^{3}J_{H3,H4}$ **(Hz)**	6.9	6.4	6.4	6.3	6.7	6.6
$^{3}J_{H4,H5}$ **(Hz)**	3.5	3.5	4.3	3.5	3.3	3.5
$^{3}J_{H5,H6}$ **(Hz)**	5.1	3.8	4.7	3.8	4.9	4.6
$^{3}J_{H5,H6'}$ **(Hz)**	6.4	7.4	7.2	7.1	7.1	7.3
$^{2}J_{H6,H6'}$ **(Hz)**	–12.1	–11.0	–11.7	–10.8	–12.1	–11.8

5.3.2. MD simulations with the original GLYCAM06 parameters

5.3.2.1. Conformation of the galactofuranose rings in 5.1 and 5.2

In MD simulations of the monosaccharide, we saw one major conformation for the furanose ring, the E_3 ring conformation, though the distribution of conformers was broad (Section 3.3.4.1). Similarly, we observe a large distribution of ring conformations for rings A and C in the methyl glycoside **5.1** (Figure 5.7), while the distribution for the central residue, ring B, is narrower. Ring A has a major peak near P = 34°, the $^{4}T_3$ conformation, and a minor peak near P = 128°, the ^{1}E conformation. These two conformers are close to those observed in simulations of the monosaccharide. Unlike the monosaccharide, there appears to be another shoulder near P = –44°, between the $^{2}T_1$ and E_1 conformations. There is only one major peak for ring B at P = 50°, the ^{4}E conformer. Ring C also has two major conformations, and both have

approximately the same populations. One is centered near P = 34°, which is the major conformation we see for ring A, and the other is centered near P = 0°, the $^{2}T_{3}$ conformation.

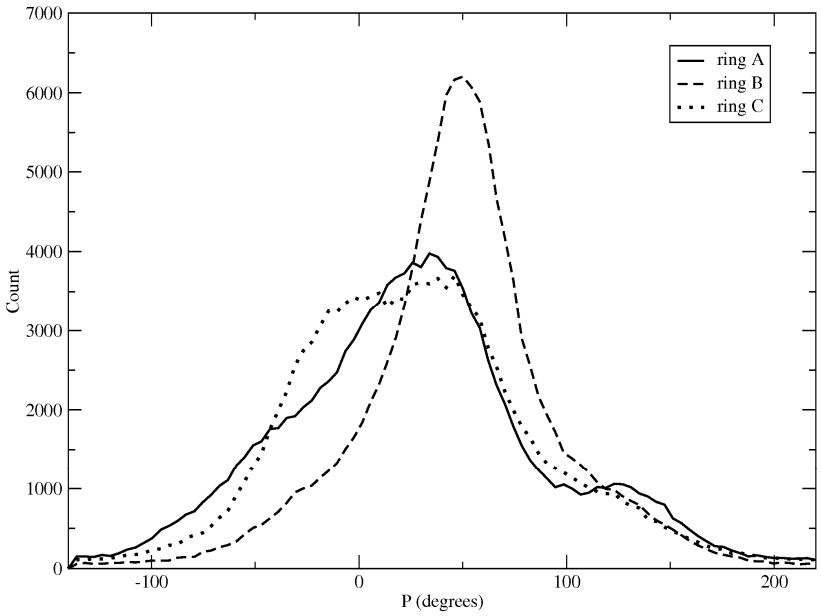

Figure 5.7. Histograms of pseudorotational phase angle P for **5.1** using the original GLYCAM06 parameters. The solid line is ring A, the dashed line is ring B, and the dotted line is ring C.

With the methyl glycoside of **5.2**, there is broad distribution of ring conformations for all three residues (Figure 5.8). Ring A has a major population centered at P = 20°, the E_3 conformer. There is also a small shoulder in the region of P = 110°–130°, the $^{1}T_{O}$ and ^{1}E conformations. As we see with **5.1**, both of these conformers are similar to the ring conformations we observed in simulations with the monosaccharide. Residue B has an O5 linkage to residue C. In **5.1**, the same linkage is found for residue A, and these rings in both trisaccharides show

similar distributions of conformations. In **5.2**, ring B has a major peak centered at P = 38°, the $^{4}T_{3}$ conformation, and a minor peak near P = 128°, the ^{1}E conformation. There is also a small shoulder at P = –40°, the $^{2}T_{1}$ conformation. The distribution for ring C is narrower than the rest, similar to ring B in **5.1**. The major population occurs at P = 50°, the ^{4}E conformer, and there is another population near P = 128°, which also overlays with the minor population for ring B. The data presented in Figure 5.7 and Figure 5.8 show having the anomeric oxygen attached to a secondary carbon center affects the ring conformation more than the groups on O5 or O6. However, whether the anomeric oxygen is attached to a methyl group or O6 of Gal*f* has little effect on the ring conformation. That is, the distribution of ring conformations for rings A and C in **5.1**, as well as rings A and B in **5.2**, are closer to the monosaccharide than those of ring B of **5.1** or ring C of **5.2**.

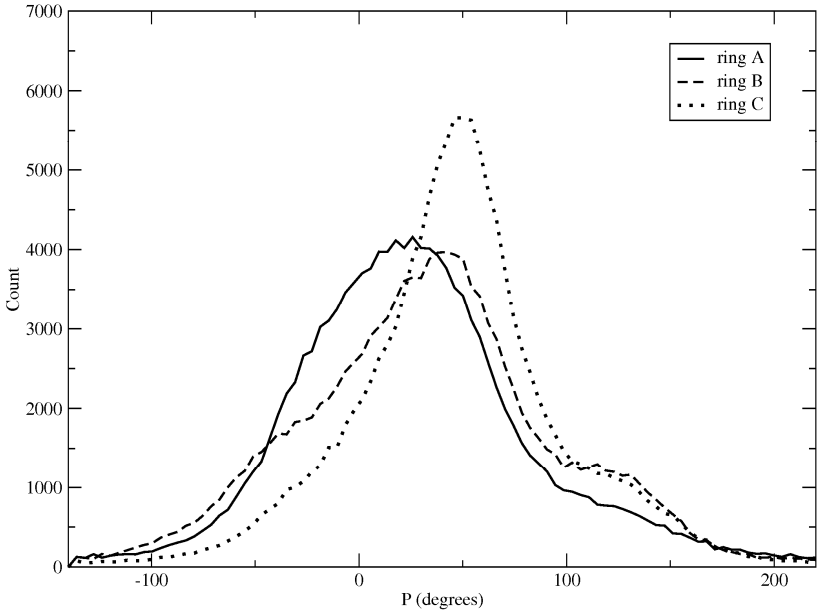

Figure 5.8. Histograms of pseudorotational phase angle *P* for **5.2** using the original GLYCAM06 parameters. The solid line is ring A, the dashed line is ring B, and the dotted line is ring C.

The distributions for the ring H–C–C–H dihedral angles do not vary significantly among the three residues of **5.1** (Figure 5.9), despite the differences in overall ring conformation described above. Similar distributions are to be expected as the vicinal coupling constants (Table 5.2) are similar for the three rings. The torsion for H1–C1–C2–H2 (solid line) shows the most obvious changes among the rings. For rings A and C, there are two distinct populations, a major population centered near 150° and a minor population centered near 100°. However, for ring B, there is only one peak, centered at 125°. The H2–C2–C3–H3 dihedral (dashed line) for all three rings shows two populations, one centered at –150° and the other at –100°. The H3–C3–C4–H4 torsion (dotted line) shows a major population centered at 160° for all three residues, but only ring A shows an obvious second population centered at 120°.

The distributions for the H–C–C–H dihedral angles of **5.2** are also similar for all three residues (Figure 5.10), corresponding to the similar values for $^{3}J_{H1,H2}$, $^{3}J_{H2,H3}$, and $^{3}J_{H3,H4}$ for the three rings (Table 5.2). For rings A and B, the H1–C1–C2–H2 torsion (solid line) shows two populations, one centered 150° and another at 100°. For ring C, there is only one broad distribution, centered at 125°. The differences observed in the H1–C1–C2–H2 correspond to the differences in distribution of the ring conformations, described above. For the H2–C2–C3–H3 dihedral angles (dashed line), there are little differences among the residues. All have two populations, a major one at –150° and a minor one at –100°. Similarly, all of the H3–C3–C4–H4 torsions (dotted line) have a major population at 160°, with a tail towards more positive values for rings A and C. Ring B has a small shoulder for a second population at 120°.

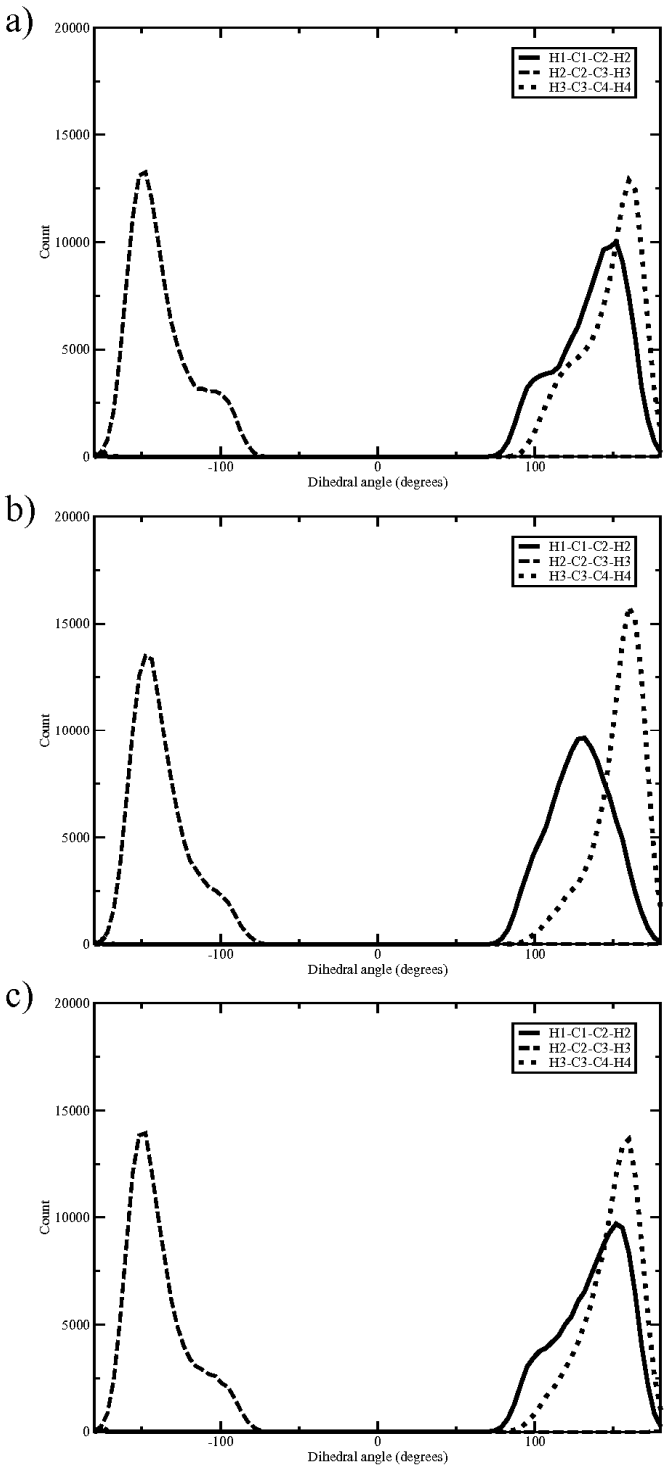

Figure 5.9. Histograms for the ring dihedral angles of **5.1** using the original GLYCAM06 parameters. Graph *a*) corresponds to ring A, graph *b*) corresponds to ring B, and graph *c*) corresponds to ring C. For all three graphs, the solid line is for H1–C1–C2–H2, the long dashed line is for H2–C2–C3–H3, and the dotted line is for H3–C3–C4–H4.

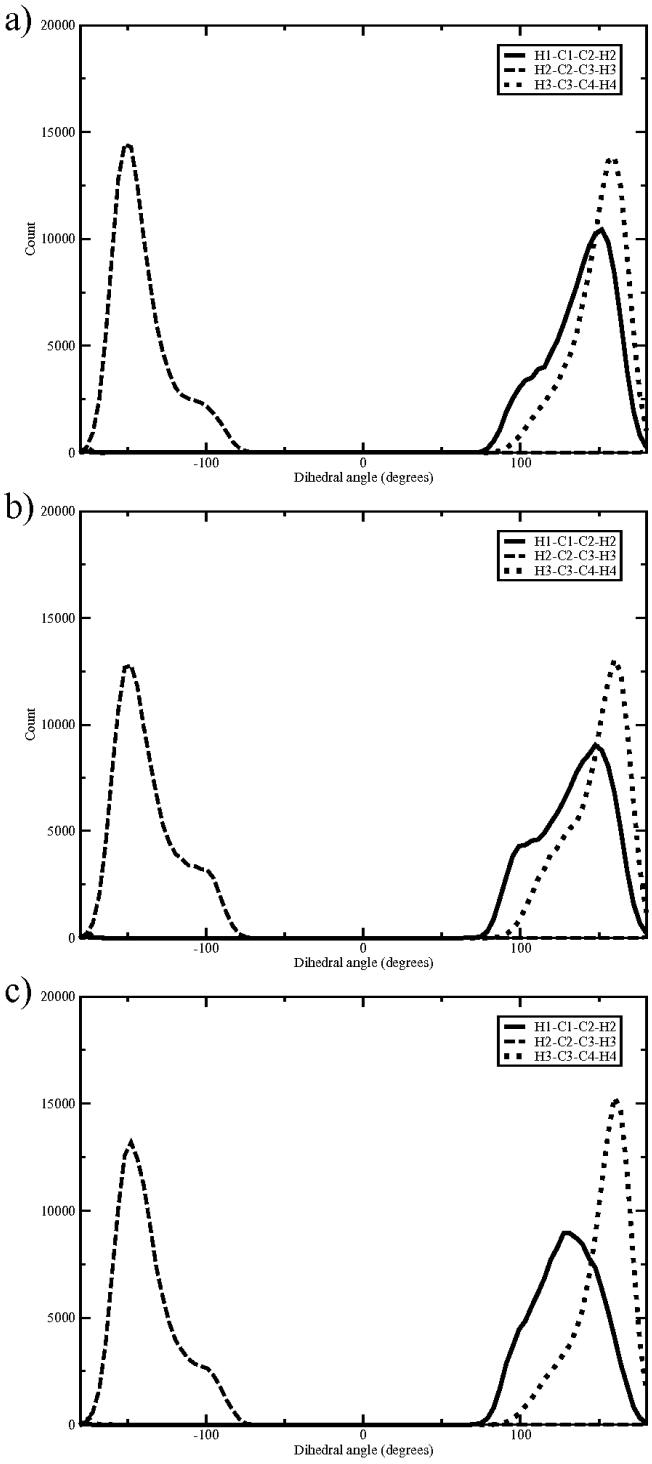

Figure 5.10. Histograms for the ring dihedral angles of **5.2** using the original GLYCAM06 parameters. Graph *a*) corresponds to ring A, graph *b*) corresponds to ring B, and graph *c*) corresponds to ring C. For all three graphs, the solid line is for H1–C1–C2–H2, the long dashed line is for H2–C2–C3–H3, and the dotted line is for H3–C3–C4–H4.

5.3.2.2. Conformation about the C4–C5 bonds of 5.1 and 5.2

In MD simulations of the monosaccharide with the original GLYCAM06 parameters, we observed mainly one rotamer about the C4–C5 bond, the *gg* rotamer (Section 3.3.4.2). We see the same thing in simulations with both of the trisaccharides. Figure 5.11 shows the C4–C5 rotamer distribution for **5.1** over the course of the simulation, and Figure 5.12 shows the same for **5.2**. All three C4–C5 bonds for both trisaccharides remain in the *gg* conformation for the majority of the simulations. The populations observed at the beginning of the calculation are unchanged from those observed at the end. Though, simulations do not converge until after 220 ns, at which point the variance in the mean is 4% or less for all 3 residues. Table 5.3 details the final C4–C5 rotamer populations for each residue of **5.1** and **5.2**.

Table 5.3. C4–C5 rotamer populations for **5.1** and **5.2** from simulations with the original GLYCAM06 parameters.

Cmpd	Residue	% *gg*	% *tg*	% *gt*
5.1	A	98 ± 3	2 ± 1	0 ± 0
5.1	B	99 ± 3	0 ± 0	1 ± 0
5.1	C	98 ± 3	0 ± 0	2 ± 1
5.2	A	94 ± 4	2 ± 1	4 ± 1
5.2	B	99 ± 4	1 ± 1	0 ± 0
5.2	C	98 ± 4	1 ± 1	1 ± 1

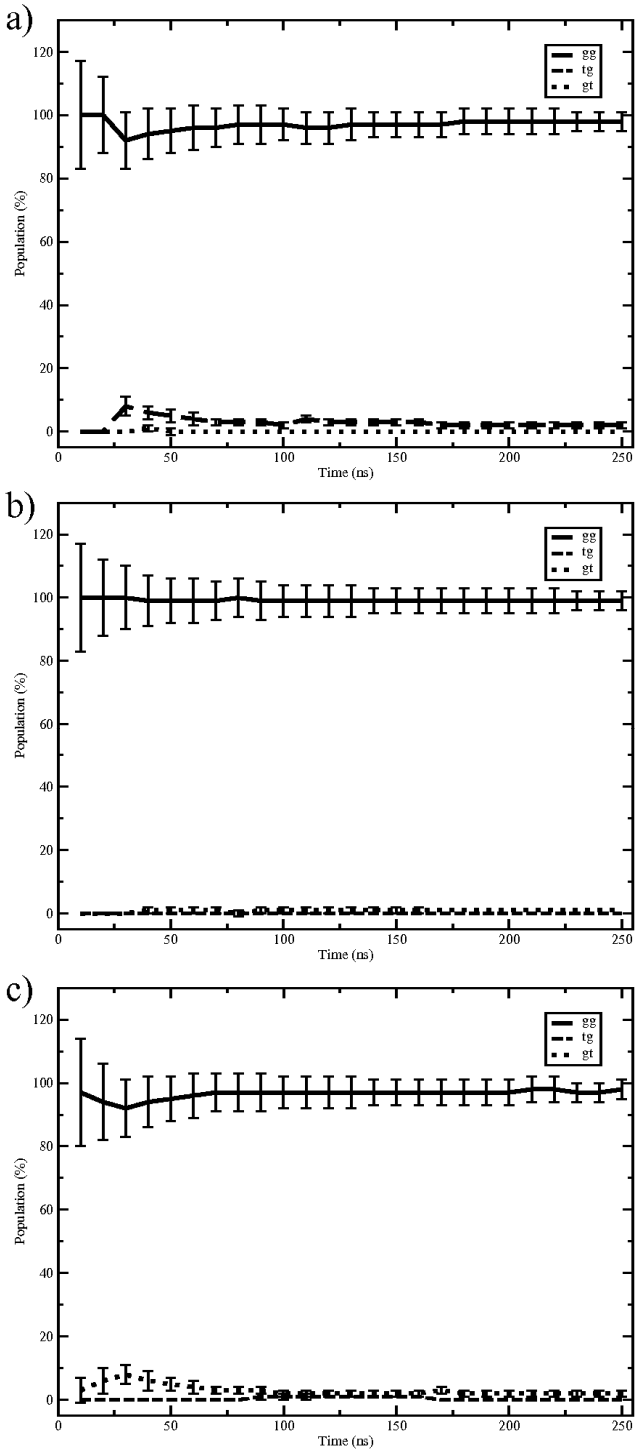

Figure 5.11. Convergence of the C4–C5 rotamer distribution of **5.1** as a function of simulation time, using the original GLYCAM06 parameters. Graph *a*) corresponds to ring A, graph *b*) corresponds to ring B, and graph *c*) corresponds to ring C.

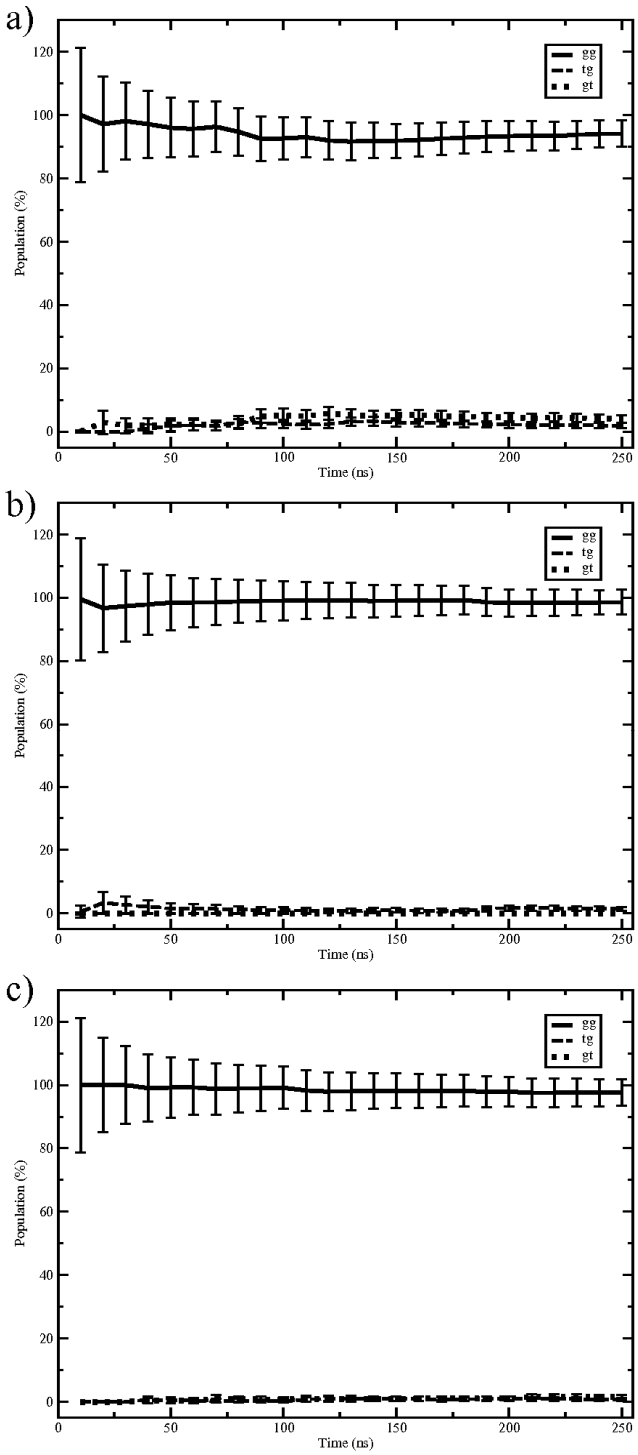

Figure 5.12. Convergence of the C4–C5 rotamer distribution of **5.2** as a function of simulation time, using the original GLYCAM06 parameters. Graph *a*) corresponds to ring A, graph *b*) corresponds to ring B, and graph *c*) corresponds to ring C.

Figure 5.13 and Figure 5.14 show the histograms for the O4–C4–C5–O5 dihedral angles for **5.1** and **5.2**, respectively. The distributions all appear fairly similar. The major populations for residues B and C in **5.1** coincide and are centered at 62°. The peak for the reducing end moiety is shifted to 68°. For **5.2**, the major populations for residues A and C overlap and are centered at 62°. The peak for residue B is shifted to 68º. In these simulations, having a large substituent on O5 increases the O4–C4–C5–O5 dihedral angle but does not affect the overall population for the *gg* rotamer.

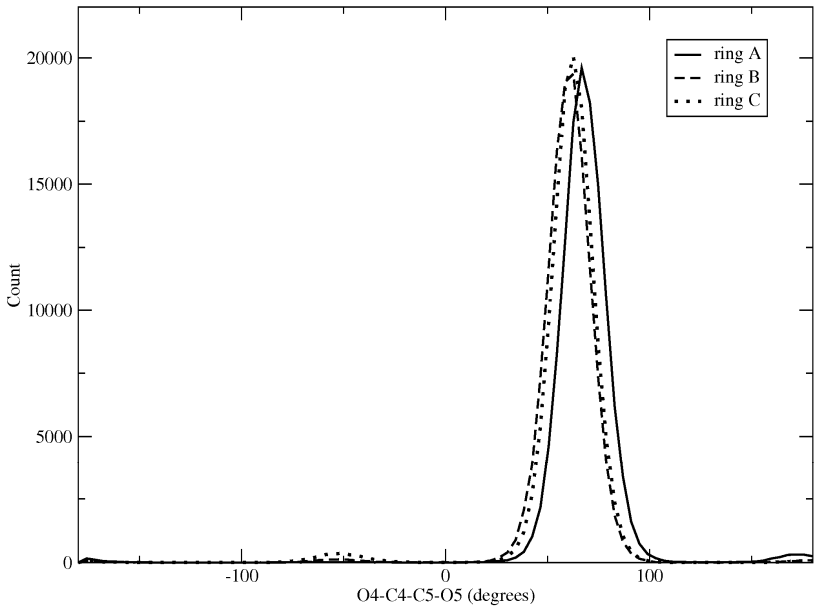

Figure 5.13. Histograms of the O4–C4–C5–O5 dihedral angle for **5.1** with the original GLYCAM06 parameters. The solid line is ring A, the dashed line is ring B, and the dotted line is ring C.

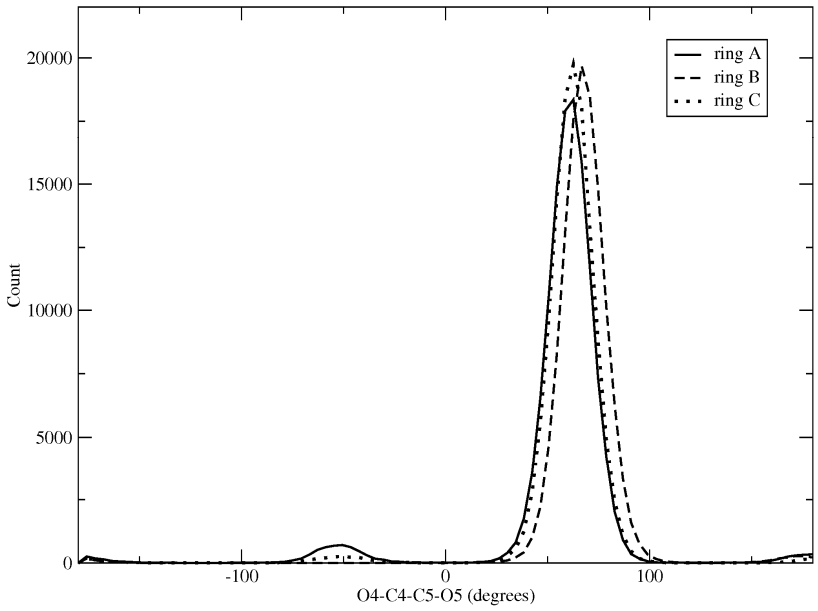

Figure 5.14. Histograms of the O4–C4–C5–O5 dihedral angle for **5.2** with the original GLYCAM06 parameters. The solid line is ring A, the dashed line is ring B, and the dotted line is ring C.

5.3.2.3. Conformation about the C5–C6 bonds of 5.1 and 5.2

The rotamers about the C5–C6 bonds of **5.1** and **5.2** took the same time to converge as the C4–C5 rotamers, more than 220 ns (Figure 5.15 for **5.1**, Figure 5.16 for **5.2**). However, unlike the C4–C5, each residue shows a different ratio among the rotamers (Table 5.7). As might be expected, the C5–C6 bonds at the non-reducing end of the trisaccharides behave quite similarly to the monosaccharides (Section 3.3.4.3), with the *gt* rotamer dominating. The residues with large substituents on O6 – ring B in **5.1** and ring A in **5.2** – have approximately the same populations for all three rotamers, though for **5.2**, the *gt* rotamer is slightly larger than the others. For residues with substituents on O5 – ring A of **5.1** and ring B of **5.2** – the *gt* rotamer dominates, and the population of the *tg* rotamer is less than that observed for the non-reducing end.

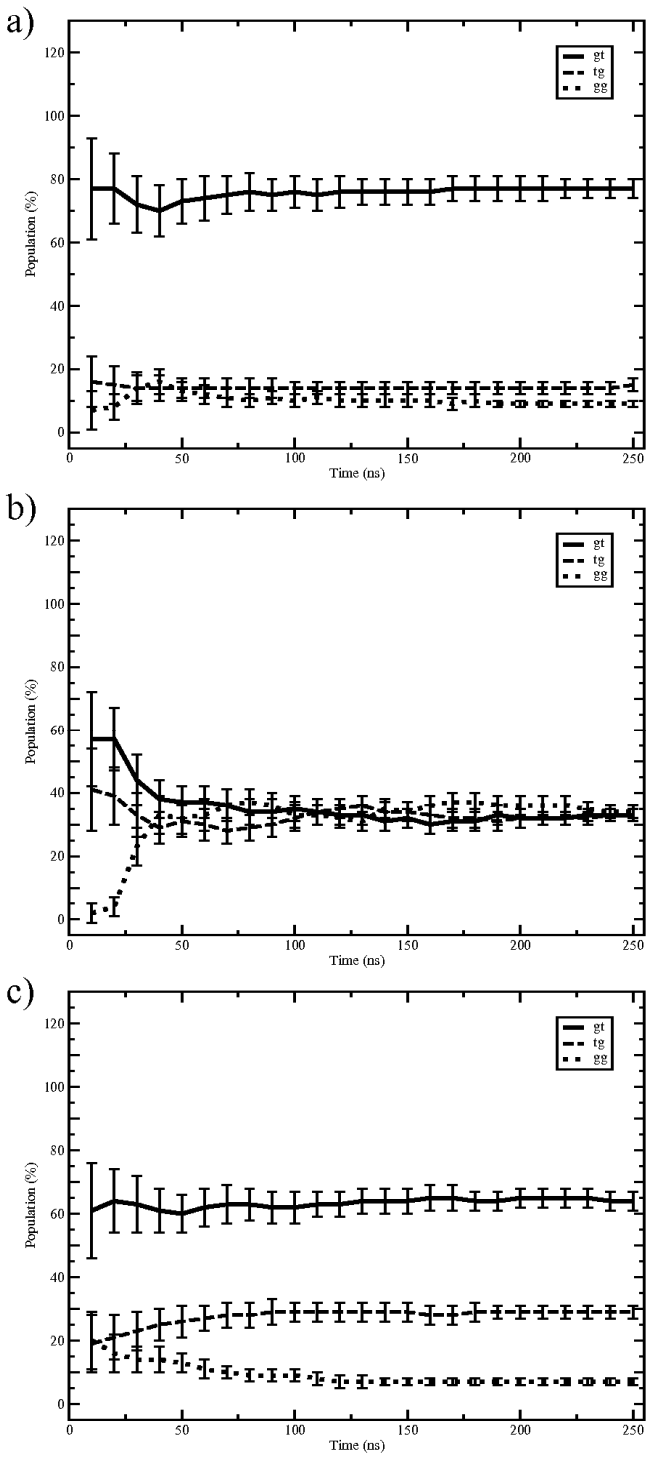

Figure 5.15. Convergence of the C5–C6 rotamer distribution of **5.1** as a function of simulation time, using the original GLYCAM06 parameters. Graph *a*) corresponds to ring A, graph *b*) corresponds to ring B, and graph *c*) corresponds to ring C.

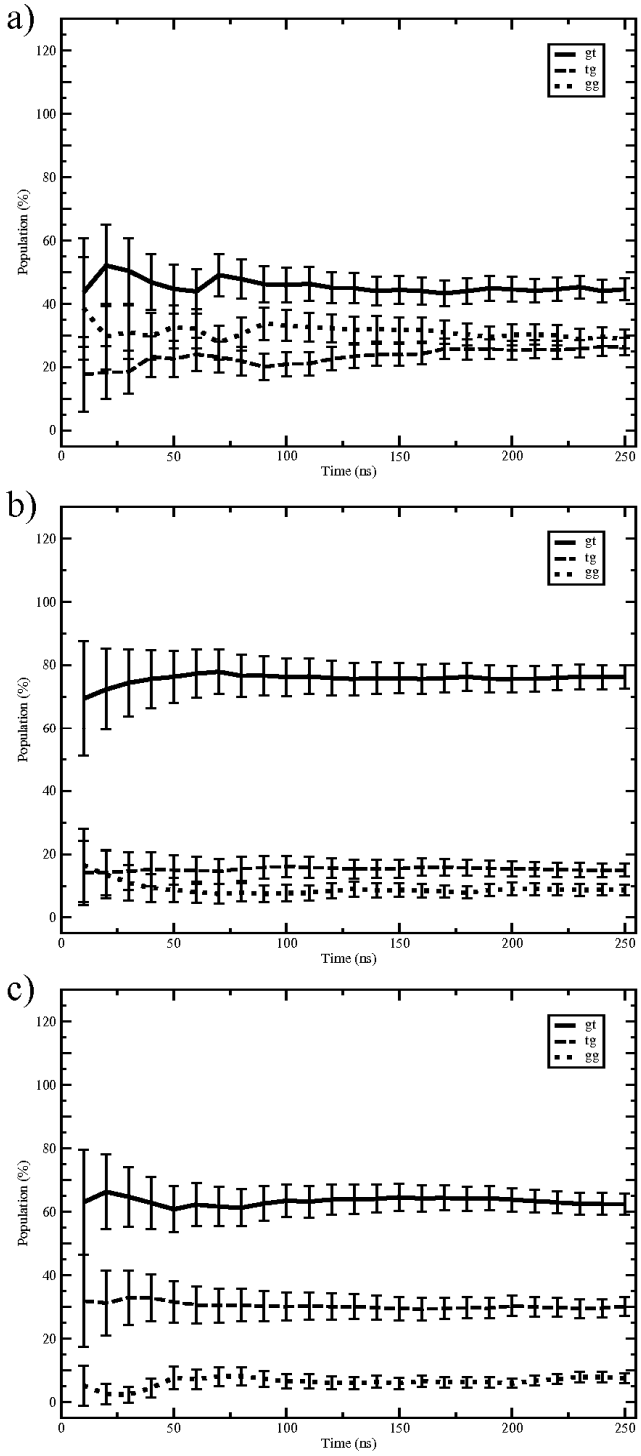

Figure 5.16. Convergence of the C5–C6 rotamer distribution of **5.2** as a function of simulation time, using the original GLYCAM06 parameters. Graph *a*) corresponds to ring A, graph *b*) corresponds to ring B, and graph *c*) corresponds to ring C.

Table 5.4. C5–C6 rotamer populations for **5.1** and **5.2** from simulations with the original GLYCAM06 parameters.

Cmpd	Residue	% *gt*	% *tg*	% *gg*
5.1	A	77 ± 3	15 ± 2	9 ± 1
5.1	B	33 ± 2	33 ± 2	34 ± 2
5.1	C	64 ± 3	29 ± 2	7 ± 1
5.2	A	45 ± 3	26 ± 3	29 ± 3
5.2	B	76 ± 4	15 ± 2	9 ± 2
5.2	C	62 ± 3	30 ± 3	8 ± 2

Having a large substituent on O5 affects the O5–C5–C6–O6 dihedral angle for the *gg* rotamers more than *gt*. Figure 5.17 and Figure 5.18 show the histograms for O5–C5–C6–O5 torsion for **5.1** and **5.2**, respectively. In **5.1**, the peaks for the *gt* conformers are close to one another, centered at 70°, 68°, and 74° for residues A, B, and C, respectively. For the *gg* rotamers in **5.1**, the distributions for residues B and C are both centered at –67°, but for ring A, with an O5 substituent, the peak shifts more positive to –54°. We observe the same pattern for **5.2**. That is, the populations for *gt* are centered at 68°, 70°, and 73° for residues A, B, and C, respectively. For the *gg* conformations, the peaks for residues A and C are centered at –64°, while ring B shifts to –54°. The O5–C5–C6–O6 dihedral angle for all residues is centered at 174°.

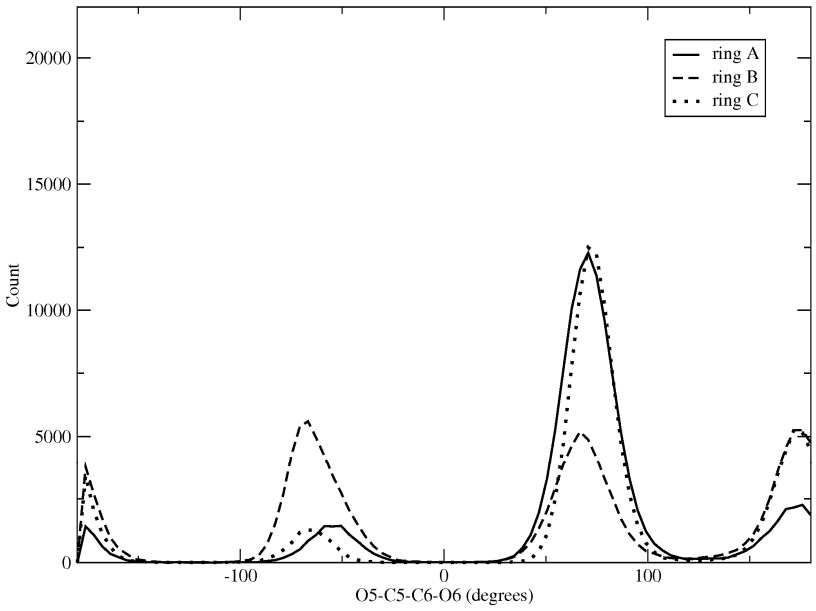

Figure 5.17. Histograms of the O5–C5–C6–O6 dihedral angle for **5.1** with the original GLYCAM06 parameters. The solid line is ring A, the dashed line is ring B, and the dotted line is ring C.

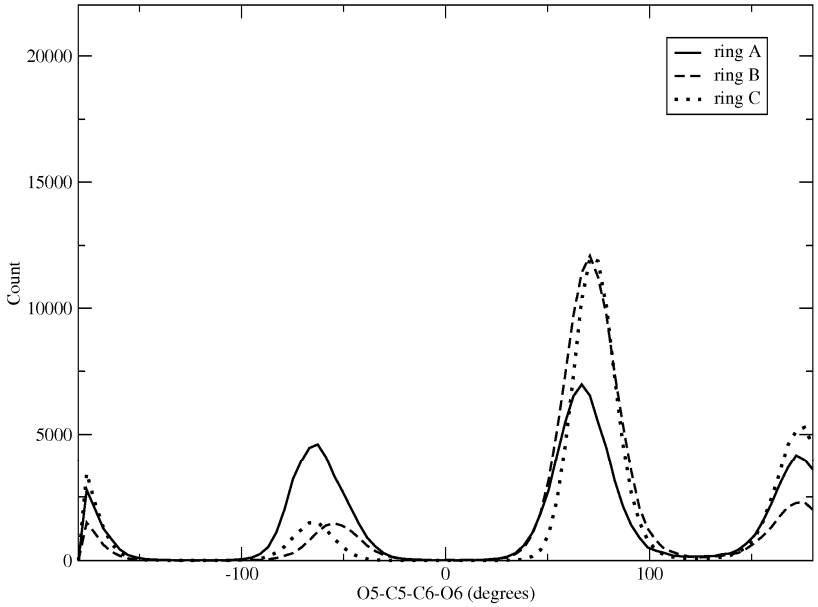

Figure 5.18. Histograms of the O5–C5–C6–O6 dihedral angle for **5.2** with the original GLYCAM06 parameters. The solid line is ring A, the dashed line is ring B, and the dotted line is ring C.

5.3.3. MD simulations with new torsion parameters for the C4–C5 bond

5.3.3.1. Conformation of the galactofuranose ring of 5.1 and 5.2

In MD simulations of the monosaccharide, the new torsion parameters for O4–C4–C5–C6 and C3–C4–C5–C6 had little effect on the furanose ring conformation (Section 4.3.3.4). We see the same trend in simulations of **5.1** and **5.2** with the new torsion parameters. Figure 5.19 shows the histograms of ring conformations for **5.1**. The distributions for rings A and C are quite broad, while the distribution for ring B is narrower – the same as we observe using the original terms (Figure 5.7). The major population for ring A is centered at P = 30°, the $^{4}T_{3}$ conformation. There is a minor population centered near P = 128°, the ^{1}E conformation, and there is a slight shoulder at P = –30°, the $^{2}T_{1}$ conformation. For ring B, there is one major peak at 52º, which is the ^{4}E conformer, the same conformer seen using the original parameters. Ring C has only one distinct population, unlike the two described earlier. The distribution is centered near P = 24°, which is between the E_3 and $^{4}T_{3}$ conformations. With the ring conformations for **5.1** varying little between the two simulations, it is not unexpected that the distributions for the ring H–C–C–H dihedral angles of **5.1** using the new parameters (Figure 5.20) are very similar to those we observe with the original parameters (Figure 5.9).

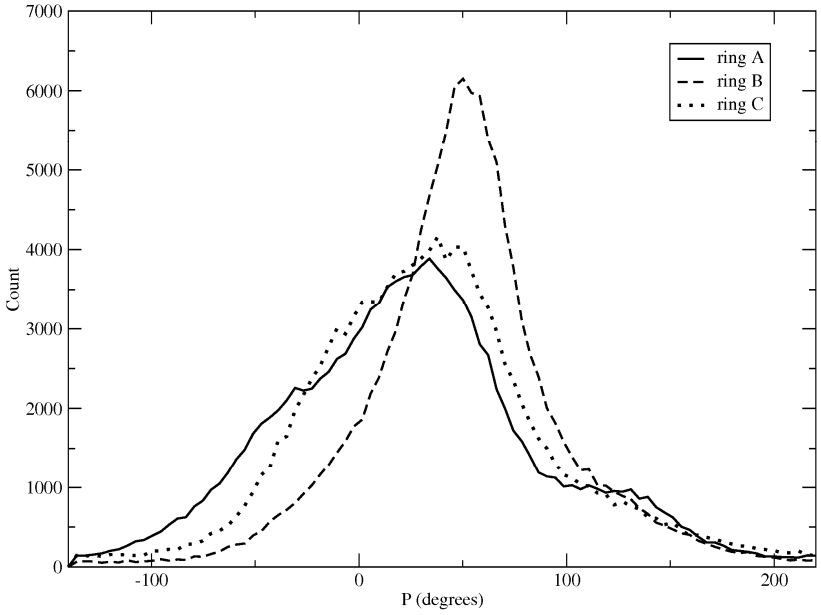

Figure 5.19. Histograms of pseudorotational phase angle *P* for **5.1** using the new torsion parameters. The solid line is ring A, the dashed line is ring B, and the dotted line is ring C.

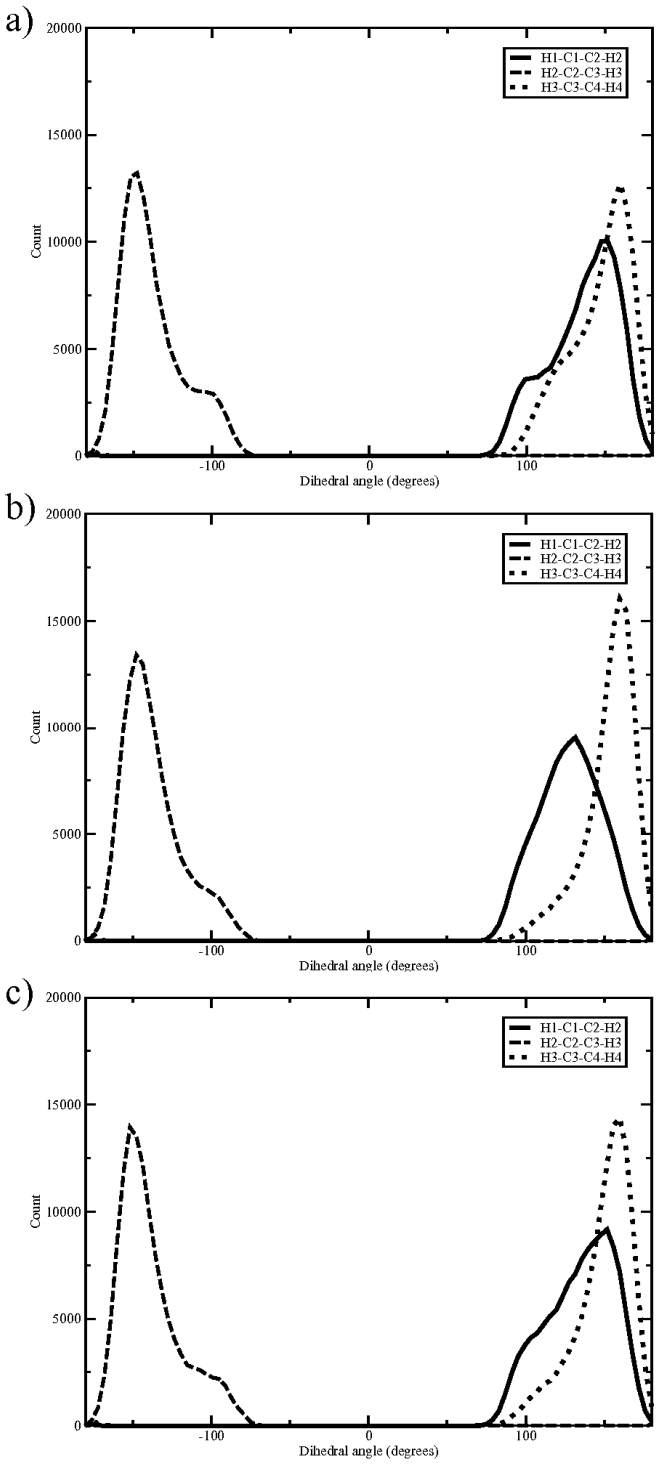

Figure 5.20. Histograms for the ring dihedral angles of **5.1** with the new torsion parameters. Graph *a*) corresponds to ring A, graph *b*) corresponds to ring B, and graph *c*) corresponds to ring C. For all three graphs, the solid line is for H1–C1–C2–H2, the long dashed line is for H2–C2–C3–H3, and the dotted line is for H3–C3–C4–H4.

The new torsion parameters for the C4–C5 bond also have little affect on the ring conformations of **5.2**. Figure 5.21 shows the populations of ring conformations from MD simulations of **5.2** with the new parameters, and they vary little from the data presented in Figure 5.8. Rings A and B have a broad distribution of conformations, but for ring C the distribution is narrower. The population for ring A is centered near $P = 24°$, which lies between the E_3 and $^4T_3$ conformations. Unlike with the original GLYCAM06 parameters, we observe no obvious second population for ring A with the new parameters. For ring B, the three conformations we see are the same as described above with the original parameters. That is, the major population is centered at $P = 40°$, the $^4T_3$ conformer, a minor conformation centered near $P = 128º$, the ^1E conformer, and a shoulder starting at $P = –32°$, the $^2T_1$ conformer. Ring C shows two populations, as well. The major one is centered at $P = 50°$, or the ^4E conformation, and the minor one is near $P = 128º$, similar to ring B. With the new parameters, the minor populations for rings B and C do not overlap as well as with the original parameters; rather, the minor population for ring C is smaller. As we see with **5.1**, the distributions of the ring H–C–C–H torsions from the simulation with the new parameters (Figure 5.22) are nearly identical to those we obtain using the original GLYCAM06 parameters (Figure 5.10).

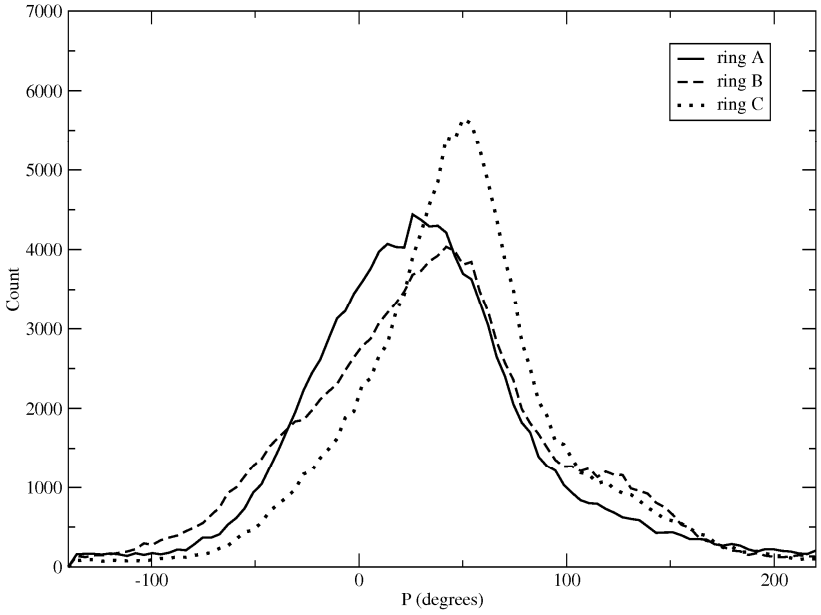

Figure 5.21. Histograms of pseudorotational phase angle *P* for **5.2** using the new torsion parameters. The solid line is ring A, the dashed line is ring B, and the dotted line is ring C.

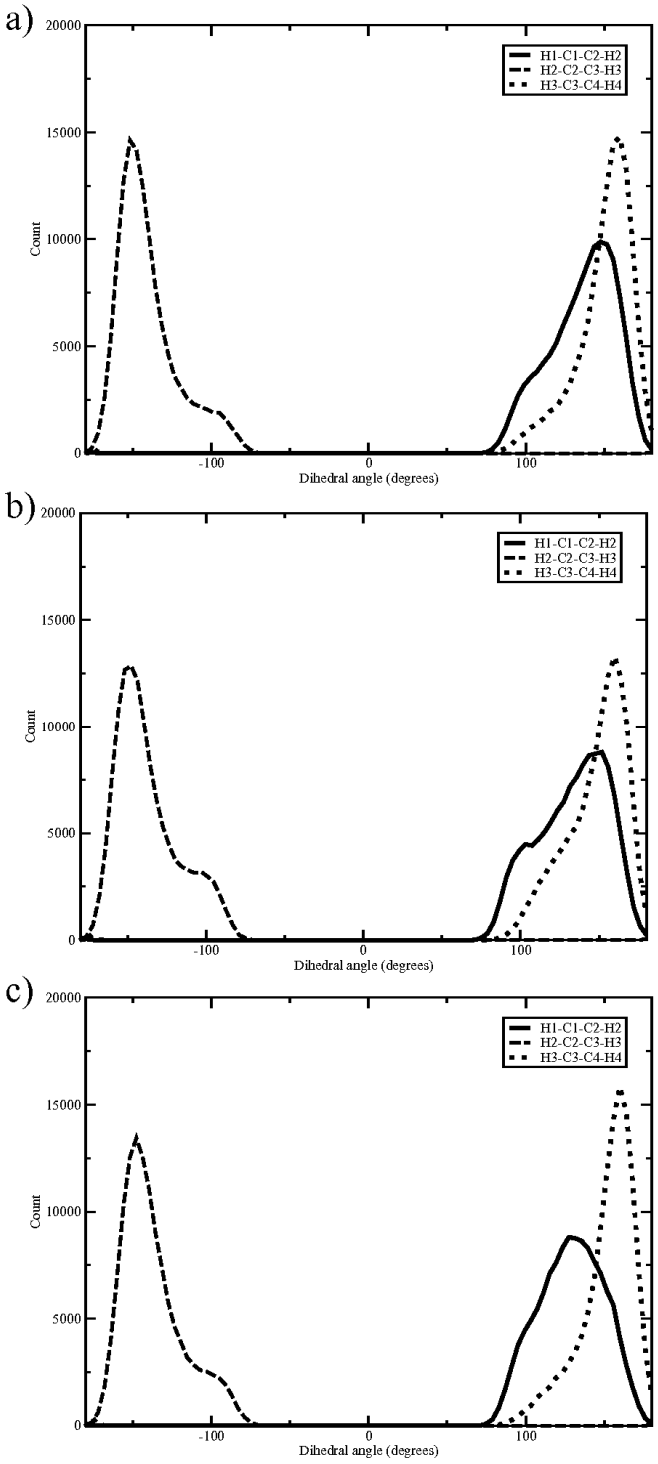

Figure 5.22. Histograms for the ring dihedral angles of **5.2** with the new torsion parameters. Graph *a*) corresponds to ring A, graph *b*) corresponds to ring B, and graph *c*) corresponds to ring C. For all three graphs, the solid line is for H1–C1–C2–H2, the long dashed line is for H2–C2–C3–H3, and the dotted line is for H3–C3–C4–H4.

5.3.3.2. Conformation about the C4–C5 bonds of 5.1 and 5.2

For both the monosaccharides and the trisaccharides **5.1** and **5.2**, the original GLYCAM06 terms O4–C4–C5–C6 and C3–C4–C5–C6 yield one conformation about the C4–C5 bond. Our new terms adjust energy differences between the *gg* and *gt* rotamers and, consequently, change their populations in MD simulations of the monosaccharides (Section 4.3.3.1). We see the same effect for the C4–C5 bonds of the trisaccharides **5.1** and **5.2** with no substituents on O5. For the residues with a large O5 substituent, the rotamer populations remain unchanged from the original GLYCAM06 parameters (Table 5.5).

Table 5.5. C4–C5 rotamer populations for **5.1** and **5.2** from simulations with the new torsion parameters.

Cmpd	Residue	% *gg*	% *tg*	% *gt*
5.1	A	96 ± 4	1 ± 1	3 ± 1
5.1	B	69 ± 4	1 ± 1	30 ± 3
5.1	C	72 ± 4	1 ± 1	27 ± 3
5.2	A	61 ± 4	3 ± 1	36 ± 3
5.2	B	89 ± 4	2 ± 1	9 ± 2
5.2	C	69 ± 4	1 ± 1	30 ± 3

Figure 5.23 shows the rotamer populations about the C4–C5 for **5.1** over the course of the simulation with the new torsion parameters. As we observe with the original terms, it takes longer than 220 ns for all the populations to converge and reach a variance in the mean of 4% or less. For residue A, the populations

vary little throughout the course of the simulation, and essentially only the *gg* rotamer is observed. The final populations for the C4–C5 rotamers of residues B and C are approximately 70% *gg* and 30% *gt*. For both residues, the populations change little from the values observed at 100 ns of simulation time. Both residues B and C have an O5 hydroxyl group, and both give similar results to the monosaccharide (Section 4.3.3.1).

The C4–C5 rotamer populations for **5.2** over the course of the simulation with the new torsion parameters are shown in Figure 5.24. Similar to **5.1**, the calculations converge after 220 ns for the three C4–C5 bonds. The overall population for residue B, which has a large O5 substituent, shows little change throughout the simulation and remains mostly in the *gg* conformation. The populations for residue A do not change much after 140 ns, and for residue C, the final values are reached by 90 ns. For both residues A and C, the *gg* conformation still dominates, but the *gt* rotamer is significantly populated: 36% for A and 30% for C. Once again, residues with an unsubstituted hydroxyl at O5 behave similarly to the monosaccharide.

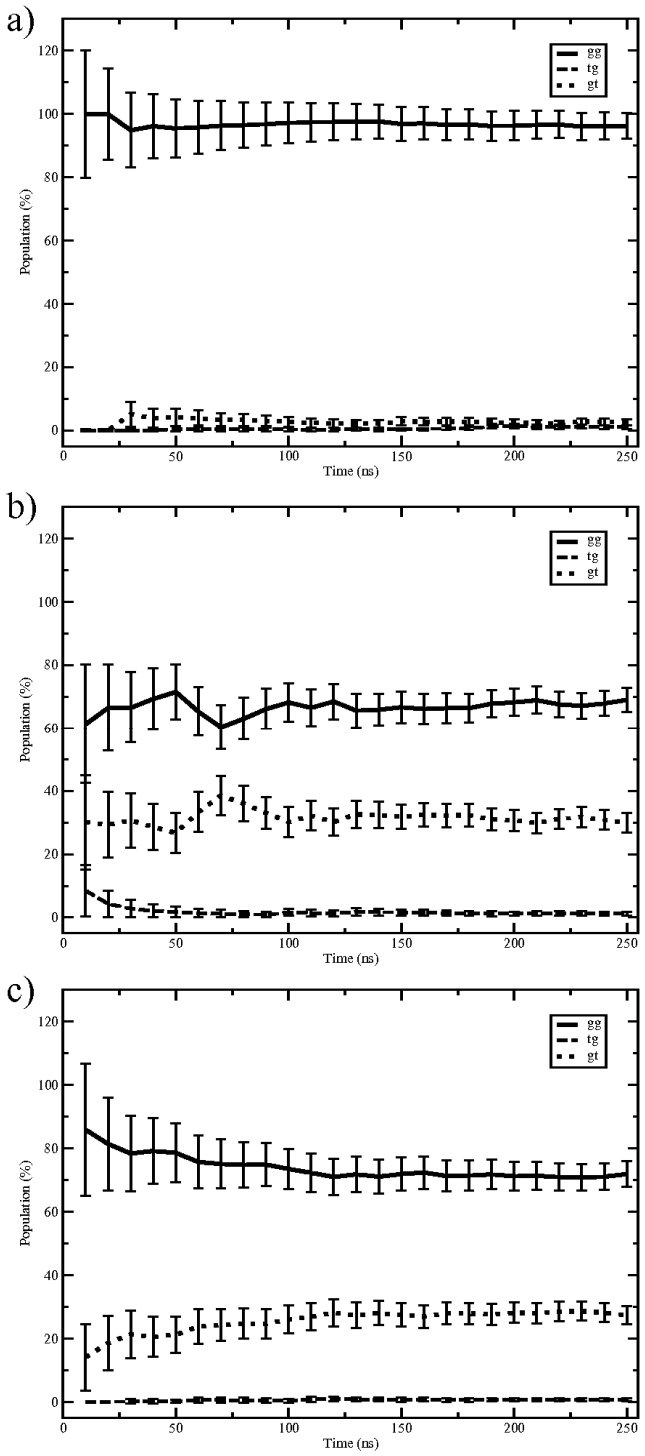

Figure 5.23. Convergence of the C4–C5 rotamer distribution of **5.1** as a function of simulation time, using the new torsion parameters. Graph *a*) corresponds to ring A, graph *b*) corresponds to ring B, and graph *c*) corresponds to ring C.

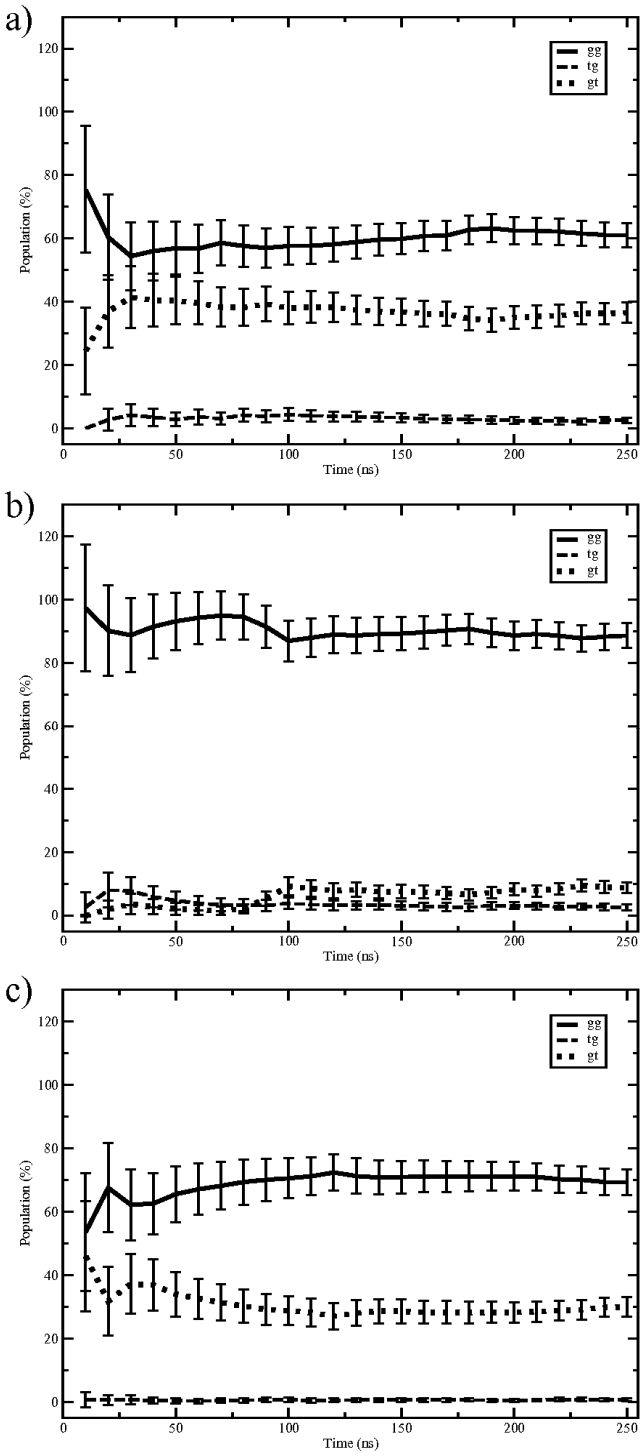

Figure 5.24. Convergence of the C4–C5 rotamer distribution of **5.2** as a function of simulation time, using the new torsion parameters. Graph *a*) corresponds to ring A, graph *b*) corresponds to ring B, and graph *c*) corresponds to ring C.

Figure 5.25 and Figure 5.26 show the distributions for the O4–C4–C5–O5 dihedral angles from simulations with the new parameters for **5.1** and **5.2**, respectively. The centers of the populations change little from those obtained with the original parameters. For the reducing end in **5.1**, the center of the *gg* conformation is 67°. For residues B and C with an O5 hydroxyl, the *gg* rotamers occur at 58° and 60°, respectively. For **5.2**, residue B has an O5 substituent, and the *gg* conformation is centered at 67°. For both of the residues where O5 is not substituted, the *gg* rotamer is at 59°. The O5 substituent also has an effect on the *gt* rotamers. In **5.1**, the center of the *gt* population is –58°, whereas it is –52° for the other residues. In **5.2**, the center of the *gt* rotamers are shifted a bit. The center for residue B is at –63° and at –54° for the others. Substitution at O5 increases the O4–C4–C5–O5 dihedral angle for both the *gg* and *gt* rotamers.

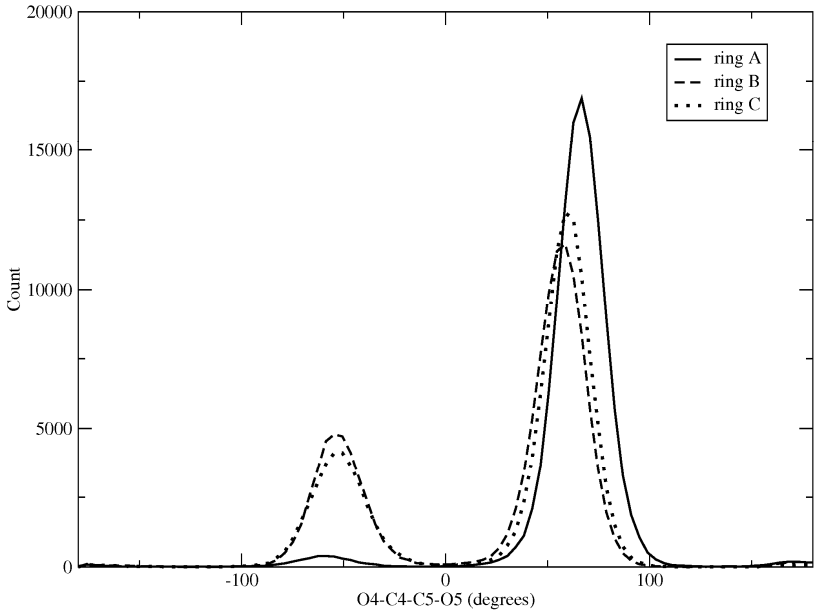

Figure 5.25. Histograms of the O4–C4–C5–O5 dihedral angle for **5.1** with the new torsion parameters. The solid line is ring A, the dashed line is ring B, and the dotted line is ring C.

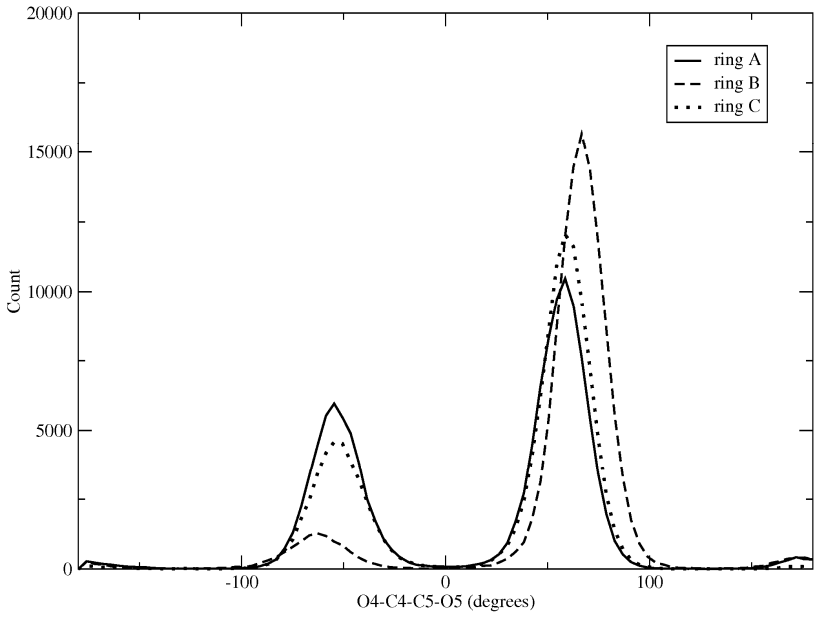

Figure 5.26. Histograms of the O4–C4–C5–O5 dihedral angle for **5.2** with the new torsion parameters. The solid line is ring A, the dashed line is ring B, and the dotted line is ring C.

5.3.3.3. Conformation about the C5–C6 bonds of 5.1 and 5.2

The new O4–C4–C5–C6 and C3–C4–C5–C6 terms also change the C5–C6 rotamer populations in MD simulations of the monosaccharide from those we observe with the original GLYCAM06 parameters (Section 4.3.3.2). We see the same effect for the rotamers about the C5–C6 bond in the trisaccharides **5.1** and **5.2** (Table 5.6). The populations for residues with an O5 substituent are essentially the same for both sets of simulation conditions. The populations for the rotamers with an O5 hydroxyl differ between the new parameters and the original ones.

Table 5.6. C5–C6 rotamer populations for **5.1** and **5.2** from simulations with the original GLYCAM06 parameters.

Cmpd	Residue	% *gt*	% *tg*	% *gg*
5.1	A	75 ± 4	14 ± 2	11 ± 2
5.1	B	22 ± 3	22 ± 3	56 ± 4
5.1	C	53 ± 3	27 ± 3	20 ± 2
5.2	A	28 ± 3	23 ± 3	49 ± 4
5.2	B	70 ± 4	15 ± 2	15 ± 2
5.2	C	47 ± 3	27 ± 3	26 ± 3

Figure 5.27 shows the populations for the C5–C6 rotamers over the course of the simulation of **5.1** with the new torsion terms. The populations all converge in 200 ns or less, as determined by a variance in the mean of less than 4%. For residue A, the populations vary little over the course of the simulation, and the *gt* rotamer dominates. The rotamer distribution is same as that from the calculation using the original parameters. For residue B, the original parameters give equal populations for all three rotamers. With the new terms, the *gg* rotamer dominates at 56%, and the other two rotamers are populated equally. For residue C, the population of the *gt* rotamer decreases from the original parameters, while the *gg* rotamer increases. These values for the non-reducing end are also similar to those observed in MD simulation of the monosaccharide with the new torsion parameters (Section 4.3.3.2).

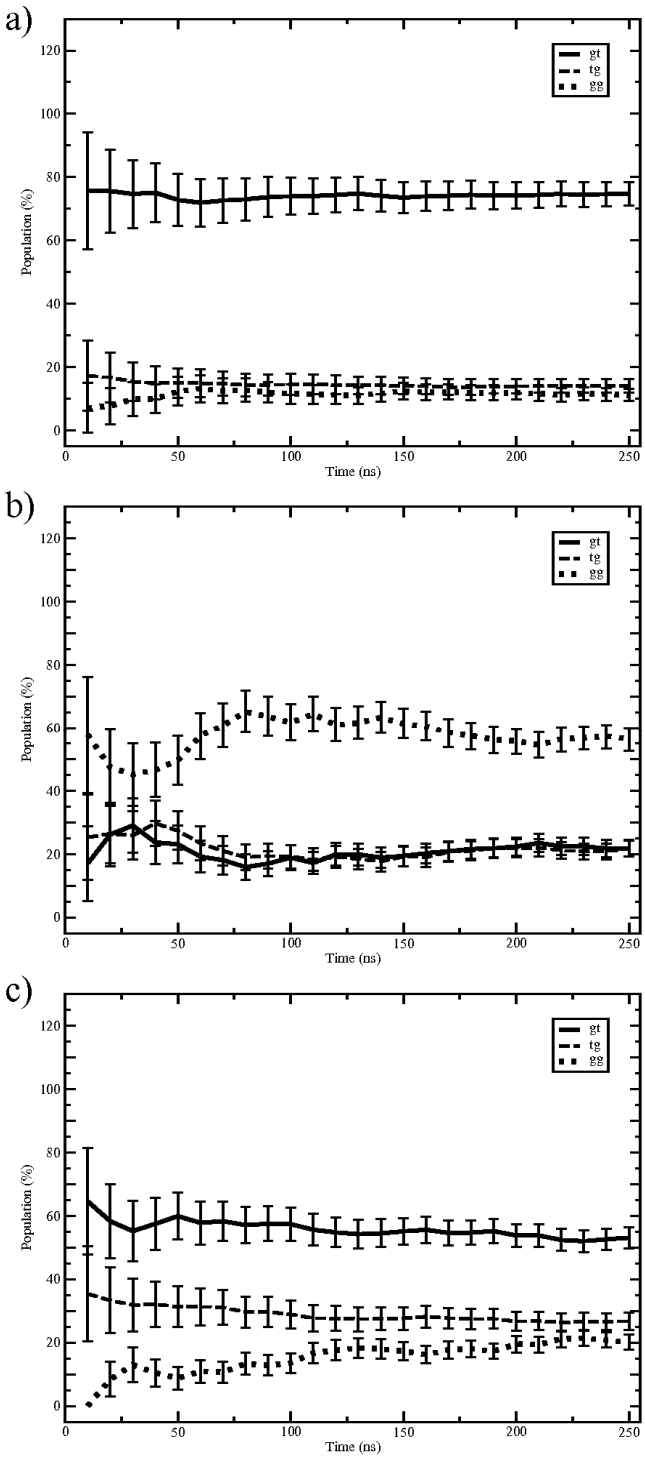

Figure 5.27. Convergence of the C5–C6 rotamer distribution of **5.1** as a function of simulation time, using the new torsion parameters. Graph *a*) corresponds to ring A, graph *b*) corresponds to ring B, and graph *c*) corresponds to ring C.

For the trisaccharide **5.2**, Figure 5.28 shows the populations of the C5–C6 rotamers throughout the MD simulation with the new torsion parameters. As with **5.1**, the calculations converge within 200 ns. For residue A, the populations change little from those present 40 ns. Both residue A in **5.2** and residue B in **5.1** have an O6 substituent, and both show a similar trend, *gg* > *gt* ≈ *tg*. For residue B in **5.2**, the C5–C6 rotamer population at the end of the simulation is the same at that at the beginning, and the *gt* rotamer dominates. The ratio among the rotamers obtained with the new parameters are not significantly different from that obtained with the original terms. Residue C again shows very similar populations to those obtained in simulations of the monosaccharide with the new torsion terms. The trend for residue C is *gt* > *tg* ≈ *gg*.

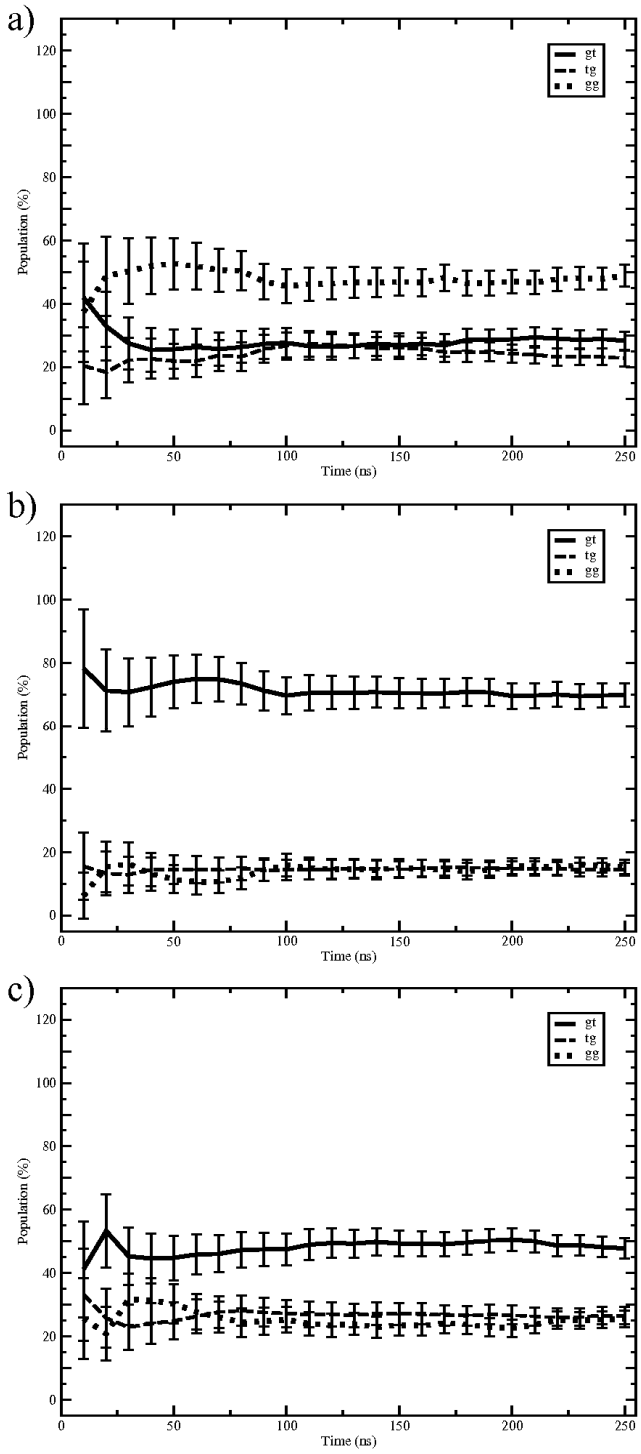

Figure 5.28. Convergence of the C5–C6 rotamer distribution of **5.2** as a function of simulation time, using the new torsion parameters. Graph *a*) corresponds to ring A, graph *b*) corresponds to ring B, and graph *c*) corresponds to ring C.

Distributions of the O5–C5–C6–O6 dihedral angles for **5.1** and **5.2** from simulations with the new torsion parameters are shown in Figure 5.29 and Figure 5.30, respectively. The values for the angles do not change significantly from those we observe with the original GLYCAM06 parameters. For **5.1**, the populations for the *tg* rotamers are all centered at 174°. The peaks for the *gt* conformation are all close to each other. They are centered at 71°, 67°, and 73° for residues A, B, and C, respectively. For the *gg* conformations, residue B is centered at –66º, and residue C is at –67°. Residue A is shifted more positive to –58º. For **5.2**, we observe the same trends. The *tg* rotamers are centered at 174º, and the peaks for the *gt* rotamers are similar. Residue A is at 66°, while residues B and C are at 71º. For the *gg* rotamers, residues A and C are at –66º and –67°, respectively, and residue B is shifted to –56º. As we observed with the original parameters, having a large substituent on O5 affects the *gg* for the C5–C6 bond more than the other rotamers.

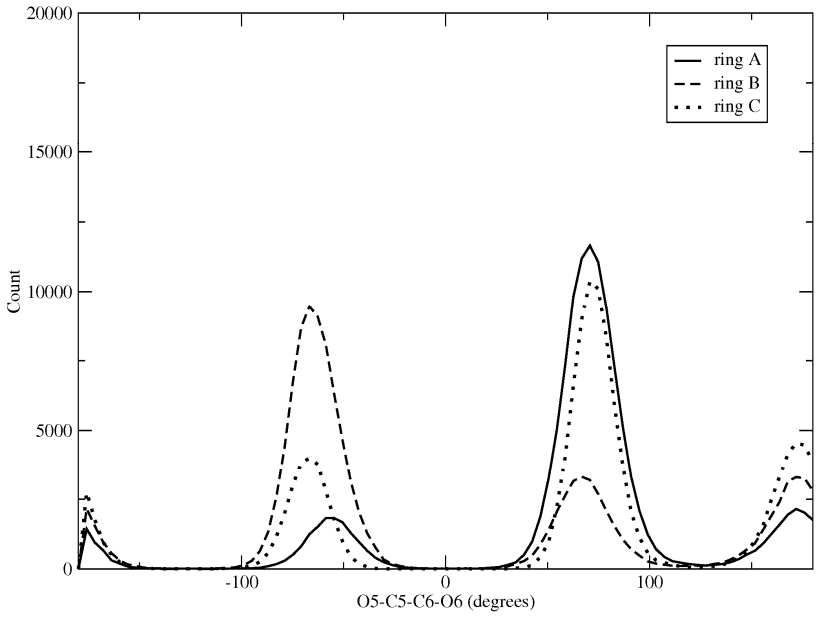

Figure 5.29. Histograms of the O5–C5–C6–O6 dihedral angle for **5.1** with the new torsion parameters. The solid line is ring A, the dashed line is ring B, and the dotted line is ring C.

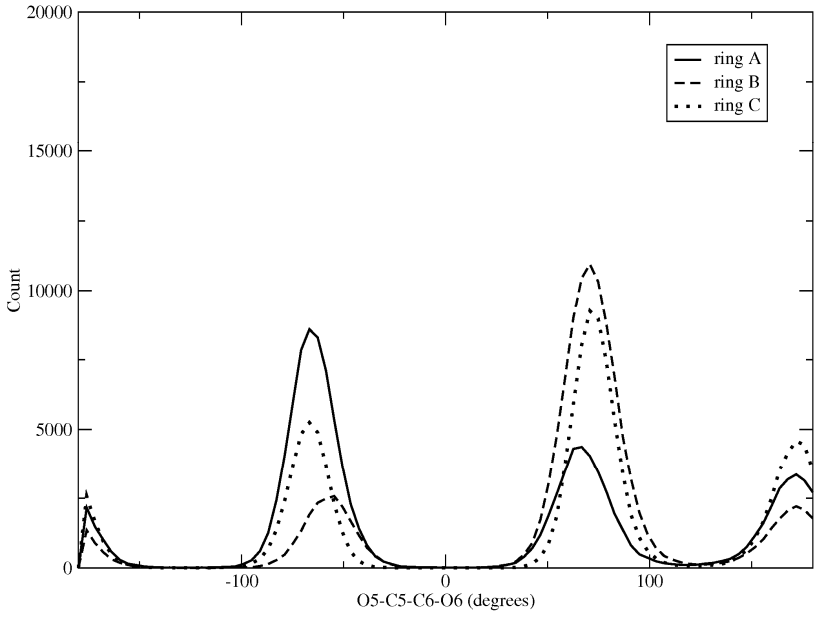

Figure 5.30. Histograms of the O5–C5–C6–O6 dihedral angle for **5.2** with the new torsion parameters. The solid line is ring A, the dashed line is ring B, and the dotted line is ring C.

5.3.4. Proton–proton coupling constants from MD simulations

To directly compare the results of our MD simulations with the experimental conformations of **5.1** and **5.2**, we determined the values for $^{3}J_{H,H}$ as described in Section 3.3.4.4. In earlier studies on arabinofuranosides, we found the Karplus-like relationships for $^{3}J_{H4,H5R}$ and $^{3}J_{H4,H5S}$ of the monosaccharide were not appreciably different from those for internal C4–C5 bond of an α-(1→5)-linked disaccharide.[29,30] Therefore, we used the Karplus-like relationships (eqs. 3.10–3.13, 3.15, and 3.16) for the monosaccharides to calculate $^{3}J_{H,H}$ from the MD simulations of the trisaccharides. Table 5.7 lists the experimental vicinal coupling constants for **5.1**, as well as those determined from MD simulations with the original and new GLYCAM06 torsion parameters. Table 5.8 lists the same values for **5.2**.

For both **5.1** and **5.2**, the values for $^{3}J_{H1,H2}$, $^{3}J_{H2,H3}$, and $^{3}J_{H3,H4}$ do not differ appreciably between the two sets of parameters. The values for $^{3}J_{H2,H3}$ all show excellent agreement to the experimental values. For the residues with a hydroxyl at O5, $^{3}J_{H3,H4}$ also agrees well with experiment. A large O5 substituent decreases this value, resulting in a worse agreement between the simulations and experiment. The values for $^{3}J_{H1,H2}$ from the simulation are larger than the experimental values, but a β-(1→5)-linkage reduces this value, bringing it closer to experiment.

In simulations with the original GLYCAM06 parameters, the values for $^{3}J_{H4,H5}$ do not agree with the experimental values, just as we observe for the monosaccharides (Section 3.3.4.4). The new torsion parameters improve

agreement for the non-reducing end moieties for both **5.1** and **5.2**. Similarly, for the residues without an O5 substituent – i.e. ring B of **5.1** and ring A of **5.2** – the new parameters improve the values for $^{3}J_{H4,H5}$. However, for both cases, the experimental coupling constants are smaller that the ones from the simulations with the new terms. For the residues with a large O5 substituent, the new parameters do not alter the values for $^{3}J_{H4,H5}$, and both conditions for the MD simulations show poor agreement to the experimental values.

In simulations with the original parameters, values for the non-reducing end residues show good agreement between experiment and calculations. The new torsion parameters show worse agreement, similar to the case with the monosaccharide (Section 4.3.3.3). For residue A of **5.1**, with an unsubstituted O6, both sets of parameters give the same values for $^{3}J_{H5,H6R}$ and $^{3}J_{H5,H6S}$, and neither agrees well with the experimental values. Similarly, for residue B of **5.2**, both sets of torsion terms give similar values for $^{3}J_{H5,H6R}$ and $^{3}J_{H5,H6S}$, but $^{3}J_{H5,H6S}$ shows poor agreement with experiment. The values for the residues with O6 substituent show poor agreement between simulation and experiment, regardless of the parameters used for the simulations.

Table 5.7. Comparison between the coupling constants from experiment and from MD simulations of **5.1** with the new and original GLYCAM06 torsion parameters.

Ring	Coupling	Expt'l[a]	Original Parameters[b]	New Parameters[b]
A	$^3J_{H1,H2}$ **(Hz)**	2.3	3.2 ± 2.2	3.2 ± 2.3
	$^3J_{H2,H3}$ **(Hz)**	4.2	3.7 ± 2.4	3.7 ± 2.4
	$^3J_{H3,H4}$ **(Hz)**	6.9	5.9 ± 2.8	5.9 ± 2.8
	$^3J_{H4,H5}$ **(Hz)**	3.5	2.0 ± 1.0	2.1 ± 1.1
	$^3J_{H5,H6R}$ **(Hz)**	6.4	7.7 ± 2.0	7.5 ± 2.0
	$^3J_{H5,H6S}$ **(Hz)**	5.1	3.7 ± 1.5	3.7 ± 1.6
B	$^3J_{H1,H2}$ **(Hz)**	1.9	2.3 ± 2.0	2.3 ± 2.0
	$^3J_{H2,H3}$ **(Hz)**	3.6	3.6 ± 2.2	3.6 ± 2.3
	$^3J_{H3,H4}$ **(Hz)**	6.4	6.8 ± 2.4	6.8 ± 2.4
	$^3J_{H4,H5}$ **(Hz)**	3.5	1.5 ± 0.6	3.8 ± 0.9
	$^3J_{H5,H6R}$ **(Hz)**	7.4	5.1 ± 1.7	5.9 ± 1.6
	$^3J_{H5,H6S}$ **(Hz)**	3.8	5.3 ± 1.5	4.9 ± 1.7
C	$^3J_{H1,H2}$ **(Hz)**	1.9	3.3 ± 2.3	3.0 ± 2.3
	$^3J_{H2,H3}$ **(Hz)**	3.6	3.9 ± 2.3	3.8 ± 2.3
	$^3J_{H3,H4}$ **(Hz)**	6.4	6.1 ± 2.6	6.3 ± 2.6
	$^3J_{H4,H5}$ **(Hz)**	4.3	1.7 ± 0.7	3.6 ± 0.9
	$^3J_{H5,H6R}$ **(Hz)**	7.2	7.0 ± 1.9	6.1 ± 1.8
	$^3J_{H5,H6S}$ **(Hz)**	4.7	4.4 ± 1.1	4.3 ± 1.2

[a] The error in the experimental values is estimated to be ± 0.2 Hz.
[b] The error analysis for the MD simulations is described in Section 3.3.4.4.

Table 5.8. Comparison between the coupling constants from experiment and from MD simulations of **5.2** with the new and original GLYCAM06 torsion parameters.

Ring	Coupling	Expt'l[a]	Original Parameters[b]	New Parameters[b]
A	$^3J_{H1,H2}$ **(Hz)**	2.2	3.4 ± 2.3	3.2 ± 2.2
	$^3J_{H2,H3}$ **(Hz)**	4.1	4.0 ± 2.3	4.0 ± 2.3
	$^3J_{H3,H4}$ **(Hz)**	6.3	6.2 ± 2.6	6.4 ± 2.5
	$^3J_{H4,H5}$ **(Hz)**	3.5	1.9 ± 0.7	4.4 ± 1.0
	$^3J_{H5,H6R}$ **(Hz)**	7.1	5.7 ± 1.8	4.4 ± 1.6
	$^3J_{H5,H6S}$ **(Hz)**	3.8	4.8 ± 1.6	4.5 ± 1.6
B	$^3J_{H1,H2}$ **(Hz)**	1.9	3.0 ± 2.3	2.9 ± 2.3
	$^3J_{H2,H3}$ **(Hz)**	3.6	3.6 ± 2.4	3.6 ± 2.4
	$^3J_{H3,H4}$ **(Hz)**	6.7	6.0 ± 2.8	6.1 ± 2.8
	$^3J_{H4,H5}$ **(Hz)**	3.3	2.0 ± 1.0	2.6 ± 1.2
	$^3J_{H5,H6R}$ **(Hz)**	7.1	7.6 ± 2.0	7.1 ± 1.9
	$^3J_{H5,H6S}$ **(Hz)**	4.9	3.7 ± 1.5	3.8 ± 1.6
C	$^3J_{H1,H2}$ **(Hz)**	2.0	2.4 ± 2.0	2.4 ± 2.1
	$^3J_{H2,H3}$ **(Hz)**	4.1	3.6 ± 2.3	3.6 ± 2.3
	$^3J_{H3,H4}$ **(Hz)**	6.6	6.6 ± 2.5	6.6 ± 2.5
	$^3J_{H4,H5}$ **(Hz)**	3.5	1.7 ± 0.7	3.8 ± 0.9
	$^3J_{H5,H6R}$ **(Hz)**	7.3	6.9 ± 1.9	5.7 ± 1.7
	$^3J_{H5,H6S}$ **(Hz)**	4.6	4.5 ± 1.1	4.3 ± 1.2

[a] The error in the experimental values is estimated to be ± 0.2 Hz.
[b] The error analysis for the MD simulations is described in Section 3.3.4.4.

5.4. Conclusions

We have presented MD simulations of the trisaccharides **5.1** and **5.2** using two sets of torsion parameters for the C4–C5 bond, and we compared the simulation results to NMR experiments. In simulations with either set of torsion parameters, the non-reducing residue of a β-(1→5) glycosidic bond (ring B of **5.1**

or ring C of **5.2**) has a narrower distribution of ring conformations than the remaining residues. When the anomeric oxygen is attached to a secondary carbon, the furanose ring is less flexible, and the major population shifts away from the E_3 conformation observed in the monosaccharide to the ^4E conformation. The anomeric linkage affects ring conformation more than large groups on O5 or O6. This shift in the population is accompanied by a change in the H1–C1–C2–H2 distribution. Also, the value for $^3J_{H1,H2}$ from the simulations is closer to experiment (0.4 Hz difference) for these rings than for the other residues (0.9–1.4 Hz difference), while the values for $^3J_{H2,H3}$ and $^3J_{H3,H4}$ are similar for all residues. The vicinal coupling constant between H1 and H2 may be more diagnostic for the ring conformation than the other ring couplings.

Our newly developed torsion parameters for O4–C4–C5–C6 and C3–C4–C5–C6 alter the rotamer populations for the trisaccharides, if there is no O5 substituent. The original GLYCAM06 terms yield one rotamer about the C4–C5 bond, the *gg* rotamer, and this is also the case for the new parameters when O5 is linked to another Gal*f* residue. For the non-reducing end or residues with an O6 substituent, the *gg* rotamer is still favored, but *gt* is also significantly populated. These changes are reflected in the improved agreement between the experimental and calculated values of $^3J_{H4,H5}$.

For residues without an O5 substituent, the new parameters also altered the rotamers about the C5–C6 bond. Based on the $^3J_{H5,H6S}$ values, the new terms do not reproduce the populations for experiment for the non-reducing end as well as the original GLYCAM06 terms do. Neither set of parameters reproduce the

experimental values for residues with an O6 substituent. This disparity may be due to poor simulation conditions or to the use of inappropriate Karplus-like equations. While there was little difference between the equations for mono- and disaccharides of Ara*f*,[30] the same may not be true for β-(1→6)-linked residues of Gal*f*. Evaluating equations specific for the β-(1→6) glycosidic linkage may be worthwhile.

5.5. References

1. Completo, G. C.; Lowary, T. L. *J. Org. Chem.* **2008**, *73*, 4513–4525.
2. Richards, M. R.; Lowary, T. L. *ChemBioChem* **2009**, *10*, 1920–1938.
3. Peltier, P.; Euzen, R.; Daniellou, R.; Nugier-Chauvin, C.; Ferrières, V. *Carbohydr. Res.* **2008**, *343*, 1897–1923.
4. Rose, N. L.; Completo, G. C.; Lin, S. J.; McNeil, M.; Palcic, M. M.; Lowary, T. L. *J. Am. Chem. Soc.* **2006**, *128*, 6721–6729.
5. Wheatley, R. W.; Zheng, R. B.; Richards, M. R.; Lowary, T. L.; Ng, K. K. S. *J. Biol. Chem. In press*, doi: 10.1074/jbc.M112.347484
6. Brennan, P. J.; Nikaido, H. *Annu. Rev. Biochem* **1995**, *64*, 29–63.
7. Brennan, P. J. *Tuberculosis* **2003**, *83*, 91–97.
8. Beláňová, M.; Dianišková, P.; Brennan, P. J.; Completo, G. C.; Rose, N. L.; Lowary, T. L.; Mikušová, K. *J. Bacteriol.* **2008**, *190*, 1141–1145.
9. Alderwick, L. J.; Dover, L. G.; Veerapen, N.; Gurcha, S. S.; Kremer, L.; Roper, D. L.; Pathak, A. K.; Reynolds, R. C.; Besra, G. S. *Protein Expression Purif.* **2008**, *58*, 332–341.
10. Mayer, M.; Meyer, B. *Angew. Chem. Int. Ed.* **1999**, *38*, 1784–1788.
11. Szczepina, M. G.; Zheng, R. B.; Completo, G. C.; Lowary, T. L.; Pinto, B. M. *ChemBioChem* **2009**, *10*, 2052–2059.
12. May, J. F.; Levengood, M. R.; Splain, R. A.; Brown, C. D.; Kiessling, L. L. *Biochemistry* **2012**, *51*, 1148–1159.

13. Szczepina, M. G.; Zheng, R. X. B.; Completo, G. C.; Lowary, T. L.; Pinto, B. M. *Bioorg. Med. Chem.* **2010**, *18*, 5123–5128.

14. Kirschner, K. N.; Yongye, A. B.; Tschampel, S. M.; González-Outeiriño, J.; Daniels, C. R.; Lachele Foley, B.; Woods, R. J. *J. Comput. Chem.* **2008**, *29*, 622–655.

15. Robinson, P. T.; Pham, T. N.; Uhrin, D. *J. Magn. Reson.* **2004**, *170*, 97–103.

16. Duncan, S. J.; Lewis, R.; Bernstein, M. A.; Sandor, P. *Magn. Reson. Chem.* **2007**, *45*, 283–288.

17. Musher, J. I.; Corey, E. J. *Tetrahedron* **1962**, *18*, 791–809.

18. Marat, K. *SpinWorks 3.1.3*, University of Manitoba: Winnipeg, 2009.

19. Reich, H. J. *WinDNMR: Dynamic NMR Spectra for Windows*, Journal of Chemical Education Software, 3D2: Madison, WI, USA, 1996.

20. Case, D. A.; Darden, T. A.; T.E. Cheatham, I.; Simmerling, C. L.; Wang, J.; Duke, R. E.; Luo, R.; Crowley, M.; Walker, R. C.; Zhang, W.; Merz, K. M.; Wang, B.; Hayik, S.; Roitberg, A.; Seabra, G.; Kolossváry, I.; Wong, K. F.; Paesani, F.; Vanicek, J.; Wu, X.; Brozell, S. R.; Steinbrecher, T.; Golke, H.; Yang, L.; Tan, C.; Mongan, J.; Hornak, V.; Cui, G.; Mathews, D. H.; Seetin, M. G.; Saugi, C.; Babin, V.; Kollman, P. A. *AMBER 10*, Univeristy of California, San Francisco: 2008.

21. Taha, H. A.; Roy, P.-N.; Lowary, T. L. *J. Chem. Theory Comput.* **2011**, *7*, 420–432.

22. Taha, H. A.; Castillo, N.; Sears, D. N.; Wasylishen, R. E.; Lowary, T. L. *J. Chem. Theory Comput.* **2010**, *6*, 212–222.

23. Cieplak, P.; Cornell, W. D.; Bayly, C.; Kollman, P. A. *J. Comput. Chem.* **1995**, *16*, 1357-1377.

24. Cornell, W. D.; Cieplak, P.; Bayly, C. I.; Gould, I. R.; Merz, K. M.; Ferguson, D. M.; Spellmeyer, D. C.; Fox, T.; Caldwell, J. W.; Kollman, P. A. *J. Am. Chem. Soc.* **1995**, *117*, 5179–5197.

25. Jorgensen, W. L.; Chandrasekhar, J.; Madura, J. D.; Impey, R. W.; Klein, M. L. *J. Chem. Phys.* **1983**, *79*, 926–935.

26. Berendsen, H. J. C.; Postma, J. P. M.; Gunsteren, W. F. v.; DiNola, A.; Haak, J. R. *J. Chem. Phys.* **1984**, *81*, 3684–3690.

27. Ryckaert, J.-P.; Ciccotti, G.; Berendsen, H. J. C. *J. Comput. Phys.* **1977**, *23*, 327–341.

28. Liu, C.; Richards, M. R.; Lowary, T. L. *Org. Biomol. Chem.* **2011**, *9*, 165–176.

29. Taha, H. A. Conformational Analysis of D-Arabinofuranosides using NMR Spectroscopy and Computational Chemistry. Ph.D. Thesis, University of Alberta, Edmonton, AB, 2010.

30. Islam, S. M.; Richards, M. R.; Taha, H. A.; Byrns, S. C.; Lowary, T. L.; Roy, P.-N. *J. Chem. Theory Comput.* **2011**, *7*, 2989–3000.

Chapter 6:

Summary and future directions

6.1. Highlights

Galactose, in its furanose form, is a component of many important bacterial and fungal glycoconjugates, including the cell wall mycolyl-arabinogalactan (mAG) of *Mycobacterium tuberculosis* (as discussed in Chapter 1).[1] The mAG complex is essential for the viability of mycobacteria,[2] yet little is known about the conformation of mAG or its constituent residues. To address this, we have developed improved methods for the conformational analysis of galactofuranosides, which we applied to the compounds shown in Figure 6.1. These methods represent an extension of earlier work in the Lowary group on arabinofuranosides.[3-5] The trisaccharides **6.3** and **6.4** represent the smallest repeating units of the galactan of mAG.

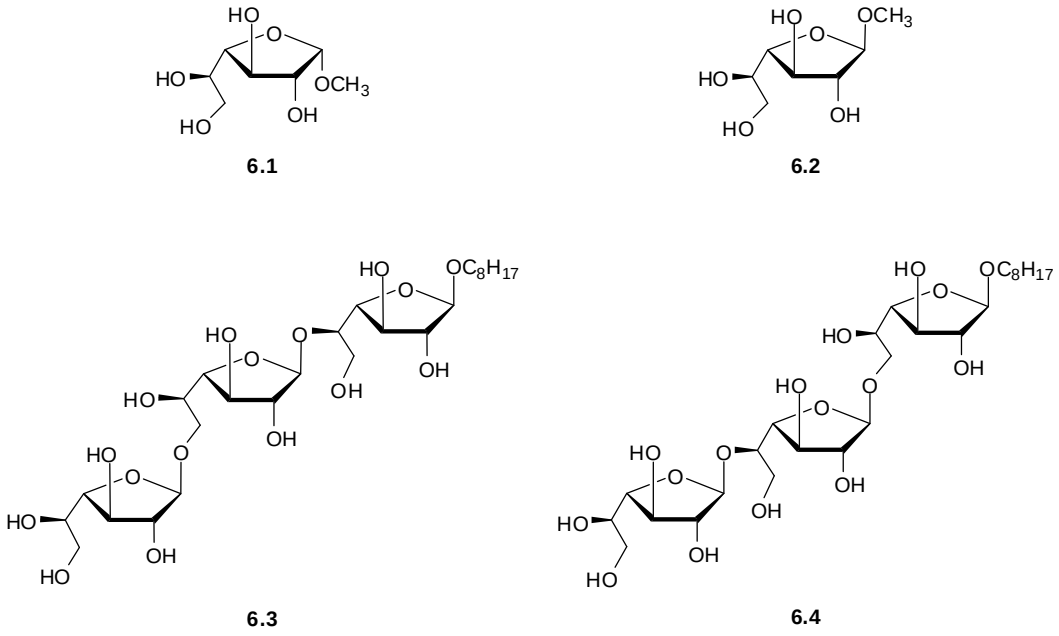

Figure 6.1. The galactofuranose-containing compounds studied in this thesis.

As a first step in these investigations, we calculated the gas-phase partial potential energy surfaces (PES) for **6.1** and **6.2** using B3LYP/6-31+G**[6-9] (Chapter 2). The PES for **6.1** and **6.2** were constructed with the ten envelope ring conformations (Figure 6.2), the three staggered rotamers about the C4–C5 bond, and the three staggered rotamers about the C5–C6 bond. The lowest energy ring conformation for **6.1** is ^{2}E (Table 2.2). The lowest energy ring conformation for **6.2** is E_O, but the ^{4}E conformer is only 0.1 kcal/mol higher in energy (Table 2.4).

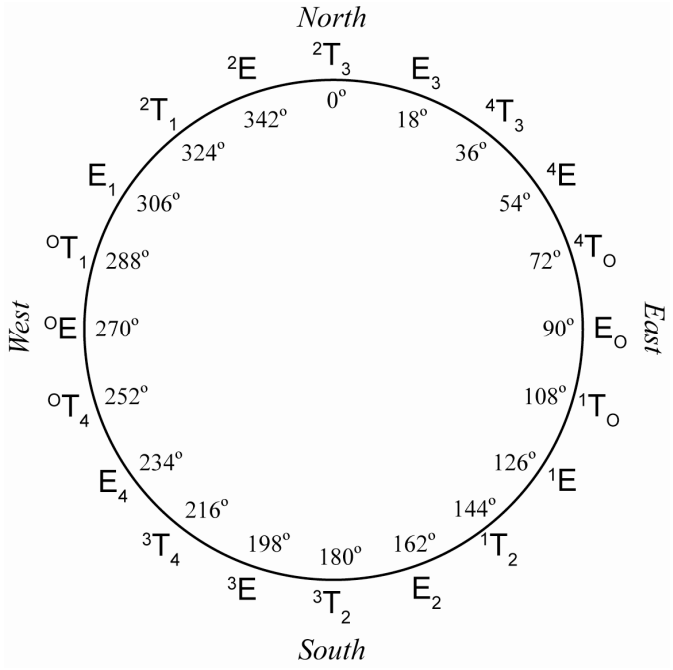

Figure 6.2. The pseudorotational itinerary for the galactose ring. The ring conformations are listed on the outside, and the corresponding pseudorotational phase angle, *P*, is listed inside.

We compared the results from the PES to the ring conformations from ^{1}H NMR spectra and PSEUROT.[10,11] The program PSEUROT assumes that the observed coupling constants for the ring dihedral angles are the average of two low energy conformations. For **6.1**, PSEUROT gave an 88:12 ratio between the ^{2}E and ^{1}E conformations (Table 2.7); thus, the major conformation agrees well

with the lowest energy conformation determined by density functional theory (DFT) calculations. For **6.2**, however, the results from four PSEUROT calculations gave three different major ring conformations (Table 2.8). Two of the PSEUROT runs predicted a 68:32 ratio between the ^{4}E and E_4 conformations, but the other two runs were not in agreement with lowest energy conformers from the DFT calculations, predicting the major conformation as either ^{1}E or ^1T_O. From these studies we conclude that the two-state model that PSEUROT employs may not be appropriate for **6.2**. Earlier, we had seen similar results when PSEUROT was used to analyze the conformation of methyl α-D-Ara*f*, which has the same relative configuration along the ring as **6.2**: four separate PSEUROT calculations gave three different answers.[12]

To address the limitations of PSEUROT, we ran molecular dynamics (MD) calculations on both **6.1** and **6.2** using the AMBER 10[13] software package and the GLYCAM06[14] force field (Chapter 3). The simulations of **6.1** gave two major populations for the ring conformation, 78:22 ratio between ^{2}E and ^{1}E, showing good agreement with both DFT and PSEUROT. For **6.2**, we observed mainly one population centered at the E_3 conformation, in contrast with the two-state model of PSEUROT. As shown in Figure 6.2, the E_3 and ^{4}E conformations are close on the pseudorotational itinerary. The differences in the low energy conformations from the DFT and MD calculations may be due to solvent interactions: We included explicit water solvation in the MD simulations, but the DFT calculations were conducted in the gas phase.

To compare directly with experiment, we developed Karplus relationships specific for galactofuranose (Gal*f*) from the PES described above (eqs. 3.10–3.16), and we used the new equations to calculate the average coupling constants from the MD simulations (Chapter 3, Table 3.5). Excellent agreement was found for $^{3}J_{H5,H6R}$ and $^{3}J_{H5,H6S}$ of both **6.1** and **6.2**. For **6.2**, good agreement was also seen for the coupling constants from the ring torsions, $^{3}J_{H1,H2,}$ $^{3}J_{H2,H3}$, and $^{3}J_{H3,H4}$, indicating the ring conformation from MD is similar to the experimental conformation. However, the same coupling constants for **6.1** showed poor agreement between experiment and simulation. This agreement could be improved in the future by restraining the simulation values for $^{3}J_{H2,H3}$ or $^{3}J_{H3,H4}$ to their experimental values,[15] and initial calculations with such *J*-restraints appear promising (data not shown). For both **6.1** and **6.2**, the values for $^{3}J_{H4,H5}$ and $^{3}J_{H4,C6}$ calculated from MD simulation were the same but did not match the experimental values obtained for either compound. To improve this agreement, we tried varying many simulation parameters, including the choice of water model, thermostat, and simulation temperature. None of these parameters significantly affected the results of the MD simulations; thus, we concluded the relative energies for each of the rotamers about the C4–C5 bond in the GLYCAM06 force field was not appropriate for **6.1** or **6.2**.

We were able to improve the agreement between MD simulations and experiment for $^{3}J_{H4,H5}$ and $^{3}J_{H4,C6}$ by developing new force field parameters for the C4–C5 bond of Gal*f* (Chapter 4, Tables 4.3 and 4.4). We used umbrella sampling[16-18] to determine the free energy of rotation about the C4–C5 bond for

6.1 and **6.2** using the original GLYCAM06 parameters (Figures 4.6 and 4.8). For both compounds, the *gg* rotamer is 2 kcal/mol lower in energy than the other two staggered conformation, which effectively restricts the C4–C5 bond to one conformations. We also used a Metropolis Monte Carlo simulated annealing algorithm[19] to determine new force field parameters for the C4–C5 bond. With the addition of these new terms, the *gg* rotamer is now only 0.3–0.5 kcal/mol lower in energy than the *gt* conformer (Figures 4.27 and 4.29), and the values of $^3J_{H4,H5}$ and $^3J_{H4,C6}$ more closely match experimental values. Unfortunately, the improvements for the C4–C5 bond came at the expense of accurate predictions of $^3J_{H5,H6R}$ and $^3J_{H5,H6S}$, though the values with the new parameters are still within error of those obtained from NMR experiments. The new terms did not have an effect on the ring conformations that we observed in the MD simulations.

Furthermore, we compared the original and improved force field parameters in MD simulations of **6.3** and **6.4** (Chapter 5). The values of $^3J_{H1,H2,}$ $^3J_{H2,H3}$, and$^3J_{H3,H4}$ from the MD simulations show good agreement with experiment (Tables 5.7 and 5.8), and the ring conformations for the trisaccharides were similar to those from simulations on **6.2**. For the non-reducing end and O6-linked residues, the new force field parameters improve the agreement between calculation and experiment for $^3J_{H4,H5}$. However, the new terms have little effect on the O5-linked residues. The new force field parameters also have little effect on $^3J_{H5,H6R}$ and $^3J_{H5,H6S}$ for both O5- and O6-linked residues, with the O6-linked moieties showing poor agreement between simulation and experiment for both the original and new terms. The original GLYCAM06 parameters show excellent

agreement to the experimental values for $^3J_{H5,H6R}$ and $^3J_{H5,H6S}$ for the non-reducing end moieties. More work will be necessary to improve the models for internal β-(1→5)- and β-(1–6)-Gal*f* linkages.

6.2. Future directions

The work detailed in this thesis sets the stage for future studies. When we noticed the discrepancy between experiment and simulation for the values of $^3J_{H4,H5}$ and $^3J_{H4,C6}$ for **6.1** and **6.2**, MD simulations were run on other hexofuranosides – allofuranose, glucofuranose, gulofuranose. None of the rotamer populations about the C4–C5 bond of these compound were the same as the distributions for **6.1** and **6.2** (Table 3.3). However, the values of $^3J_{H4,H5}$ and $^3J_{H4,C6}$ for these compounds are not available for direct comparison with the calculations, and these data will be necessary to determine the accuracy of the simulations for these hexofuranosides. Future work in this area would include measuring the vicinal coupling constants for these compounds.

Both hexofuranosides and heptopyranosides contain ethylene glycol side-chains. Initial MD simulations on β-D-*glycero*-D-*galacto*-heptopyranose (**6.5**, Figure 6.3) using GLYCAM06 indicate that the C5–C6 bond remains in essentially one conformation (data not shown), like the C4–C5 bonds of **6.1** and **6.2**. However, all three staggered rotamers for the C5–C6 bond of β-D-*glycero*-D-*gluco*-heptopyranose (**6.6**, Figure 6.3) are significantly populated in initial MD simulations (data not shown). Further work is still needed to determine if the conformations about the C5–C6 bonds of **6.5** and **6.6** in the MD calculations are

representative of their solution conformations. In particular, the 6-*O*-methyl-D-*glycero*-α-L-*gluco*-heptopyranose **6.7** (Figure 6.3) has been synthesized[20] and could serve as a starting point for studies on heptopyranosides.

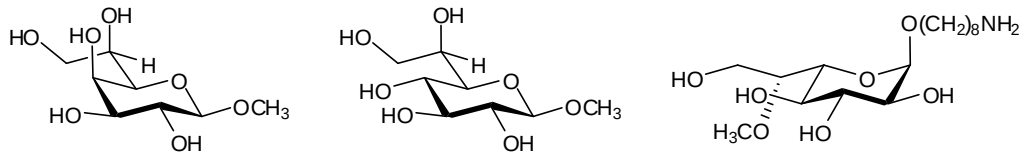

6.5 **6.6** **6.7**

Figure 6.3. Heptopyranosides for further study in MD simulations.

As noted above, the MD results for the internal β-(1→5)- and β-(1→6)-Gal*f* linkages do not agree well with experiment for **6.3** and **6.4**. Nevertheless, future studies should include simulations on longer Gal*f*-containing oligosaccharides. Dr. Maju Joe has synthesized portions of the mAG containing 4–14 Gal*f* residues. Comparison of the NMR spectra of these compounds to MD simulations may provide insight into the presence of stable secondary structure in solution, although these NMR spectra may be difficult to interpret due to spectral overlap. While oligosaccharides do not typically form rigid secondary structures as proteins do,[21] there are examples of helical conformations in solution, such as β-(1→2)-linked mannopyranosides.[22] Furthermore, the mAG complex contains 30–35 Gal*f* residues, and the arabinan chains are attached to the O3 hydroxyl group on residues 8, 10, and 12.[23] Systematic studies of galactans with defined length may provide insight into the specificity of these attachment points.

The precise mechanism of the galactofuranosyltransferase GlfT2, one of the enzymes that synthesizes mAG, remains unclear.[24,25] GlfT2 catalyzes the

formation of alternating β-(1→5)- and β-(1→6)-linkages with high fidelity; incorporation of either 5-deoxy or 6-deoxy Gal*f* residues halts chain extension.[24] The crystal structure of GlfT2 has recently been solved,[26] and docking of the trisaccharides **6.3** and **6.4**, the natural acceptor substrates, or longer galactan chains into the active site could identify key interactions responsible for determining glycosidic linkage specificity. The resulting complexes from docking simulations would also provide structures for MD simulations than could be correlated with available saturation transfer difference (STD) NMR data.[27-29]

The mechanism for galactan chain termination in GlfT2 is also unclear. The galactan chain is synthesized on decaprenyl phosphate, and it has been proposed that the lipid interacts with a second site on the enzyme to halt galactan synthesis.[30] However, there is no apparent lipid binding sight in the crystal structure of GlfT2.[26] Docking calculations, followed by MD simulations, of the full 35-residue galactan on the decaprenyl phosphate would provide insight into the mechanism of chain termination.

The studies of galactofuranosides presented here, along with our earlier work in arabinofuranosides,[3] represent advances in our understanding of the conformation of furanosides in solution. These results lay the foundation for further work on other systems, including isolated mono- and oligosaccharides and the mechanisms of carbohydrate-processing enzymes and will help elucidate the function of the galactan polymers that form part of the mycobacterial cell wall.

6.3. References

1. Richards, M. R.; Lowary, T. L. *ChemBioChem* **2009**, *10*, 1920–1938.

2. Pan, F.; Jackson, M.; Ma, Y. F.; McNeil, M. *J. Bacteriol.* **2001**, *183*, 3991–3998.

3. Taha, H. A. Conformational Analysis of D-Arabinofuranosides using NMR Spectroscopy and Computational Chemistry. Ph.D. Thesis, University of Alberta, Edmonton, AB, 2010.

4. Houseknecht, J. B.; Lowary, T. L.; Hadad, C. M. *J. Phys. Chem. A* **2003**, *107*, 5763–5777.

5. Houseknecht, J. B.; Altona, C.; Hadad, C. M.; Lowary, T. L. *J. Org. Chem.* **2002**, *67*, 4647–4651.

6. Becke, A. D. *J. Chem. Phys.* **1993**, *98*, 5648–5652.

7. Rassolov, V. A.; Ratner, M. A.; Pople, J. A.; Redfern, P. C.; Curtiss, L. A. *J. Comput. Chem.* **2001**, *22*, 976–984.

8. Clark, T.; Chandrasekhar, J.; Spitznagel, G. W.; Schleyer, P. V. *J. Comput. Chem.* **1983**, *4*, 294–301.

9. Frisch, M. J.; Pople, J. A.; Binkley, J. S. *J. Chem. Phys.* **1984**, *80*, 3265–3269.

10. van Wijk, J.; Haasnoot, C. A. G.; de Leeuw, F. A. A. M.; Huckriede, B. D.; Westra Hoekzema, A.; Altona, C. *PSEUROT 6.3*, Leiden Institute of Chemistry, Leiden University: Leiden, 1999.

11. de Leeuw, F. A. A. M.; Altona, C. *J. Comput. Chem.* **1983**, *4*, 428–437.

12. Houseknecht, J. B.; Lowary, T. L.; Hadad, C. M. *J. Phys. Chem. A* **2003**, *107*, 372–378.

13. Case, D. A.; Darden, T. A.; T.E. Cheatham, I.; Simmerling, C. L.; Wang, J.; Duke, R. E.; Luo, R.; Crowley, M.; Walker, R. C.; Zhang, W.; Merz, K. M.; Wang, B.; Hayik, S.; Roitberg, A.; Seabra, G.; Kolossváry, I.; Wong, K. F.; Paesani, F.; Vanicek, J.; Wu, X.; Brozell, S. R.; Steinbrecher, T.; Golke, H.; Yang, L.; Tan, C.; Mongan, J.; Hornak, V.; Cui, G.; Mathews, D. H.; Seetin, M. G.; Saugi, C.; Babin, V.; Kollman, P. A. *AMBER 10*, Univeristy of California, San Francisco: 2008.

14. Kirschner, K. N.; Yongye, A. B.; Tschampel, S. M.; González-Outeiriño, J.; Daniels, C. R.; Lachele Foley, B.; Woods, R. J. *J. Comput. Chem.* **2008**, *29*, 622–655.

15. Hendrickx, P. M. S.; Corzana, F.; Depraetere, S.; Tourwé, D. A.; Augustyns, K.; Martins, J. C. *J. Comput. Chem.* **2010**, *31*, 561–572.

16. Torrie, G. M.; Valleau, J. P. *J. Comput. Phys.* **1977**, *23*, 187–199.

17. Leach, A. R. Umbrella Sampling. In *Molecular Modelling: Principles and Applications*, 2nd ed.; Prentice Hall: New York, 2001; pp 581–582.

18. Kästner, J. *WIREs Comput. Mol. Sci.* **2011**, *1*, 932–942.

19. Guvench, O.; MacKerell, A. D. *J. Mol. Model.* **2008**, *14*, 667–679.

20. Peng, W.; Jayasuriya, A. B.; Imamura, A.; Lowary, T. L. *Org. Lett.* **2011**, *13*, 5290–5293.

21. DeMarco, M. L.; Woods, R. J. *Glycobiology* **2008**, *18*, 426–440.

22. Nitz, M.; Ling, C. C.; Otter, A.; Cutler, J. E.; Bundle, D. R. *J. Biol. Chem.* **2002**, *277*, 3440–3446.

23. Alderwick, L. J.; Radmacher, E.; Seidel, M.; Gande, R.; Hitchen, P. G.; Morris, H. R.; Dell, A.; Sahm, H.; Eggeling, L.; Besra, G. S. *J. Biol. Chem.* **2005**, *280*, 32362–32371.

24. Lowary, T. L.; Poulin, M. B.; Zhou, R. *Org. Biomol. Chem.* **2012**, doi: 10.1039/c2ob25159k.

25. Brown, C. D.; Rusek, M. S.; Kiessling, L. L. *J. Am. Chem. Soc.* **2012**, doi: 10.1021/ja301723p.

26. Wheatley, R. W.; Zheng, R. B.; Richards, M. R.; Lowary, T. L.; Ng, K. K. S. *J. Biol. Chem. In press*, doi: 10.1074/jbc.M112.347484

27. Szczepina, M. G.; Zheng, R. B.; Completo, G. C.; Lowary, T. L.; Pinto, B. M. *ChemBioChem* **2009**, *10*, 2052–2059.

28. Szczepina, M. G.; Zheng, R. X. B.; Completo, G. C.; Lowary, T. L.; Pinto, B. M. *Bioorg. Med. Chem.* **2010**, *18*, 5123–5128.

29. May, J. F.; Levengood, M. R.; Splain, R. A.; Brown, C. D.; Kiessling, L. L. *Biochemistry* **2012**, *51*, 1148–1159.

30. May, J. F.; Splain, R. A.; Brotschi, C.; Kiessling, L. L. *Proc. Natl. Acad. Sci. U.S.A.* **2009**, *106*, 11851–11856.

Appendix A:

Supporting information for Chapter 2

A.1. Cartesian coordinates for 2.1 (α-Gal*f*) and 2.2 (β-Gal*f*) from the gas-phase potential energy surfaces

Coordinates for α-Galf OE-gg-gg
Energy: -726.49632332 Hartrees

C	-0.8750	1.0690	-0.7150
C	-1.9770	0.1820	-0.0820
C	-1.3340	-1.2190	0.0690
C	0.1020	-1.0610	-0.4850
H	-1.2240	1.6150	-1.6050
H	-2.7760	0.0640	-0.8270
H	-1.3210	-1.4960	1.1310
H	0.2890	-1.8480	-1.2300
O	0.1110	0.1690	-1.2060
O	-0.4010	1.9670	0.2320
C	0.6510	2.7930	-0.2440
H	1.5580	2.2080	-0.4300
H	0.8390	3.5320	0.5390
H	0.3580	3.3170	-1.1690
O	-2.4780	0.7440	1.1120
H	-3.3210	0.3010	1.2950
O	-2.1260	-2.1340	-0.6890
H	-1.6750	-2.9930	-0.6920
C	1.1980	-1.2120	0.5820
H	1.0750	-2.2480	0.9590
O	0.9620	-0.2740	1.6120
H	1.5690	-0.4630	2.3450
C	2.6340	-1.1580	0.0460
H	2.7360	-1.9160	-0.7500
H	3.3060	-1.4660	0.8680
O	2.9660	0.1380	-0.4150
H	3.9130	0.1440	-0.6200

Coordinates for α-Galf OE-gg-gt
Energy: -726.50411462 Hartrees

C	-1.3990	0.7200	-0.6970
C	-2.0110	-0.4710	0.0870
C	-0.8770	-1.5170	0.1770
C	0.3230	-0.8760	-0.5570
H	-2.0310	1.0610	-1.5300
H	-2.8060	-0.9180	-0.5250
H	-0.6450	-1.7090	1.2360
H	0.7050	-1.5970	-1.2930
O	-0.2190	0.2160	-1.3090
O	-1.1800	1.7720	0.1890
C	-0.5860	2.9140	-0.4130
H	0.4420	2.7070	-0.7260
H	-0.5850	3.6980	0.3470
H	-1.1730	3.2510	-1.2820
O	-2.5050	-0.0480	1.3440
H	-3.0810	-0.7540	1.6730
O	-1.3450	-2.7080	-0.4520
H	-0.6080	-3.3360	-0.4990
C	1.5030	-0.4700	0.3560
H	1.7170	-1.3420	1.0020
O	1.2580	0.6860	1.1300
H	0.4520	0.5690	1.6570
C	2.7780	-0.2020	-0.4360
H	2.6640	0.7550	-0.9660
H	2.9060	-0.9960	-1.1910
O	3.8680	-0.1820	0.4730
H	4.6470	0.1370	-0.0070

Coordinates for α-Galf OE-gg-tg
Energy: -726.504745912 Hartrees

C	-1.3010	0.5770	-0.7890
C	-1.8370	-0.7250	-0.1400
C	-0.5840	-1.5880	0.1460
C	0.6080	-0.7440	-0.3500
H	-1.8050	0.8130	-1.7390
H	-2.4040	-1.2690	-0.9080
H	-0.5160	-1.7730	1.2260
H	1.2280	-1.3360	-1.0340
O	0.0510	0.3150	-1.1410
O	-1.4560	1.6410	0.0940
C	-1.0670	2.8900	-0.4450
H	0.0140	2.9350	-0.6300
H	-1.3390	3.6480	0.2930
H	-1.5940	3.1020	-1.3900
O	-2.6460	-0.4480	0.9830
H	-3.1560	-1.2520	1.1640
O	-0.7390	-2.8120	-0.5730
H	0.0860	-3.3150	-0.4900
C	1.5440	-0.2470	0.7560
H	1.9940	-1.1480	1.2100
O	0.7860	0.4790	1.7090
H	1.3770	0.7350	2.4340
C	2.6860	0.6060	0.2020
H	3.2460	1.0410	1.0480
H	2.2620	1.4300	-0.3870
O	3.5190	-0.2410	-0.5830
H	4.2030	0.3070	-0.9950

Coordinates for α-Galf OE-gt-gg
Energy: -726.507407646 Hartrees

C	1.7340	0.0800	-0.5290
C	1.2760	1.4430	0.0440
C	-0.2700	1.3990	-0.0440
C	-0.5800	0.0190	-0.6590
H	2.5780	0.1620	-1.2280
H	1.6030	2.2250	-0.6560
H	-0.6750	1.5000	0.9720
H	-1.3150	0.1060	-1.4630
O	0.6440	-0.3910	-1.2880
O	2.0750	-0.7770	0.5300
C	2.5030	-2.0580	0.0870
H	1.6910	-2.6010	-0.4100
H	2.8250	-2.6040	0.9780
H	3.3530	-1.9740	-0.6080
O	1.7950	1.6640	1.3400
H	1.6890	2.6100	1.5270
O	-0.7140	2.4750	-0.8610
H	-1.6700	2.3530	-0.9830
C	-1.1120	-1.0250	0.3330
H	-0.3540	-1.2020	1.1110
O	-1.3280	-2.2090	-0.4310
H	-1.6360	-2.9010	0.1740
C	-2.3930	-0.5430	1.0310
H	-2.1250	0.0980	1.8850
H	-2.9200	-1.4210	1.4390
O	-3.2130	0.1650	0.1030
H	-4.0650	0.3410	0.5290

Coordinates for α-Galf OE-gt-gt
Energy: -726.504057901 Hartrees

C	-1.7070	0.4860	-0.3900
C	-1.7870	-0.9090	0.2750
C	-0.4090	-1.5580	-0.0160
C	0.3490	-0.4810	-0.8250
H	-2.6100	0.7530	-0.9560
H	-2.5250	-1.5020	-0.2830
H	0.0910	-1.7810	0.9370
H	0.8390	-0.9320	-1.7010
O	-0.6760	0.3660	-1.3560
O	-1.4450	1.4460	0.5870
C	-1.3750	2.7730	0.0750
H	-0.5060	2.8970	-0.5780
H	-1.2830	3.4320	0.9420
H	-2.2940	3.0290	-0.4760
O	-2.1310	-0.8130	1.6410
H	-2.4130	-1.6960	1.9250
O	-0.6500	-2.7560	-0.7510
H	0.2050	-3.1170	-1.0330
C	1.4040	0.3030	-0.0060
H	0.9870	0.5660	0.9700
O	1.7220	1.5450	-0.6120
H	2.1320	1.3650	-1.4740
C	2.6560	-0.5520	0.2020
H	2.3700	-1.5390	0.6050
H	3.1310	-0.7300	-0.7820
O	3.5310	0.1290	1.0830
H	4.2790	-0.4570	1.2740

Coordinates for α-Galf OE-gt-tg
Energy: -726.507324922 Hartrees

C	1.7120	0.2150	-0.4680
C	1.1150	1.5310	0.0840
C	-0.4140	1.3810	-0.1150
C	-0.5730	-0.0140	-0.7660
H	2.5970	0.3680	-1.1030
H	1.4340	2.3450	-0.5810
H	-0.9150	1.4240	0.8580
H	-1.2550	0.0270	-1.6240
O	0.7160	-0.3150	-1.3170
O	2.0290	-0.6310	0.6010
C	2.6170	-1.8590	0.1890
H	1.9060	-2.4650	-0.3820
H	2.9070	-2.3850	1.1020
H	3.5170	-1.6800	-0.4210
O	1.5250	1.7660	1.4160
H	1.3390	2.6990	1.6060
O	-0.8620	2.4400	-0.9550
H	-1.7950	2.2650	-1.1530
C	-1.0780	-1.0860	0.2160
H	-0.5950	-0.9380	1.1920
O	-0.7420	-2.3650	-0.3180
H	-1.0570	-3.0350	0.3090
C	-2.6050	-1.0270	0.3710
H	-2.9120	-1.7780	1.1180
H	-3.0520	-1.3140	-0.5930
O	-3.0190	0.2800	0.7650
H	-3.9350	0.2260	1.0740

Coordinates for α-Galf OE-tg-gg
Energy: -726.50615388 Hartrees

C	1.5850	0.3710	-0.5220
C	0.8990	1.4240	0.3870
C	-0.6100	1.3390	0.0580
C	-0.7200	0.2430	-1.0230
H	2.4140	0.7990	-1.1040
H	1.2310	2.4180	0.0570
H	-1.1730	1.0680	0.9540
H	-1.2540	0.6490	-1.8900
O	0.6150	-0.0420	-1.4670
O	2.0750	-0.6950	0.2460
C	2.8740	-1.5980	-0.5040
H	2.2930	-2.0980	-1.2880
H	3.2540	-2.3420	0.2010
H	3.7250	-1.0790	-0.9710
O	1.2300	1.2020	1.7440
H	1.0090	2.0170	2.2210
O	-1.0100	2.6220	-0.4320
H	-1.9260	2.5380	-0.7390
C	-1.4750	-1.0450	-0.6390
H	-1.2890	-1.7560	-1.4620
O	-2.8430	-0.6510	-0.5990
H	-3.3860	-1.4440	-0.4750
C	-1.0310	-1.7430	0.6510
H	0.0620	-1.8340	0.6460
H	-1.4590	-2.7620	0.6480
O	-1.4980	-1.0160	1.7820
H	-1.1980	-1.4870	2.5730

Coordinates for α-Galf OE-tg-gt
Energy: -726.504072869 Hartrees

C	1.6600	-0.1890	-0.4980
C	1.5100	1.0150	0.4690
C	0.1000	1.5900	0.1950
C	-0.4960	0.6940	-0.9110
H	2.5770	-0.1250	-1.1000
H	2.2230	1.7910	0.1590
H	-0.4840	1.5370	1.1260
H	-0.8270	1.3310	-1.7400
O	0.5850	-0.1020	-1.4180
O	1.6680	-1.3890	0.2200
C	1.9960	-2.5170	-0.5810
H	1.2410	-2.6950	-1.3560
H	2.0390	-3.3760	0.0920
H	2.9770	-2.3860	-1.0620
O	1.7320	0.6210	1.8080
H	1.8850	1.4300	2.3190
O	0.2600	2.9470	-0.2120
H	-0.6090	3.2800	-0.4880
C	-1.7360	-0.1350	-0.5110
H	-2.0250	-0.7270	-1.3860
O	-2.8300	0.7580	-0.2980
H	-2.6480	1.2590	0.5140
C	-1.5580	-1.1110	0.6470
H	-1.4020	-0.5520	1.5880
H	-0.6560	-1.7110	0.4820
O	-2.7310	-1.9110	0.7160
H	-2.6160	-2.5310	1.4520

Coordinates for α-Galf OE-tg-tg
Energy: -726.50550362 Hartrees

C	-0.9080	-1.2140	-0.5780
C	0.2100	-1.7860	0.3340
C	1.4180	-0.8420	0.1450
C	0.9390	0.2250	-0.8620
H	-1.3290	-1.9710	-1.2560
H	0.5090	-2.7650	-0.0630
H	1.6810	-0.3840	1.1080
H	1.6580	0.2820	-1.6890
O	-0.2850	-0.2560	-1.4200
O	-1.9280	-0.6770	0.2070
C	-3.0270	-0.1940	-0.5550
H	-2.7440	0.6780	-1.1510
H	-3.8010	0.0890	0.1630
H	-3.4240	-0.9810	-1.2150
O	-0.2400	-1.8950	1.6730
H	0.3840	-2.4810	2.1300
O	2.5090	-1.6170	-0.3460
H	3.2250	-0.9990	-0.5630
C	0.8320	1.6470	-0.2850
H	0.4920	2.3150	-1.0890
O	2.1820	1.9460	0.0920
H	2.2130	2.8700	0.3820
C	-0.1440	1.8420	0.8900
H	-0.3510	0.9010	1.4130
H	0.3340	2.5290	1.6100
O	-1.3400	2.4130	0.3670
H	-1.9530	2.5360	1.1070

Coordinates for α-Galf EO-gg-gg
Energy: -726.496553163 Hartrees

C	-1.4510	0.4850	-0.4670
C	-1.7300	-0.9890	-0.0880
C	-0.3210	-1.6250	-0.1200
C	0.6140	-0.4490	-0.5140
H	-1.5510	0.5980	-1.5670
H	-2.3570	-1.4630	-0.8560
H	-0.0760	-1.9580	0.8960
H	0.7360	-0.4870	-1.6130
O	-0.0810	0.7200	-0.1300
O	-2.2810	1.3660	0.1870
C	-2.0820	2.7210	-0.1970
H	-1.0840	3.0720	0.0850
H	-2.2150	2.8490	-1.2830
H	-2.8410	3.3050	0.3280
O	-2.3440	-1.0530	1.1860
H	-2.6110	-1.9750	1.3220
O	-0.2960	-2.7080	-1.0460
H	0.5610	-3.1530	-0.9610
C	2.0110	-0.5190	0.1050
H	2.4290	-1.4850	-0.2470
O	1.8720	-0.5150	1.5150
H	2.7420	-0.6910	1.9040
C	2.9930	0.5450	-0.3990
H	3.0590	0.4560	-1.4980
H	3.9920	0.2910	0.0020
O	2.5930	1.8360	0.0090
H	3.3060	2.4510	-0.2220

Coordinates for α-Galf EO-gg-gt
Energy: -726.502540049 Hartrees

C	1.5990	-0.4630	-0.4720
C	1.7660	1.0320	-0.1000
C	0.3130	1.5650	-0.1250
C	-0.5400	0.3280	-0.5060
H	1.7150	-0.5760	-1.5680
H	2.3500	1.5490	-0.8740
H	0.0790	1.9000	0.8980
H	-0.6720	0.3710	-1.6030
O	0.2450	-0.7960	-0.1410
O	2.4890	-1.2700	0.1970
C	2.4440	-2.6320	-0.2100
H	1.4880	-3.0970	0.0570
H	2.5980	-2.7270	-1.2960
H	3.2570	-3.1390	0.3150
O	2.3780	1.1490	1.1700
H	2.5780	2.0880	1.3020
O	0.2020	2.6400	-1.0460
H	-0.6840	3.0250	-0.9600
C	-1.9290	0.2380	0.1370
H	-2.4940	1.1320	-0.1890
O	-1.8930	0.1490	1.5510
H	-1.4110	0.9110	1.9050
C	-2.6950	-0.9820	-0.3610
H	-2.2790	-1.8690	0.1330
H	-2.5380	-1.0850	-1.4470
O	-4.0710	-0.7930	-0.0580
H	-4.5300	-1.6280	-0.2360

Coordinates for α-Galf EO-gg-tg
Energy: -726.505760286 Hartrees

C	-1.4660	0.4760	-0.4620
C	-1.6470	-1.0490	-0.2680
C	-0.1910	-1.5670	-0.1980
C	0.6730	-0.2910	-0.3600
H	-1.4600	0.7010	-1.5480
H	-2.1420	-1.4830	-1.1470
H	-0.0320	-1.9960	0.7980
H	0.9320	-0.1870	-1.4260
O	-0.1660	0.7820	0.0520
O	-2.4410	1.2090	0.1760
C	-2.3740	2.6030	-0.0900
H	-1.4650	3.0480	0.3280
H	-2.4050	2.8040	-1.1730
H	-3.2510	3.0510	0.3830
O	-2.3870	-1.2990	0.9130
H	-2.5840	-2.2480	0.9240
O	0.0260	-2.5330	-1.2230
H	0.9040	-2.9200	-1.0880
C	1.9750	-0.2760	0.4330
H	2.6130	-1.0750	0.0130
O	1.6760	-0.5300	1.8000
H	2.5150	-0.5770	2.2850
C	2.7320	1.0460	0.2870
H	3.5960	1.0350	0.9750
H	2.0680	1.8680	0.5840
O	3.1570	1.1580	-1.0660
H	3.5730	2.0250	-1.1800

Coordinates for α-Galf EO-gt-gg
Energy: -726.499527771 Hartrees

C	1.7000	-0.1020	-0.4760
C	1.3470	1.3540	-0.0950
C	-0.1980	1.2880	0.0960
C	-0.5540	-0.1880	-0.1930
H	1.6710	-0.2010	-1.5800
H	1.5940	2.0350	-0.9230
H	-0.4010	1.5250	1.1520
H	-0.8440	-0.2750	-1.2510
O	0.6500	-0.9010	0.0650
O	2.9270	-0.4920	0.0140
C	3.3190	-1.7930	-0.4110
H	2.6520	-2.5620	-0.0070
H	3.3250	-1.8660	-1.5090
H	4.3320	-1.9490	-0.0340
O	2.0360	1.7120	1.0910
H	1.8930	2.6590	1.2390
O	-0.9520	2.1220	-0.7740
H	-0.7380	3.0450	-0.5690
C	-1.6680	-0.7660	0.6770
H	-1.3550	-0.6560	1.7300
O	-1.7930	-2.1360	0.3280
H	-2.4480	-2.5340	0.9220
C	-2.9920	-0.0130	0.5060
H	-2.8570	1.0420	0.7900
H	-3.7230	-0.4520	1.2090
O	-3.4290	-0.1440	-0.8360
H	-4.3240	0.2210	-0.8960

Coordinates for α-Galf EO-gt-gt
Energy: -726.499713171 Hartrees

C	1.8100	-0.1450	-0.4010
C	1.4740	1.3210	-0.0430
C	-0.0750	1.3400	-0.0640
C	-0.4690	-0.1170	-0.4320
H	1.9530	-0.2250	-1.4980
H	1.8500	1.9970	-0.8230
H	-0.4170	1.5730	0.9550
H	-0.6120	-0.1500	-1.5310
O	0.6470	-0.9060	-0.0570
O	2.9200	-0.6080	0.2670
C	3.3150	-1.9190	-0.1210
H	2.5610	-2.6620	0.1600
H	3.4890	-1.9750	-1.2070
H	4.2500	-2.1270	0.4040
O	2.0150	1.6460	1.2230
H	1.8920	2.6000	1.3470
O	-0.5220	2.3180	-0.9970
H	-1.4850	2.3980	-0.9200
C	-1.7180	-0.6820	0.2580
H	-1.5530	-0.6630	1.3400
O	-1.9150	-2.0490	-0.0570
H	-2.1110	-2.1140	-1.0060
C	-2.9660	0.1510	-0.0580
H	-2.7870	1.2040	0.2250
H	-3.1510	0.1300	-1.1480
O	-4.0570	-0.3860	0.6650
H	-4.8210	0.1930	0.5280

Coordinates for α-Galf EO-gt-tg
Energy: -726.50263147 Hartrees

C	1.7600	0.0380	0.3920
C	1.1770	-1.3830	0.2000
C	-0.3580	-1.1340	0.2390
C	-0.4940	0.3890	0.4460
H	1.9440	0.2080	1.4720
H	1.4800	-2.0310	1.0370
H	-0.7760	-1.4310	-0.7300
H	-0.6120	0.5690	1.5280
O	0.7320	0.9360	-0.0240
O	2.9160	0.2370	-0.3310
C	3.5270	1.4980	-0.0870
H	2.8950	2.3230	-0.4330
H	3.7380	1.6360	0.9850
H	4.4680	1.4980	-0.6410
O	1.6190	-1.9040	-1.0430
H	1.3360	-2.8290	-1.0890
O	-1.0440	-1.7760	1.3100
H	-0.9080	-2.7320	1.2280
C	-1.6480	1.0770	-0.2760
H	-1.4260	1.0800	-1.3540
O	-1.6950	2.4030	0.2470
H	-2.3890	2.8840	-0.2300
C	-3.0040	0.3830	-0.0740
H	-3.7890	1.1280	-0.2870
H	-3.1200	0.0640	0.9720
O	-3.1000	-0.7180	-0.9720
H	-4.0260	-0.9990	-1.0030

Coordinates for α-Galf EO-tg-gg
Energy: -726.500983718 Hartrees

C	1.6910	0.0810	-0.4560
C	1.0960	1.3520	0.1970
C	-0.4270	1.2390	-0.1040
C	-0.5640	-0.0790	-0.8970
H	2.0530	0.3320	-1.4730
H	1.5080	2.2490	-0.2890
H	-0.9690	1.1760	0.8450
H	-0.5990	0.1880	-1.9650
O	0.6060	-0.8370	-0.5970
O	2.7100	-0.4730	0.2910
C	3.3710	-1.5500	-0.3590
H	2.7020	-2.4070	-0.4970
H	3.7630	-1.2420	-1.3410
H	4.2050	-1.8360	0.2860
O	1.3890	1.3370	1.5860
H	1.1280	2.1990	1.9450
O	-0.9270	2.2870	-0.9300
H	-0.8700	3.1150	-0.4290
C	-1.7710	-0.9820	-0.6020
H	-1.6360	-1.8740	-1.2380
O	-2.9220	-0.2490	-0.9840
H	-3.6970	-0.8170	-0.8480
C	-1.8440	-1.5090	0.8360
H	-0.8600	-1.9170	1.1010
H	-2.5710	-2.3410	0.8570
O	-2.2530	-0.4760	1.7260
H	-2.2830	-0.8560	2.6170

Coordinates for α-Galf EO-tg-gt
Energy: -726.502525908 Hartrees

C	1.7440	-0.0970	-0.4240
C	1.4330	1.2180	0.3350
C	-0.0750	1.4290	0.0680
C	-0.4900	0.2270	-0.8110
H	2.1050	0.1500	-1.4410
H	1.9970	2.0500	-0.1080
H	-0.5730	1.3870	1.0500
H	-0.4310	0.5770	-1.8550
O	0.4880	-0.7780	-0.5650
O	2.6580	-0.8830	0.2390
C	3.0880	-2.0160	-0.5050
H	2.2670	-2.7230	-0.6690
H	3.5030	-1.7170	-1.4800
H	3.8710	-2.4960	0.0870
O	1.7360	1.0640	1.7090
H	1.6490	1.9390	2.1170
O	-0.2970	2.6800	-0.5650
H	-1.2580	2.8140	-0.6090
C	-1.9090	-0.3200	-0.5580
H	-2.2590	-0.8370	-1.4570
O	-2.8330	0.7630	-0.4010
H	-2.6140	1.2090	0.4330
C	-1.9970	-1.3240	0.5890
H	-1.7070	-0.8370	1.5370
H	-1.2740	-2.1300	0.4050
O	-3.3330	-1.8020	0.6400
H	-3.3870	-2.4400	1.3670

Coordinates for α-Galf EO-tg-tg
Energy: -726.497642787 Hartrees

C	-1.5800	-0.2040	-0.5080
C	-1.1240	-1.4360	0.3160
C	0.4180	-1.4670	0.1140
C	0.7170	-0.2610	-0.8030
H	-1.9460	-0.5410	-1.4980
H	-1.5740	-2.3500	-0.0960
H	0.8980	-1.3470	1.0950
H	0.8500	-0.6540	-1.8230
O	-0.4170	0.5910	-0.7180
O	-2.5580	0.5210	0.1400
C	-3.0440	1.6200	-0.6210
H	-2.2650	2.3760	-0.7680
H	-3.4140	1.2900	-1.6040
H	-3.8720	2.0490	-0.0510
O	-1.4920	-1.2460	1.6750
H	-1.3140	-2.0770	2.1420
O	0.8890	-2.6360	-0.5470
H	0.6810	-3.4020	0.0100
C	1.9520	0.5670	-0.4180
H	2.1470	1.2920	-1.2230
O	3.0180	-0.3720	-0.3030
H	3.8300	0.1280	-0.1250
C	1.7680	1.3900	0.8700
H	1.0430	0.9100	1.5440
H	2.7400	1.4180	1.3930
O	1.3490	2.6970	0.5020
H	1.2350	3.2120	1.3150

Coordinates for α-Galf 1E-gg-gg
Energy: -726.494738122 Hartrees

C	-1.5030	0.3600	-0.3950
C	-1.6060	-1.0230	0.2660
C	-0.3100	-1.6990	-0.2330
C	0.6160	-0.5010	-0.6220
H	-1.8150	0.2750	-1.4560
H	-2.4810	-1.5740	-0.1000
H	0.1310	-2.2920	0.5770
H	0.8100	-0.5890	-1.7070
O	-0.1130	0.6840	-0.3560
O	-2.2540	1.3160	0.2560
C	-2.1970	2.5960	-0.3600
H	-1.1870	3.0180	-0.3030
H	-2.8950	3.2340	0.1870
H	-2.5060	2.5440	-1.4160
O	-1.6260	-0.8620	1.6700
H	-1.8830	-1.7130	2.0550
O	-0.6400	-2.5170	-1.3560
H	0.1520	-3.0150	-1.6080
C	1.9740	-0.5080	0.0850
H	2.4470	-1.4640	-0.2200
O	1.7460	-0.4840	1.4820
H	2.5960	-0.6220	1.9280
C	2.9500	0.5810	-0.3790
H	3.0790	0.4820	-1.4720
H	3.9330	0.3600	0.0780
O	2.4950	1.8660	-0.0100
H	3.2030	2.4960	-0.2110

Coordinates for α-Galf 1E-gg-gt
Energy: -726.503045256 Hartrees

C	1.6680	-0.2790	-0.4070
C	1.6030	1.0780	0.3070
C	0.2560	1.6360	-0.1880
C	-0.5320	0.3620	-0.6370
H	1.9830	-0.1180	-1.4570
H	2.4320	1.7320	0.0150
H	-0.2490	2.1630	0.6350
H	-0.7380	0.4740	-1.7140
O	0.3190	-0.7530	-0.4000
O	2.5130	-1.1640	0.2260
C	2.6670	-2.4000	-0.4610
H	1.7310	-2.9690	-0.4710
H	3.4310	-2.9620	0.0810
H	3.0030	-2.2400	-1.4970
O	1.5640	0.8570	1.7120
H	1.7110	1.7150	2.1390
O	0.5070	2.5290	-1.2690
H	-0.3310	2.9510	-1.5130
C	-1.8510	0.1580	0.1280
H	-2.4140	1.1090	0.0540
O	-1.6340	-0.2050	1.4770
H	-1.0670	0.4580	1.9020
C	-2.7430	-0.9140	-0.4850
H	-2.3160	-1.8980	-0.2450
H	-2.7430	-0.7960	-1.5820
O	-4.0520	-0.7550	0.0450
H	-4.5750	-1.5240	-0.2250

Coordinates for α-Galf 1E-gg-tg
Energy: -726.504763318 Hartrees

C	-1.5120	0.3620	-0.4180
C	-1.5680	-1.1060	0.0280
C	-0.1680	-1.6080	-0.3880
C	0.6890	-0.3080	-0.4760
H	-1.6740	0.4120	-1.5130
H	-2.3430	-1.6580	-0.5200
H	0.2210	-2.2920	0.3750
H	1.0320	-0.1990	-1.5160
O	-0.1740	0.7770	-0.1380
O	-2.4280	1.1530	0.2430
C	-2.4730	2.4920	-0.2300
H	-1.5380	3.0230	-0.0200
H	-3.2960	2.9800	0.2970
H	-2.6670	2.5260	-1.3140
O	-1.7680	-1.1510	1.4270
H	-1.9920	-2.0650	1.6570
O	-0.2930	-2.2580	-1.6530
H	0.5630	-2.6590	-1.8710
C	1.9250	-0.2910	0.4210
H	2.6100	-1.0660	0.0330
O	1.5230	-0.5870	1.7510
H	2.3210	-0.6300	2.3000
C	2.6610	1.0500	0.3690
H	3.4670	1.0370	1.1250
H	1.9580	1.8500	0.6320
O	3.1920	1.2060	-0.9420
H	3.5960	2.0840	-1.0000

Coordinates for α-Galf 1E-gt-gg
Energy: -726.500405015 Hartrees

C	1.7200	0.0530	-0.4140
C	1.2760	1.3470	0.2770
C	-0.2390	1.3530	-0.0440
C	-0.5660	-0.1440	-0.3150
H	1.7800	0.2310	-1.5060
H	1.7850	2.2270	-0.1420
H	-0.7880	1.7500	0.8220
H	-0.9250	-0.2270	-1.3480
O	0.6600	-0.8590	-0.1500
O	2.9220	-0.4200	0.0710
C	3.3820	-1.5880	-0.5990
H	2.7100	-2.4360	-0.4280
H	4.3700	-1.8120	-0.1890
H	3.4720	-1.4150	-1.6830
O	1.5060	1.2150	1.6720
H	1.3930	2.0910	2.0710
O	-0.5580	2.0760	-1.2290
H	-0.3620	3.0120	-1.0700
C	-1.6010	-0.7590	0.6290
H	-1.2190	-0.6430	1.6570
O	-1.6990	-2.1310	0.2760
H	-2.3340	-2.5480	0.8800
C	-2.9660	-0.0670	0.5590
H	-2.8780	0.9730	0.9150
H	-3.6430	-0.5860	1.2620
O	-3.4580	-0.1280	-0.7690
H	-4.3710	0.1940	-0.7670

Coordinates for α-Galf 1E-gt-gt
Energy: -726.49979992 Hartrees

C	1.8200	0.0200	-0.3220
C	1.3470	1.3140	0.3520
C	-0.1060	1.4160	-0.1580
C	-0.4670	-0.0560	-0.5460
H	2.0520	0.2310	-1.3860
H	1.9330	2.1810	0.0230
H	-0.7450	1.7900	0.6540
H	-0.6670	-0.0660	-1.6340
O	0.6820	-0.8450	-0.2650
O	2.9040	-0.5420	0.3130
C	3.4070	-1.7050	-0.3330
H	2.6820	-2.5250	-0.2970
H	4.3120	-1.9920	0.2060
H	3.6630	-1.4960	-1.3840
O	1.3910	1.1340	1.7570
H	1.2690	2.0050	2.1640
O	-0.1300	2.3020	-1.2740
H	-1.0550	2.4410	-1.5310
C	-1.6680	-0.6530	0.2070
H	-1.5070	-0.5140	1.2810
O	-1.7620	-2.0550	0.0290
H	-1.9420	-2.2280	-0.9100
C	-2.9680	0.0510	-0.1950
H	-2.8390	1.1450	-0.1260
H	-3.1840	-0.1820	-1.2550
O	-4.0060	-0.3970	0.6570
H	-4.8030	0.1140	0.4520

Coordinates for α-Galf 1E-gt-tg
Energy: -726.504181775 Hartrees

C	1.7480	-0.1250	0.3230
C	1.0580	-1.4000	-0.1740
C	-0.3810	-1.1910	0.3520
C	-0.4880	0.3500	0.5270
H	1.9530	-0.2250	1.4070
H	1.5230	-2.3030	0.2490
H	-1.1080	-1.5750	-0.3700
H	-0.6690	0.5480	1.5950
O	0.7690	0.8940	0.1310
O	2.9070	0.1580	-0.3690
C	3.5970	1.3010	0.1220
H	3.0090	2.2130	-0.0240
H	4.5280	1.3680	-0.4450
H	3.8320	1.1940	1.1920
O	1.0900	-1.4000	-1.5930
H	0.8240	-2.2820	-1.8920
O	-0.5960	-1.7620	1.6450
H	-0.5310	-2.7260	1.5570
C	-1.5860	1.0380	-0.2810
H	-1.3590	0.9140	-1.3510
O	-1.5430	2.4110	0.1020
H	-2.2260	2.8810	-0.4020
C	-2.9940	0.4830	-0.0140
H	-3.7170	1.2490	-0.3400
H	-3.1410	0.3330	1.0670
O	-3.1890	-0.7250	-0.7440
H	-4.1370	-0.9240	-0.7460

Coordinates for α-Galf 1E-tg-gg
Energy: -726.507948243 Hartrees

C	1.6840	0.2600	-0.2320
C	0.9050	1.0290	0.8420
C	-0.4430	1.2790	0.1360
C	-0.4960	0.1660	-0.9550
H	2.0470	0.9730	-0.9970
H	1.3950	1.9760	1.1000
H	-1.2670	1.1810	0.8460
H	-0.5300	0.6700	-1.9330
O	0.7050	-0.5950	-0.8360
O	2.7300	-0.4750	0.2860
C	3.5390	-1.0930	-0.7060
H	2.9820	-1.8590	-1.2570
H	4.3750	-1.5590	-0.1790
H	3.9300	-0.3530	-1.4200
O	0.7550	0.1780	1.9700
H	0.4300	0.7270	2.6990
O	-0.4120	2.5830	-0.4450
H	-1.3000	2.7540	-0.7960
C	-1.6840	-0.7990	-0.8890
H	-1.5180	-1.5530	-1.6770
O	-2.8240	0.0030	-1.1780
H	-3.5990	-0.5760	-1.2370
C	-1.8050	-1.5700	0.4320
H	-0.8030	-1.9170	0.7160
H	-2.4410	-2.4570	0.2610
O	-2.3860	-0.7390	1.4340
H	-2.4410	-1.2680	2.2440

Coordinates for α-Galf 1E-tg-gt
Energy: -726.504524506 Hartrees

C	1.7460	0.0750	-0.2600
C	1.2040	0.9850	0.8500
C	-0.1170	1.4830	0.2290
C	-0.4590	0.3990	-0.8420
H	2.1890	0.7030	-1.0580
H	1.8780	1.8260	1.0530
H	-0.8780	1.5510	1.0210
H	-0.4520	0.9100	-1.8160
O	0.5830	-0.5740	-0.7870
O	2.6600	-0.8430	0.2070
C	3.2660	-1.6220	-0.8180
H	2.5350	-2.2740	-1.3080
H	4.0320	-2.2300	-0.3320
H	3.7400	-0.9810	-1.5770
O	0.9660	0.1960	2.0050
H	0.8030	0.8050	2.7420
O	0.1120	2.7610	-0.3560
H	-0.7430	3.1090	-0.6560
C	-1.8210	-0.2970	-0.6870
H	-1.9850	-0.9260	-1.5690
O	-2.8660	0.6730	-0.7420
H	-2.8060	1.2180	0.0600
C	-1.9190	-1.2110	0.5320
H	-1.8600	-0.6120	1.4580
H	-1.0540	-1.8860	0.5300
O	-3.1520	-1.9140	0.4490
H	-3.2090	-2.4930	1.2230

Coordinates for α-Galf 1E-tg-tg
Energy: -726.503366344 Hartrees

C	1.5970	0.2830	-0.3060
C	1.0010	1.1740	0.7940
C	-0.3910	1.5010	0.2020
C	-0.6430	0.3510	-0.8100
H	1.9430	0.9270	-1.1390
H	1.6060	2.0810	0.9410
H	-1.1520	1.5190	0.9910
H	-0.7160	0.8290	-1.8020
O	0.4950	-0.5010	-0.7640
O	2.6210	-0.5140	0.1560
C	3.2290	-1.3050	-0.8590
H	2.5270	-2.0430	-1.2610
H	4.0720	-1.8170	-0.3890
H	3.6020	-0.6760	-1.6830
O	0.9000	0.4150	1.9900
H	0.7040	1.0300	2.7120
O	-0.4100	2.7160	-0.5480
H	-0.2610	3.4510	0.0670
C	-1.9230	-0.4640	-0.5600
H	-2.0810	-1.1420	-1.4110
O	-3.0270	0.4340	-0.4150
H	-3.0610	0.9970	-1.2050
C	-1.8840	-1.3430	0.6940
H	-1.1710	-0.9480	1.4290
H	-2.8930	-1.3230	1.1320
O	-1.5220	-2.6580	0.2830
H	-1.4970	-3.2140	1.0760

Coordinates for α-Galf E1-gg-gg
Energy: -726.502062134 Hartrees

C	-0.9080	1.0710	-0.7190
C	-2.0150	0.0880	-0.3290
C	-1.2490	-1.1460	0.1770
C	0.1580	-0.9900	-0.4600
H	-1.1730	1.7310	-1.5580
H	-2.5070	-0.2220	-1.2650
H	-1.1850	-1.0920	1.2710
H	0.2880	-1.8010	-1.1910
O	0.1170	0.2200	-1.2280
O	-0.5440	1.8160	0.3940
C	0.5220	2.7250	0.1530
H	1.4560	2.1940	-0.0520
H	0.6260	3.3240	1.0620
H	0.2860	3.3940	-0.6910
O	-2.9460	0.6410	0.5750
H	-3.6620	-0.0080	0.6640
O	-1.9570	-2.3140	-0.2360
H	-1.5370	-3.0830	0.1800
C	1.3330	-1.1260	0.5220
H	1.2550	-2.1700	0.8910
O	1.1810	-0.2120	1.5920
H	1.8530	-0.4170	2.2600
C	2.7190	-1.0380	-0.1320
H	2.7560	-1.7550	-0.9700
H	3.4610	-1.3770	0.6140
O	2.9990	0.2830	-0.5530
H	3.9240	0.3120	-0.8380

Coordinates for α-Galf E1-gg-gt
Energy: -726.509711315 Hartrees

C	1.3870	0.7600	0.7210
C	2.0530	-0.5120	0.1920
C	0.8630	-1.3710	-0.2650
C	-0.3410	-0.7930	0.5230
H	1.9460	1.2580	1.5240
H	2.4910	-1.0280	1.0610
H	0.7310	-1.2280	-1.3490
H	-0.6660	-1.5680	1.2290
O	0.1890	0.2810	1.3250
O	1.1870	1.6400	-0.3460
C	0.6430	2.8970	0.0450
H	-0.3740	2.7840	0.4290
H	0.6290	3.5220	-0.8510
H	1.2800	3.3740	0.8060
O	3.0260	-0.2480	-0.7920
H	3.4620	-1.0930	-0.9860
O	1.1530	-2.7350	0.0160
H	0.4550	-3.2820	-0.3750
C	-1.5670	-0.3930	-0.3270
H	-1.7470	-1.2360	-1.0220
O	-1.4120	0.8170	-1.0390
H	-0.6110	0.7690	-1.5840
C	-2.8350	-0.2520	0.5070
H	-2.7630	0.6740	1.0950
H	-2.8980	-1.1000	1.2100
O	-3.9460	-0.2380	-0.3770
H	-4.7300	0.0030	0.1370

Coordinates for α-Galf E1-gg-tg
Energy: -726.509591373 Hartrees

C	-1.2790	0.6640	-0.8270
C	-1.8860	-0.6590	-0.3500
C	-0.7060	-1.4000	0.3050
C	0.5440	-0.7100	-0.2920
H	-1.7330	1.0510	-1.7510
H	-2.1380	-1.2350	-1.2540
H	-0.7550	-1.2410	1.3900
H	1.0720	-1.4320	-0.9260
O	0.0540	0.3090	-1.1870
O	-1.3800	1.6070	0.1900
C	-0.8460	2.8760	-0.1410
H	0.2450	2.8410	-0.2360
H	-1.1150	3.5510	0.6750
H	-1.2760	3.2580	-1.0810
O	-3.0200	-0.4750	0.4670
H	-3.4020	-1.3550	0.6110
O	-0.8200	-2.7850	-0.0110
H	-0.1460	-3.2660	0.4930
C	1.5830	-0.2060	0.7120
H	1.9470	-1.1010	1.2490
O	0.9880	0.7130	1.6150
H	1.6570	0.9570	2.2730
C	2.7890	0.4260	0.0120
H	3.4370	0.8910	0.7760
H	2.4360	1.2170	-0.6630
O	3.4770	-0.6050	-0.6850
H	4.1990	-0.2000	-1.1880

Coordinates for α-Galf E1-gt-gg
Energy: -726.505310739 Hartrees

C	1.7150	0.3450	0.5950
C	1.6630	-1.1420	0.2370
C	0.1750	-1.3450	-0.1340
C	-0.5410	-0.1820	0.5860
H	2.5100	0.6090	1.3050
H	1.8410	-1.7010	1.1700
H	0.0910	-1.2460	-1.2270
H	-1.2090	-0.5730	1.3570
O	0.4930	0.5550	1.2690
O	1.8420	1.0980	-0.5820
C	1.8730	2.5010	-0.3410
H	0.9270	2.8500	0.0880
H	2.0460	2.9790	-1.3080
H	2.6970	2.7640	0.3410
O	2.6050	-1.4880	-0.7590
H	2.6010	-2.4530	-0.8520
O	-0.3850	-2.5820	0.2950
H	0.0780	-3.2970	-0.1690
C	-1.3540	0.7090	-0.3680
H	-0.7190	0.9690	-1.2300
O	-1.7170	1.8760	0.3570
H	-2.2290	2.4450	-0.2380
C	-2.5840	-0.0300	-0.9070
H	-2.2600	-0.9120	-1.4850
H	-3.1060	0.6420	-1.6120
O	-3.4240	-0.3910	0.1760
H	-4.2530	-0.7370	-0.1880

Coordinates for α-Galf E1-gt-gt
Energy: -726.508445539 Hartrees

C	1.7020	0.6270	0.4490
C	1.9180	-0.8420	0.0800
C	0.4800	-1.3700	-0.0620
C	-0.3520	-0.3800	0.7980
H	2.5230	1.0740	1.0250
H	2.3470	-1.3340	0.9670
H	0.1920	-1.3070	-1.1210
H	-0.7650	-0.9110	1.6680
O	0.5900	0.5690	1.3300
O	1.4530	1.3610	-0.7130
C	1.2330	2.7490	-0.4690
H	0.3200	2.9060	0.1160
H	1.1340	3.2230	-1.4480
H	2.0890	3.1920	0.0620
O	2.7410	-1.0100	-1.0510
H	2.8950	-1.9640	-1.1440
O	0.4560	-2.7240	0.3820
H	-0.4190	-3.0940	0.1870
C	-1.4960	0.3160	0.0260
H	-1.1260	0.6420	-0.9500
O	-1.9300	1.5050	0.6650
H	-2.3060	1.2690	1.5280
C	-2.6510	-0.6650	-0.1880
H	-2.2570	-1.6140	-0.5960
H	-3.1030	-0.9020	0.7940
O	-3.5930	-0.0810	-1.0670
H	-4.2740	-0.7420	-1.2610

Coordinates for α-Galf E1-gt-tg
Energy: -726.507638049 Hartrees

C	1.7460	-0.3270	-0.4390
C	1.5420	1.1780	-0.2440
C	0.0030	1.3050	-0.1590
C	-0.5080	0.0290	-0.8590
H	2.6620	-0.5880	-0.9860
H	1.8560	1.6660	-1.1810
H	-0.2890	1.3210	0.8970
H	-1.0400	0.3030	-1.7760
O	0.6670	-0.6980	-1.2720
O	1.7270	-0.9620	0.8110
C	1.9230	-2.3680	0.7220
H	1.1140	-2.8490	0.1600
H	1.9390	-2.7460	1.7470
H	2.8830	-2.6030	0.2370
O	2.2700	1.6710	0.8630
H	2.1930	2.6370	0.8630
O	-0.5340	2.4390	-0.8400
H	-0.2090	3.2350	-0.3920
C	-1.4370	-0.8440	-0.0070
H	-0.9210	-1.1200	0.9230
O	-1.7260	-1.9940	-0.8000
H	-2.3250	-2.5610	-0.2880
C	-2.7510	-0.1370	0.3640
H	-3.4720	-0.9160	0.6630
H	-3.1660	0.3720	-0.5200
O	-2.5220	0.7710	1.4360
H	-3.3820	1.0260	1.8020

Coordinates for α-Galf E1-tg-gg
Energy: -726.503932503 Hartrees

C	1.5570	0.1760	-0.6470
C	1.1000	1.4320	0.1120
C	-0.4480	1.3500	0.1220
C	-0.7740	0.3120	-0.9680
H	2.4280	0.3630	-1.2900
H	1.3560	2.2930	-0.5260
H	-0.7870	1.0120	1.1050
H	-1.3060	0.8340	-1.7700
O	0.4850	-0.1300	-1.5200
O	1.8620	-0.8560	0.2510
C	2.5470	-1.9400	-0.3580
H	1.9330	-2.4320	-1.1240
H	2.7800	-2.6540	0.4360
H	3.4870	-1.6030	-0.8230
O	1.7330	1.5260	1.3730
H	1.5150	2.3930	1.7460
O	-1.0730	2.5820	-0.2430
H	-0.8710	3.2320	0.4470
C	-1.6670	-0.8830	-0.5840
H	-1.7050	-1.5210	-1.4840
O	-2.9400	-0.3120	-0.3080
H	-3.5650	-1.0350	-0.1480
C	-1.1820	-1.7900	0.5480
H	-0.1770	-2.1520	0.3060
H	-1.8570	-2.6660	0.5800
O	-1.2090	-1.0970	1.7870
H	-0.8950	-1.7040	2.4730

Coordinates for α-Galf E1-tg-gt
Energy: -726.50723846 Hartrees

C	1.5130	0.6740	0.5760
C	1.8670	-0.6340	-0.1430
C	0.5430	-1.4120	-0.1810
C	-0.3240	-0.7430	0.9090
H	2.3340	1.0610	1.1940
H	2.5300	-1.1960	0.5340
H	0.1100	-1.2710	-1.1840
H	-0.4610	-1.4820	1.7060
O	0.4800	0.3110	1.4820
O	1.1260	1.6400	-0.3590
C	1.0800	2.9570	0.1720
H	0.3460	3.0440	0.9840
H	0.7940	3.6190	-0.6490
H	2.0660	3.2630	0.5510
O	2.4830	-0.4110	-1.3910
H	2.7810	-1.2770	-1.7120
O	0.8060	-2.7900	0.0510
H	-0.0280	-3.2700	-0.0740
C	-1.7510	-0.3320	0.4830
H	-2.3170	-0.0950	1.3900
O	-2.3970	-1.4940	-0.0460
H	-2.0410	-1.6450	-0.9360
C	-1.8880	0.8720	-0.4430
H	-1.3490	0.6970	-1.3900
H	-1.4190	1.7390	0.0380
O	-3.2770	1.0780	-0.6670
H	-3.3650	1.8430	-1.2550

Coordinates for α-Galf E1-tg-tg
Energy: -726.509599367 Hartrees

C	-0.4870	-1.4310	0.6290
C	-1.7330	-0.8170	-0.0260
C	-1.3910	0.6750	-0.1570
C	-0.2300	0.8840	0.8410
H	-0.7210	-2.2600	1.3110
H	-2.5440	-0.8850	0.7160
H	-1.0540	0.8580	-1.1860
H	-0.6000	1.5350	1.6420
O	0.0250	-0.3890	1.4520
O	0.4030	-1.8660	-0.3560
C	1.4810	-2.6350	0.1650
H	2.1130	-2.0360	0.8260
H	2.0670	-2.9720	-0.6950
H	1.1050	-3.5180	0.7040
O	-2.0850	-1.4700	-1.2260
H	-2.9380	-1.0990	-1.5000
O	-2.5440	1.4580	0.1210
H	-2.3080	2.3760	-0.0870
C	1.0000	1.6070	0.2630
H	1.7050	1.8040	1.0840
O	0.4260	2.8320	-0.2200
H	1.1480	3.4090	-0.5110
C	1.8000	0.9060	-0.8440
H	1.1630	0.2490	-1.4490
H	2.2050	1.6910	-1.5070
O	2.8580	0.1810	-0.2270
H	3.3610	-0.2590	-0.9290

Coordinates for α-Galf 2E-gg-gg
Energy: -726.505955697 Hartrees

C	-1.1110	0.9850	-0.7070
C	-1.9690	-0.2680	-0.5230
C	-0.9970	-1.1700	0.2380
C	0.3340	-0.8510	-0.4770
H	-1.3980	1.6210	-1.5560
H	-2.1310	-0.7150	-1.5180
H	-0.9610	-0.8510	1.2850
H	0.4530	-1.5580	-1.3120
O	0.1790	0.4680	-1.0200
O	-1.1290	1.7160	0.4820
C	-0.2290	2.8180	0.4810
H	0.8090	2.4780	0.4170
H	-0.3910	3.3470	1.4230
H	-0.4420	3.5010	-0.3560
O	-3.1900	-0.0110	0.1290
H	-3.6570	-0.8600	0.1760
O	-1.4230	-2.5250	0.1190
H	-0.8540	-3.0710	0.6820
C	1.5780	-0.9790	0.4110
H	1.6090	-2.0470	0.7100
O	1.4070	-0.1450	1.5440
H	2.1330	-0.3190	2.1620
C	2.9080	-0.7210	-0.3090
H	2.9500	-1.3650	-1.2040
H	3.7220	-1.0540	0.3620
O	3.0470	0.6490	-0.6280
H	3.9470	0.7830	-0.9630

Coordinates for α-Galf 2E-gg-gt
Energy: -726.512297085 Hartrees

C	1.4490	0.7390	0.7400
C	1.9710	-0.6640	0.4210
C	0.7650	-1.2560	-0.3100
C	-0.4040	-0.6870	0.5200
H	1.9410	1.2350	1.5870
H	2.0810	-1.2080	1.3730
H	0.7690	-0.8710	-1.3400
H	-0.6320	-1.4130	1.3130
O	0.0950	0.5220	1.1240
O	1.5560	1.5190	-0.4160
C	1.0380	2.8360	-0.2650
H	-0.0490	2.8180	-0.1400
H	1.2970	3.3770	-1.1780
H	1.5000	3.3450	0.5950
O	3.1750	-0.6490	-0.3080
H	3.4250	-1.5770	-0.4410
O	0.8590	-2.6730	-0.3040
H	0.1410	-3.0320	-0.8490
C	-1.6850	-0.3920	-0.2790
H	-1.9680	-1.3250	-0.8030
O	-1.5210	0.6750	-1.1990
H	-0.7810	0.4730	-1.7910
C	-2.8540	-0.0230	0.6250
H	-2.6810	0.9890	1.0160
H	-2.8790	-0.7210	1.4780
O	-4.0490	-0.1050	-0.1390
H	-4.7660	0.2740	0.3920

Coordinates for α-Galf 2E-gg-tg
Energy: -726.514311122 Hartrees

C	-1.3590	0.6230	-0.8300
C	-1.7610	-0.8210	-0.5250
C	-0.6180	-1.2520	0.3950
C	0.5900	-0.5830	-0.2880
H	-1.7650	1.0270	-1.7680
H	-1.6710	-1.3990	-1.4590
H	-0.7880	-0.8330	1.3930
H	1.0200	-1.2830	-1.0150
O	0.0540	0.5470	-1.0110
O	-1.7350	1.4250	0.2480
C	-1.3180	2.7760	0.1340
H	-0.2290	2.8610	0.2140
H	-1.7890	3.3170	0.9580
H	-1.6480	3.2160	-0.8210
O	-3.0530	-0.9280	0.0240
H	-3.2120	-1.8770	0.1570
O	-0.5640	-2.6750	0.4300
H	0.1000	-2.9380	1.0860
C	1.7170	-0.1410	0.6430
H	2.1110	-1.0510	1.1290
O	1.1840	0.7610	1.6050
H	1.8940	0.9930	2.2220
C	2.8730	0.5120	-0.1210
H	3.5870	0.9320	0.6100
H	2.4760	1.3390	-0.7250
O	3.4880	-0.4930	-0.9180
H	4.1730	-0.0720	-1.4580

Coordinates for α-Galf 2E-gt-gg
Energy: -726.506589436 Hartrees

C	1.7760	-0.2920	-0.6110
C	1.4750	1.1980	-0.4620
C	0.0960	1.1440	0.2110
C	-0.5650	-0.0290	-0.5290
H	2.4930	-0.5360	-1.4070
H	1.3380	1.6130	-1.4730
H	0.2500	0.8970	1.2710
H	-1.1130	0.3440	-1.4010
O	0.5310	-0.8520	-0.9950
O	2.2330	-0.7830	0.6210
C	2.5740	-2.1620	0.5810
H	1.7060	-2.7830	0.3320
H	2.9410	-2.4230	1.5770
H	3.3700	-2.3520	-0.1550
O	2.4830	1.8940	0.2420
H	2.2570	2.8370	0.2170
O	-0.6830	2.3270	0.0790
H	-0.2420	3.0220	0.5920
C	-1.5130	-0.8690	0.3300
H	-0.9390	-1.2310	1.2010
O	-1.9440	-1.9530	-0.4780
H	-2.4890	-2.5360	0.0720
C	-2.6950	-0.0490	0.8580
H	-2.3210	0.7680	1.4950
H	-3.3090	-0.7100	1.4970
O	-3.4430	0.4430	-0.2410
H	-4.2540	0.8430	0.1030

Coordinates for α-Galf 2E-gt-gt
Energy: -726.508592761 Hartrees

C	-1.8120	-0.4900	0.5000
C	-1.7540	1.0300	0.3530
C	-0.3130	1.2250	-0.1220
C	0.4350	0.1710	0.7240
H	-2.5730	-0.8530	1.2040
H	-1.8290	1.4680	1.3620
H	-0.2620	0.9840	-1.1930
H	0.7650	0.6500	1.6600
O	-0.5470	-0.8300	1.0580
O	-2.0040	-1.0550	-0.7640
C	-2.1040	-2.4730	-0.7400
H	-1.1780	-2.9340	-0.3740
H	-2.2920	-2.7910	-1.7670
H	-2.9410	-2.7990	-0.1030
O	-2.7460	1.5390	-0.5040
H	-2.6360	2.5030	-0.5070
O	0.0620	2.5760	0.1220
H	0.9390	2.7300	-0.2620
C	1.6360	-0.5100	0.0480
H	1.2870	-0.9910	-0.8720
O	2.1460	-1.5680	0.8410
H	2.5110	-1.1860	1.6560
C	2.7310	0.4980	-0.3150
H	2.3040	1.2880	-0.9590
H	3.0970	0.9890	0.6060
O	3.7710	-0.1900	-0.9840
H	4.4190	0.4650	-1.2850

Coordinates for α-Galf 2E-gt-tg
Energy: -726.459204093 Hartrees

C	1.8060	-0.2410	-0.4940
C	1.4130	1.2140	-0.4970
C	-0.0220	1.1150	-0.0410
C	-0.4740	-0.1490	-0.7560
C	2.6080	-1.9910	0.8600
C	-1.4930	-0.9910	0.0200
C	-2.8230	-0.3320	0.3810
H	2.7040	-0.4440	-1.1180
H	1.4920	1.6460	-1.5210
H	-0.0950	1.0270	1.0670
H	-0.8960	0.1080	-1.7580
H	2.0170	-2.7410	0.2910
H	2.6650	-2.3140	1.9230
H	3.6430	-1.9180	0.4560
H	1.8620	2.9050	0.3280
H	-1.0250	3.2230	-0.4080
H	-1.0470	-1.3950	0.9560
H	-2.4290	-2.6870	-0.2750
H	-3.4780	-1.0390	0.9410
H	-3.3630	-0.0100	-0.5380
H	-3.5310	1.0490	1.5690
O	0.6770	-0.9220	-0.9990
O	1.9800	-0.7270	0.8220
O	2.1830	2.0020	0.3720
O	-0.8730	2.2890	-0.4490
O	-1.8620	-2.0980	-0.7790
O	-2.6810	0.8130	1.1890

Coordinates for α-Galf 2E-tg-gg
Energy: -726.50616917 Hartrees

C	1.6410	-0.1430	-0.6660
C	1.3910	1.2690	-0.1380
C	-0.1120	1.2330	0.1800
C	-0.6520	0.3550	-0.9580
H	2.4870	-0.2150	-1.3630
H	1.5300	1.9620	-0.9830
H	-0.2640	0.7540	1.1520
H	-0.9640	1.0140	-1.7780
O	0.4690	-0.4430	-1.4110
O	1.8370	-1.0220	0.4090
C	2.2970	-2.3050	0.0120
H	1.5630	-2.8230	-0.6190
H	2.4600	-2.8790	0.9270
H	3.2470	-2.2320	-0.5390
O	2.2530	1.5980	0.9340
H	2.0830	2.5240	1.1680
O	-0.7390	2.5100	0.1380
H	-0.4020	3.0260	0.8860
C	-1.8320	-0.5880	-0.6730
H	-1.9030	-1.2360	-1.5640
O	-2.9780	0.2400	-0.5500
H	-3.7490	-0.3320	-0.4170
C	-1.6560	-1.5330	0.5210
H	-0.6680	-2.0080	0.4460
H	-2.4180	-2.3290	0.4410
O	-1.8130	-0.8210	1.7430
H	-1.6930	-1.4560	2.4660

Coordinates for α-Galf 2E-tg-gt
Energy: -726.509039142 Hartrees

C	1.6350	0.5120	0.6510
C	1.8040	-0.9140	0.1190
C	0.3610	-1.2370	-0.2920
C	-0.4380	-0.5940	0.8510
H	2.4090	0.8160	1.3670
H	2.0640	-1.5580	0.9750
H	0.1770	-0.7330	-1.2510
H	-0.5610	-1.3490	1.6390
O	0.4100	0.4580	1.3680
O	1.5990	1.4060	-0.4260
C	1.6190	2.7710	-0.0270
H	0.7340	3.0300	0.5660
H	1.6340	3.3660	-0.9430
H	2.5220	2.9950	0.5620
O	2.7790	-1.0000	-0.8990
H	2.8750	-1.9360	-1.1360
O	0.0290	-2.6180	-0.3900
H	0.5200	-2.9900	-1.1390
C	-1.8540	-0.0810	0.5290
H	-2.1840	0.5270	1.3780
O	-2.7460	-1.1880	0.4820
H	-2.5250	-1.7130	-0.3050
C	-1.9270	0.7920	-0.7210
H	-1.8480	0.1530	-1.6180
H	-1.0680	1.4790	-0.7300
O	-3.1640	1.4900	-0.7000
H	-3.2040	2.0430	-1.4950

Coordinates for α-Galf 2E-tg-tg
Energy: -726.504388378 Hartrees

C	1.3040	0.8230	0.6580
C	1.8900	-0.5150	0.2130
C	0.6330	-1.2840	-0.2300
C	-0.4020	-0.8010	0.7970
H	1.9010	1.3480	1.4160
H	2.2750	-1.0210	1.1130
H	0.3690	-0.9700	-1.2490
H	-0.4090	-1.5180	1.6280
O	0.0770	0.4700	1.2810
O	1.1280	1.6430	-0.4630
C	0.6510	2.9450	-0.1390
H	-0.3660	2.9020	0.2650
H	0.6610	3.5200	-1.0680
H	1.3140	3.4360	0.5900
O	2.9060	-0.3640	-0.7580
H	3.2830	-1.2420	-0.9240
O	0.7690	-2.6960	-0.1570
H	1.4080	-2.9660	-0.8340
C	-1.8490	-0.6420	0.3040
H	-2.4610	-0.3420	1.1690
O	-2.2250	-1.9330	-0.1670
H	-3.1590	-1.8910	-0.4270
C	-2.0650	0.4440	-0.7680
H	-1.1420	0.6520	-1.3230
H	-2.8100	0.0630	-1.4870
O	-2.5480	1.6200	-0.1210
H	-2.6800	2.2970	-0.8020

Coordinates for α-Galf E2-gg-gg
Energy: -726.492651815 Hartrees

C	-1.4190	0.5390	-0.4620
C	-1.7100	-0.7690	0.3040
C	-0.5820	-1.7050	-0.1820
C	0.5510	-0.7510	-0.6470
H	-1.9760	0.5470	-1.4170
H	-2.6760	-1.1850	-0.0110
H	-0.2560	-2.3570	0.6390
H	0.8870	-1.0930	-1.6400
O	-0.0280	0.5360	-0.7860
O	-1.7600	1.6480	0.2910
C	-1.5000	2.8790	-0.3690
H	-0.4250	3.0270	-0.5170
H	-1.8960	3.6660	0.2770
H	-2.0090	2.9240	-1.3460
O	-1.6750	-0.5300	1.6950
H	-2.0480	-1.3120	2.1280
O	-1.1120	-2.4670	-1.2690
H	-0.4630	-3.1470	-1.5020
C	1.7940	-0.7490	0.2550
H	2.1770	-1.7890	0.2120
O	1.3950	-0.4100	1.5680
H	2.1550	-0.5300	2.1570
C	2.9490	0.1210	-0.2580
H	3.1900	-0.1970	-1.2890
H	3.8360	-0.1100	0.3600
O	2.6280	1.4950	-0.1860
H	3.4310	1.9930	-0.3990

Coordinates for α-Galf E2-gg-gt
Energy: -726.506072462 Hartrees

C	1.6880	-0.1730	-0.3690
C	1.4730	0.9880	0.6150
C	0.2940	1.7170	-0.0370
C	-0.5260	0.5610	-0.6760
H	2.2840	0.1840	-1.2280
H	2.3570	1.6310	0.6770
H	-0.2900	2.2780	0.7070
H	-0.8750	0.9000	-1.6630
O	0.3840	-0.5260	-0.8390
O	2.3140	-1.2410	0.2430
C	2.6020	-2.3170	-0.6410
H	1.6820	-2.7890	-1.0040
H	3.1840	-3.0430	-0.0680
H	3.1960	-1.9760	-1.5030
O	1.1140	0.4810	1.9010
H	1.1330	1.2280	2.5180
O	0.8450	2.5930	-1.0170
H	0.1320	3.1570	-1.3540
C	-1.7440	0.1050	0.1710
H	-2.2370	1.0230	0.5470
O	-1.3780	-0.7530	1.2260
H	-0.7010	-0.3100	1.7680
C	-2.8020	-0.6210	-0.6520
H	-2.4270	-1.6280	-0.8880
H	-2.9560	-0.0800	-1.6020
O	-4.0010	-0.6640	0.1080
H	-4.6190	-1.2530	-0.3500

Coordinates for α-Galf E2-gg-tg
Energy: -726.502781585 Hartrees

C	-1.5000	0.3320	-0.5090
C	-1.5580	-1.0610	0.1490
C	-0.2070	-1.6800	-0.2720
C	0.7260	-0.4660	-0.5000
H	-1.9160	0.2750	-1.5310
H	-2.3730	-1.6520	-0.2870
H	0.1690	-2.3430	0.5180
H	1.2580	-0.6080	-1.4510
O	-0.1180	0.6800	-0.6300
O	-2.1970	1.2720	0.2290
C	-2.2900	2.5380	-0.4060
H	-1.3080	3.0180	-0.4900
H	-2.9440	3.1530	0.2170
H	-2.7290	2.4490	-1.4130
O	-1.7030	-0.9210	1.5460
H	-1.9210	-1.7960	1.9010
O	-0.4450	-2.3990	-1.4830
H	0.3570	-2.9000	-1.6970
C	1.8040	-0.2510	0.5660
H	2.4990	-1.1060	0.4860
O	1.1950	-0.2070	1.8460
H	1.8990	-0.1230	2.5080
C	2.6050	1.0280	0.3100
H	3.2830	1.1940	1.1660
H	1.9070	1.8730	0.2570
O	3.3390	0.8540	-0.8970
H	3.7890	1.6870	-1.0970

Coordinates for α-Galf E2-gt-gg
Energy: -726.504876794 Hartrees

C	-1.7420	-0.2410	-0.3210
C	-1.0190	-1.3100	0.5060
C	0.3650	-1.3130	-0.1540
C	0.5630	0.1710	-0.5540
H	-2.1000	-0.6880	-1.2660
H	-1.5100	-2.2870	0.4230
H	1.1240	-1.6720	0.5510
H	1.0280	0.2140	-1.5450
O	-0.7500	0.7390	-0.6330
O	-2.8010	0.3180	0.3750
C	-3.5430	1.2600	-0.3870
H	-2.9400	2.1440	-0.6250
H	-4.3980	1.5530	0.2270
H	-3.9090	0.8140	-1.3250
O	-0.9280	-0.8700	1.8550
H	-0.5910	-1.6150	2.3760
O	0.3090	-2.1600	-1.2970
H	1.2170	-2.2520	-1.6250
C	1.4200	1.0230	0.3910
H	0.8470	1.1870	1.3150
O	1.6330	2.2530	-0.2980
H	2.1300	2.8420	0.2900
C	2.7430	0.3510	0.7740
H	2.5620	-0.3780	1.5800
H	3.4220	1.1190	1.1810
O	3.3100	-0.2840	-0.3700
H	4.2010	-0.5850	-0.1370

Coordinates for α-Galf E2-gt-gt
Energy: -726.499856779 Hartrees

C	1.8280	0.1150	-0.2130
C	1.1940	1.2020	0.6650
C	-0.0730	1.5280	-0.1420
C	-0.4650	0.1470	-0.7360
H	2.3650	0.5860	-1.0560
H	1.8440	2.0810	0.7500
H	-0.8510	1.9430	0.5130
H	-0.7920	0.2920	-1.7800
O	0.7290	-0.6340	-0.7420
O	2.6830	-0.6910	0.5140
C	3.3350	-1.6810	-0.2700
H	2.6210	-2.4190	-0.6520
H	4.0540	-2.1740	0.3890
H	3.8730	-1.2290	-1.1180
O	0.8700	0.6480	1.9290
H	0.5990	1.3780	2.5060
O	0.3010	2.4650	-1.1490
H	-0.5040	2.7810	-1.5860
C	-1.5660	-0.6120	0.0390
H	-1.3050	-0.6150	1.1010
O	-1.6140	-1.9780	-0.3350
H	-1.8750	-2.0250	-1.2700
C	-2.9320	0.0560	-0.1420
H	-2.8600	1.1350	0.0770
H	-3.2340	-0.0360	-1.2030
O	-3.8630	-0.5780	0.7170
H	-4.7010	-0.0950	0.6580

Coordinates for α-Galf E2-gt-tg
Energy: -726.505076193 Hartrees

C	-1.7370	-0.2630	-0.2320
C	-0.8850	-1.3340	0.4590
C	0.3840	-1.2900	-0.4030
C	0.5050	0.2160	-0.7520
H	-2.2000	-0.6860	-1.1410
H	-1.3620	-2.3200	0.4190
H	1.2560	-1.6670	0.1390
H	0.8340	0.3280	-1.7960
O	-0.8130	0.7570	-0.6250
O	-2.7110	0.2430	0.6120
C	-3.5660	1.1900	-0.0130
H	-3.0200	2.1000	-0.2860
H	-4.3450	1.4330	0.7120
H	-4.0330	0.7700	-0.9180
O	-0.6160	-0.9190	1.7890
H	-0.1900	-1.6620	2.2420
O	0.1170	-2.0770	-1.5670
H	0.9460	-2.1680	-2.0610
C	1.4550	1.0340	0.1340
H	1.0980	0.9690	1.1710
O	1.3800	2.3700	-0.3630
H	1.9330	2.9290	0.2050
C	2.9240	0.5900	0.0820
H	3.5270	1.3960	0.5320
H	3.2450	0.4960	-0.9690
O	3.1130	-0.6280	0.7990
H	4.0630	-0.7490	0.9390

Coordinates for α-Galf E2-tg-gg
Energy: -726.506270227 Hartrees

C	1.6700	0.3410	-0.1310
C	0.8120	0.8100	1.0580
C	-0.4530	1.3350	0.3500
C	-0.5440	0.4820	-0.9370
H	2.2550	1.1900	-0.5250
H	1.3070	1.6240	1.6000
H	-1.3400	1.2180	0.9800
H	-0.7790	1.1590	-1.7700
O	0.7560	-0.0720	-1.1530
O	2.5170	-0.6950	0.2270
C	3.4230	-1.0670	-0.8030
H	2.8960	-1.4910	-1.6660
H	4.0890	-1.8210	-0.3750
H	4.0210	-0.2060	-1.1390
O	0.5570	-0.3010	1.9000
H	0.1630	0.0440	2.7150
O	-0.2050	2.7090	0.0430
H	-1.0350	3.0870	-0.2850
C	-1.6030	-0.6320	-1.0020
H	-1.3570	-1.2130	-1.9050
O	-2.8430	0.0530	-1.1530
H	-3.5350	-0.6050	-1.3180
C	-1.6180	-1.6230	0.1640
H	-0.5850	-1.9190	0.3850
H	-2.1740	-2.5230	-0.1550
O	-2.2580	-1.0340	1.2940
H	-2.2410	-1.6960	2.0010

Coordinates for α-Galf E2-tg-gt
Energy: -726.504132225 Hartrees

C	1.7190	0.0960	-0.2170
C	1.1180	0.9010	0.9500
C	-0.0740	1.6010	0.2740
C	-0.4920	0.6290	-0.8590
H	2.4240	0.7330	-0.7790
H	1.8330	1.6440	1.3210
H	-0.8770	1.7740	1.0070
H	-0.6650	1.2360	-1.7590
O	0.6300	-0.2270	-1.0870
O	2.3570	-1.0460	0.2320
C	3.0460	-1.7530	-0.7930
H	2.3490	-2.1590	-1.5350
H	3.5760	-2.5720	-0.3020
H	3.7740	-1.1040	-1.3020
O	0.7070	0.0140	1.9770
H	0.4920	0.5520	2.7540
O	0.4100	2.8370	-0.2430
H	-0.3500	3.3500	-0.5590
C	-1.7750	-0.2060	-0.6620
H	-1.9170	-0.7820	-1.5830
O	-2.9070	0.6600	-0.6010
H	-2.8660	1.1400	0.2410
C	-1.7410	-1.2210	0.4760
H	-1.7980	-0.7010	1.4470
H	-0.7810	-1.7520	0.4500
O	-2.8450	-2.0990	0.2940
H	-2.8230	-2.7450	1.0160

Coordinates for α-Galf E2-tg-tg
Energy: -726.50365973 Hartrees

C	-1.4510	-0.6370	-0.3480
C	-0.6600	-1.4080	0.7310
C	0.7610	-1.4840	0.1430
C	0.8320	-0.3140	-0.8710
H	-1.9330	-1.3470	-1.0450
H	-1.0630	-2.4200	0.8530
H	1.5110	-1.3770	0.9350
H	1.2430	-0.7160	-1.8070
O	-0.5030	0.1200	-1.1010
O	-2.4070	0.1820	0.2300
C	-3.1420	0.9490	-0.7150
H	-2.5040	1.7020	-1.1890
H	-3.9430	1.4410	-0.1570
H	-3.5860	0.3080	-1.4920
O	-0.6990	-0.6920	1.9580
H	-0.3680	-1.2920	2.6450
O	0.8880	-2.7490	-0.5070
H	1.8180	-2.8490	-0.7630
C	1.7160	0.8770	-0.4630
H	1.7820	1.5560	-1.3270
O	2.9910	0.2920	-0.1780
H	3.6160	1.0130	-0.0050
C	1.1990	1.7220	0.7110
H	0.6620	1.1040	1.4410
H	2.0820	2.1560	1.2160
O	0.3680	2.7480	0.1780
H	0.0450	3.2770	0.9220

Coordinates for α-Galf 3E-gg-gg
Energy: -726.492772131 Hartrees

C	-1.1550	0.9030	-0.5800
C	-1.9030	-0.2290	0.1730
C	-1.0530	-1.4920	-0.0930
C	0.3080	-0.9670	-0.6110
H	-1.6860	1.1850	-1.5060
H	-2.8850	-0.3880	-0.2930
H	-0.9390	-2.0630	0.8380
H	0.5840	-1.5350	-1.5130
O	0.1070	0.3830	-0.9930
O	-1.0170	2.0160	0.2350
C	-0.2730	3.0650	-0.3690
H	0.7710	2.7690	-0.5170
H	-0.3260	3.9140	0.3170
H	-0.7080	3.3580	-1.3380
O	-2.0380	0.0920	1.5420
H	-2.6490	-0.5590	1.9210
O	-1.7430	-2.2580	-1.0830
H	-1.2630	-3.0910	-1.2060
C	1.4570	-1.1370	0.3960
H	1.5580	-2.2320	0.5390
O	1.0760	-0.4990	1.5990
H	1.7370	-0.7010	2.2780
C	2.8280	-0.6720	-0.1130
H	3.0310	-1.1770	-1.0740
H	3.5880	-1.0360	0.6030
O	2.8830	0.7360	-0.2290
H	3.8010	0.9760	-0.4280

Coordinates for α-Galf 3E-gg-gt
Energy: -726.507013724 Hartrees

C	1.6260	-0.3140	-0.4220
C	1.5900	0.8300	0.6220
C	0.5080	1.7570	0.0530
C	-0.4570	0.7760	-0.6470
H	2.4130	-0.1280	-1.1700
H	2.5550	1.3430	0.6750
H	0.0160	2.3350	0.8500
H	-0.8920	1.2800	-1.5210
O	0.3810	-0.2740	-1.1260
O	1.8480	-1.5260	0.2140
C	1.8980	-2.6340	-0.6750
H	0.9250	-2.8050	-1.1480
H	2.1710	-3.5020	-0.0720
H	2.6580	-2.4830	-1.4580
O	1.2210	0.3170	1.9010
H	1.3080	1.0410	2.5400
O	1.1640	2.6170	-0.8740
H	0.5200	3.2670	-1.1930
C	-1.6130	0.2320	0.2390
H	-2.0230	1.0890	0.8070
O	-1.2120	-0.8130	1.0920
H	-0.4760	-0.5000	1.6500
C	-2.7610	-0.3020	-0.6120
H	-2.4380	-1.2500	-1.0670
H	-2.9760	0.4140	-1.4230
O	-3.8950	-0.4730	0.2260
H	-4.5670	-0.9510	-0.2820

Coordinates for α-Galf 3E-gg-tg
Energy: -726.502462056 Hartrees

C	-1.4320	0.3900	-0.6480
C	-1.6510	-0.9670	0.0710
C	-0.2980	-1.6990	-0.0820
C	0.7210	-0.5990	-0.4470
H	-1.9300	0.3950	-1.6320
H	-2.4060	-1.5480	-0.4740
H	-0.0370	-2.1980	0.8610
H	1.3470	-0.9390	-1.2810
O	-0.0350	0.5210	-0.9090
O	-1.9220	1.4360	0.1220
C	-1.8840	2.6890	-0.5390
H	-0.8530	3.0180	-0.7220
H	-2.3810	3.4050	0.1200
H	-2.4190	2.6530	-1.5020
O	-2.0420	-0.7570	1.4120
H	-2.3200	-1.6180	1.7590
O	-0.4590	-2.6480	-1.1390
H	0.3550	-3.1710	-1.1980
C	1.6720	-0.2080	0.6890
H	2.2980	-1.0940	0.9020
O	0.8950	0.1550	1.8180
H	1.4990	0.3550	2.5500
C	2.6030	0.9350	0.2850
H	3.1740	1.2570	1.1740
H	1.9930	1.7820	-0.0560
O	3.4730	0.4520	-0.7330
H	4.0150	1.1930	-1.0420

Coordinates for α-Galf 3E-gt-gg
Energy: -726.504790366 Hartrees

C	1.7320	0.3170	-0.2870
C	0.9320	1.3310	0.5620
C	-0.4040	1.3930	-0.1900
C	-0.5590	-0.0480	-0.7120
H	2.3480	0.8420	-1.0350
H	1.4250	2.3110	0.5680
H	-1.2230	1.7060	0.4680
H	-1.1240	-0.0580	-1.6490
O	0.7790	-0.4610	-1.0110
O	2.5430	-0.4660	0.5290
C	3.3660	-1.3660	-0.1990
H	2.7650	-2.1060	-0.7400
H	3.9990	-1.8710	0.5340
H	4.0040	-0.8300	-0.9180
O	0.7570	0.8260	1.8790
H	0.3320	1.5290	2.3950
O	-0.2400	2.3170	-1.2610
H	-1.1020	2.4200	-1.6930
C	-1.2280	-1.0600	0.2350
H	-0.5180	-1.2930	1.0410
O	-1.4740	-2.2110	-0.5720
H	-1.8420	-2.9020	0.0010
C	-2.5090	-0.5390	0.8900
H	-2.2360	0.1410	1.7130
H	-3.0450	-1.3910	1.3400
O	-3.3130	0.1210	-0.0820
H	-4.1700	0.3240	0.3220

Coordinates for α-Galf 3E-gt-gt
Energy: -726.500113058 Hartrees

C	1.8190	0.0910	-0.1790
C	1.1960	1.1800	0.7240
C	-0.0190	1.6330	-0.1040
C	-0.4400	0.3320	-0.8220
H	2.6090	0.5180	-0.8170
H	1.8920	2.0170	0.8620
H	-0.8040	2.0420	0.5490
H	-0.8680	0.5720	-1.8090
O	0.7850	-0.3560	-1.0610
O	2.3340	-0.9380	0.5950
C	2.9260	-1.9790	-0.1700
H	2.1750	-2.5010	-0.7740
H	3.3700	-2.6750	0.5450
H	3.7140	-1.5890	-0.8340
O	0.8070	0.6120	1.9630
H	0.5130	1.3390	2.5330
O	0.4520	2.6200	-1.0160
H	-0.3090	2.9780	-1.4980
C	-1.4380	-0.5700	-0.0540
H	-1.0800	-0.7060	0.9700
O	-1.4720	-1.8730	-0.6120
H	-1.8180	-1.8030	-1.5180
C	-2.8360	0.0530	-0.0170
H	-2.7790	1.0840	0.3700
H	-3.2240	0.1190	-1.0520
O	-3.6700	-0.7540	0.7960
H	-4.5250	-0.3070	0.8810

Coordinates for α-Galf 3E-gt-tg
Energy: -726.505003502 Hartrees

C	-1.7090	-0.3460	-0.1740
C	-0.7730	-1.3620	0.5190
C	0.4360	-1.3730	-0.4290
C	0.4900	0.0920	-0.9030
H	-2.4110	-0.8620	-0.8490
H	-1.2370	-2.3550	0.5710
H	1.3490	-1.6960	0.0810
H	0.9160	0.1570	-1.9140
O	-0.8820	0.4790	-1.0000
O	-2.4140	0.3930	0.7690
C	-3.3400	1.3000	0.1900
H	-2.8270	2.0750	-0.3920
H	-3.8830	1.7620	1.0180
H	-4.0560	0.7780	-0.4650
O	-0.4230	-0.8730	1.8030
H	0.0950	-1.5640	2.2440
O	0.0970	-2.2520	-1.5030
H	0.8730	-2.3370	-2.0760
C	1.2670	1.0720	-0.0100
H	0.7850	1.1110	0.9740
O	1.1850	2.3300	-0.6840
H	1.6280	2.9910	-0.1290
C	2.7520	0.7260	0.1780
H	3.2480	1.6180	0.5920
H	3.2130	0.5260	-0.8040
O	2.9050	-0.3810	1.0640
H	3.8340	-0.4180	1.3350

Coordinates for α-Galf 3E-tg-gg
Energy: -726.504869888 Hartrees

C	1.6340	0.4250	-0.2360
C	0.7870	1.0800	0.8880
C	-0.5670	1.3770	0.2060
C	-0.6110	0.4300	-1.0090
H	2.3580	1.1430	-0.6530
H	1.2410	2.0310	1.1930
H	-1.3990	1.1940	0.8930
H	-0.9990	0.9840	-1.8730
O	0.7450	0.0800	-1.2950
O	2.3130	-0.6910	0.2480
C	3.2100	-1.2550	-0.6980
H	2.6770	-1.6590	-1.5670
H	3.7380	-2.0620	-0.1850
H	3.9420	-0.5100	-1.0460
O	0.6890	0.1850	1.9820
H	0.2810	0.6780	2.7100
O	-0.5180	2.7450	-0.2060
H	-1.3900	2.9700	-0.5660
C	-1.4820	-0.8350	-0.8980
H	-1.1970	-1.4590	-1.7610
O	-2.8210	-0.3690	-1.0200
H	-3.4080	-1.1390	-1.0680
C	-1.2690	-1.6890	0.3570
H	-0.1920	-1.7830	0.5480
H	-1.6670	-2.7000	0.1580
O	-1.9580	-1.1030	1.4570
H	-1.7970	-1.6720	2.2240

Coordinates for α-Galf 3E-tg-gt
Energy: -726.50357088 Hartrees

C	1.6910	0.0760	-0.2640
C	1.1550	0.9740	0.8810
C	-0.0660	1.6670	0.2480
C	-0.5100	0.7160	-0.8840
H	2.5530	0.5520	-0.7590
H	1.9000	1.7340	1.1450
H	-0.8490	1.8230	1.0070
H	-0.7990	1.3270	-1.7480
O	0.6610	-0.0200	-1.2470
O	2.0620	-1.1720	0.2240
C	2.6940	-1.9920	-0.7500
H	2.0080	-2.2420	-1.5680
H	3.0010	-2.9050	-0.2360
H	3.5840	-1.4970	-1.1690
O	0.8140	0.1790	2.0050
H	0.6130	0.7890	2.7310
O	0.3920	2.9150	-0.2640
H	-0.3760	3.4030	-0.5990
C	-1.7120	-0.2180	-0.6190
H	-1.8620	-0.7930	-1.5390
O	-2.9000	0.5630	-0.4850
H	-2.8490	1.0340	0.3620
C	-1.5470	-1.2390	0.5020
H	-1.5990	-0.7350	1.4810
H	-0.5540	-1.7000	0.4300
O	-2.5910	-2.1960	0.3570
H	-2.4880	-2.8460	1.0670

Coordinates for α-Galf 3E-tg-tg
Energy: -726.503486697 Hartrees

C	-1.2210	-0.9550	-0.4180
C	-0.2680	-1.6010	0.6240
C	1.1460	-1.2530	0.1180
C	0.9410	-0.0970	-0.8860
H	-1.6620	-1.7160	-1.0820
H	-0.3850	-2.6920	0.6100
H	1.7880	-0.9480	0.9530
H	1.5310	-0.3130	-1.7850
O	-0.4350	-0.1040	-1.2480
O	-2.2320	-0.2580	0.2330
C	-3.1260	0.4000	-0.6550
H	-2.6270	1.2250	-1.1720
H	-3.9420	0.7880	-0.0400
H	-3.5400	-0.3010	-1.3980
O	-0.5340	-1.0830	1.9190
H	-0.0280	-1.6250	2.5450
O	1.6680	-2.4190	-0.5190
H	2.5850	-2.2270	-0.7690
C	1.3690	1.2950	-0.3860
H	1.2720	1.9970	-1.2280
O	2.7420	1.1330	-0.0150
H	3.0910	2.0070	0.2200
C	0.5310	1.8780	0.7630
H	0.1590	1.0930	1.4310
H	1.1970	2.5350	1.3530
O	-0.5340	2.6290	0.1900
H	-1.0570	2.9950	0.9180

Coordinates for α-Galf E3-gg-gg
Energy: -726.503300352 Hartrees

C	-1.3120	0.8060	-0.6400
C	-1.8250	-0.6430	-0.5190
C	-0.6690	-1.3390	0.1910
C	0.5270	-0.6530	-0.4920
H	-1.5960	1.2970	-1.5840
H	-1.8800	-1.0700	-1.5350
H	-0.6840	-1.0820	1.2560
H	0.6670	-1.1080	-1.4880
O	0.1170	0.7060	-0.6160
O	-1.7740	1.5490	0.4420
C	-1.3020	2.8890	0.4450
H	-0.2130	2.9270	0.5610
H	-1.7820	3.3850	1.2920
H	-1.5820	3.4110	-0.4840
O	-3.0740	-0.7200	0.1260
H	-3.3180	-1.6590	0.1240
O	-0.7650	-2.7420	-0.0180
H	-0.0620	-3.1720	0.4930
C	1.8560	-0.7850	0.2560
H	2.0700	-1.8730	0.2610
O	1.6770	-0.2980	1.5750
H	2.4770	-0.5000	2.0830
C	3.0570	-0.1450	-0.4520
H	3.1170	-0.5600	-1.4730
H	3.9700	-0.4730	0.0790
O	2.9490	1.2640	-0.4510
H	3.7840	1.6210	-0.7900

Coordinates for α-Galf E3-gg-gt
Energy: -726.508707007 Hartrees

C	-1.5340	0.6540	-0.6710
C	-1.8170	-0.8480	-0.4680
C	-0.5480	-1.3360	0.2270
C	0.5170	-0.5020	-0.5000
H	-1.9090	1.0480	-1.6280
H	-1.8330	-1.3270	-1.4610
H	-0.6130	-1.0540	1.2890
H	0.7080	-0.9810	-1.4750
O	-0.1050	0.7740	-0.6780
O	-2.0830	1.3690	0.3890
C	-1.8850	2.7720	0.2940
H	-0.8240	3.0330	0.3790
H	-2.4400	3.2220	1.1200
H	-2.2760	3.1640	-0.6580
O	-3.0190	-1.0810	0.2240
H	-3.1230	-2.0450	0.2670
O	-0.4380	-2.7410	0.0650
H	0.3340	-3.0530	0.5630
C	1.8640	-0.3340	0.2150
H	2.3120	-1.3420	0.3000
O	1.7550	0.2840	1.4870
H	1.1480	-0.2320	2.0390
C	2.8260	0.5150	-0.6070
H	2.5100	1.5640	-0.5230
H	2.7520	0.2170	-1.6660
O	4.1390	0.3080	-0.1060
H	4.7220	0.9580	-0.5260

Coordinates for α-Galf E3-gg-tg
Energy: -726.512050032 Hartrees

C	1.4140	-0.6170	-0.7010
C	1.6260	0.9040	-0.5730
C	0.4320	1.3350	0.2720
C	-0.6630	0.4330	-0.3160
H	1.6940	-1.0190	-1.6870
H	1.4860	1.3510	-1.5720
H	0.6120	1.0740	1.3210
H	-1.0050	0.8540	-1.2720
O	0.0050	-0.8180	-0.5340
O	2.1330	-1.2670	0.2980
C	2.0090	-2.6800	0.2590
H	0.9850	-2.9980	0.4870
H	2.6900	-3.0740	1.0160
H	2.2960	-3.0790	-0.7270
O	2.8930	1.2270	-0.0510
H	2.9390	2.1970	-0.0430
O	0.2230	2.7320	0.1030
H	-0.4960	3.0020	0.6950
C	-1.8960	0.2220	0.5570
H	-2.4170	1.1950	0.6120
O	-1.4720	-0.2050	1.8460
H	-2.2590	-0.2810	2.4080
C	-2.8700	-0.7910	-0.0520
H	-3.6740	-0.9880	0.6800
H	-2.3340	-1.7310	-0.2330
O	-3.3920	-0.2270	-1.2480
H	-3.9530	-0.8910	-1.6740

Coordinates for α-Galf E3-gt-gg
Energy: -726.50921383 Hartrees

C	1.7650	-0.2410	-0.6190
C	1.3380	1.2350	-0.4600
C	-0.0110	1.1240	0.2440
C	-0.5880	-0.1450	-0.3920
H	2.2540	-0.4580	-1.5840
H	1.1560	1.6590	-1.4600
H	0.1820	0.9510	1.3140
H	-1.0340	0.0960	-1.3650
O	0.5600	-0.9960	-0.5690
O	2.6320	-0.5770	0.4250
C	3.0840	-1.9240	0.3690
H	2.2540	-2.6280	0.4910
H	3.7970	-2.0490	1.1870
H	3.5900	-2.1340	-0.5870
O	2.1890	2.0670	0.3000
H	3.0440	2.1330	-0.1520
O	-0.8530	2.2450	0.0460
H	-0.4390	2.9860	0.5170
C	-1.6210	-0.8910	0.4510
H	-1.1490	-1.1270	1.4220
O	-1.9410	-2.0800	-0.2560
H	-2.5860	-2.5750	0.2730
C	-2.8650	-0.0440	0.7350
H	-2.5760	0.8560	1.2960
H	-3.5390	-0.6380	1.3790
O	-3.4900	0.2830	-0.4950
H	-4.3400	0.7020	-0.2970

Coordinates for α-Galf E3-gt-gt
Energy: -726.504879842 Hartrees

C	-1.8440	-0.3780	0.5150
C	-1.5820	1.1340	0.4120
C	-0.1620	1.2000	-0.1480
C	0.4880	0.0090	0.5810
H	-2.4170	-0.6660	1.4100
H	-1.5290	1.5390	1.4370
H	-0.1950	1.0150	-1.2310
H	0.7410	0.3290	1.6080
O	-0.5470	-0.9790	0.6140
O	-2.5010	-0.8130	-0.6320
C	-2.8250	-2.1960	-0.6100
H	-1.9230	-2.8200	-0.6010
H	-3.4000	-2.3960	-1.5170
H	-3.4400	-2.4460	0.2690
O	-2.5630	1.8030	-0.3420
H	-2.3310	2.7450	-0.3080
O	0.3660	2.4850	0.1520
H	1.2420	2.5660	-0.2540
C	1.7270	-0.6330	-0.0610
H	1.4440	-1.0130	-1.0480
O	2.1420	-1.7780	0.6640
H	2.4480	-1.4870	1.5390
C	2.8750	0.3680	-0.2350
H	2.5400	1.1970	-0.8840
H	3.1400	0.8030	0.7460
O	3.9720	-0.3090	-0.8170
H	4.6630	0.3450	-1.0020

Coordinates for α-Galf E3-gt-tg
Energy: -726.453494019 Hartrees

C	1.8140	-0.2060	-0.5270
C	1.2770	1.2070	-0.5570
C	-0.1160	1.0360	-0.0010
C	-0.4850	-0.2970	-0.6240
C	3.1390	-1.6920	0.7260
C	-1.5930	-1.0740	0.0960
C	-2.9240	-0.3590	0.3220
H	2.5120	-0.4170	-1.3660
H	1.2490	1.5870	-1.6040
H	-0.1240	1.0020	1.1110
H	-0.7470	-0.1650	-1.7020
H	2.4700	-2.5460	0.4840
H	3.5520	-1.8420	1.7490
H	3.9850	-1.6420	0.0060
H	1.6100	2.9840	0.1300
H	-1.2770	3.0430	-0.4650
H	-1.2390	-1.4550	1.0800
H	-2.5610	-2.7490	-0.2110
H	-3.6460	-1.0210	0.8530
H	-3.3760	-0.0570	-0.6490
H	-3.6760	1.0900	1.3960
O	0.6880	-1.0640	-0.5710
O	2.4200	-0.4770	0.7220
O	2.0220	2.1180	0.2080
O	-1.0640	2.1210	-0.4440
O	-1.9340	-2.1990	-0.6890
O	-2.8070	0.8120	1.0970

Coordinates for α-Galf E3-tg-gg
Energy: -726.503321228 Hartrees

C	1.6980	-0.1040	-0.6470
C	1.2930	1.3090	-0.1940
C	-0.1990	1.1620	0.1390
C	-0.6410	0.1600	-0.9310
H	2.3960	-0.1060	-1.4980
H	1.3540	1.9710	-1.0740
H	-0.3090	0.7220	1.1370
H	-0.8240	0.7060	-1.8690
O	0.4830	-0.7260	-1.0730
O	2.2600	-0.8010	0.4230
C	2.7830	-2.0690	0.0620
H	1.9930	-2.7550	-0.2700
H	3.2660	-2.4750	0.9540
H	3.5320	-1.9770	-0.7400
O	2.1230	1.7870	0.8450
H	1.8680	2.7080	1.0130
O	-0.9310	2.3730	0.0250
H	-0.6540	2.9530	0.7500
C	-1.8700	-0.7240	-0.6730
H	-1.8630	-1.4700	-1.4870
O	-3.0040	0.1210	-0.7650
H	-3.7950	-0.4270	-0.6520
C	-1.8260	-1.5330	0.6270
H	-0.8530	-2.0420	0.6780
H	-2.6080	-2.3110	0.5730
O	-2.0470	-0.6880	1.7500
H	-2.0080	-1.2430	2.5430

Coordinates for α-Galf E3-tg-gt
Energy: -726.504967963 Hartrees

C	1.6920	0.3520	0.6360
C	1.6410	-1.0930	0.1040
C	0.1640	-1.2860	-0.2720
C	-0.5290	-0.4530	0.8100
H	2.3440	0.4690	1.5140
H	1.8320	-1.7680	0.9550
H	-0.0060	-0.8530	-1.2680
H	-0.5970	-1.0760	1.7200
O	0.3520	0.6540	1.0390
O	2.1040	1.2100	-0.3800
C	2.3060	2.5480	0.0520
H	1.3700	3.0110	0.3870
H	2.6990	3.0980	-0.8060
H	3.0390	2.5920	0.8730
O	2.5870	-1.3070	-0.9230
H	2.5430	-2.2450	-1.1660
O	-0.2770	-2.6340	-0.2120
H	0.1370	-3.1200	-0.9420
C	-1.9350	0.0950	0.5050
H	-2.2170	0.7490	1.3450
O	-2.8630	-0.9700	0.3460
H	-2.8920	-1.4770	1.1730
C	-1.9970	0.9480	-0.7540
H	-2.0500	0.2810	-1.6290
H	-1.0780	1.5460	-0.8210
O	-3.1530	1.7740	-0.6650
H	-3.1890	2.3140	-1.4680

Coordinates for α-Galf E3-tg-tg
Energy: -726.500154632 Hartrees

C	1.5460	0.3400	0.6710
C	1.5760	-1.1200	0.1890
C	0.1200	-1.3990	-0.2250
C	-0.6520	-0.5380	0.7820
H	2.1560	0.5220	1.5690
H	1.7690	-1.7580	1.0670
H	-0.0300	-1.0320	-1.2510
H	-0.7780	-1.1210	1.7050
O	0.1840	0.6020	1.0030
O	1.9630	1.1780	-0.3640
C	1.9010	2.5580	-0.0270
H	0.8640	2.8830	0.1180
H	2.3490	3.1020	-0.8620
H	2.4750	2.7700	0.8890
O	2.5590	-1.3310	-0.8040
H	2.5880	-2.2830	-0.9830
O	-0.2510	-2.7630	-0.1100
H	0.2220	-3.2590	-0.7950
C	-2.0270	-0.0060	0.3490
H	-2.4550	0.5360	1.2060
O	-2.8050	-1.1530	0.0270
H	-3.6990	-0.8480	-0.1940
C	-1.9830	1.0050	-0.8130
H	-1.1180	0.8250	-1.4660
H	-2.8920	0.8540	-1.4210
O	-1.9520	2.3200	-0.2690
H	-1.9240	2.9440	-1.0090

Coordinates for α-Galf 4E-gg-gg
Energy: -726.499068756 Hartrees

C	-1.3980	0.6400	-0.5390
C	-1.7610	-0.8630	-0.3590
C	-0.4310	-1.5040	0.0500
C	0.6010	-0.5050	-0.5020
H	-1.5520	0.9590	-1.5870
H	-2.0350	-1.2760	-1.3430
H	-0.3670	-1.5020	1.1450
H	0.7080	-0.6790	-1.5890
O	0.0000	0.7550	-0.2460
O	-2.1350	1.4400	0.3130
C	-1.8750	2.8280	0.1490
H	-0.8460	3.0770	0.4290
H	-2.5740	3.3520	0.8060
H	-2.0510	3.1440	-0.8910
O	-2.8120	-1.0450	0.5660
H	-3.0210	-1.9920	0.5530
O	-0.3470	-2.8220	-0.4790
H	0.4220	-3.2560	-0.0770
C	1.9970	-0.6160	0.1100
H	2.3470	-1.6290	-0.1740
O	1.8800	-0.4990	1.5180
H	2.7440	-0.6980	1.9100
C	3.0350	0.3460	-0.4810
H	3.0580	0.1960	-1.5750
H	4.0270	0.0410	-0.0980
O	2.7430	1.6820	-0.1300
H	3.4890	2.2300	-0.4150

Coordinates for α-Galf 4E-gg-gt
Energy: -726.504230917 Hartrees

C	1.5660	-0.5760	-0.5600
C	1.7800	0.9520	-0.3470
C	0.3900	1.4640	0.0560
C	-0.5480	0.3780	-0.4910
H	1.7630	-0.8600	-1.6090
H	2.0200	1.4080	-1.3200
H	0.3590	1.4680	1.1580
H	-0.6930	0.5780	-1.5680
O	0.1790	-0.8290	-0.2880
O	2.3660	-1.3120	0.2910
C	2.2880	-2.7150	0.0790
H	1.2960	-3.1040	0.3350
H	3.0390	-3.1690	0.7300
H	2.5150	-2.9710	-0.9680
O	2.7980	1.2150	0.5930
H	2.9220	2.1770	0.5960
O	0.1880	2.7660	-0.4720
H	-0.6190	3.1370	-0.0820
C	-1.9340	0.2760	0.1570
H	-2.4590	1.2260	-0.0550
O	-1.8920	0.0170	1.5510
H	-1.3740	0.7100	1.9860
C	-2.7580	-0.8410	-0.4730
H	-2.3780	-1.7990	-0.0940
H	-2.6140	-0.8210	-1.5660
O	-4.1210	-0.6310	-0.1320
H	-4.6180	-1.4170	-0.4020

Coordinates for α-Galf 4E-gg-tg
Energy: -726.507939193 Hartrees

C	1.4340	-0.5850	-0.5370
C	1.6260	0.9590	-0.4840
C	0.2780	1.4750	0.0350
C	-0.6790	0.3320	-0.3360
H	1.5150	-0.9560	-1.5750
H	1.7430	1.3290	-1.5150
H	0.3350	1.5500	1.1270
H	-0.9370	0.4060	-1.4050
O	0.0970	-0.8390	-0.0830
O	2.3500	-1.2320	0.2700
C	2.2890	-2.6480	0.1800
H	1.3490	-3.0370	0.5890
H	3.1280	-3.0330	0.7640
H	2.3910	-2.9850	-0.8640
O	2.7390	1.3230	0.3040
H	2.8310	2.2840	0.2110
O	-0.0150	2.7320	-0.5630
H	-0.7830	3.1070	-0.1060
C	-1.9890	0.2780	0.4420
H	-2.5830	1.1540	0.1240
O	-1.6950	0.3400	1.8330
H	-2.5370	0.3620	2.3140
C	-2.8020	-0.9780	0.1200
H	-3.6760	-1.0140	0.7960
H	-2.1800	-1.8610	0.3180
O	-3.2100	-0.8970	-1.2390
H	-3.6620	-1.7230	-1.4670

Coordinates for α-Galf 4E-gt-gg
Energy: -726.499791083 Hartrees

C	-1.7300	-0.1950	0.5400
C	-1.3170	1.2890	0.3240
C	0.1220	1.1890	-0.2250
C	0.5770	-0.1940	0.2570
H	-1.9290	-0.3940	1.6090
H	-1.2600	1.7830	1.3070
H	0.0540	1.1820	-1.3250
H	0.9110	-0.1310	1.3030
O	-0.6080	-0.9820	0.1390
O	-2.8410	-0.5210	-0.2170
C	-3.3190	-1.8380	0.0200
H	-2.5940	-2.5930	-0.3040
H	-4.2410	-1.9420	-0.5580
H	-3.5420	-1.9930	1.0870
O	-2.2330	1.9610	-0.5200
H	-1.9770	2.8960	-0.5400
O	1.0040	2.2070	0.2290
H	0.6970	3.0530	-0.1310
C	1.6770	-0.8570	-0.5710
H	1.3110	-0.9250	-1.6110
O	1.8730	-2.1510	-0.0200
H	2.5560	-2.5950	-0.5450
C	2.9750	-0.0450	-0.5900
H	2.7870	0.9370	-1.0470
H	3.6960	-0.5800	-1.2350
O	3.4650	0.0770	0.7350
H	4.3470	0.4740	0.6920

Coordinates for α-Galf 4E-gt-gt
Energy: -726.500938561 Hartrees

C	-1.8250	-0.2770	0.4650
C	-1.5160	1.2340	0.2840
C	-0.0210	1.2700	-0.0670
C	0.4910	-0.0790	0.4740
H	-2.1440	-0.4950	1.5000
H	-1.6260	1.7310	1.2610
H	0.0690	1.2810	-1.1640
H	0.6700	0.0300	1.5610
O	-0.5920	-0.9680	0.2280
O	-2.7900	-0.7010	-0.4280
C	-3.1810	-2.0550	-0.2430
H	-2.3590	-2.7440	-0.4660
H	-4.0090	-2.2350	-0.9330
H	-3.5260	-2.2310	0.7880
O	-2.3560	1.8340	-0.6770
H	-2.1580	2.7840	-0.6550
O	0.5510	2.4350	0.5150
H	1.4490	2.5460	0.1690
C	1.7450	-0.6790	-0.1780
H	1.5280	-0.8580	-1.2370
O	2.0360	-1.9600	0.3530
H	2.2810	-1.8510	1.2870
C	2.9560	0.2550	-0.0820
H	2.7220	1.2100	-0.5830
H	3.1650	0.4830	0.9800
O	4.0570	-0.3790	-0.7040
H	4.7960	0.2470	-0.7150

Coordinates for α-Galf 4E-gt-tg
Energy: -726.451898192 Hartrees

C	-1.7850	-0.1050	0.5100
C	-1.2160	1.2980	0.3890
C	0.2340	1.0810	0.0060
C	0.4770	-0.3360	0.4790
C	-3.4340	-1.5630	-0.3200
C	1.5950	-1.1060	-0.2340
C	3.0010	-0.5120	-0.1860
H	-2.1950	-0.3070	1.5240
H	-1.2960	1.8220	1.3690
H	0.3840	1.1690	-1.0940
H	0.6400	-0.3520	1.5830
H	-2.7220	-2.4160	-0.3410
H	-4.1490	-1.6770	-1.1650
H	-4.0080	-1.5540	0.6340
H	-1.4910	2.9890	-0.5180
H	1.4670	2.9320	0.7870
H	1.3360	-1.2880	-1.3000
H	2.3640	-2.9030	-0.1050
H	3.7230	-1.1580	-0.7360
H	3.3500	-0.4160	0.8670
H	4.0090	0.9970	-0.9100
O	-0.7290	-0.9960	0.2190
O	-2.7530	-0.3380	-0.4920
O	-1.8630	2.1030	-0.5640
O	1.1950	2.0340	0.6560
O	1.7320	-2.3700	0.3850
O	3.0870	0.7710	-0.7610

Coordinates for α-Galf 4E-tg-gg
Energy: -726.499088556 Hartrees

C	1.7040	-0.0510	-0.5660
C	1.2050	1.3480	-0.1050
C	-0.3280	1.1830	0.0100
C	-0.6040	-0.0340	-0.8790
H	2.1760	0.0090	-1.5630
H	1.4030	2.0710	-0.9120
H	-0.5770	0.9440	1.0500
H	-0.6700	0.3090	-1.9240
O	0.5360	-0.8730	-0.6820
O	2.5890	-0.6010	0.3430
C	3.1860	-1.8100	-0.1030
H	2.4480	-2.6170	-0.1920
H	3.9340	-2.0820	0.6450
H	3.6820	-1.6730	-1.0760
O	1.8540	1.7420	1.0910
H	1.5720	2.6490	1.2870
O	-1.0660	2.3020	-0.4600
H	-0.8580	3.0590	0.1090
C	-1.8430	-0.8990	-0.6060
H	-1.7520	-1.7590	-1.2940
O	-2.9740	-0.1080	-0.9280
H	-3.7580	-0.6750	-0.8790
C	-1.9140	-1.5080	0.7980
H	-0.9580	-2.0110	1.0000
H	-2.7040	-2.2810	0.7930
O	-2.2070	-0.5080	1.7650
H	-2.2390	-0.9410	2.6310

Coordinates for α-Galf 4E-tg-gt
Energy: -726.501128706 Hartrees

C	1.7300	-0.2180	-0.5550
C	1.5320	1.2050	0.0450
C	-0.0010	1.3400	0.1980
C	-0.5330	0.2840	-0.7760
H	2.1870	-0.1620	-1.5590
H	1.8520	1.9460	-0.7050
H	-0.2660	1.0770	1.2320
H	-0.5340	0.7360	-1.7850
O	0.4160	-0.7770	-0.7020
O	2.4980	-1.0120	0.2740
C	2.8240	-2.2760	-0.2880
H	1.9330	-2.9010	-0.4190
H	3.5090	-2.7590	0.4120
H	3.3250	-2.1600	-1.2620
O	2.2690	1.3530	1.2440
H	2.1880	2.2780	1.5220
O	-0.5120	2.6150	-0.1620
H	-0.1940	3.2670	0.4810
C	-1.9390	-0.2870	-0.5120
H	-2.1470	-1.0250	-1.3030
O	-2.9070	0.7540	-0.5140
H	-2.8940	1.1830	-1.3830
C	-2.0650	-1.0250	0.8140
H	-2.1610	-0.2850	1.6240
H	-1.1520	-1.6130	0.9790
O	-3.2180	-1.8560	0.7380
H	-3.2950	-2.3250	1.5820

Coordinates for α-Galf 4E-tg-tg
Energy: -726.496159933 Hartrees

C	-1.5930	0.0490	-0.6120
C	-1.3410	-1.3650	-0.0190
C	0.1930	-1.4280	0.1760
C	0.7050	-0.3250	-0.7590
H	-2.0290	-0.0160	-1.6260
H	-1.6030	-2.1150	-0.7820
H	0.4100	-1.1730	1.2240
H	0.8100	-0.7590	-1.7660
O	-0.3110	0.6710	-0.7200
O	-2.4170	0.7980	0.2100
C	-2.6860	2.0990	-0.2990
H	-1.7770	2.7110	-0.3230
H	-3.4180	2.5490	0.3760
H	-3.1120	2.0490	-1.3130
O	-2.1000	-1.5630	1.1600
H	-1.9730	-2.4840	1.4340
O	0.7680	-2.6750	-0.1830
H	0.4240	-3.3520	0.4190
C	2.0280	0.3610	-0.3870
H	2.2880	1.0460	-1.2100
O	2.9890	-0.6810	-0.2650
H	3.8520	-0.2650	-0.1150
C	1.9590	1.2330	0.8810
H	1.2120	0.8470	1.5890
H	2.9430	1.1730	1.3780
O	1.6660	2.5670	0.4900
H	1.6250	3.1080	1.2930

Coordinates for α-Galf E4-gg-gg
Energy: -726.493879604 Hartrees

C	-0.9350	1.0580	-0.6490
C	-1.9320	0.1280	0.0970
C	-1.3210	-1.2880	-0.0280
C	0.1170	-1.0600	-0.5500
H	-1.3830	1.5110	-1.5480
H	-2.8790	0.1110	-0.4600
H	-1.3230	-1.7790	0.9540
H	0.3240	-1.7760	-1.3600
O	0.1200	0.2330	-1.1360
O	-0.4940	2.0570	0.2080
C	0.4690	2.9200	-0.3790
H	1.4040	2.3870	-0.5800
H	0.6450	3.7200	0.3450
H	0.0920	3.3610	-1.3170
O	-2.1390	0.5630	1.4240
H	-2.8630	0.0260	1.7800
O	-2.1260	-2.0080	-0.9630
H	-1.7720	-2.9080	-1.0340
C	1.2020	-1.2720	0.5180
H	1.1090	-2.3370	0.8140
O	0.9150	-0.4160	1.6050
H	1.5170	-0.6280	2.3350
C	2.6410	-1.1260	0.0090
H	2.7760	-1.8040	-0.8520
H	3.3140	-1.4890	0.8080
O	2.9370	0.2170	-0.3220
H	3.8860	0.2700	-0.5120

Coordinates for α-Galf E4-gg-gt
Energy: -726.502688563 Hartrees

C	-1.4640	0.6520	-0.5500
C	-1.8580	-0.5020	0.4220
C	-0.8500	-1.6320	0.1050
C	0.2920	-0.9120	-0.6260
H	-2.2490	0.8300	-1.3030
H	-2.8880	-0.8310	0.2280
H	-0.5150	-2.1200	1.0330
H	0.6780	-1.5860	-1.3990
O	-0.3540	0.1700	-1.3060
O	-1.2420	1.8170	0.1660
C	-0.8150	2.9070	-0.6360
H	0.1860	2.7300	-1.0430
H	-0.7930	3.7810	0.0190
H	-1.5160	3.0910	-1.4660
O	-1.7160	-0.0520	1.7700
H	-2.0040	-0.7770	2.3460
O	-1.3780	-2.5870	-0.8110
H	-2.1090	-3.0530	-0.3750
C	1.4590	-0.4770	0.2910
H	1.7240	-1.3580	0.9040
O	1.1510	0.6380	1.0990
H	0.4280	0.4140	1.7100
C	2.7160	-0.1240	-0.4960
H	2.5560	0.8410	-1.0000
H	2.8790	-0.8920	-1.2700
O	3.8070	-0.0730	0.4130
H	4.6000	0.1520	-0.0950

Coordinates for α-Galf E4-gg-tg
Energy: -726.502995619 Hartrees

C	-1.3610	0.4830	-0.7220
C	-1.7440	-0.8400	-0.0030
C	-0.4410	-1.6750	0.0210
C	0.6730	-0.7000	-0.4100
H	-1.8930	0.5920	-1.6810
H	-2.4550	-1.3880	-0.6370
H	-0.2690	-2.0580	1.0360
H	1.3200	-1.1730	-1.1580
O	0.0200	0.3910	-1.0640
O	-1.6470	1.5740	0.0910
C	-1.4540	2.8210	-0.5510
H	-0.3970	2.9960	-0.7900
H	-1.7990	3.5890	0.1460
H	-2.0410	2.8900	-1.4820
O	-2.2990	-0.5790	1.2670
H	-2.6380	-1.4230	1.6010
O	-0.6160	-2.7450	-0.9090
H	0.1830	-3.2940	-0.8860
C	1.5800	-0.2390	0.7350
H	2.1230	-1.1330	1.0920
O	0.7620	0.3060	1.7570
H	1.3280	0.5500	2.5050
C	2.6210	0.7810	0.2710
H	3.1520	1.1720	1.1570
H	2.1030	1.6180	-0.2150
O	3.5180	0.1160	-0.6120
H	4.1350	0.7730	-0.9650

Coordinates for α-Galf E4-gt-gg
Energy: -726.505075524 Hartrees

C	1.7110	0.3310	-0.3690
C	0.9980	1.4690	0.4250
C	-0.4390	1.4580	-0.1410
C	-0.5680	0.0460	-0.7330
H	2.5180	0.7130	-1.0120
H	1.4630	2.4360	0.1930
H	-1.1670	1.6650	0.6540
H	-1.2530	0.0260	-1.5850
O	0.7420	-0.2090	-1.2520
O	2.2280	-0.6160	0.5220
C	2.8810	-1.6940	-0.1360
H	2.1750	-2.2760	-0.7380
H	3.3080	-2.3230	0.6490
H	3.6920	-1.3300	-0.7860
O	1.0340	1.1990	1.8180
H	0.6490	1.9710	2.2590
O	-0.5040	2.4570	-1.1520
H	-1.4140	2.4700	-1.4900
C	-1.0110	-1.0490	0.2530
H	-0.2380	-1.1620	1.0260
O	-1.1140	-2.2380	-0.5300
H	-1.3460	-2.9650	0.0680
C	-2.3240	-0.7120	0.9650
H	-2.1180	-0.0020	1.7820
H	-2.7160	-1.6320	1.4290
O	-3.2530	-0.1680	0.0310
H	-4.1110	-0.0880	0.4730

Coordinates for α-Galf E4-gt-gt
Energy: -726.50096999 Hartrees

C	1.7800	-0.1690	-0.2170
C	1.4350	1.0840	0.6450
C	0.2020	1.6900	-0.0660
C	-0.3550	0.4940	-0.8620
H	2.7540	-0.0800	-0.7210
H	2.2550	1.8120	0.5890
H	-0.5080	2.0830	0.6770
H	-0.8430	0.8300	-1.7890
O	0.8190	-0.2040	-1.2680
O	1.7550	-1.3040	0.5880
C	2.0010	-2.5100	-0.1250
H	1.1810	-2.7290	-0.8160
H	2.0720	-3.3000	0.6250
H	2.9480	-2.4550	-0.6850
O	1.1690	0.7070	1.9830
H	1.0480	1.5250	2.4880
O	0.6790	2.7280	-0.9150
H	-0.0840	3.1390	-1.3510
C	-1.3300	-0.4160	-0.0700
H	-0.9340	-0.5840	0.9350
O	-1.4170	-1.7070	-0.6520
H	-1.7980	-1.6110	-1.5400
C	-2.7090	0.2390	0.0400
H	-2.6040	1.2690	0.4220
H	-3.1470	0.3140	-0.9740
O	-3.5190	-0.5470	0.8960
H	-4.3580	-0.0790	1.0250

Coordinates for α-Galf E4-gt-tg
Energy: -726.50502534 Hartrees

C	1.6810	0.4550	-0.2600
C	0.8030	1.5240	0.4590
C	-0.5620	1.4210	-0.2590
C	-0.5170	0.0140	-0.8830
H	2.5230	0.9010	-0.8100
H	1.2140	2.5250	0.2810
H	-1.3880	1.5430	0.4490
H	-1.0900	-0.0390	-1.8170
O	0.8550	-0.1400	-1.2490
O	2.1580	-0.4660	0.6750
C	2.9340	-1.5030	0.0890
H	2.3200	-2.1330	-0.5630
H	3.3310	-2.0970	0.9160
H	3.7740	-1.0920	-0.4940
O	0.7200	1.2390	1.8450
H	0.2380	1.9760	2.2520
O	-0.5810	2.4390	-1.2590
H	-1.4440	2.4030	-1.7000
C	-0.9930	-1.1100	0.0570
H	-0.5350	-0.9670	1.0450
O	-0.5650	-2.3380	-0.5330
H	-0.8300	-3.0550	0.0630
C	-2.5200	-1.1710	0.2090
H	-2.7610	-2.0760	0.7930
H	-2.9690	-1.2960	-0.7890
O	-3.0140	-0.0070	0.8640
H	-3.9230	-0.1830	1.1450

Coordinates for α-Galf E4-tg-gg
Energy: -726.505152505 Hartrees

C	1.6010	0.4560	-0.3470
C	0.7870	1.2800	0.6910
C	-0.6400	1.3660	0.0980
C	-0.6560	0.3340	-1.0440
H	2.4050	1.0520	-0.8030
H	1.1880	2.3010	0.7350
H	-1.3910	1.1360	0.8600
H	-1.1490	0.7680	-1.9210
O	0.7140	0.1230	-1.4040
O	2.1600	-0.6760	0.2560
C	3.0330	-1.3920	-0.6060
H	2.4990	-1.8010	-1.4720
H	3.4560	-2.2080	-0.0160
H	3.8500	-0.7480	-0.9670
O	0.8530	0.6510	1.9590
H	0.4340	1.2560	2.5890
O	-0.7920	2.6990	-0.3980
H	-1.6930	2.7750	-0.7490
C	-1.3810	-1.0000	-0.7740
H	-1.0580	-1.6780	-1.5810
O	-2.7660	-0.6860	-0.8890
H	-3.2700	-1.5130	-0.8380
C	-1.0530	-1.6950	0.5530
H	0.0340	-1.6930	0.7020
H	-1.3830	-2.7470	0.4760
O	-1.7400	-1.0460	1.6180
H	-1.5050	-1.5140	2.4330

Coordinates for α-Galf E4-tg-gt
Energy: -726.503307429 Hartrees

C	1.6800	-0.0080	-0.3570
C	1.2870	1.0210	0.7400
C	-0.0290	1.6540	0.2300
C	-0.5000	0.7290	-0.9090
H	2.6210	0.2720	-0.8540
H	2.0420	1.8160	0.7820
H	-0.7550	1.7120	1.0550
H	-0.8520	1.3440	-1.7440
O	0.6800	0.0570	-1.3650
O	1.8170	-1.2840	0.1920
C	2.3260	-2.2370	-0.7320
H	1.6350	-2.3930	-1.5690
H	2.4510	-3.1710	-0.1800
H	3.3020	-1.9190	-1.1300
O	1.1540	0.3770	1.9950
H	1.0190	1.0730	2.6560
O	0.2980	2.9600	-0.2390
H	-0.5210	3.3850	-0.5400
C	-1.6690	-0.2290	-0.5870
H	-1.8240	-0.8480	-1.4770
O	-2.8700	0.5330	-0.4620
H	-2.8100	1.0490	0.3570
C	-1.4680	-1.1830	0.5870
H	-1.4550	-0.6130	1.5330
H	-0.4920	-1.6740	0.4980
O	-2.5420	-2.1170	0.5640
H	-2.4130	-2.7220	1.3100

Coordinates for α-Galf E4-tg-tg
Energy: -726.504102099 Hartrees

C	-1.0110	-1.1450	-0.4760
C	0.0480	-1.6880	0.5240
C	1.3710	-1.0020	0.1210
C	0.9620	0.0980	-0.8820
H	-1.4120	-1.9400	-1.1230
H	0.1720	-2.7680	0.3700
H	1.8600	-0.5720	1.0040
H	1.6380	0.0560	-1.7450
O	-0.3390	-0.2440	-1.3490
O	-2.0560	-0.5450	0.2210
C	-3.0840	-0.0480	-0.6260
H	-2.7300	0.8010	-1.2180
H	-3.8960	0.2740	0.0310
H	-3.4590	-0.8350	-1.2980
O	-0.3460	-1.4130	1.8590
H	0.2840	-1.8740	2.4340
O	2.2000	-1.9950	-0.4800
H	3.0410	-1.5680	-0.7090
C	1.0350	1.5360	-0.3350
H	0.7900	2.2210	-1.1600
O	2.4030	1.6830	0.0590
H	2.5390	2.6060	0.3240
C	0.0700	1.8780	0.8130
H	-0.1740	0.9980	1.4210
H	0.5840	2.6060	1.4670
O	-1.0970	2.4570	0.2390
H	-1.7030	2.6710	0.9640

Coordinates for β-Galf OE-gg-gg
Energy: -726.502784639 Hartrees

C	-1.0070	0.7140	0.1750
C	-1.6160	-0.6880	0.3270
C	-0.5790	-1.6480	-0.2990
C	0.5660	-0.7080	-0.7690
H	-0.5510	1.0410	1.1210
H	-2.5190	-0.7290	-0.2960
H	-0.2280	-2.3600	0.4600
H	0.8730	-0.9650	-1.7920
O	0.0040	0.5930	-0.8270
O	-1.9820	1.6130	-0.2420
C	-1.5390	2.9630	-0.2560
H	-0.7430	3.1170	-0.9940
H	-2.4060	3.5740	-0.5210
H	-1.1690	3.2690	0.7340
O	-1.9110	-0.9220	1.6920
H	-2.5030	-1.6890	1.7340
O	-1.2180	-2.3260	-1.3800
H	-0.5480	-2.8490	-1.8460
C	1.8190	-0.8060	0.1180
H	2.2170	-1.8270	-0.0430
O	1.4080	-0.6350	1.4650
H	2.1650	-0.8030	2.0480
C	2.9520	0.1540	-0.2690
H	3.1480	0.0480	-1.3500
H	3.8670	-0.1790	0.2540
O	2.6250	1.4820	0.0890
H	3.4140	2.0260	-0.0560

Coordinates for β-Galf OE-gg-gt
Energy: -726.51001245 Hartrees

C	-1.2320	0.6240	0.1790
C	-1.5720	-0.8640	0.3610
C	-0.4080	-1.6350	-0.2940
C	0.5350	-0.5210	-0.8140
H	-0.8180	1.0430	1.1070
H	-2.4990	-1.0890	-0.1790
H	0.0900	-2.2730	0.4530
H	0.8570	-0.7370	-1.8420
O	-0.2420	0.6730	-0.8550
O	-2.3690	1.3180	-0.2150
C	-2.1940	2.7280	-0.2570
H	-1.4860	3.0200	-1.0420
H	-3.1740	3.1580	-0.4740
H	-1.8370	3.1120	0.7100
O	-1.6890	-1.1150	1.7590
H	-2.1040	-1.9840	1.8720
O	-0.9560	-2.4390	-1.3350
H	-0.2230	-2.8460	-1.8230
C	1.7830	-0.3560	0.0780
H	2.3660	-1.2930	0.0210
O	1.4420	-0.0540	1.4280
H	0.8670	-0.7500	1.7870
C	2.6780	0.7720	-0.4160
H	2.1850	1.7260	-0.1890
H	2.7790	0.6930	-1.5110
O	3.9400	0.6530	0.2260
H	4.4490	1.4520	0.0270

Coordinates for β-Galf OE-gg-tg
Energy: -726.512216171 Hartrees

C	-1.2910	0.5560	0.1810
C	-1.5580	-0.9530	0.1020
C	-0.2310	-1.5830	-0.3730
C	0.7310	-0.3800	-0.5400
H	-1.1580	0.8690	1.2270
H	-2.3030	-1.1210	-0.6850
H	0.1390	-2.2810	0.3900
H	1.2420	-0.4190	-1.5090
O	-0.0830	0.7930	-0.5450
O	-2.3460	1.2480	-0.4070
C	-2.2620	2.6570	-0.2580
H	-1.4110	3.0700	-0.8120
H	-3.1910	3.0710	-0.6580
H	-2.1690	2.9400	0.8020
O	-2.0200	-1.4040	1.3640
H	-2.4090	-2.2820	1.2340
O	-0.4920	-2.2620	-1.6010
H	0.3550	-2.5680	-1.9610
C	1.8140	-0.3100	0.5410
H	2.4350	-1.2180	0.4480
O	1.1580	-0.2670	1.8040
H	1.8320	-0.2670	2.5010
C	2.7250	0.9050	0.3660
H	3.3860	0.9830	1.2470
H	2.1020	1.8080	0.3220
O	3.4790	0.7110	-0.8250
H	4.0050	1.5080	-0.9820

Coordinates for β-Galf OE-gt-gg
Energy: -726.508132122 Hartrees

C	1.6270	-0.1530	0.2420
C	1.1320	1.3010	0.2570
C	-0.3360	1.2290	-0.2130
C	-0.5860	-0.2790	-0.4670
H	1.6470	-0.5550	1.2720
H	1.7090	1.8700	-0.4820
H	-0.9720	1.6160	0.5950
H	-1.0610	-0.4260	-1.4400
O	0.7010	-0.8880	-0.5490
O	2.8970	-0.2180	-0.3180
C	3.4770	-1.5150	-0.2690
H	2.9170	-2.2270	-0.8860
H	4.4940	-1.4170	-0.6570
H	3.5200	-1.8920	0.7640
O	1.2970	1.8160	1.5720
H	1.1930	2.7780	1.5240
O	-0.4980	2.0150	-1.3850
H	-1.4030	1.8490	-1.6980
C	-1.4890	-0.9700	0.5680
H	-0.9810	-0.9880	1.5480
O	-1.6800	-2.2940	0.0830
H	-2.2200	-2.7750	0.7290
C	-2.8200	-0.2250	0.7570
H	-2.6830	0.6010	1.4710
H	-3.5510	-0.9210	1.2000
O	-3.2760	0.2640	-0.5040
H	-4.1730	0.6110	-0.3860

Coordinates for β-Galf OE-gt-gt
Energy: -726.505243727 Hartrees

C	1.5030	-0.3160	0.2160
C	1.2980	1.1900	0.4410
C	-0.0670	1.5060	-0.2160
C	-0.5240	0.1290	-0.7640
H	1.1910	-0.8850	1.1080
H	2.0760	1.7300	-0.1120
H	-0.7660	1.8910	0.5420
H	-0.9360	0.2220	-1.7790
O	0.6590	-0.6460	-0.8880
O	2.8260	-0.5830	-0.0960
C	3.1320	-1.9700	-0.1620
H	2.6090	-2.4550	-0.9950
H	4.2110	-2.0440	-0.3160
H	2.8630	-2.4800	0.7750
O	1.3550	1.4480	1.8350
H	1.4460	2.4050	1.9560
O	0.1600	2.4790	-1.2310
H	-0.6670	2.6050	-1.7210
C	-1.5750	-0.5510	0.1680
H	-1.4040	-0.2450	1.2060
O	-1.4450	-1.9590	0.1860
H	-1.6320	-2.2930	-0.7060
C	-2.9760	-0.0950	-0.2380
H	-2.9790	1.0030	-0.3610
H	-3.2130	-0.5290	-1.2270
O	-3.9030	-0.5070	0.7490
H	-4.7690	-0.1390	0.5210

Coordinates for β-Galf OE-gt-tg
Energy: -726.507992848 Hartrees

C	-1.5960	0.1210	0.2250
C	-1.0550	-1.3110	0.3340
C	0.3960	-1.2410	-0.1880
C	0.5870	0.2560	-0.5650
H	-1.5970	0.6040	1.2190
H	-1.6370	-1.9520	-0.3390
H	1.0850	-1.5320	0.6130
H	1.0240	0.3530	-1.5660
O	-0.7160	0.8160	-0.6490
O	-2.8830	0.1070	-0.3000
C	-3.5050	1.3850	-0.3220
H	-2.9890	2.0700	-1.0040
H	-4.5300	1.2280	-0.6660
H	-3.5260	1.8320	0.6840
O	-1.1650	-1.7260	1.6900
H	-1.0370	-2.6870	1.7120
O	0.5310	-2.1160	-1.3000
H	1.4180	-1.9620	-1.6630
C	1.4940	0.9980	0.4390
H	1.2920	0.6260	1.4570
O	1.2110	2.3890	0.3510
H	1.7820	2.8450	0.9900
C	2.9760	0.7790	0.1000
H	3.5950	1.2550	0.8780
H	3.1790	1.2950	-0.8510
O	3.2630	-0.6150	0.0040
H	4.2240	-0.7290	0.0220

Coordinates for β-Galf OE-tg-gg
Energy: -726.507338364 Hartrees

C	1.3580	-0.2390	0.0920
C	0.8400	1.0960	0.6400
C	-0.4930	1.3510	-0.0990
C	-0.6520	0.1250	-1.0350
H	1.1710	-1.0480	0.8180
H	1.5430	1.8750	0.3170
H	-1.3210	1.4140	0.6140
H	-0.8810	0.4950	-2.0420
O	0.6330	-0.4900	-1.1180
O	2.7180	-0.1500	-0.1800
C	3.3100	-1.3800	-0.5710
H	2.9220	-1.7240	-1.5370
H	4.3840	-1.1990	-0.6540
H	3.1340	-2.1630	0.1840
O	0.7720	1.0210	2.0540
H	0.6950	1.9280	2.3870
O	-0.3530	2.5680	-0.8300
H	-1.1480	2.6700	-1.3770
C	-1.7700	-0.8910	-0.7220
H	-1.7540	-1.6240	-1.5460
O	-2.9700	-0.1230	-0.7520
H	-3.7230	-0.7300	-0.6830
C	-1.6140	-1.7020	0.5600
H	-0.6970	-2.3060	0.4750
H	-2.4630	-2.4080	0.6270
O	-1.5820	-0.8270	1.6700
H	-1.4830	-1.3460	2.4810

Coordinates for β-Galf OE-tg-gt
Energy: -726.506234885 Hartrees

C	1.3970	-0.4230	0.1280
C	1.1430	0.9410	0.7850
C	-0.0970	1.5140	0.0670
C	-0.4810	0.4290	-0.9700
H	1.0410	-1.2360	0.7830
H	1.9990	1.5940	0.5770
H	-0.8930	1.6790	0.8100
H	-0.6280	0.9060	-1.9460
O	0.6610	-0.4200	-1.0990
O	2.7520	-0.5770	-0.1280
C	3.1020	-1.8610	-0.6300
H	2.6700	-2.0330	-1.6230
H	4.1920	-1.8820	-0.6980
H	2.7680	-2.6580	0.0510
O	0.9590	0.7300	2.1790
H	1.0180	1.5910	2.6200
O	0.2770	2.7490	-0.5340
H	-0.4680	3.0560	-1.0750
C	-1.7930	-0.3390	-0.6820
H	-1.9770	-1.0020	-1.5350
O	-2.8830	0.5770	-0.6990
H	-2.8090	1.1480	0.0820
C	-1.7850	-1.2180	0.5680
H	-1.5810	-0.6100	1.4670
H	-0.9680	-1.9490	0.4730
O	-3.0470	-1.8630	0.6540
H	-3.0380	-2.4190	1.4470

Coordinates for β-Galf OE-tg-tg
Energy: -726.509825662 Hartrees

C	1.3380	-0.1600	0.0810
C	0.8250	1.1140	0.7710
C	-0.5300	1.4310	0.1060
C	-0.7180	0.3050	-0.9400
H	1.2280	-1.0330	0.7410
H	1.5210	1.9330	0.5570
H	-1.3330	1.4160	0.8520
H	-0.9710	0.7440	-1.9130
O	0.5330	-0.3520	-1.0810
O	2.6720	0.0130	-0.2790
C	3.2740	-1.1570	-0.8150
H	2.8180	-1.4410	-1.7700
H	4.3300	-0.9220	-0.9710
H	3.1910	-2.0020	-0.1150
O	0.7320	0.8490	2.1680
H	0.6290	1.7010	2.6190
O	-0.4380	2.7250	-0.4870
H	-1.2530	2.8690	-0.9920
C	-1.8540	-0.6770	-0.5970
H	-1.8710	-1.4550	-1.3750
O	-3.0340	0.1310	-0.6430
H	-3.8020	-0.4470	-0.5220
C	-1.7590	-1.3920	0.7600
H	-1.4710	-0.6910	1.5560
H	-2.7670	-1.7710	1.0030
O	-0.8320	-2.4650	0.6500
H	-0.7850	-2.9030	1.5130

Coordinates for β-Galf EO-gg-gg
Energy: -726.505915365 Hartrees

C	1.4020	0.6910	-0.5310
C	1.8670	-0.7410	-0.2270
C	0.6310	-1.3910	0.4370
C	-0.4280	-0.2550	0.4460
H	1.7350	1.0490	-1.5130
H	2.6990	-0.7210	0.4870
H	0.2830	-2.2050	-0.2130
H	-0.3760	0.2310	1.4340
O	-0.0110	0.6450	-0.5750
O	1.8790	1.5210	0.5010
C	1.4970	2.8810	0.3390
H	0.4070	2.9910	0.3180
H	1.9100	3.4260	1.1920
H	1.9120	3.3000	-0.5910
O	2.2410	-1.3510	-1.4540
H	2.6460	-2.2060	-1.2420
O	0.9690	-1.8730	1.7330
H	0.2090	-2.3690	2.0740
C	-1.8640	-0.7280	0.2260
H	-2.0410	-1.4890	1.0140
O	-1.9440	-1.3120	-1.0620
H	-2.8160	-1.7260	-1.1510
C	-2.9340	0.3420	0.4690
H	-2.8530	0.6700	1.5200
H	-3.9220	-0.1430	0.3620
O	-2.7910	1.4200	-0.4340
H	-3.5600	1.9990	-0.3240

Coordinates for β-Galf EO-gg-gt
Energy: -726.511733047 Hartrees

C	1.6040	0.5660	-0.5320
C	1.8660	-0.8940	-0.1280
C	0.5280	-1.3510	0.5020
C	-0.3840	-0.1020	0.4010
H	2.0130	0.8140	-1.5190
H	2.6590	-0.9380	0.6260
H	0.1390	-2.1690	-0.1270
H	-0.3180	0.4120	1.3720
O	0.1970	0.7020	-0.6280
O	2.1570	1.3840	0.4680
C	2.0220	2.7730	0.1990
H	0.9690	3.0730	0.1450
H	2.5110	3.3000	1.0210
H	2.5160	3.0430	-0.7470
O	2.2100	-1.6180	-1.3020
H	2.4940	-2.5020	-1.0260
O	0.7410	-1.8010	1.8310
H	-0.0880	-2.1830	2.1600
C	-1.8610	-0.3640	0.0850
H	-2.2650	-0.9770	0.9120
O	-2.0670	-1.0000	-1.1660
H	-1.5690	-1.8310	-1.1820
C	-2.6620	0.9330	0.0570
H	-2.4260	1.4590	-0.8780
H	-2.3450	1.5680	0.9000
O	-4.0410	0.6030	0.1540
H	-4.5500	1.4090	-0.0160

Coordinates for β-Galf EO-gg-tg
Energy: -726.514916591 Hartrees

C	1.4760	0.6000	-0.5610
C	1.8590	-0.7800	-0.0050
C	0.5370	-1.3200	0.5900
C	-0.4880	-0.1900	0.3180
H	1.9270	0.8070	-1.5400
H	2.6010	-0.6680	0.7930
H	0.2520	-2.2180	0.0290
H	-0.5640	0.4310	1.2200
O	0.0750	0.5710	-0.7580
O	1.8670	1.5600	0.3900
C	1.5720	2.8930	0.0010
H	0.4930	3.0500	-0.1120
H	1.9550	3.5420	0.7920
H	2.0680	3.1480	-0.9480
O	2.3570	-1.5610	-1.0830
H	2.7130	-2.3800	-0.7070
O	0.7150	-1.6090	1.9730
H	-0.0890	-2.0470	2.2920
C	-1.8910	-0.6510	-0.0580
H	-2.3130	-1.1480	0.8340
O	-1.7950	-1.5590	-1.1490
H	-2.6860	-1.8890	-1.3420
C	-2.8120	0.5180	-0.4180
H	-3.7730	0.1100	-0.7790
H	-2.3540	1.0870	-1.2370
O	-2.9980	1.3060	0.7510
H	-3.5210	2.0840	0.5100

Coordinates for β-Galf EO-gt-gg
Energy: -726.508501256 Hartrees

C	-1.8500	-0.2710	-0.3340
C	-1.5910	1.2200	-0.0700
C	-0.0470	1.2910	0.1100
C	0.4230	-0.1700	-0.0670
H	-2.5970	-0.4410	-1.1200
H	-2.1020	1.5360	0.8480
H	0.3460	1.9150	-0.7100
H	0.5200	-0.6270	0.9240
O	-0.6300	-0.7950	-0.8120
O	-2.2520	-0.8470	0.8840
C	-2.4960	-2.2450	0.7890
H	-1.5960	-2.7900	0.4850
H	-2.8090	-2.5750	1.7830
H	-3.3010	-2.4580	0.0680
O	-2.0550	1.9380	-1.2100
H	-1.9950	2.8850	-1.0140
O	0.4000	1.7640	1.3720
H	0.0920	2.6770	1.4800
C	1.7310	-0.3400	-0.8340
H	1.6000	0.1300	-1.8250
O	1.9530	-1.7360	-0.9640
H	2.7560	-1.8610	-1.4930
C	2.9040	0.3600	-0.1400
H	2.6930	1.4380	-0.0560
H	3.7950	0.2490	-0.7850
O	3.1130	-0.2340	1.1290
H	3.9330	0.1250	1.4970

Coordinates for β-Galf EO-gt-gt
Energy: -726.508884351 Hartrees

C	-1.8800	-0.2310	-0.4430
C	-1.5980	1.2550	-0.1790
C	-0.1020	1.2830	0.2180
C	0.3360	-0.2050	0.1430
H	-2.5030	-0.3940	-1.3310
H	-2.2060	1.6110	0.6610
H	0.4340	1.8660	-0.5460
H	0.2580	-0.6230	1.1620
O	-0.6240	-0.8260	-0.7140
O	-2.4870	-0.7590	0.7090
C	-2.8330	-2.1320	0.5820
H	-1.9490	-2.7550	0.4050
H	-3.3070	-2.4240	1.5220
H	-3.5440	-2.2850	-0.2440
O	-1.8760	1.9710	-1.3750
H	-1.8150	2.9170	-1.1690
O	0.0390	1.8710	1.5040
H	0.9840	1.9810	1.6890
C	1.7340	-0.4820	-0.4210
H	1.7820	-0.0890	-1.4430
O	1.9760	-1.8730	-0.5550
H	1.9880	-2.2620	0.3350
C	2.8250	0.1980	0.4130
H	2.6150	1.2810	0.4810
H	2.8010	-0.2060	1.4420
O	4.0740	-0.0350	-0.2090
H	4.7480	0.4670	0.2740

Coordinates for β-Galf EO-gt-tg
Energy: -726.512057812 Hartrees

C	1.8290	-0.0320	-0.4670
C	1.2530	-1.4100	-0.1070
C	-0.2150	-1.0980	0.2970
C	-0.3380	0.4300	0.1300
H	2.4580	-0.0540	-1.3660
H	1.8090	-1.8400	0.7360
H	-0.8830	-1.6190	-0.4010
H	-0.1760	0.8890	1.1150
O	0.7190	0.7890	-0.7680
O	2.5540	0.4250	0.6480
C	3.1260	1.7130	0.4570
H	2.3560	2.4710	0.2740
H	3.6690	1.9530	1.3740
H	3.8300	1.7110	-0.3900
O	1.3500	-2.2200	-1.2750
H	1.0920	-3.1230	-1.0370
O	-0.5500	-1.4100	1.6460
H	-0.4080	-2.3590	1.7820
C	-1.6520	0.9560	-0.4350
H	-1.7140	0.6740	-1.4970
O	-1.5990	2.3730	-0.2790
H	-2.4040	2.7450	-0.6720
C	-2.8940	0.3950	0.2760
H	-3.7250	1.0950	0.0880
H	-2.7280	0.3540	1.3620
O	-3.1910	-0.8920	-0.2580
H	-4.0870	-1.1320	0.0210

Coordinates for β-Galf EO-tg-gg
Energy: -726.516851876 Hartrees

C	-1.6800	0.0460	-0.5700
C	-1.1100	1.3550	-0.0000
C	0.2150	0.9270	0.6710
C	0.2790	-0.5980	0.4200
H	-2.1030	0.1650	-1.5760
H	-1.7960	1.7640	0.7510
H	1.0340	1.4240	0.1430
H	-0.1250	-1.0860	1.3190
O	-0.5770	-0.8430	-0.7000
O	-2.6440	-0.4310	0.3320
C	-3.2750	-1.6300	-0.0930
H	-2.5560	-2.4530	-0.1890
H	-4.0190	-1.8800	0.6670
H	-3.7810	-1.4890	-1.0610
O	-0.9270	2.2510	-1.0920
H	-0.6870	3.1120	-0.7170
O	0.2200	1.2560	2.0520
H	1.1190	1.0590	2.3650
C	1.6630	-1.1950	0.1530
H	1.5460	-2.2910	0.1150
O	2.4380	-0.8060	1.2870
H	3.3040	-1.2380	1.2320
C	2.3120	-0.7970	-1.1760
H	1.5890	-1.0020	-1.9780
H	3.1880	-1.4510	-1.3370
O	2.7090	0.5670	-1.1490
H	3.1120	0.7740	-2.0050

Coordinates for β-Galf EO-tg-gt
Energy: -726.511045443 Hartrees

C	1.6870	-0.4320	0.5180
C	1.4460	1.0850	0.6050
C	0.1200	1.2950	-0.1630
C	-0.2870	-0.1230	-0.6260
H	2.0270	-0.8640	1.4680
H	2.2550	1.6220	0.0990
H	-0.6050	1.6920	0.5670
H	0.0680	-0.2250	-1.6600
O	0.4240	-1.0190	0.2370
O	2.6190	-0.6530	-0.5050
C	2.9610	-2.0230	-0.6740
H	2.0890	-2.6240	-0.9550
H	3.7070	-2.0630	-1.4710
H	3.3960	-2.4380	0.2490
O	1.3570	1.4320	1.9820
H	1.3290	2.4000	2.0360
O	0.3070	2.2010	-1.2380
H	-0.5670	2.3860	-1.6170
C	-1.7970	-0.4260	-0.5890
H	-2.0110	-1.2590	-1.2670
O	-2.5280	0.6710	-1.1460
H	-2.4350	1.4200	-0.5350
C	-2.3240	-0.8330	0.7860
H	-2.1800	-0.0040	1.5030
H	-1.7310	-1.6820	1.1500
O	-3.6980	-1.1590	0.6420
H	-4.0290	-1.4180	1.5150

Coordinates for β-Galf EO-tg-tg
Energy: -726.506784593 Hartrees

C	1.5390	-0.4620	0.4130
C	1.3070	1.0130	0.7730
C	-0.0000	1.3890	0.0180
C	-0.4050	0.0900	-0.7110
H	1.8230	-1.0710	1.2800
H	2.1480	1.6230	0.4220
H	-0.7600	1.6830	0.7560
H	-0.0830	0.1900	-1.7550
O	0.3030	-0.9620	-0.0490
O	2.5390	-0.4980	-0.5760
C	2.8670	-1.8150	-0.9980
H	2.0020	-2.3230	-1.4410
H	3.6580	-1.7170	-1.7450
H	3.2380	-2.4190	-0.1560
O	1.1620	1.0720	2.1920
H	1.1290	2.0060	2.4510
O	0.1710	2.4000	-0.9650
H	0.4570	3.2120	-0.5200
C	-1.9000	-0.2570	-0.6700
H	-2.0740	-1.1130	-1.3390
O	-2.5700	0.9090	-1.1410
H	-3.5160	0.7010	-1.1940
C	-2.4060	-0.6880	0.7200
H	-1.8020	-0.2310	1.5180
H	-3.4390	-0.3140	0.8320
O	-2.3660	-2.1060	0.7850
H	-2.6850	-2.3730	1.6600

Coordinates for β-Galf 1E-gg-gg
Energy: -726.502622783 Hartrees

C	1.3820	0.4950	-0.6520
C	1.5690	-1.0130	-0.4590
C	0.5290	-1.3570	0.6300
C	-0.4480	-0.1420	0.6250
H	1.5580	0.8200	-1.6860
H	2.5790	-1.2350	-0.0960
H	0.0020	-2.2750	0.3400
H	-0.3850	0.3320	1.6170
O	0.0260	0.7620	-0.3710
O	2.2590	1.1450	0.2370
C	2.1860	2.5610	0.1600
H	1.1850	2.9280	0.4140
H	2.9130	2.9520	0.8750
H	2.4450	2.9180	-0.8490
O	1.2920	-1.6380	-1.7030
H	1.6090	-2.5520	-1.6490
O	1.2040	-1.5240	1.8730
H	0.5560	-1.8340	2.5240
C	-1.9110	-0.5230	0.3820
H	-2.1620	-1.2240	1.2040
O	-1.9940	-1.1710	-0.8740
H	-2.8890	-1.5300	-0.9700
C	-2.9140	0.6280	0.5280
H	-2.7970	1.0580	1.5380
H	-3.9290	0.1890	0.4850
O	-2.7340	1.5940	-0.4870
H	-3.4680	2.2240	-0.4240

Coordinates for β-Galf 1E-gg-gt
Energy: -726.510449275 Hartrees

C	1.5860	0.3550	-0.6680
C	1.5910	-1.1220	-0.2630
C	0.4660	-1.2090	0.7860
C	-0.3780	0.0760	0.5400
H	1.8670	0.5140	-1.7170
H	2.5540	-1.4150	0.1670
H	-0.1260	-2.1190	0.5990
H	-0.3420	0.6780	1.4600
O	0.2450	0.7790	-0.5400
O	2.4610	1.0290	0.2000
C	2.5600	2.4210	-0.0670
H	1.5940	2.9250	0.0600
H	3.2810	2.8260	0.6460
H	2.9210	2.6040	-1.0910
O	1.2620	-1.8800	-1.4270
H	1.4590	-2.8090	-1.2340
O	1.0430	-1.2600	2.0840
H	0.3310	-1.4120	2.7240
C	-1.8400	-0.2110	0.1600
H	-2.2590	-0.8570	0.9550
O	-1.9510	-0.8270	-1.1100
H	-1.4120	-1.6340	-1.1250
C	-2.7020	1.0430	0.1230
H	-2.4450	1.6130	-0.7810
H	-2.4660	1.6660	1.0020
O	-4.0660	0.6420	0.1330
H	-4.6050	1.4270	-0.0430

Coordinates for β-Galf 1E-gg-tg
Energy: -726.512282414 Hartrees

C	1.4800	0.3670	-0.6750
C	1.6420	-1.0450	-0.1010
C	0.4500	-1.1690	0.8750
C	-0.5220	-0.0390	0.4390
H	1.8120	0.4460	-1.7180
H	2.5870	-1.1340	0.4460
H	-0.0160	-2.1540	0.7440
H	-0.6330	0.6640	1.2740
O	0.0930	0.6310	-0.6720
O	2.2020	1.2450	0.1530
C	2.1250	2.6000	-0.2590
H	1.0940	2.9730	-0.2260
H	2.7440	3.1750	0.4330
H	2.5130	2.7280	-1.2820
O	1.5600	-1.9530	-1.1910
H	1.8710	-2.8150	-0.8770
O	0.9350	-1.0030	2.2040
H	0.2000	-1.1790	2.8120
C	-1.9180	-0.5100	0.0380
H	-2.3880	-0.9230	0.9490
O	-1.7870	-1.5090	-0.9650
H	-2.6740	-1.8420	-1.1700
C	-2.8000	0.6370	-0.4610
H	-3.7460	0.2120	-0.8430
H	-2.2900	1.1380	-1.2940
O	-3.0380	1.5140	0.6340
H	-3.5340	2.2770	0.3040

Coordinates for β-Galf 1E-gt-gg
Energy: -726.507300317 Hartrees

C	-1.8180	-0.1760	-0.4680
C	-1.4410	1.2940	-0.2780
C	-0.0440	1.2040	0.3890
C	0.4430	-0.2270	0.0480
H	-2.4620	-0.3480	-1.3410
H	-2.1680	1.8120	0.3610
H	0.6020	1.9720	-0.0650
H	0.5870	-0.7730	0.9850
O	-0.6030	-0.8350	-0.7300
O	-2.4450	-0.6050	0.7150
C	-2.8050	-1.9790	0.6930
H	-1.9260	-2.6220	0.5750
H	-3.2900	-2.1910	1.6490
H	-3.5120	-2.1910	-0.1250
O	-1.3620	1.8690	-1.5790
H	-1.3110	2.8310	-1.4770
O	-0.0620	1.3280	1.8030
H	-0.3920	2.2130	2.0240
C	1.7310	-0.2900	-0.7770
H	1.5590	0.2830	-1.7040
O	1.9590	-1.6620	-1.0630
H	2.7410	-1.7200	-1.6330
C	2.9320	0.3360	-0.0590
H	2.7600	1.4160	0.0850
H	3.8090	0.2400	-0.7250
O	3.1430	-0.3310	1.1720
H	3.9780	-0.0150	1.5480

Coordinates for β-Galf 1E-gt-gt
Energy: -726.506929098 Hartrees

C	-1.8310	-0.1730	-0.5520
C	-1.4110	1.2940	-0.4340
C	-0.1200	1.2200	0.4100
C	0.3360	-0.2640	0.2690
H	-2.3500	-0.3980	-1.4930
H	-2.1740	1.8890	0.0780
H	0.6210	1.9010	-0.0320
H	0.3070	-0.7210	1.2720
O	-0.6260	-0.9090	-0.5720
O	-2.6390	-0.4730	0.5580
C	-3.1040	-1.8150	0.5690
H	-2.2740	-2.5290	0.6230
H	-3.7370	-1.9200	1.4540
H	-3.7010	-2.0360	-0.3290
O	-1.1500	1.7570	-1.7540
H	-1.0770	2.7220	-1.7180
O	-0.4160	1.5990	1.7480
H	0.4180	1.6410	2.2410
C	1.7290	-0.4590	-0.3530
H	1.7740	0.1040	-1.2910
O	1.9630	-1.8060	-0.7220
H	1.9710	-2.3430	0.0880
C	2.8230	0.0600	0.5860
H	2.5780	1.0840	0.9200
H	2.8460	-0.5780	1.4900
O	4.0600	0.0290	-0.1020
H	4.7300	0.4360	0.4680

Coordinates for β-Galf 1E-gt-tg
Energy: -726.511288859 Hartrees

C	1.7810	-0.0270	-0.5670
C	1.1160	-1.3930	-0.3890
C	-0.1470	-1.0580	0.4420
C	-0.3450	0.4620	0.2220
H	2.3410	0.0630	-1.5060
H	1.7810	-2.0930	0.1340
H	-0.9960	-1.6350	0.0600
H	-0.2520	0.9570	1.1980
O	0.7150	0.8930	-0.6460
O	2.6170	0.1850	0.5430
C	3.2700	1.4460	0.5210
H	2.5500	2.2720	0.5370
H	3.8980	1.4900	1.4140
H	3.9060	1.5490	-0.3720
O	0.7730	-1.8480	-1.6950
H	0.5260	-2.7820	-1.6300
O	0.0070	-1.2560	1.8450
H	0.1710	-2.1990	1.9960
C	-1.6700	0.8830	-0.4080
H	-1.7200	0.4720	-1.4280
O	-1.6520	2.3090	-0.4230
H	-2.4660	2.6110	-0.8560
C	-2.9050	0.4020	0.3700
H	-3.7510	1.0440	0.0740
H	-2.7480	0.5420	1.4510
O	-3.1800	-0.9600	0.0520
H	-4.0740	-1.1660	0.3650

Coordinates for β-Galf 1E-tg-gg
Energy: -726.513891867 Hartrees

C	-1.6080	0.3980	-0.5730
C	-0.8720	1.3190	0.4040
C	0.1370	0.3740	1.0910
C	0.2350	-0.8300	0.1140
H	-1.9480	0.9140	-1.4800
H	-1.5580	1.7620	1.1330
H	1.1020	0.8780	1.1870
H	-0.1160	-1.7210	0.6510
O	-0.6410	-0.5490	-0.9890
O	-2.6850	-0.1850	0.1110
C	-3.4490	-1.0750	-0.6880
H	-2.8500	-1.9280	-1.0270
H	-4.2710	-1.4310	-0.0620
H	-3.8630	-0.5610	-1.5700
O	-0.2170	2.3020	-0.3960
H	0.0890	3.0030	0.1990
O	-0.3690	-0.0040	2.3670
H	0.3320	-0.5130	2.8030
C	1.6230	-1.1490	-0.4520
H	1.4840	-1.9710	-1.1740
O	2.3850	-1.5760	0.6720
H	3.2490	-1.8820	0.3580
C	2.2860	-0.0010	-1.2260
H	1.5320	0.4400	-1.8920
H	3.0890	-0.4250	-1.8540
O	2.8260	0.9570	-0.3220
H	3.2300	1.6570	-0.8560

Coordinates for β-Galf 1E-tg-gt
Energy: -726.510651546 Hartrees

C	1.6100	-0.5520	0.5400
C	1.1620	0.8080	1.0820
C	0.1660	1.3020	0.0110
C	-0.2390	0.0080	-0.7530
H	1.8560	-1.2720	1.3320
H	2.0060	1.4990	1.1780
H	-0.6920	1.7610	0.5270
H	0.0930	0.1350	-1.7910
O	0.4800	-1.0730	-0.1380
O	2.7030	-0.3310	-0.3080
C	3.2200	-1.5200	-0.8890
H	2.4770	-2.0130	-1.5260
H	4.0810	-1.2240	-1.4930
H	3.5490	-2.2300	-0.1140
O	0.5130	0.5630	2.3270
H	0.4020	1.4170	2.7730
O	0.8090	2.2560	-0.8220
H	0.1410	2.6220	-1.4220
C	-1.7400	-0.3250	-0.7750
H	-1.8940	-1.1650	-1.4600
O	-2.4610	0.7550	-1.3670
H	-2.4140	1.5090	-0.7580
C	-2.3100	-0.7500	0.5770
H	-2.2540	0.0890	1.2920
H	-1.6840	-1.5580	0.9780
O	-3.6530	-1.1640	0.3690
H	-4.0100	-1.4340	1.2280

Coordinates for β-Galf 1E-tg-tg
Energy: -726.508668272 Hartrees

C	1.4640	-0.6230	0.4170
C	1.0700	0.6320	1.2030
C	0.1110	1.3650	0.2290
C	-0.3270	0.2620	-0.7650
H	1.6570	-1.4920	1.0600
H	1.9540	1.2380	1.4390
H	-0.7470	1.7720	0.7820
H	0.0110	0.5760	-1.7600
O	0.3330	-0.9460	-0.3630
O	2.5940	-0.3010	-0.3520
C	3.0590	-1.3810	-1.1500
H	2.3010	-1.7010	-1.8740
H	3.9430	-1.0200	-1.6800
H	3.3370	-2.2440	-0.5260
O	0.4020	0.1880	2.3830
H	0.3230	0.9450	2.9830
O	0.7520	2.3810	-0.5310
H	1.0490	3.0730	0.0800
C	-1.8350	-0.0180	-0.8230
H	-2.0160	-0.7370	-1.6350
O	-2.4340	1.2440	-1.1160
H	-3.3840	1.0960	-1.2410
C	-2.4180	-0.6550	0.4540
H	-1.7890	-0.4390	1.3280
H	-3.4090	-0.2010	0.6310
O	-2.5320	-2.0550	0.2290
H	-2.8970	-2.4540	1.0330

Coordinates for β-Galf E1-gg-gg
Energy: -726.505210204 Hartrees

C	-1.0770	0.7440	0.1330
C	-1.7610	-0.6160	0.0230
C	-0.5940	-1.5980	-0.1340
C	0.5790	-0.7010	-0.6300
H	-0.7530	0.9490	1.1650
H	-2.3320	-0.6150	-0.9170
H	-0.3600	-2.0200	0.8520
H	0.8660	-1.0100	-1.6450
O	0.0670	0.6240	-0.7210
O	-1.9100	1.7480	-0.3350
C	-1.3910	3.0560	-0.1330
H	-1.1890	3.2420	0.9320
H	-2.1570	3.7530	-0.4810
H	-0.4660	3.2110	-0.7010
O	-2.5940	-0.8540	1.1410
H	-3.0770	-1.6760	0.9660
O	-0.9780	-2.6260	-1.0450
H	-0.2850	-3.3040	-1.0440
C	1.8250	-0.8100	0.2620
H	2.1250	-1.8770	0.2250
O	1.4410	-0.4420	1.5790
H	2.1810	-0.6190	2.1800
C	3.0460	-0.0250	-0.2310
H	3.2610	-0.3380	-1.2670
H	3.9130	-0.3360	0.3820
O	2.8280	1.3680	-0.1270
H	3.6670	1.8090	-0.3270

Coordinates for β-Galf E1-gg-gt
Energy: -726.509737451 Hartrees

C	-1.2780	0.6580	0.1340
C	-1.7420	-0.7960	0.0740
C	-0.4470	-1.5910	-0.1380
C	0.5580	-0.5380	-0.6800
H	-0.9630	0.9370	1.1530
H	-2.3580	-0.9060	-0.8290
H	-0.1240	-1.9870	0.8390
H	0.8360	-0.8110	-1.7060
O	-0.1500	0.7060	-0.7470
O	-2.2790	1.4990	-0.3200
C	-1.9880	2.8830	-0.1620
H	-1.7520	3.1200	0.8850
H	-2.8870	3.4260	-0.4610
H	-1.1480	3.1890	-0.7970
O	-2.4580	-1.1350	1.2470
H	-2.8150	-2.0270	1.1190
O	-0.7110	-2.6710	-1.0250
H	0.0750	-3.2380	-1.0590
C	1.8420	-0.3960	0.1590
H	2.3960	-1.3500	0.0990
O	1.5770	-0.0520	1.5160
H	1.0070	-0.7310	1.9080
C	2.7360	0.6990	-0.4050
H	2.2780	1.6680	-0.1690
H	2.7750	0.5980	-1.5030
O	4.0290	0.5600	0.1690
H	4.5460	1.3420	-0.0730

Coordinates for β-Galf E1-gg-tg
Energy: -726.514319257 Hartrees

C	-1.3060	0.5740	0.1000
C	-1.6270	-0.9050	-0.0900
C	-0.2500	-1.5840	-0.1100
C	0.7300	-0.4280	-0.4470
H	-1.1820	0.8230	1.1650
H	-2.0700	-1.0140	-1.0910
H	-0.0440	-1.9790	0.8930
H	1.2140	-0.6140	-1.4120
O	-0.0630	0.7570	-0.5910
O	-2.2920	1.3580	-0.4810
C	-2.1480	2.7480	-0.2250
H	-2.0980	2.9500	0.8560
H	-3.0320	3.2370	-0.6400
H	-1.2490	3.1530	-0.7050
O	-2.5040	-1.3600	0.9220
H	-2.7580	-2.2670	0.6920
O	-0.2740	-2.6360	-1.0720
H	0.5530	-3.1350	-0.9910
C	1.8340	-0.2350	0.5970
H	2.4300	-1.1650	0.6260
O	1.2060	0.0060	1.8540
H	1.8960	0.0820	2.5310
C	2.7740	0.9150	0.2390
H	3.4490	1.1040	1.0930
H	2.1740	1.8190	0.0700
O	3.5060	0.5280	-0.9170
H	4.0520	1.2780	-1.1940

Coordinates for β-Galf E1-gt-gg
Energy: -726.502991095 Hartrees

C	1.6430	-0.2250	0.1780
C	1.3300	1.2630	0.0370
C	-0.2120	1.3020	-0.0230
C	-0.6140	-0.1420	-0.4080
H	1.6300	-0.5250	1.2430
H	1.7300	1.5900	-0.9340
H	-0.5700	1.5500	0.9900
H	-1.1020	-0.1420	-1.3850
O	0.6060	-0.8820	-0.5390
O	2.8770	-0.5170	-0.3830
C	3.2850	-1.8670	-0.1980
H	3.3130	-2.1290	0.8710
H	4.2930	-1.9470	-0.6120
H	2.6160	-2.5610	-0.7190
O	1.9100	1.9780	1.1170
H	1.7770	2.9260	0.9640
O	-0.7590	2.2050	-0.9750
H	-0.4860	3.1030	-0.7320
C	-1.5630	-0.8030	0.6060
H	-1.1030	-0.7430	1.6100
O	-1.7130	-2.1530	0.2010
H	-2.2770	-2.5980	0.8530
C	-2.9150	-0.0810	0.6830
H	-2.7680	0.9480	1.0470
H	-3.5360	-0.6020	1.4350
O	-3.5240	-0.1060	-0.5950
H	-4.4270	0.2340	-0.5060

Coordinates for β-Galf E1-gt-gt
Energy: -726.505878594 Hartrees

C	1.6120	-0.2980	0.2340
C	1.4320	1.2120	0.1120
C	-0.0730	1.3780	-0.1400
C	-0.5200	-0.0200	-0.6580
H	1.4020	-0.6410	1.2630
H	1.9660	1.5310	-0.7940
H	-0.5560	1.6020	0.8240
H	-0.8520	0.0690	-1.7030
O	0.6480	-0.8400	-0.6730
O	2.8890	-0.6700	-0.1480
C	3.1770	-2.0470	0.0680
H	3.0260	-2.3210	1.1230
H	4.2280	-2.1890	-0.1930
H	2.5510	-2.6890	-0.5620
O	1.9150	1.8690	1.2670
H	1.8680	2.8220	1.0960
O	-0.2700	2.4520	-1.0520
H	-1.2210	2.6320	-1.1120
C	-1.6500	-0.6620	0.1810
H	-1.4040	-0.5870	1.2470
O	-1.7720	-2.0500	-0.0630
H	-2.0400	-2.1730	-0.9880
C	-2.9710	0.0760	-0.0560
H	-2.8140	1.1640	0.0530
H	-3.2910	-0.1000	-1.1000
O	-3.9310	-0.3970	0.8710
H	-4.7350	0.1330	0.7690

Coordinates for β-Galf E1-gt-tg
Energy: -726.506721179 Hartrees

C	-1.5990	-0.1140	-0.2720
C	-1.1390	1.3080	0.0460
C	0.3650	1.1490	0.3510
C	0.5380	-0.3600	0.6390
H	-1.4740	-0.3270	-1.3500
H	-1.6580	1.6240	0.9630
H	0.9320	1.4470	-0.5380
H	0.8450	-0.4910	1.6830
O	-0.7530	-0.9610	0.5000
O	-2.9250	-0.2890	0.0990
C	-3.4600	-1.5540	-0.2680
H	-3.3630	-1.7250	-1.3510
H	-4.5200	-1.5320	-0.0030
H	-2.9630	-2.3690	0.2690
O	-1.4460	2.1530	-1.0520
H	-1.2320	3.0660	-0.8060
O	0.8260	1.8690	1.4940
H	0.6880	2.8150	1.3280
C	1.5740	-1.0760	-0.2360
H	1.2360	-1.0710	-1.2850
O	1.6460	-2.4040	0.2750
H	2.2660	-2.9040	-0.2790
C	2.9690	-0.4290	-0.1870
H	3.7020	-1.1990	-0.4780
H	3.2060	-0.1190	0.8420
O	3.0160	0.6720	-1.0920
H	3.9450	0.9170	-1.2180

Coordinates for β-Galf E1-tg-gg
Energy: -726.512305341 Hartrees

C	1.3800	-0.1640	0.0450
C	0.9200	1.2630	0.3260
C	-0.5560	1.2860	-0.0960
C	-0.7050	0.0310	-0.9990
H	1.2080	-0.8080	0.9230
H	1.4760	1.9220	-0.3570
H	-1.1810	1.1920	0.7960
H	-0.9350	0.3800	-2.0130
O	0.5730	-0.6100	-1.0560
O	2.7200	-0.1820	-0.3140
C	3.2610	-1.4860	-0.4580
H	3.1100	-2.0820	0.4560
H	4.3330	-1.3650	-0.6300
H	2.8130	-2.0160	-1.3070
O	1.1680	1.5930	1.6810
H	0.9710	2.5370	1.7830
O	-0.8340	2.5060	-0.7770
H	-1.7940	2.5320	-0.9140
C	-1.8230	-0.9560	-0.6100
H	-1.9240	-1.6740	-1.4410
O	-2.9940	-0.1470	-0.5040
H	-3.7570	-0.7280	-0.3680
C	-1.5530	-1.8020	0.6310
H	-0.6830	-2.4400	0.4170
H	-2.4200	-2.4680	0.7910
O	-1.3340	-0.9700	1.7590
H	-1.1650	-1.5320	2.5290

Coordinates for β-Galf E1-tg-gt
Energy: -726.507453464 Hartrees

C	1.4390	-0.4120	0.1210
C	1.3260	1.0730	0.4620
C	-0.0860	1.4670	0.0070
C	-0.5300	0.3170	-0.9340
H	1.1240	-1.0340	0.9790
H	2.0460	1.6100	-0.1720
H	-0.7180	1.5110	0.9090
H	-0.6440	0.7350	-1.9400
O	0.5530	-0.6220	-0.9830
O	2.7400	-0.7210	-0.2410
C	2.9690	-2.1090	-0.4520
H	2.6860	-2.6960	0.4350
H	4.0400	-2.2240	-0.6310
H	2.4110	-2.4780	-1.3200
O	1.5850	1.2730	1.8390
H	1.6120	2.2300	1.9920
O	-0.0390	2.7440	-0.6170
H	-0.9520	3.0260	-0.7840
C	-1.8750	-0.3490	-0.5720
H	-2.1660	-0.9960	-1.4070
O	-2.8980	0.6440	-0.5160
H	-2.7270	1.2020	0.2600
C	-1.8450	-1.2340	0.6720
H	-1.6230	-0.6240	1.5680
H	-1.0320	-1.9650	0.5580
O	-3.1100	-1.8680	0.7860
H	-3.0880	-2.4290	1.5760

Coordinates for β-Galf E1-tg-tg
Energy: -726.510687834 Hartrees

C	1.3530	-0.0830	0.0270
C	0.9290	1.3390	0.3910
C	-0.5680	1.3800	0.0570
C	-0.7750	0.1730	-0.8930
H	1.2050	-0.7760	0.8710
H	1.4530	2.0230	-0.2920
H	-1.1320	1.2420	0.9890
H	-1.0770	0.5560	-1.8750
O	0.4920	-0.4580	-1.0530
O	2.6760	-0.0990	-0.3900
C	3.1900	-1.4050	-0.6150
H	3.0860	-2.0320	0.2830
H	4.2510	-1.2860	-0.8490
H	2.6820	-1.8960	-1.4530
O	1.2410	1.6100	1.7470
H	1.0490	2.5480	1.9000
O	-0.9000	2.6370	-0.5210
H	-1.8670	2.6610	-0.5980
C	-1.8810	-0.8040	-0.4560
H	-1.9380	-1.6030	-1.2100
O	-3.0640	0.0040	-0.4640
H	-3.8280	-0.5680	-0.2920
C	-1.7340	-1.4760	0.9150
H	-1.5370	-0.7240	1.6930
H	-2.7060	-1.9430	1.1580
O	-0.7060	-2.4540	0.8530
H	-0.6340	-2.8630	1.7290

Coordinates for β-Galf 2E-gg-gg
Energy: -726.506604913 Hartrees

C	-1.2880	0.6490	0.2090
C	-1.7390	-0.7670	-0.1330
C	-0.4350	-1.5520	-0.0500
C	0.6130	-0.5220	-0.5380
H	-1.2350	0.7990	1.3000
H	-2.0850	-0.7640	-1.1780
H	-0.2470	-1.8050	1.0010
H	0.7880	-0.6830	-1.6130
O	0.0250	0.7630	-0.3480
O	-2.1420	1.5800	-0.3670
C	-1.8520	2.9220	0.0020
H	-1.8810	3.0460	1.0960
H	-2.6280	3.5450	-0.4500
H	-0.8680	3.2330	-0.3660
O	-2.7490	-1.2100	0.7510
H	-2.9990	-2.1020	0.4640
O	-0.5350	-2.7280	-0.8460
H	0.2640	-3.2580	-0.7060
C	1.9610	-0.6530	0.1850
H	2.2870	-1.6990	0.0140
O	1.7290	-0.4160	1.5650
H	2.5430	-0.6170	2.0500
C	3.0880	0.2140	-0.3850
H	3.2130	-0.0470	-1.4500
H	4.0250	-0.0770	0.1260
O	2.8130	1.5880	-0.2010
H	3.6060	2.0810	-0.4590

Coordinates for β-Galf 2E-gg-gt
Energy: -726.511072449 Hartrees

C	-1.4490	0.6030	0.2010
C	-1.7590	-0.8580	-0.1100
C	-0.3820	-1.5120	-0.0540
C	0.5550	-0.3940	-0.5590
H	-1.4000	0.7790	1.2890
H	-2.1270	-0.9070	-1.1460
H	-0.1800	-1.7540	1.0040
H	0.7130	-0.5520	-1.6360
O	-0.1570	0.8370	-0.3720
O	-2.4010	1.4270	-0.3790
C	-2.2730	2.7980	-0.0210
H	-2.3010	2.9260	1.0710
H	-3.1240	3.3170	-0.4660
H	-1.3400	3.2260	-0.4080
O	-2.6960	-1.3840	0.8060
H	-2.8680	-2.3010	0.5390
O	-0.3830	-2.6970	-0.8350
H	0.4670	-3.1490	-0.7140
C	1.9320	-0.3240	0.1250
H	2.4720	-1.2590	-0.1130
O	1.8470	-0.1300	1.5290
H	1.3290	-0.8520	1.9160
C	2.7510	0.8340	-0.4320
H	2.3330	1.7670	-0.0330
H	2.6450	0.8510	-1.5290
O	4.1070	0.6440	-0.0500
H	4.5920	1.4520	-0.2730

Coordinates for β-Galf 2E-gg-tg
Energy: -726.51563998 Hartrees

C	1.4260	-0.5380	0.1830
C	1.6250	0.9150	-0.2350
C	0.2370	1.5140	-0.0350
C	-0.6970	0.3320	-0.3760
H	1.5130	-0.6550	1.2760
H	1.8590	0.9220	-1.3100
H	0.1250	1.7920	1.0210
H	-1.0210	0.4100	-1.4210
O	0.0900	-0.8590	-0.2220
O	2.3430	-1.3540	-0.4660
C	2.3190	-2.7060	-0.0300
H	2.4690	-2.7750	1.0580
H	3.1440	-3.2130	-0.5370
H	1.3740	-3.1950	-0.2920
O	2.6480	1.5260	0.5260
H	2.7390	2.4320	0.1920
O	0.0930	2.6530	-0.8780
H	-0.7550	3.0770	-0.6720
C	-1.9470	0.2510	0.5010
H	-2.5370	1.1680	0.3210
O	-1.5220	0.1740	1.8580
H	-2.3110	0.1710	2.4210
C	-2.8280	-0.9480	0.1460
H	-3.6310	-1.0350	0.8990
H	-2.2150	-1.8580	0.1920
O	-3.3640	-0.7210	-1.1510
H	-3.8640	-1.5070	-1.4130

Coordinates for β-Galf 2E-gt-gg
Energy: -726.510165457 Hartrees

C	1.7420	-0.1720	0.2230
C	1.3000	1.2460	-0.1180
C	-0.2030	1.1820	0.1680
C	-0.5700	-0.2550	-0.2550
H	1.9050	-0.2870	1.3090
H	1.4700	1.3950	-1.1970
H	-0.3290	1.3080	1.2510
H	-0.9180	-0.2610	-1.2980
O	0.6530	-1.0030	-0.1960
O	2.8980	-0.5030	-0.4700
C	3.4270	-1.7780	-0.1290
H	3.6240	-1.8490	0.9520
H	4.3700	-1.8800	-0.6710
H	2.7450	-2.5850	-0.4220
O	1.9960	2.2000	0.6570
H	1.6710	3.0740	0.3880
O	-0.9790	2.2150	-0.4130
H	-1.0640	2.0260	-1.3620
C	-1.6650	-0.9100	0.5880
H	-1.3090	-0.9630	1.6330
O	-1.8640	-2.2100	0.0560
H	-2.5300	-2.6580	0.6000
C	-2.9540	-0.0810	0.5800
H	-2.7790	0.8790	1.0890
H	-3.7190	-0.6280	1.1600
O	-3.3720	0.1150	-0.7640
H	-4.2500	0.5230	-0.7470

Coordinates for β-Galf 2E-gt-gt
Energy: -726.507334194 Hartrees

C	1.7300	-0.2750	0.2890
C	1.4810	1.1880	-0.0570
C	-0.0410	1.2890	-0.0130
C	-0.4940	-0.1100	-0.4960
H	1.7440	-0.4310	1.3820
H	1.8120	1.3460	-1.0940
H	-0.3420	1.4450	1.0360
H	-0.6850	-0.0570	-1.5800
O	0.6220	-0.9830	-0.2800
O	2.9230	-0.7050	-0.2720
C	3.2930	-2.0250	0.1060
H	3.3550	-2.1210	1.2010
H	4.2800	-2.2070	-0.3250
H	2.5820	-2.7650	-0.2780
O	2.1500	2.0460	0.8440
H	1.9710	2.9540	0.5520
O	-0.4540	2.3820	-0.8220
H	-1.4100	2.5020	-0.7190
C	-1.7390	-0.6850	0.2030
H	-1.5490	-0.7320	1.2810
O	-1.9770	-2.0270	-0.1820
H	-2.1980	-2.0360	-1.1280
C	-2.9730	0.1940	-0.0330
H	-2.7560	1.2270	0.2940
H	-3.1900	0.2310	-1.1160
O	-4.0570	-0.3480	0.6980
H	-4.8080	0.2580	0.6120

Coordinates for β-Galf 2E-gt-tg
Energy: -726.508081818 Hartrees

C	1.6770	-0.1050	0.3050
C	1.2020	1.2590	-0.1860
C	-0.3230	1.0980	-0.2040
C	-0.5180	-0.3930	-0.5230
H	1.6940	-0.1440	1.4090
H	1.5640	1.3860	-1.2170
H	-0.7060	1.3330	0.7980
H	-0.6920	-0.5020	-1.6020
O	0.7200	-1.0410	-0.1920
O	2.9420	-0.3800	-0.1990
C	3.5040	-1.5900	0.2930
H	3.5480	-1.5880	1.3930
H	4.5190	-1.6480	-0.1060
H	2.9290	-2.4610	-0.0410
O	1.6940	2.2790	0.6690
H	1.3970	3.1350	0.3260
O	-1.0070	1.8710	-1.1850
H	-0.8200	2.8080	-1.0160
C	-1.6750	-1.0850	0.2020
H	-1.4150	-1.1780	1.2680
O	-1.7960	-2.3650	-0.4140
H	-2.4910	-2.8550	0.0540
C	-3.0080	-0.3260	0.1070
H	-3.8160	-1.0540	0.2870
H	-3.1450	0.0830	-0.9040
O	-3.0260	0.7010	1.0950
H	-3.9380	1.0140	1.1850

Coordinates for β-Galf 2E-tg-gg
Energy: -726.506857345 Hartrees

C	1.4430	-0.1980	0.1010
C	1.0400	1.2690	0.1930
C	-0.4780	1.2550	-0.0580
C	-0.6730	0.0070	-0.9390
H	1.3680	-0.6890	1.0850
H	1.5230	1.7970	-0.6430
H	-0.9990	1.1440	0.8980
H	-0.7490	0.3460	-1.9800
O	0.5030	-0.8030	-0.7930
O	2.7370	-0.3080	-0.3970
C	3.2440	-1.6340	-0.3950
H	3.1950	-2.0770	0.6110
H	4.2890	-1.5710	-0.7070
H	2.6930	-2.2750	-1.0950
O	1.4510	1.7950	1.4450
H	1.2250	2.7370	1.4650
O	-0.9520	2.3930	-0.7720
H	-0.8150	3.1740	-0.2130
C	-1.9090	-0.8610	-0.6270
H	-2.0280	-1.5660	-1.4690
O	-3.0130	0.0310	-0.5620
H	-3.8210	-0.4980	-0.4710
C	-1.7690	-1.7420	0.6150
H	-0.9660	-2.4690	0.4260
H	-2.7110	-2.3060	0.7370
O	-1.4970	-0.9530	1.7660
H	-1.4160	-1.5480	2.5260

Coordinates for β-Galf 2E-tg-gt
Energy: -726.508754572 Hartrees

C	1.5170	-0.4340	0.1770
C	1.4680	1.0920	0.2170
C	-0.0170	1.3890	0.0330
C	-0.5100	0.2290	-0.8530
H	1.3280	-0.8660	1.1750
H	2.0120	1.4640	-0.6640
H	-0.4750	1.3450	1.0360
H	-0.4910	0.5850	-1.8910
O	0.4600	-0.8240	-0.7150
O	2.7450	-0.8590	-0.3050
C	2.9290	-2.2680	-0.2600
H	2.7740	-2.6560	0.7590
H	3.9610	-2.4580	-0.5620
H	2.2460	-2.7820	-0.9470
O	2.0210	1.5820	1.4210
H	1.9860	2.5500	1.3730
O	-0.1890	2.6750	-0.5380
H	-1.1410	2.8650	-0.5510
C	-1.9440	-0.2620	-0.5440
H	-2.3490	-0.7570	-1.4330
O	-2.8130	0.8570	-0.3440
H	-2.5460	1.2860	0.4860
C	-2.0340	-1.2740	0.5960
H	-1.6930	-0.8090	1.5400
H	-1.3520	-2.1060	0.3760
O	-3.3850	-1.6990	0.6920
H	-3.4400	-2.3420	1.4150

Coordinates for β-Galf 2E-tg-tg
Energy: -726.505210194 Hartrees

C	1.4780	-0.2340	0.0700
C	1.1480	1.2530	0.0790
C	-0.3860	1.2560	0.0290
C	-0.7010	0.0090	-0.8160
H	1.4300	-0.6620	1.0840
H	1.5370	1.6870	-0.8540
H	-0.7410	1.1360	1.0620
H	-0.8430	0.3290	-1.8570
O	0.4610	-0.8280	-0.7380
O	2.7340	-0.4420	-0.4880
C	3.1710	-1.7930	-0.4270
H	3.1660	-2.1660	0.6080
H	4.1950	-1.8080	-0.8090
H	2.5420	-2.4460	-1.0440
O	1.7160	1.8800	1.2180
H	1.5070	2.8260	1.1770
O	-0.9740	2.4010	-0.5740
H	-0.7550	3.1730	-0.0290
C	-1.9420	-0.8300	-0.4550
H	-1.7230	-1.8450	-0.8180
O	-3.0450	-0.2600	-1.1580
H	-3.8160	-0.8300	-1.0160
C	-2.2910	-0.9070	1.0340
H	-2.6130	0.0910	1.3690
H	-3.1530	-1.5850	1.1540
O	-1.1650	-1.3770	1.7630
H	-1.4100	-1.4170	2.7000

Coordinates for β-Galf E2-gg-gg
Energy: -726.500901219 Hartrees

C	1.3070	0.5160	-0.5390
C	1.4820	-1.0060	-0.4530
C	0.4420	-1.4530	0.5970
C	-0.5300	-0.2500	0.7310
H	1.2890	0.8680	-1.5800
H	2.4870	-1.2380	-0.0850
H	-0.0830	-2.3450	0.2310
H	-0.6130	0.0070	1.7980
O	0.0590	0.8460	0.0400
O	2.3760	1.1080	0.1570
C	2.3470	2.5260	0.1300
H	2.3630	2.9050	-0.9050
H	3.2460	2.8690	0.6490
H	1.4580	2.9210	0.6340
O	1.2520	-1.5480	-1.7450
H	1.5650	-2.4650	-1.7360
O	1.1390	-1.7320	1.8100
H	0.5110	-2.1340	2.4300
C	-1.9450	-0.5490	0.2170
H	-2.2940	-1.4110	0.8200
O	-1.8400	-0.8970	-1.1510
H	-2.7060	-1.2110	-1.4530
C	-2.9760	0.5570	0.4740
H	-2.9970	0.7610	1.5600
H	-3.9700	0.1500	0.2090
O	-2.6840	1.7160	-0.2790
H	-3.4300	2.3260	-0.1780

Coordinates for β-Galf E2-gg-gt
Energy: -726.511366728 Hartrees

C	1.5130	0.3040	-0.6680
C	1.3640	-1.1900	-0.3520
C	0.4300	-1.1960	0.8680
C	-0.4050	0.0990	0.6860
H	1.6020	0.4990	-1.7460
H	2.3330	-1.6390	-0.1180
H	-0.2110	-2.0910	0.8490
H	-0.4720	0.6090	1.6570
O	0.3150	0.9230	-0.2390
O	2.6450	0.7670	0.0160
C	2.8960	2.1500	-0.1820
H	3.0300	2.3820	-1.2500
H	3.8210	2.3790	0.3530
H	2.0810	2.7670	0.2130
O	0.7440	-1.8260	-1.4760
H	0.8060	-2.7840	-1.3360
O	1.2350	-1.1820	2.0390
H	0.6540	-1.3160	2.8030
C	-1.8270	-0.1550	0.1310
H	-2.2670	-0.9720	0.7340
O	-1.8140	-0.4770	-1.2430
H	-1.2280	-1.2410	-1.3880
C	-2.7540	1.0420	0.3020
H	-2.4610	1.8140	-0.4220
H	-2.6260	1.4550	1.3180
O	-4.0890	0.5990	0.0990
H	-4.6560	1.3820	0.0580

Coordinates for β-Galf E2-gg-tg
Energy: -726.510695218 Hartrees

C	1.4300	0.3660	-0.5900
C	1.5210	-1.0850	-0.1020
C	0.3380	-1.2310	0.8810
C	-0.6050	-0.0520	0.5430
H	1.5910	0.4460	-1.6740
H	2.4610	-1.2310	0.4420
H	-0.1600	-2.1960	0.7120
H	-0.8520	0.4880	1.4660
O	0.1190	0.8320	-0.3220
O	2.3990	1.1110	0.1030
C	2.4330	2.4790	-0.2690
H	2.6170	2.5950	-1.3490
H	3.2580	2.9350	0.2850
H	1.4960	2.9890	-0.0140
O	1.4270	-1.9320	-1.2370
H	1.6890	-2.8230	-0.9600
O	0.8630	-1.1490	2.2040
H	0.1480	-1.3680	2.8210
C	-1.9270	-0.4590	-0.1110
H	-2.4840	-1.0540	0.6340
O	-1.6360	-1.2290	-1.2680
H	-2.4760	-1.5280	-1.6490
C	-2.7870	0.7530	-0.4770
H	-3.6600	0.4020	-1.0560
H	-2.1970	1.4220	-1.1170
O	-3.1940	1.3810	0.7330
H	-3.6770	2.1880	0.5050

Coordinates for β-Galf E2-gt-gg
Energy: -726.509830838 Hartrees

C	-1.7450	0.1380	0.5340
C	-1.1060	-1.2500	0.6180
C	0.1050	-1.1360	-0.3220
C	0.4620	0.3680	-0.2630
H	-2.1990	0.4520	1.4850
H	-1.8010	-2.0300	0.2930
H	0.9150	-1.7670	0.0660
H	0.6530	0.7310	-1.2780
O	-0.6950	1.0450	0.2570
O	-2.7110	0.0990	-0.4830
C	-3.3530	1.3470	-0.6970
H	-3.8510	1.7010	0.2200
H	-4.1050	1.1830	-1.4730
H	-2.6420	2.1120	-1.0290
O	-0.6790	-1.4270	1.9690
H	-0.4120	-2.3530	2.0720
O	-0.2600	-1.5550	-1.6280
H	0.5620	-1.5870	-2.1420
C	1.6790	0.7400	0.5920
H	1.4170	0.5820	1.6500
O	1.9200	2.1210	0.3330
H	2.6560	2.4060	0.8950
C	2.9100	-0.1220	0.2820
H	2.8380	-1.0760	0.8270
H	3.8050	0.3990	0.6590
O	3.0000	-0.3450	-1.1240
H	3.8490	-0.7750	-1.3070

Coordinates for β-Galf E2-gt-gt
Energy: -726.505427575 Hartrees

C	-1.7290	0.2140	0.5990
C	-1.1880	-1.2150	0.6650
C	-0.1280	-1.2340	-0.4510
C	0.3570	0.2380	-0.4950
H	-2.0240	0.5990	1.5850
H	-1.9780	-1.9490	0.4730
H	0.6840	-1.9210	-0.1720
H	0.4260	0.5620	-1.5460
O	-0.6550	1.0200	0.1500
O	-2.8210	0.2220	-0.2810
C	-3.4120	1.5020	-0.4360
H	-3.7530	1.9040	0.5310
H	-4.2740	1.3720	-1.0940
H	-2.7120	2.2170	-0.8860
O	-0.5910	-1.3750	1.9480
H	-0.3820	-2.3150	2.0630
O	-0.7540	-1.6570	-1.6550
H	-0.0640	-1.7910	-2.3220
C	1.7100	0.4890	0.2100
H	1.6890	0.0030	1.1900
O	1.9140	1.8640	0.4850
H	1.9740	2.3350	-0.3620
C	2.8670	-0.0880	-0.6100
H	2.6520	-1.1340	-0.8860
H	2.9490	0.4820	-1.5550
O	4.0560	0.0050	0.1560
H	4.7630	-0.4380	-0.3360

Coordinates for β-Galf E2-gt-tg
Energy: -726.509924161 Hartrees

C	-1.7180	0.1650	0.5290
C	-1.0180	-1.1730	0.7650
C	0.1390	-1.1530	-0.2500
C	0.4310	0.3620	-0.4180
H	-2.1320	0.5940	1.4530
H	-1.6960	-2.0130	0.5820
H	1.0030	-1.6800	0.1650
H	0.5500	0.5980	-1.4850
O	-0.7230	1.0590	0.0690
O	-2.7360	-0.0440	-0.4150
C	-3.4480	1.1370	-0.7470
H	-3.9120	1.5870	0.1460
H	-4.2330	0.8440	-1.4480
H	-2.7960	1.8820	-1.2170
O	-0.5240	-1.1520	2.1040
H	-0.2200	-2.0470	2.3160
O	-0.2910	-1.7670	-1.4570
H	0.4930	-1.8530	-2.0200
C	1.6760	0.8450	0.3380
H	1.6360	0.4480	1.3630
O	1.6420	2.2700	0.3400
H	2.4150	2.5820	0.8370
C	2.9870	0.4200	-0.3410
H	3.8220	0.8440	0.2420
H	3.0170	0.8790	-1.3410
O	3.0990	-1.0000	-0.4180
H	4.0190	-1.2170	-0.6320

Coordinates for β-Galf E2-tg-gg
Energy: -726.511217807 Hartrees

C	-1.5360	0.4170	-0.5240
C	-0.7750	1.1890	0.5590
C	0.1270	0.1130	1.2010
C	0.3040	-0.9360	0.0790
H	-1.6990	1.0180	-1.4300
H	-1.4680	1.6040	1.2980
H	1.0890	0.5430	1.4970
H	0.1300	-1.9280	0.5160
O	-0.7190	-0.6830	-0.8960
O	-2.7620	0.0080	0.0190
C	-3.5660	-0.7300	-0.8870
H	-3.7790	-0.1470	-1.7980
H	-4.5060	-0.9410	-0.3720
H	-3.0870	-1.6720	-1.1760
O	-0.0340	2.2030	-0.1140
H	0.3150	2.8050	0.5600
O	-0.5690	-0.4190	2.3240
H	0.0500	-0.9970	2.7960
C	1.6690	-1.0250	-0.6210
H	1.5170	-1.7050	-1.4760
O	2.5360	-1.6060	0.3480
H	3.3860	-1.7940	-0.0770
C	2.2260	0.2810	-1.1970
H	1.4210	0.8000	-1.7310
H	3.0110	0.0260	-1.9310
O	2.7750	1.0780	-0.1530
H	3.1120	1.8880	-0.5640

Coordinates for β-Galf E2-tg-gt
Energy: -726.509161531 Hartrees

C	1.5120	-0.6740	0.3260
C	1.0230	0.4570	1.2370
C	0.1710	1.3320	0.2960
C	-0.2860	0.3550	-0.8140
H	1.5500	-1.6430	0.8450
H	1.8690	1.0280	1.6330
H	-0.6790	1.7480	0.8590
H	-0.1060	0.8460	-1.7790
O	0.5620	-0.8000	-0.7200
O	2.7820	-0.3200	-0.1470
C	3.3550	-1.2870	-1.0150
H	3.4380	-2.2670	-0.5190
H	4.3550	-0.9270	-1.2670
H	2.7640	-1.4040	-1.9310
O	0.2440	-0.1360	2.2720
H	0.0790	0.5430	2.9430
O	0.9980	2.3750	-0.2010
H	0.4350	2.9970	-0.6880
C	-1.7690	-0.0700	-0.8240
H	-1.9080	-0.7220	-1.6940
O	-2.5870	1.0670	-1.0910
H	-2.5570	1.6450	-0.3110
C	-2.2400	-0.8640	0.3900
H	-2.2690	-0.2130	1.2800
H	-1.5140	-1.6610	0.5960
O	-3.5280	-1.3840	0.0860
H	-3.8280	-1.8890	0.8570

Coordinates for β-Galf E2-tg-tg
Energy: -726.509831501 Hartrees

C	1.4070	-0.5400	0.2540
C	0.8760	0.5310	1.2170
C	-0.0910	1.3670	0.3550
C	-0.4420	0.4400	-0.8330
H	1.4690	-1.5300	0.7260
H	1.7000	1.1570	1.5740
H	-0.9870	1.6260	0.9330
H	-0.3060	1.0120	-1.7610
O	0.4830	-0.6450	-0.8140
O	2.6750	-0.1230	-0.1830
C	3.2870	-1.0280	-1.0880
H	3.3940	-2.0290	-0.6390
H	4.2780	-0.6270	-1.3100
H	2.7110	-1.1190	-2.0170
O	0.2180	-0.1360	2.2930
H	0.0600	0.5220	2.9870
O	0.5910	2.5460	-0.0610
H	-0.0640	3.1180	-0.4900
C	-1.8830	-0.0950	-0.8500
H	-1.9970	-0.7190	-1.7490
O	-2.6900	1.0850	-0.9360
H	-3.6130	0.8090	-1.0420
C	-2.3100	-0.9510	0.3500
H	-1.9560	-0.5080	1.2890
H	-3.4160	-0.9500	0.3710
O	-1.8080	-2.2660	0.1720
H	-2.0860	-2.7920	0.9370

Coordinates for β-Galf 3E-gg-gg
Energy: -726.497415047 Hartrees

C	1.3010	0.4020	-0.5650
C	1.3940	-1.1200	-0.3690
C	0.4470	-1.3780	0.8150
C	-0.5860	-0.2240	0.7020
H	1.2130	0.6640	-1.6290
H	2.4180	-1.3810	-0.0770
H	-0.0300	-2.3670	0.7260
H	-0.8610	0.0930	1.7190
O	0.1180	0.8480	0.0900
O	2.4420	0.9900	-0.0070
C	2.4740	2.4020	-0.1460
H	2.4030	2.6990	-1.2050
H	3.4340	2.7350	0.2560
H	1.6570	2.8780	0.4090
O	1.0090	-1.7700	-1.5670
H	1.2020	-2.7140	-1.4570
O	1.2200	-1.2870	2.0040
H	0.6500	-1.5240	2.7510
C	-1.9010	-0.5590	-0.0390
H	-2.1930	-1.5800	0.2780
O	-1.6530	-0.5110	-1.4290
H	-2.4530	-0.8080	-1.8890
C	-3.0690	0.3400	0.3800
H	-3.2880	0.1470	1.4470
H	-3.9630	0.0240	-0.1890
O	-2.7600	1.6990	0.1460
H	-3.5620	2.2180	0.3020

Coordinates for β-Galf 3E-gg-gt
Energy: -726.512346616 Hartrees

C	1.4060	0.4210	-0.5490
C	1.3110	-1.1140	-0.4900
C	0.4160	-1.3750	0.7310
C	-0.4520	-0.0990	0.8100
H	1.2800	0.7950	-1.5760
H	2.3050	-1.5470	-0.3460
H	-0.1960	-2.2780	0.5820
H	-0.6310	0.1470	1.8660
O	0.3400	0.9420	0.2360
O	2.6540	0.7940	-0.0410
C	2.8740	2.1970	-0.0500
H	2.7610	2.6100	-1.0640
H	3.9000	2.3540	0.2900
H	2.1810	2.7140	0.6230
O	0.7140	-1.5840	-1.7040
H	0.7670	-2.5530	-1.7010
O	1.2760	-1.5230	1.8530
H	0.7320	-1.7650	2.6180
C	-1.8130	-0.2010	0.0780
H	-2.3020	-1.1340	0.4170
O	-1.6770	-0.1700	-1.3270
H	-1.0840	-0.8900	-1.6100
C	-2.7460	0.9420	0.4600
H	-2.3700	1.8620	-0.0100
H	-2.7200	1.0790	1.5550
O	-4.0560	0.6130	0.0200
H	-4.6090	1.4010	0.1280

Coordinates for β-Galf 3E-gg-tg
Energy: -726.506817475 Hartrees

C	1.3970	0.2770	-0.5860
C	1.4000	-1.1680	-0.0600
C	0.3270	-1.1430	1.0450
C	-0.6390	-0.0240	0.5800
H	1.4310	0.3030	-1.6850
H	2.3750	-1.3730	0.4000
H	-0.1800	-2.1180	1.1150
H	-0.9990	0.5210	1.4630
O	0.1740	0.8820	-0.1720
O	2.5010	0.9480	-0.0470
C	2.6120	2.2940	-0.4800
H	2.6540	2.3580	-1.5790
H	3.5450	2.6820	-0.0630
H	1.7720	2.9020	-0.1230
O	1.1340	-2.0480	-1.1340
H	1.2780	-2.9510	-0.8120
O	0.9820	-0.8110	2.2610
H	0.3300	-0.8690	2.9750
C	-1.9030	-0.4350	-0.1830
H	-2.4740	-1.1070	0.4820
O	-1.5490	-1.0810	-1.3930
H	-2.3680	-1.3590	-1.8320
C	-2.7810	0.7860	-0.4770
H	-3.6080	0.4720	-1.1380
H	-2.1770	1.5300	-1.0140
O	-3.2770	1.2840	0.7610
H	-3.7720	2.0970	0.5810

Coordinates for β-Galf 3E-gt-gg
Energy: -726.508551667 Hartrees

C	-1.6660	0.1710	0.4990
C	-1.0050	-1.2070	0.6450
C	0.1440	-1.1690	-0.3720
C	0.4950	0.3310	-0.4400
H	-1.9100	0.6080	1.4800
H	-1.7190	-2.0050	0.4150
H	0.9820	-1.7860	-0.0240
H	0.7950	0.6040	-1.4560
O	-0.7260	1.0200	-0.1460
O	-2.8310	0.0210	-0.2640
C	-3.5230	1.2410	-0.4820
H	-3.7850	1.7260	0.4710
H	-4.4400	0.9890	-1.0200
H	-2.9260	1.9390	-1.0810
O	-0.5080	-1.2930	1.9820
H	-0.1750	-2.1940	2.1120
O	-0.3470	-1.6550	-1.6140
H	0.4090	-1.6980	-2.2200
C	1.6090	0.8130	0.5050
H	1.2330	0.7690	1.5380
O	1.8700	2.1590	0.1180
H	2.5330	2.5210	0.7250
C	2.8720	-0.0530	0.4410
H	2.7170	-0.9640	1.0400
H	3.7010	0.5030	0.9090
O	3.1660	-0.3720	-0.9160
H	4.0330	-0.8040	-0.9430

Coordinates for β-Galf 3E-gt-gt
Energy: -726.504907271 Hartrees

C	1.6350	-0.2730	0.5320
C	1.0960	1.1540	0.7180
C	0.0870	1.3130	-0.4330
C	-0.3940	-0.1370	-0.6660
H	1.7020	-0.8040	1.4930
H	1.9060	1.8850	0.6260
H	-0.7330	1.9800	-0.1290
H	-0.5740	-0.3080	-1.7390
O	0.7040	-0.9660	-0.2910
O	2.8940	-0.1960	-0.0720
C	3.5020	-1.4620	-0.2780
H	3.5970	-2.0160	0.6690
H	4.4990	-1.2670	-0.6810
H	2.9320	-2.0700	-0.9890
O	0.4640	1.2030	1.9930
H	0.2110	2.1230	2.1650
O	0.7920	1.8470	-1.5460
H	0.1520	2.0250	-2.2520
C	-1.6670	-0.5210	0.1320
H	-1.5780	-0.1390	1.1530
O	-1.7940	-1.9240	0.2740
H	-1.9140	-2.3080	-0.6100
C	-2.9120	0.0900	-0.5170
H	-2.7490	1.1640	-0.7090
H	-3.0700	-0.3910	-1.5010
O	-4.0200	-0.1150	0.3430
H	-4.7820	0.3470	-0.0370

Coordinates for β-Galf 3E-gt-tg
Energy: -726.508794749 Hartrees

C	1.5950	0.0910	-0.5720
C	0.8320	-1.2420	-0.5830
C	-0.1580	-1.0960	0.5840
C	-0.4180	0.4240	0.6130
H	1.7370	0.4810	-1.5920
H	1.5140	-2.0830	-0.4230
H	-1.0710	-1.6730	0.4040
H	-0.5800	0.7700	1.6440
O	0.7960	1.0220	0.1500
O	2.8350	-0.1090	0.0450
C	3.6250	1.0670	0.1200
H	3.7950	1.4980	-0.8800
H	4.5860	0.7710	0.5490
H	3.1560	1.8260	0.7570
O	0.1590	-1.3170	-1.8380
H	-0.2550	-2.1920	-1.9000
O	0.5130	-1.5410	1.7610
H	-0.1280	-1.5260	2.4880
C	-1.6040	0.9180	-0.2320
H	-1.4410	0.6280	-1.2790
O	-1.6130	2.3370	-0.0770
H	-2.3250	2.6910	-0.6320
C	-2.9710	0.3790	0.2190
H	-3.7440	1.0030	-0.2590
H	-3.0780	0.5100	1.3080
O	-3.1280	-0.9840	-0.1660
H	-4.0640	-1.2150	-0.0770

Coordinates for β-Galf 3E-tg-gg
Energy: -726.50960361 Hartrees

C	-1.5030	0.2170	-0.5050
C	-0.7950	1.1890	0.4540
C	0.2360	0.3250	1.2090
C	0.3790	-0.9480	0.3470
H	-1.5270	0.6140	-1.5310
H	-1.5170	1.6100	1.1610
H	1.1910	0.8530	1.3030
H	0.3430	-1.8230	1.0070
O	-0.7630	-0.9980	-0.5130
O	-2.8080	0.0110	-0.0420
C	-3.5740	-0.8530	-0.8670
H	-3.6190	-0.4800	-1.9020
H	-4.5840	-0.8720	-0.4500
H	-3.1630	-1.8700	-0.8750
O	-0.2010	2.1960	-0.3630
H	0.1370	2.8880	0.2260
O	-0.3220	0.0340	2.4900
H	0.3540	-0.4420	2.9960
C	1.6690	-1.1020	-0.4800
H	1.4860	-1.9550	-1.1530
O	2.6790	-1.4060	0.4760
H	3.4950	-1.6250	-0.0000
C	2.0490	0.0880	-1.3700
H	1.1510	0.4440	-1.8940
H	2.7600	-0.2680	-2.1360
O	2.6470	1.1110	-0.5840
H	2.8690	1.8380	-1.1840

Coordinates for β-Galf 3E-tg-gt
Energy: -726.507931779 Hartrees

C	1.4610	-0.5910	0.2780
C	1.0280	0.6240	1.1150
C	0.0900	1.4230	0.1900
C	-0.3480	0.4080	-0.8910
H	1.3410	-1.5290	0.8410
H	1.9020	1.2310	1.3720
H	-0.7630	1.8060	0.7720
H	-0.2850	0.9020	-1.8690
O	0.6170	-0.6480	-0.8670
O	2.7990	-0.4150	-0.0870
C	3.3290	-1.4940	-0.8450
H	3.2320	-2.4460	-0.3010
H	4.3880	-1.2760	-0.9990
H	2.8280	-1.5850	-1.8150
O	0.3650	0.1270	2.2750
H	0.2070	0.8780	2.8680
O	0.8440	2.4990	-0.3540
H	0.2430	3.0530	-0.8760
C	-1.7850	-0.1500	-0.7920
H	-1.9280	-0.8130	-1.6520
O	-2.7220	0.9060	-0.9920
H	-2.6880	1.4870	-0.2150
C	-2.0910	-0.9800	0.4510
H	-2.0820	-0.3410	1.3490
H	-1.2960	-1.7280	0.5800
O	-3.3600	-1.5890	0.2570
H	-3.5530	-2.1170	1.0470

Coordinates for β-Galf 3E-tg-tg
Energy: -726.509406138 Hartrees

C	1.3720	-0.4210	0.1800
C	0.8070	0.6310	1.1480
C	-0.2490	1.3990	0.3280
C	-0.5400	0.4800	-0.8780
H	1.3590	-1.4260	0.6260
H	1.6060	1.3170	1.4490
H	-1.1540	1.5720	0.9240
H	-0.5520	1.0880	-1.7920
O	0.5360	-0.4480	-0.9680
O	2.6810	-0.0500	-0.1520
C	3.3290	-0.9730	-1.0140
H	3.3490	-1.9820	-0.5740
H	4.3540	-0.6170	-1.1410
H	2.8350	-1.0240	-1.9920
O	0.2580	-0.0520	2.2740
H	0.0390	0.6190	2.9380
O	0.3330	2.6380	-0.0670
H	-0.3570	3.1520	-0.5150
C	-1.8880	-0.2610	-0.8300
H	-1.9360	-0.9070	-1.7190
O	-2.8680	0.7800	-0.8910
H	-3.7420	0.3660	-0.9570
C	-2.1440	-1.1450	0.3970
H	-1.9350	-0.5910	1.3200
H	-3.2210	-1.4000	0.3940
O	-1.3460	-2.3150	0.3020
H	-1.5260	-2.8550	1.0860

Coordinates for β-Galf E3-gg-gg
Energy: -726.508257729 Hartrees

C	-1.3990	0.6180	0.3110
C	-1.7450	-0.8040	-0.1330
C	-0.4040	-1.5210	-0.0310
C	0.5660	-0.4070	-0.4670
H	-1.5860	0.7640	1.3860
H	-2.0430	-0.7670	-1.1920
H	-0.2130	-1.7800	1.0190
H	0.5700	-0.3640	-1.5700
O	0.0030	0.7820	0.0820
O	-2.1490	1.5280	-0.4360
C	-1.9670	2.8780	-0.0290
H	-2.2330	3.0120	1.0310
H	-2.6360	3.4840	-0.6450
H	-0.9310	3.2030	-0.1790
O	-2.7720	-1.3450	0.6750
H	-2.9470	-2.2390	0.3390
O	-0.4160	-2.6780	-0.8570
H	0.4200	-3.1520	-0.7260
C	2.0120	-0.6150	-0.0100
H	2.3220	-1.5750	-0.4720
O	2.0190	-0.7090	1.4040
H	2.9100	-0.9690	1.6850
C	3.0090	0.4200	-0.5440
H	2.9510	0.4140	-1.6460
H	4.0250	0.0730	-0.2760
O	2.7490	1.6980	-0.0020
H	3.4760	2.2820	-0.2660

Coordinates for β-Galf E3-gg-gt
Energy: -726.512930388 Hartrees

C	-1.5600	0.5740	0.3030
C	-1.7720	-0.8710	-0.1540
C	-0.3730	-1.4730	-0.0520
C	0.5080	-0.2770	-0.4450
H	-1.7760	0.6970	1.3750
H	-2.0630	-0.8520	-1.2150
H	-0.2060	-1.7480	1.0030
H	0.5250	-0.2240	-1.5470
O	-0.1710	0.8600	0.0990
O	-2.3760	1.4140	-0.4530
C	-2.3610	2.7680	-0.0220
H	-2.6560	2.8510	1.0350
H	-3.0870	3.3010	-0.6390
H	-1.3700	3.2180	-0.1520
O	-2.7500	-1.5080	0.6430
H	-2.8480	-2.4100	0.2980
O	-0.2790	-2.6080	-0.8970
H	0.5920	-3.0170	-0.7740
C	1.9620	-0.3050	0.0460
H	2.4610	-1.1520	-0.4620
O	2.0850	-0.4180	1.4560
H	1.6240	-1.2180	1.7500
C	2.7000	0.9640	-0.3600
H	2.3600	1.7780	0.2940
H	2.4290	1.2200	-1.3980
O	4.0960	0.7240	-0.2380
H	4.5520	1.5710	-0.3480

Coordinates for β-Galf E3-gg-tg
Energy: -726.516992037 Hartrees

C	-1.4980	0.5200	0.3180
C	-1.6540	-0.8820	-0.2710
C	-0.2690	-1.4910	-0.0770
C	0.6330	-0.2680	-0.3070
H	-1.8130	0.5550	1.3720
H	-1.8420	-0.7790	-1.3500
H	-0.1700	-1.8340	0.9610
H	0.7690	-0.1130	-1.3870
O	-0.1000	0.8250	0.2650
O	-2.2500	1.4210	-0.4380
C	-2.2800	2.7340	0.1010
H	-2.6660	2.7320	1.1320
H	-2.9540	3.3180	-0.5310
H	-1.2840	3.1930	0.0940
O	-2.7040	-1.5780	0.3730
H	-2.7590	-2.4490	-0.0500
O	-0.0900	-2.5610	-0.9950
H	0.7680	-2.9750	-0.8130
C	2.0200	-0.3480	0.3250
H	2.5670	-1.1510	-0.2020
O	1.8680	-0.6550	1.7060
H	2.7540	-0.7590	2.0870
C	2.8150	0.9480	0.1460
H	3.7470	0.8730	0.7330
H	2.2250	1.7820	0.5470
O	3.0930	1.0970	-1.2400
H	3.5320	1.9510	-1.3700

Coordinates for β-Galf E3-gt-gg
Energy: -726.506944808 Hartrees

C	-1.7960	-0.1880	-0.2780
C	-1.3520	1.2200	0.1120
C	0.1410	1.2160	-0.2380
C	0.5360	-0.2240	0.1110
H	-2.2140	-0.2150	-1.2970
H	-1.4540	1.3190	1.2030
H	0.2360	1.3710	-1.3260
H	0.7230	-0.3050	1.1900
O	-0.6200	-0.9950	-0.2590
O	-2.7480	-0.6340	0.6400
C	-3.2880	-1.9100	0.3240
H	-3.7490	-1.9100	-0.6760
H	-4.0560	-2.1190	1.0720
H	-2.5170	-2.6890	0.3620
O	-2.1350	2.1890	-0.5690
H	-1.8340	3.0680	-0.2900
O	0.9280	2.1580	0.4760
H	0.6500	3.0460	0.2020
C	1.7470	-0.7790	-0.6390
H	1.5270	-0.7110	-1.7190
O	1.8840	-2.1330	-0.2360
H	2.6140	-2.5210	-0.7430
C	3.0250	0.0240	-0.3760
H	2.8890	1.0580	-0.7290
H	3.8360	-0.4270	-0.9770
O	3.3240	-0.0230	1.0080
H	4.1980	0.3730	1.1400

Coordinates for β-Galf E3-gt-gt
Energy: -726.509178796 Hartrees

C	-1.8120	-0.2520	-0.3470
C	-1.5060	1.1800	0.0820
C	0.0100	1.2780	-0.0780
C	0.4520	-0.1450	0.3140
H	-2.1000	-0.3090	-1.4080
H	-1.7440	1.2720	1.1520
H	0.2410	1.4660	-1.1390
H	0.4950	-0.2010	1.4170
O	-0.5940	-0.9870	-0.1810
O	-2.8330	-0.7610	0.4560
C	-3.2740	-2.0550	0.0660
H	-3.6260	-2.0560	-0.9770
H	-4.1060	-2.3140	0.7250
H	-2.4750	-2.7990	0.1750
O	-2.2410	2.1050	-0.6940
H	-2.0170	2.9890	-0.3610
O	0.4800	2.3350	0.7470
H	1.4320	2.4460	0.6030
C	1.7810	-0.6580	-0.2620
H	1.7020	-0.6680	-1.3550
O	2.0050	-2.0100	0.0970
H	2.1270	-2.0510	1.0590
C	2.9660	0.2300	0.1320
H	2.7930	1.2560	-0.2410
H	3.0350	0.2880	1.2340
O	4.1410	-0.3160	-0.4350
H	4.8720	0.2940	-0.2540

Coordinates for β-Galf E3-gt-tg
Energy: -726.509696275 Hartrees

C	-1.7450	-0.0630	-0.3740
C	-1.2160	1.2660	0.1660
C	0.3080	1.0880	0.1340
C	0.4680	-0.4170	0.3780
H	-1.9880	0.0020	-1.4460
H	-1.5370	1.3550	1.2150
H	0.6770	1.3560	-0.8660
H	0.4760	-0.5980	1.4630
O	-0.6940	-1.0130	-0.2160
O	-2.8840	-0.4230	0.3520
C	-3.5110	-1.6060	-0.1240
H	-3.7950	-1.5060	-1.1830
H	-4.4130	-1.7450	0.4770
H	-2.8570	-2.4780	-0.0100
O	-1.7210	2.3350	-0.6220
H	-1.3900	3.1680	-0.2540
O	1.0140	1.8060	1.1390
H	0.8300	2.7510	1.0240
C	1.7080	-1.0840	-0.2170
H	1.5660	-1.1530	-1.3060
O	1.7680	-2.3780	0.3790
H	2.5110	-2.8550	-0.0210
C	3.0160	-0.3190	0.0350
H	3.8450	-1.0390	-0.0790
H	3.0480	0.0690	1.0620
O	3.1210	0.7260	-0.9270
H	4.0330	1.0520	-0.9170

Coordinates for β-Galf E3-tg-gg
Energy: -726.507307332 Hartrees

C	1.6000	-0.2290	0.2730
C	1.1930	1.2280	0.0610
C	-0.3320	1.1650	-0.1300
C	-0.5150	-0.2090	-0.7890
H	1.7040	-0.4710	1.3420
H	1.6470	1.5710	-0.8800
H	-0.8180	1.1810	0.8520
H	-0.3910	-0.0800	-1.8740
O	0.5390	-1.0270	-0.2570
O	2.8050	-0.4690	-0.3910
C	3.3340	-1.7670	-0.1650
H	3.4850	-1.9540	0.9100
H	4.3000	-1.8060	-0.6730
H	2.6760	-2.5450	-0.5720
O	1.6370	2.0070	1.1630
H	1.3910	2.9300	0.9970
O	-0.8500	2.1800	-0.9800
H	-0.7190	3.0330	-0.5390
C	-1.8340	-0.9680	-0.5700
H	-1.7220	-1.9180	-1.1230
O	-2.8570	-0.1670	-1.1370
H	-3.6790	-0.6800	-1.1260
C	-2.1270	-1.3800	0.8750
H	-1.2670	-1.9570	1.2450
H	-3.0000	-2.0560	0.8610
O	-2.3930	-0.2410	1.6850
H	-2.5700	-0.5560	2.5840

Coordinates for β-Galf E3-tg-gt
Energy: -726.508593754 Hartrees

C	1.6150	-0.4420	0.2670
C	1.4780	1.0830	0.2790
C	-0.0250	1.3310	0.0670
C	-0.4610	0.0960	-0.7310
H	1.6740	-0.8520	1.2870
H	2.0200	1.4740	-0.5950
H	-0.5230	1.3600	1.0470
H	-0.3110	0.3340	-1.7980
O	0.4300	-0.9580	-0.3450
O	2.7590	-0.7860	-0.4540
C	3.0530	-2.1770	-0.4310
H	3.1680	-2.5410	0.6010
H	3.9990	-2.3050	-0.9630
H	2.2710	-2.7590	-0.9310
O	2.0150	1.5890	1.4920
H	1.9480	2.5560	1.4750
O	-0.3290	2.4950	-0.6920
H	-0.0490	3.2740	-0.1880
C	-1.9280	-0.3450	-0.5440
H	-2.1610	-1.0990	-1.3130
O	-2.7860	0.7820	-0.6590
H	-2.6170	1.2120	-1.5130
C	-2.2140	-0.9990	0.8010
H	-2.1920	-0.2290	1.5890
H	-1.4240	-1.7330	1.0060
O	-3.4930	-1.6160	0.7180
H	-3.6730	-2.0310	1.5740

Coordinates for β-Galf E3-tg-tg
Energy: -726.503580078 Hartrees

C	1.5110	-0.3350	0.2050
C	1.3360	1.1820	0.2630
C	-0.1810	1.3950	0.1100
C	-0.6010	0.1770	-0.7280
H	1.6080	-0.7740	1.2100
H	1.8330	1.6120	-0.6190
H	-0.6370	1.3560	1.1120
H	-0.5070	0.4560	-1.7870
O	0.3280	-0.8580	-0.3930
O	2.6470	-0.6290	-0.5540
C	2.9620	-2.0140	-0.5920
H	3.1130	-2.4150	0.4220
H	3.8930	-2.1080	-1.1560
H	2.1720	-2.5900	-1.0880
O	1.9000	1.6800	1.4680
H	1.8050	2.6450	1.4710
O	-0.5350	2.5920	-0.5620
H	-0.2510	3.3410	-0.0160
C	-2.0200	-0.3690	-0.5060
H	-2.1790	-1.1780	-1.2360
O	-2.8950	0.7270	-0.7540
H	-3.8040	0.3920	-0.7140
C	-2.2740	-0.9920	0.8790
H	-1.6790	-0.4880	1.6560
H	-3.3360	-0.8220	1.1270
O	-1.9810	-2.3790	0.8120
H	-2.1450	-2.7600	1.6880

Coordinates for β-Galf 4E-gg-gg
Energy: -726.509031416 Hartrees

C	1.4040	0.7240	-0.4140
C	1.8770	-0.6770	0.0160
C	0.5700	-1.4690	0.1410
C	-0.4520	-0.3450	0.3980
H	1.7740	1.0040	-1.4080
H	2.3390	-0.6020	1.0100
H	0.3430	-1.9280	-0.8300
H	-0.3530	-0.0090	1.4440
O	-0.0140	0.6700	-0.5040
O	1.8330	1.6450	0.5570
C	1.4740	2.9860	0.2480
H	1.9280	3.3090	-0.7020
H	1.8600	3.6090	1.0590
H	0.3860	3.0990	0.1770
O	2.7920	-1.1910	-0.9390
H	3.1020	-2.0450	-0.6000
O	0.6860	-2.4440	1.1690
H	-0.0880	-3.0260	1.1170
C	-1.9120	-0.7280	0.1690
H	-2.1040	-1.5530	0.8850
O	-2.0490	-1.1810	-1.1680
H	-2.9420	-1.5440	-1.2720
C	-2.9240	0.3620	0.5400
H	-2.7830	0.6080	1.6070
H	-3.9350	-0.0760	0.4440
O	-2.7760	1.4940	-0.2920
H	-3.5140	2.0940	-0.1030

Coordinates for β-Galf 4E-gg-gt
Energy: -726.51371834 Hartrees

C	-1.5990	0.6150	0.4080
C	-1.8730	-0.8210	-0.0720
C	-0.4740	-1.4420	-0.1910
C	0.4190	-0.2010	-0.3580
H	-2.0220	0.8100	1.4020
H	-2.3170	-0.7740	-1.0760
H	-0.2550	-1.9330	0.7710
H	0.3360	0.1380	-1.4030
O	-0.1850	0.7440	0.5320
O	-2.1320	1.4980	-0.5430
C	-2.0300	2.8650	-0.1670
H	-2.5540	3.0550	0.7820
H	-2.5070	3.4440	-0.9610
H	-0.9840	3.1760	-0.0630
O	-2.7340	-1.4780	0.8430
H	-2.9310	-2.3520	0.4710
O	-0.4450	-2.3690	-1.2650
H	0.3890	-2.8610	-1.2270
C	1.9050	-0.3670	-0.0250
H	2.3240	-1.0740	-0.7650
O	2.1460	-0.8170	1.3000
H	1.6800	-1.6560	1.4380
C	2.6560	0.9490	-0.1860
H	2.4130	1.5860	0.6750
H	2.3030	1.4540	-1.1000
O	4.0450	0.6600	-0.2640
H	4.5260	1.4990	-0.2130

Coordinates for β-Galf 4E-gg-tg
Energy: -726.517596597 Hartrees

C	1.4890	0.6120	-0.4410
C	1.8080	-0.7620	0.1770
C	0.4420	-1.4550	0.2450
C	-0.5230	-0.2570	0.2640
H	1.9750	0.7540	-1.4150
H	2.1740	-0.6060	1.2010
H	0.2890	-2.0150	-0.6850
H	-0.5410	0.1900	1.2670
O	0.0850	0.6410	-0.6760
O	1.8970	1.6020	0.4680
C	1.7340	2.9240	-0.0240
H	2.3080	3.0760	-0.9520
H	2.1170	3.5960	0.7470
H	0.6800	3.1520	-0.2190
O	2.7730	-1.4320	-0.6190
H	2.9880	-2.2600	-0.1620
O	0.3860	-2.3050	1.3830
H	-0.4180	-2.8430	1.3120
C	-1.9620	-0.5510	-0.1420
H	-2.4000	-1.1630	0.6670
O	-1.9520	-1.2670	-1.3730
H	-2.8680	-1.4990	-1.5890
C	-2.8020	0.7230	-0.2690
H	-3.7890	0.4510	-0.6850
H	-2.3090	1.4020	-0.9760
O	-2.9310	1.2900	1.0280
H	-3.3990	2.1330	0.9430

Coordinates for β-Galf 4E-gt-gg
Energy: -726.508969612 Hartrees

C	-1.8330	-0.2290	-0.3040
C	-1.4770	1.2220	0.0620
C	0.0480	1.2910	-0.1720
C	0.4650	-0.1830	-0.0420
H	-2.5110	-0.2880	-1.1660
H	-1.6800	1.3750	1.1300
H	0.2120	1.6190	-1.2120
H	0.5290	-0.4620	1.0170
O	-0.6230	-0.8600	-0.6890
O	-2.4150	-0.8250	0.8260
C	-2.8140	-2.1730	0.6090
H	-3.5540	-2.2400	-0.2040
H	-3.2710	-2.5170	1.5390
H	-1.9550	-2.8070	0.3620
O	-2.2460	2.1070	-0.7450
H	-2.0530	3.0150	-0.4670
O	0.7610	2.1100	0.7440
H	0.4520	3.0230	0.6360
C	1.7600	-0.5780	-0.7460
H	1.6500	-0.3140	-1.8130
O	1.8920	-1.9840	-0.5860
H	2.6800	-2.2650	-1.0760
C	2.9800	0.1730	-0.2070
H	2.8520	1.2520	-0.3780
H	3.8610	-0.1550	-0.7890
O	3.1350	-0.1250	1.1700
H	3.9800	0.2460	1.4640

Coordinates for β-Galf 4E-gt-gt
Energy: -726.510530877 Hartrees

C	-1.8660	-0.2580	-0.3880
C	-1.5940	1.2000	0.0140
C	-0.0620	1.3170	-0.0300
C	0.3780	-0.1520	0.1490
H	-2.4300	-0.3360	-1.3270
H	-1.9190	1.3420	1.0540
H	0.2280	1.6620	-1.0340
H	0.2910	-0.4140	1.2180
O	-0.5970	-0.8590	-0.6230
O	-2.5600	-0.8770	0.6630
C	-2.9350	-2.2180	0.3770
H	-3.5880	-2.2660	-0.5070
H	-3.4840	-2.5820	1.2480
H	-2.0560	-2.8510	0.2040
O	-2.2760	2.0790	-0.8640
H	-2.1300	2.9790	-0.5320
O	0.3540	2.2300	0.9770
H	1.2940	2.4250	0.8490
C	1.7640	-0.5620	-0.3630
H	1.7960	-0.3940	-1.4450
O	1.9720	-1.9560	-0.2070
H	1.9980	-2.1500	0.7450
C	2.8900	0.2490	0.2870
H	2.7420	1.3210	0.0670
H	2.8460	0.1310	1.3850
O	4.1240	-0.2030	-0.2380
H	4.8240	0.3680	0.1120

Coordinates for β-Galf 4E-gt-tg
Energy: -726.511479992 Hartrees

C	-1.8000	-0.0020	-0.4280
C	-1.2410	1.3410	0.0730
C	0.2830	1.1050	0.1590
C	0.3910	-0.4240	0.2230
H	-2.2860	0.0900	-1.4080
H	-1.6350	1.5290	1.0810
H	0.7490	1.4770	-0.7630
H	0.2540	-0.7440	1.2670
O	-0.6960	-0.8760	-0.5940
O	-2.7130	-0.4700	0.5330
C	-3.3380	-1.6920	0.1660
H	-3.8900	-1.5860	-0.7810
H	-4.0420	-1.9360	0.9650
H	-2.6060	-2.5010	0.0610
O	-1.6340	2.3620	-0.8390
H	-1.3280	3.2130	-0.4920
O	0.9080	1.6630	1.3090
H	0.7630	2.6210	1.3020
C	1.6750	-1.0560	-0.3070
H	1.6540	-0.9930	-1.4050
O	1.6450	-2.4130	0.1330
H	2.4190	-2.8620	-0.2410
C	2.9620	-0.3680	0.1730
H	3.7840	-1.0940	0.0570
H	2.8900	-0.1080	1.2380
O	3.1870	0.7830	-0.6360
H	4.0980	1.0760	-0.4910

Coordinates for β-Galf 4E-tg-gg
Energy: -726.508480766 Hartrees

C	1.6740	-0.1420	0.4340
C	1.2150	1.2680	0.0360
C	-0.2790	1.1030	-0.3340
C	-0.3960	-0.4050	-0.6050
H	1.9890	-0.1960	1.4850
H	1.7730	1.5780	-0.8570
H	-0.8880	1.3740	0.5360
H	-0.1080	-0.5850	-1.6510
O	0.5490	-1.0000	0.2960
O	2.7290	-0.5120	-0.4160
C	3.2960	-1.7740	-0.0970
H	3.6850	-1.7860	0.9330
H	4.1240	-1.9310	-0.7930
H	2.5650	-2.5840	-0.2090
O	1.4610	2.1450	1.1330
H	1.2310	3.0440	0.8560
O	-0.6730	1.8220	-1.4940
H	-0.5810	2.7680	-1.3070
C	-1.7400	-1.1080	-0.3690
H	-1.5490	-2.1780	-0.5680
O	-2.6490	-0.5690	-1.3150
H	-3.4680	-1.0860	-1.2680
C	-2.2680	-1.0540	1.0670
H	-1.4750	-1.4160	1.7370
H	-3.1150	-1.7590	1.1420
O	-2.6890	0.2630	1.4030
H	-3.0110	0.2430	2.3160

Coordinates for β-Galf 4E-tg-gt
Energy: -726.510141622 Hartrees

C	1.6740	-0.4490	0.3850
C	1.5130	1.0810	0.3790
C	0.0330	1.3170	-0.0030
C	-0.3810	-0.0210	-0.6310
H	1.9310	-0.8350	1.3800
H	2.1560	1.4940	-0.4100
H	-0.5400	1.5110	0.9150
H	-0.1030	0.0270	-1.6970
O	0.4100	-1.0050	0.0410
O	2.6680	-0.7810	-0.5470
C	2.9740	-2.1690	-0.5790
H	3.3170	-2.5220	0.4050
H	3.7800	-2.2950	-1.3050
H	2.1060	-2.7640	-0.8870
O	1.8810	1.5710	1.6630
H	1.8400	2.5400	1.6430
O	-0.1700	2.3460	-0.9640
H	0.1120	3.1900	-0.5810
C	-1.8750	-0.3880	-0.5380
H	-2.0580	-1.2520	-1.1970
O	-2.6700	0.7250	-0.9260
H	-2.3950	1.0050	-1.8130
C	-2.3280	-0.8060	0.8550
H	-2.3640	0.0830	1.5040
H	-1.5930	-1.5090	1.2670
O	-3.6130	-1.4040	0.7270
H	-3.8990	-1.6710	1.6130

Coordinates for β-Galf 4E-tg-tg
Energy: -726.505095322 Hartrees

C	1.5640	-0.4150	0.3110
C	1.4250	1.1120	0.4070
C	-0.0590	1.3910	0.0660
C	-0.4900	0.1040	-0.6590
H	1.8320	-0.8700	1.2740
H	2.0570	1.5700	-0.3660
H	-0.6100	1.5010	1.0120
H	-0.2330	0.2190	-1.7220
O	0.2890	-0.9260	-0.0460
O	2.5400	-0.6990	-0.6570
C	2.8110	-2.0870	-0.7940
H	3.1690	-2.5160	0.1550
H	3.5960	-2.1810	-1.5480
H	1.9210	-2.6390	-1.1180
O	1.8200	1.5210	1.7120
H	1.7930	2.4890	1.7470
O	-0.2610	2.5090	-0.7830
H	0.0370	3.3040	-0.3150
C	-1.9660	-0.3050	-0.5570
H	-2.1110	-1.1840	-1.2060
O	-2.7090	0.8120	-1.0320
H	-3.6420	0.5490	-1.0630
C	-2.4190	-0.7420	0.8490
H	-1.8230	-0.2490	1.6310
H	-3.4640	-0.4100	0.9800
O	-2.3180	-2.1560	0.9290
H	-2.6050	-2.4250	1.8150

Coordinates for β-Galf E4-gg-gg
Energy: -726.50101748 Hartrees

C	-1.2000	0.5910	0.3550
C	-1.5080	-0.9150	0.3970
C	-0.4230	-1.5780	-0.4780
C	0.5970	-0.4450	-0.7670
H	-0.9760	0.9680	1.3640
H	-2.4800	-1.0840	-0.0830
H	0.0460	-2.4040	0.0730
H	0.8440	-0.4380	-1.8390
O	-0.0510	0.7780	-0.4620
O	-2.2990	1.2640	-0.1840
C	-2.1540	2.6770	-0.1820
H	-1.9610	3.0550	0.8340
H	-3.0990	3.0890	-0.5450
H	-1.3370	2.9970	-0.8400
O	-1.5160	-1.3340	1.7520
H	-1.8230	-2.2530	1.7690
O	-1.0640	-2.0530	-1.6610
H	-0.3950	-2.4950	-2.2060
C	1.9120	-0.6220	0.0100
H	2.3120	-1.6080	-0.3000
O	1.5810	-0.6200	1.3880
H	2.3720	-0.8490	1.8990
C	3.0130	0.3860	-0.3380
H	3.2050	0.3250	-1.4240
H	3.9400	0.0510	0.1660
O	2.6590	1.6920	0.0680
H	3.4360	2.2570	-0.0580

Coordinates for β-Galf E4-gg-gt
Energy: -726.512359428 Hartrees

C	-1.2790	0.5490	0.3340
C	-1.3690	-0.9750	0.5660
C	-0.4080	-1.5870	-0.4680
C	0.4930	-0.3950	-0.8570
H	-0.9080	1.0590	1.2340
H	-2.3910	-1.3200	0.3880
H	0.1690	-2.4150	-0.0260
H	0.7840	-0.4760	-1.9130
O	-0.3500	0.7490	-0.7350
O	-2.5380	1.0270	-0.0220
C	-2.5880	2.4390	-0.1770
H	-2.2370	2.9500	0.7330
H	-3.6350	2.6960	-0.3520
H	-1.9830	2.7700	-1.0280
O	-0.9570	-1.2430	1.9120
H	-1.0870	-2.1900	2.0780
O	-1.2040	-2.0460	-1.5530
H	-0.6170	-2.4600	-2.2040
C	1.7720	-0.2670	0.0010
H	2.3220	-1.2230	-0.0790
O	1.4950	0.0550	1.3520
H	0.9040	-0.6170	1.7420
C	2.6940	0.8220	-0.5340
H	2.2350	1.7970	-0.3150
H	2.7740	0.7200	-1.6300
O	3.9630	0.6750	0.0860
H	4.4930	1.4540	-0.1400

Coordinates for β-Galf E4-gg-tg
Energy: -726.510796545 Hartrees

C	1.3620	0.4960	-0.3550
C	1.5220	-1.0150	-0.1260
C	0.2440	-1.4570	0.6190
C	-0.6890	-0.2260	0.5750
H	1.3550	0.7260	-1.4310
H	2.3770	-1.1770	0.5430
H	-0.2080	-2.3140	0.1010
H	-1.1040	-0.0240	1.5700
O	0.1130	0.8940	0.2020
O	2.4160	1.1620	0.2770
C	2.4170	2.5640	0.0570
H	2.4280	2.7990	-1.0190
H	3.3290	2.9540	0.5170
H	1.5440	3.0430	0.5160
O	1.7210	-1.6370	-1.3850
H	1.9360	-2.5670	-1.2190
O	0.6280	-1.8090	1.9480
H	-0.1650	-2.1140	2.4160
C	-1.8680	-0.3840	-0.3910
H	-2.4800	-1.2310	-0.0320
O	-1.3300	-0.6490	-1.6800
H	-2.0660	-0.7960	-2.2950
C	-2.7580	0.8580	-0.4240
H	-3.4990	0.7430	-1.2340
H	-2.1330	1.7320	-0.6510
O	-3.3970	0.9660	0.8430
H	-3.9060	1.7900	0.8550

Coordinates for β-Galf E4-gt-gg
Energy: -726.507621738 Hartrees

C	-1.6060	0.1680	0.3580
C	-1.0170	-1.2470	0.5180
C	0.2580	-1.2390	-0.3450
C	0.5470	0.2640	-0.5410
H	-1.6530	0.6720	1.3380
H	-1.7260	-1.9950	0.1430
H	1.0700	-1.7660	0.1710
H	0.9750	0.4580	-1.5280
O	-0.7370	0.8870	-0.5100
O	-2.8830	0.0820	-0.1950
C	-3.5290	1.3390	-0.3320
H	-3.5920	1.8600	0.6360
H	-4.5390	1.1330	-0.6940
H	-3.0070	1.9820	-1.0490
O	-0.7300	-1.4260	1.9050
H	-0.4200	-2.3370	2.0240
O	-0.0470	-1.8800	-1.5770
H	0.7690	-1.8930	-2.1020
C	1.4950	0.8920	0.4980
H	1.0080	0.8750	1.4860
O	1.6980	2.2310	0.0610
H	2.2550	2.6780	0.7170
C	2.8170	0.1260	0.6360
H	2.6620	-0.7540	1.2790
H	3.5450	0.7760	1.1500
O	3.2850	-0.2550	-0.6540
H	4.1780	-0.6170	-0.5570

Coordinates for β-Galf E4-gt-gt
Energy: -726.504953387 Hartrees

C	1.5290	-0.3180	0.3550
C	1.1090	1.1240	0.7090
C	0.0030	1.4670	-0.3120
C	-0.4540	0.0730	-0.7880
H	1.3320	-0.9900	1.2060
H	1.9590	1.8010	0.5710
H	-0.8090	2.0300	0.1740
H	-0.7790	0.0950	-1.8390
O	0.7240	-0.7200	-0.7550
O	2.8760	-0.3460	0.0110
C	3.3750	-1.6540	-0.2330
H	3.1940	-2.3150	0.6280
H	4.4520	-1.5530	-0.3890
H	2.9170	-2.0980	-1.1250
O	0.6440	1.1130	2.0530
H	0.4470	2.0280	2.3080
O	0.6080	2.2340	-1.3450
H	-0.0800	2.4810	-1.9820
C	-1.5890	-0.5220	0.0990
H	-1.4720	-0.1700	1.1290
O	-1.5100	-1.9310	0.1900
H	-1.6470	-2.3010	-0.6980
C	-2.9450	-0.0480	-0.4240
H	-2.9070	1.0410	-0.6040
H	-3.1320	-0.5280	-1.4040
O	-3.9480	-0.3810	0.5190
H	-4.7850	-0.0010	0.2130

Coordinates for β-Galf E4-gt-tg
Energy: -726.507972228 Hartrees

C	-1.5680	0.1410	0.3630
C	-0.9070	-1.2310	0.5910
C	0.3120	-1.2440	-0.3530
C	0.5160	0.2530	-0.6780
H	-1.5710	0.7230	1.2990
H	-1.6020	-2.0320	0.3170
H	1.1860	-1.6810	0.1410
H	0.8700	0.4010	-1.7060
O	-0.7870	0.8200	-0.6150
O	-2.8720	-0.0360	-0.0970
C	-3.5800	1.1820	-0.2780
H	-3.6030	1.7710	0.6520
H	-4.6020	0.9100	-0.5550
H	-3.1340	1.7900	-1.0730
O	-0.5360	-1.2920	1.9670
H	-0.1840	-2.1790	2.1370
O	-0.0540	-1.9960	-1.5060
H	0.7200	-2.0280	-2.0900
C	1.4980	0.9490	0.2890
H	1.3010	0.5990	1.3140
O	1.2720	2.3510	0.1770
H	1.8680	2.7940	0.8020
C	2.9680	0.6750	-0.0590
H	3.5950	1.2710	0.6250
H	3.1560	1.0410	-1.0810
O	3.2680	-0.7120	0.0620
H	4.2320	-0.8130	0.0640

Coordinates for β-Galf E4-tg-gg
Energy: -726.505067346 Hartrees

C	-1.4380	0.0870	-0.4570
C	-0.7580	1.2020	0.3610
C	0.2590	0.4510	1.2500
C	0.4410	-0.9010	0.5400
H	-1.2690	0.2430	-1.5370
H	-1.5030	1.6880	1.0010
H	1.2020	1.0030	1.3310
H	0.5820	-1.6900	1.2870
O	-0.8460	-1.1470	-0.0520
O	-2.8050	0.0770	-0.1920
C	-3.5280	-0.8830	-0.9470
H	-3.3620	-0.7470	-2.0270
H	-4.5860	-0.7230	-0.7250
H	-3.2470	-1.9060	-0.6700
O	-0.1850	2.1180	-0.5640
H	0.1730	2.8610	-0.0560
O	-0.3640	0.2880	2.5210
H	0.2710	-0.1590	3.1020
C	1.6130	-1.1000	-0.4470
H	1.3060	-1.9480	-1.0810
O	2.7190	-1.4500	0.3820
H	3.4520	-1.7230	-0.1910
C	1.9730	0.0510	-1.3900
H	1.0720	0.4110	-1.9030
H	2.6550	-0.3500	-2.1620
O	2.6140	1.0900	-0.6620
H	2.8230	1.7930	-1.2940

Coordinates for β-Galf E4-tg-gt
Energy: -726.507183132 Hartrees

C	1.4550	-0.4950	0.2320
C	1.0910	0.8210	0.9390
C	-0.0250	1.4570	0.0860
C	-0.4090	0.3720	-0.9470
H	1.2660	-1.3560	0.8930
H	1.9620	1.4850	0.9420
H	-0.8700	1.7220	0.7410
H	-0.4170	0.8270	-1.9450
O	0.6280	-0.6110	-0.9220
O	2.8030	-0.4550	-0.1250
C	3.2730	-1.6590	-0.7170
H	3.0990	-2.5200	-0.0540
H	4.3470	-1.5330	-0.8680
H	2.7870	-1.8470	-1.6810
O	0.6700	0.4920	2.2600
H	0.5320	1.3240	2.7400
O	0.5100	2.6280	-0.5210
H	-0.1960	3.0460	-1.0380
C	-1.7970	-0.2770	-0.7490
H	-1.9590	-0.9640	-1.5860
O	-2.8160	0.7080	-0.8920
H	-2.7630	1.3090	-0.1310
C	-1.9420	-1.0990	0.5300
H	-1.8240	-0.4540	1.4180
H	-1.1310	-1.8410	0.5580
O	-3.2190	-1.7200	0.5050
H	-3.3060	-2.2420	1.3170

Coordinates for β-Galf E4-tg-tg
Energy: -726.509626693 Hartrees

C	1.3440	-0.2930	0.1380
C	0.7900	0.8430	1.0170
C	-0.3860	1.4440	0.2200
C	-0.6290	0.4320	-0.9230
H	1.2560	-1.2620	0.6480
H	1.5620	1.6080	1.1450
H	-1.2750	1.5500	0.8550
H	-0.7780	0.9770	-1.8630
O	0.5590	-0.3360	-1.0510
O	2.6790	-0.0180	-0.1660
C	3.3150	-1.0470	-0.9100
H	3.2480	-2.0140	-0.3870
H	4.3660	-0.7620	-1.0040
H	2.8730	-1.1530	-1.9070
O	0.4020	0.2800	2.2690
H	0.1510	1.0150	2.8500
O	0.0330	2.7170	-0.2660
H	-0.7160	3.1050	-0.7440
C	-1.8720	-0.4600	-0.7430
H	-1.8960	-1.1600	-1.5910
O	-2.9710	0.4560	-0.7940
H	-3.7920	-0.0590	-0.7820
C	-1.9500	-1.2930	0.5430
H	-1.7200	-0.6770	1.4210
H	-2.9940	-1.6440	0.6420
O	-1.0580	-2.3950	0.4340
H	-1.1220	-2.9060	1.2540

Appendix B:

Supporting information for Chapter 3

B.1. Calculated spin-spin coupling constants

The dihedral angles $\phi_{H,H}$ and vicinal coupling constants $^3J_{H,H}$ or $^3J_{H,C}$ that were calculated in Gaussian 03[1] at the B3LYP/[5s2p1d|3s1p][2,3] level of theory for **3.1** and **3.2** are shown in Tables B.1 through B.4 below. The ^{2}E-*gt-tg*, E_3-*gt-tg*, and ^{4}E-*gt-tg* conformation of **3.1** are excluded, as their single point energies (B3LYP/6-31+G**, Chapter 2) were all greater than 34 kcal/mol above the global minimum.

Table B.1. $\phi_{H,H}$ (in degrees) and $J_{H,H}$ (in Hz) for the ring dihedral angles of **3.1**.

Conformer	$\phi_{1,2}$	$J_{1,2}$	$\phi_{2,3}$	$J_{2,3}$	$\phi_{3,4}$	$J_{3,4}$
^{O}E-*gg-gg*	16.4	6.8	-127.1	1.1	113.7	0.9
^{O}E-*gg-gt*	16.5	6.7	-125.3	1.1	112.7	1.1
^{O}E-*gg-tg*	15.5	7.1	-127.1	1.1	114.5	1.1
^{O}E-*gt-gg*	22.8	6.4	-126.8	1.2	109.7	0.8
^{O}E-*gt-gt*	23.4	6.3	-127.0	1.0	108.4	0.3
^{O}E-*gt-tg*	22.7	6.4	-127.2	1.2	108.7	0.5
^{O}E-*tg-gg*	14.2	7.3	-126.0	1.2	115.0	1.1
^{O}E-*tg-gt*	14.1	7.3	-125.5	1.1	116.2	1.3
^{O}E-*tg-tg*	13.7	7.1	-125.8	1.3	114.5	1.2
E_O-*gg-gg*	-24.2	5.5	-127.2	1.2	150.9	6.6
E_O-*gg-gt*	-23.4	5.5	-125.8	1.1	150.9	7.2
E_O-*gg-tg*	-24.2	5.5	-126.7	1.2	150.3	6.8
E_O-*gt-gg*	-25.6	5.1	-126.2	0.8	151.3	7.0
E_O-*gt-gt*	-23.5	5.5	-126.5	1.2	150.8	6.5
E_O-*gt-tg*	-24.7	5.2	-124.9	0.8	148.8	6.9
E_O-*tg-gg*	-22.2	5.6	-124.6	0.7	145.3	5.8
E_O-*tg-gt*	-22.9	5.6	-125.6	1.1	150.5	7.0
E_O-*tg-tg*	-19.6	5.7	-123.9	0.7	142.5	5.4
^{1}E-*gg-gg*	-37.5	3.6	-101.8	-0.1	124.7	2.1
^{1}E-*gg-gt*	-39.8	3.3	-99.1	-0.1	123.3	2.3
^{1}E-*gg-tg*	-38.4	3.6	-101.0	-0.1	124.2	2.2
^{1}E-*gt-gg*	-42.4	3.0	-98.0	-0.2	123.8	2.4
^{1}E-*gt-gt*	-40.2	3.3	-99.6	-0.1	125.5	2.1
^{1}E-*gt-tg*	-42.5	3.0	-97.8	-0.1	123.0	2.4
^{1}E-*tg-gg*	-41.1	3.2	-99.0	0.0	123.2	2.0
^{1}E-*tg-gt*	-40.5	3.3	-98.5	0.0	124.7	2.3
^{1}E-*tg-tg*	-41.0	3.3	-99.4	-0.2	123.4	2.1
E_1-*gg-gg*	36.6	5.6	-151.3	4.9	131.0	3.3
E_1-*gg-gt*	38.3	5.7	-150.9	5.1	130.9	3.6

Conformer	$\phi_{1,2}$	$J_{1,2}$	$\phi_{2,3}$	$J_{2,3}$	$\phi_{3,4}$	$J_{3,4}$
E_1-*gg-tg*	35.3	5.9	-150.1	4.7	130.5	3.4
E_1-*gt-gg*	40.8	5.1	-152.8	4.8	129.9	3.5
E_1-*gt-gt*	41.7	5.0	-153.5	5.2	130.5	2.8
E_1-*gt-tg*	39.5	5.2	-151.4	4.9	129.0	3.6
E_1-*tg-gg*	30.1	6.7	-145.0	3.8	127.9	3.3
E_1-*tg-gt*	34.4	6.4	-148.2	4.7	131.8	3.7
E_1-*tg-tg*	33.6	6.4	-148.8	5.3	130.8	3.5
^2E-*gg-gg*	43.2	4.7	-169.8	7.8	154.0	6.9
^2E-*gg-gt*	44.4	4.7	-168.5	7.5	154.0	7.5
^2E-*gg-tg*	43.3	4.8	-169.8	7.8	153.8	7.3
^2E-*gt-gg*	43.8	4.9	-170.3	7.8	154.5	7.8
^2E-*gt-gt*	43.4	4.9	-168.7	7.7	154.0	6.9
^2E-*tg-gg*	40.7	5.6	-166.5	7.8	151.0	7.2
^2E-*tg-gt*	43.3	5.2	-169.7	7.9	156.3	8.3
^2E-*tg-tg*	41.0	5.4	-166.1	7.5	151.1	7.1
E_2-*gg-gg*	-24.2	5.1	-99.1	0.0	108.8	0.5
E_2-*gg-gt*	-36.9	3.6	-87.3	0.6	100.8	0.1
E_2-*gg-tg*	-26.7	4.9	-96.7	0.1	107.2	0.4
E_2-*gt-gg*	-37.7	3.4	-86.0	0.8	101.5	0.3
E_2-*gt-gt*	-37.7	3.3	-86.3	0.7	102.0	0.0
E_2-*gt-tg*	-38.9	3.2	-84.7	1.0	99.1	0.0
E_2-*tg-gg*	-31.1	4.4	-92.4	0.3	104.1	0.2
E_2-*tg-gt*	-31.1	4.4	-91.6	0.3	105.0	0.3
E_2-*tg-tg*	-24.0	5.1	-99.4	0.0	108.8	0.6
^3E-*gg-gg*	-9.2	6.3	-108.0	-0.1	108.7	0.5
^3E-*gg-gt*	-23.6	4.9	-88.9	0.5	92.4	0.0
^3E-*gg-tg*	-10.6	6.4	-106.1	-0.1	106.8	0.4
^3E-*gt-gg*	-24.4	4.7	-86.4	0.7	89.5	0.1
^3E-*gt-gt*	-23.2	4.8	-88.2	0.6	92.7	-0.1
^3E-*gt-tg*	-25.0	4.5	-85.6	0.9	88.9	0.1
^3E-*tg-gg*	-13.4	6.0	-101.2	-0.1	102.5	0.2
^3E-*tg-gt*	-16.2	5.8	-96.9	0.1	100.3	0.1
^3E-*tg-tg*	-11.1	6.2	-105.5	-0.1	106.5	0.5
E_3-*gg-gg*	30.3	6.3	-169.9	8.3	166.6	8.3
E_3-*gg-gt*	29.9	6.4	-167.8	7.5	166.7	9.0
E_3-*gg-tg*	30.3	6.4	-169.6	8.3	166.4	8.6
E_3-*gt-gg*	27.1	5.9	-165.8	7.5	164.5	9.0
E_3-*gt-gt*	29.8	6.5	-167.9	7.8	165.6	8.3
E_3-*tg-gg*	28.3	6.8	-166.3	8.0	162.5	8.5
E_3-*tg-gt*	28.1	6.8	-164.8	7.4	162.8	8.5
E_3-*tg-tg*	27.6	6.6	-163.2	7.2	159.9	8.0
^4E-*gg-gg*	3.2	7.5	-153.8	6.0	166.6	8.7
^4E-*gg-gt*	3.5	7.4	-151.3	5.3	165.3	9.3
^4E-*gg-tg*	3.1	7.5	-153.4	5.9	166.1	9.0
^4E-*gt-gg*	3.4	7.4	-152.4	5.2	164.7	8.9
^4E-*gt-gt*	3.7	7.5	-151.3	5.5	163.9	8.5
^4E-*tg-gg*	2.6	7.4	-150.1	5.0	161.7	8.3
^4E-*tg-gt*	2.9	7.4	-149.1	4.7	162.2	8.4

Conformer	$\phi_{1,2}$	$J_{1,2}$	$\phi_{2,3}$	$J_{2,3}$	$\phi_{3,4}$	$J_{3,4}$
^{4}E-*tg-tg*	3.4	7.3	-148.4	4.5	159.6	7.9
E_4-*gg-gg*	1.2	6.7	-112.8	0.0	106.3	0.3
E_4-*gg-gt*	-6.2	6.0	-101.7	-0.3	96.3	0.2
E_4-*gg-tg*	1.3	7.0	-113.8	0.1	107.4	0.5
E_4-*gt-gg*	-1.1	6.1	-100.1	-0.1	90.3	0.0
E_4-*gt-gt*	-0.9	6.0	-101.2	-0.1	92.2	-0.1
E_4-*gt-tg*	-0.7	6.0	-101.3	-0.1	91.2	0.0
E_4-*tg-gg*	0.9	6.8	-110.5	0.0	103.8	0.2
E_4-*tg-gt*	0.0	6.9	-108.6	-0.1	103.6	0.2
E_4-*tg-tg*	0.0	6.8	-112.6	0.1	107.0	0.5
^{2}E-*gg-gg*	49.0	4.6	-179.9	8.3	155.1	6.8
^{2}E-*gt-gg*	47.8	4.7	-180.0	8.4	156.5	6.4
$^{2}T_3$-*tg-gt*	43.9	5.2	-179.9	8.6	165.9	8.8
E_3-*gg-gt*	41.6	4.9	-178.0	6.7	179.9	9.7
E_3-*gt-gt*	39.3	5.4	-177.8	7.3	180.0	9.2
E_3-*tg-gt*	39.9	5.4	-178.5	7.4	180.0	9.8

Table B.2. $\phi_{H,H}$ (in degrees), $J_{H,H}$ (in Hz), and $J_{H,C}$ (in Hz) for the exocyclic dihedral angles of **3.1**.

Conformer	$\phi_{4,5}$	$J_{4,5}$	$\phi_{H4,C6}$	$J_{H4,C6}$	$\phi_{5,6R}$	$J_{5,6R}$	$\phi_{5,6S}$	$J_{5,6S}$
^{O}E-*gg-gg*	-58.3	2.3	55.9	0.2	59.4	1.1	-55.6	4.2
^{O}E-*gg-gt*	-72.2	0.6	43.8	0.4	-170.8	9.5	71.9	1.6
^{O}E-*gg-tg*	-57.6	2.3	59.5	0.9	-70.8	4.1	171.5	10.2
^{O}E-*gt-gg*	175.1	9.6	-66.0	0.2	36.4	3.3	-80.1	0.6
^{O}E-*gt-gt*	-167.6	11.1	-47.7	0.4	-174.4	9.3	69.0	2.1
^{O}E-*gt-tg*	-163.5	10.2	-41.8	0.4	-56.2	5.7	-172.4	9.9
^{O}E-*tg-gg*	68.4	4.3	-173.4	0.7	69.6	0.6	-47.4	5.1
^{O}E-*tg-gt*	60.9	6.0	-179.4	0.8	-172.2	10.1	70.8	2.4
^{O}E-*tg-tg*	59.2	5.4	179.0	0.7	-99.3	0.1	142.6	7.1
E_O-*gg-gg*	-59.8	1.8	54.8	0.2	57.9	1.2	-56.9	3.9
E_O-*gg-gt*	-58.5	1.3	58.2	0.2	-167.8	8.2	74.8	1.2
E_O-*gg-tg*	-55.1	2.3	62.7	0.6	-69.4	4.4	173.2	10.1
E_O-*gt-gg*	-179.5	9.0	-61.3	0.1	57.8	1.0	-58.6	3.5
E_O-*gt-gt*	178.8	9.4	-61.8	0.2	-179.3	10.1	63.4	2.8
E_O-*gt-tg*	168.5	8.0	-71.6	0.1	-81.1	2.4	161.6	9.8
E_O-*tg-gg*	61.2	5.1	177.1	0.6	67.2	0.7	-49.1	4.8
E_O-*tg-gt*	37.2	8.7	156.4	0.5	-176.9	10.8	66.2	3.3
E_O-*tg-tg*	50.9	6.2	168.7	0.6	-95.6	0.4	147.0	7.4
^{1}E-*gg-gg*	-58.0	2.0	56.5	0.2	58.6	1.1	-56.2	4.0
^{1}E-*gg-gt*	-67.4	0.6	49.2	0.3	-168.4	8.9	74.1	1.3
^{1}E-*gg-tg*	-53.5	2.5	64.3	0.6	-69.5	4.3	173.1	10.1
^{1}E-*gt-gg*	-179.0	9.4	-60.3	0.2	53.7	1.2	-62.1	2.9
^{1}E-*gt-gt*	-172.6	10.5	-53.1	0.3	-174.0	9.3	69.3	1.9
^{1}E-*gt-tg*	175.2	8.8	-64.0	0.2	-79.3	2.6	164.2	9.9
^{1}E-*tg-gg*	63.9	4.9	-178.7	0.6	73.6	0.5	-43.3	5.6
^{1}E-*tg-gt*	53.3	6.9	172.0	0.7	-174.5	10.3	68.8	2.8
^{1}E-*tg-tg*	53.0	6.3	171.8	0.6	-96.6	0.3	144.9	6.4
E_1-*gg-gg*	-55.5	2.7	58.5	0.2	61.4	0.9	-53.8	4.5
E_1-*gg-gt*	-73.1	0.6	42.6	0.4	-170.9	9.6	71.7	1.7
E_1-*gg-tg*	-58.3	2.4	58.2	0.1	-71.7	4.0	170.6	10.2
E_1-*gt-gg*	-171.1	10.1	-52.9	0.3	56.9	1.1	-59.3	3.4
E_1-*gt-gt*	-166.9	10.9	-47.7	0.4	-173.3	9.0	70.3	1.9
E_1-*gt-tg*	-179.5	9.4	-59.0	0.3	-77.7	2.8	165.9	9.7
E_1-*tg-gg*	63.8	5.5	-178.8	0.7	62.0	1.0	-54.4	4.0
E_1-*tg-gt*	49.0	8.2	169.4	0.8	-179.2	10.9	63.5	3.7
E_1-*tg-tg*	55.5	6.1	176.8	0.7	-90.0	0.9	151.9	8.4
^{2}E-*gg-gg*	-57.6	1.9	57.5	0.2	62.2	0.9	-53.0	4.6
^{2}E-*gg-gt*	-66.1	0.6	50.9	0.3	-169.8	8.9	72.9	1.4
^{2}E-*gg-tg*	-59.6	1.6	58.1	0.1	-70.3	4.2	172.2	10.1
^{2}E-*gt-gg*	-179.9	9.0	-61.7	0.1	56.8	1.1	-59.8	3.3
^{2}E-*gt-gt*	179.2	9.6	-61.3	0.2	-179.8	10.2	63.1	2.8
^{2}E-*tg-gg*	68.2	4.3	-175.5	0.6	68.2	0.7	-48.2	5.0
^{2}E-*tg-gt*	71.5	3.9	-169.4	0.7	-165.9	8.6	76.9	1.4
^{2}E-*tg-tg*	55.8	5.9	173.7	0.6	-99.3	0.1	142.8	6.8
E_2-*gg-gg*	-57.1	2.0	57.3	0.2	59.8	1.0	-55.0	4.3

Conformer	$\phi_{4,5}$	$J_{4,5}$	$\phi_{H4,C6}$	$J_{H4,C6}$	$\phi_{5,6R}$	$J_{5,6R}$	$\phi_{5,6S}$	$J_{5,6S}$
E_2-*gg*-*gt*	-77.9	0.7	37.8	0.5	-169.3	9.5	73.0	1.6
E_2-*gg*-*tg*	-53.6	2.5	63.8	0.8	-69.9	4.2	172.7	10.0
E_2-*gt*-*gg*	166.7	7.7	-74.1	0.3	38.5	3.0	-77.9	0.8
E_2-*gt*-*gt*	-171.4	10.5	-51.2	0.3	-174.3	9.5	68.9	2.0
E_2-*gt*-*tg*	177.0	8.9	-61.0	0.2	-73.1	3.6	171.0	10.4
E_2-*tg*-*gg*	70.0	4.5	-172.4	0.6	72.1	0.6	-45.1	5.5
E_2-*tg*-*gt*	57.4	7.0	175.4	0.7	-169.0	9.7	73.9	2.0
E_2-*tg*-*tg*	52.5	6.6	171.3	0.7	-89.1	1.1	153.1	8.8
^3E-*gg*-*gg*	-57.0	2.0	57.9	0.2	61.5	0.9	-53.4	4.5
^3E-*gg*-*gt*	-78.0	0.7	37.8	0.5	-171.1	9.6	71.4	1.7
^3E-*gg*-*tg*	-56.2	2.1	61.5	0.9	-69.8	4.2	172.7	10.2
^3E-*gt*-*gg*	162.9	7.1	-78.0	0.2	41.8	2.7	-74.4	1.2
^3E-*gt*-*gt*	-172.8	10.5	-52.5	0.3	-175.8	9.6	67.4	2.2
^3E-*gt*-*tg*	173.5	8.7	-64.5	0.2	-73.0	3.7	171.1	10.4
^3E-*tg*-*gg*	70.5	4.2	-171.7	0.7	73.3	0.5	-43.8	5.7
^3E-*tg*-*gt*	58.8	6.8	176.9	0.8	-168.5	9.7	74.3	1.9
^3E-*tg*-*tg*	53.4	6.4	172.2	0.7	-89.9	1.0	152.3	8.7
E_3-*gg*-*gg*	-57.3	1.8	57.4	0.2	60.2	1.0	-54.8	4.3
E_3-*gg*-*gt*	-57.6	1.2	59.0	0.2	-168.1	8.3	74.5	1.2
E_3-*gg*-*tg*	-54.9	2.0	62.8	0.7	-69.6	4.4	173.0	10.1
E_3-*gt*-*gg*	179.7	8.7	-62.1	0.1	57.1	1.1	-59.6	3.3
E_3-*gt*-*gt*	175.8	8.8	-64.4	0.1	177.0	10.6	59.7	3.4
E_3-*tg*-*gg*	66.4	4.3	-177.9	0.5	66.3	0.8	-49.8	4.7
E_3-*tg*-*gt*	63.9	5.0	-178.5	0.6	-161.6	7.6	80.2	0.9
E_3-*tg*-*tg*	54.0	5.9	171.3	0.5	-95.9	0.4	146.8	7.3
^4E-*gg*-*gg*	-57.3	2.0	57.4	0.2	59.6	1.0	-55.3	4.3
^4E-*gg*-*gt*	-57.3	1.3	59.4	0.2	-167.9	8.1	74.7	1.2
^4E-*gg*-*tg*	-53.6	2.3	64.1	0.6	-69.2	4.4	173.3	10.2
^4E-*gt*-*gg*	179.0	8.6	-62.7	0.1	56.6	1.1	-60.0	3.2
^4E-*gt*-*gt*	175.5	8.8	-64.8	0.1	177.5	10.6	60.2	3.3
^4E-*tg*-*gg*	62.9	4.8	178.4	0.5	64.5	0.9	-51.7	4.4
^4E-*tg*-*gt*	58.7	5.7	176.3	0.6	-163.5	8.0	78.1	1.1
^4E-*tg*-*tg*	52.2	6.0	169.5	0.5	-94.9	0.5	148.0	7.5
E_4-*gg*-*gg*	-58.2	2.0	56.5	0.2	60.4	1.0	-54.5	4.4
E_4-*gg*-*gt*	-72.3	0.6	43.3	0.4	-171.0	9.5	71.5	1.8
E_4-*gg*-*tg*	-56.7	2.2	60.9	0.8	-70.2	4.1	172.2	10.1
E_4-*gt*-*gg*	170.3	8.6	-70.7	0.8	40.7	2.9	-75.5	1.1
E_4-*gt*-*gt*	-168.6	10.8	-48.4	0.4	-174.4	9.3	69.0	2.1
E_4-*gt*-*tg*	-171.4	10.0	-49.4	0.4	-65.2	4.7	179.0	10.2
E_4-*tg*-*gg*	72.3	3.7	-169.4	0.7	71.5	0.6	-45.5	5.5
E_4-*tg*-*gt*	62.7	5.7	-177.9	0.8	-171.8	10.1	71.1	2.3
E_4-*tg*-*tg*	55.5	6.0	174.8	0.7	-93.3	0.7	148.7	8.2
^2E-*gg*-*gg*	-67.3	0.6	49.8	0.4	-172.2	9.0	70.5	1.7
^2E-*gt*-*gg*	179.4	9.6	-61.2	0.2	-179.9	10.2	63.0	2.8
$^2T_3$-*tg*-*gt*	70.1	4.0	-171.3	0.6	-166.5	8.8	76.2	1.6
E_3-*gg*-*gt*	-61.8	0.8	55.2	0.2	-168.7	8.4	73.9	1.3
E_3-*gt*-*gt*	173.5	10.0	-66.8	0.1	177.2	10.6	60.0	3.4
E_3-*tg*-*gt*	67.2	4.0	-174.9	0.7	-163.9	7.9	78.1	1.1

Table B.3. $\phi_{H,H}$ (in degrees) and $J_{H,H}$ (in Hz) for the ring dihedral angles of **3.2**.

Conformer	$\phi_{1,2}$	$J_{1,2}$	$\phi_{2,3}$	$J_{2,3}$	$\phi_{3,4}$	$J_{3,4}$
^{O}E-*gg-gg*	145.3	4.5	-126.1	1.0	108.4	0.5
^{O}E-*gg-gt*	142.0	4.1	-123.1	0.8	107.3	0.7
^{O}E-*gg-tg*	141.8	4.2	-126.1	1.1	110.6	0.8
^{O}E-*gt-gg*	141.6	4.3	-125.1	1.2	111.7	1.3
^{O}E-*gt-gt*	147.9	5.0	-125.6	0.9	105.8	0.1
^{O}E-*gt-tg*	141.6	4.3	-125.7	1.3	111.1	0.8
^{O}E-*tg-gg*	143.5	4.7	-126.5	1.1	110.4	0.8
^{O}E-*tg-gt*	141.2	4.3	-123.9	0.9	111.1	0.9
^{O}E-*tg-tg*	138.1	3.8	-124.0	1.1	111.3	1.0
E_O-*gg-gg*	104.3	0.0	-126.7	1.2	149.2	6.3
E_O-*gg-gt*	105.1	0.0	-125.3	1.1	149.2	6.9
E_O-*gg-tg*	104.7	0.0	-126.2	1.1	148.2	6.4
E_O-*gt-gg*	102.9	-0.1	-125.7	0.7	149.6	6.7
E_O-*gt-gt*	104.8	0.0	-126.0	1.2	149.6	6.3
E_O-*gt-tg*	103.3	-0.1	-124.3	0.7	147.4	6.8
E_O-*tg-gg*	104.3	0.0	-125.9	1.2	149.1	6.4
E_O-*tg-gt*	105.5	0.1	-125.1	1.1	149.0	6.7
E_O-*tg-tg*	105.4	0.1	-123.1	0.6	142.9	5.5
^{1}E-*gg-gg*	95.7	-0.1	-106.3	-0.1	125.6	2.4
^{1}E-*gg-gt*	93.1	-0.1	-103.2	-0.1	124.4	2.6
^{1}E-*gg-tg*	95.5	-0.1	-105.8	-0.1	125.2	2.5
^{1}E-*gt-gg*	90.4	0.0	-102.0	-0.3	125.2	2.7
^{1}E-*gt-gt*	92.7	-0.1	-103.7	-0.1	126.7	2.4
^{1}E-*gt-tg*	90.5	-0.1	-101.6	-0.2	124.4	2.8
^{1}E-*tg-gg*	91.5	-0.1	-102.4	-0.1	124.6	2.3
^{1}E-*tg-gt*	92.2	-0.1	-102.1	-0.1	126.0	2.6
^{1}E-*tg-tg*	91.9	-0.1	-102.5	-0.3	123.0	2.3
E_1-*gg-gg*	162.0	6.7	-149.9	4.9	128.5	3.0
E_1-*gg-gt*	160.2	6.6	-147.3	4.8	128.4	3.4
E_1-*gg-tg*	160.9	6.6	-149.1	4.8	127.9	3.1
E_1-*gt-gg*	158.3	6.2	-147.9	4.4	129.2	3.7
E_1-*gt-gt*	161.3	6.8	-149.6	5.1	129.9	3.0
E_1-*gt-tg*	156.0	6.0	-145.5	4.2	128.0	3.9
E_1-*tg-gg*	156.4	6.3	-146.2	4.6	128.5	3.1
E_1-*tg-gt*	154.1	6.2	-144.2	4.2	129.7	3.5
E_1-*tg-tg*	157.7	6.5	-146.5	4.9	128.4	3.2
^{2}E-*gg-gg*	161.9	6.5	-163.7	7.6	149.3	6.6
^{2}E-*gg-gt*	161.1	6.5	-161.6	7.2	150.2	7.5
^{2}E-*gg-tg*	161.6	6.5	-162.9	7.5	148.4	6.8
^{2}E-*gt-gg*	161.9	6.4	-165.0	8.2	152.5	8.5
^{2}E-*gt-gt*	161.0	6.5	-162.6	7.5	150.2	6.8
^{2}E-*gt-tg*	158.3	6.1	-159.9	7.2	147.7	7.7
^{2}E-*tg-gg*	156.0	6.0	-155.8	6.1	143.8	6.3
^{2}E-*tg-gt*	159.4	6.4	-160.3	7.0	150.2	7.4
^{2}E-*tg-tg*	161.0	6.4	-161.9	7.0	150.2	7.3
E_2-*gg-gg*	108.5	0.3	-107.7	0.0	114.3	1.2
E_2-*gg-gt*	94.9	-0.1	-93.8	0.2	105.9	0.5

Conformer	$\phi_{1,2}$	$J_{1,2}$	$\phi_{2,3}$	$J_{2,3}$	$\phi_{3,4}$	$J_{3,4}$
E_2-*gg-tg*	106.6	0.2	-105.5	-0.1	112.8	1.1
E_2-*gt-gg*	93.9	-0.1	-92.9	0.3	107.8	0.9
E_2-*gt-gt*	94.0	-0.1	-92.5	0.3	107.2	0.3
E_2-*gt-tg*	94.4	-0.1	-93.8	0.3	107.5	0.5
E_2-*tg-gg*	98.0	-0.1	-96.5	0.1	108.1	0.6
E_2-*tg-gt*	98.5	-0.1	-96.5	0.1	109.4	0.7
E_2-*tg-tg*	103.5	0.1	-102.4	-0.1	110.6	0.9
^3E-*gg-gg*	107.9	0.2	-96.2	0.1	97.1	0.0
^3E-*gg-gt*	105.6	0.1	-94.6	0.1	96.7	0.1
^3E-*gg-tg*	108.4	0.3	-96.7	0.2	97.7	0.1
^3E-*gt-gg*	103.4	0.0	-91.8	0.3	96.1	0.2
^3E-*gt-gt*	104.8	0.0	-93.1	0.2	97.4	-0.1
^3E-*gt-tg*	103.1	0.0	-90.5	0.5	94.2	0.1
^3E-*tg-gg*	111.8	0.6	-104.0	-0.1	106.1	0.5
^3E-*tg-gt*	111.1	0.5	-102.2	-0.1	105.9	0.5
^3E-*tg-tg*	113.4	0.7	-105.5	-0.1	105.7	0.5
E_3-*gg-gg*	151.2	5.1	-166.4	8.0	163.7	8.5
E_3-*gg-gt*	150.8	5.1	-164.4	7.3	164.2	9.3
E_3-*gg-tg*	151.0	5.1	-165.8	8.0	163.2	8.8
E_3-*gt-gg*	150.6	5.0	-166.0	7.6	163.9	9.2
E_3-*gt-gt*	150.8	5.3	-164.6	7.6	163.2	8.6
E_3-*gt-tg*	147.4	4.7	-159.9	7.1	158.0	9.1
E_3-*tg-gg*	147.6	4.8	-159.9	6.9	157.8	8.4
E_3-*tg-gt*	145.5	4.6	-155.9	6.3	155.6	8.4
E_3-*tg-tg*	146.2	4.7	-157.3	6.4	155.9	8.1
^4E-*gg-gg*	128.0	1.7	-155.0	5.9	169.4	9.0
^4E-*gg-gt*	128.3	1.9	-152.5	5.2	168.0	9.6
^4E-*gg-tg*	128.1	1.8	-154.1	5.8	167.9	9.3
^4E-*gt-gg*	127.7	1.7	-153.2	5.0	167.0	9.2
^4E-*gt-gt*	128.5	2.0	-152.9	5.5	167.5	8.9
^4E-*gt-tg*	126.8	1.7	-148.1	4.5	160.3	9.2
^4E-*tg-gg*	126.8	1.8	-147.4	4.3	159.1	8.3
^4E-*tg-gt*	126.8	1.8	-145.1	4.0	157.7	8.4
^4E-*tg-tg*	127.0	1.8	-146.6	4.1	158.6	8.1
E_4-*gg-gg*	126.0	2.0	-114.9	0.2	108.4	0.6
E_4-*gg-gt*	122.7	1.4	-102.7	-0.2	94.2	0.1
E_4-*gg-tg*	125.9	2.0	-115.7	0.3	109.4	0.8
E_4-*gt-gg*	122.2	1.4	-102.5	-0.1	95.3	0.2
E_4-*gt-gt*	124.1	1.6	-102.7	-0.2	93.7	-0.1
E_4-*gt-tg*	122.9	1.5	-103.5	-0.1	95.3	0.0
E_4-*tg-gg*	124.2	1.7	-103.1	-0.1	95.0	0.1
E_4-*tg-gt*	123.8	1.9	-113.5	0.2	111.1	1.0
E_4-*tg-tg*	124.7	1.8	-111.2	0.1	104.3	0.4
$^2T_1$-*gg-tg*	180.0	7.7	-166.7	7.0	142.6	5.5
$^2T_1$-*gt-tg*	179.9	7.5	-169.8	7.3	149.3	7.8
^2E-*tg-tg*	180.0	7.5	-171.5	7.1	153.2	7.6
E_3-*gg-tg*	152.8	4.6	-180.0	8.9	173.3	8.5
E_3-*gt-tg*	155.7	4.9	-180.0	8.8	169.4	8.9

Conformer	$\phi_{1,2}$	$J_{1,2}$	$\phi_{2,3}$	$J_{2,3}$	$\phi_{3,4}$	$J_{3,4}$
E_3-*tg-tg*	152.7	4.5	180.0	8.6	174.6	8.6
$^4T_3$-*gg-tg*	134.1	2.4	-163.1	6.1	180.0	10.0
$^4T_3$-*gt-tg*	129.0	1.8	-158.2	5.1	180.0	10.5
$^4T_3$-*tg-tg*	134.5	2.5	-163.5	6.2	-180.0	9.8

Table B.4. $\phi_{H,H}$ (in degrees), $J_{H,H}$ (in Hz), and $J_{H,C}$ (in Hz) for the exocyclic dihedral angles of **3.2**.

Conformer	$\phi_{4,5}$	$J_{4,5}$	$\phi_{H4,C6}$	$J_{H4,C6}$	$\phi_{5,6R}$	$J_{5,6R}$	$\phi_{5,6S}$	$J_{5,6S}$
^{O}E-*gg-gg*	-54.9	2.5	61.3	0.1	65.2	0.7	-50.0	5.0
^{O}E-*gg-gt*	-58.6	1.2	59.3	0.2	-169.4	8.6	73.5	1.3
^{O}E-*gg-tg*	-60.0	1.8	58.5	1.0	-69.9	4.0	172.5	10.1
^{O}E-*gt-gg*	171.4	9.3	-69.8	0.1	36.7	3.2	-80.1	0.6
^{O}E-*gt-gt*	-153.9	10.5	-35.5	0.6	-171.6	8.7	72.3	1.9
^{O}E-*gt-tg*	-160.0	10.2	-39.3	0.5	-55.0	5.7	-171.5	9.6
^{O}E-*tg-gg*	55.3	7.1	172.7	0.7	55.4	1.5	-60.3	2.8
^{O}E-*tg-gt*	54.7	7.0	173.8	0.9	178.8	11.2	61.4	3.8
^{O}E-*tg-tg*	61.7	4.8	-177.8	0.7	-78.0	2.6	164.9	9.9
E_O-*gg-gg*	-63.7	1.4	50.7	0.2	54.2	1.5	-60.7	3.2
E_O-*gg-gt*	-58.6	1.3	58.1	0.2	-168.1	8.2	74.4	1.2
E_O-*gg-tg*	-54.8	2.4	63.1	0.6	-68.4	4.5	174.2	10.1
E_O-*gt-gg*	-180.0	9.3	-61.8	0.2	58.2	1.0	-58.2	3.6
E_O-*gt-gt*	178.2	9.9	-62.3	0.2	-178.8	10.1	64.0	2.7
E_O-*gt-tg*	168.1	8.3	-72.0	0.1	-81.4	2.4	161.3	9.7
E_O-*tg-gg*	53.5	6.3	171.3	0.6	66.6	0.7	-49.6	4.5
E_O-*tg-gt*	39.0	8.6	158.3	0.6	-177.1	10.7	66.0	3.3
E_O-*tg-tg*	50.8	6.2	168.8	0.6	-95.8	0.3	146.9	7.3
^{1}E-*gg-gg*	-60.0	1.8	54.6	0.2	58.0	1.2	-56.7	3.9
^{1}E-*gg-gt*	-65.8	0.7	51.0	0.3	-168.7	8.9	73.7	1.4
^{1}E-*gg-tg*	-55.3	2.3	62.5	0.7	-69.2	4.4	173.3	10.2
^{1}E-*gt-gg*	-179.1	9.5	-60.5	0.2	54.1	1.2	-61.8	3.0
^{1}E-*gt-gt*	-173.2	10.7	-53.8	0.3	-174.2	9.3	69.1	1.9
^{1}E-*gt-tg*	174.3	9.0	-64.9	0.2	-79.8	2.5	163.7	9.8
^{1}E-*tg-gg*	63.3	5.0	-179.2	0.6	72.7	0.5	-44.0	5.5
^{1}E-*tg-gt*	52.0	7.1	170.7	0.7	-175.6	10.4	67.6	2.9
^{1}E-*tg-tg*	53.8	6.2	171.9	0.7	-99.8	0.1	142.4	6.7
E_1-*gg-gg*	-60.3	1.7	55.5	0.2	61.2	0.9	-53.6	4.3
E_1-*gg-gt*	-56.9	1.3	61.0	0.2	-169.0	8.3	73.9	1.2
E_1-*gg-tg*	-60.3	1.7	58.2	0.1	-70.2	4.0	172.2	10.1
E_1-*gt-gg*	-176.2	10.1	-58.0	0.2	55.8	1.1	-60.4	3.1
E_1-*gt-gt*	-169.7	11.2	-50.8	0.4	-173.1	8.8	70.4	1.8
E_1-*gt-tg*	173.2	9.2	-66.3	0.2	-81.4	2.2	161.8	9.4
E_1-*tg-gg*	49.8	7.8	167.0	0.7	54.6	1.6	-61.3	2.6
E_1-*tg-gt*	49.5	8.1	168.2	0.8	-176.2	10.7	66.4	3.0
E_1-*tg-tg*	59.9	5.3	-178.7	0.7	-71.4	3.6	172.4	10.3
^{2}E-*gg-gg*	-62.9	1.2	52.3	0.2	58.0	1.2	-56.8	3.8
^{2}E-*gg-gt*	-56.7	1.2	60.6	0.3	-168.9	8.2	73.8	1.2
^{2}E-*gg-tg*	-59.2	1.5	59.1	0.1	-69.9	4.2	172.6	10.1
^{2}E-*gt-gg*	176.9	8.8	-65.0	0.1	52.4	1.4	-64.5	2.6
^{2}E-*gt-gt*	-179.7	9.7	-60.2	0.2	-178.7	9.9	64.2	2.6
^{2}E-*gt-tg*	168.0	8.0	-72.0	0.9	-81.6	2.3	161.2	9.7
^{2}E-*tg-gg*	46.7	7.6	162.7	0.6	52.9	1.8	-63.3	2.4
^{2}E-*tg-gt*	37.5	9.0	156.6	0.6	-176.6	10.8	66.3	3.3
^{2}E-*tg-tg*	84.3	1.7	-155.4	0.4	-58.0	5.7	-174.1	10.3
E_2-*gg-gg*	-60.9	1.6	54.0	0.2	58.7	1.1	-56.0	4.0

Conformer	$\phi_{4,5}$	$J_{4,5}$	$\phi_{H4,C6}$	$J_{H4,C6}$	$\phi_{5,6R}$	$J_{5,6R}$	$\phi_{5,6S}$	$J_{5,6S}$
E_2-*gg*-*gt*	-73.1	0.6	43.1	0.4	-169.6	9.3	72.8	1.5
E_2-*gg*-*tg*	-56.7	2.1	61.2	0.9	-69.7	4.2	172.8	10.1
E_2-*gt*-*gg*	167.9	8.2	-73.0	0.5	37.0	3.2	-79.5	0.6
E_2-*gt*-*gt*	-169.9	10.8	-50.1	0.3	-174.0	9.3	69.3	1.9
E_2-*gt*-*tg*	-169.9	10.0	-47.8	0.3	-61.2	5.1	-177.0	10.1
E_2-*tg*-*gg*	68.4	4.7	-173.8	0.7	72.2	0.5	-44.7	5.5
E_2-*tg*-*gt*	57.7	6.8	176.1	0.8	-171.5	10.0	71.4	2.3
E_2-*tg*-*tg*	59.1	5.4	179.3	0.7	-79.1	2.5	163.6	9.9
^3E-*gg*-*gg*	-80.6	0.6	34.4	0.4	51.5	1.8	-63.6	2.4
^3E-*gg*-*gt*	-72.2	0.6	44.2	0.4	-170.7	9.3	71.8	1.6
^3E-*gg*-*tg*	-62.4	1.6	54.6	0.2	-70.8	4.1	171.8	10.1
^3E-*gt*-*gg*	166.7	7.9	-74.2	0.4	40.1	2.9	-76.2	1.0
^3E-*gt*-*gt*	-167.0	10.9	-47.3	0.4	-173.1	9.1	70.3	1.9
^3E-*gt*-*tg*	177.2	9.2	-61.1	0.2	-73.7	3.5	170.4	10.1
^3E-*tg*-*gg*	69.3	4.4	-172.8	0.7	72.7	0.5	-43.9	5.6
^3E-*tg*-*gt*	57.2	6.9	175.6	0.8	-173.3	10.3	69.6	2.5
^3E-*tg*-*tg*	61.9	5.0	-177.6	0.7	-72.9	3.5	170.1	10.4
E_3-*gg*-*gg*	-60.1	1.5	54.5	0.2	58.1	1.1	-56.7	4.0
E_3-*gg*-*gt*	-55.2	1.4	61.6	0.2	-168.1	8.1	74.5	1.2
E_3-*gg*-*tg*	-55.6	1.9	62.1	0.8	-69.9	4.3	172.6	10.1
E_3-*gt*-*gg*	178.6	8.6	-63.1	0.1	56.4	1.1	-60.2	3.2
E_3-*gt*-*gt*	176.0	8.9	-64.3	0.1	177.5	10.6	60.2	3.3
E_3-*gt*-*tg*	164.5	7.3	-75.9	0.5	-81.3	2.4	161.2	9.8
E_3-*tg*-*gg*	58.3	5.8	173.9	0.6	61.2	1.0	-54.7	3.9
E_3-*tg*-*gt*	48.9	7.2	167.1	0.6	-168.7	9.0	73.1	1.6
E_3-*tg*-*tg*	54.2	6.0	171.9	0.6	-92.6	0.7	150.8	7.9
^4E-*gg*-*gg*	-60.8	1.6	53.7	0.2	55.8	1.3	-59.0	3.6
^4E-*gg*-*gt*	-56.6	1.4	60.1	0.2	-167.8	8.1	74.8	1.2
^4E-*gg*-*tg*	-53.8	2.4	63.9	0.6	-69.9	4.4	172.7	10.1
^4E-*gt*-*gg*	178.2	8.8	-63.5	0.1	56.4	1.2	-60.3	3.2
^4E-*gt*-*gt*	174.0	9.0	-66.1	0.1	177.3	10.6	60.1	3.4
^4E-*gt*-*tg*	163.2	7.4	-77.3	0.5	-81.0	2.5	161.5	9.9
^4E-*tg*-*gg*	60.4	5.2	176.0	0.6	63.0	0.9	-53.0	4.2
^4E-*tg*-*gt*	48.3	7.2	166.5	0.6	-168.3	8.9	73.5	1.6
^4E-*tg*-*tg*	52.6	6.1	170.0	0.5	-96.4	0.3	146.5	7.2
E_4-*gg*-*gg*	-62.1	1.5	53.4	0.2	59.2	1.0	-55.5	4.0
E_4-*gg*-*gt*	-66.5	0.7	50.3	0.3	-170.9	9.1	71.7	1.5
E_4-*gg*-*tg*	-60.1	1.7	58.4	0.1	-69.8	4.1	172.7	10.2
E_4-*gt*-*gg*	169.9	8.6	-71.3	0.7	39.7	2.9	-76.6	0.9
E_4-*gt*-*gt*	-156.1	10.6	-37.2	0.6	-171.5	8.9	72.3	1.9
E_4-*gt*-*tg*	-165.9	10.0	-44.7	0.4	-63.3	4.8	-179.3	9.9
E_4-*tg*-*gg*	78.4	2.8	-162.7	0.7	67.6	0.6	-49.1	4.8
E_4-*tg*-*gt*	55.2	7.0	173.7	0.8	-178.0	10.8	64.9	3.2
E_4-*tg*-*tg*	62.0	4.9	-177.4	0.7	-74.6	3.3	168.1	10.4
$^2T_1$-*gg*-*tg*	-60.0	1.5	58.5	0.1	172.4	10.1	62.0	1.0
$^2T_1$-*gt*-*tg*	167.4	7.9	-72.4	0.9	161.1	9.6	-70.7	0.7
^2E-*tg*-*tg*	87.3	1.3	-152.3	0.4	-176.0	10.4	-151.1	4.2
E_3-*gg*-*tg*	-54.2	2.2	63.4	0.6	172.5	10.1	70.1	0.7

Conformer	$\phi_{4,5}$	$J_{4,5}$	$\phi_{H4,C6}$	$J_{H4,C6}$	$\phi_{5,6R}$	$J_{5,6R}$	$\phi_{5,6S}$	$J_{5,6S}$
E_3-*gt-tg*	159.8	6.5	-80.6	0.2	160.9	9.9	-75.2	0.4
E_3-*tg-tg*	97.2	0.3	-142.3	0.3	176.4	10.4	-137.7	3.1
$^4T_1$-*gg-tg*	-58.6	2.1	59.9	0.7	173.9	10.5	67.0	0.7
$^4T_1$-*gt-tg*	155.6	7.4	-85.1	0.2	161.3	10.0	-76.6	0.2
$^4T_1$-*tg-tg*	98.6	0.2	-141.1	0.3	175.0	10.4	-135.0	2.8

B.2. Partial charges for 3.1–3.10

Table B.5. Partial charges for **3.1** determined by RESP charge fitting[4] of 200 conformations.

Atom	Partial charge	Standard deviation
CH_3	0.264	0.000
C1	0.394	0.000
O1	–0.458	0.000
C2	0.295	0.000
O2	–0.690	0.000
H (O2)	0.422	0.000
C3	0.277	0.000
O3	–0.719	0.000
H (O3)	0.432	0.000
C4	0.270	0.000
O4	–0.482	0.000
C5	0.232	0.077
O5	–0.609	0.070
H (O5)	0.393	0.044
C6	0.217	0.066
O6	–0.643	0.041
H (O6)	0.405	0.031

Table B.6. Partial charges for **3.2** determined by RESP charge fitting[4] of 200 conformations.

Atom	Partial charge	Standard deviation
CH_3	0.264	0.000
O1	–0.458	0.000
C1	0.368	0.000
C2	0.278	0.000
O2	–0.688	0.000
H (O2)	0.430	0.000
C3	0.370	0.000
O3	–0.703	0.000
H (O3)	0.404	0.000
C4	0.147	0.000
O4	–0.453	0.000
C5	0.307	0.069
O5	–0.659	0.054
H (O5)	0.392	0.029
C6	0.259	0.055
O6	–0.664	0.050
H (O6)	0.406	0.036

Table B.7. Partial charges for **3.3** determined by RESP charge fitting[4] of 200 conformations.

Atom	Partial charge	Standard deviation
CH_3	0.264	0.000
C1	0.409	0.049
O1	–0.458	0.000
C2	0.264	0.075
O2	–0.700	0.030
H (O2)	0.432	0.020
C3	0.296	0.083
O3	–0.736	0.030
H (O3)	0.445	0.021
C4	0.288	0.105
O4	–0.511	0.052
C5	0.315	0.118
O5	–0.729	0.049
H (O5)	0.436	0.029
C6	0.257	0.056
O6	–0.698	0.030
H (O6)	0.424	0.025

Table B.8. Partial charges for **3.4** determined by RESP charge fitting[4] of 200 conformations.

Atom	Partial charge	Standard deviation
CH_3	0.264	0.000
C1	0.403	0.043
O1	–0.458	0.000
C2	0.272	0.067
O2	–0.707	0.035
H (O2)	0.434	0.021
C3	0.281	0.089
O3	–0.740	0.033
H (O3)	0.448	0.024
C4	0.286	0.102
O4	0.000	0.000
C5	–0.502	0.041
O5	0.340	0.123
H (O5)	–0.734	0.047
C6	0.437	0.024
O6	0.246	0.058
H (O6)	–0.696	0.036

Table B.9. Partial charges for **3.5** determined by RESP charge fitting[4] of 200 conformations.

Atom	Partial charge	Standard deviation
CH_3	0.264	0.000
C1	0.417	0.067
O1	–0.458	0.000
C2	0.226	0.070
O2	–0.669	0.041
H (O2)	0.429	0.022
C3	0.273	0.111
O3	–0.723	0.035
H (O3)	0.443	0.027
C4	0.386	0.148
O4	–0.543	0.075
C5	0.258	0.111
O5	–0.727	0.050
H (O5)	0.438	0.029
C6	0.261	0.056
O6	–0.708	0.038
H (O6)	0.432	0.024

Table B.10. Partial charges for **3.6** determined by RESP charge fitting[4] of 200 conformations.

Atom	Partial charge	Standard deviation
CH_3	0.264	0.000
C1	0.413	0.048
O1	–0.458	0.000
C2	0.217	0.063
O2	–0.661	0.037
H (O2)	0.430	0.018
C3	0.242	0.104
O3	–0.712	0.033
H (O3)	0.444	0.027
C4	0.387	0.134
O4	–0.528	0.048
C5	0.254	0.114
O5	–0.714	0.039
H (O5)	0.434	0.021
C6	0.260	0.053
O6	–0.698	0.035
H (O6)	0.426	0.024

Table B.11. Partial charges for **3.7** determined by RESP charge fitting[4] of 200 conformations.

Atom	Partial charge	Standard deviation
CH3	0.264	0.000
C1	0.435	0.061
O1	–0.458	0.000
C2	0.272	0.076
O2	–0.695	0.028
H (O2)	0.431	0.027
C3	0.260	0.079
O3	–0.717	0.042
H (O3)	0.456	0.030
C4	0.211	0.096
O4	–0.526	0.056
C5	0.362	0.111
O5	–0.709	0.057
H (O5)	0.437	0.032
C6	0.257	0.067
O6	–0.714	0.037
H (O6)	0.433	0.024

Table B.12. Partial charges for **3.8** determined by RESP charge fitting[4] of 200 conformations.

Atom	Partial charge	Standard deviation
CH3	0.264	0.000
C1	0.428	0.056
O1	–0.458	0.000
C2	0.251	0.067
O2	–0.682	0.031
H (O2)	0.431	0.017
C3	0.252	0.070
O3	–0.686	0.041
H (O3)	0.439	0.020
C4	0.177	0.097
O4	–0.466	0.042
C5	0.327	0.105
O5	–0.702	0.056
H (O5)	0.431	0.027
C6	0.274	0.061
O6	–0.713	0.032
H (O6)	0.432	0.025

Table B.13. Partial charges for **3.9** determined by RESP charge fitting[4] of 200 conformations.

Atom	Partial charge	Standard deviation
CH_3	0.264	0.000
C1	0.381	0.065
O1	–0.458	0.000
C2	0.377	0.098
O2	–0.729	0.018
H (O2)	0.431	0.016
C3	0.235	0.093
O3	–0.697	0.023
H (O3)	0.431	0.016
C4	0.279	0.078
O4	–0.681	0.029
H (O4)	0.435	0.019
C5	0.100	0.094
O5	–0.437	0.046
C6	0.362	0.110
O6	–0.691	0.033
H (O6)	0.416	0.018
H6	0.000	0.000
C7	0.250	0.045
O7	–0.680	0.031
H (O7)	0.412	0.026

Table B.14. Partial charges for **3.10** determined by RESP charge fitting[4] of 200 conformations.

Atom	Partial charge	Standard deviation
CH3	0.264	0.000
C1	0.381	0.065
O1	–0.458	0.000
C2	0.377	0.098
O2	–0.729	0.018
H (O2)	0.431	0.016
C3	0.235	0.093
O3	–0.697	0.023
H (O3)	0.431	0.016
C4	0.279	0.078
O4	–0.681	0.029
H (O4)	0.435	0.019
C5	0.100	0.094
O5	–0.437	0.046
C6	0.362	0.110
O6	–0.691	0.033
H (O6)	0.416	0.018
H6	0.000	0.000
C7	0.250	0.045
O7	–0.680	0.031
H (O7)	0.412	0.026

B.3. References

1. Frisch, M. J.; Trucks, G. W.; Schlegel, H. B.; Scuseria, G. E.; Robb, M. A.; Cheeseman, J. R.; Montgomery, J. A., Jr.; Vreven, T.; Kudin, K. N.; Burant, J. C.; Millam, J. M.; Iyengar, S. S.; Tomasi, J.; Barone, V.; Mennucci, B.; Cossi, M.; Scalmani, G.; Rega, N.; Petersson, G. A.; Nakatsuji, H.; Hada, M.; Ehara, M.; Toyota, K.; Fukuda, R.; Hasegawa, J.; Ishida, M.; Nakajima, T.; Honda, Y.; Kitao, O.; Nakai, H.; Klene, M.; Li, X.; Knox, J. E.; Hratchian, H. P.; Cross, J. B.; Bakken, V.; Adamo, C.; Jaramillo, J.; Gomperts, R.; Stratmann, R. E.; Yazyev, O.; Austin, A. J.; Cammi, R.; Pomelli, C.; Ochterski, J. W.; Ayala, P. Y.; Morokuma, K.; Voth, G. A.; Salvador, P.; Dannenberg, J. J.; Zakrzewski, V. G.; Dapprich, S.; Daniels, A. D.; Strain, M. C.; Farkas, O.; Malick, D. K.; Rabuck, A. D.; Raghavachari, K.; Foresman, J. B.; Ortiz, J. V.; Cui, Q.; Baboul, A. G.; Clifford, S.; Cioslowski, J.; Stefanov, B. B.; Liu, G.; Liashenko, A.; Piskorz, P.; Komaromi, I.; Martin, R. L.; Fox, D. J.; Keith, T.; Al-Laham, M. A.; Peng, C. Y.; Nanayakkara, A.; Challacombe, M.; Gill, P. M. W.; Johnson, B.; Chen, W.; Wong, M. W.; Gonzalez, C.; Pople, J. A. *Gaussian 03* Revision C.02; Gaussian, Inc.: Wallingford, CT, 2004.

2. Becke, A. D. *J. Chem. Phys.* **1993**, *98*, 5648–5652.

3. Stenutz, R.; Carmichael, I.; Widmalm, G.; Serianni, A. S. *J. Org. Chem.* **2002**, *67*, 949–958.

4. Bayly, C. I.; Cieplak, P.; Cornell, W.; Kollman, P. A. *J. Phys. Chem.* **1993**, *97*, 10269–10280.

Appendix C:

Supporting information for Chapter 4

C.1. Relative energies used to develop new torsion parameters

The tables below show O4–C4–C5–O5 and O5–C5–C6–O6 dihedral angles for **4.1** and **4.2** that are shown in Figures 4.10 and 4.11 in Section 4.3.2.1. The C3–C4–C5–C6 and O4–C4–C5–C6 dihedrals angles that were used in the Metropolis Monte Carlo simulated annealing procedure[1] are also included. The QM relative energies were calculated in Gaussian 03[2] at the B3LYP/6-31++G(2d,2p)[3-5] level of theory. The MM1 relative energies were calculated using the Sander module of the AMBER 10[6] program and the GLYCAM06[7] force field. The MM2 relative energies are from GLYCAM06 without the terms for the O4–C4–C5–C6 and C3–C4–C5–C6 dihedral angles. The MM3 relative energies are from GLYCAM06 with the new parameters described in Section 4.3.2.2. The relative energies are scaled independently with the lowest energy conformation set to 0 kcal/mol.

Table C.1. Dihedral angles and relative energies for **4.1** with the ^{2}E ring conformation.

O4-C4-C5-O5 (degrees)	O5-C5-C6-O6 (degrees)	C3-C4-C5-C6 (degrees)	O4-C4-C5-C6 (degrees)	QM rel. E (kcal/mol)	MM1 rel. E (kcal/mol)	MM2 rel. E (kcal/mol)	MM3 rel. E (kcal/mol)
0.02	0.01	113.01	-126.58	14.34	20.09	19.49	18.56
0.01	14.93	112.77	-126.84	12.71	17.95	17.34	16.41
-0.04	29.95	113.4	-126.15	9.80	14.18	13.58	12.65
-0.04	45.01	114.87	-124.58	6.95	10.22	9.64	8.71
0.02	60.0	116.32	-123.03	5.45	7.47	6.90	5.98
-0.05	75.03	116.72	-122.59	5.82	6.69	6.12	5.20
-0.04	89.94	116.42	-122.97	7.49	7.83	7.26	6.34
-0.06	105.01	115.75	-123.82	9.35	9.54	8.96	8.03
0.01	120.03	115.32	-124.45	10.35	10.56	9.98	9.05
-0.03	134.99	115.47	-124.5	10.17	10.07	9.49	8.56
-0.01	149.98	116.9	-123.34	9.23	8.89	8.32	7.39
-0.04	164.99	119.22	-121.38	8.28	8.15	7.61	6.69
-0.05	-179.95	121.36	-119.52	8.21	8.74	8.22	7.31
-0.01	-165.03	122.27	-118.78	9.35	10.80	10.29	9.38

O4-C4-C5-O5 (degrees)	O5-C5-C6-O6 (degrees)	C3-C4-C5-C6 (degrees)	O4-C4-C5-C6 (degrees)	QM rel. E (kcal/mol)	MM1 rel. E (kcal/mol)	MM2 rel. E (kcal/mol)	MM3 rel. E (kcal/mol)
-0.02	-150.01	121.54	-119.66	11.28	13.75	13.23	12.31
0.05	-134.98	119.7	-121.53	12.84	16.12	15.59	14.66
-0.0	-120.0	117.3	-123.81	13.14	16.70	16.14	15.20
-0.03	-104.99	115.39	-125.45	12.06	14.89	14.31	13.37
0.09	-90.04	114.81	-125.66	10.25	12.55	11.96	11.02
0.01	-75.0	115.15	-124.94	8.83	11.19	10.61	9.68
0.01	-60.0	115.54	-124.12	8.71	11.96	11.38	10.45
0.02	-45.0	115.26	-124.13	10.10	14.45	13.87	12.95
-0.03	-29.99	114.47	-124.84	12.30	17.51	16.92	15.99
-0.05	-15.02	113.65	-125.8	14.08	19.77	19.17	18.24
0.02	0.01	113.01	-126.58	14.34	20.11	19.50	18.57
15.15	-0.01	130.16	-110.46	13.54	19.92	19.50	18.71
15.13	14.95	129.99	-110.54	11.76	17.77	17.34	16.56
15.11	29.91	130.62	-109.77	8.81	13.91	13.49	12.72
15.15	44.96	132.01	-108.25	6.00	9.85	9.45	8.71
15.08	59.98	133.23	-107.01	4.66	6.87	6.48	5.77
15.12	75.02	133.81	-106.53	5.15	6.04	5.65	4.95
15.06	89.99	133.54	-106.99	6.88	7.12	6.73	6.02
15.13	104.97	133.03	-107.68	8.64	8.85	8.45	7.72
15.08	119.98	132.49	-108.32	9.44	9.90	9.50	8.75
15.05	134.98	132.6	-108.28	9.01	9.26	8.86	8.12
15.1	149.95	133.76	-107.23	7.80	7.95	7.56	6.84
15.06	165.03	135.61	-105.5	6.69	7.12	6.75	6.06
15.01	-179.98	137.43	-103.87	6.60	7.62	7.27	6.63
15.12	-164.97	138.47	-103.12	7.82	9.77	9.43	8.81
15.07	-150.0	137.78	-103.98	9.78	12.84	12.49	11.85
15.08	-135.0	136.0	-105.8	11.40	15.17	14.81	14.11
15.13	-119.98	133.89	-107.79	11.83	15.62	15.23	14.49
15.08	-104.98	132.1	-109.29	10.93	13.93	13.52	12.75
15.0	-90.0	131.32	-109.71	9.37	11.82	11.40	10.63
15.13	-74.97	131.68	-108.96	8.17	10.88	10.47	9.72
15.09	-60.02	131.93	-108.44	8.24	11.78	11.37	10.63
15.1	-45.0	131.78	-108.52	9.70	14.26	13.85	13.11
15.04	-30.02	131.22	-109.2	11.85	17.41	17.00	16.24
15.04	-14.99	130.63	-109.95	13.49	19.72	19.30	18.53
15.15	-0.01	130.16	-110.46	13.54	19.90	19.48	18.70
29.92	0.02	145.98	-95.07	11.54	18.32	18.04	17.66
29.89	14.9	145.88	-95.03	9.71	16.21	15.94	15.56
29.91	30.02	146.51	-94.25	6.79	12.40	12.13	11.78
29.94	44.98	147.78	-92.92	4.18	8.17	7.92	7.61
29.83	60.03	148.96	-91.79	2.95	5.15	4.91	4.63
29.92	75.02	149.59	-91.27	3.48	4.19	3.95	3.69
29.87	90.02	149.3	-91.7	5.16	5.07	4.83	4.55
29.91	104.98	148.76	-92.37	6.74	6.79	6.55	6.25
29.86	119.98	148.17	-92.96	7.34	7.71	7.46	7.14
29.88	135.03	148.22	-92.9	6.71	7.27	7.02	6.70
29.89	150.04	149.11	-92.01	5.36	5.95	5.71	5.42
29.93	165.0	150.89	-90.36	4.24	5.06	4.83	4.59
29.92	-179.98	152.7	-88.77	4.21	5.49	5.27	5.09
29.87	-164.96	153.52	-88.19	5.51	7.59	7.38	7.21
29.92	-149.97	152.97	-88.89	7.53	10.55	10.34	10.15
29.91	-135.0	151.23	-90.64	9.21	12.83	12.60	12.36
29.92	-119.97	149.1	-92.59	9.81	13.41	13.16	12.85

O4-C4-C5-O5 (degrees)	O5-C5-C6-O6 (degrees)	C3-C4-C5-C6 (degrees)	O4-C4-C5-C6 (degrees)	QM rel. E (kcal/mol)	MM1 rel. E (kcal/mol)	MM2 rel. E (kcal/mol)	MM3 rel. E (kcal/mol)
29.9	-105.01	147.25	-94.17	9.16	12.03	11.77	11.41
29.89	-89.97	146.23	-94.81	7.86	10.42	10.15	9.78
29.85	-74.96	146.18	-94.56	6.87	9.70	9.43	9.06
29.91	-60.02	146.77	-93.89	7.00	10.56	10.30	9.96
29.93	-45.01	147.08	-93.69	8.36	12.93	12.67	12.33
29.91	-29.94	146.86	-94.07	10.27	15.88	15.61	15.26
29.93	-15.0	146.42	-94.62	11.66	18.12	17.86	17.49
29.92	-0.04	145.98	-95.07	11.55	18.28	18.01	17.63
44.97	0.02	160.74	-79.86	9.29	15.86	15.71	15.79
44.96	15.07	160.52	-79.99	7.46	13.83	13.68	13.76
45.04	30.02	161.09	-79.33	4.72	10.02	9.87	9.97
44.94	45.04	162.19	-78.22	2.24	6.10	5.97	6.10
45.08	59.96	163.61	-76.82	1.05	2.85	2.72	2.89
45.03	75.01	164.2	-76.28	1.52	1.84	1.72	1.90
45.03	90.02	164.04	-76.53	3.01	2.75	2.62	2.79
45.06	105.02	163.48	-77.15	4.44	4.17	4.05	4.20
45.0	120.04	162.81	-77.78	4.94	5.16	5.02	5.16
45.02	134.99	162.61	-77.94	4.28	4.82	4.68	4.82
45.07	150.04	163.3	-77.26	2.99	3.60	3.47	3.63
45.0	164.97	164.88	-75.85	2.00	2.69	2.57	2.76
45.01	-179.98	166.7	-74.21	2.03	3.09	2.98	3.21
45.0	-164.99	167.61	-73.45	3.29	5.05	4.94	5.19
45.02	-150.03	167.1	-74.05	5.33	7.96	7.85	8.08
45.02	-134.98	165.22	-75.84	7.17	10.41	10.29	10.47
45.01	-120.04	162.61	-78.18	8.08	11.31	11.17	11.30
45.03	-105.07	160.15	-80.3	7.82	10.41	10.26	10.33
45.04	-90.05	158.86	-81.32	6.77	8.99	8.83	8.88
45.02	-75.01	159.08	-81.03	5.84	8.24	8.08	8.14
44.99	-60.0	160.14	-80.04	5.82	8.92	8.77	8.85
45.03	-45.01	161.2	-79.18	6.83	11.05	10.91	11.01
44.98	-30.01	161.51	-79.05	8.44	13.72	13.58	13.68
45.01	-14.99	161.27	-79.38	9.54	15.74	15.60	15.70
44.94	0.0	160.73	-79.9	9.30	15.94	15.79	15.87
60.02	0.01	174.67	-65.17	7.93	14.22	14.16	14.54
59.99	15.02	173.88	-65.77	6.24	12.02	11.95	12.33
60.07	30.03	174.07	-65.47	3.66	8.31	8.25	8.63
60.0	45.01	175.16	-64.37	1.23	4.27	4.22	4.61
60.03	60.03	176.62	-62.91	0.00	1.24	1.19	1.60
60.07	74.99	177.47	-62.09	0.33	0.16	0.11	0.53
60.01	90.0	177.45	-62.17	1.65	0.97	0.93	1.35
60.08	105.0	176.95	-62.68	2.96	2.53	2.48	2.89
60.0	119.98	176.04	-63.56	3.46	3.47	3.42	3.82
60.03	134.98	175.49	-64.04	2.93	3.28	3.23	3.63
60.06	150.03	176.0	-63.58	1.79	2.09	2.04	2.45
60.03	165.0	177.53	-62.17	0.90	1.26	1.22	1.64
60.05	-179.95	179.39	-60.45	0.98	1.66	1.63	2.05
60.03	-164.98	-179.64	-59.59	2.25	3.58	3.55	3.98
60.02	-150.02	179.7	-60.17	4.41	6.75	6.71	7.14
60.03	-135.01	177.2	-62.37	6.68	9.35	9.31	9.72
60.02	-120.01	173.74	-65.38	8.13	10.38	10.32	10.71
59.99	-104.97	170.89	-67.96	8.13	9.77	9.69	10.04
60.03	-90.06	169.95	-68.86	7.08	8.47	8.39	8.73
60.08	-75.01	170.83	-68.11	5.90	7.71	7.64	7.98

O4-C4-C5-O5 (degrees)	O5-C5-C6-O6 (degrees)	C3-C4-C5-C6 (degrees)	O4-C4-C5-C6 (degrees)	QM rel. E (kcal/mol)	MM1 rel. E (kcal/mol)	MM2 rel. E (kcal/mol)	MM3 rel. E (kcal/mol)
60.04	-59.97	172.49	-66.62	5.45	7.87	7.81	8.18
60.04	-45.07	174.11	-65.25	6.04	9.50	9.44	9.82
60.01	-30.0	175.18	-64.51	7.29	11.98	11.92	12.32
59.98	-15.05	175.37	-64.54	8.19	14.04	13.99	14.38
60.05	0.03	174.71	-65.14	7.93	14.13	14.07	14.46
75.02	0.03	-172.72	-51.47	8.15	13.75	13.75	14.17
75.06	14.93	-173.78	-52.31	6.65	11.75	11.74	12.17
75.03	30.04	-173.97	-52.3	4.04	8.00	7.99	8.42
74.97	44.97	-172.86	-51.14	1.56	4.06	4.06	4.48
75.05	59.97	-171.22	-49.48	0.24	1.00	1.00	1.41
75.01	74.96	-170.26	-48.58	0.43	0.00	0.00	0.40
74.96	89.93	-170.21	-48.59	1.66	0.95	0.95	1.36
74.99	105.0	-170.91	-49.26	3.01	2.55	2.55	2.96
75.01	119.95	-172.02	-50.27	3.64	3.58	3.58	4.00
74.97	134.99	-172.72	-50.94	3.22	3.36	3.35	3.77
74.98	150.02	-172.26	-50.51	2.21	2.30	2.30	2.72
75.06	165.0	-170.6	-48.95	1.41	1.40	1.40	1.81
74.98	-179.97	-168.91	-47.31	1.53	1.82	1.83	2.22
74.99	-164.99	-168.07	-46.41	2.99	4.25	4.25	4.63
74.99	-150.05	-169.36	-47.36	5.67	7.60	7.61	8.00
75.05	-135.05	-172.62	-49.97	8.67	10.35	10.35	10.76
75.02	-120.01	-176.3	-53.29	10.37	11.41	11.40	11.83
74.96	-105.02	-178.69	-55.75	10.13	10.95	10.93	11.37
74.96	-89.94	-179.07	-56.34	8.63	9.48	9.46	9.90
75.02	-74.94	-177.85	-55.26	6.96	8.31	8.30	8.74
75.0	-60.03	-175.92	-53.46	6.06	8.04	8.03	8.46
74.97	-44.98	-173.96	-51.81	6.25	9.22	9.21	9.64
74.98	-30.03	-172.47	-50.78	7.20	11.52	11.51	11.93
74.99	-15.01	-172.04	-50.71	8.12	13.42	13.42	13.84
75.02	0.04	-172.7	-51.46	8.16	13.77	13.76	14.19
89.91	-0.03	-160.6	-38.15	9.77	14.89	14.91	15.17
89.94	14.96	-161.67	-39.04	8.36	12.85	12.87	13.14
89.91	29.95	-161.97	-39.07	5.56	9.00	9.02	9.29
89.92	44.96	-160.55	-37.65	2.90	4.81	4.83	5.08
89.84	60.01	-158.73	-35.91	1.42	1.84	1.86	2.08
89.85	75.04	-157.72	-34.95	1.56	1.03	1.05	1.25
89.91	90.0	-157.81	-35.04	2.86	2.13	2.15	2.35
89.88	105.0	-158.85	-35.92	4.37	3.99	4.01	4.22
89.89	119.98	-160.03	-37.01	5.16	5.01	5.03	5.26
89.85	135.04	-160.72	-37.67	4.81	4.77	4.79	5.03
89.94	150.0	-160.11	-37.09	3.77	3.46	3.48	3.72
89.98	165.01	-158.4	-35.46	3.02	2.75	2.77	2.98
89.94	179.97	-156.71	-33.75	3.36	3.60	3.62	3.80
89.92	-165.02	-156.5	-33.12	5.43	6.53	6.55	6.71
89.93	-150.07	-158.48	-34.31	8.98	10.06	10.08	10.26
89.94	-135.01	-161.77	-37.07	12.36	12.90	12.92	13.15
89.88	-119.99	-164.98	-40.34	13.81	14.10	14.12	14.41
89.86	-104.97	-167.05	-42.66	12.98	13.10	13.11	13.44
89.89	-90.03	-167.4	-43.13	10.82	11.25	11.27	11.60
89.89	-75.02	-166.22	-41.99	8.63	9.52	9.54	9.86
89.94	-60.02	-164.05	-39.94	7.35	8.99	9.01	9.29
89.88	-44.99	-161.91	-38.18	7.26	10.03	10.05	10.30
89.89	-30.07	-160.46	-37.26	8.18	12.33	12.35	12.59

O4-C4-C5-O5 (degrees)	O5-C5-C6-O6 (degrees)	C3-C4-C5-C6 (degrees)	O4-C4-C5-C6 (degrees)	QM rel. E (kcal/mol)	MM1 rel. E (kcal/mol)	MM2 rel. E (kcal/mol)	MM3 rel. E (kcal/mol)
89.91	-14.99	-160.11	-37.37	9.39	14.33	14.35	14.59
89.87	-0.03	-160.63	-38.18	9.76	14.93	14.94	15.20
105.02	-0.05	-146.95	-23.8	11.94	16.97	16.97	16.97
104.95	15.0	-148.23	-24.86	10.33	14.47	14.48	14.49
104.97	30.0	-147.84	-24.5	7.47	10.39	10.39	10.40
104.94	44.98	-145.81	-22.76	4.66	6.30	6.30	6.28
104.99	60.0	-143.58	-20.71	3.10	3.55	3.54	3.49
104.93	75.05	-142.86	-19.94	3.29	2.82	2.82	2.75
104.99	90.01	-143.49	-20.29	4.79	4.23	4.22	4.16
105.01	104.98	-144.76	-21.32	6.48	6.30	6.30	6.25
105.01	119.99	-145.99	-22.43	7.28	7.40	7.40	7.37
104.99	135.04	-146.51	-22.97	6.88	6.82	6.82	6.80
104.93	149.96	-145.8	-22.41	5.85	5.47	5.48	5.45
104.99	165.0	-143.85	-20.61	5.18	4.93	4.93	4.87
104.99	179.99	-142.39	-18.85	6.08	6.57	6.56	6.48
104.96	-165.04	-142.61	-18.2	9.12	9.85	9.84	9.75
104.93	-149.99	-144.49	-19.37	13.26	13.70	13.70	13.62
104.99	-134.97	-147.46	-22.12	16.40	16.65	16.66	16.61
105.01	-120.04	-150.81	-25.45	17.20	17.14	17.16	17.17
105.07	-105.01	-153.26	-27.92	15.78	15.66	15.68	15.74
104.95	-89.96	-153.96	-28.66	13.10	13.22	13.24	13.31
104.96	-75.0	-152.42	-27.27	10.58	11.15	11.17	11.21
104.95	-59.97	-149.76	-24.93	9.08	10.54	10.55	10.55
105.0	-45.03	-147.55	-23.18	8.90	11.57	11.58	11.55
104.98	-29.94	-146.67	-22.71	9.97	13.89	13.89	13.86
105.01	-15.0	-146.54	-23.04	11.44	16.22	16.23	16.20
104.96	-0.02	-147.01	-23.86	11.93	16.87	16.87	16.87
120.04	-0.01	-131.42	-8.34	13.60	18.76	18.70	18.54
120.07	15.02	-131.67	-8.82	11.92	16.11	16.05	15.90
120.04	30.04	-130.43	-8.04	8.90	11.96	11.90	11.74
120.09	44.96	-127.96	-6.01	5.99	7.82	7.74	7.59
120.04	60.02	-126.05	-4.23	4.39	5.02	4.93	4.79
120.01	74.99	-125.84	-3.75	4.81	4.53	4.44	4.29
120.08	89.93	-126.88	-4.32	6.49	6.27	6.19	6.04
120.04	105.02	-128.44	-5.5	8.21	8.52	8.45	8.29
120.04	120.04	-129.55	-6.52	8.95	9.35	9.28	9.12
120.08	135.05	-129.52	-6.73	8.49	8.65	8.59	8.43
120.08	149.96	-128.2	-5.78	7.50	7.42	7.34	7.19
120.04	165.0	-126.37	-3.92	7.18	7.33	7.25	7.09
120.05	-179.98	-125.03	-1.96	8.85	9.30	9.20	9.06
120.06	-165.0	-125.2	-1.23	12.54	13.04	12.95	12.80
120.06	-150.03	-127.51	-2.71	16.54	17.05	16.97	16.80
120.04	-135.0	-131.11	-5.8	19.15	19.72	19.66	19.48
120.06	-120.02	-134.64	-9.17	19.62	19.94	19.90	19.72
120.07	-104.96	-136.84	-11.54	17.90	17.88	17.86	17.69
120.11	-90.01	-136.78	-11.8	14.99	14.93	14.90	14.74
120.07	-75.02	-134.98	-10.29	12.14	12.58	12.54	12.37
120.09	-60.01	-132.5	-8.15	10.45	11.75	11.70	11.53
120.06	-45.01	-130.69	-6.83	10.39	13.10	13.04	12.87
120.07	-30.0	-130.09	-6.7	11.68	15.73	15.67	15.51
120.09	-14.99	-130.54	-7.38	13.29	18.49	18.43	18.26
120.04	-0.01	-131.42	-8.33	13.59	18.69	18.63	18.47
134.97	-0.06	-113.29	8.45	14.04	19.49	19.32	19.33

O4-C4-C5-O5 (degrees)	O5-C5-C6-O6 (degrees)	C3-C4-C5-C6 (degrees)	O4-C4-C5-C6 (degrees)	QM rel. E (kcal/mol)	MM1 rel. E (kcal/mol)	MM2 rel. E (kcal/mol)	MM3 rel. E (kcal/mol)
135.01	15.0	-113.21	8.19	12.25	16.73	16.56	16.56
134.96	30.02	-112.08	8.93	9.00	12.45	12.26	12.29
135.03	45.02	-110.1	10.66	5.95	8.13	7.93	8.00
135.05	60.01	-108.59	12.19	4.56	5.29	5.08	5.18
135.0	74.96	-108.49	12.57	5.22	5.05	4.83	4.94
135.06	90.03	-109.4	12.06	7.07	6.94	6.73	6.82
134.96	104.98	-110.69	11.01	8.76	9.12	8.92	8.99
134.99	120.01	-111.34	10.29	9.40	9.89	9.70	9.75
135.02	134.96	-111.1	10.25	8.85	9.08	8.88	8.94
135.02	149.98	-109.85	11.32	7.93	8.14	7.94	8.01
134.95	164.97	-108.03	13.37	8.11	8.34	8.12	8.24
135.0	179.97	-106.88	15.35	10.33	10.83	10.60	10.77
135.0	-164.97	-107.31	15.89	14.02	14.80	14.57	14.75
134.97	-149.94	-109.27	14.51	17.72	18.87	18.66	18.79
134.99	-135.01	-112.29	11.82	20.14	21.29	21.10	21.16
135.02	-120.01	-115.75	8.64	20.48	21.24	21.09	21.08
134.99	-104.97	-118.52	6.08	18.59	18.73	18.59	18.53
134.97	-89.97	-119.38	5.32	15.47	15.36	15.23	15.16
135.01	-75.06	-118.02	6.58	12.49	12.68	12.54	12.49
134.96	-60.01	-115.59	8.43	10.75	11.86	11.70	11.69
135.01	-44.96	-113.37	9.65	10.83	13.59	13.42	13.44
134.99	-29.96	-112.45	9.75	12.33	16.69	16.51	16.54
135.0	-15.0	-112.72	9.21	13.89	19.40	19.22	19.24
134.98	-0.03	-113.28	8.45	14.03	19.55	19.37	19.38
150.0	0.01	-95.6	25.11	12.83	18.09	17.76	18.23
150.03	15.02	-95.98	24.68	10.91	15.42	15.09	15.55
150.05	29.99	-95.27	25.18	7.77	11.29	10.95	11.43
150.02	44.97	-93.86	26.43	5.01	6.93	6.58	7.10
150.07	60.03	-92.43	27.84	3.89	4.05	3.69	4.25
150.04	75.03	-92.0	28.4	4.62	3.81	3.45	4.03
150.06	89.99	-92.55	28.11	6.37	5.67	5.31	5.88
150.04	104.99	-93.52	27.33	7.91	7.70	7.35	7.89
150.03	120.02	-94.22	26.64	8.41	8.49	8.15	8.67
149.99	135.0	-93.96	26.67	7.88	8.02	7.67	8.20
150.04	149.97	-92.57	27.98	7.25	7.21	6.85	7.41
150.06	165.03	-90.98	30.08	7.86	7.88	7.50	8.13
150.04	179.94	-89.15	32.33	10.07	10.31	9.91	10.60
150.02	-165.01	-89.07	33.0	13.49	14.24	13.84	14.55
150.0	-149.98	-91.62	31.49	16.94	18.11	17.73	18.39
150.0	-135.0	-95.59	28.61	19.30	20.48	20.14	20.70
150.05	-119.99	-99.61	25.38	19.59	20.31	20.01	20.46
150.05	-104.99	-102.34	22.97	17.69	17.70	17.42	17.79
150.01	-90.02	-102.74	22.4	14.54	14.15	13.88	14.23
149.99	-75.05	-100.86	23.63	11.48	11.31	11.03	11.43
150.07	-60.04	-98.17	25.19	9.79	10.55	10.24	10.69
150.04	-45.01	-96.13	25.96	10.00	12.26	11.93	12.42
150.07	-30.02	-94.48	26.45	11.52	15.49	15.15	15.66
150.05	-15.0	-94.55	26.05	12.92	18.14	17.80	18.30
150.0	0.01	-95.61	25.1	12.82	18.02	17.69	18.16
165.02	-0.06	-79.8	40.78	10.84	15.70	15.21	16.13
165.01	14.98	-80.55	40.05	9.08	13.36	12.87	13.77
164.98	30.03	-80.36	40.13	6.34	9.20	8.71	9.62
164.97	45.02	-79.17	41.17	3.96	5.15	4.65	5.58

O4-C4-C5-O5 (degrees)	O5-C5-C6-O6 (degrees)	C3-C4-C5-C6 (degrees)	O4-C4-C5-C6 (degrees)	QM rel. E (kcal/mol)	MM1 rel. E (kcal/mol)	MM2 rel. E (kcal/mol)	MM3 rel. E (kcal/mol)
164.97	60.06	-77.78	42.55	2.93	2.39	1.87	2.84
165.0	74.99	-77.23	43.32	3.50	1.91	1.39	2.37
164.99	90.01	-77.61	43.2	4.98	3.57	3.05	4.03
164.96	104.99	-78.23	42.65	6.32	5.58	5.07	6.03
165.0	119.99	-78.44	42.21	6.78	6.66	6.15	7.10
165.0	134.98	-78.1	42.33	6.41	6.38	5.86	6.82
164.95	149.98	-77.32	43.41	6.14	5.73	5.21	6.19
164.99	165.02	-75.37	45.69	6.93	6.39	5.85	6.86
165.02	-180.0	-74.13	47.67	8.91	8.56	8.00	9.04
165.07	-165.04	-74.79	48.27	11.89	12.16	11.61	12.66
165.04	-149.95	-77.34	47.06	15.11	15.99	15.46	16.49
165.06	-134.97	-80.8	44.64	17.40	18.29	17.79	18.77
165.06	-120.01	-83.99	41.91	17.64	18.06	17.59	18.52
164.98	-104.98	-85.87	39.81	15.65	15.29	14.85	15.72
165.05	-90.04	-85.81	39.18	12.42	11.55	11.11	11.97
165.0	-74.93	-84.37	39.56	9.41	8.67	8.22	9.10
165.02	-60.03	-81.79	40.71	7.93	7.80	7.32	8.23
165.06	-45.01	-79.19	41.83	8.11	9.47	8.97	9.91
164.96	-29.99	-78.39	42.02	9.50	12.70	12.19	13.14
164.99	-14.99	-78.8	41.63	10.85	15.42	14.92	15.86
165.02	-0.03	-79.81	40.77	10.84	15.72	15.23	16.15
-179.92	-0.04	-65.77	55.15	9.30	13.71	13.05	14.16
-179.98	15.03	-67.03	54.0	7.96	11.42	10.78	11.89
-179.94	29.95	-67.07	53.9	5.65	7.85	7.22	8.32
-179.98	45.0	-66.02	54.89	3.41	4.17	3.52	4.63
-179.99	60.04	-64.54	56.46	2.26	1.53	0.87	1.97
180.0	74.96	-63.63	57.51	2.54	1.05	0.37	1.48
-179.95	89.95	-63.4	57.76	3.68	2.23	1.55	2.65
-179.93	105.0	-63.64	57.36	4.85	4.16	3.49	4.59
-179.96	119.98	-64.09	56.65	5.44	5.16	4.49	5.60
-179.96	134.99	-64.49	56.55	5.45	5.16	4.49	5.60
179.99	150.0	-63.88	57.6	5.54	4.69	4.02	5.13
-179.96	165.03	-62.5	59.73	6.28	5.31	4.61	5.71
-179.97	179.98	-61.55	61.8	7.83	7.17	6.47	7.55
-179.96	-165.03	-61.74	62.79	10.34	10.42	9.71	10.79
-179.98	-150.01	-63.37	62.15	13.17	13.70	13.00	14.09
179.99	-135.02	-66.04	60.08	15.09	15.71	15.04	16.14
-179.98	-120.02	-68.85	57.36	15.05	14.98	14.34	15.45
-179.92	-105.03	-70.98	54.77	13.12	12.15	11.54	12.65
-179.98	-90.04	-71.59	53.18	10.21	8.94	8.34	9.43
-179.98	-74.97	-69.99	53.35	7.59	6.57	5.96	7.06
-179.98	-59.97	-67.55	54.43	6.23	6.13	5.50	6.60
-179.97	-44.99	-65.66	55.59	6.44	7.69	7.03	8.14
-179.96	-30.0	-64.62	56.27	7.77	10.50	9.84	10.95
-179.98	-15.01	-64.66	56.12	9.12	13.25	12.59	13.70
-179.92	-0.05	-65.77	55.15	9.30	13.56	12.91	14.02
-165.04	0.02	-53.65	67.99	9.25	13.04	12.25	13.23
-165.06	15.01	-55.03	66.74	8.25	11.45	10.68	11.68
-165.08	30.04	-54.92	66.73	6.01	8.22	7.45	8.45
-165.03	45.0	-53.29	68.24	3.61	4.87	4.08	5.06
-165.06	59.99	-51.18	70.24	2.14	2.08	1.27	2.20
-165.06	75.07	-49.87	71.46	2.09	1.16	0.33	1.23
-165.0	90.07	-49.75	71.57	3.10	2.16	1.33	2.22

O4-C4-C5-O5 (degrees)	O5-C5-C6-O6 (degrees)	C3-C4-C5-C6 (degrees)	O4-C4-C5-C6 (degrees)	QM rel. E (kcal/mol)	MM1 rel. E (kcal/mol)	MM2 rel. E (kcal/mol)	MM3 rel. E (kcal/mol)
-165.03	105.01	-50.6	70.66	4.47	4.04	3.23	4.14
-164.98	119.94	-51.76	69.75	5.45	5.34	4.53	5.47
-165.04	134.97	-52.37	69.66	5.78	5.54	4.74	5.68
-165.06	150.0	-51.64	70.97	5.85	5.35	4.54	5.46
-165.01	164.96	-49.99	73.45	6.17	5.56	4.73	5.58
-165.08	180.0	-48.52	75.84	7.19	6.92	6.07	6.85
-165.03	-165.02	-48.17	77.09	9.12	9.26	8.40	9.14
-164.99	-150.03	-49.66	76.4	11.38	11.83	10.98	11.76
-165.01	-135.02	-52.76	73.82	13.01	13.26	12.44	13.30
-165.07	-119.99	-56.26	70.26	13.20	12.87	12.09	13.04
-165.02	-105.02	-58.49	67.16	11.80	10.99	10.24	11.25
-165.05	-90.0	-58.68	65.64	9.28	8.61	7.87	8.90
-164.98	-75.02	-56.88	66.12	6.94	6.96	6.20	7.22
-165.01	-60.02	-54.38	67.69	5.65	6.41	5.63	6.62
-165.04	-44.99	-52.2	69.24	5.84	7.52	6.72	7.67
-165.04	-29.98	-51.15	69.96	7.17	10.07	9.26	10.19
-165.04	-14.95	-51.8	69.47	8.68	12.43	11.63	12.57
-165.04	-0.06	-53.64	68.0	9.24	12.99	12.20	13.18
-150.08	-0.03	-41.68	80.93	10.74	14.75	13.84	14.43
-150.07	15.04	-42.54	79.97	9.65	13.53	12.62	13.25
-150.08	29.95	-41.64	80.5	7.11	10.20	9.29	9.89
-150.08	45.04	-39.11	82.51	4.24	6.33	5.39	5.92
-150.09	60.03	-36.58	84.68	2.51	3.38	2.42	2.85
-150.04	74.97	-35.77	85.63	2.41	2.38	1.41	1.80
-150.05	89.94	-36.67	85.14	3.73	3.50	2.54	2.96
-150.1	105.01	-38.36	83.7	5.59	5.84	4.90	5.38
-150.07	120.01	-39.57	82.88	6.80	7.39	6.46	6.97
-150.07	135.01	-39.55	83.25	7.02	7.49	6.56	7.06
-150.06	149.96	-38.07	85.02	6.67	6.63	5.68	6.11
-150.08	165.01	-35.73	87.78	6.31	6.15	5.17	5.49
-150.09	-179.98	-33.97	90.24	6.72	6.83	5.84	6.05
-150.08	-165.02	-34.37	90.9	8.28	8.78	7.78	7.97
-150.12	-150.01	-37.07	89.32	10.63	11.33	10.35	10.61
-150.09	-134.99	-40.6	86.22	12.74	13.33	12.38	12.78
-150.04	-120.02	-43.73	82.61	13.40	14.03	13.12	13.67
-150.08	-105.0	-45.49	79.72	12.12	12.71	11.82	12.47
-150.05	-90.01	-45.04	78.84	9.69	10.48	9.60	10.27
-150.14	-75.02	-42.82	79.86	7.33	8.35	7.45	8.08
-150.06	-60.02	-39.74	81.95	6.03	7.46	6.53	7.07
-150.05	-45.05	-37.86	83.38	6.31	8.48	7.54	8.03
-150.11	-29.98	-38.04	83.49	7.93	11.15	10.21	10.69
-150.06	-15.01	-39.67	82.52	9.89	13.73	12.80	13.33
-150.06	0.02	-41.65	80.95	10.74	14.84	13.92	14.51
-135.02	-0.08	-27.32	95.79	12.65	18.04	16.99	16.96
-135.06	14.96	-27.36	95.28	11.10	16.23	15.19	15.17
-135.05	29.95	-25.53	96.28	8.05	12.35	11.30	11.23
-135.07	45.01	-22.79	98.4	4.93	7.99	6.92	6.76
-135.05	60.03	-21.08	100.2	3.23	4.91	3.83	3.59
-135.03	75.03	-21.34	100.63	3.52	4.23	3.14	2.89
-135.11	89.99	-22.82	99.88	5.33	5.83	4.75	4.53
-135.04	105.01	-24.28	98.64	7.43	8.46	7.39	7.23
-135.04	120.0	-24.96	97.8	8.47	9.89	8.83	8.70
-135.04	134.99	-24.14	98.38	8.18	9.30	8.23	8.08

O4-C4-C5-O5 (degrees)	O5-C5-C6-O6 (degrees)	C3-C4-C5-C6 (degrees)	O4-C4-C5-C6 (degrees)	QM rel. E (kcal/mol)	MM1 rel. E (kcal/mol)	MM2 rel. E (kcal/mol)	MM3 rel. E (kcal/mol)
-135.04	149.96	-21.91	100.35	7.19	7.67	6.59	6.35
-135.07	164.96	-19.68	102.95	6.34	6.67	5.57	5.23
-135.08	-179.98	-19.25	104.65	6.68	7.32	6.21	5.81
-135.06	-165.05	-20.72	104.69	8.67	9.79	8.68	8.29
-135.03	-150.0	-23.27	103.04	11.60	13.29	12.20	11.88
-135.05	-135.08	-26.04	100.25	13.92	16.16	15.09	14.88
-135.04	-120.02	-28.48	97.11	14.55	16.84	15.80	15.71
-135.12	-104.97	-29.68	94.71	13.12	15.04	14.01	14.03
-135.09	-89.98	-28.73	94.3	10.55	12.08	11.04	11.07
-135.09	-75.0	-26.14	95.63	8.15	9.44	8.39	8.35
-135.06	-59.99	-23.75	97.4	6.97	8.76	7.70	7.58
-135.04	-45.02	-23.33	98.23	7.62	10.48	9.41	9.26
-135.05	-30.06	-24.45	97.95	9.79	13.65	12.58	12.45
-135.07	-14.99	-26.13	96.9	12.02	16.83	15.77	15.68
-135.04	0.02	-27.35	95.76	12.64	17.93	16.88	16.85
-120.04	0.03	-9.3	112.77	13.48	20.16	18.99	18.31
-120.0	14.99	-8.61	112.7	11.46	17.78	16.61	15.93
-119.98	29.99	-6.98	113.69	8.13	13.32	12.15	11.44
-120.04	45.02	-5.54	115.23	5.13	8.94	7.76	7.01
-119.95	59.95	-4.66	116.77	3.86	6.09	4.90	4.11
-119.99	75.0	-4.88	117.29	4.60	5.66	4.47	3.68
-119.96	89.98	-5.63	116.93	6.56	7.40	6.21	5.42
-120.0	105.01	-6.38	115.98	8.39	9.69	8.51	7.74
-120.01	120.07	-6.59	115.08	9.05	10.58	9.40	8.65
-120.0	134.99	-5.61	115.3	8.32	9.58	8.40	7.65
-119.98	149.97	-4.12	116.76	6.95	7.77	6.58	5.79
-119.98	164.98	-3.37	118.69	6.12	6.90	5.70	4.88
-120.0	179.98	-3.29	120.32	6.92	8.19	6.99	6.13
-119.99	-164.99	-3.71	120.89	9.39	11.56	10.35	9.49
-119.97	-150.0	-5.01	119.76	12.43	15.53	14.33	13.49
-119.99	-135.04	-7.06	117.27	14.69	18.21	17.02	16.23
-119.97	-119.93	-9.1	114.37	15.15	18.40	17.22	16.50
-119.95	-104.98	-10.3	112.11	13.65	15.78	14.61	13.95
-120.01	-89.98	-10.02	111.29	11.03	12.25	11.09	10.45
-119.94	-75.0	-8.49	112.15	8.72	9.82	8.65	7.98
-119.98	-60.0	-7.55	113.37	7.96	9.84	8.67	7.97
-119.97	-45.02	-7.55	114.17	9.20	12.33	11.16	10.44
-119.97	-30.03	-8.09	114.19	11.51	16.16	14.99	14.27
-119.99	-15.01	-8.85	113.57	13.40	19.50	18.32	17.62
-120.04	-0.01	-9.3	112.77	13.49	20.17	19.00	18.32
-104.98	-0.03	10.52	130.32	12.53	19.86	18.63	17.68
-104.98	14.98	10.47	129.96	10.39	17.14	15.90	14.96
-105.0	30.03	10.84	130.52	7.27	12.83	11.60	10.65
-105.01	44.99	11.79	132.04	4.67	8.60	7.36	6.42
-104.96	60.07	13.16	133.86	3.66	5.89	4.64	3.70
-104.97	75.01	13.83	134.7	4.47	5.38	4.13	3.19
-104.96	90.01	13.65	134.42	6.22	6.82	5.57	4.63
-104.95	104.99	13.23	133.48	7.69	8.49	7.25	6.31
-105.0	120.0	12.94	132.51	7.97	8.95	7.71	6.76
-105.01	134.99	13.07	132.34	6.99	8.01	6.77	5.83
-104.96	149.99	13.53	133.53	5.60	6.45	5.21	4.27
-104.99	165.0	14.46	135.7	5.20	6.09	4.84	3.90
-104.98	-179.97	15.86	137.95	6.38	7.97	6.72	5.80

O4-C4-C5-O5 (degrees)	O5-C5-C6-O6 (degrees)	C3-C4-C5-C6 (degrees)	O4-C4-C5-C6 (degrees)	QM rel. E (kcal/mol)	MM1 rel. E (kcal/mol)	MM2 rel. E (kcal/mol)	MM3 rel. E (kcal/mol)
-104.98	-165.01	16.48	138.7	8.93	11.37	10.11	9.20
-104.96	-150.0	15.57	137.45	11.90	15.00	13.74	12.82
-104.99	-134.97	13.23	134.62	14.09	17.10	15.85	14.91
-104.99	-119.96	10.57	131.36	14.54	16.78	15.54	14.60
-104.99	-104.93	8.66	128.76	13.11	14.19	12.96	12.01
-104.99	-90.0	8.24	127.8	10.75	11.25	10.02	9.08
-104.97	-75.03	9.18	128.68	8.86	9.50	8.27	7.33
-104.93	-60.01	10.59	130.44	8.45	9.97	8.74	7.79
-104.96	-44.98	11.36	131.6	9.60	12.94	11.70	10.75
-105.01	-30.03	11.24	131.68	11.46	16.69	15.45	14.50
-104.98	-15.06	10.88	131.13	12.83	19.64	18.40	17.46
-104.98	0.03	10.52	130.32	12.53	19.82	18.58	17.64
-90.12	-0.01	28.02	146.16	10.60	17.66	16.42	15.62
-90.11	15.01	27.5	145.81	8.66	15.41	14.16	13.36
-90.12	29.97	27.81	146.58	5.92	11.36	10.12	9.32
-90.12	45.05	29.2	148.33	3.50	7.32	6.08	5.31
-90.14	60.03	30.87	150.11	2.44	4.47	3.23	2.50
-90.13	75.01	31.62	150.78	3.03	3.56	2.32	1.60
-90.14	90.01	31.29	150.19	4.53	4.45	3.21	2.48
-90.11	105.04	30.56	149.01	5.78	6.07	4.83	4.08
-90.12	120.01	29.88	147.95	5.93	6.69	5.45	4.68
-90.09	134.99	29.77	148.03	5.00	5.81	4.57	3.81
-90.1	149.98	30.6	149.66	3.85	4.57	3.33	2.58
-90.09	165.03	32.52	152.33	3.59	4.39	3.15	2.45
-90.04	-179.99	34.29	154.48	4.76	6.07	4.84	4.18
-90.13	-164.99	34.45	154.57	7.26	9.06	7.83	7.17
-90.12	-150.02	33.25	152.91	10.27	12.24	11.01	10.32
-90.04	-134.99	31.15	150.2	12.59	14.22	12.98	12.25
-90.11	-120.03	28.65	147.1	13.27	14.33	13.09	12.31
-90.05	-105.04	26.98	144.9	12.14	12.50	11.25	10.44
-90.09	-90.04	26.84	144.46	10.05	9.84	8.60	7.77
-90.1	-75.01	28.53	146.06	8.22	8.38	7.14	6.34
-90.08	-59.97	30.39	148.07	7.47	8.93	7.69	6.93
-90.14	-45.01	30.67	148.77	8.14	11.65	10.41	9.65
-90.08	-29.98	29.96	148.34	9.65	15.03	13.79	13.03
-90.13	-14.98	28.93	147.21	10.84	17.51	16.27	15.49
-90.11	0.03	28.0	146.13	10.59	17.65	16.41	15.61
-75.02	-0.06	43.59	161.17	8.89	15.76	14.56	14.04
-75.04	14.99	43.2	161.05	7.23	13.49	12.29	11.77
-75.02	30.01	43.73	161.94	4.63	9.92	8.72	8.21
-75.01	45.0	44.95	163.47	2.20	5.85	4.65	4.17
-74.98	59.98	46.3	164.88	1.02	2.75	1.56	1.10
-75.01	75.0	46.89	165.3	1.44	1.82	0.64	0.18
-75.02	90.0	46.62	164.7	2.79	2.74	1.55	1.08
-75.04	104.99	45.89	163.63	3.95	4.29	3.10	2.62
-75.02	120.02	45.17	162.78	4.11	4.80	3.61	3.12
-75.09	135.03	45.1	163.04	3.30	4.04	2.84	2.35
-75.05	150.02	46.16	164.79	2.29	2.91	1.72	1.26
-75.06	165.03	47.64	166.98	2.13	2.75	1.57	1.13
-75.03	-179.98	48.92	168.47	3.40	4.17	2.99	2.58
-75.05	-165.0	49.58	168.61	5.95	6.86	5.68	5.27
-75.04	-150.01	49.17	167.32	9.01	10.16	8.98	8.56
-75.01	-134.97	47.79	165.05	11.40	12.59	11.41	10.95

O4-C4-C5-O5 (degrees)	O5-C5-C6-O6 (degrees)	C3-C4-C5-C6 (degrees)	O4-C4-C5-C6 (degrees)	QM rel. E (kcal/mol)	MM1 rel. E (kcal/mol)	MM2 rel. E (kcal/mol)	MM3 rel. E (kcal/mol)
-75.02	-119.96	46.02	162.59	12.10	12.74	11.55	11.06
-75.03	-104.98	44.96	161.03	10.99	11.02	9.82	9.31
-75.05	-89.95	45.44	161.28	8.67	8.44	7.24	6.74
-74.98	-75.05	46.91	162.96	6.40	7.01	5.82	5.34
-75.1	-60.02	47.27	164.07	5.36	7.59	6.41	5.94
-75.04	-45.06	46.59	164.1	5.99	9.98	8.79	8.32
-75.0	-29.99	45.6	163.26	7.64	12.96	11.77	11.29
-75.07	-14.99	44.47	162.02	8.98	15.34	14.14	13.64
-74.98	-0.06	43.62	161.2	8.89	15.75	14.55	14.03
-60.03	0.0	57.35	175.44	8.45	14.82	13.68	13.35
-59.97	14.93	56.91	175.29	6.86	12.79	11.65	11.32
-60.01	30.02	57.04	175.81	4.30	9.35	8.21	7.88
-59.96	44.98	58.12	177.1	1.91	5.31	4.18	3.85
-59.98	60.02	59.52	178.43	0.69	2.31	1.19	0.87
-59.96	75.03	60.37	179.02	1.01	1.43	0.32	0.00
-60.0	90.0	60.28	178.63	2.20	2.37	1.26	0.94
-59.98	105.05	59.61	177.8	3.30	3.85	2.73	2.41
-59.98	120.02	58.72	176.96	3.56	4.34	3.21	2.89
-59.97	135.03	58.29	176.98	2.94	3.63	2.50	2.18
-59.97	149.98	58.7	178.16	2.20	2.67	1.55	1.22
-59.99	165.01	60.05	179.93	2.31	2.62	1.51	1.19
-59.95	-179.99	62.11	-178.42	3.68	4.10	3.00	2.68
-59.99	-165.0	63.69	-177.87	6.18	6.95	5.86	5.55
-59.93	-150.06	64.17	-178.58	9.05	10.35	9.27	8.95
-60.0	-134.96	63.29	179.54	11.16	12.51	11.42	11.11
-59.96	-120.04	61.97	177.6	11.54	12.43	11.33	11.01
-60.0	-105.0	60.86	176.27	10.01	10.36	9.25	8.92
-60.0	-89.98	60.36	176.22	7.34	7.93	6.82	6.49
-60.0	-74.96	60.21	177.06	5.01	6.56	5.45	5.13
-60.01	-59.99	60.13	177.87	4.23	6.99	5.87	5.55
-59.96	-44.99	59.92	178.01	5.14	9.25	8.13	7.81
-60.0	-29.99	59.21	177.29	6.95	12.28	11.16	10.83
-59.96	-14.99	58.31	176.32	8.40	14.69	13.56	13.23
-60.04	0.02	57.36	175.44	8.46	14.88	13.74	13.41
-45.06	0.08	69.88	-170.75	9.48	15.40	14.36	14.02
-45.05	15.0	69.07	-171.28	8.02	13.27	12.22	11.88
-45.03	29.97	69.26	-170.89	5.51	9.86	8.81	8.47
-45.05	44.96	70.61	-169.57	3.10	6.11	5.08	4.72
-45.05	60.03	72.35	-168.02	1.79	3.24	2.22	1.85
-45.14	75.02	73.24	-167.31	1.92	2.52	1.51	1.13
-45.01	90.0	73.25	-167.39	3.02	3.44	2.42	2.05
-45.09	104.99	72.25	-168.34	4.19	4.80	3.78	3.41
-45.1	120.01	70.87	-169.49	4.71	5.32	4.29	3.94
-45.12	135.02	69.88	-169.99	4.47	4.93	3.89	3.54
-45.07	149.99	70.5	-169.0	4.10	4.10	3.07	2.71
-45.08	165.03	72.74	-167.04	4.35	4.24	3.23	2.85
-45.09	179.99	75.73	-165.0	5.62	5.85	4.86	4.46
-45.13	-165.0	78.05	-163.91	7.75	8.68	7.71	7.29
-45.07	-150.02	78.85	-164.23	10.12	11.59	10.62	10.20
-45.05	-134.97	77.85	-165.91	11.73	13.27	12.30	11.90
-45.12	-120.01	75.77	-168.15	11.68	12.70	11.70	11.33
-45.08	-104.99	73.51	-169.88	9.85	10.70	9.69	9.33
-45.06	-90.01	71.98	-170.46	7.33	8.51	7.49	7.14

O4-C4-C5-O5 (degrees)	O5-C5-C6-O6 (degrees)	C3-C4-C5-C6 (degrees)	O4-C4-C5-C6 (degrees)	QM rel. E (kcal/mol)	MM1 rel. E (kcal/mol)	MM2 rel. E (kcal/mol)	MM3 rel. E (kcal/mol)
-45.09	-74.97	71.79	-169.75	5.41	7.21	6.19	5.83
-45.02	-59.98	72.49	-168.6	4.93	7.71	6.69	6.32
-45.07	-45.03	72.66	-168.25	5.96	9.97	8.95	8.58
-45.01	-30.06	72.16	-168.68	7.80	13.03	12.01	11.65
-45.07	-15.02	71.09	-169.73	9.34	15.25	14.22	13.87
-45.06	-0.05	69.89	-170.74	9.49	15.35	14.31	13.96
-30.08	-0.01	82.44	-156.88	11.56	16.75	15.82	15.30
-30.08	14.96	81.72	-157.52	10.18	14.77	13.83	13.32
-30.12	29.99	82.27	-157.06	7.61	11.33	10.40	9.88
-30.09	45.01	83.98	-155.48	5.03	7.69	6.78	6.23
-30.04	59.98	85.77	-153.75	3.56	4.93	4.04	3.46
-30.02	74.99	86.6	-152.92	3.58	4.23	3.34	2.75
-30.07	89.97	86.19	-153.23	4.76	5.18	4.29	3.70
-30.05	104.95	85.01	-154.23	6.24	6.63	5.73	5.16
-30.08	119.99	83.49	-155.54	7.14	7.38	6.47	5.92
-30.15	135.02	82.79	-156.11	7.21	7.11	6.18	5.65
-30.06	149.98	84.26	-154.9	6.93	6.38	5.47	4.92
-30.07	165.03	87.39	-152.53	6.96	6.39	5.51	4.91
-30.09	179.99	90.84	-150.13	7.71	7.65	6.80	6.14
-30.07	-165.0	93.06	-148.83	9.22	10.02	9.19	8.51
-30.07	-150.05	93.11	-149.38	11.07	12.57	11.74	11.07
-30.1	-135.01	91.1	-151.47	12.42	13.96	13.11	12.47
-30.05	-120.04	88.15	-154.04	12.36	13.89	13.01	12.42
-30.09	-105.01	85.37	-156.14	10.79	12.33	11.43	10.88
-30.13	-90.0	84.14	-156.72	8.63	10.28	9.36	8.83
-30.04	-74.95	84.73	-155.69	6.96	8.91	8.00	7.45
-30.0	-60.02	85.66	-154.43	6.57	9.27	8.38	7.80
-30.16	-44.96	85.7	-154.12	7.64	11.60	10.71	10.13
-30.12	-29.99	85.03	-154.59	9.57	14.68	13.77	13.21
-30.09	-14.96	83.75	-155.69	11.22	16.74	15.83	15.28
-30.1	0.07	82.39	-156.93	11.55	16.75	15.82	15.30
-15.07	0.01	96.59	-142.27	13.57	18.71	17.93	17.15
-15.12	14.99	96.19	-142.79	12.15	16.74	15.95	15.18
-15.06	30.03	97.02	-142.07	9.37	13.11	12.33	11.55
-15.08	44.96	98.65	-140.44	6.60	9.31	8.55	7.74
-15.08	60.01	100.21	-138.83	5.01	6.65	5.91	5.08
-15.06	74.96	100.75	-138.16	5.13	5.88	5.14	4.31
-15.09	89.98	100.21	-138.56	6.58	7.04	6.30	5.47
-15.07	105.05	99.27	-139.51	8.37	8.54	7.79	6.97
-15.07	120.0	98.36	-140.51	9.47	9.45	8.69	7.89
-15.06	134.99	98.39	-140.67	9.53	9.20	8.44	7.64
-15.1	149.95	100.03	-139.49	8.96	8.28	7.53	6.71
-15.07	164.98	103.13	-137.08	8.44	7.88	7.16	6.30
-15.08	179.93	106.06	-134.82	8.59	8.71	8.02	7.13
-15.04	-164.99	107.37	-133.89	9.72	10.69	10.02	9.12
-15.11	-150.0	106.56	-134.83	11.55	13.32	12.64	11.75
-15.11	-135.0	104.25	-137.02	13.00	15.22	14.51	13.64
-15.06	-120.0	101.5	-139.47	13.13	15.64	14.90	14.07
-15.0	-105.03	99.35	-141.26	11.88	14.15	13.39	12.58
-15.09	-90.0	98.53	-141.72	9.93	11.89	11.12	10.32
-15.08	-75.05	99.11	-140.78	8.37	10.46	9.71	8.90
-15.02	-60.08	99.88	-139.62	8.07	10.96	10.21	9.39
-15.08	-44.97	99.68	-139.44	9.27	13.39	12.64	11.82

O4-C4-C5-O5 (degrees)	O5-C5-C6-O6 (degrees)	C3-C4-C5-C6 (degrees)	O4-C4-C5-C6 (degrees)	QM rel. E (kcal/mol)	MM1 rel. E (kcal/mol)	MM2 rel. E (kcal/mol)	MM3 rel. E (kcal/mol)
-15.04	-30.03	98.82	-140.04	11.37	16.27	15.51	14.70
-15.09	-15.05	97.61	-141.21	13.16	18.44	17.67	16.88
-15.07	0.01	96.6	-142.27	13.58	18.66	17.88	17.10
0.14	0.04	113.13	-126.45	14.35	20.10	19.50	18.57
0.09	15.01	112.85	-126.77	12.69	17.97	17.36	16.43
0.12	30.0	113.56	-125.99	9.79	14.26	13.66	12.73
0.16	45.0	115.09	-124.35	6.94	10.30	9.72	8.79
0.12	60.0	116.42	-122.93	5.45	7.43	6.87	5.95
0.05	75.02	116.83	-122.49	5.82	6.79	6.23	5.31
0.11	89.93	116.61	-122.81	7.49	7.78	7.21	6.29
0.07	105.02	115.9	-123.68	9.35	9.59	9.02	8.09
0.15	120.05	115.47	-124.31	10.36	10.52	9.94	9.01
0.07	134.98	115.57	-124.4	10.18	10.07	9.50	8.57
0.18	149.97	117.1	-123.16	9.22	8.95	8.38	7.45
0.09	165.01	119.35	-121.25	8.26	8.15	7.61	6.69
0.1	-180.0	121.52	-119.37	8.19	8.85	8.33	7.42
0.12	-165.02	122.42	-118.65	9.35	10.78	10.27	9.36
0.08	-150.03	121.66	-119.55	11.27	13.76	13.25	12.33
0.21	-135.03	119.87	-121.36	12.83	16.14	15.61	14.68
0.05	-119.99	117.36	-123.76	13.15	16.62	16.06	15.12
0.1	-104.98	115.55	-125.31	12.05	14.89	14.31	13.37
0.16	-90.04	114.91	-125.59	10.24	12.46	11.87	10.94
0.17	-75.0	115.31	-124.77	8.83	11.22	10.63	9.70
0.08	-60.0	115.63	-124.04	8.70	11.99	11.41	10.48
0.09	-44.97	115.34	-124.05	10.11	14.52	13.94	13.02
0.14	-29.97	114.66	-124.67	12.30	17.52	16.94	16.01
0.14	-15.08	113.87	-125.57	14.08	19.81	19.21	18.29
0.14	0.04	113.15	-126.45	14.34	20.10	19.49	18.57

Table C.2. Dihedral angles and relative energies for **4.1** with the ^{1}E ring conformation.

O4-C4-C5-O5 (degrees)	O5-C5-C6-O6 (degrees)	C3-C4-C5-C6 (degrees)	O4-C4-C5-C6 (degrees)	QM rel. E (kcal/mol)	MM1 rel. E (kcal/mol)	MM2 rel. E (kcal/mol)	MM3 rel. E (kcal/mol)
-0.06	0.05	112.09	-126.73	17.09	25.81	25.87	23.85
-0.02	14.96	112.01	-126.88	15.41	23.57	23.63	21.61
-0.02	30.01	112.76	-126.07	12.42	19.76	19.82	17.80
-0.05	45.07	114.13	-124.53	9.50	15.68	15.76	13.74
-0.02	59.97	115.45	-123.04	7.98	12.74	12.83	10.82
-0.05	75.04	115.81	-122.62	8.29	11.88	11.98	9.97
-0.04	90.02	115.49	-123.07	9.89	12.77	12.87	10.86
-0.04	105.01	114.79	-124.04	11.60	14.21	14.30	12.28
-0.0	119.95	114.08	-124.93	12.34	14.91	14.99	12.96
-0.03	134.97	113.82	-125.28	11.79	13.89	13.97	11.94
0.04	149.99	114.79	-124.43	10.49	12.42	12.51	10.48
-0.03	164.97	116.7	-122.68	9.42	11.59	11.69	9.67
-0.07	-179.97	118.87	-120.71	9.48	12.51	12.64	10.63
0.02	-165.02	120.31	-119.58	10.95	14.79	14.93	12.93
-0.05	-150.03	120.04	-120.18	13.19	18.12	18.26	16.24
-0.01	-135.01	118.51	-121.9	15.00	20.84	20.96	18.94
-0.07	-119.96	116.29	-124.11	15.56	21.51	21.60	19.57
-0.04	-105.03	114.61	-125.59	14.62	19.99	20.07	18.03
0.04	-90.02	114.09	-125.76	12.88	17.80	17.88	15.84
-0.02	-75.03	114.44	-124.96	11.48	16.74	16.83	14.80
-0.06	-60.02	114.7	-124.17	11.37	17.65	17.74	15.72
-0.01	-44.94	114.35	-124.17	12.80	20.27	20.36	18.34
0.01	-29.97	113.63	-124.84	15.06	23.39	23.47	21.45
-0.06	-15.01	112.74	-125.87	16.85	25.54	25.61	23.59
-0.03	-0.0	112.13	-126.69	17.10	25.84	25.90	23.88
14.9	-0.02	129.06	-110.65	16.61	25.82	26.06	24.17
14.92	15.02	128.99	-110.65	14.74	23.43	23.67	21.79
14.92	30.01	129.67	-109.79	11.73	19.51	19.76	17.90
14.9	44.98	130.94	-108.36	8.92	15.25	15.51	13.68
14.89	59.96	132.2	-107.08	7.55	12.09	12.37	10.56
14.91	74.98	132.76	-106.67	8.03	11.15	11.43	9.64
14.98	90.0	132.65	-107.03	9.67	11.99	12.27	10.46
14.95	104.99	131.96	-107.94	11.27	13.44	13.71	11.88
14.89	119.96	131.24	-108.75	11.83	14.19	14.45	12.61
14.89	135.01	131.12	-108.87	11.13	13.27	13.53	11.68
14.97	150.02	132.09	-107.91	9.72	11.83	12.09	10.27
14.92	164.96	133.87	-106.21	8.64	11.01	11.30	9.51
14.97	179.96	136.06	-104.3	8.71	11.68	11.98	10.24
14.93	-165.01	137.22	-103.48	10.16	14.08	14.40	12.67
14.9	-149.99	136.81	-104.18	12.33	17.52	17.83	16.08
14.92	-134.98	135.19	-105.89	14.18	20.07	20.36	18.57
14.9	-120.0	133.05	-107.92	14.73	20.81	21.08	19.25
14.92	-104.97	131.34	-109.36	13.92	19.27	19.52	17.66
14.93	-90.0	130.61	-109.68	12.36	17.36	17.61	15.74
14.91	-74.96	130.72	-109.13	11.20	16.57	16.82	14.97
14.96	-59.96	131.02	-108.48	11.29	17.61	17.87	16.03
14.88	-44.92	130.71	-108.65	12.80	20.28	20.54	18.70
14.94	-30.0	130.28	-109.2	14.95	23.42	23.67	21.82
14.9	-14.94	129.62	-110.04	16.58	25.64	25.88	24.01
14.95	-0.06	129.13	-110.58	16.61	25.81	26.05	24.17

O4-C4-C5-O5 (degrees)	O5-C5-C6-O6 (degrees)	C3-C4-C5-C6 (degrees)	O4-C4-C5-C6 (degrees)	QM rel. E (kcal/mol)	MM1 rel. E (kcal/mol)	MM2 rel. E (kcal/mol)	MM3 rel. E (kcal/mol)
29.99	-0.06	145.63	-94.83	14.64	23.67	24.07	22.60
29.96	15.09	145.49	-94.79	12.70	21.30	21.70	20.22
29.97	29.99	146.11	-94.0	9.74	17.35	17.76	16.31
29.95	45.0	147.32	-92.74	7.07	12.99	13.40	12.00
29.94	60.02	148.69	-91.51	5.80	9.86	10.29	8.92
30.0	74.99	149.44	-91.01	6.30	8.60	9.04	7.68
29.98	89.98	149.26	-91.38	7.83	9.48	9.91	8.54
29.99	104.98	148.63	-92.14	9.29	10.88	11.30	9.91
29.95	120.02	147.92	-92.81	9.72	11.56	11.98	10.57
29.97	135.01	147.71	-92.91	8.96	10.92	11.34	9.92
30.02	150.03	148.55	-92.05	7.55	9.56	9.98	8.59
29.99	164.98	150.3	-90.43	6.53	8.72	9.16	7.82
29.94	-179.99	152.31	-88.78	6.63	9.23	9.68	8.40
29.98	-165.02	153.52	-87.91	8.02	11.50	11.96	10.71
29.92	-149.97	153.05	-88.59	10.14	14.71	15.17	13.89
29.99	-134.97	151.46	-90.2	11.98	17.22	17.67	16.33
30.02	-119.99	149.28	-92.18	12.70	18.05	18.47	17.08
29.94	-104.98	147.14	-93.93	12.19	16.97	17.38	15.93
29.91	-90.01	145.89	-94.71	10.95	15.57	15.97	14.50
30.05	-75.04	145.9	-94.35	10.00	14.91	15.31	13.85
29.99	-59.98	146.35	-93.78	10.14	15.95	16.36	14.92
29.91	-44.97	146.61	-93.62	11.50	18.45	18.86	17.43
29.9	-30.02	146.46	-93.91	13.41	21.45	21.86	20.41
29.97	-14.99	146.08	-94.41	14.78	23.55	23.95	22.49
29.98	-0.01	145.64	-94.82	14.63	23.62	24.02	22.55
45.05	0.05	160.54	-79.88	12.19	20.63	21.15	20.14
44.94	15.03	160.22	-80.05	10.34	18.36	18.88	17.85
45.05	30.04	160.87	-79.36	7.53	14.34	14.87	13.87
45.02	45.0	162.19	-78.15	4.96	10.10	10.63	9.67
45.06	59.98	163.72	-76.76	3.67	6.87	7.42	6.48
45.05	75.02	164.51	-76.14	4.02	5.62	6.17	5.25
45.05	89.94	164.44	-76.33	5.40	6.27	6.82	5.90
44.98	105.02	163.76	-77.06	6.74	7.74	8.28	7.34
45.0	120.0	162.98	-77.75	7.16	8.56	9.10	8.14
44.99	134.96	162.56	-78.03	6.47	7.97	8.51	7.54
44.99	150.02	163.12	-77.47	5.22	6.74	7.28	6.33
45.04	165.0	164.95	-75.88	4.27	5.77	6.33	5.41
45.01	-179.96	166.98	-74.19	4.36	6.27	6.83	5.96
44.97	-165.01	168.13	-73.29	5.64	8.31	8.88	8.02
45.01	-149.97	167.8	-73.76	7.77	11.61	12.18	11.31
44.96	-135.03	165.87	-75.57	9.71	14.23	14.78	13.88
45.07	-119.98	163.17	-77.92	10.79	15.12	15.66	14.69
45.04	-104.95	160.43	-80.22	10.66	14.60	15.12	14.10
45.02	-89.98	158.89	-81.35	9.75	13.59	14.10	13.05
45.0	-74.92	158.91	-81.12	8.84	13.09	13.60	12.55
44.99	-60.05	159.82	-80.22	8.83	14.00	14.52	13.49
45.01	-44.96	160.78	-79.41	9.90	16.08	16.60	15.60
45.01	-29.95	161.18	-79.19	11.49	18.70	19.23	18.23
45.06	-14.99	161.0	-79.45	12.57	20.67	21.19	20.19
44.98	-0.0	160.49	-79.93	12.22	20.77	21.29	20.28
59.9	-0.01	173.46	-66.05	10.66	18.14	18.75	18.02
59.91	14.96	173.09	-66.39	8.84	15.95	16.56	15.83
59.94	29.97	173.67	-65.89	6.09	11.96	12.56	11.84

O4-C4-C5-O5 (degrees)	O5-C5-C6-O6 (degrees)	C3-C4-C5-C6 (degrees)	O4-C4-C5-C6 (degrees)	QM rel. E (kcal/mol)	MM1 rel. E (kcal/mol)	MM2 rel. E (kcal/mol)	MM3 rel. E (kcal/mol)
59.96	45.0	175.13	-64.54	3.53	7.83	8.44	7.74
59.93	59.94	176.81	-62.98	2.15	4.62	5.25	4.55
59.89	75.0	177.77	-62.17	2.37	3.32	3.95	3.27
59.94	90.01	177.89	-62.14	3.63	4.02	4.65	3.96
59.9	104.99	177.18	-62.83	4.92	5.48	6.11	5.42
59.86	119.99	176.1	-63.8	5.43	6.28	6.90	6.20
59.92	135.02	175.49	-64.3	4.90	5.91	6.52	5.82
59.91	149.96	176.01	-63.86	3.79	4.83	5.45	4.75
59.89	165.02	177.78	-62.33	2.90	3.97	4.60	3.91
59.94	179.96	179.89	-60.46	2.97	4.37	5.01	4.33
59.88	-165.0	-178.93	-59.47	4.26	6.60	7.24	6.57
59.93	-150.0	-179.5	-60.02	6.58	9.85	10.49	9.82
59.97	-135.03	177.91	-62.25	9.02	12.62	13.25	12.56
59.91	-120.02	174.2	-65.41	10.58	13.80	14.41	13.69
59.91	-104.98	171.13	-68.05	10.66	13.50	14.09	13.34
59.95	-90.01	169.83	-69.11	9.63	12.72	13.31	12.54
59.91	-74.99	170.25	-68.6	8.60	12.24	12.83	12.07
59.91	-59.98	171.68	-67.21	8.26	12.70	13.30	12.57
59.89	-44.94	173.18	-65.94	8.97	14.44	15.04	14.32
59.92	-29.96	174.14	-65.26	10.15	16.70	17.31	16.59
59.89	-14.96	174.09	-65.44	11.02	18.50	19.11	18.39
59.9	-0.01	173.46	-66.04	10.66	18.28	18.89	18.17
74.99	-0.0	-174.42	-52.59	10.62	17.14	17.80	17.13
75.01	15.0	-174.91	-53.11	8.82	14.94	15.60	14.93
75.05	29.93	-174.23	-52.58	6.04	11.16	11.82	11.15
75.02	45.0	-172.5	-51.03	3.36	7.02	7.69	7.01
75.05	60.04	-170.51	-49.21	1.89	3.72	4.39	3.70
75.0	75.01	-169.45	-48.27	2.01	2.58	3.25	2.55
74.99	90.03	-169.46	-48.33	3.23	3.44	4.11	3.42
74.98	104.98	-170.41	-49.17	4.60	4.89	5.56	4.87
74.98	120.0	-171.7	-50.34	5.25	5.76	6.43	5.75
75.04	134.95	-172.36	-50.93	4.86	5.60	6.26	5.59
74.97	150.0	-171.77	-50.46	3.79	4.50	5.17	4.49
74.98	165.04	-169.89	-48.78	2.96	3.65	4.32	3.63
74.98	179.97	-167.82	-46.88	3.14	4.37	5.04	4.33
75.02	-165.0	-166.89	-45.99	4.74	6.87	7.54	6.82
74.99	-150.02	-168.28	-46.99	7.66	10.33	11.00	10.29
74.97	-135.0	-171.85	-49.82	10.75	13.19	13.86	13.18
74.95	-119.97	-175.91	-53.29	12.50	14.67	15.33	14.66
74.99	-105.02	-178.77	-55.89	12.39	14.59	15.24	14.58
75.0	-90.03	-179.66	-56.7	11.07	13.65	14.30	13.64
75.0	-75.03	-178.67	-55.75	9.56	12.78	13.43	12.77
75.05	-60.03	-176.59	-53.83	8.85	12.71	13.37	12.70
75.03	-44.98	-174.53	-52.14	9.20	14.16	14.82	14.15
75.0	-29.98	-173.31	-51.33	10.20	16.06	16.72	16.05
74.98	-14.97	-173.48	-51.65	10.97	17.56	18.22	17.55
74.99	0.06	-174.44	-52.6	10.62	17.27	17.93	17.26
90.02	-0.01	-161.86	-38.91	11.82	17.88	18.57	17.74
89.99	15.04	-162.32	-39.5	9.95	15.55	16.24	15.42
89.98	29.97	-161.45	-38.88	7.01	11.64	12.32	11.49
89.95	45.02	-159.41	-37.11	4.19	7.47	8.16	7.30
90.04	59.96	-157.16	-35.08	2.67	4.39	5.08	4.18
90.02	75.01	-156.17	-34.18	2.82	3.51	4.20	3.29

O4-C4-C5-O5 (degrees)	O5-C5-C6-O6 (degrees)	C3-C4-C5-C6 (degrees)	O4-C4-C5-C6 (degrees)	QM rel. E (kcal/mol)	MM1 rel. E (kcal/mol)	MM2 rel. E (kcal/mol)	MM3 rel. E (kcal/mol)
89.98	90.0	-156.58	-34.5	4.15	4.42	5.11	4.20
89.97	105.03	-157.87	-35.54	5.72	6.17	6.86	5.97
89.96	120.02	-159.22	-36.73	6.40	7.10	7.78	6.92
90.01	135.0	-159.68	-37.24	6.00	6.67	7.36	6.50
90.02	149.96	-158.85	-36.56	4.94	5.64	6.33	5.46
89.99	165.02	-156.87	-34.81	4.21	5.04	5.72	4.82
89.98	-179.97	-155.01	-33.0	4.67	6.24	6.92	5.99
90.01	-164.98	-154.76	-32.35	7.00	9.16	9.85	8.90
89.97	-150.01	-157.03	-33.69	10.75	12.82	13.51	12.58
90.02	-135.05	-160.87	-36.68	14.18	16.00	16.69	15.82
90.05	-120.01	-164.78	-40.19	15.76	17.51	18.20	17.38
90.03	-105.01	-167.4	-42.77	15.25	17.01	17.69	16.92
90.02	-90.01	-167.87	-43.32	13.34	15.52	16.21	15.44
90.04	-75.02	-166.23	-41.92	11.39	14.18	14.87	14.08
90.04	-59.98	-163.58	-39.65	10.28	13.65	14.34	13.52
90.04	-44.99	-161.17	-37.77	10.32	14.68	15.37	14.52
90.0	-30.0	-160.13	-37.13	11.22	16.73	17.42	16.55
90.06	-15.05	-160.66	-37.73	12.10	18.07	18.75	17.90
90.03	-0.02	-161.85	-38.9	11.81	17.82	18.50	17.67
105.0	0.02	-147.31	-24.13	13.35	19.86	20.54	19.44
105.08	15.03	-147.47	-24.55	11.39	17.28	17.95	16.86
105.05	30.03	-146.32	-23.8	8.30	13.20	13.88	12.77
105.06	44.98	-143.99	-21.86	5.36	9.03	9.69	8.56
105.04	60.02	-141.78	-19.9	3.81	6.05	6.71	5.56
105.09	75.01	-141.08	-19.11	4.11	5.36	6.01	4.84
105.07	89.97	-142.03	-19.67	5.68	6.52	7.18	6.02
105.01	104.98	-143.6	-20.88	7.31	8.45	9.12	7.97
105.03	120.01	-144.75	-21.96	8.02	9.44	10.11	8.97
105.07	135.01	-144.93	-22.29	7.52	8.91	9.58	8.45
105.0	149.99	-143.89	-21.54	6.45	7.75	8.41	7.27
105.08	164.96	-141.76	-19.62	5.88	7.62	8.28	7.11
105.07	-179.96	-140.23	-17.81	7.02	9.32	9.97	8.78
104.98	-164.98	-140.74	-17.31	10.29	12.73	13.39	12.18
104.99	-150.01	-143.33	-18.77	14.57	16.90	17.57	16.37
105.02	-134.99	-147.11	-21.87	17.90	20.11	20.79	19.63
104.99	-120.01	-150.85	-25.4	19.09	21.08	21.77	20.67
105.01	-105.01	-153.15	-27.86	18.04	19.91	20.60	19.55
104.96	-90.01	-153.23	-28.25	15.60	17.69	18.38	17.34
105.05	-74.96	-151.02	-26.47	13.17	15.66	16.35	15.28
105.01	-59.93	-147.96	-23.98	11.63	14.77	15.45	14.34
105.0	-44.96	-145.7	-22.25	11.49	16.00	16.67	15.54
105.03	-29.95	-145.23	-22.03	12.49	18.36	19.03	17.89
105.03	-15.0	-146.21	-22.97	13.56	19.88	20.55	19.43
105.0	0.08	-147.31	-24.13	13.35	19.87	20.55	19.45
119.98	0.04	-130.46	-8.09	14.14	21.68	22.29	21.04
119.99	14.98	-130.3	-8.38	12.11	18.96	19.57	18.32
119.95	30.03	-128.82	-7.45	8.87	14.63	15.23	13.98
119.97	44.99	-126.35	-5.49	5.85	10.31	10.89	9.65
119.99	59.99	-124.41	-3.66	4.34	7.50	8.08	6.85
119.99	74.98	-124.33	-3.2	4.82	7.04	7.61	6.38
119.98	90.02	-125.71	-3.95	6.60	8.51	9.09	7.85
119.99	105.0	-127.21	-5.1	8.29	10.65	11.24	9.99
119.99	119.96	-128.08	-6.03	8.90	11.46	12.06	10.81

O4-C4-C5-O5 (degrees)	O5-C5-C6-O6 (degrees)	C3-C4-C5-C6 (degrees)	O4-C4-C5-C6 (degrees)	QM rel. E (kcal/mol)	MM1 rel. E (kcal/mol)	MM2 rel. E (kcal/mol)	MM3 rel. E (kcal/mol)
119.97	134.97	-127.88	-6.2	8.31	10.64	11.23	9.98
119.98	149.96	-126.4	-5.12	7.31	9.70	10.28	9.04
119.96	165.0	-124.46	-3.16	7.11	9.95	10.52	9.28
119.99	180.0	-123.31	-1.26	9.01	12.29	12.85	11.62
119.98	-165.01	-124.11	-0.77	12.94	16.36	16.93	15.69
119.99	-149.97	-126.72	-2.35	17.29	20.63	21.22	19.96
119.98	-135.02	-130.21	-5.37	20.41	23.76	24.37	23.09
120.06	-120.05	-133.4	-8.58	21.23	24.10	24.72	23.45
120.04	-104.99	-135.43	-10.9	19.67	21.97	22.61	21.34
119.93	-90.01	-135.3	-11.22	16.74	18.97	19.60	18.34
120.0	-74.95	-132.67	-9.22	13.78	16.34	16.96	15.70
119.97	-60.0	-129.68	-6.79	11.96	15.63	16.23	14.97
119.99	-45.02	-128.27	-5.68	11.89	17.18	17.78	16.52
119.99	-29.99	-128.66	-6.09	13.14	19.74	20.33	19.08
119.94	-14.97	-129.71	-7.13	14.34	21.72	22.32	21.06
120.0	0.04	-130.41	-8.04	14.14	21.74	22.35	21.09
134.89	-0.07	-111.91	8.81	13.36	21.57	22.05	20.98
134.87	15.03	-111.44	8.69	11.17	18.77	19.25	18.18
134.9	30.01	-109.93	9.65	7.94	14.36	14.82	13.78
134.91	45.03	-108.01	11.3	4.90	10.11	10.56	9.56
134.94	59.98	-106.68	12.78	3.62	7.11	7.55	6.58
134.92	75.02	-106.86	13.1	4.33	6.77	7.22	6.25
134.89	90.05	-108.12	12.38	6.15	8.56	9.01	8.02
134.93	104.95	-109.3	11.4	7.70	10.66	11.13	10.11
134.93	119.99	-109.76	10.69	8.21	11.37	11.84	10.81
134.9	135.0	-109.22	10.77	7.63	10.70	11.16	10.14
134.93	149.96	-107.82	11.9	6.81	10.01	10.46	9.47
134.92	165.02	-106.26	13.87	7.16	10.81	11.25	10.30
134.9	-179.99	-105.38	15.78	9.65	13.66	14.09	13.18
134.92	-165.04	-105.96	16.32	13.64	17.83	18.26	17.36
134.91	-150.0	-108.23	14.82	17.74	21.98	22.43	21.48
134.93	-134.98	-111.22	12.11	20.44	24.56	25.04	24.01
134.89	-119.96	-114.13	9.1	20.91	24.37	24.87	23.78
134.94	-105.03	-115.71	7.19	18.99	21.64	22.15	21.03
134.91	-89.98	-115.41	7.08	15.69	17.88	18.39	17.26
134.93	-75.01	-113.44	8.75	12.49	14.90	15.40	14.31
134.92	-59.98	-111.66	10.32	10.74	14.48	14.96	13.91
134.93	-45.01	-110.9	10.77	10.99	16.25	16.72	15.68
134.91	-30.0	-110.98	10.37	12.44	19.33	19.80	18.76
134.91	-14.98	-111.59	9.52	13.60	21.74	22.22	21.16
134.97	-0.01	-111.79	8.89	13.34	21.67	22.15	21.08
150.08	0.01	-93.06	25.9	10.84	18.56	18.88	18.29
150.09	14.96	-93.25	25.52	8.77	15.56	15.88	15.29
150.01	30.03	-92.78	25.87	5.73	11.31	11.63	11.04
150.03	45.09	-91.6	27.1	3.07	7.15	7.45	6.90
150.08	59.97	-90.43	28.49	1.98	4.48	4.77	4.26
150.06	75.02	-90.15	29.0	2.68	4.17	4.46	3.97
150.05	89.96	-90.69	28.63	4.31	6.04	6.33	5.82
150.08	104.99	-91.36	27.91	5.76	7.99	8.29	7.76
150.08	119.95	-91.82	27.27	6.16	8.82	9.12	8.58
150.06	134.99	-91.79	27.12	5.65	8.50	8.81	8.25
150.06	149.97	-90.97	28.11	5.15	8.14	8.43	7.91
150.06	164.99	-89.49	30.23	6.06	9.26	9.54	9.08

O4-C4-C5-O5 (degrees)	O5-C5-C6-O6 (degrees)	C3-C4-C5-C6 (degrees)	O4-C4-C5-C6 (degrees)	QM rel. E (kcal/mol)	MM1 rel. E (kcal/mol)	MM2 rel. E (kcal/mol)	MM3 rel. E (kcal/mol)
150.07	-179.98	-87.96	32.47	8.67	12.03	12.30	11.90
150.06	-164.99	-87.7	33.29	12.30	15.98	16.23	15.86
150.04	-150.01	-89.23	32.18	15.92	19.69	19.96	19.55
150.09	-135.02	-91.94	29.79	18.23	21.85	22.15	21.66
150.04	-119.96	-95.08	26.93	18.36	21.02	21.35	20.77
150.05	-105.02	-97.37	24.86	16.30	17.79	18.14	17.50
150.03	-90.03	-97.97	24.38	12.99	14.05	14.40	13.74
150.07	-75.0	-97.09	25.31	10.02	11.67	12.02	11.39
150.05	-60.02	-95.98	26.16	8.66	11.24	11.58	10.98
150.02	-44.96	-94.54	26.66	8.98	12.97	13.30	12.72
150.0	-30.0	-93.2	26.83	10.24	16.23	16.54	15.98
150.05	-14.97	-92.75	26.53	11.22	18.86	19.17	18.60
150.02	-0.02	-93.15	25.82	10.86	18.65	18.96	18.37
165.05	0.04	-77.52	41.2	8.03	14.03	14.19	14.03
165.06	15.04	-78.56	40.38	6.36	11.73	11.90	11.72
165.06	29.94	-78.59	40.46	3.81	8.06	8.22	8.04
165.08	45.01	-77.57	41.55	1.53	4.20	4.35	4.20
165.08	59.98	-76.23	42.92	0.49	1.47	1.61	1.49
165.08	74.98	-75.51	43.63	0.95	1.25	1.38	1.27
165.06	89.98	-75.64	43.48	2.32	2.75	2.89	2.77
165.03	105.03	-76.33	42.81	3.56	4.59	4.73	4.60
165.06	119.99	-77.07	42.11	4.04	5.70	5.85	5.71
165.13	135.01	-77.34	41.95	3.87	5.98	6.13	5.98
165.12	150.0	-76.56	43.04	3.88	5.98	6.12	5.99
165.09	164.95	-74.77	45.31	4.88	6.87	6.99	6.90
165.06	179.96	-72.76	47.62	7.04	8.97	9.07	9.01
165.08	-164.94	-71.97	48.68	10.01	12.07	12.16	12.12
165.09	-150.05	-73.4	47.86	13.05	15.16	15.26	15.21
165.09	-135.0	-76.48	45.6	15.10	16.86	17.00	16.91
165.06	-120.02	-79.84	42.88	15.19	16.48	16.65	16.51
165.03	-104.99	-82.39	40.71	13.28	14.23	14.43	14.24
165.05	-90.01	-83.6	39.75	10.37	11.46	11.66	11.45
165.09	-74.98	-83.3	39.97	7.87	8.86	9.06	8.86
165.06	-60.01	-81.39	40.87	6.62	8.08	8.27	8.09
165.08	-45.04	-78.77	41.86	6.60	9.22	9.38	9.23
165.07	-30.04	-76.74	42.39	7.47	11.93	12.08	11.94
165.07	-15.01	-76.39	42.17	8.28	14.09	14.23	14.09
165.06	0.03	-77.52	41.2	8.03	13.97	14.12	13.96
179.96	-0.03	-64.77	54.9	6.66	11.45	11.47	11.47
179.94	14.97	-66.02	53.86	5.47	9.74	9.77	9.77
179.99	30.06	-66.11	53.83	3.33	6.51	6.54	6.54
-179.99	44.97	-65.02	54.83	1.18	2.89	2.90	2.91
180.0	60.01	-63.56	56.19	0.00	0.53	0.53	0.53
179.95	74.97	-62.77	56.98	0.18	0.00	0.00	0.00
179.99	89.94	-62.78	57.04	1.28	1.18	1.17	1.17
179.97	104.97	-63.46	56.54	2.50	3.20	3.20	3.20
179.98	119.98	-64.3	55.87	3.28	4.89	4.89	4.90
-179.99	134.99	-64.6	55.7	3.58	5.44	5.45	5.46
-179.99	150.0	-63.74	56.85	3.89	5.26	5.26	5.26
179.97	165.02	-61.9	58.98	4.70	5.55	5.53	5.53
179.99	-179.96	-60.16	61.07	6.28	6.83	6.79	6.77
179.99	-165.0	-59.9	62.04	8.52	9.09	9.04	9.02
179.99	-149.97	-61.29	61.53	11.02	11.94	11.91	11.89

O4-C4-C5-O5 (degrees)	O5-C5-C6-O6 (degrees)	C3-C4-C5-C6 (degrees)	O4-C4-C5-C6 (degrees)	QM rel. E (kcal/mol)	MM1 rel. E (kcal/mol)	MM2 rel. E (kcal/mol)	MM3 rel. E (kcal/mol)
179.98	-135.04	-63.87	59.69	12.86	14.17	14.16	14.16
179.98	-119.98	-67.11	56.99	13.02	14.91	14.94	14.94
179.97	-104.97	-70.41	54.26	11.45	12.82	12.88	12.88
-179.98	-90.01	-71.55	53.02	9.04	9.55	9.62	9.62
179.97	-74.99	-70.04	53.37	6.62	6.93	6.99	6.99
179.98	-60.03	-67.1	54.53	5.08	5.86	5.89	5.90
179.97	-45.0	-64.48	55.54	4.76	6.73	6.74	6.75
-179.99	-30.01	-63.14	56.1	5.47	8.67	8.67	8.67
179.99	-14.99	-63.44	55.89	6.42	10.81	10.81	10.82
-180.0	0.01	-64.72	54.95	6.65	11.43	11.45	11.45
-165.0	0.02	-52.74	68.03	7.26	11.62	11.50	11.38
-165.0	15.04	-54.09	66.77	6.42	10.02	9.91	9.81
-164.98	29.97	-54.08	66.59	4.43	7.18	7.07	6.98
-165.02	45.04	-52.84	67.57	2.08	3.97	3.85	3.73
-165.01	60.01	-51.11	69.16	0.66	1.38	1.25	1.09
-165.03	75.04	-50.23	70.15	0.61	0.85	0.70	0.52
-165.03	90.02	-50.22	70.41	1.65	2.08	1.94	1.75
-164.96	105.01	-50.84	70.08	3.08	4.27	4.13	3.96
-165.04	119.99	-51.89	69.26	4.27	5.91	5.78	5.63
-165.01	134.99	-52.32	68.96	4.93	6.47	6.34	6.20
-164.98	149.98	-51.57	69.89	5.25	6.23	6.09	5.93
-165.0	165.01	-50.01	71.82	5.70	6.20	6.04	5.83
-165.04	-179.96	-48.77	73.83	6.65	6.84	6.67	6.41
-165.03	-165.04	-48.64	74.97	8.29	8.67	8.50	8.20
-165.01	-149.97	-49.96	74.58	10.43	11.80	11.63	11.35
-165.05	-134.96	-52.98	72.44	12.17	14.55	14.41	14.19
-164.99	-119.95	-56.72	69.46	12.63	14.46	14.35	14.22
-165.03	-105.02	-58.81	66.95	11.37	11.93	11.85	11.77
-165.02	-89.99	-58.41	65.85	8.81	8.94	8.87	8.80
-164.99	-74.97	-56.18	66.19	6.18	6.76	6.67	6.59
-165.01	-60.04	-53.58	67.24	4.50	5.87	5.76	5.65
-164.97	-45.0	-51.6	68.46	4.16	6.43	6.30	6.16
-165.01	-30.02	-50.79	69.22	5.10	8.27	8.13	7.98
-165.03	-14.97	-51.27	69.11	6.56	10.54	10.40	10.25
-164.94	-0.02	-52.7	68.07	7.25	11.59	11.46	11.34
-149.96	0.01	-40.49	81.17	9.42	13.70	13.45	12.93
-149.98	15.04	-41.83	79.73	8.61	12.53	12.30	11.83
-149.94	29.96	-41.5	79.66	6.35	9.82	9.58	9.11
-150.0	45.0	-39.72	81.08	3.68	6.41	6.16	5.63
-149.98	60.0	-37.53	83.14	2.01	3.83	3.56	2.95
-149.96	75.0	-36.44	84.39	1.90	3.20	2.92	2.26
-149.99	90.04	-36.76	84.49	3.15	4.51	4.22	3.56
-149.98	105.02	-37.92	83.82	5.02	6.70	6.42	5.79
-149.98	120.01	-39.21	82.83	6.62	8.55	8.29	7.70
-149.97	135.01	-39.83	82.3	7.33	9.21	8.95	8.38
-149.97	149.99	-39.1	83.18	7.32	8.88	8.61	8.01
-149.95	164.99	-37.5	85.29	7.17	8.15	7.87	7.19
-149.96	179.98	-36.22	87.5	7.54	8.35	8.05	7.28
-149.97	-165.03	-36.27	88.61	8.93	10.41	10.10	9.29
-149.96	-150.0	-38.21	87.97	11.18	13.41	13.12	12.34
-149.97	-135.03	-41.07	85.79	13.21	15.25	14.98	14.30
-149.97	-120.0	-43.44	82.8	13.62	14.89	14.65	14.08
-149.94	-105.0	-44.64	80.1	12.11	12.97	12.75	12.28

O4-C4-C5-O5 (degrees)	O5-C5-C6-O6 (degrees)	C3-C4-C5-C6 (degrees)	O4-C4-C5-C6 (degrees)	QM rel. E (kcal/mol)	MM1 rel. E (kcal/mol)	MM2 rel. E (kcal/mol)	MM3 rel. E (kcal/mol)
-149.95	-90.01	-44.35	78.66	9.39	10.61	10.40	9.97
-149.98	-75.01	-42.55	78.99	6.72	8.67	8.44	8.00
-149.99	-60.01	-39.98	80.67	5.06	7.45	7.20	6.68
-150.0	-45.0	-38.03	82.35	4.97	7.90	7.63	7.05
-149.95	-29.98	-37.46	83.2	6.38	10.04	9.77	9.16
-149.95	-15.03	-38.52	82.72	8.38	12.56	12.29	11.70
-150.0	0.04	-40.54	81.11	9.41	13.64	13.39	12.87
-135.0	-0.03	-27.0	95.26	12.16	17.58	17.20	16.08
-135.02	15.01	-27.87	94.11	11.00	16.43	16.06	14.99
-134.97	29.96	-26.83	94.58	8.19	13.40	13.02	11.93
-135.01	45.01	-24.29	96.57	5.17	9.31	8.92	7.74
-134.99	60.04	-21.9	98.82	3.39	6.44	6.03	4.75
-135.02	74.99	-21.44	99.71	3.56	5.76	5.34	4.03
-134.99	90.0	-22.47	99.41	5.39	7.48	7.07	5.77
-135.02	104.98	-24.05	98.42	7.72	10.07	9.67	8.42
-134.99	120.0	-25.21	97.49	9.31	12.28	11.89	10.68
-135.01	134.98	-25.43	97.25	9.63	12.49	12.10	10.90
-135.0	150.01	-24.2	98.44	9.01	11.34	10.94	9.69
-135.02	165.03	-22.14	100.87	8.30	10.02	9.60	8.24
-135.01	179.98	-20.71	103.23	8.44	10.29	9.85	8.41
-135.03	-164.97	-21.09	104.12	10.01	12.32	11.88	10.41
-134.99	-150.06	-22.63	103.19	12.61	15.21	14.78	13.35
-134.97	-134.98	-25.03	100.47	14.66	17.42	17.01	15.69
-135.0	-120.02	-27.7	96.92	14.89	17.84	17.46	16.28
-135.04	-105.04	-29.5	93.94	13.23	16.45	16.09	15.04
-134.98	-90.07	-29.2	92.99	10.45	13.67	13.31	12.29
-135.02	-74.98	-26.92	94.16	7.66	10.85	10.48	9.40
-135.02	-59.99	-24.07	96.37	6.13	9.29	8.90	7.72
-135.03	-44.96	-22.73	97.84	6.48	10.10	9.70	8.46
-135.03	-29.98	-23.36	97.94	8.57	13.00	12.60	11.36
-135.01	-14.93	-25.11	96.89	11.05	15.98	15.59	14.40
-135.0	-0.03	-27.0	95.26	12.15	17.55	17.17	16.05
-119.98	-0.02	-10.53	111.5	14.01	21.44	20.95	19.20
-120.05	15.05	-10.65	110.87	12.32	19.76	19.27	17.54
-120.04	30.01	-8.98	111.81	9.07	15.70	15.20	13.44
-120.06	45.03	-6.55	113.86	5.87	11.35	10.84	9.03
-120.11	60.03	-5.18	115.53	4.33	8.35	7.83	5.98
-120.07	74.98	-5.41	116.03	5.05	7.92	7.41	5.54
-120.05	90.04	-6.57	115.57	7.32	10.04	9.53	7.67
-120.04	104.97	-7.64	114.8	9.73	12.98	12.47	10.64
-120.03	119.97	-8.13	114.19	10.90	14.76	14.26	12.44
-120.04	134.99	-7.46	114.48	10.55	14.08	13.57	11.74
-120.04	150.01	-5.36	116.2	9.33	12.01	11.49	9.62
-120.02	165.0	-3.07	118.82	8.25	10.69	10.16	8.23
-120.06	179.99	-2.41	120.54	8.59	11.32	10.79	8.83
-120.04	-165.0	-2.95	120.77	10.69	14.12	13.58	11.62
-120.05	-149.97	-4.61	119.19	13.55	17.90	17.37	15.44
-120.06	-134.99	-7.16	116.29	15.55	20.86	20.35	18.48
-120.07	-119.98	-9.73	113.1	15.71	21.35	20.85	19.07
-120.06	-104.98	-11.15	110.81	13.88	18.95	18.46	16.74
-120.04	-90.02	-10.43	110.45	10.86	14.98	14.49	12.78
-120.02	-75.03	-7.95	112.04	8.06	11.27	10.77	9.00
-120.05	-60.03	-6.17	113.82	6.86	10.14	9.64	7.82

O4-C4-C5-O5 (degrees)	O5-C5-C6-O6 (degrees)	C3-C4-C5-C6 (degrees)	O4-C4-C5-C6 (degrees)	QM rel. E (kcal/mol)	MM1 rel. E (kcal/mol)	MM2 rel. E (kcal/mol)	MM3 rel. E (kcal/mol)
-120.07	-44.97	-6.64	114.21	8.01	12.27	11.77	9.94
-120.04	-30.01	-7.98	113.69	10.75	16.15	15.64	13.84
-120.05	-14.99	-9.48	112.6	13.30	19.90	19.40	17.62
-120.04	-0.03	-10.6	111.43	14.02	21.51	21.02	19.28
-104.99	0.02	8.88	129.3	13.99	22.95	22.38	20.34
-104.96	14.98	9.39	129.27	11.83	20.36	19.79	17.75
-105.02	30.01	10.55	130.17	8.38	15.98	15.41	13.37
-104.94	45.02	11.75	131.73	5.51	11.58	11.01	8.96
-104.97	59.95	12.45	133.01	4.57	8.86	8.28	6.24
-104.95	75.02	12.57	133.58	5.70	8.79	8.21	6.17
-104.99	90.02	12.11	133.28	7.97	10.98	10.41	8.36
-105.0	105.01	11.65	132.63	9.92	13.36	12.79	10.74
-104.99	120.02	11.81	132.27	10.45	13.99	13.42	11.37
-104.96	135.01	13.21	133.01	9.43	12.49	11.92	9.88
-104.93	150.02	14.92	134.72	7.79	10.50	9.93	7.89
-104.96	165.02	15.64	136.42	6.90	9.82	9.24	7.21
-105.0	180.0	16.22	137.78	7.83	11.40	10.82	8.80
-104.93	-164.98	16.47	138.12	10.23	15.03	14.45	12.43
-104.91	-150.02	15.52	136.85	13.01	19.05	18.47	16.44
-104.97	-134.96	13.48	134.32	14.89	21.57	21.00	18.95
-105.0	-120.0	11.4	131.63	14.84	21.03	20.46	18.42
-104.95	-104.97	10.4	129.88	12.79	17.42	16.85	14.81
-104.95	-89.97	10.97	129.77	9.74	12.71	12.15	10.11
-105.04	-75.03	11.85	130.71	7.31	10.03	9.47	7.43
-104.97	-59.98	11.68	131.47	6.97	10.54	9.97	7.92
-105.02	-44.98	10.75	131.34	8.85	13.74	13.17	11.12
-104.98	-29.96	10.03	130.89	11.68	18.23	17.66	15.61
-104.99	-14.95	9.31	130.11	13.84	22.06	21.50	19.45
-104.99	0.04	8.89	129.32	13.99	22.99	22.42	20.38
-90.01	0.0	28.39	146.86	12.12	21.22	20.65	18.76
-90.01	15.04	28.39	146.8	9.81	18.75	18.18	16.29
-89.99	30.03	28.45	147.43	6.81	14.77	14.20	12.32
-90.01	45.07	29.04	148.64	4.56	10.79	10.22	8.35
-90.01	60.03	30.32	150.12	3.92	8.27	7.70	5.86
-89.95	75.02	31.3	150.99	4.92	7.78	7.21	5.39
-90.02	89.96	31.25	150.69	6.77	9.15	8.58	6.75
-89.97	105.0	31.17	150.1	8.12	10.56	9.99	8.15
-89.98	119.97	31.43	149.73	8.06	10.64	10.08	8.24
-90.0	135.03	31.8	150.03	6.79	9.55	8.98	7.15
-90.02	150.01	31.99	151.1	5.36	8.26	7.69	5.87
-90.02	165.0	33.1	153.0	5.03	8.22	7.66	5.87
-90.04	179.96	34.83	154.76	6.15	10.04	9.48	7.72
-89.99	-164.97	35.91	155.37	8.36	13.11	12.55	10.81
-90.04	-150.03	35.4	154.22	10.84	16.20	15.64	13.88
-89.98	-135.06	33.95	152.11	12.39	17.65	17.09	15.30
-90.0	-120.02	32.05	149.65	12.20	16.34	15.78	13.94
-90.02	-104.98	30.51	147.76	10.26	13.00	12.43	10.57
-89.98	-89.97	29.67	147.15	7.71	9.96	9.39	7.51
-90.04	-74.96	29.37	147.67	6.21	8.88	8.31	6.43
-89.97	-59.97	29.55	148.58	6.54	10.18	9.61	7.75
-89.96	-44.97	29.5	148.75	8.41	13.77	13.20	11.34
-90.02	-29.97	29.1	148.25	10.85	17.86	17.29	15.42
-90.01	-14.97	28.65	147.5	12.46	20.92	20.35	18.47

O4-C4-C5-O5 (degrees)	O5-C5-C6-O6 (degrees)	C3-C4-C5-C6 (degrees)	O4-C4-C5-C6 (degrees)	QM rel. E (kcal/mol)	MM1 rel. E (kcal/mol)	MM2 rel. E (kcal/mol)	MM3 rel. E (kcal/mol)
-90.01	0.0	28.39	146.86	12.12	21.23	20.66	18.77
-75.02	-0.08	44.66	162.37	9.82	19.02	18.49	16.89
-75.07	15.07	43.79	162.02	7.94	16.86	16.32	14.72
-75.15	30.02	43.73	162.58	5.56	13.37	12.84	11.24
-75.06	45.01	45.02	164.14	3.59	9.63	9.10	7.53
-75.05	60.04	46.8	165.77	2.77	6.97	6.45	4.90
-75.09	75.01	47.9	166.55	3.38	5.93	5.42	3.88
-75.05	90.0	48.06	166.31	4.72	6.52	6.01	4.47
-75.05	105.05	47.62	165.41	5.61	7.65	7.13	5.58
-75.05	119.94	46.9	164.51	5.43	7.97	7.45	5.89
-75.08	134.96	46.35	164.53	4.41	7.21	6.69	5.12
-75.06	149.95	46.98	165.95	3.46	6.24	5.72	4.18
-75.06	164.98	49.04	168.23	3.32	6.09	5.58	4.06
-75.17	-179.97	51.29	170.09	4.20	7.31	6.82	5.33
-75.07	-165.02	52.69	170.78	5.95	9.47	8.98	7.50
-75.13	-149.96	52.3	169.6	8.07	11.86	11.37	9.88
-75.06	-134.97	50.61	167.3	9.47	12.94	12.44	10.93
-75.05	-120.0	48.25	164.6	9.48	12.41	11.90	10.35
-75.09	-105.0	46.03	162.51	8.13	10.52	10.00	8.41
-75.04	-90.0	45.01	162.12	6.38	8.77	8.25	6.65
-75.1	-75.0	45.41	163.14	5.38	8.08	7.56	5.97
-75.05	-59.97	46.34	164.4	5.63	9.54	9.02	7.45
-75.12	-44.97	46.54	164.62	7.08	12.60	12.08	10.52
-75.07	-29.99	46.17	164.13	9.05	16.12	15.60	14.03
-75.1	-14.98	45.46	163.17	10.26	18.69	18.16	16.58
-75.04	-0.04	44.63	162.35	9.82	19.00	18.47	16.87
-60.04	-0.01	57.55	175.99	9.02	18.12	17.65	16.22
-59.98	15.01	56.9	175.79	7.60	16.16	15.69	14.26
-60.04	30.04	57.34	176.48	5.42	12.88	12.42	10.99
-60.01	44.99	58.93	178.01	3.32	9.17	8.71	7.29
-60.03	60.0	60.73	179.59	2.18	6.23	5.79	4.37
-60.04	75.0	61.66	-179.71	2.38	5.16	4.72	3.31
-60.05	90.0	61.47	179.87	3.37	5.65	5.22	3.80
-60.0	104.99	60.52	178.77	4.22	6.83	6.39	4.97
-59.99	120.02	59.3	177.71	4.32	7.24	6.80	5.37
-60.0	135.07	58.99	177.88	3.69	6.38	5.93	4.50
-59.98	149.97	60.2	179.47	2.96	5.30	4.86	3.44
-60.0	165.0	62.57	-178.27	2.66	4.65	4.22	2.80
-60.02	179.98	64.88	-176.47	3.19	5.42	5.00	3.59
-59.99	-165.0	66.05	-176.02	4.65	7.29	6.88	5.47
-60.03	-149.95	65.59	-177.25	6.59	9.69	9.28	7.87
-60.03	-134.99	63.79	-179.61	8.18	11.69	11.27	9.86
-60.03	-120.0	61.28	177.75	8.61	11.97	11.54	10.12
-60.03	-104.97	59.28	176.05	7.75	10.68	10.23	8.80
-59.99	-90.04	58.8	176.07	6.27	9.18	8.73	7.30
-60.05	-75.01	59.53	177.24	5.16	8.50	8.06	6.63
-59.99	-60.0	60.58	178.52	5.02	9.48	9.04	7.62
-60.05	-44.99	60.71	178.8	6.19	12.22	11.78	10.36
-60.04	-30.01	60.04	178.18	7.91	15.35	14.91	13.49
-60.05	-15.05	58.83	177.0	9.11	17.74	17.29	15.86
-60.02	0.01	57.56	176.0	9.01	18.03	17.57	16.14
-44.98	0.04	69.37	-170.77	10.30	19.01	18.63	17.19
-44.99	15.0	68.93	-171.13	9.05	17.15	16.77	15.33

O4-C4-C5-O5 (degrees)	O5-C5-C6-O6 (degrees)	C3-C4-C5-C6 (degrees)	O4-C4-C5-C6 (degrees)	QM rel. E (kcal/mol)	MM1 rel. E (kcal/mol)	MM2 rel. E (kcal/mol)	MM3 rel. E (kcal/mol)
-44.98	30.04	69.62	-170.48	6.74	13.87	13.50	12.05
-44.97	44.99	71.27	-168.96	4.37	10.19	9.83	8.37
-44.94	59.96	72.93	-167.39	2.98	7.15	6.81	5.33
-44.97	74.97	73.61	-166.73	2.95	6.16	5.82	4.34
-44.97	90.06	73.21	-167.1	3.88	6.86	6.52	5.04
-45.04	104.98	71.96	-168.31	4.92	7.99	7.63	6.17
-45.01	120.0	70.7	-169.44	5.39	8.31	7.95	6.49
-44.94	134.98	70.59	-169.36	4.99	7.45	7.08	5.63
-45.04	150.02	71.92	-168.05	4.20	5.99	5.63	4.16
-45.06	165.01	74.23	-166.0	3.70	5.22	4.88	3.39
-44.99	180.0	76.48	-164.27	4.01	5.87	5.56	4.05
-45.0	-164.94	77.7	-163.75	5.38	8.23	7.92	6.40
-44.92	-150.01	77.48	-164.62	7.41	11.22	10.91	9.40
-44.99	-134.99	75.71	-166.79	9.25	13.42	13.09	11.61
-44.93	-120.02	73.44	-169.08	9.92	13.75	13.41	11.95
-44.99	-104.98	71.58	-170.64	9.11	12.58	12.22	10.77
-44.94	-90.09	71.18	-170.65	7.51	10.96	10.59	9.15
-44.97	-75.04	71.91	-169.56	6.12	10.12	9.76	8.31
-44.99	-59.97	72.77	-168.34	5.85	10.84	10.49	9.03
-44.96	-45.09	72.78	-167.97	6.88	13.37	13.02	11.55
-45.0	-29.96	71.91	-168.6	8.66	16.42	16.06	14.60
-44.97	-15.01	70.64	-169.69	10.08	18.65	18.29	16.83
-44.99	0.02	69.39	-170.76	10.31	18.93	18.56	17.12
-30.1	-0.0	81.66	-157.18	12.99	21.29	21.02	19.41
-30.04	14.93	81.43	-157.6	11.65	19.41	19.15	17.54
-30.07	30.0	82.16	-157.04	9.08	15.92	15.66	14.04
-30.12	45.01	83.69	-155.56	6.46	11.96	11.71	10.07
-30.06	60.0	85.28	-153.86	4.88	9.25	9.02	7.34
-30.09	74.96	85.78	-153.19	4.84	8.40	8.17	6.49
-30.1	90.0	85.26	-153.54	5.91	9.15	8.93	7.25
-30.08	104.98	84.11	-154.64	7.29	10.38	10.14	8.48
-30.07	120.0	82.88	-155.94	7.99	10.64	10.38	8.75
-30.08	135.01	82.63	-156.33	7.65	9.80	9.54	7.91
-30.04	149.96	83.91	-155.21	6.74	8.32	8.08	6.43
-30.11	165.03	86.09	-153.36	6.01	7.51	7.29	5.60
-30.09	180.0	88.45	-151.49	6.22	8.36	8.16	6.44
-30.14	-164.98	89.87	-150.63	7.58	11.01	10.83	9.08
-30.1	-149.99	89.76	-151.18	9.80	13.97	13.79	12.05
-30.08	-134.99	88.19	-152.99	11.74	16.10	15.90	14.19
-30.1	-120.01	85.87	-155.27	12.37	16.52	16.30	14.64
-30.07	-104.97	84.12	-156.84	11.43	15.45	15.20	13.57
-30.07	-89.96	83.62	-157.03	9.65	13.68	13.43	11.80
-30.06	-75.0	84.32	-155.94	8.18	12.70	12.45	10.81
-30.07	-60.04	85.03	-154.75	7.88	13.41	13.18	11.51
-30.05	-45.02	84.98	-154.32	9.00	15.85	15.61	13.94
-30.11	-30.0	83.98	-154.96	10.92	18.91	18.67	17.02
-30.15	-14.95	82.68	-156.12	12.59	21.01	20.76	19.13
-30.0	-0.01	81.76	-157.09	13.01	21.28	21.01	19.40
-15.01	-0.01	95.98	-142.38	15.69	23.93	23.81	21.94
-15.02	15.04	95.78	-142.81	14.20	21.86	21.75	19.88
-14.98	29.98	96.58	-142.07	11.38	18.18	18.07	16.19
-14.95	44.97	98.17	-140.41	8.55	14.35	14.26	12.35
-15.0	59.98	99.52	-138.88	6.93	11.53	11.45	9.52

O4-C4-C5-O5 (degrees)	O5-C5-C6-O6 (degrees)	C3-C4-C5-C6 (degrees)	O4-C4-C5-C6 (degrees)	QM rel. E (kcal/mol)	MM1 rel. E (kcal/mol)	MM2 rel. E (kcal/mol)	MM3 rel. E (kcal/mol)
-14.98	74.99	99.88	-138.28	7.02	10.73	10.66	8.73
-15.02	89.99	99.33	-138.74	8.39	11.68	11.60	9.68
-14.98	104.94	98.47	-139.74	10.04	12.88	12.79	10.88
-14.96	119.97	97.52	-140.91	10.84	13.32	13.22	11.33
-15.02	135.01	97.13	-141.49	10.41	12.40	12.29	10.40
-15.0	150.04	98.1	-140.69	9.33	11.00	10.90	9.00
-15.01	164.99	100.25	-138.83	8.42	10.11	10.04	8.11
-15.04	179.99	102.62	-136.81	8.50	11.13	11.08	9.12
-15.02	-164.99	104.1	-135.66	9.91	13.57	13.53	11.56
-14.99	-149.99	104.04	-136.05	12.20	16.64	16.61	14.63
-15.0	-134.94	102.41	-137.87	14.09	19.03	18.97	17.02
-15.01	-120.06	100.29	-140.06	14.63	19.64	19.56	17.64
-14.97	-105.04	98.59	-141.62	13.62	18.36	18.26	16.37
-15.03	-89.98	97.98	-141.91	11.85	16.45	16.35	14.46
-15.03	-74.99	98.52	-140.93	10.38	15.33	15.23	13.33
-15.01	-60.01	99.04	-139.84	10.11	15.98	15.90	13.98
-15.01	-45.06	98.77	-139.61	11.33	18.47	18.38	16.47
-15.03	-29.94	97.81	-140.28	13.48	21.58	21.49	19.59
-15.01	-15.07	96.79	-141.34	15.29	23.72	23.62	21.73
-14.99	0.01	95.99	-142.37	15.69	24.00	23.89	22.02
-0.01	0.03	112.17	-126.64	17.10	25.82	25.87	23.85
0.04	15.05	112.09	-126.81	15.40	23.65	23.71	21.69
-0.01	29.97	112.74	-126.07	12.43	19.81	19.88	17.86
-0.0	45.02	114.16	-124.49	9.52	15.69	15.78	13.76
-0.06	60.04	115.41	-123.09	7.98	12.78	12.87	10.86
0.07	74.98	115.95	-122.5	8.29	11.92	12.03	10.02
0.01	89.98	115.56	-123.02	9.89	12.90	12.99	10.98
-0.04	104.97	114.79	-124.01	11.61	14.25	14.33	12.32
-0.01	119.94	114.07	-124.93	12.34	14.82	14.90	12.88
0.03	135.04	113.9	-125.22	11.78	13.91	13.99	11.96
-0.02	150.0	114.74	-124.47	10.49	12.39	12.47	10.45
0.05	164.99	116.79	-122.59	9.42	11.58	11.69	9.67
0.05	179.98	119.0	-120.58	9.46	12.42	12.55	10.54
-0.03	-164.99	120.25	-119.64	10.94	14.81	14.95	12.94
0.0	-150.0	120.07	-120.15	13.19	18.12	18.26	16.25
0.03	-135.02	118.57	-121.87	15.00	20.79	20.91	18.89
0.05	-120.07	116.45	-123.96	15.56	21.54	21.64	19.60
-0.02	-104.97	114.63	-125.58	14.62	20.06	20.14	18.11
0.0	-90.01	114.04	-125.8	12.87	17.72	17.80	15.77
0.05	-74.99	114.52	-124.88	11.48	16.70	16.78	14.76
0.05	-60.02	114.81	-124.09	11.36	17.61	17.70	15.68
0.03	-45.02	114.41	-124.11	12.79	20.29	20.37	18.36
0.01	-29.95	113.63	-124.83	15.05	23.45	23.53	21.51
0.03	-15.07	112.88	-125.76	16.87	25.69	25.76	23.74
-0.02	-0.05	112.16	-126.65	17.11	25.98	26.04	24.02

Table C.3. Dihedral angles and relative energies for **4.2** with the E_3 ring conformation.

O4-C4-C5-O5 (degrees)	O5-C5-C6-O6 (degrees)	C3-C4-C5-C6 (degrees)	O4-C4-C5-C6 (degrees)	QM rel. E (kcal/mol)	MM1 rel. E (kcal/mol)	MM2 rel. E (kcal/mol)	MM3 rel. E (kcal/mol)
-0.04	0.04	115.4	-126.78	15.56	22.69	22.11	20.75
-0.1	14.98	115.05	-127.12	13.90	20.36	19.77	18.42
-0.08	29.97	115.72	-126.33	10.95	16.66	16.08	14.72
-0.02	44.96	117.25	-124.7	8.10	12.61	12.05	10.70
-0.06	60.04	118.64	-123.25	6.62	9.73	9.18	7.83
-0.02	74.95	119.21	-122.66	7.03	8.83	8.28	6.94
-0.1	89.99	118.89	-123.11	8.78	9.82	9.27	7.92
-0.06	104.97	118.41	-123.78	10.73	11.63	11.08	9.73
-0.06	119.97	117.99	-124.39	11.78	12.75	12.19	10.84
-0.06	134.97	118.32	-124.27	11.66	12.53	11.97	10.61
-0.09	149.99	119.84	-123.08	10.71	11.73	11.19	9.84
-0.11	165.01	122.15	-121.16	9.74	11.17	10.65	9.30
0.01	179.97	124.24	-119.33	9.59	11.85	11.35	10.01
-0.05	-164.93	124.89	-118.86	10.71	13.99	13.50	12.17
-0.05	-150.02	124.13	-119.78	12.56	16.85	16.34	15.00
-0.03	-135.01	122.24	-121.73	14.10	19.18	18.66	17.30
-0.04	-120.01	119.87	-123.99	14.40	19.72	19.18	17.81
-0.04	-104.97	117.96	-125.6	13.29	17.96	17.40	16.03
-0.09	-89.97	117.19	-125.98	11.51	15.59	15.01	13.65
-0.03	-74.99	117.66	-125.09	10.08	14.57	14.00	12.64
0.04	-60.0	118.1	-124.21	9.96	15.32	14.76	13.41
-0.09	-45.01	117.64	-124.34	11.35	17.67	17.11	15.76
-0.07	-29.96	116.94	-125.01	13.55	20.56	19.99	18.64
-0.06	-14.96	116.11	-125.96	15.33	22.71	22.13	20.78
-0.07	0.03	115.34	-126.84	15.55	22.65	22.06	20.70
15.05	0.02	132.97	-110.66	14.35	22.26	21.85	20.63
15.01	14.95	132.73	-110.76	12.57	19.83	19.42	18.20
15.0	30.0	133.31	-109.99	9.63	15.91	15.51	14.31
15.03	45.02	134.67	-108.5	6.88	11.75	11.36	10.19
15.04	60.01	136.05	-107.16	5.57	8.69	8.32	7.18
15.03	75.04	136.67	-106.72	6.07	7.66	7.29	6.16
14.97	89.99	136.49	-107.12	7.79	8.74	8.36	7.22
15.05	104.99	136.09	-107.71	9.55	10.33	9.95	8.79
14.98	120.05	135.57	-108.31	10.37	11.38	11.00	9.83
15.06	134.95	135.83	-108.11	9.94	11.10	10.72	9.56
15.07	149.96	136.85	-107.14	8.73	9.99	9.62	8.48
15.04	164.96	138.61	-105.51	7.63	9.37	9.02	7.91
14.95	179.97	140.36	-104.01	7.54	9.93	9.59	8.52
14.95	-164.98	141.27	-103.41	8.75	12.06	11.73	10.68
15.02	-150.02	140.81	-104.13	10.65	15.18	14.85	13.77
15.02	-135.0	139.08	-105.93	12.26	17.63	17.27	16.15
15.04	-120.0	136.96	-107.92	12.69	18.07	17.69	16.52
15.06	-105.04	135.23	-109.34	11.81	16.52	16.13	14.93
15.05	-90.02	134.46	-109.68	10.25	14.73	14.33	13.13
15.04	-74.96	134.59	-109.15	9.09	13.78	13.39	12.20
15.02	-60.01	134.82	-108.59	9.14	14.68	14.29	13.12
15.02	-45.03	134.65	-108.68	10.57	16.91	16.52	15.35
15.0	-29.94	134.14	-109.34	12.71	20.03	19.63	18.44
15.02	-15.03	133.54	-110.06	14.31	22.09	21.69	20.48
15.1	-0.03	133.04	-110.6	14.35	22.22	21.81	20.60

O4-C4-C5-O5 (degrees)	O5-C5-C6-O6 (degrees)	C3-C4-C5-C6 (degrees)	O4-C4-C5-C6 (degrees)	QM rel. E (kcal/mol)	MM1 rel. E (kcal/mol)	MM2 rel. E (kcal/mol)	MM3 rel. E (kcal/mol)
29.95	-0.04	149.23	-95.04	11.91	19.82	19.56	18.76
29.95	14.96	149.12	-95.02	10.09	17.43	17.17	16.37
29.93	30.0	149.71	-94.28	7.25	13.66	13.41	12.63
29.93	45.02	150.97	-93.0	4.63	9.36	9.12	8.38
29.95	59.96	152.37	-91.7	3.40	6.22	6.00	5.30
29.94	74.97	153.03	-91.25	3.88	5.14	4.91	4.23
29.92	89.99	152.85	-91.57	5.45	5.96	5.73	5.04
29.93	104.98	152.32	-92.19	7.01	7.57	7.33	6.62
29.97	119.99	151.82	-92.69	7.64	8.50	8.26	7.53
29.91	135.0	151.69	-92.74	7.09	8.20	7.97	7.24
29.87	149.99	152.46	-91.97	5.82	7.28	7.05	6.34
29.92	165.01	154.15	-90.42	4.76	6.49	6.27	5.62
29.91	179.98	156.01	-88.87	4.75	6.98	6.78	6.17
29.96	-165.03	157.02	-88.14	5.93	9.06	8.86	8.28
29.92	-150.03	156.48	-88.87	7.85	12.07	11.86	11.25
29.96	-135.01	154.87	-90.51	9.52	14.43	14.22	13.55
29.96	-120.0	152.75	-92.46	10.15	15.13	14.90	14.18
29.91	-105.02	150.75	-94.11	9.54	14.18	13.93	13.15
29.94	-89.97	149.67	-94.78	8.28	12.68	12.42	11.63
29.99	-75.0	149.64	-94.48	7.32	11.96	11.71	10.92
29.89	-59.98	149.99	-94.0	7.45	12.70	12.45	11.68
29.99	-45.02	150.35	-93.7	8.74	14.90	14.66	13.90
29.94	-30.02	150.13	-94.06	10.64	17.70	17.45	16.68
29.9	-15.03	149.64	-94.64	12.01	19.79	19.54	18.75
29.96	-0.01	149.26	-95.04	11.90	19.75	19.49	18.69
45.01	-0.01	163.85	-79.89	9.43	16.67	16.53	16.21
44.95	15.04	163.66	-80.02	7.64	14.45	14.30	13.97
44.94	29.94	164.2	-79.45	4.93	10.70	10.56	10.24
45.02	44.95	165.55	-78.17	2.43	6.54	6.41	6.13
44.89	60.01	166.84	-76.96	1.18	3.33	3.20	2.96
44.95	75.04	167.63	-76.27	1.54	2.15	2.04	1.81
45.02	89.98	167.63	-76.37	2.94	2.75	2.64	2.40
44.96	104.98	167.0	-77.0	4.35	4.25	4.13	3.88
44.97	120.01	166.38	-77.6	4.89	5.21	5.08	4.81
45.03	134.99	166.1	-77.81	4.34	5.06	4.94	4.67
45.0	149.96	166.63	-77.27	3.16	4.10	3.98	3.72
44.98	165.01	168.23	-75.88	2.21	3.29	3.18	2.95
45.01	179.98	170.17	-74.19	2.23	3.84	3.74	3.56
44.94	-165.0	171.1	-73.47	3.40	5.93	5.83	5.67
44.93	-150.02	170.7	-73.99	5.33	8.93	8.83	8.65
44.98	-135.01	168.87	-75.7	7.18	11.49	11.38	11.16
45.01	-119.98	166.21	-78.08	8.14	12.47	12.35	12.07
45.02	-105.01	163.63	-80.24	7.93	11.69	11.55	11.21
44.99	-89.99	162.16	-81.35	6.89	10.37	10.22	9.85
45.03	-74.99	162.2	-81.12	6.01	9.70	9.55	9.19
44.99	-60.07	163.08	-80.23	5.95	10.25	10.11	9.77
44.94	-45.02	163.95	-79.49	6.98	12.19	12.05	11.73
44.93	-29.98	164.31	-79.29	8.56	14.77	14.63	14.32
44.96	-15.02	164.19	-79.54	9.69	16.68	16.54	16.22
45.03	-0.04	163.87	-79.87	9.43	16.69	16.55	16.23
60.04	-0.01	176.82	-65.59	8.15	14.39	14.33	14.31
59.98	15.04	176.35	-66.07	6.46	12.13	12.06	12.04
60.01	30.0	176.82	-65.63	3.81	8.49	8.43	8.41

O4-C4-C5-O5 (degrees)	O5-C5-C6-O6 (degrees)	C3-C4-C5-C6 (degrees)	O4-C4-C5-C6 (degrees)	QM rel. E (kcal/mol)	MM1 rel. E (kcal/mol)	MM2 rel. E (kcal/mol)	MM3 rel. E (kcal/mol)
59.98	45.01	178.15	-64.37	1.32	4.43	4.38	4.37
60.01	60.02	179.77	-62.83	0.00	1.16	1.12	1.13
59.96	75.01	-179.33	-62.01	0.22	0.07	0.03	0.04
60.04	90.0	-179.13	-61.89	1.48	0.73	0.69	0.70
60.0	105.01	-179.77	-62.54	2.81	2.27	2.22	2.23
60.02	119.97	179.26	-63.42	3.41	3.36	3.31	3.32
60.06	135.04	178.64	-63.93	2.96	3.19	3.13	3.13
59.99	149.98	179.03	-63.62	1.91	2.22	2.17	2.17
59.95	165.02	-179.37	-62.2	1.05	1.54	1.49	1.51
59.97	179.97	-177.42	-60.44	1.06	2.07	2.03	2.06
59.98	-164.96	-176.29	-59.45	2.26	4.29	4.26	4.29
60.02	-150.02	-176.87	-60.0	4.41	7.65	7.62	7.65
59.98	-135.01	-179.54	-62.26	6.76	10.15	10.10	10.12
59.99	-119.98	176.89	-65.34	8.22	11.12	11.06	11.05
59.93	-104.99	173.87	-67.99	8.22	10.53	10.46	10.40
60.06	-89.99	172.68	-68.97	7.15	9.29	9.22	9.15
60.01	-75.01	173.16	-68.44	6.00	8.53	8.46	8.40
59.99	-59.98	174.63	-67.05	5.64	8.74	8.67	8.63
60.02	-45.01	176.25	-65.68	6.30	10.29	10.23	10.21
60.0	-30.03	177.24	-64.97	7.53	12.67	12.61	12.60
60.05	-15.0	177.44	-64.96	8.44	14.40	14.35	14.33
59.97	-0.01	176.74	-65.66	8.15	14.43	14.37	14.34
74.97	0.03	-171.26	-52.16	8.54	13.93	13.92	13.95
75.03	14.98	-171.87	-52.75	6.95	11.76	11.75	11.79
75.01	30.03	-171.39	-52.38	4.30	8.00	7.99	8.02
75.02	45.06	-169.83	-50.93	1.71	4.17	4.17	4.19
75.06	59.99	-167.95	-49.13	0.31	1.17	1.16	1.18
75.03	75.0	-166.91	-48.18	0.43	0.00	0.00	0.00
75.01	89.99	-166.93	-48.25	1.64	0.89	0.89	0.90
75.03	105.03	-167.81	-49.02	3.01	2.26	2.26	2.27
75.01	120.06	-169.08	-50.15	3.74	3.27	3.26	3.28
75.04	135.01	-169.77	-50.77	3.41	3.13	3.12	3.15
75.0	149.98	-169.26	-50.37	2.40	2.33	2.33	2.35
75.02	165.02	-167.47	-48.76	1.62	1.68	1.68	1.69
75.04	-179.99	-165.45	-46.92	1.72	2.58	2.58	2.58
75.03	-165.02	-164.61	-46.06	3.20	5.13	5.13	5.12
74.99	-150.02	-166.05	-47.06	5.95	8.38	8.38	8.37
75.06	-135.0	-169.52	-49.8	8.94	10.98	10.98	11.00
75.0	-120.05	-173.43	-53.21	10.60	11.94	11.92	11.96
75.0	-105.02	-176.19	-55.77	10.40	11.53	11.51	11.55
75.02	-89.94	-176.93	-56.54	8.93	10.10	10.08	10.12
75.07	-74.98	-175.77	-55.5	7.38	8.99	8.98	9.02
75.08	-60.01	-173.64	-53.57	6.61	8.86	8.85	8.88
75.01	-45.01	-171.51	-51.86	6.90	10.12	10.11	10.14
75.03	-30.0	-170.12	-50.9	7.88	12.34	12.33	12.36
75.04	-14.98	-170.14	-51.1	8.74	14.02	14.01	14.04
75.07	0.0	-171.16	-52.05	8.56	13.78	13.77	13.81
90.01	-0.04	-158.56	-38.39	10.34	15.16	15.17	15.04
90.03	15.03	-159.22	-39.06	8.71	12.99	13.00	12.88
90.06	29.95	-158.61	-38.58	5.97	9.41	9.42	9.29
89.98	44.96	-156.85	-37.03	3.25	5.34	5.35	5.20
90.04	59.98	-154.78	-35.1	1.76	2.49	2.50	2.31
90.03	75.03	-153.86	-34.23	1.88	1.62	1.63	1.43

O4-C4-C5-O5 (degrees)	O5-C5-C6-O6 (degrees)	C3-C4-C5-C6 (degrees)	O4-C4-C5-C6 (degrees)	QM rel. E (kcal/mol)	MM1 rel. E (kcal/mol)	MM2 rel. E (kcal/mol)	MM3 rel. E (kcal/mol)
90.07	89.96	-154.18	-34.43	3.19	2.47	2.48	2.28
90.02	104.99	-155.43	-35.45	4.76	4.15	4.16	3.98
90.02	120.05	-156.72	-36.59	5.56	5.20	5.21	5.05
90.0	135.02	-157.23	-37.15	5.22	4.96	4.97	4.82
89.99	150.02	-156.5	-36.56	4.21	4.06	4.07	3.91
90.03	164.98	-154.59	-34.86	3.43	3.56	3.57	3.38
90.02	180.0	-152.76	-33.09	3.82	4.85	4.86	4.64
90.03	-165.02	-152.54	-32.47	5.99	7.72	7.73	7.49
90.0	-150.03	-154.74	-33.74	9.58	11.14	11.15	10.93
90.01	-134.98	-158.41	-36.65	12.89	13.86	13.88	13.71
89.98	-120.03	-162.11	-40.07	14.32	14.70	14.72	14.61
90.04	-104.98	-164.44	-42.46	13.64	13.93	13.94	13.87
90.02	-90.0	-164.71	-42.95	11.65	12.05	12.06	11.99
90.04	-75.03	-162.94	-41.48	9.63	10.44	10.45	10.37
90.01	-59.97	-160.13	-39.16	8.41	10.03	10.05	9.93
89.97	-44.99	-157.65	-37.24	8.37	11.15	11.16	11.01
90.03	-30.02	-156.44	-36.46	9.28	13.53	13.54	13.38
90.02	-15.01	-157.17	-37.13	10.30	15.21	15.22	15.07
90.01	0.03	-158.57	-38.39	10.32	15.20	15.21	15.08
105.06	0.02	-143.87	-23.45	12.62	17.77	17.76	17.37
105.01	15.02	-144.52	-24.17	10.98	15.48	15.48	15.09
105.03	29.98	-143.69	-23.59	8.10	11.58	11.57	11.19
105.07	44.98	-141.62	-21.82	5.26	7.63	7.61	7.20
104.96	59.97	-139.7	-20.06	3.70	4.77	4.75	4.31
105.01	75.05	-139.04	-19.31	3.94	4.12	4.10	3.65
105.02	90.02	-139.81	-19.75	5.46	5.25	5.22	4.78
104.96	105.04	-141.24	-20.85	7.16	7.10	7.08	6.65
104.98	120.02	-142.38	-21.87	7.93	8.02	8.01	7.59
104.98	135.01	-142.64	-22.29	7.50	7.77	7.76	7.35
104.99	149.97	-141.66	-21.56	6.45	6.68	6.67	6.25
105.02	165.04	-139.72	-19.8	5.83	6.51	6.49	6.05
104.98	-179.99	-138.29	-18.11	6.76	8.12	8.10	7.63
104.96	-164.97	-138.59	-17.5	9.85	11.41	11.39	10.91
104.98	-149.96	-140.89	-18.76	13.99	15.09	15.08	14.60
104.99	-135.04	-144.3	-21.64	17.18	17.78	17.77	17.33
105.0	-120.04	-147.64	-24.95	18.22	18.30	18.31	17.92
104.99	-104.99	-149.66	-27.27	16.97	16.83	16.84	16.50
105.0	-89.98	-149.37	-27.45	14.42	14.28	14.29	13.96
105.01	-75.03	-146.87	-25.59	11.79	12.10	12.10	11.73
104.95	-59.95	-143.52	-22.97	10.10	11.62	11.61	11.21
104.97	-44.97	-141.21	-21.21	9.86	13.22	13.20	12.78
105.01	-29.95	-141.0	-21.08	11.01	15.72	15.70	15.28
105.01	-15.04	-142.4	-22.17	12.42	17.60	17.59	17.17
104.99	-0.01	-143.92	-23.5	12.61	17.76	17.76	17.36
119.99	0.0	-127.29	-7.44	14.36	20.47	20.39	19.85
120.01	14.97	-127.62	-7.97	12.66	17.91	17.83	17.30
120.03	30.0	-126.57	-7.29	9.63	13.89	13.81	13.28
120.02	45.0	-124.47	-5.55	6.69	9.76	9.67	9.14
119.97	60.02	-122.75	-3.9	5.18	7.06	6.95	6.43
119.97	74.92	-122.59	-3.39	5.64	6.41	6.30	5.79
120.02	90.0	-123.64	-3.93	7.42	7.83	7.73	7.20
120.02	104.99	-125.01	-4.96	9.14	9.87	9.77	9.24
119.98	119.94	-125.96	-5.93	9.81	10.77	10.68	10.15

O4-C4-C5-O5 (degrees)	O5-C5-C6-O6 (degrees)	C3-C4-C5-C6 (degrees)	O4-C4-C5-C6 (degrees)	QM rel. E (kcal/mol)	MM1 rel. E (kcal/mol)	MM2 rel. E (kcal/mol)	MM3 rel. E (kcal/mol)
119.96	135.03	-125.92	-6.16	9.25	10.16	10.07	9.54
119.96	149.99	-124.69	-5.28	8.19	9.12	9.03	8.50
120.01	165.02	-122.83	-3.43	7.91	9.39	9.28	8.76
120.03	179.96	-121.7	-1.59	9.63	11.48	11.37	10.85
119.95	-164.98	-122.2	-0.97	13.38	15.05	14.94	14.41
120.0	-150.01	-124.14	-2.15	17.53	18.65	18.55	18.01
119.96	-135.0	-127.06	-4.91	20.37	21.18	21.10	20.55
119.98	-119.95	-129.78	-7.91	20.88	21.23	21.17	20.62
119.97	-105.04	-131.19	-9.89	19.07	18.99	18.94	18.39
120.0	-89.98	-130.24	-9.73	15.85	15.78	15.72	15.19
120.0	-74.99	-127.12	-7.49	12.61	13.39	13.31	12.78
119.97	-59.97	-123.88	-4.98	10.56	13.13	13.03	12.51
119.99	-45.03	-122.94	-4.14	10.58	15.19	15.08	14.57
120.0	-30.04	-124.06	-4.85	12.27	18.03	17.94	17.41
120.02	-14.97	-125.87	-6.17	14.05	20.27	20.18	19.65
119.99	-0.06	-127.27	-7.42	14.37	20.49	20.41	19.87
135.05	0.04	-109.27	9.37	14.68	21.65	21.45	21.10
134.99	14.97	-109.48	8.87	12.93	19.05	18.84	18.50
134.97	30.02	-108.37	9.53	9.80	15.00	14.79	14.46
135.05	45.04	-106.49	11.19	6.89	10.95	10.72	10.43
134.99	60.02	-105.37	12.52	5.60	8.17	7.93	7.67
135.01	74.97	-105.45	12.95	6.36	7.52	7.28	7.02
135.01	90.02	-106.52	12.38	8.18	9.06	8.84	8.56
135.04	104.96	-107.6	11.49	9.82	11.07	10.86	10.56
134.97	120.03	-108.28	10.66	10.32	11.86	11.65	11.33
135.02	134.98	-107.86	10.67	9.70	11.20	10.98	10.67
135.01	149.97	-106.63	11.65	8.80	10.60	10.37	10.08
135.03	164.95	-105.05	13.59	9.07	11.16	10.92	10.67
135.05	-179.98	-103.88	15.66	11.43	13.46	13.21	13.01
135.04	-164.98	-103.83	16.47	15.18	16.90	16.65	16.47
135.08	-150.02	-105.04	15.46	18.84	20.48	20.23	20.02
134.98	-134.93	-107.25	13.0	21.11	22.55	22.32	22.05
135.03	-120.04	-109.09	10.58	20.99	22.08	21.88	21.55
135.0	-104.98	-109.88	9.05	18.57	19.19	18.99	18.64
134.98	-90.01	-108.63	9.45	14.81	15.57	15.36	15.03
135.03	-75.02	-106.18	11.35	11.20	13.04	12.81	12.52
135.0	-60.0	-104.8	12.65	9.47	13.26	13.02	12.76
134.98	-44.99	-105.09	12.58	10.21	15.68	15.44	15.18
134.99	-30.05	-106.54	11.63	12.42	18.93	18.70	18.41
135.03	-15.0	-108.19	10.42	14.36	21.38	21.17	20.85
135.01	-0.01	-109.33	9.32	14.68	21.72	21.51	21.17
149.89	0.03	-91.58	25.7	13.39	20.65	20.28	20.40
149.97	14.96	-91.72	25.32	11.57	18.26	17.90	18.01
149.88	30.01	-91.22	25.63	8.60	14.42	14.06	14.18
149.94	45.04	-90.13	26.84	6.06	10.46	10.08	10.23
149.94	60.01	-89.25	28.11	5.09	7.56	7.17	7.36
149.88	75.04	-89.18	28.59	5.84	6.94	6.55	6.75
149.86	90.03	-89.75	28.26	7.49	8.41	8.02	8.21
149.91	104.97	-90.38	27.62	8.91	10.19	9.81	9.99
149.93	120.0	-90.71	26.98	9.34	11.04	10.67	10.82
149.91	135.01	-90.46	26.9	8.82	10.71	10.34	10.49
149.95	150.07	-89.52	27.96	8.33	10.43	10.05	10.23
149.9	165.01	-88.11	30.01	9.14	10.97	10.57	10.82

O4-C4-C5-O5 (degrees)	O5-C5-C6-O6 (degrees)	C3-C4-C5-C6 (degrees)	O4-C4-C5-C6 (degrees)	QM rel. E (kcal/mol)	MM1 rel. E (kcal/mol)	MM2 rel. E (kcal/mol)	MM3 rel. E (kcal/mol)
149.89	179.98	-86.42	32.3	11.45	12.96	12.54	12.85
149.91	-164.99	-85.43	33.37	14.52	15.98	15.55	15.89
149.92	-150.04	-85.71	32.71	17.35	19.23	18.81	19.13
149.95	-134.98	-87.07	30.84	18.82	20.75	20.34	20.61
149.93	-119.99	-88.81	28.63	18.16	19.77	19.37	19.58
149.98	-105.01	-90.03	27.08	15.38	16.35	15.97	16.13
149.91	-89.95	-90.64	26.46	11.56	12.60	12.23	12.37
149.89	-74.95	-90.61	26.74	8.56	10.47	10.10	10.25
149.89	-59.96	-90.19	27.34	7.73	10.91	10.53	10.69
149.92	-44.99	-89.8	27.65	9.01	13.68	13.30	13.47
149.87	-29.98	-90.03	27.34	11.34	17.51	17.13	17.29
149.94	-15.04	-90.67	26.68	13.19	20.45	20.08	20.22
149.93	0.0	-91.52	25.77	13.39	20.66	20.29	20.41
164.93	-0.03	-75.81	40.89	11.39	18.46	17.93	18.47
164.95	15.03	-76.79	39.99	9.75	16.39	15.87	16.39
164.91	30.0	-77.07	39.94	7.27	12.82	12.31	12.82
164.94	45.0	-76.38	40.94	5.13	8.98	8.46	9.00
164.93	60.01	-75.17	42.38	4.12	6.33	5.79	6.36
164.92	75.03	-74.38	43.26	4.65	5.58	5.04	5.62
164.93	90.02	-74.15	43.34	5.96	6.79	6.24	6.83
164.95	105.02	-74.4	42.87	7.19	8.51	7.96	8.54
164.92	120.02	-75.01	42.11	7.68	9.51	8.97	9.53
164.95	134.95	-75.42	41.81	7.54	9.63	9.10	9.65
164.93	150.01	-74.95	42.8	7.58	9.33	8.79	9.36
164.92	165.01	-73.22	45.12	8.46	9.48	8.92	9.53
164.89	179.98	-70.88	47.53	10.11	10.83	10.25	10.90
164.93	-164.98	-69.1	48.82	12.08	12.94	12.33	13.00
164.93	-150.02	-68.83	48.46	13.91	15.41	14.81	15.47
164.97	-135.01	-70.33	46.7	14.77	16.41	15.82	16.46
164.94	-119.99	-73.27	44.01	13.95	15.10	14.55	15.14
164.92	-104.99	-76.43	41.32	11.53	12.07	11.55	12.09
164.89	-89.94	-78.65	39.6	8.70	9.60	9.10	9.61
164.95	-75.04	-79.03	39.5	6.85	8.38	7.88	8.38
164.91	-59.94	-77.96	40.38	6.55	8.87	8.37	8.89
164.92	-45.04	-76.37	41.42	7.70	11.31	10.79	11.33
164.94	-30.02	-75.25	41.93	9.64	14.95	14.42	14.98
164.9	-14.96	-75.06	41.72	11.26	18.03	17.49	18.05
164.93	-0.03	-75.82	40.88	11.38	18.44	17.92	18.45
179.96	-0.0	-63.34	54.1	10.16	16.81	16.15	16.85
179.92	14.99	-64.91	52.86	9.03	15.29	14.65	15.34
179.95	30.02	-65.13	52.87	6.90	12.32	11.67	12.37
179.93	45.0	-63.94	54.13	4.71	8.80	8.14	8.84
179.9	59.96	-62.0	55.91	3.47	6.08	5.40	6.10
179.95	75.02	-60.59	57.09	3.58	5.14	4.45	5.15
179.94	90.0	-60.18	57.29	4.62	5.95	5.25	5.95
179.98	104.97	-60.8	56.73	5.86	7.60	6.91	7.61
179.97	120.0	-62.12	55.7	6.73	8.89	8.21	8.91
179.95	135.01	-62.98	55.28	7.12	9.28	8.61	9.31
179.95	150.02	-62.18	56.53	7.35	8.85	8.17	8.88
179.97	165.02	-59.7	59.08	7.72	8.53	7.82	8.51
179.98	179.96	-56.71	61.55	8.34	8.97	8.23	8.90
179.93	-164.99	-54.75	62.79	9.33	10.19	9.43	10.09
179.92	-149.95	-55.35	62.17	10.50	11.70	10.95	11.61

O4-C4-C5-O5 (degrees)	O5-C5-C6-O6 (degrees)	C3-C4-C5-C6 (degrees)	O4-C4-C5-C6 (degrees)	QM rel. E (kcal/mol)	MM1 rel. E (kcal/mol)	MM2 rel. E (kcal/mol)	MM3 rel. E (kcal/mol)
-180.0	-135.04	-58.51	59.77	11.33	12.35	11.63	12.32
179.94	-120.05	-63.0	56.16	11.17	11.85	11.18	11.88
179.98	-105.01	-66.87	52.85	9.82	10.43	9.80	10.50
179.98	-90.04	-68.48	51.33	8.04	9.13	8.52	9.21
179.99	-74.98	-67.64	51.86	6.58	8.31	7.69	8.38
179.97	-60.03	-65.4	53.41	6.10	8.88	8.24	8.94
179.98	-45.0	-63.14	54.84	6.84	10.75	10.09	10.79
179.92	-30.02	-61.76	55.55	8.36	13.68	13.00	13.71
179.93	-15.0	-61.77	55.36	9.82	16.29	15.61	16.31
179.96	-0.0	-63.32	54.1	10.17	16.84	16.18	16.88
-164.97	-0.02	-52.13	66.79	10.68	17.47	16.68	17.27
-165.0	14.96	-53.34	65.74	9.75	16.38	15.60	16.21
-165.02	29.96	-52.75	66.11	7.47	13.51	12.73	13.33
-165.01	44.94	-50.6	67.85	4.89	9.85	9.05	9.61
-164.96	59.95	-48.07	69.97	3.28	6.90	6.07	6.59
-164.96	74.95	-46.83	71.08	3.18	5.78	4.94	5.43
-164.96	89.99	-47.25	70.94	4.29	6.52	5.68	6.18
-165.07	105.02	-48.78	69.96	5.90	8.26	7.44	7.96
-164.96	120.01	-50.17	69.03	7.21	9.81	9.00	9.55
-165.0	135.01	-50.51	68.87	7.69	10.15	9.34	9.89
-165.04	150.02	-48.89	70.32	7.52	9.29	8.46	8.98
-165.03	165.01	-45.62	72.96	7.06	8.35	7.50	7.94
-164.97	179.96	-42.4	75.43	6.84	7.94	7.05	7.41
-165.0	-165.03	-42.06	76.06	7.40	8.55	7.66	8.00
-165.03	-149.97	-44.95	74.48	8.85	10.08	9.21	9.61
-165.0	-134.99	-49.48	71.33	10.50	11.76	10.93	11.43
-164.97	-120.02	-53.79	67.68	11.22	12.48	11.69	12.28
-165.05	-104.99	-56.44	64.85	10.49	12.15	11.39	12.03
-165.02	-89.94	-56.5	64.14	8.77	10.74	9.99	10.64
-165.0	-74.97	-54.57	65.22	7.11	9.79	9.02	9.65
-164.99	-59.98	-51.8	67.04	6.31	9.79	8.99	9.58
-165.0	-45.02	-49.57	68.51	6.76	11.51	10.70	11.25
-165.02	-30.01	-48.97	68.99	8.24	14.18	13.36	13.90
-165.0	-15.06	-50.15	68.29	9.95	16.47	15.66	16.22
-165.02	0.0	-52.18	66.74	10.69	17.49	16.71	17.30
-149.91	0.03	-39.36	80.74	12.34	20.04	19.11	19.29
-149.98	15.07	-39.61	80.1	11.06	18.76	17.84	18.04
-149.95	29.99	-38.08	80.92	8.30	15.30	14.37	14.54
-149.93	44.99	-35.33	83.0	5.37	11.36	10.41	10.49
-149.94	60.04	-33.13	85.02	3.60	8.16	7.19	7.19
-149.9	74.94	-32.87	85.75	3.71	7.03	6.05	6.02
-149.96	89.99	-34.18	85.25	5.22	7.90	6.93	6.93
-149.95	105.01	-35.63	84.36	7.18	9.97	9.01	9.04
-149.97	120.03	-36.48	83.56	8.46	11.49	10.54	10.61
-149.95	135.0	-35.86	83.7	8.55	11.32	10.36	10.43
-149.97	150.02	-33.39	85.27	7.67	9.88	8.91	8.90
-149.97	164.98	-30.2	87.65	6.50	8.24	7.24	7.12
-149.95	179.99	-29.07	89.28	5.98	7.76	6.75	6.57
-149.95	-165.02	-30.87	89.21	7.05	8.86	7.86	7.69
-149.98	-149.96	-34.41	87.45	9.47	11.52	10.54	10.45
-149.95	-135.04	-38.02	84.69	11.82	14.23	13.28	13.33
-149.95	-120.0	-40.97	81.59	12.78	15.33	14.41	14.58
-149.95	-105.04	-42.46	79.28	11.98	14.64	13.74	13.99

O4-C4-C5-O5 (degrees)	O5-C5-C6-O6 (degrees)	C3-C4-C5-C6 (degrees)	O4-C4-C5-C6 (degrees)	QM rel. E (kcal/mol)	MM1 rel. E (kcal/mol)	MM2 rel. E (kcal/mol)	MM3 rel. E (kcal/mol)
-149.96	-90.0	-41.92	78.73	10.01	12.94	12.04	12.30
-149.99	-75.0	-39.66	79.88	8.07	11.53	10.61	10.82
-149.94	-60.02	-37.05	81.7	7.15	11.57	10.63	10.76
-149.92	-45.03	-35.79	82.88	7.73	13.28	12.33	12.42
-149.96	-29.93	-36.42	82.87	9.61	16.17	15.22	15.31
-149.96	-15.03	-38.0	81.94	11.61	18.96	18.02	18.15
-149.94	0.01	-39.36	80.72	12.33	20.09	19.17	19.35
-135.04	0.02	-23.27	96.52	13.72	22.90	21.84	21.35
-135.01	15.04	-22.7	96.36	11.94	20.83	19.77	19.28
-135.03	30.05	-21.05	97.28	8.79	16.79	15.71	15.19
-135.09	45.01	-19.04	99.06	5.75	12.42	11.33	10.72
-135.02	59.98	-17.71	100.8	4.19	9.15	8.05	7.38
-135.01	74.99	-17.89	101.39	4.67	8.24	7.14	6.44
-135.04	89.97	-18.79	101.05	6.53	9.61	8.51	7.83
-134.97	104.96	-19.5	100.38	8.45	11.69	10.60	9.95
-135.05	119.94	-19.61	99.69	9.35	12.73	11.64	11.01
-135.05	135.03	-18.47	99.85	8.82	11.82	10.73	10.10
-135.06	150.02	-16.51	100.98	7.33	9.90	8.80	8.12
-135.07	165.03	-15.33	102.58	5.94	8.20	7.09	6.35
-135.0	179.97	-15.73	103.92	6.05	8.31	7.19	6.40
-135.02	-165.0	-17.22	104.23	8.06	10.52	9.40	8.61
-135.02	-149.99	-19.2	103.12	11.05	14.24	13.13	12.39
-135.02	-134.99	-21.74	100.63	13.53	17.32	16.23	15.58
-135.08	-119.95	-24.25	97.57	14.40	18.15	17.08	16.56
-134.99	-105.04	-25.63	95.3	13.42	16.92	15.87	15.44
-135.06	-90.02	-25.54	94.4	11.27	14.65	13.60	13.21
-135.08	-75.0	-23.87	95.25	9.27	13.25	12.20	11.76
-135.07	-59.97	-22.18	96.77	8.49	13.47	12.40	11.90
-135.08	-45.01	-21.72	97.74	9.42	15.62	14.55	14.00
-135.06	-29.98	-22.13	97.88	11.59	19.02	17.94	17.40
-135.06	-14.97	-22.85	97.28	13.46	21.99	20.92	20.41
-135.08	0.07	-23.33	96.47	13.72	22.76	21.69	21.21
-119.95	-0.01	-4.54	113.59	13.93	24.11	22.94	21.83
-119.92	14.96	-4.52	113.22	11.90	21.66	20.49	19.39
-119.94	29.94	-3.84	113.83	8.75	17.35	16.17	15.05
-119.94	45.03	-2.56	115.43	5.88	12.79	11.61	10.45
-119.88	59.99	-1.16	117.23	4.65	9.69	8.49	7.30
-119.94	74.95	-0.54	118.11	5.22	8.81	7.61	6.40
-119.92	89.98	-0.69	117.99	7.00	9.93	8.74	7.52
-119.94	105.0	-1.17	117.1	8.65	11.80	10.61	9.41
-119.91	120.0	-1.4	116.22	9.10	12.34	11.15	9.97
-119.87	134.95	-1.03	115.95	8.18	11.21	10.02	8.85
-119.94	149.98	-0.46	116.66	6.52	9.15	7.96	6.77
-119.87	164.94	0.15	118.51	5.58	7.84	6.64	5.42
-119.96	-179.95	0.77	120.44	6.35	8.78	7.57	6.32
-119.87	-165.03	1.11	121.5	8.77	12.01	10.80	9.53
-119.95	-149.99	-0.38	120.28	11.94	16.05	14.84	13.58
-119.98	-134.96	-3.19	117.45	14.47	19.02	17.82	16.62
-119.91	-119.99	-6.14	114.17	15.38	19.60	18.42	17.30
-119.94	-104.96	-8.33	111.4	14.38	18.00	16.84	15.79
-119.93	-90.0	-8.67	110.42	12.30	15.95	14.79	13.77
-119.92	-74.99	-7.48	111.27	10.43	14.51	13.35	12.30
-119.9	-60.0	-5.96	112.88	9.91	14.92	13.74	12.65

O4-C4-C5-O5 (degrees)	O5-C5-C6-O6 (degrees)	C3-C4-C5-C6 (degrees)	O4-C4-C5-C6 (degrees)	QM rel. E (kcal/mol)	MM1 rel. E (kcal/mol)	MM2 rel. E (kcal/mol)	MM3 rel. E (kcal/mol)
-119.92	-45.03	-4.69	114.14	10.93	17.53	16.35	15.23
-119.96	-30.03	-4.01	114.69	12.74	21.10	19.92	18.78
-119.87	-15.01	-4.01	114.47	14.10	23.77	22.59	21.46
-119.95	-0.03	-4.54	113.58	13.93	24.16	22.99	21.88
-104.97	-0.01	13.14	129.84	12.96	23.53	22.30	20.96
-104.94	14.98	12.63	129.4	11.04	21.03	19.80	18.47
-104.97	29.98	13.01	130.02	8.12	16.75	15.52	14.19
-104.96	45.0	14.63	131.82	5.47	12.21	10.97	9.64
-104.97	59.98	16.6	133.77	4.19	8.98	7.74	6.41
-104.98	75.03	17.4	134.57	4.66	7.74	6.51	5.18
-105.01	90.05	16.87	134.02	6.26	8.72	7.48	6.15
-105.03	104.99	15.95	132.81	7.68	10.27	9.03	7.70
-105.0	119.98	15.28	131.67	7.95	10.93	9.69	8.36
-105.05	135.0	15.05	131.27	6.94	9.83	8.60	7.26
-104.96	149.96	15.82	132.61	5.49	7.86	6.62	5.29
-104.97	164.99	17.55	135.09	4.83	6.83	5.59	4.26
-104.98	-179.98	19.27	137.46	5.84	8.46	7.22	5.91
-104.99	-165.0	18.94	137.85	8.45	11.84	10.59	9.28
-105.03	-150.03	16.96	136.2	11.83	15.89	14.65	13.32
-104.98	-134.97	14.18	133.32	14.59	18.78	17.54	16.20
-104.99	-119.94	11.25	130.06	15.67	19.61	18.38	17.03
-105.03	-105.04	9.16	127.52	14.79	18.25	17.03	15.69
-104.99	-89.94	8.89	126.82	12.79	16.26	15.04	13.71
-104.94	-75.05	10.56	128.07	11.02	14.91	13.68	12.35
-104.95	-60.06	13.46	130.18	10.32	15.52	14.28	12.95
-105.02	-44.97	15.36	131.68	10.76	17.91	16.67	15.34
-104.99	-29.97	15.32	131.85	12.02	21.02	19.79	18.45
-105.0	-14.97	14.18	130.91	13.15	23.28	22.05	20.71
-104.96	-0.0	13.14	129.84	12.96	23.39	22.16	20.83
-90.09	0.08	29.68	145.43	11.43	21.87	20.64	19.44
-90.01	15.07	29.42	145.32	9.71	19.57	18.33	17.13
-90.01	30.01	30.21	146.21	6.91	15.31	14.07	12.89
-89.96	44.93	31.93	147.96	4.23	10.88	9.65	8.49
-90.01	60.01	33.3	149.48	2.88	7.41	6.18	5.05
-89.99	75.01	33.6	149.91	3.30	6.06	4.84	3.71
-90.05	89.97	33.0	149.2	4.84	6.90	5.67	4.54
-90.02	104.97	32.13	148.03	6.16	8.60	7.37	6.21
-90.07	120.04	31.35	146.96	6.35	9.18	7.95	6.78
-90.03	135.0	31.42	147.03	5.37	8.01	6.78	5.61
-90.08	149.99	32.69	148.65	4.03	6.17	4.94	3.80
-90.0	164.98	34.46	151.15	3.56	5.64	4.41	3.31
-90.0	179.96	34.98	152.73	4.81	7.39	6.16	5.08
-90.03	-164.98	34.59	152.85	7.80	10.82	9.59	8.51
-89.98	-149.99	33.49	151.53	11.39	14.88	13.65	12.54
-90.04	-134.98	31.46	149.02	14.26	17.98	16.74	15.60
-89.98	-120.02	29.3	146.36	15.34	18.91	17.67	16.48
-89.98	-105.05	27.78	144.37	14.43	17.70	16.46	15.24
-90.02	-90.01	28.36	144.13	12.36	15.54	14.31	13.09
-90.03	-74.97	31.69	146.12	10.13	14.34	13.11	11.94
-90.07	-59.97	34.19	148.19	8.67	14.62	13.39	12.26
-89.99	-44.99	33.66	148.53	8.75	16.42	15.19	14.06
-90.01	-30.05	32.12	147.69	10.16	19.23	18.00	16.84
-90.03	-14.95	30.77	146.46	11.47	21.51	20.28	19.10

O4-C4-C5-O5 (degrees)	O5-C5-C6-O6 (degrees)	C3-C4-C5-C6 (degrees)	O4-C4-C5-C6 (degrees)	QM rel. E (kcal/mol)	MM1 rel. E (kcal/mol)	MM2 rel. E (kcal/mol)	MM3 rel. E (kcal/mol)
-90.06	-0.02	29.72	145.46	11.43	21.94	20.71	19.51
-75.08	0.01	45.43	160.72	10.12	20.35	19.15	18.24
-75.0	14.98	45.37	160.73	8.45	17.95	16.76	15.85
-75.03	29.97	45.86	161.44	5.62	13.72	12.53	11.63
-75.12	45.01	46.67	162.63	2.99	9.33	8.14	7.26
-75.04	60.03	47.76	163.94	1.74	5.93	4.75	3.88
-75.03	74.99	48.28	164.38	2.20	4.73	3.55	2.69
-75.1	89.98	48.01	163.82	3.61	5.76	4.57	3.71
-75.09	105.0	47.37	162.9	4.81	7.29	6.10	5.23
-75.05	120.0	46.76	162.1	4.96	7.74	6.55	5.66
-75.0	134.97	46.77	162.23	4.04	6.46	5.28	4.39
-75.08	150.0	47.29	163.46	2.93	4.99	3.80	2.93
-75.04	165.0	47.87	165.26	2.88	5.00	3.82	2.97
-75.03	179.99	48.8	166.8	4.56	6.92	5.74	4.92
-75.07	-165.03	49.63	167.29	7.63	10.51	9.33	8.51
-75.04	-150.0	49.58	166.46	11.12	14.50	13.33	12.50
-75.04	-135.01	48.39	164.52	13.75	17.49	16.31	15.45
-75.09	-119.98	46.83	162.23	14.61	18.25	17.07	16.18
-75.04	-104.96	46.81	160.98	13.43	16.95	15.77	14.87
-75.06	-89.98	48.7	161.56	10.69	14.77	13.60	12.71
-75.06	-75.04	50.04	162.98	7.72	12.96	11.80	10.93
-75.07	-59.97	49.39	163.61	6.25	12.72	11.55	10.69
-75.05	-44.99	48.16	163.36	6.87	14.67	13.49	12.62
-75.09	-30.04	47.09	162.49	8.58	17.56	16.38	15.50
-75.07	-15.01	46.16	161.47	10.04	19.99	18.80	17.90
-75.05	-0.02	45.45	160.75	10.13	20.46	19.27	18.35
-59.99	-0.03	59.6	175.38	9.74	19.40	18.28	17.56
-59.96	15.0	59.03	175.07	8.04	16.86	15.73	15.00
-60.0	29.98	58.9	175.41	5.37	12.88	11.75	11.02
-59.98	44.99	59.78	176.58	2.95	8.74	7.62	6.90
-60.0	60.02	61.2	177.96	1.74	5.69	4.58	3.86
-60.0	74.97	62.1	178.59	2.10	4.78	3.68	2.96
-60.0	89.96	62.12	178.34	3.32	5.76	4.66	3.94
-60.0	104.99	61.48	177.54	4.43	6.93	5.83	5.11
-60.02	120.02	60.43	176.56	4.65	7.17	6.06	5.33
-59.98	135.05	59.52	176.2	4.03	6.20	5.08	4.35
-59.95	149.96	59.28	177.06	3.46	5.39	4.27	3.54
-59.99	164.97	60.36	178.82	3.89	5.80	4.69	3.97
-59.96	-180.0	62.55	-179.26	5.70	8.07	6.97	6.26
-60.01	-164.99	64.36	-178.35	8.52	11.68	10.60	9.88
-60.02	-149.99	64.93	-178.86	11.56	15.52	14.44	13.73
-59.99	-135.04	64.7	179.59	13.72	18.25	17.17	16.46
-60.03	-120.01	64.56	177.92	14.03	18.68	17.60	16.89
-59.99	-105.01	64.12	176.78	11.99	16.70	15.61	14.90
-60.0	-89.98	63.04	176.33	8.74	13.63	12.54	11.82
-60.0	-75.02	62.17	176.79	6.17	11.67	10.57	9.85
-59.97	-60.05	61.89	177.53	5.39	11.78	10.67	9.95
-60.02	-44.96	61.65	177.59	6.37	14.15	13.04	12.32
-60.0	-30.03	61.19	177.03	8.22	17.21	16.11	15.38
-59.98	-15.04	60.39	176.16	9.70	19.54	18.43	17.70
-60.01	-0.07	59.59	175.36	9.74	19.43	18.32	17.59
-45.03	0.02	72.02	-170.74	10.68	19.27	18.25	17.50
-45.04	14.98	71.0	-171.4	9.19	16.90	15.87	15.13

O4-C4-C5-O5 (degrees)	O5-C5-C6-O6 (degrees)	C3-C4-C5-C6 (degrees)	O4-C4-C5-C6 (degrees)	QM rel. E (kcal/mol)	MM1 rel. E (kcal/mol)	MM2 rel. E (kcal/mol)	MM3 rel. E (kcal/mol)
-45.04	30.02	71.1	-171.04	6.72	13.27	12.23	11.49
-45.09	44.98	72.45	-169.73	4.29	9.42	8.40	7.64
-45.09	60.07	74.29	-168.1	2.97	6.58	5.58	4.81
-45.07	75.02	75.32	-167.25	3.12	5.68	4.68	3.90
-45.09	90.02	75.25	-167.46	4.25	6.59	5.59	4.81
-45.06	105.03	74.21	-168.34	5.45	7.58	6.57	5.80
-45.04	119.96	72.56	-169.6	6.00	8.13	7.11	6.35
-45.08	134.94	71.15	-170.28	5.92	7.71	6.68	5.93
-45.12	150.01	71.46	-169.39	5.85	7.44	6.41	5.65
-45.13	165.0	73.77	-167.28	6.45	8.24	7.23	6.46
-45.01	179.96	77.13	-164.85	7.99	10.50	9.52	8.72
-45.03	-164.98	80.01	-163.46	10.24	14.06	13.11	12.27
-45.06	-149.97	81.53	-163.57	12.56	17.53	16.58	15.74
-45.08	-134.99	81.03	-165.15	13.93	19.33	18.38	17.56
-45.05	-119.99	78.86	-167.5	13.48	18.49	17.52	16.74
-45.1	-105.01	75.97	-169.69	11.30	15.95	14.95	14.19
-45.06	-89.95	73.93	-170.5	8.60	13.26	12.25	11.50
-45.05	-75.01	73.71	-169.81	6.67	11.79	10.78	10.02
-45.04	-60.01	74.53	-168.65	6.24	12.16	11.16	10.39
-45.05	-44.97	74.83	-168.22	7.30	14.67	13.67	12.90
-45.07	-30.01	74.35	-168.67	9.17	17.74	16.73	15.96
-45.06	-14.97	73.31	-169.68	10.61	19.72	18.70	17.95
-45.07	0.01	72.01	-170.79	10.68	19.30	18.28	17.53
-29.97	0.01	84.41	-156.89	12.80	20.29	19.38	18.45
-29.94	14.99	83.72	-157.48	11.41	17.98	17.06	16.14
-30.03	30.05	84.29	-157.01	8.84	14.57	13.66	12.73
-30.01	44.97	86.05	-155.4	6.26	10.81	9.91	8.95
-30.01	60.0	87.86	-153.67	4.74	7.98	7.10	6.11
-29.99	74.99	88.64	-152.86	4.79	7.07	6.20	5.20
-29.97	89.99	88.25	-153.12	6.06	7.89	7.02	6.02
-30.03	105.04	86.85	-154.26	7.60	9.16	8.28	7.30
-29.99	119.98	85.3	-155.44	8.66	10.06	9.16	8.20
-30.0	135.0	84.76	-155.74	8.95	10.04	9.13	8.18
-29.99	149.98	86.46	-154.33	8.97	10.08	9.18	8.21
-30.0	165.0	89.91	-151.76	9.19	10.69	9.84	8.81
-30.04	-179.99	93.82	-149.19	9.96	12.54	11.72	10.63
-30.01	-165.01	96.28	-147.92	11.32	15.27	14.47	13.35
-30.04	-150.01	96.13	-148.72	12.96	17.70	16.90	15.79
-29.97	-134.97	93.84	-151.01	14.04	18.83	18.00	16.94
-29.97	-120.0	90.43	-153.88	13.75	18.37	17.51	16.50
-29.96	-105.04	87.41	-156.09	12.11	16.45	15.56	14.60
-29.99	-90.03	86.18	-156.65	9.94	14.30	13.40	12.45
-30.01	-75.03	86.82	-155.67	8.28	12.94	12.05	11.09
-30.04	-59.95	87.82	-154.42	7.91	13.39	12.51	11.53
-29.99	-45.0	88.03	-153.92	8.98	15.82	14.94	13.95
-30.0	-29.99	87.24	-154.49	10.91	18.65	17.76	16.79
-29.98	-15.03	85.89	-155.64	12.52	20.32	19.43	18.47
-29.98	0.01	84.39	-156.92	12.79	20.10	19.19	18.25
-15.15	-0.04	98.52	-142.54	14.84	21.63	20.86	19.67
-15.06	14.98	98.29	-142.89	13.33	19.63	18.86	17.67
-15.09	29.97	99.08	-142.21	10.56	15.94	15.17	13.98
-15.09	45.01	100.73	-140.55	7.76	12.05	11.31	10.08
-15.18	60.0	102.21	-138.99	6.20	9.18	8.45	7.21

O4-C4-C5-O5 (degrees)	O5-C5-C6-O6 (degrees)	C3-C4-C5-C6 (degrees)	O4-C4-C5-C6 (degrees)	QM rel. E (kcal/mol)	MM1 rel. E (kcal/mol)	MM2 rel. E (kcal/mol)	MM3 rel. E (kcal/mol)
-15.12	74.99	102.76	-138.3	6.39	8.42	7.70	6.45
-15.1	89.97	102.28	-138.66	7.96	9.32	8.60	7.35
-15.12	105.01	101.3	-139.6	9.85	10.93	10.20	8.96
-15.16	119.99	100.46	-140.48	11.07	11.98	11.24	10.02
-15.15	134.96	100.82	-140.36	11.29	12.12	11.38	10.16
-15.14	150.0	102.94	-138.81	10.82	11.63	10.91	9.66
-15.12	165.04	106.27	-136.35	10.34	11.81	11.12	9.83
-15.12	-180.0	109.12	-134.24	10.39	12.80	12.14	10.82
-15.15	-165.03	110.09	-133.65	11.41	14.82	14.17	12.84
-15.07	-150.0	109.07	-134.71	13.12	17.29	16.63	15.31
-15.22	-134.95	106.36	-137.22	14.45	19.02	18.32	17.04
-15.15	-120.05	103.52	-139.73	14.51	19.20	18.48	17.23
-15.14	-104.96	101.32	-141.57	13.23	17.70	16.96	15.74
-15.15	-89.98	100.62	-141.94	11.26	15.41	14.66	13.45
-15.05	-75.01	101.38	-140.85	9.71	14.04	13.30	12.07
-15.12	-60.01	102.02	-139.8	9.41	14.62	13.89	12.65
-15.13	-44.91	101.79	-139.6	10.60	17.01	16.28	15.04
-15.09	-30.0	100.87	-140.24	12.69	19.71	18.96	17.74
-15.09	-15.04	99.66	-141.37	14.49	21.69	20.93	19.72
-15.12	-0.01	98.54	-142.52	14.85	21.64	20.87	19.68
0.05	-0.02	115.46	-126.7	15.55	22.67	22.09	20.73
0.11	14.95	115.26	-126.89	13.91	20.57	19.98	18.63
0.12	30.03	115.96	-126.14	10.94	16.71	16.13	14.77
0.12	45.01	117.41	-124.58	8.09	12.56	11.99	10.64
0.08	59.97	118.77	-123.11	6.62	9.61	9.06	7.71
0.05	75.03	119.28	-122.6	7.04	8.77	8.22	6.88
0.12	89.98	119.16	-122.86	8.78	9.91	9.36	8.02
0.13	104.99	118.62	-123.6	10.74	11.63	11.07	9.72
0.13	119.99	118.23	-124.17	11.78	12.70	12.14	10.79
0.09	134.99	118.51	-124.09	11.66	12.58	12.02	10.66
0.04	149.99	119.97	-122.96	10.71	11.67	11.13	9.78
0.12	165.01	122.38	-120.92	9.72	11.12	10.60	9.26
0.13	179.98	124.37	-119.18	9.58	11.77	11.27	9.93
0.13	-164.97	125.07	-118.68	10.69	14.01	13.52	12.18
0.1	-149.97	124.28	-119.64	12.56	16.80	16.30	14.95
0.04	-135.0	122.32	-121.67	14.08	19.24	18.72	17.36
0.01	-119.99	119.93	-123.92	14.39	19.66	19.11	17.74
0.11	-105.01	118.12	-125.44	13.29	18.06	17.49	16.13
0.02	-89.99	117.31	-125.89	11.51	15.70	15.13	13.76
0.12	-75.04	117.81	-124.95	10.08	14.41	13.84	12.48
0.1	-60.02	118.19	-124.14	9.96	15.36	14.80	13.45
0.04	-44.98	117.79	-124.22	11.36	17.69	17.13	15.78
0.12	-29.97	117.16	-124.81	13.56	20.52	19.95	18.60
0.0	-14.98	116.18	-125.89	15.34	22.65	22.07	20.72
0.09	0.0	115.53	-126.65	15.56	22.67	22.09	20.73

Table C.4. Dihedral angles and relative energies for **4.2** with the ^{1}E ring conformation.

O4-C4-C5-O5 (degrees)	O5-C5-C6-O6 (degrees)	C3-C4-C5-C6 (degrees)	O4-C4-C5-C6 (degrees)	QM rel. E (kcal/mol)	MM1 rel. E (kcal/mol)	MM2 rel. E (kcal/mol)	MM3 rel. E (kcal/mol)
-0.01	0.03	112.45	-126.67	16.24	25.80	25.77	23.86
0.01	14.99	112.29	-126.88	14.54	23.30	23.27	21.36
0.05	30.02	113.07	-126.04	11.49	19.36	19.33	17.43
-0.01	45.02	114.43	-124.52	8.56	15.10	15.10	13.20
0.11	59.92	115.87	-122.95	7.04	11.97	11.98	10.09
0.05	75.0	116.23	-122.53	7.34	10.90	10.92	9.02
0.03	90.02	115.85	-123.03	8.97	11.62	11.63	9.73
0.02	105.01	115.14	-123.97	10.71	13.00	13.00	11.10
0.03	119.99	114.42	-124.87	11.47	13.69	13.69	11.78
0.04	135.05	114.27	-125.14	10.99	13.00	12.99	11.08
0.02	150.0	115.18	-124.34	9.78	11.81	11.81	9.90
-0.01	164.98	117.14	-122.54	8.75	11.30	11.32	9.42
0.05	179.99	119.44	-120.47	8.83	12.37	12.41	10.52
0.04	-165.01	120.73	-119.48	10.28	15.17	15.22	13.34
0.02	-149.96	120.46	-120.09	12.53	18.67	18.72	16.83
0.05	-135.01	118.92	-121.81	14.33	21.62	21.65	19.74
0.13	-120.0	116.83	-123.88	14.81	22.32	22.33	20.42
0.04	-105.0	115.01	-125.49	13.85	21.10	21.09	19.18
0.1	-90.03	114.48	-125.66	12.05	18.96	18.95	17.04
0.03	-75.0	114.81	-124.86	10.62	17.82	17.81	15.91
0.03	-60.03	115.14	-124.03	10.51	18.55	18.55	16.65
0.06	-44.94	114.78	-124.04	11.95	21.00	20.99	19.09
0.03	-29.98	113.95	-124.8	14.18	23.76	23.75	21.85
0.12	-15.02	113.26	-125.66	16.00	25.80	25.78	23.88
-0.01	-0.03	112.45	-126.66	16.23	25.75	25.72	23.82
15.04	-0.06	129.58	-110.47	15.57	25.17	25.32	23.56
15.07	14.94	129.51	-110.48	13.73	22.63	22.78	21.02
15.02	29.99	130.13	-109.7	10.66	18.59	18.75	17.01
15.06	44.96	131.48	-108.21	7.82	14.17	14.35	12.64
15.05	60.03	132.78	-106.92	6.40	10.89	11.08	9.39
15.02	74.98	133.3	-106.55	6.85	9.72	9.91	8.24
15.12	90.01	133.15	-106.92	8.52	10.53	10.72	9.03
15.04	104.97	132.43	-107.82	10.19	11.91	12.09	10.38
15.03	120.01	131.78	-108.56	10.82	12.63	12.81	11.08
15.11	135.01	131.81	-108.57	10.17	12.00	12.17	10.45
15.07	150.0	132.67	-107.71	8.85	10.84	11.02	9.32
15.04	165.0	134.52	-105.99	7.78	10.29	10.49	8.82
15.06	180.0	136.64	-104.12	7.87	11.34	11.57	9.94
15.05	-165.04	137.8	-103.3	9.31	13.96	14.19	12.59
15.08	-150.0	137.44	-103.94	11.46	17.59	17.82	16.20
15.05	-135.04	135.75	-105.71	13.24	20.42	20.63	18.96
15.04	-119.99	133.61	-107.73	13.76	21.34	21.53	19.82
15.09	-105.0	131.96	-109.08	12.88	19.99	20.16	18.42
15.0	-90.01	131.13	-109.49	11.28	18.01	18.18	16.43
15.12	-75.02	131.41	-108.77	10.08	17.19	17.36	15.64
15.08	-59.95	131.53	-108.28	10.16	18.03	18.21	16.49
15.09	-44.95	131.33	-108.4	11.69	20.38	20.56	18.84
15.05	-30.03	130.77	-109.06	13.85	23.05	23.22	21.49
15.1	-15.03	130.22	-109.79	15.51	25.12	25.28	23.53
15.11	-0.07	129.66	-110.41	15.56	25.11	25.27	23.51

O4-C4-C5-O5 (degrees)	O5-C5-C6-O6 (degrees)	C3-C4-C5-C6 (degrees)	O4-C4-C5-C6 (degrees)	QM rel. E (kcal/mol)	MM1 rel. E (kcal/mol)	MM2 rel. E (kcal/mol)	MM3 rel. E (kcal/mol)
30.06	0.01	146.17	-94.71	13.39	22.39	22.70	21.35
30.04	15.05	146.05	-94.68	11.43	19.91	20.23	18.87
29.96	29.97	146.57	-94.01	8.53	15.92	16.24	14.91
29.98	45.01	147.86	-92.69	5.86	11.45	11.78	10.50
29.97	59.95	149.21	-91.49	4.58	8.12	8.46	7.21
29.97	74.97	149.9	-91.0	5.02	6.72	7.07	5.83
29.95	90.02	149.68	-91.41	6.61	7.47	7.81	6.57
29.95	105.0	149.06	-92.12	8.09	8.87	9.20	7.93
29.92	120.01	148.39	-92.79	8.61	9.69	10.02	8.73
29.98	135.02	148.27	-92.82	7.91	9.22	9.55	8.26
29.97	150.0	149.03	-92.02	6.56	8.21	8.54	7.27
30.01	164.98	150.86	-90.36	5.53	7.52	7.88	6.66
29.97	179.98	152.89	-88.66	5.62	8.52	8.89	7.72
30.03	-164.99	154.07	-87.82	7.01	10.91	11.28	10.14
29.96	-149.98	153.57	-88.5	9.10	14.38	14.75	13.59
29.95	-135.01	151.92	-90.15	10.89	17.25	17.61	16.39
29.91	-119.98	149.69	-92.15	11.59	18.13	18.47	17.19
29.99	-105.02	147.72	-93.72	10.97	17.18	17.50	16.18
30.02	-89.99	146.49	-94.46	9.66	15.75	16.06	14.72
29.99	-74.97	146.31	-94.26	8.69	14.92	15.24	13.90
30.05	-60.02	146.81	-93.67	8.86	15.65	15.97	14.65
29.91	-44.96	147.01	-93.6	10.23	17.64	17.97	16.65
29.98	-30.03	146.95	-93.83	12.15	20.45	20.77	19.45
30.03	-15.01	146.61	-94.31	13.54	22.51	22.83	21.49
30.02	0.01	146.13	-94.77	13.41	22.31	22.62	21.27
44.98	0.03	161.06	-79.87	10.87	18.73	19.16	18.26
44.98	14.97	160.87	-79.95	9.00	16.39	16.82	15.92
44.97	29.99	161.4	-79.36	6.22	12.35	12.78	11.90
45.01	45.01	162.73	-78.12	3.65	7.99	8.43	7.58
45.05	59.99	164.26	-76.73	2.36	4.55	5.00	4.19
44.99	75.0	164.99	-76.15	2.72	3.19	3.65	2.85
45.03	90.0	164.96	-76.31	4.11	3.96	4.42	3.62
44.95	104.99	164.3	-77.0	5.49	5.23	5.69	4.86
45.0	120.02	163.58	-77.64	5.95	6.15	6.60	5.76
45.02	135.02	163.19	-77.93	5.31	5.88	6.33	5.48
44.98	150.01	163.73	-77.4	4.08	4.93	5.38	4.55
44.98	164.99	165.44	-75.89	3.15	4.26	4.72	3.93
45.04	-179.96	167.55	-74.09	3.22	4.95	5.42	4.67
45.03	-165.03	168.73	-73.17	4.52	7.35	7.82	7.09
44.98	-149.98	168.34	-73.66	6.59	10.81	11.28	10.54
45.0	-135.0	166.47	-75.4	8.52	13.80	14.27	13.48
45.06	-120.04	163.71	-77.77	9.53	14.83	15.28	14.43
45.0	-105.02	160.86	-80.12	9.32	14.15	14.59	13.68
45.01	-90.05	159.29	-81.28	8.39	12.92	13.34	12.41
44.97	-75.01	159.21	-81.17	7.49	12.09	12.51	11.58
45.04	-60.05	160.21	-80.21	7.48	12.60	13.03	12.12
45.04	-45.0	161.19	-79.42	8.52	14.45	14.89	14.00
45.04	-29.99	161.69	-79.17	10.12	17.05	17.48	16.61
45.01	-15.08	161.53	-79.42	11.21	18.79	19.23	18.34
45.08	-0.01	161.17	-79.77	10.87	18.61	19.04	18.15
59.95	-0.0	174.15	-65.91	9.29	15.88	16.39	15.79
60.03	14.97	173.81	-66.2	7.51	13.40	13.92	13.31
59.97	29.99	174.22	-65.82	4.80	9.46	9.97	9.37

O4-C4-C5-O5 (degrees)	O5-C5-C6-O6 (degrees)	C3-C4-C5-C6 (degrees)	O4-C4-C5-C6 (degrees)	QM rel. E (kcal/mol)	MM1 rel. E (kcal/mol)	MM2 rel. E (kcal/mol)	MM3 rel. E (kcal/mol)
59.96	44.99	175.63	-64.52	2.23	5.30	5.83	5.24
59.97	60.05	177.3	-62.96	0.89	2.01	2.54	1.97
59.93	74.97	178.26	-62.11	1.13	0.65	1.19	0.62
59.98	89.96	178.42	-62.05	2.38	1.28	1.81	1.25
59.99	105.05	177.8	-62.68	3.70	2.72	3.25	2.68
59.96	120.04	176.73	-63.63	4.24	3.60	4.13	3.55
59.96	134.99	176.1	-64.2	3.73	3.54	4.07	3.48
59.98	149.95	176.6	-63.75	2.62	2.66	3.19	2.61
59.98	164.96	178.32	-62.22	1.76	2.14	2.67	2.11
59.97	-179.99	-179.65	-60.42	1.82	2.81	3.35	2.80
59.95	-165.0	-178.48	-59.4	3.11	5.43	5.97	5.43
59.95	-149.94	-179.02	-59.91	5.33	8.96	9.50	8.96
60.01	-134.94	178.36	-62.14	7.73	11.82	12.35	11.79
59.98	-119.99	174.59	-65.31	9.24	12.76	13.29	12.69
60.02	-105.06	171.47	-67.95	9.33	12.31	12.81	12.18
59.98	-90.0	170.04	-69.16	8.36	11.17	11.67	11.02
59.92	-75.01	170.42	-68.72	7.26	10.37	10.87	10.23
59.96	-60.0	171.96	-67.29	6.93	10.68	11.19	10.57
59.98	-45.1	173.58	-65.94	7.57	12.12	12.64	12.04
59.93	-29.96	174.62	-65.25	8.77	14.38	14.90	14.31
59.99	-15.05	174.81	-65.24	9.63	15.98	16.50	15.90
59.96	-0.03	174.18	-65.88	9.28	15.72	16.24	15.64
75.05	0.03	-173.8	-52.44	9.31	14.43	15.00	14.45
75.02	15.05	-174.45	-53.09	7.54	12.23	12.80	12.25
75.08	29.96	-173.87	-52.6	4.81	8.50	9.07	8.53
75.09	44.95	-172.19	-51.06	2.18	4.27	4.85	4.29
75.08	59.95	-170.27	-49.27	0.74	1.16	1.74	1.17
75.1	75.0	-169.08	-48.23	0.90	0.00	0.58	0.00
75.11	90.03	-169.04	-48.26	2.12	0.59	1.18	0.60
75.1	104.97	-169.92	-49.06	3.50	2.09	2.67	2.10
75.04	120.04	-171.27	-50.27	4.17	3.13	3.71	3.15
75.04	134.96	-172.0	-50.93	3.79	3.15	3.73	3.17
75.0	150.01	-171.43	-50.46	2.76	2.34	2.92	2.36
75.03	164.99	-169.59	-48.79	1.92	1.92	2.50	1.92
75.05	179.99	-167.52	-46.87	2.05	3.05	3.63	3.04
75.05	-165.05	-166.64	-45.97	3.57	5.70	6.28	5.68
75.04	-149.98	-168.07	-47.0	6.42	9.34	9.93	9.34
75.05	-135.01	-171.7	-49.85	9.48	11.85	12.43	11.86
75.04	-120.0	-175.88	-53.39	11.29	13.10	13.67	13.12
75.04	-105.02	-178.8	-56.06	11.18	12.66	13.22	12.68
75.06	-90.03	-179.6	-56.84	9.81	11.41	11.97	11.43
75.06	-75.05	-178.52	-55.87	8.35	10.32	10.88	10.34
75.06	-60.03	-176.36	-53.97	7.61	10.20	10.76	10.22
75.07	-45.02	-174.13	-52.15	7.90	11.27	11.84	11.29
75.01	-30.03	-172.77	-51.26	8.86	13.34	13.91	13.36
75.06	-15.07	-172.76	-51.44	9.64	14.87	15.44	14.89
75.08	0.02	-173.79	-52.43	9.31	14.40	14.97	14.42
90.03	-0.05	-161.49	-38.9	10.64	15.25	15.84	15.13
89.97	14.94	-162.14	-39.62	8.87	12.96	13.55	12.86
89.95	30.0	-161.37	-39.07	5.97	9.19	9.79	9.08
90.01	45.02	-159.33	-37.25	3.21	5.01	5.61	4.87
90.02	60.06	-157.13	-35.27	1.71	1.99	2.59	1.82
90.02	74.94	-156.06	-34.32	1.87	0.98	1.57	0.78

O4-C4-C5-O5 (degrees)	O5-C5-C6-O6 (degrees)	C3-C4-C5-C6 (degrees)	O4-C4-C5-C6 (degrees)	QM rel. E (kcal/mol)	MM1 rel. E (kcal/mol)	MM2 rel. E (kcal/mol)	MM3 rel. E (kcal/mol)
89.98	90.01	-156.45	-34.6	3.22	1.97	2.57	1.78
90.02	104.94	-157.7	-35.59	4.79	3.54	4.14	3.37
89.96	120.0	-159.13	-36.85	5.56	4.67	5.26	4.52
89.94	135.0	-159.68	-37.43	5.19	4.53	5.13	4.40
89.98	150.01	-158.83	-36.73	4.13	3.82	4.42	3.67
89.99	165.0	-156.89	-34.97	3.36	3.53	4.13	3.35
90.03	179.98	-155.02	-33.12	3.74	4.94	5.54	4.73
90.02	-165.0	-154.91	-32.55	6.00	8.01	8.60	7.78
90.02	-149.99	-157.26	-33.92	9.72	11.39	11.99	11.19
90.01	-135.0	-161.27	-37.04	13.18	14.17	14.77	14.02
89.98	-120.01	-165.17	-40.6	14.75	15.40	16.00	15.32
89.94	-104.95	-167.71	-43.18	14.13	14.54	15.14	14.49
89.99	-90.03	-167.89	-43.58	12.21	12.89	13.49	12.85
90.0	-74.96	-166.09	-42.09	10.24	11.35	11.95	11.29
89.95	-60.02	-163.28	-39.76	9.07	10.84	11.44	10.74
90.05	-45.0	-160.6	-37.66	9.02	12.02	12.62	11.88
90.0	-30.04	-159.51	-36.98	9.89	14.03	14.63	13.89
89.94	-14.95	-160.24	-37.75	10.81	15.41	16.01	15.28
90.03	-0.07	-161.49	-38.9	10.64	15.19	15.79	15.08
104.94	0.02	-147.29	-24.29	12.47	17.46	18.04	17.06
104.97	15.03	-147.65	-24.85	10.57	15.02	15.60	14.64
104.96	29.98	-146.58	-24.14	7.52	10.96	11.54	10.56
104.94	44.97	-144.29	-22.24	4.60	6.79	7.36	6.36
104.96	59.93	-142.04	-20.23	3.04	3.90	4.47	3.44
104.92	74.98	-141.41	-19.5	3.36	3.10	3.66	2.62
104.97	90.02	-142.24	-19.96	4.97	4.21	4.78	3.74
104.96	105.02	-143.77	-21.12	6.68	6.18	6.76	5.73
104.94	120.01	-145.01	-22.26	7.44	7.32	7.90	6.89
104.9	135.05	-145.28	-22.68	6.94	6.97	7.55	6.55
104.94	150.05	-144.18	-21.83	5.85	6.16	6.74	5.73
104.94	164.98	-142.22	-20.03	5.25	6.20	6.77	5.73
105.01	179.97	-140.82	-18.25	6.30	7.96	8.53	7.46
104.95	-165.02	-141.39	-17.78	9.51	11.32	11.89	10.81
105.01	-150.02	-143.96	-19.19	13.83	15.12	15.70	14.64
104.95	-134.99	-147.7	-22.36	17.17	17.97	18.56	17.54
104.95	-119.95	-151.19	-25.81	18.30	18.70	19.30	18.33
105.0	-105.03	-153.2	-28.1	17.15	17.19	17.79	16.87
105.0	-90.04	-152.97	-28.31	14.66	14.87	15.47	14.56
104.94	-75.02	-150.65	-26.54	12.08	12.67	13.26	12.32
104.93	-59.98	-147.35	-23.88	10.41	12.00	12.58	11.60
104.97	-45.04	-145.03	-22.09	10.21	13.31	13.89	12.88
104.98	-29.97	-144.77	-21.96	11.30	15.71	16.29	15.28
104.98	-15.02	-145.94	-22.99	12.53	17.36	17.94	16.94
104.97	0.04	-147.26	-24.27	12.47	17.43	18.01	17.03
120.03	-0.05	-130.48	-8.15	13.55	19.60	20.12	18.99
120.05	14.95	-130.45	-8.5	11.62	17.01	17.53	16.40
120.07	29.94	-129.03	-7.63	8.39	12.81	13.33	12.20
120.03	45.05	-126.57	-5.67	5.34	8.67	9.17	8.04
120.06	60.04	-124.62	-3.83	3.86	5.87	6.35	5.24
120.02	74.99	-124.59	-3.39	4.37	5.21	5.69	4.58
120.02	90.01	-125.95	-4.14	6.19	6.57	7.06	5.94
120.05	104.98	-127.43	-5.26	7.89	8.67	9.18	8.04
120.01	120.05	-128.42	-6.26	8.55	9.63	10.14	9.01

O4-C4-C5-O5 (degrees)	O5-C5-C6-O6 (degrees)	C3-C4-C5-C6 (degrees)	O4-C4-C5-C6 (degrees)	QM rel. E (kcal/mol)	MM1 rel. E (kcal/mol)	MM2 rel. E (kcal/mol)	MM3 rel. E (kcal/mol)
120.01	135.0	-128.27	-6.44	7.95	9.11	9.61	8.48
120.1	149.95	-126.77	-5.32	6.89	8.34	8.84	7.71
120.02	165.0	-125.02	-3.5	6.67	8.77	9.26	8.14
120.05	-179.97	-124.0	-1.64	8.63	11.19	11.67	10.55
120.02	-164.97	-124.78	-1.14	12.57	14.79	15.28	14.15
120.05	-149.99	-127.11	-2.61	16.87	18.74	19.25	18.10
120.06	-135.0	-130.25	-5.5	19.86	21.41	21.93	20.78
120.08	-120.02	-133.21	-8.66	20.50	21.52	22.06	20.90
120.08	-105.02	-134.93	-10.83	18.77	19.22	19.77	18.62
120.04	-90.03	-134.45	-10.93	15.68	16.00	16.54	15.40
120.06	-74.98	-131.71	-8.85	12.52	13.37	13.90	12.76
120.01	-60.0	-128.79	-6.46	10.69	12.92	13.43	12.30
120.09	-44.99	-127.58	-5.42	10.71	14.70	15.20	14.07
120.04	-30.01	-128.3	-5.97	12.16	17.30	17.81	16.67
120.04	-14.96	-129.51	-7.07	13.58	19.52	20.03	18.90
120.07	-0.02	-130.43	-8.11	13.56	19.66	20.17	19.04
135.08	-0.01	-111.89	8.88	12.91	20.00	20.39	19.44
135.08	14.95	-111.51	8.72	10.89	17.21	17.60	16.65
135.09	30.01	-110.0	9.65	7.63	13.19	13.57	12.65
135.06	44.99	-108.06	11.31	4.68	8.94	9.30	8.42
135.08	59.95	-106.73	12.79	3.41	6.07	6.43	5.58
135.0	74.99	-107.0	13.05	4.13	5.51	5.86	5.01
135.07	90.04	-108.26	12.38	5.97	7.19	7.56	6.69
135.06	105.01	-109.55	11.35	7.59	9.21	9.58	8.69
135.03	120.04	-110.11	10.56	8.12	10.01	10.39	9.48
135.08	135.01	-109.55	10.65	7.49	9.47	9.84	8.93
135.07	149.98	-108.15	11.81	6.63	9.06	9.42	8.54
135.04	165.03	-106.61	13.77	7.02	9.84	10.19	9.36
135.08	180.0	-105.56	15.84	9.56	12.42	12.76	11.97
135.04	-165.0	-106.01	16.34	13.49	16.23	16.58	15.79
135.1	-149.96	-107.85	15.01	17.40	20.05	20.41	19.59
135.08	-135.01	-110.54	12.37	19.86	22.17	22.56	21.66
135.07	-120.0	-113.11	9.53	20.05	21.62	22.02	21.06
135.07	-104.98	-114.56	7.64	17.89	18.61	19.02	18.03
135.05	-90.01	-114.14	7.62	14.46	14.79	15.20	14.22
135.05	-74.95	-112.29	9.24	11.13	12.02	12.41	11.46
135.06	-60.02	-110.79	10.7	9.54	11.84	12.22	11.30
135.1	-45.0	-110.31	11.08	10.02	14.00	14.38	13.47
135.04	-30.02	-110.68	10.53	11.69	17.31	17.69	16.77
135.1	-15.01	-111.38	9.7	13.00	19.81	20.20	19.26
135.07	0.01	-111.89	8.87	12.92	20.07	20.46	19.51
149.96	-0.03	-93.32	25.75	10.59	17.65	17.88	17.40
149.97	15.03	-93.48	25.34	8.58	14.83	15.06	14.58
149.95	30.0	-92.92	25.74	5.53	10.69	10.92	10.44
149.97	45.08	-91.67	27.03	2.90	6.57	6.78	6.35
149.94	59.98	-90.63	28.3	1.91	3.97	4.18	3.78
149.95	75.0	-90.37	28.86	2.66	3.50	3.70	3.32
149.98	90.04	-90.97	28.51	4.34	5.20	5.41	5.02
149.98	104.95	-91.74	27.74	5.79	7.23	7.44	7.03
150.01	119.96	-92.15	27.1	6.22	8.01	8.23	7.79
149.95	134.97	-92.09	26.97	5.71	7.65	7.86	7.43
149.93	149.97	-91.21	27.98	5.23	7.53	7.73	7.33
149.98	165.01	-89.57	30.21	6.08	8.41	8.60	8.26

O4-C4-C5-O5 (degrees)	O5-C5-C6-O6 (degrees)	C3-C4-C5-C6 (degrees)	O4-C4-C5-C6 (degrees)	QM rel. E (kcal/mol)	MM1 rel. E (kcal/mol)	MM2 rel. E (kcal/mol)	MM3 rel. E (kcal/mol)
149.97	-180.0	-87.9	32.5	8.61	10.86	11.03	10.75
149.98	-164.98	-87.34	33.39	12.03	14.46	14.63	14.37
149.98	-149.98	-88.57	32.31	15.32	17.70	17.87	17.59
149.95	-134.98	-91.08	29.92	17.35	19.22	19.42	19.06
149.98	-119.99	-93.89	27.24	17.20	18.01	18.24	17.80
149.94	-104.98	-96.12	25.15	14.91	14.63	14.89	14.38
149.97	-89.97	-96.69	24.75	11.54	10.95	11.21	10.69
149.96	-75.03	-96.29	25.46	8.76	8.85	9.10	8.60
149.94	-60.04	-95.53	26.19	7.67	8.90	9.15	8.67
149.98	-45.0	-94.18	26.74	8.27	11.06	11.29	10.84
149.97	-30.0	-92.98	26.93	9.70	14.80	15.02	14.58
149.98	-15.03	-92.8	26.51	10.84	17.68	17.90	17.45
149.91	0.04	-93.38	25.67	10.60	17.65	17.88	17.40
164.98	0.01	-77.5	41.18	7.89	13.54	13.61	13.57
164.97	15.0	-78.56	40.28	6.19	11.36	11.43	11.37
164.99	29.98	-78.54	40.39	3.71	7.77	7.85	7.79
164.98	44.99	-77.63	41.42	1.46	4.04	4.10	4.07
164.97	59.99	-76.36	42.78	0.50	1.52	1.57	1.56
165.01	74.98	-75.6	43.57	1.00	1.07	1.11	1.11
164.97	90.06	-75.72	43.46	2.38	2.40	2.44	2.44
164.99	104.98	-76.31	42.87	3.59	4.28	4.33	4.32
164.94	120.0	-77.07	42.09	4.09	5.25	5.31	5.29
164.96	134.99	-77.31	41.91	3.92	5.52	5.58	5.55
164.96	150.02	-76.47	43.06	3.92	5.45	5.51	5.50
164.97	164.99	-74.51	45.41	4.82	6.06	6.08	6.12
164.96	179.98	-72.28	47.78	6.77	7.77	7.78	7.85
164.94	-165.01	-71.27	48.8	9.41	10.39	10.38	10.47
165.0	-149.99	-72.41	48.01	12.08	12.79	12.79	12.87
164.95	-135.0	-75.19	45.78	13.78	13.84	13.87	13.91
164.97	-120.0	-77.9	43.38	13.57	13.06	13.12	13.11
165.0	-105.02	-79.87	41.72	11.49	10.99	11.07	11.03
164.99	-90.01	-81.2	40.83	8.66	7.84	7.94	7.88
164.98	-75.01	-81.26	41.01	6.48	4.68	4.78	4.72
164.97	-59.94	-80.64	41.42	5.88	3.92	4.00	3.96
164.96	-45.05	-80.31	41.58	7.12	6.47	6.56	6.51
165.02	-29.96	-80.31	41.6	9.38	10.17	10.26	10.22
164.97	-14.98	-76.38	42.13	8.04	13.44	13.49	13.47
164.97	0.05	-77.54	41.15	7.89	13.61	13.67	13.63
180.0	0.03	-64.65	54.89	6.48	11.43	11.35	11.48
180.0	14.95	-65.89	53.85	5.39	9.88	9.82	9.94
-179.98	29.96	-66.0	53.8	3.27	6.79	6.73	6.85
180.0	45.01	-64.98	54.77	1.16	3.34	3.27	3.39
180.0	59.99	-63.44	56.21	0.00	0.85	0.75	0.88
-179.97	75.0	-62.57	57.11	0.18	0.10	0.00	0.13
179.99	90.07	-62.57	57.18	1.25	1.29	1.19	1.31
179.99	105.0	-63.15	56.73	2.48	3.16	3.07	3.19
179.99	120.06	-63.98	55.99	3.26	4.53	4.44	4.57
-179.99	134.97	-64.25	55.87	3.52	5.03	4.94	5.07
179.99	149.97	-63.38	56.99	3.70	4.80	4.70	4.83
180.0	164.99	-61.37	59.17	4.38	4.82	4.70	4.82
179.99	-179.98	-59.41	61.24	5.65	5.56	5.42	5.52
-179.98	-164.98	-58.94	62.18	7.56	7.16	7.01	7.11
-179.96	-149.99	-59.94	61.7	9.64	9.07	8.93	9.03

O4-C4-C5-O5 (degrees)	O5-C5-C6-O6 (degrees)	C3-C4-C5-C6 (degrees)	O4-C4-C5-C6 (degrees)	QM rel. E (kcal/mol)	MM1 rel. E (kcal/mol)	MM2 rel. E (kcal/mol)	MM3 rel. E (kcal/mol)
-179.94	-134.98	-61.51	60.38	10.89	10.80	10.67	10.79
-179.99	-119.98	-65.29	57.61	10.82	10.68	10.60	10.73
180.0	-105.01	-68.6	54.87	9.32	8.38	8.34	8.46
-179.96	-90.03	-70.15	53.4	7.26	4.73	4.70	4.82
179.98	-75.0	-69.99	53.22	5.68	2.60	2.57	2.69
179.98	-59.93	-68.99	53.99	5.50	3.11	3.06	3.19
-179.99	-45.03	-67.54	55.11	6.65	5.34	5.28	5.41
180.0	-30.01	-63.14	56.03	5.14	8.33	8.24	8.36
-180.0	-14.99	-63.35	55.89	6.24	10.64	10.55	10.68
179.99	0.01	-64.64	54.89	6.48	11.34	11.26	11.39
-164.97	-0.02	-52.67	67.91	7.16	12.11	11.89	11.89
-165.01	15.01	-54.07	66.63	6.30	10.80	10.60	10.63
-165.06	30.01	-54.13	66.4	4.25	8.02	7.82	7.85
-165.03	44.96	-52.76	67.52	2.01	4.94	4.73	4.73
-165.02	60.01	-50.97	69.18	0.55	2.39	2.17	2.13
-164.99	74.97	-49.91	70.32	0.53	1.60	1.37	1.31
-165.01	89.98	-49.88	70.55	1.50	2.49	2.25	2.18
-165.02	105.0	-50.54	70.13	2.92	4.35	4.12	4.06
-165.02	120.04	-51.56	69.34	4.09	5.82	5.60	5.56
-164.95	134.92	-51.97	69.06	4.70	6.27	6.05	6.02
-164.99	150.03	-51.15	69.95	4.87	5.91	5.68	5.63
-165.05	165.01	-49.43	71.85	5.10	5.55	5.30	5.20
-164.98	179.98	-47.99	73.86	5.75	5.64	5.38	5.23
-165.04	-165.05	-47.77	74.85	7.12	6.74	6.46	6.29
-164.98	-150.05	-47.73	74.99	8.33	7.94	7.66	7.48
-165.02	-135.0	-51.21	72.89	9.73	9.80	9.55	9.44
-165.01	-119.95	-55.38	69.57	10.28	9.04	8.84	8.81
-165.02	-105.03	-58.48	66.53	9.55	6.84	6.68	6.72
-165.05	-89.99	-59.53	64.95	8.06	4.89	4.73	4.80
-165.04	-74.97	-58.8	65.28	6.82	4.23	4.07	4.13
-165.05	-60.0	-56.77	66.89	6.43	4.60	4.42	4.45
-165.01	-45.03	-51.69	68.26	3.89	6.42	6.20	6.19
-165.05	-29.98	-50.82	69.07	4.93	8.58	8.35	8.32
-165.03	-15.03	-51.18	69.01	6.43	11.03	10.80	10.77
-165.03	0.08	-52.73	67.84	7.14	12.02	11.81	11.80
-150.02	-0.01	-40.57	80.92	9.30	14.87	14.53	14.14
-150.02	15.07	-41.83	79.56	8.50	13.90	13.58	13.23
-150.01	30.01	-41.48	79.53	6.14	11.30	10.97	10.62
-149.93	44.98	-39.53	81.13	3.49	7.88	7.54	7.13
-149.99	60.01	-37.31	83.17	1.77	5.17	4.80	4.31
-149.97	74.96	-36.17	84.44	1.65	4.11	3.73	3.19
-149.98	90.01	-36.5	84.52	2.90	5.13	4.75	4.21
-149.99	105.01	-37.66	83.82	4.77	7.12	6.75	6.24
-149.98	119.99	-38.99	82.79	6.30	8.74	8.39	7.92
-149.99	135.0	-39.54	82.27	6.96	9.30	8.95	8.50
-150.01	149.95	-38.72	83.11	6.72	8.55	8.19	7.71
-149.95	164.96	-36.98	85.2	6.37	7.64	7.26	6.70
-149.98	-179.95	-35.61	87.34	6.57	7.31	6.92	6.27
-149.97	-165.02	-35.75	88.33	7.76	8.66	8.26	7.58
-149.93	-150.01	-37.84	87.59	9.93	11.25	10.86	10.22
-149.95	-135.0	-40.79	85.47	12.08	13.06	12.70	12.15
-150.01	-120.02	-43.27	82.48	12.70	13.06	12.73	12.30
-149.99	-105.05	-44.6	79.73	11.37	11.64	11.33	11.00

O4-C4-C5-O5 (degrees)	O5-C5-C6-O6 (degrees)	C3-C4-C5-C6 (degrees)	O4-C4-C5-C6 (degrees)	QM rel. E (kcal/mol)	MM1 rel. E (kcal/mol)	MM2 rel. E (kcal/mol)	MM3 rel. E (kcal/mol)
-149.97	-90.02	-44.41	78.3	8.78	9.88	9.58	9.29
-149.97	-74.98	-42.69	78.7	6.28	8.39	8.08	7.76
-150.02	-59.97	-40.16	80.41	4.84	7.85	7.51	7.13
-149.95	-45.07	-38.06	82.21	4.86	8.75	8.39	7.94
-149.99	-30.04	-37.51	82.99	6.33	11.07	10.70	10.22
-149.97	-15.03	-38.57	82.51	8.30	13.65	13.29	12.83
-149.99	0.01	-40.52	80.95	9.30	14.78	14.45	14.05
-135.09	-0.01	-27.03	95.09	12.04	19.26	18.79	17.80
-135.08	15.07	-27.85	94.01	10.82	18.31	17.86	16.91
-135.07	30.03	-26.77	94.5	7.95	15.06	14.59	13.62
-135.11	45.01	-24.21	96.51	4.90	11.11	10.62	9.56
-135.07	60.04	-21.77	98.8	3.11	7.94	7.44	6.28
-135.11	74.99	-21.32	99.67	3.25	6.95	6.44	5.25
-135.08	89.99	-22.36	99.33	5.06	8.27	7.77	6.60
-135.08	104.94	-23.89	98.37	7.36	10.60	10.11	8.97
-135.11	120.08	-25.1	97.34	8.91	12.60	12.12	11.03
-135.04	135.0	-25.13	97.22	9.07	12.64	12.15	11.07
-135.12	150.03	-23.92	98.29	8.30	11.15	10.66	9.53
-135.05	165.03	-21.71	100.75	7.47	9.67	9.16	7.93
-135.08	-179.94	-20.35	103.04	7.44	9.27	8.74	7.42
-135.06	-164.99	-20.78	103.92	8.98	11.00	10.48	9.13
-135.07	-149.99	-22.49	102.88	11.62	13.65	13.14	11.83
-135.14	-135.01	-25.08	100.07	13.74	16.01	15.52	14.33
-135.07	-119.99	-27.74	96.59	14.17	16.93	16.46	15.41
-135.11	-104.98	-29.64	93.61	12.66	15.78	15.33	14.41
-135.1	-89.94	-29.48	92.62	10.02	13.65	13.20	12.32
-135.08	-75.03	-27.19	93.86	7.50	11.52	11.06	10.12
-135.07	-60.0	-24.25	96.14	6.06	10.35	9.87	8.82
-135.07	-44.98	-22.84	97.63	6.48	11.62	11.13	10.02
-135.06	-30.0	-23.44	97.74	8.58	14.58	14.10	12.98
-135.13	-14.95	-25.26	96.61	11.01	17.64	17.16	16.10
-135.09	-0.0	-27.07	95.07	12.03	19.27	18.81	17.81
-119.99	0.01	-10.34	111.55	13.79	23.70	23.12	21.50
-119.95	14.94	-10.26	111.11	12.06	21.94	21.36	19.74
-119.96	29.97	-8.63	112.04	8.74	17.85	17.26	15.62
-119.99	45.02	-6.16	114.11	5.49	13.15	12.56	10.85
-120.0	59.99	-4.82	115.78	3.98	10.05	9.44	7.70
-119.99	74.97	-5.07	116.24	4.71	9.19	8.59	6.83
-119.99	89.99	-6.21	115.76	6.95	11.02	10.41	8.67
-119.95	104.98	-7.22	115.0	9.25	13.78	13.18	11.46
-119.97	119.99	-7.69	114.34	10.34	15.15	14.56	12.85
-119.97	135.02	-6.96	114.63	9.86	14.14	13.54	11.83
-119.96	149.97	-4.73	116.41	8.47	11.84	11.24	9.48
-120.01	164.98	-2.57	118.9	7.31	10.12	9.50	7.69
-120.0	-179.98	-2.01	120.57	7.63	10.54	9.92	8.08
-119.98	-165.02	-2.64	120.74	9.77	13.21	12.58	10.74
-119.97	-149.97	-4.42	119.13	12.70	17.07	16.45	14.64
-119.98	-135.01	-7.05	116.26	14.83	20.36	19.75	18.00
-120.04	-119.96	-9.75	113.01	15.17	21.08	20.49	18.82
-119.96	-104.98	-11.12	110.8	13.47	19.20	18.62	17.02
-119.99	-90.03	-10.51	110.4	10.62	15.68	15.10	13.51
-119.99	-74.98	-7.98	112.01	7.97	12.60	12.01	10.37
-120.05	-60.0	-6.22	113.73	6.84	12.04	11.45	9.76

O4-C4-C5-O5 (degrees)	O5-C5-C6-O6 (degrees)	C3-C4-C5-C6 (degrees)	O4-C4-C5-C6 (degrees)	QM rel. E (kcal/mol)	MM1 rel. E (kcal/mol)	MM2 rel. E (kcal/mol)	MM3 rel. E (kcal/mol)
-120.02	-45.02	-6.54	114.2	8.01	14.30	13.71	12.00
-120.06	-29.95	-7.9	113.65	10.69	18.29	17.70	16.01
-119.94	-14.97	-9.17	112.76	13.15	22.21	21.62	19.96
-119.94	-0.01	-10.26	111.63	13.79	23.68	23.10	21.47
-105.07	0.04	9.11	129.39	13.64	25.30	24.64	22.72
-105.08	15.03	9.59	129.33	11.40	22.67	22.01	20.09
-105.03	30.04	10.9	130.39	7.92	18.05	17.39	15.47
-105.04	45.02	11.94	131.84	5.05	13.53	12.87	10.94
-105.01	60.03	12.74	133.2	4.10	10.56	9.90	7.97
-105.0	75.0	12.91	133.77	5.20	10.03	9.37	7.44
-105.01	89.93	12.49	133.46	7.41	11.85	11.19	9.26
-105.02	105.04	11.99	132.75	9.32	14.02	13.35	11.43
-104.99	119.99	12.23	132.41	9.72	14.29	13.63	11.71
-105.0	135.0	13.63	133.11	8.62	12.55	11.89	9.97
-105.03	150.01	15.16	134.69	6.88	10.27	9.61	7.70
-104.99	165.02	15.83	136.39	5.98	9.45	8.78	6.87
-104.95	179.99	16.41	137.81	6.94	10.92	10.25	8.35
-104.97	-165.0	16.49	138.05	9.41	14.54	13.86	11.96
-104.96	-150.03	15.45	136.76	12.30	18.74	18.07	16.16
-105.02	-134.98	13.38	134.25	14.32	21.48	20.82	18.89
-105.09	-120.0	11.21	131.49	14.44	21.31	20.65	18.73
-105.01	-105.02	10.24	129.79	12.56	18.26	17.61	15.69
-104.97	-90.03	10.88	129.72	9.64	14.23	13.58	11.66
-105.02	-75.0	11.88	130.72	7.27	12.07	11.42	9.49
-105.03	-60.01	11.74	131.43	6.94	12.93	12.27	10.35
-105.02	-45.01	11.0	131.42	8.75	16.30	15.64	13.71
-105.02	-30.02	10.31	130.98	11.49	20.77	20.11	18.18
-105.06	-15.03	9.54	130.18	13.54	24.45	23.80	21.87
-105.06	0.01	9.13	129.41	13.63	25.32	24.66	22.74
-90.03	-0.02	28.75	147.05	11.59	23.53	22.87	21.10
-90.01	15.02	28.7	146.99	9.27	20.99	20.33	18.57
-90.0	30.02	28.69	147.57	6.26	16.83	16.17	14.41
-90.03	45.03	29.33	148.79	4.01	12.55	11.89	10.14
-90.02	59.97	30.68	150.33	3.32	9.76	9.10	7.39
-89.98	75.02	31.63	151.16	4.28	8.92	8.26	6.56
-90.03	90.05	31.61	150.84	6.06	9.98	9.33	7.62
-89.98	105.0	31.53	150.25	7.33	11.04	10.39	8.68
-90.01	119.98	31.73	149.79	7.24	10.84	10.18	8.47
-89.96	134.99	32.01	150.05	5.85	9.43	8.77	7.06
-90.05	150.01	32.06	151.04	4.39	7.91	7.26	5.56
-90.02	165.02	33.15	152.98	4.11	7.82	7.16	5.50
-89.99	-179.99	34.9	154.81	5.29	9.68	9.02	7.39
-90.07	-165.01	35.73	155.24	7.66	12.98	12.33	10.71
-90.02	-149.99	35.3	154.2	10.30	16.36	15.71	14.08
-90.02	-134.98	33.75	152.01	12.01	18.12	17.47	15.79
-90.06	-120.02	31.82	149.52	11.96	17.38	16.73	15.01
-90.0	-105.01	30.43	147.71	10.14	14.64	13.98	12.23
-90.02	-89.98	29.66	147.09	7.65	12.15	11.49	9.73
-90.01	-74.94	29.62	147.77	6.12	11.42	10.76	9.01
-90.02	-60.01	29.83	148.65	6.37	12.94	12.28	10.54
-89.97	-45.02	29.84	148.89	8.13	16.44	15.78	14.04
-90.05	-30.01	29.38	148.35	10.45	20.52	19.85	18.11
-89.98	-15.0	29.03	147.71	11.97	23.50	22.84	21.09

O4-C4-C5-O5 (degrees)	O5-C5-C6-O6 (degrees)	C3-C4-C5-C6 (degrees)	O4-C4-C5-C6 (degrees)	QM rel. E (kcal/mol)	MM1 rel. E (kcal/mol)	MM2 rel. E (kcal/mol)	MM3 rel. E (kcal/mol)
-90.03	-0.02	28.73	147.04	11.59	23.65	22.99	21.23
-74.93	-0.05	44.91	162.52	9.18	21.13	20.51	19.03
-75.02	14.99	44.03	162.15	7.32	18.80	18.18	16.70
-75.02	29.98	44.04	162.79	4.90	15.02	14.40	12.93
-74.95	44.99	45.37	164.34	2.88	11.19	10.57	9.12
-75.01	60.02	47.11	165.93	2.03	8.13	7.52	6.09
-74.96	74.97	48.28	166.78	2.59	6.78	6.18	4.76
-75.0	90.02	48.34	166.42	3.88	7.11	6.51	5.10
-74.98	104.95	47.83	165.46	4.74	7.95	7.35	5.92
-75.0	120.0	46.98	164.47	4.53	7.89	7.28	5.84
-75.04	134.97	46.36	164.45	3.48	6.92	6.31	4.87
-74.98	150.0	47.01	165.94	2.54	5.77	5.16	3.74
-75.0	165.01	49.01	168.2	2.43	5.72	5.12	3.72
-74.96	-179.96	51.34	170.2	3.43	7.07	6.48	5.12
-75.01	-165.01	52.53	170.73	5.35	9.63	9.05	7.69
-75.01	-150.0	52.16	169.6	7.60	12.35	11.77	10.40
-74.98	-135.04	50.52	167.31	9.19	14.00	13.41	12.02
-75.0	-120.02	48.24	164.62	9.32	14.04	13.44	12.01
-75.01	-104.97	46.18	162.61	8.02	12.75	12.14	10.68
-75.0	-90.02	45.3	162.24	6.26	11.36	10.75	9.27
-75.0	-75.01	45.84	163.35	5.12	10.95	10.34	8.88
-75.0	-60.08	46.74	164.59	5.25	12.42	11.81	10.37
-75.02	-44.98	46.95	164.85	6.62	15.36	14.75	13.32
-75.02	-29.97	46.51	164.31	8.49	18.80	18.19	16.74
-75.03	-14.98	45.76	163.34	9.63	21.06	20.45	18.98
-75.03	0.02	44.83	162.43	9.17	21.13	20.51	19.04
-60.07	-0.05	57.64	175.97	8.37	19.87	19.32	18.00
-60.01	14.99	57.04	175.78	6.96	17.83	17.28	15.96
-60.04	30.06	57.5	176.51	4.72	14.28	13.73	12.42
-59.93	44.98	59.13	178.09	2.59	10.46	9.92	8.62
-60.02	60.02	60.84	179.59	1.40	7.23	6.70	5.40
-60.02	75.02	61.73	-179.75	1.55	5.65	5.12	3.83
-60.0	90.05	61.54	179.82	2.52	5.94	5.42	4.12
-60.03	105.01	60.46	178.58	3.40	6.68	6.15	4.85
-59.96	119.98	59.29	177.59	3.47	6.90	6.36	5.06
-59.97	135.0	58.91	177.77	2.85	6.04	5.49	4.19
-59.92	149.97	60.16	179.42	2.15	4.95	4.42	3.12
-59.98	164.98	62.38	-178.39	1.93	4.50	3.98	2.69
-60.03	-179.99	64.67	-176.59	2.61	5.54	5.04	3.74
-60.03	-164.98	65.84	-176.16	4.24	7.85	7.35	6.06
-60.0	-149.98	65.48	-177.31	6.36	10.80	10.31	9.01
-60.02	-135.01	63.79	-179.62	8.05	13.21	12.71	11.41
-60.01	-119.98	61.4	177.79	8.51	13.95	13.43	12.13
-60.05	-104.93	59.46	176.09	7.61	13.06	12.52	11.22
-59.97	-90.01	59.11	176.19	6.03	11.69	11.15	9.84
-59.95	-75.02	59.88	177.44	4.75	11.21	10.68	9.37
-59.97	-60.03	60.79	178.6	4.56	12.25	11.72	10.42
-59.98	-45.03	60.91	178.9	5.62	14.71	14.18	12.89
-59.99	-29.96	60.2	178.24	7.30	17.74	17.20	15.90
-60.02	-15.02	58.96	177.04	8.47	19.77	19.22	17.92
-60.05	0.01	57.65	175.98	8.36	19.84	19.29	17.98
-45.06	-0.03	69.45	-170.84	9.64	20.40	19.94	18.62
-45.01	14.98	69.02	-171.17	8.38	18.32	17.85	16.53

O4-C4-C5-O5 (degrees)	O5-C5-C6-O6 (degrees)	C3-C4-C5-C6 (degrees)	O4-C4-C5-C6 (degrees)	QM rel. E (kcal/mol)	MM1 rel. E (kcal/mol)	MM2 rel. E (kcal/mol)	MM3 rel. E (kcal/mol)
-45.02	29.99	69.7	-170.55	6.03	14.84	14.38	13.05
-45.01	44.95	71.27	-169.08	3.64	10.87	10.42	9.08
-45.01	59.96	72.9	-167.53	2.19	7.73	7.30	5.94
-45.07	74.98	73.55	-166.9	2.14	6.29	5.86	4.50
-45.01	90.04	73.18	-167.25	3.07	6.83	6.39	5.04
-45.05	104.99	71.92	-168.45	4.14	7.59	7.15	5.81
-45.06	120.01	70.61	-169.6	4.62	7.79	7.34	6.00
-44.97	135.01	70.52	-169.5	4.24	6.95	6.50	5.16
-45.03	150.01	71.8	-168.16	3.53	5.67	5.23	3.88
-45.01	165.02	74.1	-166.09	3.17	5.21	4.78	3.41
-45.04	179.97	76.32	-164.4	3.64	6.36	5.95	4.56
-45.0	-164.99	77.71	-163.76	5.11	9.05	8.66	7.26
-44.98	-149.96	77.53	-164.63	7.23	12.59	12.19	10.80
-45.04	-135.02	75.84	-166.77	9.06	15.14	14.72	13.36
-45.0	-120.01	73.59	-169.07	9.68	15.67	15.23	13.89
-45.01	-105.03	71.8	-170.59	8.80	14.72	14.27	12.94
-45.08	-90.01	71.23	-170.73	7.06	13.24	12.79	11.46
-45.02	-74.99	72.02	-169.59	5.62	12.64	12.20	10.87
-45.04	-59.96	72.8	-168.41	5.29	13.24	12.80	11.46
-45.01	-45.03	72.85	-168.01	6.25	15.53	15.10	13.75
-45.02	-30.02	72.01	-168.59	7.98	18.43	17.98	16.64
-45.0	-15.03	70.71	-169.73	9.39	20.32	19.87	18.54
-45.06	-0.03	69.46	-170.84	9.63	20.38	19.92	18.59
-29.95	-0.02	81.93	-157.07	12.28	22.09	21.74	20.24
-29.97	15.0	81.59	-157.6	10.94	20.07	19.72	18.23
-29.96	29.93	82.32	-157.01	8.40	16.37	16.02	14.52
-29.99	45.05	83.87	-155.49	5.73	12.34	12.01	10.48
-29.99	60.01	85.4	-153.89	4.13	9.31	9.00	7.44
-29.99	75.07	85.94	-153.17	4.06	8.20	7.88	6.32
-29.96	90.0	85.46	-153.48	5.15	8.76	8.44	6.88
-30.02	104.98	84.21	-154.67	6.55	9.73	9.40	7.86
-29.98	119.99	83.01	-155.93	7.33	9.98	9.64	8.12
-29.96	135.02	82.78	-156.26	7.05	9.19	8.85	7.34
-29.96	149.99	84.01	-155.19	6.26	8.05	7.71	6.18
-30.01	165.03	86.24	-153.29	5.62	7.45	7.14	5.57
-30.03	-179.99	88.63	-151.41	5.86	8.88	8.59	6.98
-29.96	-165.02	90.24	-150.38	7.28	11.77	11.50	9.87
-29.98	-149.96	90.09	-150.98	9.49	15.25	14.98	13.36
-29.99	-135.0	88.5	-152.85	11.43	17.58	17.29	15.70
-29.93	-120.0	86.24	-155.08	11.98	18.24	17.92	16.38
-29.91	-105.05	84.45	-156.65	11.01	17.26	16.93	15.42
-29.94	-90.05	83.9	-156.91	9.17	15.63	15.30	13.79
-30.05	-74.95	84.44	-155.97	7.60	14.70	14.37	12.85
-29.99	-59.93	85.23	-154.7	7.27	15.31	14.99	13.45
-30.01	-44.96	85.09	-154.31	8.31	17.58	17.26	15.71
-29.93	-30.04	84.3	-154.75	10.23	20.33	20.00	18.46
-30.02	-14.99	82.95	-155.99	11.88	22.15	21.81	20.29
-29.94	0.02	81.94	-157.05	12.28	22.16	21.81	20.31
-15.02	0.11	96.17	-142.41	14.93	24.41	24.21	22.45
-14.96	15.03	96.02	-142.77	13.40	22.08	21.87	20.12
-14.99	30.01	96.71	-142.14	10.58	18.29	18.09	16.33
-14.96	44.99	98.32	-140.48	7.74	14.21	14.03	12.25
-14.88	60.03	99.78	-138.82	6.10	11.13	10.97	9.16

O4-C4-C5-O5 (degrees)	O5-C5-C6-O6 (degrees)	C3-C4-C5-C6 (degrees)	O4-C4-C5-C6 (degrees)	QM rel. E (kcal/mol)	MM1 rel. E (kcal/mol)	MM2 rel. E (kcal/mol)	MM3 rel. E (kcal/mol)
-14.97	75.0	100.07	-138.31	6.20	10.14	9.98	8.17
-14.96	90.0	99.57	-138.73	7.60	10.85	10.69	8.88
-15.01	104.95	98.6	-139.81	9.23	12.03	11.85	10.06
-15.04	120.01	97.58	-141.04	10.08	12.37	12.18	10.41
-15.04	135.02	97.29	-141.51	9.77	11.72	11.52	9.75
-14.95	149.99	98.43	-140.58	8.75	10.53	10.35	8.56
-14.9	165.01	100.66	-138.63	7.92	10.22	10.06	8.25
-14.96	-179.95	103.03	-136.6	8.02	11.56	11.43	9.59
-14.97	-165.0	104.5	-135.49	9.43	14.25	14.13	12.27
-15.01	-149.96	104.3	-136.01	11.71	17.53	17.40	15.55
-14.94	-134.95	102.75	-137.77	13.60	20.11	19.97	18.14
-14.95	-120.05	100.59	-139.98	14.08	20.98	20.81	19.01
-15.01	-104.98	98.77	-141.68	13.02	19.89	19.71	17.93
-15.0	-89.98	98.21	-141.9	11.17	17.94	17.76	15.98
-14.95	-75.05	98.78	-140.87	9.65	16.72	16.54	14.75
-14.96	-59.97	99.35	-139.75	9.38	17.45	17.28	15.48
-14.94	-44.99	99.06	-139.51	10.64	19.76	19.59	17.79
-14.94	-29.97	98.13	-140.17	12.76	22.56	22.38	20.60
-14.98	-14.98	97.05	-141.3	14.57	24.30	24.10	22.34
-15.02	0.09	96.15	-142.44	14.93	24.38	24.18	22.43
-0.02	-0.04	112.45	-126.65	16.23	25.71	25.68	23.77
-0.05	14.95	112.21	-126.93	14.54	23.41	23.38	21.47
-0.07	29.98	112.92	-126.17	11.50	19.47	19.44	17.54
0.04	44.95	114.53	-124.44	8.58	15.08	15.08	13.18
0.0	60.0	115.75	-123.06	7.03	11.97	11.97	10.08
0.0	74.99	116.17	-122.59	7.34	10.90	10.91	9.01
0.06	89.96	115.89	-122.99	8.97	11.67	11.68	9.78
-0.02	104.99	115.09	-124.0	10.70	13.05	13.05	11.15
0.02	119.93	114.41	-124.88	11.46	13.63	13.62	11.72
-0.08	134.96	114.13	-125.27	10.99	12.94	12.93	11.02
0.0	149.98	115.19	-124.35	9.79	11.82	11.82	9.91
0.01	164.98	117.2	-122.5	8.75	11.28	11.30	9.40
-0.01	179.98	119.34	-120.56	8.83	12.46	12.50	10.61
-0.02	-165.02	120.65	-119.55	10.26	15.14	15.20	13.31
-0.07	-150.01	120.37	-120.15	12.52	18.68	18.74	16.84
-0.05	-135.01	118.8	-121.92	14.34	21.48	21.52	19.61
-0.08	-119.98	116.62	-124.09	14.81	22.44	22.45	20.53
0.02	-105.03	114.98	-125.51	13.85	21.11	21.10	19.18
-0.03	-90.01	114.33	-125.81	12.04	18.90	18.89	16.98
-0.03	-74.98	114.73	-124.93	10.62	17.81	17.81	15.90
0.01	-60.06	115.12	-124.03	10.51	18.66	18.66	16.76
-0.06	-44.99	114.63	-124.17	11.93	21.02	21.02	19.12
-0.04	-30.0	113.87	-124.85	14.16	23.75	23.74	21.84
-0.02	-15.03	113.1	-125.8	15.98	25.70	25.68	23.77
-0.02	0.05	112.43	-126.67	16.22	25.75	25.72	23.82

C.2. References

1. Guvench, O.; MacKerell, A. D. *J. Mol. Model.* **2008**, *14*, 667–679.

2. Frisch, M. J.; Trucks, G. W.; Schlegel, H. B.; Scuseria, G. E.; Robb, M. A.; Cheeseman, J. R.; Montgomery, J. A., Jr.; Vreven, T.; Kudin, K. N.; Burant, J. C.; Millam, J. M.; Iyengar, S. S.; Tomasi, J.; Barone, V.; Mennucci, B.; Cossi, M.; Scalmani, G.; Rega, N.; Petersson, G. A.; Nakatsuji, H.; Hada, M.; Ehara, M.; Toyota, K.; Fukuda, R.; Hasegawa, J.; Ishida, M.; Nakajima, T.; Honda, Y.; Kitao, O.; Nakai, H.; Klene, M.; Li, X.; Knox, J. E.; Hratchian, H. P.; Cross, J. B.; Bakken, V.; Adamo, C.; Jaramillo, J.; Gomperts, R.; Stratmann, R. E.; Yazyev, O.; Austin, A. J.; Cammi, R.; Pomelli, C.; Ochterski, J. W.; Ayala, P. Y.; Morokuma, K.; Voth, G. A.; Salvador, P.; Dannenberg, J. J.; Zakrzewski, V. G.; Dapprich, S.; Daniels, A. D.; Strain, M. C.; Farkas, O.; Malick, D. K.; Rabuck, A. D.; Raghavachari, K.; Foresman, J. B.; Ortiz, J. V.; Cui, Q.; Baboul, A. G.; Clifford, S.; Cioslowski, J.; Stefanov, B. B.; Liu, G.; Liashenko, A.; Piskorz, P.; Komaromi, I.; Martin, R. L.; Fox, D. J.; Keith, T.; Al-Laham, M. A.; Peng, C. Y.; Nanayakkara, A.; Challacombe, M.; Gill, P. M. W.; Johnson, B.; Chen, W.; Wong, M. W.; Gonzalez, C.; Pople, J. A. *Gaussian 03* Revision C.02; Gaussian, Inc.: Wallingford, CT, 2004.

3. Becke, A. D. *J. Chem. Phys.* **1993**, *98*, 5648–5652.

4. Clark, T.; Chandrasekhar, J.; Spitznagel, G. W.; Schleyer, P. V. *J. Comput. Chem.* **1983**, *4*, 294–301.

5. Frisch, M. J.; Pople, J. A.; Binkley, J. S. *J. Chem. Phys.* **1984**, *80*, 3265–3269.

6. Case, D. A.; Darden, T. A.; T.E. Cheatham, I.; Simmerling, C. L.; Wang, J.; Duke, R. E.; Luo, R.; Crowley, M.; Walker, R. C.; Zhang, W.; Merz, K. M.; Wang, B.; Hayik, S.; Roitberg, A.; Seabra, G.; Kolossváry, I.; Wong, K. F.; Paesani, F.; Vanicek, J.; Wu, X.; Brozell, S. R.; Steinbrecher, T.; Golke, H.; Yang, L.; Tan, C.; Mongan, J.; Hornak, V.; Cui, G.; Mathews, D. H.; Seetin, M. G.; Saugi, C.; Babin, V.; Kollman, P. A. *AMBER 10*, Univeristy of California, San Francisco: 2008.

7. Kirschner, K. N.; Yongye, A. B.; Tschampel, S. M.; González-Outeiriño, J.; Daniels, C. R.; Lachele Foley, B.; Woods, R. J. *J. Comput. Chem.* **2008**, *29*, 622–655.